VOLUME 121 NUMBER 1

THE ASTROPHYSICAL JOURNAL

AN INTERNATIONAL REVIEW OF SPECTROSCOPY AND ASTRONOMICAL PHYSICS

JANUARY 1955

A CATALOGUE OF RELIABLY KNOWN DISCRETE SOURCES OF COSMIC RADIO WAVES . . . . . *J. L. Pawsey* 1

ACCELERATION OF INTERSTELLAR CLOUDS BY O-TYPE STARS *Jan H. Oort and Lyman Spitzer, Jr.* 6

THE ASSOCIATION I GEMINORUM *D. Crawford, D. Nelson Limber, E. Mendoza, D. Schulte, H. Steinman, and T. Swihart* 24

SPECTRAL AND LUMINOSITY CLASSIFICATION OF THE BRIGHT SEQUENCE STARS IN THE C REGIONS . . . . . *J. J. Nassau and Donald A. MacRae* 32

PRELIMINARY LIST OF PHOTOELECTRIC CLASSIFICATION INDICES FOR 234 BRIGHT NORTHERN G AND K STARS . . . . . *K. Gyldenkerne* 38

SPECTRAL CLASSIFICATION OF G AND K STARS THROUGH PHOTOELECTRIC PHOTOMETRY WITH INTERFERENCE FILTERS *Bengt Strömgren and K. Gyldenkerne* 43

THE COLORS OF THE BETA CANIS MAJORIS STARS *D. H. McNamara and A. D. Williams* 51

THE ECLIPSING BINARY V356 SAGITTARII . . . . . *Daniel M. Popper* 56

ON THE SUBGIANT COMPONENTS OF ECLIPSING BINARY SYSTEMS *J. A. Crawford* 71

A SPECTROSCOPIC STUDY OF THE DOUBLE STAR DELTA EQUULEI *William H. Wehlau* 77

STUDY OF DOPPLER VELOCITIES IN STELLAR ATMOSPHERES: THE SPECTRUM OF ALPHA CYGNI . . . . . *Su-Shu Huang and Otto Struve* 84

AXIAL ROTATION IN THE BRIGHTER STARS OF DRAPER TYPES B2–B5 *Arne Slettebak and Robert F. Howard* 102

AXIAL ROTATION AND LINE BROADENING IN STARS OF SPECTRAL TYPES F0–K5 *George H. Herbig and John F. Spalding, Jr.* 118

(Continued on inside page)

THE UNIVERSITY OF CHICAGO PRESS
CHICAGO, ILLINOIS, U.S.A.

January 1955 Vol. 121, No. 1

THE ASTROPHYSICAL JOURNAL

AN INTERNATIONAL REVIEW OF SPECTROSCOPY AND ASTRONOMICAL PHYSICS

Founded in 1895 by George E. Hale and James E. Keeler

Published in Collaboration with the American Astronomical Society

S. CHANDRASEKHAR
Managing Editor

GERARD P. KUIPER
Associate Editor

Yerkes Observatory of the University of Chicago

EDITORIAL BOARD

LEO GOLDBERG (1955-59)
The Observatory of the University of Michigan

H. W. BABCOCK (1953-57)
Mount Wilson Observatory of the Carnegie Institution of Washington

MARTIN SCHWARZSCHILD, JR. (1954-58)
Princeton University Observatory

O. HERZBERG (1952-56)
National Research Council, Ottawa

C. D. SHANE (1952-55)
Lick Observatory, University of California

The Astrophysical Journal is published bimonthly by the University of Chicago at the University of Chicago Press, 5750 Ellis Avenue, Chicago 37, Illinois, during January, March, May, July, September, and November. ¶Two volumes are published per year, one beginning with the January issue and the other beginning with the July issue. On all orders from the United States and its possessions the subscription price is $7.50 per volume or $15.00 per year; the price of single copies is $3.50. ¶On all orders from Canada the subscription price is $8.00 per volume or $16.00 per year; the price of single copies is $3.65. On all orders from all other countries the subscription price is $8.25 per volume or $16.50 per year; the price of single copies is $3.75. (Orders for service of less than a volume will be charged at the single-copy rate.) ¶Postage is prepaid by the publishers on all orders from the United States and its possessions. No extra charge is made for postage to countries in the Pan American Postal Union. ¶Postage is charged extra as follows: for Canada, 20 cents per volume, 40 cents per year (total $8.20 per volume, $16.40 per year), on single copies 5 cents ($3.70); for all other countries in the Postal Union, 40 cents per volume, 75 cents per year (total $8.65 per volume, $17.25 per year), on single copies 10 cents (total $3.85). ¶Subscriptions are payable in advance. Please make all remittances payable to The University of Chicago Press, in United States currency or its equivalent by postal or express money orders or bank drafts. (Exception: members of The American Astronomical Society must send their subscriptions and remittances to the Treasurer of the Society.)

The following is an authorized agent:

For the British Commonwealth, except North America and Australasia: The Cambridge University Press, Bentley House, 200 Euston Road, London, N.W. 1, England. Prices of yearly subscriptions and of single copies may be had on application.

Claims for missing numbers should be made within the month following the regular month of publication. The publishers expect to supply missing numbers free only when losses have been sustained in transit, and when the reserve stock will permit.

Business correspondence should be addressed to The University of Chicago Press, Chicago 37, Illinois.

Communications for the editors and manuscripts should be addressed to: S. Chandrasekhar, Editor of THE ASTROPHYSICAL JOURNAL, Yerkes Observatory, Williams Bay, Wisconsin.

Line drawings and photographs should be made by the author, and all marginal notes such as co-ordinates, wave lengths, etc., should be included in the cuts. It will not be possible to set up such material in type.

One copy of the corrected galley proof should be returned as soon as possible to the editor, Yerkes Observatory, Williams Bay, Wisconsin. Authors should take notice that the manuscript will not be sent to them with the proof.

The cable address is "Observatory, Williamsbay, Wisconsin."

The articles in this journal are indexed in the *International Index to Periodicals*, New York, N.Y.

Applications for permission to quote from this journal should be addressed to The University of Chicago Press, and will be freely granted.

Microfilms of complete journal volumes are available to regular subscribers only and may be obtained at the end of the year. Orders and inquiries should be addressed to University Microfilms, 313 North First Street, Ann Arbor, Michigan.

Notice to subscribers: If you change your address, please notify us and your local postmaster immediately.

Entered as second-class matter, July 31, 1940, at the Post-Office at Chicago, Ill., under the Act of March 3, 1879.
Acceptance for mailing at special rate of postage provided for in United States Postal Act of October 3, 1917, Section 1103, amended February 28, 1925.
Copyright 1955 by the University of Chicago.

[PRINTED IN U.S.A.]

(*Continued from front cover*)

ORIGIN OF ANOMALOUS ABUNDANCES OF THE ELEMENTS IN GIANT STARS
A. G. W. Cameron 144

THE LUMINOSITY FUNCTION AND STELLAR EVOLUTION . . *Edwin E. Salpeter* 161

ON TOROIDAL MAGNETIC FIELDS IN THE SUN AND STARS
C. Plumpton and V. C. A. Ferraro 168

THE TRANSFER OF RADIATION BY AN EMITTING ATMOSPHERE. IV
Charles A. Lundquist and Henry G. Horak 175

THE TRANSFER OF RADIATION BY AN EMITTING ATMOSPHERE. V
Charles A. Lundquist 183

FORMATION OF ABSORPTION LINES . . . . . *James W. Warwick* 190

QUANTUM THEORY OF LINE BROADENING BY AN IONIC PLASMA
H. Margenau and R. Meyerott 194

A STATISTICAL ANALYSIS OF SPECTROHELIOGRAMS . . . *John B. Rogerson, Jr.* 204

ADDITIONAL DATA FOR TURBULENCE SPECTRUM OF SOLAR PHOTOSPHERE AT LONG WAVE LENGTHS . . . . . *F. N. Frenkiel and M. Schwarzschild* 216

THE PROMINENCE OF JULY 25, 1951
Kurt Rothschild, Jean-Claude Pecker, and Walter Orr Roberts 224

CORONAL LINE INTENSITIES AT THE KHARTOUM ECLIPSE
R. G. Athay and W. O. Roberts 231

THE PHYSICAL THEORY OF METEORS. VII. ON METEOR LUMINOSITY AND IONIZATION . . . . . *Fred L. Whipple* 241

PHOTOMETRIC ANALYSIS OF A SPECTROGRAM OF A PERSEID METEOR
Allan F. Cook and Peter M. Millman 250

SUPPRESSION OF *AlO* IN THE WAKE OF ULTRASPEED PELLETS *William C. White* 271

THE ULTRAVIOLET AIRGLOW SPECTRUM . . . . . *Joseph W. Chamberlain* 277

NOTES

AN IDENTIFICATION OF THE CORONAL LINE λ 5694 . . . . *Ali M. Naqvi and S. P. Talwar* 287

ANNOUNCEMENT 290

THE ASTROPHYSICAL JOURNAL

AN INTERNATIONAL REVIEW OF SPECTROSCOPY AND ASTRONOMICAL PHYSICS

VOLUME 121 JANUARY 1955 NUMBER 1

A CATALOGUE OF RELIABLY KNOWN DISCRETE SOURCES OF COSMIC RADIO WAVES

J. L. Pawsey

President, Commission 40 of the International Astronomical Union

Received August 2, 1954

ABSTRACT

As a part of the work of Commission 40 of the International Astronomical Union, a list of reliably known discrete sources of cosmic radio waves has been prepared by a committee consisting of J. G. Bolton, R. Hanbury Brown, F. G. Smith, and B. Y. Mills. In this paper this list is published, with a short description of the catalogue by the president of the commission, J. L. Pawsey.

INTRODUCTION

Observations of discrete sources of cosmic radio waves (sometimes called "radio stars") are severely limited by the relatively poor resolving power of radio instruments. The more intense or more favorably situated ones can be located with certainty and precision, but there remains a large number whose positions are known very imperfectly. Indeed, where a number of sources are close together, the resulting confusion can lead to an assigned position where no source exists, the observation referring to a "blend" of several sources each slightly removed from the assigned position. In these circumstances it is most difficult for an astronomer who has no direct access to the radio observers to know what certainty to attach to a published location of a radio source.

In an attempt partly to overcome this difficulty, it was suggested by the radio astronomy commission of the Union Radio Scientifique Internationale (U.R.S.I.) that the corresponding commission (Commission 40) of the International Astronomical Union (I.A.U.) should prepare and publish a list of sources whose existence was certain and should supplement this list from time to time as better observations became available.

The members of Commission 40 considered this suggestion sound and have taken steps to prepare an initial list, which is given below.

The list was prepared, on the invitation of the president of Commission 40, by a committee consisting of J. G. Bolton (*convenor*) (Sydney), R. Hanbury Brown (Manchester), F. G. Smith (Cambridge), and B. Y. Mills (Sydney). These men were selected because they include representatives of each of the laboratories which have published major contributions to this subject. Further, they were already engaged in the preparation of a special report for the U.R.S.I. on the discrete sources.

It will be noted that different observers have given their own catalogue numbers to

TABLE 1

I.A.U. Catalogue of Discrete Sources of Cosmic Radio Waves (1954), List 1

Constellation	I.A.U. No.	Observer's Catalogue No.	Position (1950 Epoch) R.A.	Position (1950 Epoch) Dec.	Flux Density Frequency (Mc/Sec)	Flux Density Watts M^{-2} (C/Sec)$^{-1}$ $\times 10^{-24}$	Angular Size Dimensions	Angular Size Position Angle	Optical Identifications* Object	Mag-nitude	Position (1950): R.A., Dec.	Angular Size
Andromeda	00N4A	R 00.01 HB 2	00h40m15s ± 30s 00h42m ± 6m	40°50′ ± 20′ p 38° ± 5° k	81.5 158	0.4 k 1.6 p			M31 NGC 224	5.0	00h40m00s +41°00′	
Perseus	03N4A	BSS 40 R 03.02 M 03+4 HB 6	03h15m15s ± 1½m 03h12m ± 3m 03h10m ± 4m 03h16m37s ± 4s	41°22′ ± 30′ p 43°45′ ± 30′ k 42° ± 20′ b 41°25′ ± 6′ x	81.5 81.5 100 101 158	0.95 k 1.2 z 0.9 r 2.4 b 0.6 p			NGC 1275, colliding galaxies	13.28	03h16m31s 41°19′	
Taurus	05N2A	BSS 2 R 05.01 M 05+2 NRL 2	05h31m29s ± 2½s 05h31m25s ± 30s 05h31m35s ± 5s	22°00′ ± 3′ c 22°02′ ± 8′ a 22°04′ ± 5′ d	60 81.5 100 101 160 3200	18.5 a 12.5 k 18.5 a 19.0 b 18.5 a 8.0 y	3½′×5½′†	140° n	M1 NGC1952 Crab Nebula	9	05h31m30s 21°59′.3	4′×6′ position angle 120°
Puppis	08S4A	BSS 21 M 08−4 S 08−4	08h20m ± 4m	−42°30′ ± 1° r	18.3 100 101	70 s 35 r 5.0 b	33′ >1° but <2°	E.-W.‡ b g	Galactic nebulosity		08h27m.3 −42°48′	50′×80′ position angle 145°
Virgo	12N1A	BSS 4 R 12.01 M 12+1 S 12+1 NRL 8	12h28m15½s ± 2½s 12h28m18s ± 3s 12h28m11s ± 37s	12°44′ ± 6′ c 12°37′ ± 10′ d 12°41′ ± 10′ a	18.3 60 81.5 100 101 3200	110 s 25.0 a 10.5 k 12.5 a 12 b 1.4 y	2½′×5′†	50° n	M87 NGC 4486	9.9	12h28m18s 12°40′.1	5′
Centaurus	13S4A	BSS 6 M 13−4 S 13−4 NRL 7	13h22m30s ± 4s 13h22m24s ± 1m	−42°46′ ± 2′ c −42°37′ ± 8′ a	60 100 101 3200	32.0 a 18.5 a 16.0 b 2.0 y	3′×6½′	130° n	NGC 5128	6.1	13h22m28s −42°45′.6	20′
Cygnus	19N4A	BSS 1 R 19.01 M 19+4 HB 19 (S 20+X) NRL 3	19h57m45.3s ± 1s 19h57m44s ± 2½s	40°35′ ± 1′ d 40°35′ ± 1½′ c	60 81.5 100 101 158 3200	220 a 135 k 125 a 130 b 57 p 7.0 y	2′10″×35″ 0′.9 3′.5	120°‡ e E.-W.§ n E.-W.‖ j	Colliding gallaxies	17.9	19h57m44s.5 40°35′46′.3	18″×30″ position angle 150° nucleus, 3″×5″ position angle 115°
Cassiopeia	23N5A	R 23.01 HB 23 NRL 1	23h21m12s ± 1s 23h21m36s ± 30s	58°32′.1 ± 0′.7 d 58°35′ ± 10′ p	81.5 158 3200	220 k 93 p 15.0 y	3′×4′ 5′	25°‡ e E.-W.‖ j	Galactic nebulosity		23h21m11s.4 58°31′52′.9	6′.3 in diameter

* Optical identifications are discussed by W. Baade and R. Minkowski, *Ap. J.*, **119**, 206 and 215, 1954.

† The width between the half-brightness isophotes along the minor and major axes.

‡ The equivalent rectangular strip of constant surface intensity.

§ The width between half-intensity points of the measured distribution of intensity across the equivalent strip source.

‖ The equivalent circular disk of constant surface intensity (measured in the specified direction).

particular sources. In an attempt to gain a measure of uniformity, a new designation, headed "I.A.U. Number," has been allotted to each source. This system is based on position in the sky, the five symbols being allocated as indicated below.

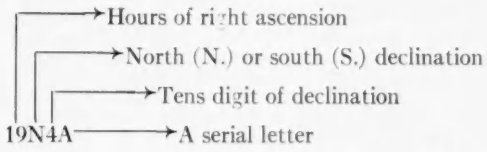

At present the major sources are well known by their constellation names, e.g., Cygnus and Cassiopeia, and there is every reason to expect that this will continue. Catalogue numbers are essential for the minor sources. The commission hopes to publish supplementary lists of sources from time to time.

TABLE 2

I.A.U. CATALOGUE OF DISCRETE SOURCES OF COSMIC RADIO WAVES, LIST 2*a*

CONSTELLATION	I.A.U. No.	OBSERVER'S CATALOGUE No.	POSITION (1950 EPOCH) R.A.	POSITION (1950 EPOCH) Dec.	FLUX DENSITY Frequency (Mc/Sec)	FLUX DENSITY Watts M^{-2} (C/Sec)$^{-1}$ $\times 10^{-24}$	SUGGESTED IDENTIFICATIONS AND REMARKS
Cassiopeia	00N6A	HB 1	$00^h22^m \pm 2^m$	$64°15' \pm 35'$ q	158	1.7 q	Supernova 1572 (no visible remnants)
Auriga	04N4A	BSS 76 (M 05+4) HB 9	$04^h57^m \pm 2^m$ $05^h08^m \pm 4^m$	$46\frac{1}{2}° \pm 1°$ p $46° \pm 1°$ r	100 158	0.7 r 0.8 p	Angular size of source is 1°.4; identified with galactic nebulosity w
Orion	05S0A	NRL 6	$05^h33^m0 \pm 0^m2$	$-05°27' \pm 5'$ y	3200	4.5 y	Orion Nebula M42, NGC 1976
Gemini	06N2A	R 06.01	$06^h13^m37^s \pm 4^s$	$22°38' \pm 5'$ z	38 81.5	6.5 z 4.2 z	IC 443
Ursa Major	09N6A		$09^h51^m20^s \pm 2^m$	$69° \pm 1°$ t	158	0.12 t	NGC 3031
Canes Venatici	12N4A	HB 15	$12^h15^m \pm 3^m$	$47° \pm 1\frac{1}{2}°$ p	158	0.5 p	NGC 4258
Canes Venatici	13N4A	R 13.01 HB 17	$13^h27^m30^s \pm 3^m$ $13^h26^m \pm 4^m$	$47° \pm 1°$ p $48° \pm 3°$ k	81.5 158	0.35 k 0.055 p	NGC 5194–5195
Boötes	14N5A	(R 14.01) M 14+5 HB 18	$14^h10^m \pm 2^m$ $14^h20^m \pm 8^m$	$51°30' \pm 1°$ p $51° \pm 40'$ b	101 158	2.0 b 0.4 p	NGC 5457
Sagittarius	18S1A	NRL 4	$18^h17^m9 \pm 0^m2$	$-16°14' \pm 5'$ y	3200	6.8 y	Omega Nebula, M17, NGC 6618

I.A.U. CATALOGUE OF DISCRETE SOURCES OF COSMIC RADIO WAVES (1954)

This short catalogue is divided into two lists. List 1 (Table 1) contains those sources whose existence has been definitely established, for which accurate positions have been given by a number of observers, and for which optical identifications have been secured. In some cases the identifications are supported by agreement between the radio and optical sizes.

List 2 (Tables 2 and 3) contains sources for which the radio positions are not known so accurately. Their inclusion is considered justified because either a reasonable identification has been suggested for the source (List 2*a* [Table 2]) or there is good agreement between the positions and flux densities given in surveys by two or more independent

TABLE 3

I.A.U. CATALOGUE OF DISCRETE SOURCES OF COSMIC RADIO WAVES, LIST 2*b*

CONSTELLATION	I.A.U. No.	OBSERVER'S CATALOGUE No.	POSITION (1950 EPOCH) R.A.	POSITION (1950 EPOCH) Dec.	FLUX DENSITY Frequency (Mc/Sec)	FLUX DENSITY Watts M^{-2} $(C/Sec)^{-1}$ $\times 10^{-24}$	REMARKS
Cetus	02S0A	BSS 97 M 02−0	$02^h36^m \pm 10^m$ $02^h35^m \pm 4^m$	$-3° \pm 3°$ r $-4° \pm 1°.5$ b	100 101	0.7 r 0.5 b	
Cetus	02S1A	BSS 62 M 02−1	$02^h04^m \pm 5^m$ $02^h00^m \pm 4^m$	$-10° \pm 2°$ r $-11° \pm 40'$ b	100 101	0.85 r 1.0 b	
Fornax	03S3A	BSS 10 M 03−3 S 03−4	$03^h19^m30^s \pm 6^s$ $03^h17^m \pm 5^m$	$-37°18' \pm 3'$ c $-37°15' \pm 1°$ r	18.3 100 101	35 s 2.4 r 2.4 b	Apparent extended source with complicated brightness distribution; may be a blend
Perseus	04N3A	BSS 8 M 04+3 R 04.01	$04^h30^m \pm 8^m$ $04^h30^m \pm 4^m$	$31° \pm 40'$ b $31° \pm 1°$ r	81.5 100 101	3.3 k 3.0 r 3.0 b	
Pictor	05S4A	BSS 22 M 05−4 S 05−4	$05^h09^m \pm 4^m$ $05^h30^m \pm 4^m$ 05^h12^m	$-43\frac{1}{2}° \pm 1°$ r $-46\frac{2}{3}° \pm 20'$ b $-45°$ s	18.3 100 101	35 s 18 r 2.5 b	Extended source
Lynx	08N4A	R 08.01 HB 11	$08^h09^m \pm 2^m$ $08^h08^m \pm 15^s$	$48° \pm 1°$ k $48°15' \pm 30'$ p	81.5 158	1.0 k 0.4 p	
Monoceros	08S0A	BSS 99 M 08−0	$08^h08^m \pm 10^m$ $08^h10^m \pm 8^m$	$-6° \pm 3°$ r $-4° \pm 1°.5$ b	100 101	0.6 r 0.5 b	
Lynx	09N4A	BSS 86 R 09.01 (M 09+4) HB 12	$09^h16^m \pm 8^m$ $09^h16^m \pm 4^m$ $09^h16^m \pm 2^m$	$46° \pm 2°$ r $47° \pm 1°$ k $45° \pm 1°$ p	81.5 100 158	0.5 k 0.7 r 0.3 p	
Hydra	09S1A	BSS 26 M 09−1A S 09−1	$09^h16^m \pm 2^m$ $09^h15^m46^s \pm 4^s$	$-12° \pm 2°$ r $-11°55' \pm 8'$ c	18.3 100 101	40 s 2.8 r 2.5 b	
Ursa Major	10N5B	R 10.03 HB 13	$10^h30^m \pm 2^m.5$ $10^h33^m \pm 4^m$	$57° \pm 2°$ p $56° \pm 1°$ k	81.5 158	0.33 k 0.05 p	
Vela	10S4A	BSS 50 M 10−4	$10^h10^m \pm 4^m$ $10^h20^m \pm 5^m$	$-42\frac{1}{2}° \pm 20'$ b $-43\frac{1}{2}° \pm 1°$ r	100 101	0.8 r 1.0 b	
Crater	11S1A	BSS 56 M 11−1	$11^h38^m \pm 8^m$ $11^h45^m \pm 8^m$	$-15° \pm 2°$ r $-14° \pm 40'$ b	100 101	0.5 r 0.5 b	
Canes Venatici	12N4B	M 12+4 HB 16	$12^h49^m \pm 2^m$ $12^h55^m \pm 8^m$	$47\frac{1}{2}° \pm \frac{1}{2}°$ p $49° \pm 40'$ b	101 158	1.2 b 0.18 p	
Centaurus	13S6A	BSS 28 M 13−6	$13^h35^m \pm 8^m$	$-60\frac{1}{4}° \pm 5'$ b	101	7.5 b	
Serpens Caput	15N1A	BSS 80 M 15+1	$15^h10^m \pm 4^m$ $15^h10^m \pm 6^m$	$11° \pm 1\frac{1}{2}°$ b $11° \pm 1\frac{1}{2}°$ r	100 101	0.6 r 1.0 b	
Hercules	16N4A	M 16+4 R 16.03 BSS 81	$16^h36^m \pm 10^m$ $16^h40^m \pm 4^m$	$41° \pm 2°$ r $41° \pm 40'$ b	100 101	0.8 r 0.8 b	
Hercules	16N0A	BSS 7 M 16+0 R 16.01	$16^h45^m \pm 2^m$ $16^h49^m \pm 2^m$	$6° \pm 1°.5$ b $6° \pm 1°$ r	81.5 100 101	3.0 k 4.0 r 4.0 b	
Triangulum Australis	16S6A	BSS 27 M 16−6	$16^h10^m \pm 8^m$	$-60\frac{3}{4}° \pm 5'$ b	101	8.5 b	
Sagittarius	17S2A	M 17−2B BSS 68 NRL 5	$17^h44^m \pm 2^m$ $17^h42^m \pm 1^m$ $17^h42^m.5 \pm 0^m.2$	$-30° \pm 1°$ aa $-28°.5 \pm 0°.2$ bb $-29°01' \pm 5'$ y	100 101 400 1200 3200	1.2 r .3 b 14 bb 26 aa 4.8 y	May be associated with the galactic nucleus; the presence of neighboring intense emission regions makes the measurements of flux density difficult
Ophiuchus	18S0A	BSS 120 M 18−0	$18^h16^m \pm 4^m$ $18^h10^m \pm 4^m$	$-8° \pm 2°$ r $-6° \pm 1°.5$ b	100 101	1.5 r 2.5 b	
Cygnus	20N4A	HB 20 Cyg-X	20^h22^m $20^h27^m \pm 3^m$	$40°$ p $40\frac{1}{2}° \pm 1°$ m	158 1210	3.0 p 8.7 m	Extended source possibly associated with galactic nebulosity

REFERENCES TO TABLES

a Stanley, G. J., and Slee, O. B. 1950, *Australian J. Sci. Res.*, **A3**, 234.
b Mills, B. Y. 1952, *Australian J. Sci. Res.*, **A5**, 266.
c Mills, B. Y. 1952, *ibid.*, p. 456.
d Smith, F. G. 1951, *Nature*, **168**, 555.
e Brown, R. Hanbury, Jennison, R. C., and Das Gupta, M. K. 1952, *Nature*, **170**, 1061.
g Bolton, J. G., Westfold, K. C., Stanley, G. J., and Slee, O. B. 1954, *Australian J. Phys.*, **7**, 96.
j Smith, F. G. 1952, *Nature*, **170**, 1065.
k Ryle, M., Smith, F. G., and Elsmore, B. 1950, *M.N.*, **110**, 508.
m Piddington, J. H., and Minnett, H. C. 1952, *Australian J. Sci. Res.*, **A5**, 17.
n Mills, B. Y. 1953, *Australian J. Phys.*, **6**, 452.
p Brown, R. Hanbury, and Hazard, C. 1953, *M.N.*, **113**, 123.
q Brown, R. Hanbury, and Hazard, C. 1952, *Nature*, **170**, 364.
r Bolton, J. G., Stanley, G. J., and Slee, O. B. 1954, *Australian J. Phys.*, **7**, 110.
s Shain, C. A., and Higgins, C. S. 1954, *Australian J. Phys.*, **7**, 130.
t Brown, R. Hanbury, and Hazard, C. 1953, *Nature*, **172**, 853.
w Brown, R. Hanbury, Palmer, H. P., and Thompson, A. R. 1954, *Nature*, **173**, 945.
x Baldwin, J. E., and Elsmore, B. 1954, *Nature*, **173**, 818.
y Haddock, F. T., Mayer, C. H., and Sloanaker, R. M. 1954, *Ap. J.*, **119**, 456.
z Baldwin, J. E., and Dewhirst, D. W. 1954, *Nature*, **173**, 164.
aa Piddington, J. H., and Minnett, H. C. 1951, *Australian J. Sci. Res.*, **A4**, 459.
bb McGee, R. X., and Bolton, J. G. 1954, *Nature*, **173**, 985.

observers. The catalogue numbers of the independent observers have been given with an identifying prefix, e.g., BSS 50 is source number 50 in the list compiled by Bolton, Stanley, and Slee.

Letters alongside data in the list denote the sources of the data, explained in a key at the end. Where the uncertainty in the observational data can be indicated simply, it has been done, e.g., in the measured positions of the sources.

The catalogue was compiled early in 1954 on the basis of observations published at that time. More detailed and reliable observations are rapidly becoming available as better equipment is put into operation. Such unpublished results are not included in the catalogue but have been used to check the reality of the great majority of those sources included. In this respect, data supplied by J. P. Hagen and J. D. Kraus and preliminary observations obtained by B. Y. Mills have been particularly helpful.

In conclusion, I wish to express the thanks of the members of Commission 40 to those who have contributed to the computation and checking of this list: to the members of the committee, named above, and also to J. P. Hagen, J. D. Kraus, R. Minkowski, and M. Ryle, who helped in the checking.

ACCELERATION OF INTERSTELLAR CLOUDS BY O-TYPE STARS

JAN H. OORT* AND LYMAN SPITZER, JR.
Leiden Observatory and Princeton University Observatory
Received June 18, 1954

ABSTRACT

A possible mechanism is proposed for the acceleration of interstellar clouds. The ultraviolet light from a newly born O star heats the gas in a dense interstellar cloud from 100° to 10,000° K. The resultant increase in pressure leads to high accelerations, and in this way an appreciable fraction of the radiant energy from a hot star may be converted into kinetic energy of cloud motions.

Since a detailed treatment of this problem would be very intricate, involving an integration through time both of the hydrodynamic equations and of the equation of radiative transfer, a preliminary analysis is carried through. When the side of the cloud facing the O star is heated, the heated cloud gases expand into the less dense material between the cloud and the O star. The momentum carried away by these gases is computed approximately, on the assumption that the pressure of the gas originally surrounding the cloud is negligible. The acceleration of the cloud is then found from the momentum carried away, with the use of Newton's third law of motion but with complete neglect of all detailed hydrodynamic effects within the cloud.

The analysis is applied to three physical situations: (*a*) formation of an O star near a single dense cloud, which then becomes accelerated; (*b*) approach of a cloud to an O star in a steady state, with repulsion of the cloud by the "rocket effect" of the expelled gases; (*c*) formation of an O star in an extended cloud complex of such large mass that the O star can ionize only part of it; the outside cool shell may then be driven away. In all three cases, the mass of the neutral cloud decreases during the interaction with the radiation field, and very high velocities may be attained. It seems possible to explain by such mechanisms the high velocities that are observed in the faint components of interstellar lines. It may be, even, that all random cloud motions in the interstellar gas originate in this way.

I. INTRODUCTION

The multiplicity of the interstellar K and H lines, investigated first by Beals (1936), then very extensively by Adams (1949), demonstrates that interstellar gas clouds have appreciable random motions with respect to one another. The distribution of cloud velocities has been considered by Whipple (1948), Blaauw (1952*b*), Searle (1952), and Schlüter, Schmidt, and Stumpff (1953) on the basis of the data by Adams. Whipple showed that the distribution was non-Maxwellian; he fitted the observations with two Maxwellian distributions: large clouds, with a root-mean-square radial velocity in the neighborhood of 8 km/sec, and small clouds, with a corresponding velocity of about 25 km/sec. In the analysis by Blaauw, which takes into account the overlapping of components produced in different clouds, the observations are fitted with a distribution function proportional to $\exp(-v/\eta)$, where η is 5 km/sec; the corresponding root-mean-square velocity is 7 km/sec. However, neither of these two theoretical distributions provides a fit for the few clouds observed with very high velocities, between 50 and 100 km/sec. As shown by Spitzer (1948*b*), a root-mean-square random cloud velocity of 9 km/sec is consistent also with the observed equivalent widths of the interstellar D lines. Searle and Schlüter, Schmidt, and Stumpff discuss the prevalence of negative values among the clouds with random velocities in excess of 15 km/sec, a problem that had also been indicated by Blaauw.

Observations of the hydrogen line near 21 cm give slightly higher random velocities. From extensive measures in the northern Milky Way, van de Hulst, Muller, and Oort (1954) have derived $\eta = 8.5$ km/sec. This value is in good agreement with the mean velocity found by Blaauw from his more distant group of stars.

* Visiting professor at Princeton University when this work was undertaken. The authors have shared evenly in the work; their names appear in alphabetical order.

Very little work has been done on the origin of these motions. Von Weizsäcker (1948, 1949) has proposed that the motions can be regarded as turbulence generated by the differential galactic rotation, and he suggests that the spread of relative velocities within a region will vary as the cube root of the size of the region, as in isotropic turbulence. Such a picture has been applied by Jentzsch and Unsöld (1948) to an explanation of the equivalent widths of interstellar *Na* I and *Ca* II. However, there is some question as to whether the theory of isotropic turbulence in an incompressible fluid can actually be applied to supersonic motions of a gas with large density fluctuations in a rotating galaxy.

Moreover, if we combine the evidence from interstellar lines with that of other observational data on dark clouds and luminous nebulae, the picture we obtain looks rather different from what would be expected on the theory of turbulent motion. Instead of more or less contiguous vortices, we find concentrated clouds that are often separated by much larger spaces of negligible density. Whenever two such clouds collide, there will be considerable losses of kinetic energy, and it is uncertain whether the transfer of energy from the rotation of the Galaxy, regarded as the largest eddy, to smaller and smaller eddies, as envisaged in the theory of isotropic turbulence, can maintain the velocities of the clouds at their observed level.

It would seem a priori that stellar radiation would, in principle, provide a much more abundant source of energy for the maintenance of cloud velocities. Spitzer and Savedoff (1950) have suggested that temperature differences between *H* I and *H* II regions might provide the driving force for the cloud motions, in much the same way as thermal effects produce terrestrial winds. No quantitative analysis along these lines was given.

It now seems probable that the major part of the kinetic energy of clouds may come from the formation of O stars. The fact that O stars are frequently found imbedded in, or associated with, large and dense cloud complexes indicates that they form preferentially in such extended nebulous regions. The newly born O star will ionize the hydrogen in its immediate surroundings up to the radius of the Strömgren sphere. In many cases the cloud agglomerations exceed this radius, and dense cool clouds remain at the outside, showing as dark nebulae. The ionization of the parts near the O star raises their temperature by a factor of 100. The consequent increase of the pressure will cause the ionized parts of the cloud complex to expand and to push away the nonionized parts, which will, in general, be set moving with sensible velocities. These velocities will be increased by the circumstance that during the expansion the radius of the Strömgren sphere will increase faster than the radius of the expanding region and that, consequently, new parts of the neutral clouds will continually be ionized; the region of ionized *H* will gradually eat its way into the *H* I clouds.

A survey of various aspects of these phenomena has been given by Oort (1954), who discusses the observational material bearing upon the problem. Although the data are much too scant to permit a definite conclusion, it is indicated that the birth of O stars may well provide sufficient kinetic energy to maintain the random cloud motions and, besides, cause enough compression to explain the continued existence of compact interstellar clouds. It would also explain the phenomenon of the expansion of the associations of young stars.

To work out the actual details of what happens in a cloud complex subsequent to the birth of an O star would require much study. In the present article we wish to limit ourselves to one particular phase of the problem, namely, the calculation of the acceleration which the neutral part of a cloud undergoes as a consequence of the "evaporation" of neutral hydrogen by the radiation from the O star. The problem will be further simplified by assuming that the density in the region between the O star and the cloud is much lower than that of the cloud, so that the ionized layers can expand more or less freely in the direction toward the O star. The idealized case that we shall first consider is that

of an O star that has been formed at a certain distance from a dense cloud. It may be expected that the results obtained will, at least to some extent, be applicable to the more realistic case of O stars forming in a field of heavy, but irregularly distributed, clouds. We shall refer to this as case *a*. The second case (*b*) which we propose to treat is that of a neutral cloud moving with a certain velocity into an *H* II region. In the third place, we shall consider the effects of the birth of O stars within a large, more or less homogeneous, mass of interstellar gas (case *c*). This last case, presumably the most realistic, is treated only very roughly here.

The general operation of the mechanism mentioned above is explained in Section II, while the detailed analysis is given in the following two sections. The final section gives some considerations relating to the distribution of high interstellar velocities.

II. PROPOSED MECHANISM

According to present theory, a typical cloud of neutral *H* has a temperature in the general neighborhood of 100° K and a density of about 10 *H* atoms/cm^3. This low temperature, predicted theoretically by Spitzer and Savedoff (1950), has since been confirmed by radio measures of the *H* I emission line reported by Oort (1952), Wild (1952), and van de Hulst, Muller, and Oort (1954). An analysis by Strömgren (1948) shows that these assumed values of temperature and density are consistent with the observations of interstellar *Na* I and *Ca* II, provided that the composition of the interstellar gas is assumed to be about the same as in the stars. If the material between the clouds has a density of 0.1 *H* atoms/cm^3, and a temperature of 10,000° K, a cloud of density 10 and $T = 100^{\circ}$ would be in pressure equilibrium with its surroundings.

Now consider what happens to a cloud when it becomes exposed to ultraviolet radiation from an O star. The *H* atoms near the surface will evidently become ionized. The photoelectrons will escape with several volts of kinetic energy, and the kinetic temperature of the gas will rise, approaching some 10,000° as the ionization approaches completeness. As the surface layer of gas becomes ionized, it will become transparent to ultraviolet radiation, and the region of ionized *H* will eat its way into the *H* I cloud.

The heating of the dense gas in the surface layer of the cloud will produce large dynamical effects. Evidently, an increase of temperature by a factor of 100 will increase the pressure by the same factor, and the gas will tend to expand vigorously. Expansion into the material of the cloud is soon stopped by the large amount of dense material there. In the direction away from the cloud, toward the O star, the heated gas "sees" only a low-density medium and expands in very much the same way as it would into a vacuum. Thus most of the cloud material ionized by the O star will escape from the cloud. This material will be moving preponderantly in the direction of the O star, with a mean velocity relative to the cloud which we shall denote by *V*. Evidently, the escaping material must have an equal and opposite reaction on the cloud; in other words, it behaves precisely as a jet from a rocket and will accelerate the cloud away from the ionizing star.

In the simple one-dimensional case, the relation between the mass change and the velocity is the same as that used in all rocket computations. If *M* is the mass of the cloud and *v* the cloud velocity relative to the star, counted positive in the direction away from the star, then we have

$$M \frac{dv}{dt} = - V \frac{dM}{dt}, \tag{1}$$

where the left-hand side is the rate of change of the cloud's momentum, while the right-hand side is the momentum, relative to the cloud, carried away, per second, by the escaping gases. We have the usual solution

$$M = M_0 e^{-(v - v_0)/V}, \tag{2}$$

where v_0 is the velocity at the time when the mass was M_0. In case *a* we shall take $v_0 = 0$; in case *b* we shall take it to be the velocity with which the cloud enters the *H* II region.

In either of these two cases, it is evident from equation (2) that, to obtain velocity changes of the order of V or larger, the mass of the cloud must decrease considerably. This is particularly true with case *b;* if the initial velocity of approach v_0 is small compared to V, it is readily shown that the final velocity is equal to v_0 but opposite in sign, and the collision is effectively elastic. If v_0 is comparable with V, the cloud mass M is much greater during the initial deceleration than during the subsequent acceleration, and the cloud gains greater velocity than it loses; i.e., the collision will be superelastic in the sense that the cloud gains kinetic energy per unit mass by the encounter.[1]

III. EJECTION OF GAS FROM A HEATED CLOUD

We consider what happens to a relatively dense cloud of neutral *H* when its surface becomes exposed to a flux F_u ergs cm^{-2} sec^{-1} of radiation beyond the Lyman limit. A detailed solution of this problem would evidently require a direct integration, with respect to time, of the hydrodynamic and thermal equations, since the problem can apparently not be idealized in terms of a steady-state solution. Evidently, a shock wave will advance into the neutral gas, the front of ultraviolet radiation will also move toward the rear of the cloud, while heated gas will stream out forward toward the star. No attempt at a detailed solution will be made here, and approximate estimates will be obtained for the quantities of interest.

We consider the amount of gas escaping per second and the mean velocity with which the gas escapes. If M is the mass of the cloud, then $-dM/dt$ is the amount of material escaping per second. We may suppose that, on the average, u ergs of ultraviolet energy are required for each *H* atom (neutral or ionized) that escapes. Then, if A is the projected area of the cloud, as seen from the central star,

$$\frac{dM}{dt} = -\frac{AF_u m_H}{u}. \tag{3}$$

The presence of atoms other than *H* may safely be ignored in this preliminary analysis.

To evaluate dM/dt, we must know u, the mean energy absorbed per escaping particle. The energy u_0 absorbed by a single *H* atom, when it becomes photoionized, exceeds 13.5 ev by the kinetic energy of the ejected photoelectron. If the ionizing radiation is dilute black-body radiation with the color temperature T_c, the mean electron kinetic energy is nearly equal to kT_c, or about 2.5 ev near a star of surface temperature 30,000° (Spitzer 1948*a*). Thus u_0 may be set equal to 16 ev, or 2.6×10^{-11} ergs.

The ratio u/u_0, which we denote by f, equals the number of times an electron will be recaptured and reionized as the heated gas expands. This quantity is given by

$$f = n\overline{\sigma_p v}\, t, \tag{4}$$

where n is the electron density, equal, of course, to the proton density; σ_p is the capture cross-section of a proton for an electron; and the bar denotes an average over all values of the electron velocity, v. The quantity t is the time which an electron spends in the region of density n. It seems scarcely worth while to carry out the more refined computation, in which the variation of n along the electron path is considered.

The effective recombination coefficient, $\overline{\sigma_p v}$, for capture of electrons by protons has been computed by Spitzer (1948*a*) and others, and may be written

$$\overline{\sigma_p v} = 2A\left(\frac{2kT}{\pi m_e}\right)^{1/2} \beta\phi(\beta), \tag{5}$$

[1] As pointed out to us by Dr. Burgers, it may be shown generally that, because of the decrease of mass, the total kinetic energy of the cloud, measured relative to the O star, always decreases. Relative to the local standard of rest, however, the energies of the clouds may be increased by these encounters.

where A is 2.11×10^{-22} cm^2, β equals $158{,}000/T$, and $\phi(\beta)$ is given in Table 1 of the paper by Spitzer (1948*a*). If T is 10,000°, we find

$$\overline{\sigma_p v} = 4.5 \times 10^{-13} \text{cm}^3/\text{sec}. \tag{6}$$

Thus a typical electron will recombine in a time equal to $(n\overline{\sigma_p v})^{-1}$, or $7 \times 10^4/n$ years.

The factors n and t entering into the expression for f may be estimated from the following simple argument. Suppose a dense cloud to become exposed to radiation from an O star that has been formed in its vicinity. The radiation will at first ionize the cloud at a rapid rate, causing a stream of ionized particles to proceed from the cloud. As the stream develops, it will absorb more and more of the ultraviolet radiation coming from the O star, thereby diminishing the amount available for ionization of the cool cloud. The stream will form an insulating shell around the cool cloud. A semistationary state may be reached when the density in the stream has become such that the intensity of the radiation penetrating to the surface of the cool cloud is just sufficient to maintain the stream.

To deal properly with the problem of this "insulating" layer would seem to require an extensive investigation, which we have not yet been able to carry out. We realize that it introduces a serious uncertainty in some of the results derived. Since our analysis was carried out, Dr. Kahn (1954*a*) has investigated the expansional and compressional motions that will be set up in a plane, cool cloud as a consequence of the heating of its surface by the radiation of an O star. In the present investigation we have confined ourselves to a rather simple estimate of the total outward momentum which will be imparted to the part of the cloud that remains un-ionized, as a consequence of the evaporation of particles from the surface exposed to the radiation of the O star.

To obtain a rough estimate of the influence of the insulating shell, we assume that the stream of ionized matter proceeds relative to the cloud with a velocity of the order of V, for which we shall take 20 km/sec. The amount of material in the shell may be computed in the following manner. If the outward velocity of the material in the shell is constant and directed radially outward from the cloud center, then the equation of continuity requires that the density of matter vary as $1/R^2$, where R is the distance from the center of the cloud. The total amount of material per square centimeter in the line of sight between the cloud surface and the star is then equal to the density at the cloud surface multiplied by the "effective thickness," which in this case is the cloud radius, R_c. If the absorption coefficient per gram varies as some power of the density, the effective thickness will be reduced below R_c, and we shall here take an effective thickness equal to $\frac{1}{2}R_c$.

We now consider a cloud of radius R_c subjected to the radiation of an O star at a distance r. Suppose that without absorption this radiation were capable of ionizing a mass g/r^2cm^{-2}sec^{-1}. Suppose, further, that the radiation is reduced by a factor f through absorption in the ionized shell. The number of protons and electrons developed per square centimeter per second is then $g/(fm_H r^2)$. The number n of protons per cubic centimeter of the stream is

$$n = \frac{g}{f m_H V r^2}. \tag{7}$$

With a thickness of $R_c/2$ for the shell, the expansion through this thickness will require that

$$t = \frac{R_c}{2V}. \tag{8}$$

Per electron, the number of recombinations during its passage through the shell (which

number is at the same time the factor by which the radiation effective for the ionization is reduced) will be, on substitution of equations (6), (7), and (8) in equation (4),

$$f = \frac{2.3 \times 10^{-13} g R_c}{f m_H V^2 r^2}. \tag{9}$$

Hence

$$f = \frac{1}{Vr}\left(\frac{2.3 \times 10^{-13} g R_c}{m_H}\right)^{1/2} = 0.18\,\frac{(gR_c)^{1/2}}{r}. \tag{10}$$

Values of g have been tabulated in Table 1, appearing in the next section. With R_c = 5 pc, r = 10 pc, we obtain for an O5 star, f = 66; for O7, f = 28; and for O9, f = 9. For larger r, f diminishes proportional to r. Considering, similarly, a small dense cloud, with R_c = 1 pc, we obtain, at r = 2 pc, values of f equal to 147, 63, and 22 for stars of types O5, O7, and O9, respectively. We may also express these results by saying that the effective value of u should be taken larger than 2.6×10^{-11} by the factors mentioned.

In the case of an O5 star the density in the insulating shell would become 40 for the first cloud and 452 for the second. Considering that the shell is formed only on that half of the cloud's surface that receives radiation from the O star, the volume of the shell is 1.2 times that of the original cloud. This means that, in the two examples considered, the original density of the cloud should be at least 50 and 550 H/cm^3 in order not to be vaporized entirely before the insulating shell has been formed. For O stars of later type the minimum densities are smaller.

We turn to a consideration of the mean ejection velocity. The gas may be assumed to leave the cloud at a velocity V_e normal to the cloud's surface; the mean component of this velocity in the direction of the central star will be $V_e \cos\theta$ where θ is the angle which the direction to the star makes with the outward normal. Evidently, V_e will depend on the temperature to which the ionized gas is heated. Two situations will be considered—one in which the photoelectrons are not recaptured by protons before the gas escapes; the other, in which they are recaptured and re-emitted a number of times.

In the first of these situations the temperature will depend entirely on the initial kinetic energy of the photoelectrons. The mean energy of a photoelectron from H is equal to kT_{ep}, where T_{ep} is roughly the color temperature of the ionizing radiation (Spitzer 1948*a*). In this case we may assume that virtually all this electron energy goes into the expansion velocity, with electrons and protons accelerated equally, and write

$$V_e^2 = \frac{2kT_{ep}}{m_H}. \tag{11}$$

Values of V_e obtained from this equation range from 19 km/sec for a star of type B0 to 26 km/sec for type O7 and up to 31 km/sec for type O5.

It is readily shown that if electron captures by protons are negligible, excitation of forbidden lines by electron impact will also have a negligible effect. However, the possible presence of H_2 molecules must be considered, since, as shown by Spitzer (1949), the rate of radiation by H_2 molecules is very rapid when the temperature is high. Because of the high cosmic abundance of H, encounters between electrons and H_2 molecules may dissipate appreciable energy, even though there is not sufficient time for electrons to lose energy in collisions with oxygen and other atoms.

While radiation by H_2 molecules may be appreciable, it appears possible that this loss of energy may be offset by the corresponding energy gain resulting from dissociative recombination,

$$H_2^+ + e \rightarrow 2H\,.$$

As pointed out by Bates (1950), this process may have a very high rate coefficient (greater by a factor of some 10^5 than the rate coefficient for electron capture by protons). If the two H atoms are both in their ground states, each atom will have a kinetic energy of 5.5 volts, plus half the kinetic energy of the incident electron. Some of this energy will be radiated in impacts with other H_2 or H_2^+ molecules, and it is not clear whether, on the whole, the presence of molecules will increase or decrease V_e. For preliminary results we shall assume that equation (11) is valid even if some H_2 molecules are present.

When the electrons recombine with protons and absorb ultraviolet photons several times in the course of the expansion, we may assume that the temperature is determined not solely by the initial electron energy but rather by the condition of equilibrium between the gains and losses of kinetic energy. The kinetic temperature is then about the same as in planetary nebulae and H II regions generally; we may take 10,000° as a representative value. In this situation the temperature tends to remain constant as the gas expands.

The final expansion velocity may be computed very simply. As a gram of matter expands, it does work equal to $pd(1/\rho)$. If we assume that this work goes entirely into increasing the expansion velocity of this particular gram, then we find

$$V^2 + \frac{2kT}{m} \ln \rho = \text{Constant}. \tag{12}$$

If we let the original density be ρ_0, the final density be ρ_1, and again let m, the mean mass per particle, equal $m_H/2$, then

$$V_e^2 = \frac{4kT}{m_H} \ln \left(\frac{\rho_0}{\rho_1} \right). \tag{13}$$

If ρ_0 and ρ_1 correspond to particle densities of 10 and 0.1 H atoms/cm^3, typical values for H I clouds and for the regions between the clouds (Strömgren 1948), we find that equation (13) gives a value of 39 km/sec for V_e, if T is set equal to 10^4.

It may be remarked that in this case, where the expansion is assumed to occur relatively slowly compared to the ionization, the presence of H_2 molecules may be neglected. Any molecules present will be dissociated relatively early and can have no effect on the temperature during most of the gradual expansion.

Finally, we must average V, or $V_e \cos \theta$ over a hemisphere. If we assume that the loss of mass per unit cloud surface is proportional to the projected area, or to $\cos \theta$, we must average $\cos \theta$ over $\cos \theta \, d\omega$, where $d\omega$ is an element of solid angle. In this way we obtain, for a spherical cloud,

$$V = \tfrac{2}{3} V_e. \tag{14}$$

While interstellar clouds are probably not even remotely spherical, equation (14) should provide a fair approximation, on the average. In conclusion, we have the following range of values for V,

$$1.3 \leq V \leq 2.6 \text{ km/sec}. \tag{15}$$

A value of 20 km/sec for V has been adopted throughout most of this paper.

IV. DYNAMICS OF CLOUDS ACCELERATED BY RADIATION

If the gas in the H II region is assumed initially homogeneous, the ultraviolet flux depends on the distance, r, from the central star, according to the equation

$$F_u = \frac{L_u}{4\pi r^2} \left(1 - \frac{r^3}{s_0^3} \right) \qquad (r < s_0), \tag{16}$$

where L_u, the luminosity of the star beyond the Lyman limit, is related to the stellar radius R and the surface temperature T_e by the approximate relationship

$$L_u = 4\pi R^2 \times \frac{2\pi h}{c^2} \int_{\nu_0}^{\infty} \nu^3 e^{-h\nu/kT_e} d\nu , \tag{17}$$

where ν_0 is the frequency at the Lyman limit. In the following discussion we shall, in general, suppose the medium to have a density of 1 proton and electron per cubic centimeter. We define s_0 as the radius of the Strömgren sphere in such a medium. Equation (16), together with values of s_0 for stars of different spectral type, may be taken from Strömgren (1939). Evidently F_u vanishes for r greater than s_0. If equations (3), (16), and (17) are combined, we may write the resultant equation in the form

$$\frac{dM}{dt} = -\frac{\pi g R_c^2}{f r^2}\left(1 - \frac{r^3}{s_0^3}\right), \tag{18}$$

where M and R_c are the cloud's mass and radius. The constant g is given by

$$g = \frac{m_H L_u}{4\pi u_0} = \frac{2\pi R^2 m_H h}{u_0 c^2} \int_{\nu_0}^{\infty} \nu^3 e^{-h\nu/kT_e} d\nu \tag{19}$$

$$= \frac{2\pi R^2 m_H k T_e \nu_0^3 e^{-\beta}}{u_0 c^2}\left(1 + \frac{3}{\beta} + \frac{6}{\beta^2} + \frac{6}{\beta^3}\right),$$

where

$$\beta = \frac{h\nu_0}{kT_e} = 1.58 \times 10^5 T_e^{-1} . \tag{20}$$

Again f is the factor by which the radiation is reduced by absorption in the stream of ionized particles developing from the cloud's surface. In the case of an isolated cloud we shall use equation (10) for f. Equation (18) may then be written

$$\frac{dM}{dt} = -5.5\pi (gR_c^3)^{1/2} \frac{1}{r}\left(1 - \frac{r^3}{s_0^3}\right). \tag{21}$$

It should be noted that, in the computation of f from equation (10), the effect of the reduction of the radiation by the general interstellar medium has been neglected. This medium gives an additional factor $(1 - r^3/s_0^3)^{1/2}$ in f, and strictly, therefore, in equation (21) the factor $(1 - r^3/s_0^3)$ should be replaced by $(1 - r^3/s_0^3)^{1/2}$. In reality, however, the phenomena will be more complicated, because the insulating layer will dissipate only gradually after the radiation has been cut off. We have therefore left the factor as in equation (21). The change to a square root would not have produced a very great change in the results.

Values of g computed from equation (19) are given in Table 1, for stars of different spectral type. The values of T_e and R are practically those used by Strömgren (1939); the values of s_0, also from Strömgren, are for a gas density of one H atom/cm^3. The value of V is set equal to 20 km/sec, while u_0 has been set equal to 3×10^{-11} ergs.

We shall now consider three different cases of acceleration of interstellar clouds:

a) An O star is formed at a distance r_0 from an isolated cloud, where r_0 is smaller than the radius of the Strömgren sphere in the average interstellar medium (supposed to have a density of 1 proton and electron per cubic centimeter). It will be assumed that the O star suddenly begins to radiate at full strength. This supposition simplifies the analysis but is not essential for the theory.

b) An isolated cloud moves into an *H* II region.

c) An O star, or a group of O stars, is formed inside a homogeneous cloud of large dimension and considerable density.

CASE *a*. REPULSION OF AN ISOLATED CLOUD BY A NEWLY FORMED O STAR

We shall first consider the case where, in the space between the O star and the cloud, the influence of the general medium is negligible. If we assume, for simplicity, that the cloud radius R_c is constant during the acceleration and combine equations (1), (2), and (21), we find

$$\frac{dv}{dt} = -\frac{V}{M}\frac{dM}{dt} = \frac{5.5\pi V (gR_c^3)^{1/2}}{M_0 r} e^{(v-v_0)/V} . \tag{22}$$

If we substitute $v dv/dr$ for d/dt, equation (22) can be integrated directly, to give

$$(v+V) e^{-(v-v_0)/V} = -17.2 \frac{(gR_c^3)^{1/2}}{M_0} \ln\left(\frac{r}{r_0}\right) + v_0 + V , \tag{23}$$

where ln is the natural logarithm.

TABLE 1

VALUES OF g AND γ

Type	T_e	s_0 (Pc)	β	g	γ
O5	79,000°	140	1.99	8.4×10^{24}	35.8
O6	63,000	110	2.49	3.6	19.3
O7	50,000	87	3.14	1.50	10.3
O8	40,000	66	3.92	0.63	5.7
O9	32,000	46	4.91	0.20	2.6
B0	25,000	26	6.28	0.033	0.76
B1	23,000	17	6.83	0.010	0.35
B2	20,000	11	7.85	0.0020	0.11
B3	18,600	7.2	8.44	0.0007	0.06

So far, the effect of the reduction of the radiation by the general interstellar medium has been neglected. Should we assume that, in addition to the protective layer surrounding the cloud, there is an ionized medium of density 1 hydrogen particle/cm^3, the ultraviolet radiation would be cut off at $r = s_0$. Integration of equations (1), (2), and (21) then gives, for $r = s_0$,

$$(v+V) e^{-(v-v_0)/V} = -17.2 \frac{(gR_c^3)^{1/2}}{M_0} \left\{\ln\left(\frac{s_0}{r_0}\right) - \frac{1}{3}\left(1 - \frac{r_0^3}{s_0^3}\right)\right\} + v_0 + V . \tag{24}$$

In most relevant cases s_0/r_0 will be larger than 10, and the second term within the braces will be small compared to the first. In order to compute the final velocities obtained, we may therefore safely use equation (23), putting $r = s_0$.

Even if the general ionized medium between the cloud and the star should remain negligible, there will be a limit to the distance up to which the cloud is accelerated. This limit will be set by the finite lifetime of the O star. If for the brightest O stars we put this at 5 million years and if we suppose the average velocity of the cloud to be 30 km/sec, the cloud travels to a distance of 150 pc before the O star declines in brightness.

A third factor which may limit the acceleration of the cloud is the sweeping-up of "ordinary" interstellar material. According to equation (7), the number of protons and

electrons evaporated per second from 1 cm² of the cloud, if there is no general medium between the cloud and the O star, is $g/(fm_H r^2)$, or 5.6 $g^{1/2}/(rm_H R_c^{1/2})$. If the medium in front of the cloud has a density of 1 atom/cm³, the number of atoms swept up at the front side is $v\text{cm}^{-2}\text{sec}^{-1}$. Each evaporating proton carries away a momentum $m_H V$, while each atom swept up adds a momentum $m_H v$ in the same direction. The two amounts of momentum will be equal when 5.6 $g^{1/2}V/(rR_c^{1/2}) = m_H v^2$. For an O5 star and a cloud of 5-pc radius the braking action will become of the same order as the acceleration at $r = 180$ pc if $v = 30$ km/sec, and at 410 pc if $v = 20$ km/sec. This effect may therefore be of the same order as the first two effects.

From equation (23) we can derive the limiting original mass that a cloud must have in order to escape total ionization. This limiting mass, M_0, is obtained by putting the right-hand member equal to zero. As an example, we may consider the case of a cloud of 5-pc radius accelerated from $r_0 = 10$ to $r = 100$ pc. If $v_0 = 0$ and $V = 20$ km/sec, we find, from equation (23) and Table 1, that $M_0 = 1700$ solar masses for an O5 star, and 700 solar masses for an O7 star.

Clouds with original masses slightly exceeding these values will attain high velocities. It is tempting to think that the high interstellar velocities observed in some cases are due to this rocket effect. It may be seen from equation (23) that there is a considerable range of M_0 where the accelerations will be large. Acceleration to rather high velocities will therefore occur not infrequently.

One of the most interesting cases observed is that of the California nebula NGC 1499. Mayall (1953) has recently measured a radial velocity of +53 km/sec for this nebula; the velocity is rather uncertain, and Mayall thinks that it is likely to be the same as that of the exciting O star ξ Persei, which has a radial velocity of +67 km/sec. It is probable that, notwithstanding its large velocity of 49 km/sec with respect to the center of the ζ Persei association, ξ Persei belongs to this group (Blaauw 1952*a;* Delhaye and Blaauw 1953), in which case NGC 1499 should also belong to it. If we think of NGC 1499 as having been expelled from the center of the group by the ionization effects of an early O star, it is natural to suppose that ξ Persei likewise obtained its high velocity in this manner. It should then have been formed in the cloud after this had obtained most of its acceleration, and probably as a consequence of the compression accompanying this acceleration (Oort 1954). At present, the ζ Persei association contains no O stars besides ξ Persei itself. If the foregoing supposition concerning the origin of the high velocities of NGC 1499 and ξ Persei is correct, there should originally have been an O star, which must have faded during the 1.5 million years elapsed since the origin of the association.

The dimensions of NGC 1499 are roughly 13 × 4 pc. A thickness of 10 pc in the radial direction and a density of 20 H/cm³ might be reasonable estimates, in view of the observed brightness. With these estimates, the mass of the luminous nebula would be 130 solar masses. The total mass may be larger, as not all of the cloud may be ionized. For the present we shall assume a mass equal to 130 times that of the sun. Equation (2) then enables us to determine M_0. With $v_0 = 0$, $v = 49$ km/sec, $V = 20$ km/sec, we find $M/M_0 = 0.086$, or $M_0 = 1500$ solar masses.

As we shall see in the discussion of case *c*, it may well be that the clouds, before they become isolated, have already obtained a velocity v_0 of the order of the velocity of sound in an H II region, or about 11 km/sec. Also, V may, in reality, be as high as 30 km/sec. With these values for v_0 and V, we would get

$$\frac{M}{M_0} = 0.28\,, \qquad \text{or} \qquad M_0 = 460 \text{ solar masses}\,.$$

Supposing that the cloud was accelerated without expansion from $r_0 = 8$ to $r = 50$ pc, we can now derive, from equation (23), the value of g that would have been needed to accelerate the cloud to a velocity $v = 49$ km/sec. Taking $R_c = 4$ pc, we find, for the

two cases considered, $g = 9.8 \times 10^{24}$ and $g = 1.6 \times 10^{24}$, respectively. From Table 1 we see that the first value corresponds to a star of type O5, while in the second case a star of type O7 would have sufficed. With an O5 star at 8-pc distance, the density in the insulating layer, by equations (10) and (7), would be roughly 60 H/cm^3. As the density in the original cloud would in this case be $20/0.086 = 233$ cm^{-3}, the mass of the insulating shell would be about one-third that of the cloud. The velocity imparted to the cloud as a consequence of the formation of the insulating shell has been neglected in the foregoing estimates. If we had taken it into account, we would have found that a star of slightly lower temperature would have sufficed to give the cloud the required velocity. With somewhat different assumptions, as, for example, the assumption that R_c changes as the cloud accelerates outward, the computed value of g will be altered by a factor of 2 or more.

Strictly, this analysis applies to a neutral cloud, while what we see of NGC 1499 is an ionized mass. The picture would be that the nebula has been accelerated by the rocket effect while it was still in the neutral state. Evidently, ξ Persei was formed after the acceleration was practically finished, for it has the same velocity as the nebula. It is this star which afterward ionized the cloud.

A much more extreme case of high velocity is presented by the O star AE Aurigae. The unusual motion of this star has been discussed by Blaauw and Morgan (1953), who point to the possibility that the star originated in the Orion association. The star has a space velocity of 128 km/sec (corrected for standard solar motion) that appears to be pointed away from the Orion group; it is situated at a distance of 350 pc from the center of this group. Like ξ Persei, it appears to be associated with a rather dense, bright nebula, IC 405. It is not unlikely that this nebula moves with the star. The radius of the cloud is estimated by Blaauw and Morgan to be 2.8 pc, its density 50 H/cm^3, which would correspond to a total mass of 80 times that of the sun. We again make two estimates of the original mass, M_0. If we take $v_0 = 0$, $V = 20$ km/sec, the mass reduction factor needed to reach a velocity of 128 km/sec is $M/M_0 = 0.0017$, so that $M_0 = 48{,}000$ solar masses. If, on the other hand, we assume $v_0 = 11$ km/sec, $V = 30$ km/sec, we get $M/M_0 = 0.020$, and $M_0 = 4000$ solar masses. The first value is improbably high. It seems that if the velocity of AE Aurigae were to be explained by the rocket mechanism, V would have to be at least 30 km/sec. Entering equation (23) with this value, with $v_0 = 11$ km/sec, $v = 128$ km/sec, $M_0 = 4000$ solar masses, $R_c = 2.8$ pc, $r_0 = 2R_c = 5.6$ pc, and $r = 350$ pc, we find $g = 280 \times 10^{24}$. Comparing this with the values given in Table 1, we see that it would require 34 O5 stars to give to a cloud of 80 solar masses a velocity of 128 km/sec. Such a collection of early O stars appears very improbable.

The exceptional character of this case has been shown to be still more remarkable by Blaauw and Morgan's (1954) determination of the motion of μ Columbae. They point out that the B0 V star μ Columbae moves away from the Orion association with the same speed as AE Aurigae and that the two motions are almost exactly opposite. They suggest that the stars were formed in the same physical process and that this took place in the Orion nebula. This phenomenon indicates that the mechanism of the formation of these two high-velocity stars has been radically different from the processes considered in the present article.

In most other cases of high-velocity O stars or of high-velocity clouds found from interstellar absorption lines, the velocities lie between 50 and 75 km/sec; i.e., in a range where they can be explained without difficulty by rocket effects.

CASE *b*. ENCOUNTER OF A CLOUD WITH AN *H* II REGION

Because case *b* is probably less important for the dynamics of interstellar space than cases *a* and *c*, we shall slightly simplify the discussion by limiting ourselves to a consideration of "standard" clouds and "standard" *H* II regions. Following Strömgren (1948), we assume a "typical" cloud to have a thickness, d, of 5 parsecs and a gas density, n_H, of

10 H atoms/cm^3. If we call $n_H d$ the mass thickness, this mass thickness is therefore 50, or 2.7×10^{-4} gm/cm^2.

We may now define a dimensionless quantity, γ, as follows:

$$\gamma = \frac{g A_0}{V M_0 s_0}, \tag{25}$$

in which A_0 and M_0 are the cloud's original projected area and mass, which were assumed to be those of the "typical" cloud discussed above. Values of γ have been given in Table 1. The various constants involved were given the same values as for the computation of g. As we shall see later, encounters between a cloud and an H II region are relatively ineffective in accelerating clouds to high velocities, unless γ exceeds unity. Evidently, the early B stars yield so low a value of γ that they may safely be neglected.

In the present computation we shall set f equal to unity and neglect the formation of the insulating layer. Mechanism b is important only when γ is larger than unity, and in such a case the cloud does not come very far inside the Strömgren sphere. The evaporation rate then remains relatively low, and f will, in fact, not much exceed unity.

Equation (18) may now be written

$$\frac{dM}{dt} = -\frac{\gamma s_0 V M_0}{r^2}\left(1 - \frac{r^3}{s_0^3}\right)\frac{A}{A_0}, \tag{26}$$

A being the area at the time t which is considered. As before, we shall assume that A remains constant during the acceleration.

While the general problem is, of course, two-dimensional, we shall gain adequate insight into the physical situation by considering the simple one-dimensional case of a direct central collision. In this case v is dr/dt, equation (2) is applicable, and, if equations (1), (2), and (26) are combined, we obtain, for $r < s_0$

$$\frac{dv}{dt} = -\frac{V}{M}\frac{dM}{dt} = \gamma s_0 V^2 e^{(v-v_0)/V}\frac{1}{r^2}\left(1 - \frac{r^3}{s_0^3}\right). \tag{27}$$

Integration with respect to r gives

$$\left(1 + \frac{v}{V}\right)e^{-(v-v_0)/V} - \left(1 + \frac{v_0}{V}\right) = \gamma\left\{\frac{s_0}{r} + \frac{1}{2}\left(\frac{r}{s_0}\right)^2 - \frac{3}{2}\right\}, \tag{28}$$

where use has been made of the boundary condition that $v = v_0$, the initial velocity of approach, when $r = s_0$. The velocity is taken positive when directed away from the star; thus v_0 is negative.

At the boundary of the H II region the right-hand side of equation (28) vanishes; if we denote by v_1 the velocity of the outgoing cloud when $r = s_0$ again, it is evident that v_1 must be such that the left-hand side of equation (28) vanishes for $v = v_1$. It is readily seen that if $|v_0| > V$, the left-hand side vanishes only for the one value $v = v_0$. This corresponds to the physical fact that, for such large velocities of approach, the cloud loses all its mass before it escapes from the H II region. For v_0 negative and with an absolute value less than V, a positive value of v_1 can be found for which this left-hand side vanishes. Values of v_1/V for different v_0/V are given in Table 2. For small v_0/V we have

$$\frac{v_1}{V} = \frac{|v_0|}{V} + \frac{2}{3}\left(\frac{v_0}{V}\right)^2 \cdots, \tag{29}$$

while, for $|v_0|/V$ very near unity,

$$\frac{v_1}{V} = \ln\frac{1}{1 + v_0/V}. \tag{30}$$

Equation (28) also indicates how close to the central star the cloud comes before its velocity vanishes. If we denote this distance of closest approach by r_m, we have

$$\frac{r_m/s_0}{1+0.5\,(r_m/s_0)^3} = \frac{1}{1.5+0.5\Psi\,(v_0/V)}\,, \tag{31}$$

where

$$\Psi(y) = e^y - (1+y)\,. \tag{32}$$

For small v_0/V, Ψ varies as $\frac{1}{2}(v_0/V)^2$, but increases to 0.368 for v_0 equal to $-V$. The values of r_m/s_0 found from equation (31) for different values of γ and $|v_0|/V$ are given in Table 3. Evidently, for γ large compared to unity, the right-hand side of equation

TABLE 2

EMERGENT VELOCITY FOR DIRECT CENTRAL ENCOUNTER

$-v_0/V$	0.10	0.20	0.30	0.40	0.50	0.60	0.65	0.70	0.75	0.80
v_1/V	0.107	0.231	0.376	0.547	0.756	1.02	1.18	1.36	1.59	1.86
$-v_0/V$	0.82	0.84	0.86	0.88	0.90	0.92	0.94	0.96	0.98	0.99
v_1/V	1.99	2.14	2.30	2.49	2.72	2.99	3.34	3.83	4.67	5.48

TABLE 3

VALUE OF r_m/s_0 FOR CENTRAL ENCOUNTERS

γ	$-v_0/V$						
	0.1	0.2	0.3	0.4	0.6	0.8	1.0
0.1	0.831	0.690	0.574	0.479	0.341	0.252	0.194
0.3	.900	.810	.730	.659	.541	.435	.368
1.0	.944	.893	.844	.800	.719	.650	.591
3	.968	.937	.908	.880	.830	.784	.742
10	0.982	0.965	0.949	0.933	0.904	0.877	0.852

(31) is nearly equal to 1/1.5, and r_m is only slightly less than s_0; in this case one may expect equation (28) to be valid for noncentral encounters. For γ less than unity and v_0 comparable with $-V$, r_m is much less than s_0; these results are applicable only to the improbably few direct central encounters.

While this mechanism (*b*) can account qualitatively for the existence of high-velocity clouds, the number of such clouds appears to be greater by about an order of magnitude than would be expected from the mechanism. The number of O stars per cubic parsec in the solar neighborhood ranges from about 2×10^{-9} at O5 to 1.6×10^{-8} at O9. The radius of the *H* II sphere around each star may be taken from Table 1. With conventional values for the cloud velocity, for the number of clouds per kiloparsec, and for the mean free path of a cloud, it is readily shown that the number of high-velocity clouds produced by mechanism *b* is smaller by a factor of 20 than the number computed from the observations by Adams.

CASE *c*. BIRTH OF O STARS INSIDE A LARGE CLOUD

Interstellar clouds sometimes seem to collect together and to form a conglomerate, with a mass that is vastly greater than that of a "typical" cloud. We thus find cloud

complexes with masses of several ten thousand times the mass of the sun. Apparently, O stars can be formed in such cloud complexes, for we observe several instances where O stars are imbedded in dense clouds of very large dimensions.

We now wish to consider what happens when an O star is formed in such a dense medium. We shall first take an idealized case, where an O star is suddenly born in the central part of a vast, homogeneous, spherical cloud with a density of n_0 hydrogen atoms/cm^3. As before, let s_0 denote the radius that the Strömgren sphere around the O star would have if it were situated in a medium with a density of 1 hydrogen atom/cm^3. The newly born O star will start to ionize the hydrogen in its surroundings. If the ionization could be assumed to happen instantaneously, the radius of the Strömgren sphere would become $r_0 = s_0 n_0^{-2/3}$.

Actually, the mass ionized per second may be found from equations (3), (16), and (19), taking the area $4\pi r^2$ instead of πR_c^2, and r_0 instead of s_0. We obtain

$$\frac{dM}{dt} = \frac{L_u m_H}{u}\left(1 - \frac{r^3}{r_0^3}\right) = 4\pi g\left(1 - \frac{r^3}{r_0^3}\right). \tag{33}$$

As an example we consider the propagation of the ionization front around an O5 star formed in a cloud with a density of 50 hydrogen atoms/cm^3. In this case r_0 is 13.6 pc. The speed of the ionization front is given by

$$\frac{dr}{dt} = \frac{1}{4\pi r^2 n_H m_H}\frac{dM}{dt}.$$

For $r = 0.5r_0$, this becomes 1950 km/sec; for $r = 0.9r_0$, 185 km/sec. These velocities are, respectively, two and one orders larger than the velocity of sound in the ionized mass. For all practical purposes the ionization may therefore be said to be instantaneous up to a distance very close to the radius of the Strömgren sphere. The same conclusion probably holds for all observed large emission nebulae. For the following discussion we shall assume that the ionization front coincides with the Strömgren sphere at all times during the development of a nebula. If the radius of the ionized sphere at an arbitrary time is called r, and its density n, we have, therefore,

$$r = s_0 n^{-2/3}. \tag{34}$$

Let us assume that the dense nebula extends everywhere beyond the limit of the Strömgren sphere. The ionization by the newly born O star will increase the pressure in the inner part by a factor of about 100 over that in the cool surrounding mass. It has been shown elsewhere that, in actually observed nebulae, the gravitational forces are small compared to this pressure. As a consequence, the hot inner mass will expand into the cool shell. By the decrease in density in the inner mass, the radius of the Strömgren sphere will grow. It will grow faster than the radius of the original ionized mass, so that additional parts of the cool shell will become ionized. It would be outside the scope of the present article to attempt to discuss in detail the phenomena that will be caused by this expansion. We shall make two simplifying assumptions, which we hope will give a usable approximation for our very limited purpose. We assume that the ionized sphere remains homogeneous during the expansion. In order to have a concrete model, it will further be surmised that a compression region proceeds into the cool shell, probably with a velocity of the order of that of sound in the hot inner mass.[2] It is not unlikely that the radiation will be sufficient to keep the compression region at a temperature

[2] The case of an *H* II region expanding into a neutral shell has been discussed along similar lines by Schatzman and Kahn (1953). They have paid more attention to the progress of the shock front, without considering the probably very important effects of cooling by radiation.

comparable to that in the cool shell. The compression would then be approximately a hundred fold.

After the compression front has reached the outer surface of the nebula, the compressed shell will continue to expand. The expansion velocity will be determined by the pressure in the inner sphere as well as by the rocket effect of the matter ionized from the inner surface of the shell. In order to find the amount of acceleration, we shall need the mass of the neutral shell before and after the expansion. Let us denote these by $M_0^{(n)}$ and $M^{(n)}$, respectively. If, similarly, $M_0^{(i)}$ and $M^{(i)}$ are the masses of the ionized sphere before and after the expansion and M is the total mass, we have, evidently,

$$\frac{M^{(n)}}{M_0^{(n)}} = \frac{M - M^{(i)}}{M - M_0^{(i)}} = \frac{1 - M^{(i)}M^{-1}}{1 - M_0^{(i)}M^{-1}}. \tag{35}$$

Using equation (34), we can write

$$M_0^{(i)} = \tfrac{4}{3}\pi n_0 m_H r_0^3 = \tfrac{4}{3}\pi m_H n_0^{-1} s_0^3 \tag{36}$$

and

$$M^{(i)} = \tfrac{4}{3}\pi n m_H r^3 = \tfrac{4}{3}\pi m_H s_0^{3/2} r^{3/2}. \tag{37}$$

In the present section we are interested in very large and dense cloud complexes having densities between, say, 20 and 100 atoms/cm^3 and masses in excess of 20,000 solar masses. In these cases $M_0^{(i)}$ is rather smaller than M, as shown by the accompanying values of $M_0^{(i)}$. In the relevant cases the second term in the denominator of equation (35)

Sp.	$n_H = 20$	$n_H = 100$
O5	13,700	2,700
O7	3,300	660
O9	480	100

will thus be small and may be omitted for the present rough estimates. If the original outer radius of the entire cloud is called R, we then obtain

$$\frac{M^{(n)}}{M_0^{(n)}} = \frac{M^{(n)}}{M} = 1 - \frac{M^{(i)}}{M} = 1 - \frac{s_0^{3/2} r^{3/2}}{n_0 R^3}. \tag{38}$$

In this case the process of acceleration may well be limited by the sweeping-up of ordinary interstellar matter outside the cloud complex. If the average density of this matter is supposed to correspond to 1 hydrogen atom/cm^3, the amount swept up during an increase of the radius by dr is $4\pi m_H r^2 dr$. The mass ionized in the same interval from the inner surface of the neutral shell is given by the differential of equation (37). The two are equal for

$$r = 2^{-2/3} s_0 = 0.63\, s_0. \tag{39}$$

The velocity of the shell will reach its maximum around this point.

In view of the chaotic conditions that we find in actual interstellar space, it would seem an adequate simplification to consider separately the effects of acceleration by the radiation of the O star and the slowing-down by sweeping up other clouds. Accordingly, we assume that, up to $r = 0.5 s_0$, the collisions with other clouds are negligible and that beyond this distance the acceleration by the O star's radiation is negligible.

On this basis we can compute the minimum mass that will escape total "evaporation" by the O star. This is equal to the mass within a Strömgren sphere having a radius $r =$

$\frac{1}{2}s_0$ and may be found by inserting this value of r in equation (37). Expressed in the mass of the sun as unit we derive the minimum masses given in the accompanying table.

O5	100,000	O7	24,000	O9	3,500
O6	48,000	O8	10,400	B0	640

From the little that we know about the masses of large cloud complexes it seems probable that the masses of the larger ones are of the order of the first four numbers given in the table. The cloud complexes are always extremely uneven, so that probably in some parts the mass thickness will considerably exceed the limits required to escape total ionization, while in other directions they will be ionized completely. Owing to the irregularity, the neutral shell is likely to be broken up in the process of expansion, and we may imagine the various parts to form separate condensations in the interstellar matter that will resemble "ordinary" interstellar clouds. Through the expansion and evaporation process, these will be endowed with considerable velocity.

In order to obtain an estimate of this velocity, we combine equation (2) with equation (38). Again putting $r = 0.5s_0$, we find

$$e^{-(v-v_0)/V} = 1 - \frac{0.35\, s_0^3}{n_0 R^3}. \tag{40}$$

In the discussion concerning V given in Section III, it was tacitly supposed that the ionized particles escape into a practical vacuum. In the present case the inner sphere is filled with dense gas; yet the conditions resemble those discussed in Section III, because the compressed layer from which the "evaporation" takes place must have a density considerably exceeding that in the ionized inner mass. We do not know exactly what values to use for v_0 and V. We shall probably get too low values for v if we assume $V = 20$ km/sec, $v_0 = 0$. On the other hand, it seems unlikely that V would have to be taken larger than 30 km/sec and v_0 larger than 11 km/sec, the velocity of sound in the ionized sphere. We shall assume that v lies between the extremes corresponding to these two suppositions.

Each of the large nebulae must put a considerable amount of kinetic energy into the interstellar medium. If the nebulae are large enough, much of this energy will be in the form of translational motion of compressed clouds. Very little is at present known about the masses of these large cloud complexes or about the frequency of their occurrence. In an article by Oort (1954) an estimate has been attempted. This indicated that the energy provided by the disruption of the large nebulae in the way discussed may well be of the right order to maintain the cloudy structure and the random motions in the interstellar medium.

V. DISTRIBUTION OF CLOUD VELOCITIES

As a working hypothesis we shall start from the assumption that the process just discussed is the principal cause of cloud motions. We may then inquire whether it can explain the observed distribution of high interstellar velocities.

To compute the entire velocity distribution would be an enormous labor. Even if sufficient data were available to make any such calculation, it would far surpass the scope of the present article.[3] All we wish to do now is to see whether the mechanism could produce enough high velocities and whether the frequency and the distribution of the high velocities that would follow from it agree with those observed. In this discussion we shall once more use a drastic simplification. We shall assume that the clouds lose their high velocities when, after their acceleration, they collide for the first time with another cloud.

[3] Some calculations on the statistical effects of cloud collisions have been made by Kahn (1954*b*) and by Parker (1953).

The distribution law of interstellar velocities has recently been investigated by Blaauw (1952*b*), Searle (1952), and Schlüter, Schmidt, and Stumpff (1953), all investigations being based on data obtained by Adams (1949). Table 4, taken from a preliminary communication by Schlüter, Schmidt, and Stumpff, shows the observed distribution. The low-velocity part of the table has little significance, as it is greatly distorted by blending. The numbers of clouds with positive and negative velocities are given separately under n^+ and n^-. All velocities were corrected for the effect of solar motion and differential galactic rotation. The moderately large velocities are preponderantly negative, as has been extensively commented upon by most authors (cf. the references given above). In accordance with our working hypothesis, we shall consider this as a consequence of the fact that the high-velocity clouds will often be observed against the background of the stars associated with the cloud complex from which they originated.

An individual inspection of the velocities in excess of 20 km/sec already suffices to show that the large nebulae and the stellar associations which are probably directly related to them produce high-velocity clouds in the right order of frequency. For it appears that no less than two-thirds of the known residual velocities between 20 and 30 km/sec are related to known stellar associations (Oort 1954).

TABLE 4

DISTRIBUTION OF INTERSTELLAR VELOCITIES

v (Km/Sec)	n^+	n^-	n	$257e^{-v/12}$
<10	143	164	(307)	(145)
10–20	21	37	58:	65
20–30	4	30	34	27
30–70	7	10	17	20
>70	1	2	3	1

The theory of the origin of high-velocity clouds worked out in the present article appears to fit satisfactorily the type of distribution observed for these high velocities. As may be seen from Table 4, we can fit the observed distribution well enough with a function of the form $e^{-v/\eta}$, where $\eta = 12$ km/sec. This is the same velocity law as was proposed by Blaauw (1952*b*) for all interstellar velocities; the value of η adopted by Blaauw, however, was about 7 km/sec.

The way in which the velocity of a cloud escaping from the sphere of influence of an O star depends upon its original mass is given by equation (40) for the case of a large spherical cloud surrounding the O star, and by equation (23) for an isolated cloud. As the spherical shell will ultimately be broken up into separate parts, we shall in most cases have to deal with some kind of combination of equations (23) and (40). The velocity distribution is determined by the distribution of the masses of the original clouds.

The general character of the distribution law of high velocities that one would obtain is given in Table 5, which shows for one special case the velocities to which the clouds are accelerated. It refers to an O5 star. For v_0 and V we have used 11 and 20 km/sec, respectively. For the isolated cloud we assumed a constant radius of 5 pc and $r_0 = 10$ pc, while r in equation (23) was taken equal to s_0, or 140 pc. In the case of the shell the original radius of the spherical cloud was taken to be 20 pc. The final velocities are tabulated as a function of n_0, the number of hydrogen atoms per cubic centimeter in the original cloud.

As the spherical shell will always break up into separate units, the case of the isolated

cloud may be more representative. It is evident from a comparison of Tables 4 and 5 that the observed velocity distribution can be produced by a plausible distribution of n_0. The comparison applies only to the high velocities. Because of collisions during the later stages of a cloud's existence, there must, of course, be many more low velocities.

Moreover, examination of equations (23) and (40) shows that in each case the number of clouds of very high velocity varies asymptotically as $\exp(-v/V)$. Elsewhere in this paper we have set V equal to 20 km/sec. It is readily shown that, for clouds of velocity 30 km/sec or higher, this larger value of V provides a better fit with Adams' data than is found with the value 12 km/sec adopted in Table 4.

TABLE 5

FINAL VELOCITY v (IN KM/SEC) AS FUNCTION OF NUMBER OF HYDROGEN ATOMS PER CM^3 (n_0) IN ORIGINAL CLOUD

ISOLATED CLOUD			SPHERICAL SHELL		
log n_0	n_0	v	log n_0	n_0	v
2.00	100	∞	2.079	120	∞
2.10	126	62	2.179	151	43
2.20	159	46	2.280	191	31
2.30	200	37	2.380	240	25
2.60	400	24	2.681	480	17
2.90	800	17	2.982	960	14

REFERENCES

Adams, W. S. 1949, *Ap. J.*, **109**, 354.
Bates, D. R. 1950, *Phys. Rev.*, **78**, 492.
Beals, C. S. 1936, *M.N.*, **96**, 661.
Blaauw, A. 1952*a*, *B.A.N.*, **11**, 405 (No. 433).
———. 1952*b*, *ibid.*, p. 459 (No. 436).
———. 1954, *A.J.*, **119**, 625.
Blaauw, A., and Morgan, W. W. 1953, *B.A.N.*, **12**, 76 (No. 448).
Delhaye, J., and Blaauw, A. 1953, *B.A.N.*, **12**, 72 (No. 448).
Jentzsch, C., and Unsöld, A. 1948, *Zs. f. Phys.*, **125**, 370.
Kahn, F. D. 1954*a*, *B.A.N.*, **12**, 187 (No. 456).
———. 1954*b*, *M.N.*, **114** (in press).
Mayall, N.U. 1953, *Pub. A.S.P.*, **65**, 152.
Oort, J. H. 1952, *Ap. J.*, **116**, 233.
———. 1954, *B.A.N.*, **12**, 177 (No. 455).
Parker, E. 1953, *Ap. J.*, **117**, 169.
Schatzman, E., and Kahn, F. D. 1953, Paper read at Cambridge Symposium on Gas Dynamics of Interstellar Clouds.
Schlüter, A., Schmidt, H., and Stumpff, P. 1953, *Zs. f. Ap.*, **33**, 194.
Searle, L. T. 1952, *Ap. J.*, **116**, 650.
Spitzer, L., Jr. 1948*a*, *Ap. J.*, **107**, 6.
———. 1948*b*, *ibid.*, **108**, 276.
———. 1949, *Ap. J.*, **109**, 337.
Spitzer, L., Jr., and Savedoff, M. P. 1950, *Ap. J.*, **111**, 593.
Strömgren, B. 1939, *Ap. J.*, **89**, 526.
———. 1948, *Ap. J.*, **108**, 242.
Van de Hulst, H. C., Muller, C. A., and Oort, J. H. 1954, *B.A.N.*, **12**, 117 (No. 452).
Weizsäcker, C. F. von. 1948, *Naturwiss.*, **35**, 188.
———. 1949, *Problems of Cosmical Aerodynamics* (Dayton, Ohio: Central Air Documents Office); *Proceedings of the Paris Symposium on the Motion of Gaseous Masses of Cosmical Dimensions*, chap. 22.
Whipple, F. 1948, *Centennial Symposia* (Cambridge: Harvard College Observatory), sec. I, 8.
Wild, J. P. 1952, *Ap. J.*, **115**, 206.

THE ASSOCIATION I GEMINORUM

D. Crawford, D. Nelson Limber, E. Mendoza V.,* D. Schulte,
H. Steinman, and T. Swihart
Yerkes Observatory
Received July 14, 1954; revised July 30, 1954

ABSTRACT

A study of the O association I Geminorum is made. This association has an apparent diameter of about 5°. A distance of 1400 parsecs is obtained, giving a true diameter of 120 parsecs. Thirty-two stars are found to be members of the association; these stars range in spectral type from C6 to B9 and in apparent magnitude from 4.7 to 10.2. Several special features of the association are discussed, and a comparison with I Orionis and I Persei is made.

I. INTRODUCTION

In the field of galactic structure the study of stellar associations as outlined by Morgan, Whitford, and Code (1953) has proved to be of great importance. As these associations are composed of population I objects, accurate distances provide definitive information on the spiral structure of the Milky Way system. These observations are independent of any assumed model of the Galaxy and thus provide a check on the results of radio astronomy.

A detailed study of individual associations is also important. Considerations of the internal motion of associations and of energy generation indicate that associations are very young objects. The applications to stellar evolution are apparent; furthermore, the clustering tendency exhibited by early-type stars makes possible an accurate calibration of the luminosity of supergiants. The present paper is an investigation of the association in Gemini, near the nebulosity NGC 2175. The association I Geminorum is No. 25 in the list of Morgan, Whitford, and Code.

A plot of HD and HDE O–B5 stars in the region bounded by $5^h30^m \leq \alpha \leq 6^h40^m$ and $+15° \leq \delta \leq +30°$ (Fig. 1) reveals a marked clustering. This clustering has a diameter of around 5° and is centered near $\alpha(1900) = 6^h8^m$, $\delta(1900) = +23°31'$; the galactic co-ordinates are $l = 156.°0$ and $b = +4.°0$ on the Lund system.

An observing program was carried out for the determination of spectroscopic parallaxes. Over one-half of the stars plotted in Figure 1 were observed.

II. OBSERVATIONS

Spectra of seventy-five stars were taken with the one-prism spectrograph attached to the Yerkes 40-inch telescope. The dispersion is about 125 A/mm at $H\gamma$. Many of the plates were taken for the general Yerkes spectroscopic parallax program and were classified by W. W. Morgan. The remainder were taken by Limber and were classified by Limber and Morgan. The spectra were classified on the MK system (see Johnson and Morgan 1953). The provisional calibration of spectral-luminosity types into absolute visual magnitudes was furnished by Morgan and Keenan and differs only slightly from that published by Keenan and Morgan (1951).

The apparent magnitudes used were those given in the *Henry Draper Catalogue* and *Henry Draper Extension*. The magnitudes in the latter catalogue are photographic, but, since the color indices of these objects are very nearly zero, no corrections were made. The colors of thirty-two of the stars were taken from the list of Stebbins, Huffer, and

* Fellow of the University of Mexico.

Whitford (1940). The apparent magnitudes of these stars were then corrected for absorption by using the intrinsic colors and the ratio of reddening to total visual absorption given by Morgan, Harris, and Johnson (1953). True distance moduli were then computed.

An inspection of the distance moduli of these thirty-two stars showed that ten of them are definitely foreground objects. These ten stars were eliminated from further consideration. The data concerning the remaining twenty-two stars are given in Table 1. The first two columns give the HD number and the apparent visual magnitude. The third column gives the revised color excess on the C_1 system of Stebbins, Huffer, and Whitford (1940).

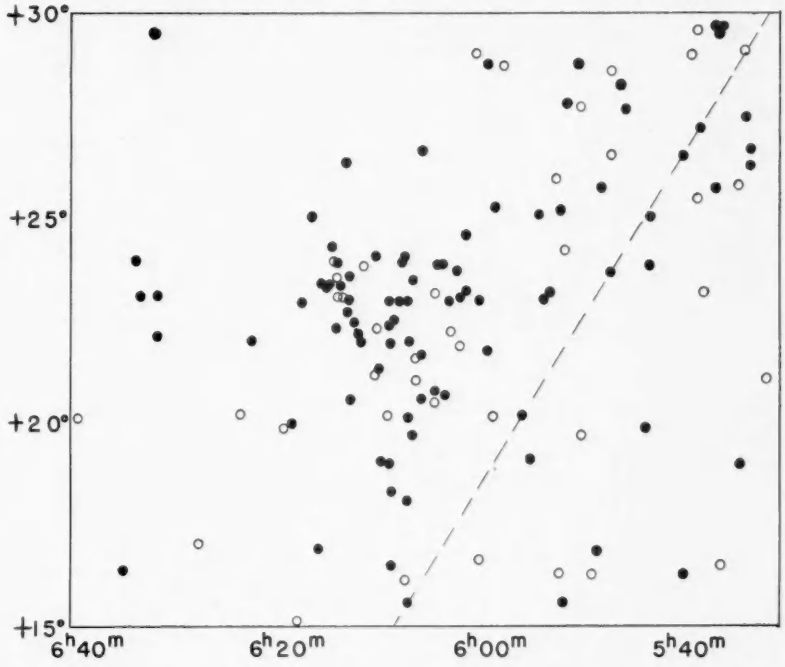

FIG. 1.—Plot of HD and HDE stars of classes O–B5, in the region bounded by $5^h30^m \leq \alpha \leq 6^h40^m$ and $+15° \leq \delta \leq +30°$. Open circles represent HD stars; filled circles represent HDE stars. The dashed line indicates the galactic equator.

The next three columns list the apparent visual magnitude corrected for absorption, the spectral type on the MK system, and the true distance modulus. The final column gives the radial velocity, taken from the catalogue of Wilson (1953).

Of the stars listed in Table 1, fourteen are grouped very close together in the sky, while nine are scattered over a much larger area. These nine stars were not considered in determining the characteristics of the association, although they are possibly outlying members. The color excesses of the fourteen remaining stars, indicated by an asterisk (*) in Table 1, were plotted as a function of position on the sky. From this plot (see Fig. 2, which also includes the nine outlying members) the approximate color excesses of the stars not in the Stebbins, Huffer, and Whitford list could be obtained. The area of the sky was divided into two regions: in one region the color excesses were all approximately 0.25 mag., while in the other region they were about 0.20 mag. The dividing line between

TABLE 1

OBSERVED STARS WITH COLORS

HD	m	E_1	m_0	Sp.	m_0-M	V (Km/Sec)
38010	6.86	0.15	5.9	B1 Vep	9.1	+19
38191	9.5	.19	8.3	B1 V	10.6	.....
39340	8.1	.10	7.5	B3 V	9.5	.....
39746	7.7	.18	6.6	B1 II	11.7	.....
39970	6.02	.18	4.9	A0 I*a*	11.9	+ 0.5
40111	4.90	.08	4.4	B1 I*b*	10.4	+ 8
41117*	4.71	.21	3.4	B2 I*a*	10.4	+16.8
41398	7.45	.21	6.2	B2 I*b*	11.9	+17.9
41690*	8.0	.20	6.8	B1 V	10.0	+15.5
42087*	5.76	.18	4.7	B2.5 I*b*	10.4	+16
42088*	7.40	.17	6.4	O6	.....	+23.4
42379*	7.8	.24	6.3	B1 II	11.4	.....
42400*	6.9	.16	5.9	B5 II	10.4	.....
43078*	8.6	.27	7.0	B0.5 III	11.4	.....
43384*	6.26	.23	4.9	B3 I*ab*	11.3	+13.2
43703*	8.7	.28	7.0	B1 IVp(e)	10.8	.....
43753*	8.1	.22	6.8	B0.5 III	11.2	.....
43818*	7.03	.26	5.4	B0 II	10.6	+18.2
43836*	7.03	.25	5.5	B9 II	9.5	.....
48532	8.60	.08	8.1	B2 V?	10.7:	.....
248753	8.5	.18	7.4	B1 Venn	10.6	.....
253214*	9.5	0.25	8.0	B2 Vnn	10.6	.....

* See text.

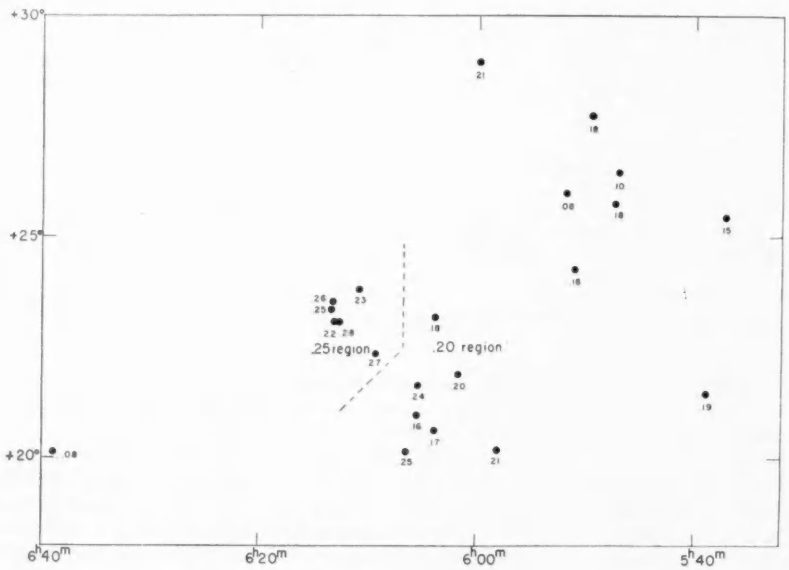

FIG. 2.—Positions and color excesses of stars with colors in the Stebbins, Huffer, and Whitford table. The dashed line represents the division into 0.20 and 0.25 mag. regions for color excesses of stars without measured colors.

the two regions is shown in the figure. These color excesses were applied to the stars for which colors were not available and which were within about three degrees of the center of the main concentration.

The data for these stars are shown in Table 2, the arrangement of which, with the addition of a "Remarks" column, is the same as that of Table 1. The estimated E_1's in the fourth column are, of course, less accurate than the measured ones. Three of the four stars without distance moduli were omitted because their spectra were blended with moonlight, making the spectral type uncertain; the fourth is a peculiar emission-line star.

TABLE 2

PROBABLE ASSOCIATION MEMBERS WITHOUT COLORS

HD	m	E_1	m_0	Sp.	m_0-M	V (Km/Sec)	Remarks
41831	9.0	0.20	7.8	B3 V	9.8	.....	
249788	9.4	.20	8.2	B1 V	11.4	.....	
250163	10.2	.20	9.0	B2 Vpe	11.6	.....	
250310	9.0	.20	7.8	B3 V	9.8	.....	
251670	9.0	.20	7.8	B1–2 V?	.....	.....	Moonlight
251726	10.0	.20	8.8	B2 III–Vpe	.....	.....	Peculiar
251847	8.7	.20	7.5	B1 IV	11.3	.....	
252321	8.9	.20	7.7	B1 V	10.9	.....	
253180	9.6	.20	8.4	B0.5 V	12.0	.....	
253236	9.6	.20	8.4	B1 V:	11.6:	.....	
253591	9.8	.25	8.3	B1 V	11.5	.....	
253683	9.5	.20	8.3	B3 III:	12.0:	.....	
253981	9.4	.20	8.2	.....	.....	.....	Moonlight
254042	8.8	.25	7.3	B1 III	11.6	.....	
254346	9.6	.25	8.1	B2–3 III?	.....	.....	Moonlight
254577	9.5	.25	8.0	B0.5 II–III	12.8	+18	Strong K
254699	9.3	.25	7.8	B1 V	11.0	.....	
254755	9.0	.25	7.5	O9 Vp	11.7	+ 9	
255055	9.1	.25	7.6	O9 Vp(e?)	11.8	.....	
255091	9.4	.25	7.9	B2 V	10.5	.....	
255093	9.4	.25	7.9	B1.5 V	10.8	.....	
255134	9.2	.25	7.7	B1 IVp	11.5	.....	
255168	9.6	.25	8.1	B1 V	11.3	.....	
256035	9.6	0.25	8.1	O9 V:p	12.3:	.....	

III. DISCUSSION

The distance moduli of the probable association members in Table 1 range between 9.5 and 11.4 mag.; the mean distance modulus is 10.7 mag., with an estimated probable error of ± 0.2 mag. As would be expected, the distance moduli from the stars without colors, given in Table 2, are not so consistent as those of Table 1. The mean value for the former is 11.2 mag.; however, either the spectra of seven of these stars are peculiar, or the types are somewhat uncertain. If these seven are excluded, the mean distance modulus becomes 11.0 mag. In view of the fact that the stars in Table 1 carry a much greater weight than those in Table 2, the distance modulus of the association is taken as 10.7 mag. This corresponds to a distance of about 1400 parsecs. The apparent diameter of I Gem, around 5°, corresponds to a linear diameter of about 120 parsecs.

The radial velocities offer further evidence that we are dealing with a physically connected group of stars; the radial velocities of these stars are all approximately +17 km/sec.

Figure 3 gives an H-R diagram for the stars in the central condensation. The agreement between luminosity class and position on the diagram is satisfactory.

IV. OBJECTS OF SPECIAL INTEREST

In the study of the I Persei association by Bidelman (1943), the Double Cluster was found to be physically connected with the group of supergiants in the neighborhood. In the region of I Gem, Trumpler (1930) lists several galactic clusters. However, using the criteria of position and distance as listed by Trumpler, it seems that none of these clusters is related to the Gemini association.

One of the most interesting objects in this region is the O6 star, HD 42088, and the

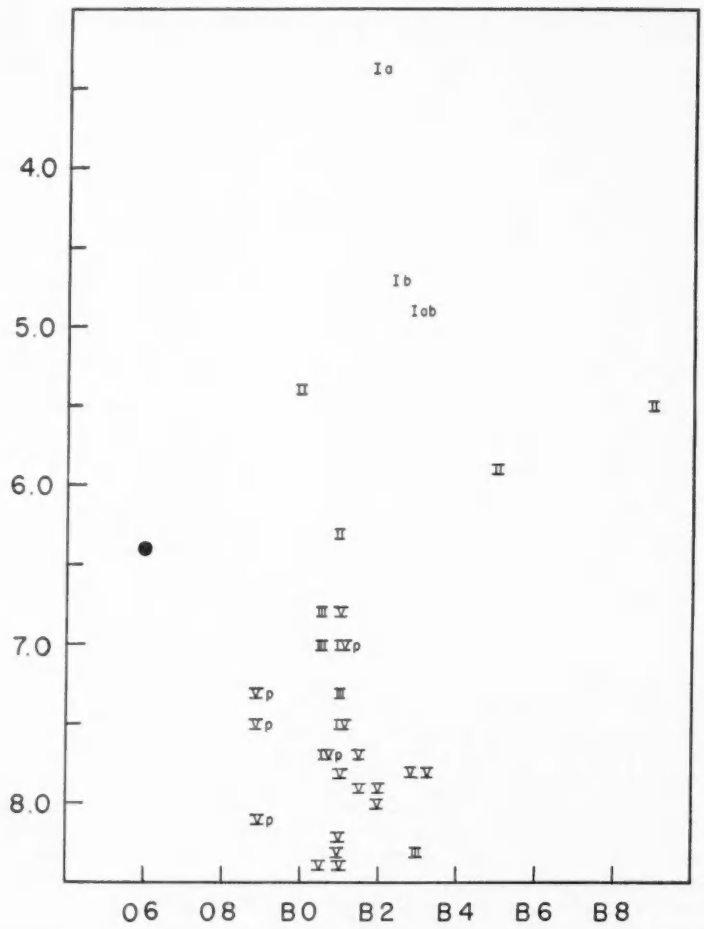

FIG. 3.—H-R diagram with corrected apparent magnitudes and spectral types for members of I Gem. Roman numerals indicate the luminosity classes of the stars in the association. The filled circle represents the O6 star HD 42088.

surrounding nebulosity NGC 2175. According to Collinder (1931), the nebulosity NGC 2175 is a nebulous cluster containing about sixteen members. This cluster has $\alpha(1900) = 6^h04^m8$ and $\delta(1900) = +20°31'$ and is 15 minutes in diameter. Collinder gives its distance as 2700 parsecs, but this measure is based on a mean of parallaxes derived from integrated magnitudes and apparent dimension. Since the nebulosity and hence the cluster are connected with the O6 star discussed in this section, the question of whether the cluster is physically related to I Gem depends on whether the O star is.

The color of HD 42088 is given in the Stebbins, Huffer, and Whitford list and, with the HD magnitude, gives a corrected apparent magnitude of 6.4. Now, if we assume that $M = -5.0$ for a main-sequence O6 star,[1] we find a distance modulus of 11.4 mag., which is within the range of distances for the association members. The intensity of the interstellar K line in the spectrum of HD 42088 also suggests a distance of the same order as that of the association. This is in agreement with the relatively small absorption, of about one magnitude, found for the star.

The apparent radius of the nebulosity NGC 2175 is 13 minutes. Thus the linear radius, s, of the nebula is related to the distance, r, by the formula $s = 0.0038r$, where s and r are measured in the same units. If one applies the analysis of Strömgren (1939) on *H* II regions to the nebula, using Kuiper's (1938) values for the temperature and bolometric correction, one obtains the values shown in Table 3 for the radius in terms of the number

TABLE 3

	M			
	−6.0	−5.5	−5.0	−4.5
$sN^{2/3}$	160	136	117	100

of hydrogen atoms and ions per cubic centimeter, N. In this table s is given in parsecs. One finds that the absolute magnitude is very sensitive to the value of N; thus, if $M = -6.0$, the hydrogen density is about 50 cm^{-3}, while for $M = -4.5$ one finds that N is about 80 cm^{-3}. Thus an independent measure of N is needed to determine the distance accurately, for example, an observation of the emission measure of the nebula (see Strömgren 1951).

Another star in this region which deserves special attention is HD 254577. Figure 4 shows the spectrum of this star and that of HD 255091 for comparison. These two stars have nearly the same line of sight and were taken during the same night on the same plate. The distance modulus for HD 254577, computed by the method described in section II of this paper, with $E_1 = 0.25$, is 12.8 mag. (3630 parsecs). The assumption of this color excess seems valid, since the blend at λ 4430, which is closely related to the interstellar reddening, is similar to that for the stars of the association. However, the interstellar H and K lines are much stronger than for the association members, indicating a larger distance for HD 254577. This would lead us to believe that the distance is as large as computed. Because of the great strength of the interstellar calcium lines, HD 254577 deserves further observation.

We can almost definitely relate several M supergiant irregular variable stars with I Gem. The two stars BU Gem and TV Gem have the magnitudes listed below, according to Kukarkin and Parenago (1949). The radial velocities (V) are from Wilson's catalogue

[1] This is in approximate agreement with Roman's estimate (1951).

(1953). BU Gem is a standard on the MK system, whereas TV Gem was classified by the authors.

Star	α(1900)	δ(1900)	m	Sp.	V (Km/Sec)
BU Gem	6^h06^m2	22° 56′	6.1–7.5	M1 I*a*	+21.5
TV Gem	6 05.8	21 53	6.6–8.0	M1 I*ab*	+17

If we accept the luminosities of Keenan and Morgan and correct for absorption according to Figure 2, using m_{max}, we obtain the following:

Star	E_1	A_1	m_0	M	$m_0 - M$
BU Gem	0.25	1.5	4.6	−7.0	11.6
TV Gem	0.20	1.2	5.4	−5.7	11.1

The resulting distance moduli place the stars within the range of the association. If the distance for the association is correctly taken as 10.7 mag., and we assume that these stars are in the association, we obtain a luminosity of −6.1 for BU Gem, a class I*a* star, and −5.3 for TV Gem, a class I*ab* star.

Bidelman (1954) suggests that WY Gem may also be connected with the association. The spectral class given below is from Kukarkin and Parenago:

Star	α(1900)	δ(1900)	m	Sp.	V (Km/Sec)
WY Gem	6^h05^m9	23° 14′	7.4	M3 ep	+16

The radial velocity is similar to those of the association stars. On following the procedure outlined above, we find the spectroscopic absolute magnitude would have to be about −4.5 for WY Gem to be in I Gem.

V. COMPARISON WITH OTHER ASSOCIATIONS

From the data derived in this investigation, a comparison can be made between I Gem and two other OB associations. Table 4 gives this comparison. On the basis of this table,

TABLE 4

COMPARISON OF THREE ASSOCIATIONS

	Association		
	I Gem	I Ori*	I Per
Diameter (parsecs)	120	125	160
Distance (parsecs)	1400	500	2300
Spectral type of class I supergiants	B2–B3	O9.5–B8	B0.5–A2
Number of stars earlier than B0	4	6	3
Number of late-type supergiants	2–3	1?	13
Earliest spectral type	O6	O6	O7

* Data from Sharpless (1952, 1954).

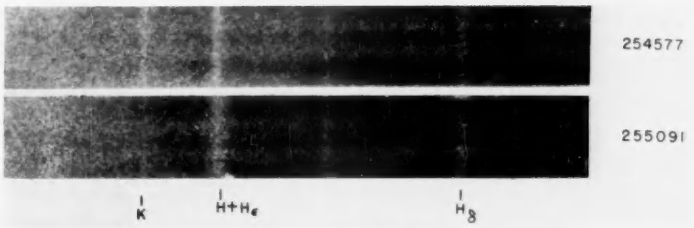

FIG. 4.—Spectra of B0.5 II–III star HD 254577 with strong K line, and B2 V star HD 255091.

I Gem can be placed somewhere between I Ori and I Per in a possible evolutionary sequence. All three are large associations. The associations I Ori and I Gem contain an O6 star imbedded in a gaseous nebula. The association I Per is somewhat peculiar, in that it contains the Double Cluster. There seems to be a transition in spectral type of the supergiants, earliest-type stars, the number of late-type supergiants, and the number of O stars. Also, the number of dark clouds in each association decreases in the same way, but this could be an observational effect due to increasing distance. In general, therefore, I Gem appears to be older than I Ori and younger than I Per.

The authors are deeply indebted to Dr. W. W. Morgan both for suggesting this investigation and for his valuable advice and helpful discussions.

REFERENCES

Barnard, E. E. 1927, *Atlas of Selected Regions of the Milky Way* (Washington, D.C.: Carnegie Institution of Washington), Pls. 9 and 10.
Bidelman, W. P. 1943, *Ap. J.*, **98**, 61.
———. 1947, *ibid.*, **105**, 492.
———. 1954, "The Space Distribution of Supergiant Stars of Types Later than B" (paper presented at the June meeting of the American Astronomical Society in Ann Arbor, Michigan).
Collinder, P. 1931, *Ann. Lund Obs.*, **2**, B6.
Johnson, H. L., and Morgan, W. W. 1953, *Ap. J.*, **117**, 313.
Keenan, P. C., and Morgan, W. W. 1951, in J. A. Hynek (ed.), *Astrophysics* (New York: McGraw-Hill Book Co., Inc.), p. 23.
Kuiper, G. P. 1938, *Ap. J.*, **88**, 429.
Kukarkin, B. V., and Parenago, P. P. 1948, *General Catalogue of Variable Stars* (Moscow).
Morgan, W. W., Harris, D. L., and Johnson, H. L. 1953, *Ap. J.*, **118**, 92.
Morgan, W. W., Whitford, A. E., and Code, A. D. 1953, *Ap. J.*, **118**, 318.
Roman, N. 1951, *Ap. J.*, **114**, 492.
Sharpless, S. 1952, *Ap. J.*, **116**, 251.
———. 1954, *ibid.*, **119**, 200.
Stebbins, J., Huffer, C. M., and Whitford, A. E. 1940, *Ap. J.*, **92**, 193.
Strömgren, B. 1939, *Ap. J.*, **89**, 526.
———. 1951, *Problems of Cosmical Aerodynamics* (Dayton: Central Air Documents Office,), chap. ii.
Trumpler, R. L. 1930, *Lick Obs. Bull.*, **14**, 154.
Wilson, R. E. 1953, *General Catalogue of Stellar Radial Velocities* (Washington, D.C.: Carnegie Institution of Washington).

SPECTRAL AND LUMINOSITY CLASSIFICATION OF THE BRIGHT SEQUENCE STARS IN THE C REGIONS

J. J. NASSAU AND DONALD A. MACRAE*
Warner and Swasey Observatory, Case Institute of Technology
Received August 16, 1954

ABSTRACT

Spectral types and luminosities on the system of the Yerkes *Atlas* have been obtained for the sequence stars in the Harvard Standard C regions from objective-prism photographs at the Warner and Swasey Observatory.

The magnitude sequences in the Harvard C regions at declination +15° and odd-numbered hours of right ascension have been the focus of much attention in photometric work. One of the chief reasons for this interest is that they can be reached from both Northern and Southern hemispheres. In view of the importance of these regions, a series of objective-prism photographs of all twelve fields has been obtained with the Burrell telescope. As the first step in the utilization of this material, the stars which form the photometric sequences have been classified according to spectral type and luminosity, and the results are presented in Table 1.

The 4° prism gives a dispersion of 283 A/mm at $H\gamma$. The emulsion used was Kodak Spectroscopic IIa-O. On every region two or more good plates (diameter 5°) were available with each of the following exposure times: 2^m, 5^m, 15^m, 30^m; in addition, shorter exposures were made to obtain spectra of the stars at the bright end of the sequences. The faint-magnitude limit ranges from 12 to 12.5.

Each star was classified from at least two plates, and sometimes from four or five plates, by each author independently. These results were then examined jointly, and a final classification was adopted for each star.

An effort was made to have both luminosity and spectral-type classification conform to the MK system (Johnson and Morgan 1953), although, in general, the criteria used on objective-prism spectra must be quite different from those used on slit spectra. In order to achieve this aim, continuous reference was made to the observatory's collection of objective-prism spectra of stars with published Yerkes classifications. In fact, virtually every star was compared directly with appropriate standard stars by superposition of plates with emulsions in contact. The objective-prism spectra of a standard star consist of a series of varying exposure times, so that a close match of density could always be obtained in making this comparison. The standards are also on the IIa-O emulsion.

The following information is listed in Table 1: column 1: the letter designation of the sequence star (co-ordinates are given in *Harvard Ann.*, **71**, 269, 1917, and charts appear in *Harvard Ann.*, **108**, 1, 1939); column 2: the number in the *Bonner Durchmusterung;* column 3: the photographic magnitude and Miss Cannon's revised spectral type from *Harvard Ann.*, **89**, 123, 1937 (the magnitudes are simply Miss Leavitt's reduced to the "1922 system"); column 4: the spectral type and luminosity determined at the Warner and Swasey Observatory.

The letter "m" following the spectral class designates an A-type star which shows the G band. The letter "p" designates a star which shows features not present in a normal star of its class. This includes the A-type stars which show the silicon, strontium, and europium characteristics. The colon (:) indicates a doubtful classification due to faintness or the overlap of a neighboring star. An asterisk (*) following the star letter

* Now at the David Dunlap Observatory, University of Toronto.

TABLE 1

Region	Star	B. D.	Ipg	Sp. (HD)	Sp. & Lum. (W&S)
C 1	A	14° 169	7.19	F2	F2 V
	B	13 165	7.41	F2	F2 V
	C	14 175	7.53	K5	M0 III
	D	16 97	8.02	G5	K2 III
	E	15 159	8.43	F0	F0 V
	F	15 164	8.58	G0	G5 III
	G	15 156	8.78	M0	M2 III
	H	15 149	8.98	A5	F0 III
	I	15 161	9.34	F2	F2 III
	K	14 161	9.44	G5	G8 V
	L*	14 167	9.68	K2	K2 V
	M	14 164	9.87	G5	F5 III
	N	14 171	10.23	A2	A3 p
	O	14 168	10.37	K5	K2 III
	P		10.66	G0	F5 V
	Q	15 162	10.84	G0	G0 V
	R	14 170	11.28	F5	G0
	S	14 160	11.44	F8	G0:
	T		11.74		G0:
C 2	A	15 450	6.94	A0	A0
	B	15 447	7.25	A2	A5
	C	15 430	7.67	K0	K3 III
	D	13 496	8.24	G5	G8 III
	E	14 518	8.29	G0	G8 V
	F	13 494	8.78	K0	K0 IV
	G	14 511	9.20	F5	F5 V
	H	13 501	9.26	F5	F2 V
	I	14 513	9.40	K5	K3 III
	K	14 516	9.52	F8	F8 V
	L	14 509	9.92	K0	K0 III
	M	14 507	10.17	G5	G2 V
	N	14 515	10.63	F5	F8 V
	O	14 514	10.64	K0	G8 V
	P	14 519	10.76	K	G5 V
	Q	14 505	11.02	F0	F0
	R	15 429	11.27	F5	F8
	S		11.42	F8	F8
	T		11.67		F2
	U	14 510	11.75		K
	V		12.07		G
	W		12.45		A
C 3	A	14 825	6.62	A2	A3 p
	B	15 713	6.94	F5	F5 V
C 3 (Cont'd.)	C	14° 804	7.23	G0	G5 V
	D	15 735	7.47	A0	A0 p
	E	14 843	7.62	B9	A0
	F	14 839	7.75	A0	A2
	G	14 834	8.12	A0	A2 p
	H	14 831	8.31	G5	K0 V
	I	14 836	8.80	G5	G5 III
	K	15 721	8.85	K0	G8 III
	L	14 812	9.10	F0	F0 III
	M	14 832	9.19	K0	K0 III
	N	14 813	9.47	F8	F5 V
	O	15 733	9.60	A5	F0 V
	P	15 730	10.05	A2	A2 m
	Q*	14 816	10.36	F5	F5
	R	14 822	10.54	K2	G8 III
	S	14 828	10.63	K5	K0 III
	T	14 830	10.79	K0	F8
	U		10.90	G5	G5
	V	15 731	11.29	K5	G8
	W		11.29	G0	F5
	X		11.44	G5	G2
	Y		11.85		F0
	Z	14 827	12.06		K
	a		12.12		F
	b		12.38		G
C 4	A	14 1558	6.70	B8	B8
	B	15 1444	7.22	A2	A3
	C	15 1494	7.34	F0	F2 III
	D	15 1461	7.78	K0	K0 III
	E	15 1473	8.01	F8	G0 V
	F	15 1445	8.46	K0	K2 III
	G	15 1447	8.51	B9	B8
	H	14 1545	8.86	K0	K0 III
	I	15 1443	8.99	A0	B9
	K	15 1459	9.51	K0	K2 III
	L	15 1456	9.80	F5	F8 V
	M	15 1457	10.02	F8	F8 V
	N	15 1440	10.06	A2	A0
	O	15 1458	10.25	F5	G5 V
	P	14 1556	10.41	K0	K0 III
	Q	15 1464	10.97	G0	F5 V
	R		11.28	G0	G0
	S		11.34	F2	F5
	T		11.74	G5	G5
	U		12.17		F8

TABLE 1

Region	Star	B. D.	Ipg	Sp. (HD)	Sp. & Lum. (W&S)
C 5	A	15° 2003	7.17	G5	K0 V
	B	15 1981	8.09	F5	F5 V
	C	13 2021	8.09	K2	K5 III
	D	13 2036	8.29	G5	G8 III
	E	15 1960	8.48	F5	F2 V
	F	15 1962	9.07	F5	F8 V
	G	14 2024	9.31	A3	A3
	H	14 2018	9.34	K7	K3 III
	I	15 1969	9.73	F5	F5 V
	K	14 2025	9.91	K0	K2 III
	L	15 1976	10.13	K0	G5 V
	M	14 2022	10.32	G5	G5 V
	N	15 1971	10.43	G5	G8 V
	O	15 1972	10.68	K0	G5 III
	P	15 1974	10.78	M0	M3 III
	Q		11.18		F5
	R	14 2020	11.40		M5 III
	S		11.60		F5
	T	15 1970	11.99		K2
	U	15 1980	12.06		G2:
	V		12.29		K
	W		12.46		G
C 6	A	13 2348	6.75	A0	A3 p
	B	12 2284	6.88	F5	F5 III
	C	16 2224	7.54	F0	F2 V
	D	14 2345	7.59	F5	G0 V
	E	13 2350	7.81	F5	F5 V
	F	14 2344	8.30	F5	F5 V
	G	13 2358	8.61	K0	K2 III
	H	15 2283	8.69	K0	K0 III
	I	15 2302	8.73	F2	F5 III
	K	15 2290	9.03	M1	M2 III
	L	15 2294	9.20	F8	G0 III
	M	15 2282	9.51	K2	K3 III
	N	14 2338	9.58	F2	F0 V
	O	15 2288	9.87	K0	K2 V
	P	15 2281	10.27	G5	G2 V
	Q*	15 2289	10.27	K5	M0 II:
	R	14 2337	10.74	G5	G0 V
	S	15 2286	11.01		G0 V
	T	15 2284	11.16		G5
	U		11.35		F5
	V	15 2285	11.35		G0
	W	15 2287	11.50		G0
	X		11.78		G2:
	Y		12.07		F8:
	Z		12.40		K
C 7	A	17° 2573	6.85	G5	K0 III
	B	16 2476	7.75	F2	F5 V
	C	14 2585	8.19	F2	F2 IV:
	D	15 2541	8.29	F8	F5 V
	E	16 2466	8.66	K0	K2 III
	F	15 2542	9.07	F8	G0 V
	G	16 2459	9.36	G5	G8 V
	H	16 2461	9.78	F2	F5 V
	I	15 2523	10.01	F2	F5 V
	K	16 2448	10.30	F8	G0 V
	L	15 2535	10.33	K7	K3 III
	M	15 2545	10.58	G5	G8 V
	N	15 2538	10.88	F2	G0 V
	O	15 2537	11.05	G0	G5 V
	P	15 2543	11.23	G0	G0 V
	Q	15 2536	11.47	G5	G2
	R		11.80	F8	F5
	S		11.93	K0	G5
	T*		12.25		F8:
	U*		12.50		
	GA*		11.82		K
	GB*		12.23		F
C 8	A	16 2725	7.21	F8	G0 V
	B	13 2899	7.25	A5	A7 p
	C*	15 2792	7.76	K0	K0 III
	D	14 2812	7.98	K2	K3 III
	E	15 2808	8.16	F0	F0 III
	F	15 2803	8.19	K0	K2 III
	G	13 2879	8.91	F0	F0 p:
	H*	14 2850	8.93	F8	G0 V
	I	14 2828	9.10	K0	K2 III
	K	14 2823	9.38	K0	K2 III
	L	14 2824	9.69	F8	F8 V
	M	15 2810	9.70	F2	F2 III
	N	15 2814	9.94	K2	K2 III
	O	15 2807	10.09	K2	K2 III
	P	14 2839	10.18	G0	G0 V
	Q	15 2816	10.58	G0	G2 V
	R	14 2835	10.74	F5	F0
	S	14 2827	10.79	K0	K5 III
	T	15 2818	10.86	K7	K5 III
	U		10.90	G0	F8 V
	V	15 2809	10.90	G5	G5 V
	W	15 2815	11.46	G0	G2
	X	15 2817	11.61	F8	G2
	Y		11.66		F8
	Z		12.06		F8
	a		12.23		F5
	b		12.33		F8

TABLE 1

Region	Star	B. D.	Ipg	Sp. (HD)	Sp. & Lum. (W&S)
C 9	A*	14°3180	7.04	G5	G5 IV:
	B	16 3083	7.19	A0	A0
	C	15 3089	7.24	G0	G5 V
	D	14 3161	7.37	F0	F2 IV
	E	15 3108	7.87	G5	K0 V
	F	15 3116	8.13	F5	F8 V
	G	15 3090	8.57	G5	G5 V
	H*	16 3091	8.75	K5	K0 III
	I	14 3178	9.18	K7	K5 III
	K	15 3096	9.71	K0	K0 III
	L	15 3101	9.86	F8	G2 V
	M	15 3104	10.30	G0	G0 V
	N	15 3106	10.72	M0	K5 III
	O	14 3183	10.79	K0	G8 III
	P	15 3109	10.88	G5	G2 V
	Q	15 3107	10.94	K0	K2 III
	R	14 3187	11.02	G5	G5 V
	S		11.27	K5	K3 III
	T		11.84		F8
	U		12.07		F5
C 10	A	15 3683	6.84	A0	A2
	B	14 3755	7.36	G0	G2 V
	C	15 3690	7.43	A5	F0 p
	D*	14 3745	7.89	B9	B5
	E	14 3771	8.38	K0	G8 IV
	F	14 3744	8.53	F2	F2 III
	G*	14 3768	8.60	F5	
	H	15 3681	9.25	A0	A0
	I	14 3790	9.57	K0	G8 V
	K	14 3782	9.87	B9	B8
	L	14 3772	10.25	F8	F5 V
	M	14 3776	10.71	A2	A0
	N*	14 3775	10.96	A2	A2
	O	15 3680	11.25	A3	A5
	P	15 3676	11.41	F0	F0
	Q*	15 3677	11.76	F8	
	R*		12.14		
C 11	A	14 4530	6.81	F5	F5 III
	B	15 4340	7.08	K0	K2 IV
	C	13 4607	7.70	A0	A2
	D	14 4518	7.97	M1	M1 III
C 11 (Cont'd.)	E*	15°4320	8.40	G5p	
	F	14 4537	8.56	F5	F2 III
	G*	15 4325	8.95	A2	A5 p
	H	14 4520	9.17	A0	A3 p
	I	14 4516	9.51	F5	F2 III
	K	14 4528	9.62	A3	A5
	L	14 4522	10.02	K5	K5 III
	M	14 4519	10.04	F0	F2 V
	N	14 4531	10.05	K0	K2 III
	O	15 4331	10.18	K7	K5 III
	P		10.62	F8	F2 V
	Q	14 4533	10.93	G0	G5 V
	R*	14 4523	11.20		G5
	S	15 4322	11.26	K0	G8 V
	T		11.56		F0
	U		11.63		F5
	V*		12.10		F:
	W		12.10		K
	X		12.13		F
C 12	A*	14 4929	6.59	A0	A0
	B	13 5059	6.99	G0	G0 V
	C	15 4752	7.29	A2	A3
	D	15 4751	7.59	K0	K0 III
	E*	14 4916	7.89	K0	K0 III
	F	15 4748	8.31	A0	A0 p
	G	14 4902	8.53	F0	F0 p
	H	14 4894	8.71	A2	A0
	I	14 4912	9.12	K2	K3 III
	K	15 4764	9.16	F5	F5 V
	L	15 4750	9.48	F5	F5 III
	M	15 4753	9.79	K2	K3 III
	N	14 4924	10.00	F8	F5 III
	O	15 4761	10.12	K2	K0 III
	P	15 4756	10.05	K0	K0 III
	Q	14 4932	10.60	K5	K2 III
	R	15 4755	10.87	K5	K5 III
	S	15 4754	11.32	K7	K3 III
	T	14 4925	11.54		G2 V
	U*		11.71		
	V		12.06		F8
	W		12.14		F8

REMARKS ON TABLE 1

C1—L: Double star, ADS 895.
C3—Q: Double star, not in *ADS*.
C6—Q: Overlapping spectra.
C7—T: Overlapping spectra.
C7—U: Double star (Gossner and Gossner 1947); also double on our plates.
C7—GA, GB: These are the stars designated as "A" and "B" by Gossner and Gossner (1947) and as "1" and "2" by van Rhijn and Plaut (1950).
C8—C: The *CN* in the blue region is weak.
C8—H: Because of the off-center position of this star the classification was made from one plate only.
C9—A: On objective-prism plates the spectrum shows peculiarities in the luminosity characteristics. Slit spectrograms at the David Dunlap Observatory confirm the classifications given here. The space motion is probably about 70 km/sec.
C9—H: λ 4150 is strong.
C10—D: This star has a peculiar spectrum. *H* and *Hε* have the strength of a B5 star, and the K line is equivalent to that of an A2 star.
G10—G: Double star, ADS 11999.
C10—N: Overlapping spectra.
C10—Q, R: Overlapping spectra.
C11—E: Composite (G plus A); HD 200428–200429.
C11—G: The G band is also present.
C11—R: Overlapping spectra.
C11—V: Overlapping spectra.
C12—A: Variable; see Kron, White, and Gascoigne (1953).
C12—E: The *CN* in the blue region is weak.
C12—F: The peculiarity is striking; the color of this star (Fig. 1) corresponds to spectral class F1.
C12—U: Double star, separation about 7″ at 100°.

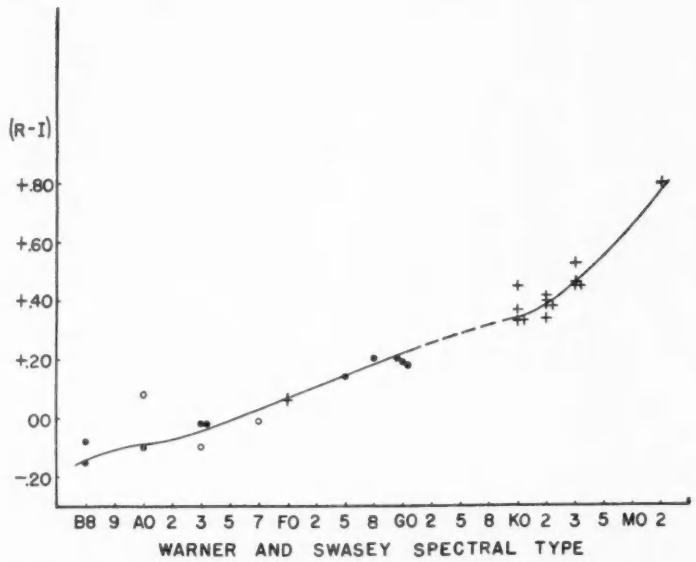

FIG. 1.—Photoelectric colors $(R - I)$ plotted against Warner and Swasey spectral classes for stars in the regions C4, C6, C8, and C12. *Crosses:* class III stars; *open circles:* peculiar stars; *filled circles:* class V stars or stars unclassified according to luminosity. The line indicates the variation of $(R - I)$ with spectral class on the MK or MKK system and was obtained from the $(R - I)$ color standards published by Kron, White, and Gascoigne (1953, Table 4). The red A0p star is C12 F, and the red K0 III star is C12 D.

directs attention to the remarks at the end of the table. For the early-type stars up to F0 no luminosity class has been assigned. All appear to be main-sequence stars.

In Figure 1 photoelectric colors from Kron, White, and Gascoigne (1953) are plotted against our spectral types. The line is the relation between the same color system and the Yerkes spectral types. The agreement of the plotted points and the curve speaks well for the systematic accuracy of our spectral classification.

This investigation was supported by the Office of Naval Research; a photometric investigation in the C regions is being carried out at the Leander McCormick Observatory under the same contract, and the results will be presented separately. We are indebted to Dr. A. N. Vyssotsky for checking the identification of the stars given in the catalogue.

REFERENCES

Gossner, S. D., and Gossner, J. L. 1947, *A.J.*, **53**, 209.
Johnson, H. L., and Morgan, W. W. 1953, *Ap. J.*, **117**, 313.
Kron, G. E., White, H. S., and Gascoigne, S. C. B. 1953, *Ap. J.*, **118**, 502.
Van Rhijn, P. J., and Plaut, L. 1950, *B.A.N.*, **11**, 245.

PRELIMINARY LIST OF PHOTOELECTRIC CLASSIFICATION INDICES FOR 234 BRIGHT NORTHERN G AND K STARS

K. GYLDENKERNE
Copenhagen Observatory
Received July 28, 1954

ABSTRACT

A list is given of values for the classification indices k (K-line index), g (G-discontinuity index), and n (cyanogen index) for 234 bright northern G and K stars. The indices were determined through photoelectric photometry with interference filters made with a 10-inch reflector at the Sophienholm station of the Copenhagen Observatory.

In Table 1 are tabulated values for the classification indices k, n, and g as defined in B. Strömgren and K. Gyldenkerne (*Ap. J.*, in preparation), according to observations made by the author with a 10-inch reflector at the Sophienholm station of the Copenhagen Observatory.

The first four columns give the "Revised Harvard Photometry" or "Bright Star" number and the star name and co-ordinates of the star (1900.0). The remaining columns are: (5) visual magnitude; (6) spectral class and luminosity class in the Yerkes MK system. The sources are as follows: "JM," H. L. Johnson and W. W. Morgan, *Ap. J.*, **117,** 320, 1953; "MHJ," W. W. Morgan, D. L. Harris, and H. L. Johnson, *Ap. J.*, **118,** 92, 1953; "M," W. W. Morgan, private communication; (7) number of nights on which the star has been measured; (8) $k = 2.5\ [\log I(3910 - \log I(4030)] + \text{const.}$, K-line index; (9) $n = 2.5\ [\log I(4240) - \log I(4170)] + \text{const.}$, cyanogen index; (10) $g = 2.5\ [\log I(4360) - \log I(4240)] + \text{const.}$, G-discontinuity index; (11) "hv" indicates that the star is a high-luminosity star according to P. C. Keenan and G. Keller, *Ap. J.*, **117,** 241, 1953.

The observations are discussed in the paper by B. Strömgren and K. Gyldenkerne, quoted above.

Table 1

Photoelectric Classification Indices for 234 Bright Northern G and K Stars

HR		(1900)		m	Sp		N	k	n	g	
163	ϵ And	0^h33^m3	+28°46'	4.5	G8 III p	M	3	0^m432	0^m081	0^m220	hv
165	δ And	0 34.0	30 19	3.5	K3 III	M	3	.449	.300	.393	
166	54 Psc	0 34.2	20 43	6.1	KO V	JM	2	.344	.117	.256	
168	α Cas	0 34.8	55 59	2.5	KO II-III	M	10	.222	.281	.318	
175	32 And	0 35.7	38 55	5.4	G8 III		2	.365	.144	.240	
244		0 47.1	60 34	4.9	F8 IV		1	.603	.083	.155	
253	υ^1 Cas	0 49.1	58 26	4.9	K2 III		1	.200	.245	.352	
265	υ^2 Cas	0 50.7	58 38	4.8	G8 III-IV		2	.341	.121	.256	
285		0 55.0	85 43	4.5	K2 III	M	2	.180	.288	.348	
294	ϵ Psc	0 57.7	7 21	4.4	KO III		3	.327	.138	.267	
321	μ Cas	1 1.6	54 26	5.3	G5 V p	JM	1	.552	.045	.190	hv
351	χ Psc	1 6.1	20 30	4.9	G8 III	M	2	.309	.211	.270	
352	τ Psc	1 6.1	29 34	4.7	KO III-IV		2	.245	.215	.309	
360	ϕ Psc	1 8.3	24 03	4.6	KO III		3	.291	.214	.296	
390	ξ And	1 16.4	45 00	5.0	KO III-IV		2	.238	.224	.312	
430	49 And	1 24.1	46 30	5.3	G9 III	M	4	.293	.207	.274	
434	μ Psc	1 24.9	5 38	5.1	K4 III	M	2	.085	.248	.396	
437	η Psc	1 26.1	14 50	3.7	G8 III	JM	2	.339	.190	.250	
442	χ Cas	1 27.4	58 43	4.9	G8 III	M	2	.321	.160	.251	
458	υ And	1 30.9	40 54	4.2	F8 V	JM	2	.606	.079	.150	
464	51 And	1 31.9	48 07	3.8	K3 III	JM	3	.165	.288	.366	
469	χ And	1 33.3	43 52	5.2	G8 III		4	.393	.143	.242	
483		1 35.7	42 07	5.1	G2 V	JM	1	.562	.075	.175	
489	ν Psc	1 36.2	4 59	4.7	K3 III		2	.124	.270	.425	
493	107 Psc	1 37.1	19 47	5.3	K1 V	JM	2	.372	.071	.248	
510	o Psc	1 40.1	8 39	4.5	G8 III	M	2	.335	.187	.255	
511		1 40.5	63 22	5.7	KO V	MHJ	2	.420	.084	.246	
549	ξ Psc	1 48.4	2 42	4.8	KO III		3	.312	.178	.272	
592	49 Cas	1 56.0	75 38	5.3	G8 III		3	.348	.180	.258	
617	α Ari	2 1.5	22 59	2.2	K2 III	JM	4	.208	.211	.324	
643	60 And	2 6.9	43 46	5.1	K4 III		2	.125	.292	.444	
645		2 6.9	50 36	5.4	KO III		2	.354	.201	.254	hv
694	64 And	2 17.8	49 33	5.5	G8 III	M	3	.316	.187	.262	
743		2 28.5	72 23	5.3	G8 III		3	.371	.161	.234	
800	14 Per	2 37.6	43 52	5.6	G0 Ib	M	3	.447	.146	.203	
824	39 Ari	2 41.9	28 50	4.6	K1 III	M	2	.216	.235	.319	
843	17 Per	2 45.3	34 39	4.7	K5 III		1	.138	.268	.462	
882	24 Per	2 52.9	34 47	5.0	K2 III	M	2	.188	.246	.351	
918		2 58.0	56 19	5.1	KO II-III		2	.290	.192	.272	
941	κ Per	3 2.7	44 29	4.0	KO III		3	.292	.210	.283	
947	ω Per	3 4.8	39 14	4.8	KO III	M	2	.245	.230	.311	
951	δ Ari	3 5.9	19 21	4.5	K2 III		2	.282	.198	.292	
969		3 9.0	50 34	5.3	G5 II	M	4	.354	.198	.253	
999		3 14.3	28 41	4.7	K4 III	M	2	.121	.315	.434	
1017	α Per	3 17.2	49 30	1.9	F5 Ib	JM	21	.610	.100	.112	
1030	o Tau	3 19.4	8 41	3.8	G8 III	JM	2	.364	.154	.252	
1052	σ Per	3 23.5	47 39	4.5	K3 III	M	3	.128	.257	.402	
1135	ν Per	3 38.4	42 16	3.9	F5 II	M	2	.656	.099	.089	
1256	37 Tau	3 58.8	21 49	4.5	KO III		2	.248	.228	.311	
1303	μ Per	4 7.5	48 09	4.3	G0 Ib	M	1	.460	.160	.208	
1327		4 11.3	64 54	5.4	G5 III	M	2	.428	.135	.210	
1343	54 Per	4 13.9	34 20	5.1	G8 III		2	.336	.195	.270	
1346	γ Tau	4 14.1	15 23	3.9	KO III	JM	2	.359	.180	.252	
1348	Φ Tau	4 14.2	27 07	5.1	K1 III		2		.184	.335	
1373	δ Tau	4 17.2	17 18	3.9	KO III	JM	5	.292	.216	.266	
1396	π Tau	4 20.9	14 29	4.9	G8 III	M	2	.325	.189	.252	
1407	75 Tau	4 22.7	16 08	5.3	K2 III	M	2	.222	.221	.320	
1409	ϵ Tau	4 22.8	18 58	3.6	KO III	JM	5	.292	.225	.291	
1411	θ^1 Tau	4 22.9	15 44	4.0	KO III	M	2	.349	.198	.257	
1523		4 41.6	81 02	5.3	K3 III		2	.146	.258	.385	

Table 1 (continued)

HR		(1900)		m	Sp		N	k	n	g	
1577	ι Aur	4^h50^m5	+33°00'	2.9	K3 II	M	3	0^m147	0^m320	0^m432	
1603	10 Cam	4 54.5	60 18	4.2	G0 Ib	M	1	.461	.152	.196	
1729	λ Aur	5 12.1	40 01	4.9	G0 V	JM	2	.558	.065	.170	
1739	109 Tau	5 13.3	22 00	5.1	G8 III		2	.359	.172	.256	
1907	ϕ^2 Ori	5 31.4	9 14	4.4	G8 III p	M	2	.371	.105	.244	hv
1963	51 Ori	5 37.3	1 26	5.2	K0 III	M	2	.224	.184	.308	
1995	τ Aur	5 42.2	39 09	4.6	G8 III		2	.371	.161	.251	
2002	132 Tau	5 42.9	24 32	5.0	G8 III		2	.354	.234	.289	
2012	χ^1 Aur	5 44.6	39 07	4.2	K0 III		2	.230	.248	.320	
2047	X^1 Ori	5 48.5	20 16	4.6	G0 V	M	2	.595	.062	.178	
2077	δ Aur	5 51.3	54 17	3.9	K0 III	JM	9	.286	.190	.275	
2152	37 Cam	6 1.2	58 57	5.4	G8 III		2	.300	.185	.274	
2219	κ Aur	6 9.0	29 32	4.4	G8 III		3	.300	.154	.260	
2289	ψ^1 Aur	6 17.2	49 20	5.1	M0 Iab	M	1	.192	.349	.474	
2427	ψ^2 Aur	6 32.2	42 35	5.1	K3 II-III	M	2	.178	.266	.345	
2459	ψ^4 Aur	6 35.8	44 37	5.2	K5 III	M	2	.104	.292	.472	
2473	ϵ Gem	6 37.8	25 14	3.2	G8 Ib	M	3	.174	.350	.379	
2477	13 Lyn	6 38.3	57 16	5.5	K0 III-IV	M	2	.332	.148	.260	
2478	30 Gem	6 38.4	13 20	4.6	K1 III		2	.202	.239	.336	
2487	ψ^6 Aur	6 40.0	48 54	5.3	K1 III		2	.236	.246	.308	
2506	18 Mon	6 42.6	2 31	4.7	K0 III		2	.235	.220	.344	
2516	ψ^7 Aur	6 43.7	41 54	5.0	K3 III	M	2	.174	.279	.349	
2527		6 45.5	77 06	4.7	K4 III		2	.128	.321	.432	
2649		6 58.1	11 06	5.2	K3 III		2	.103	.302	.426	
2697	τ Gem	7 4.8	30 25	4.5	K2 III		2	.172	.272	.380	
2715	18 Lyn	7 7.2	59 49	5.3	K2 III		2	.249	.215	.316	
2793	65 Aur	7 15.4	36 57	5.2	G8 III		2	.284	.181	.302	
2805	66 Aur	7 17.2	40 52	5.3	K0 III	M	2	.216	.235	.341	
2808	57 Gem	7 17.4	25 15	5.1	G8 III		2	.390	.125	.248	
2821	ι Gem	7 19.5	28 00	3.9	K0 III	M	3	.293	.181	.274	
2864	6 CMi	7 24.2	12 13	4.8	K2 III		2	.165	.276	.382	
2990	β Gem	7 39.2	28 16	1.2	K0 III	JM	5	.292	.198	.279	
3149	X Gem	7 57.4	28 04	5.0	K2 III		2	.235	.246	.334	
3176	μ Cnc	8 1.9	21 52	5.4	G2 IV		2	.519	.062	.176	
3249	β Cnc	8 11.1	9 30	3.8	K4 III	JM	4	.086	.285	.445	
3275	31 Lyn	8 16.0	43 31	4.4	K5 III		2	.078	.296	.472	
3403	π^2 UMa	8 31.5	64 41	4.8	K2 III	M	2	.207	.210	.330	
3418	σ Hya	8 33.5	3 42	4.5	K2 III		2	.195	.284	.355	
3461	δ Cnc	8 39.0	18 31	4.2	K0 III		2	.248	.220	.320	
3508	35 Lyn	8 45.3	44 06	5.2	K0 III		2	.332	.145	.245	
3547	ζ Hya	8 50.1	6 20	3.3	K0 II-III	M	5	.313	.196	.280	
3612		9 0.2	38 51	4.7	G8 Ib-II		2	.318	.209	.274	
3627	ξ Cnc	9 3.6	22 27	5.2	K0 III		2	.314	.215	.280	
3731	κ Leo	9 18.8	26 37	4.6	K2 III		2	.188	.249	.357	
3751		9 22.9	81 46	4.6	K3 III		2	.145	.341	.436	
3771	24 UMa	9 25.6	70 16	4.6	G2 IV	M	2	.476	.100	.209	
3773	λ Leo	9 26.0	23 25	4.5	K5 III		2	.110	.299	.498	
3800	10 LMi	9 28.1	36 51	4.6	G8 III		3	.375	.160	.243	
3815	11 LMi	9 29.7	36 16	5.5	G8 IV-V	JM	2	.416	.090	.225	
3839	27 UMa	9 33.8	72 42	5.4	K0 III		2	.272	.234	.284	
3851	43 Lyn	9 35.8	40 13	5.5	G8 III		2	.344	.184	.263	
3873	ϵ Leo	9 40.2	24 14	3.1	G0 II	M	3	.459	.127	.202	
3905	μ Leo	9 47.1	26 29	4.1	K2 III		2	.152	.318	.380	
4126		10 26.6	76 14	5.0	K0 III		2	.319	.189	.266	
4178	38 UMa	10 35.1	66 14	5.1	K2 III		2	.186	.285	.352	
4181		10 35.9	69 36	5.2	K3 III		3	.132	.268	.398	
4246	44 UMa	10 47.5	55 07	5.4	K3 III		2	.142	.280	.385	
4247	46 LMi	10 47.7	34 45	3.9	K0 III-IV	JM	2	.258	.184	.286	
4258	46 UMa	10 50.2	34 02	5.2	K1 III		2	.241	.205	.301	
4291	58 Leo	10 55.4	4 09	5.0	K1 III		3	.222	.211	.342	

Table 1 (continued)

HR		(1900)		m	Sp		N	k	n	g	
4301	α UMa	$10^h57\overset{m}{.}6$	+62°17'	2.0	K0 III	JM	13	0$\overset{m}{.}$334	0$\overset{m}{.}$226	0$\overset{m}{.}$273	
4335	ψ UMa	11 4.0	45 02	3.1	K1 III	JM	2	.238	.240	.311	
4365	73 Leo	11 10.6	13 51	5.5	K3 III		2	.326	.225	.318	
4377	ν UMa	11 13.1	33 38	3.7	K3 III	JM	2	.164	.279	.408	
4461	2 Dra	11 30.2	69 53	5.4	K0 III		3	.322	.164	.264	
4495	92 Leo	11 35.6	21 54	5.4	K0 III		2	.321	.172	.260	
4496	61 UMa	11 35.8	34 46	5.5	G8 V	JM	2	.482	.064	.208	
4504	3 Dra	11 36.9	67 18	5.5	K3 III		3	.172	.267	.353	
4518	χ UMa	11 40.8	48 20	3.8	K0 III		2	.210	.209	.319	
4521		11 41.6	56 11	5.4	K3 III		2	.164	.315	.376	
4608	o Vir	12 0.1	9 17	4.2	G8 III		3	.385	.132	.251	
4667	7 Com	12 11.3	24 30	5.1	K0 III		2	.334	.149	.272	
4668		12 11.5	33 37	5.1	K1 III		2	.219	.202	.319	
4695	16 Vir	12 15.3	3 52	5.1	K0 III		3	.207	.189	.327	hv
4697	11 Com	12 15.7	18 21	4.9	G8 III		3	.325	.142	.275	
4716	5 CVn	12 19.2	52 07	5.0	G7 III		2	.370	.151	.226	
4728	6 CVn	12 20.9	39 34	5.2	G8 III-IV		2	.335	.182	.254	
4737	15 Com	12 21.9	28 49	4.6	K1 III-IV		2	.208	.279	.336	
4783		12 28.7	33 48	5.4	K0 III		2	.299	.181	.280	
4785	8 CVn	12 29.0	41 54	4.3	G0 V	JM	1	.602	.052	.160	
4883	31 Com	12 46.8	28 05	5.1	G0 III	M	1	.592	.078	.168	
4928	9 Dra	12 56.1	67 08	5.5	G8 III		2	.205	.210	.330	
4932	ϵ Vir	12 57.2	11 30	2.9	G9 II-III	M	3	.350	.186	.264	
4954	41 Com	13 2.4	28 10	4.9	K5 III		3	.110	.302	.459	
4983	β Com	13 7.2	28 23	4.3	G0 V	JM	1	.595	.065	.158	
4997		13 9.2	40 41	5.0	K0 III		3	.278	.243	.292	
5072	70 Vir	13 23.5	14 19	5.2	G5 IV-V		1	.508	.068	.190	
5200	υ Boo	13 44.6	16 18	4.3	K5 III		2	.109	.300	.472	
5201	6 Boo	13 45.0	21 46	5.1	K4 III		2	.118	.286	.426	
5247	9 Boo	13 52.0	27 59	5.2	K3 III		4	.099	.283	.428	
5330	15 Boo	14 9.9	10 34	5.4	K0 III		2	.319	.181	.292	
5340	α Boo	14 11.1	19 42	0.2	K2 III p	JM	12	.174	.207	.339	hv
5370	20 Boo	14 15.0	16 46	5.0	K3 III		2	.171	.285	.366	
5429	ρ Boo	14 27.5	30 49	3.8	K3 III	JM	2	.125	.258	.381	
5430	5 UMi	14 27.7	76 08	4.4	K4 III		2	.112	.284	.432	
5480	31 Boo	14 36.7	8 35	5.0	G8 III		2	.348	.214	.271	
5502	o Boo	14 40.6	17 23	4.7	K0 III		2	.329	.174	.265	
5541		14 46.5	37 41	5.5	K0 III-IV		4	.301	.154	.288	
5563	β UMi	14 51.0	74 34	2.2	K4 III	MHJ	2	.100	.288	.444	
5600	ω Boo	14 57.7	25 24	4.9	K4 III		3	.108	.298	.458	
5601	110 Vir	14 57.9	2 29	4.6	K0 III		2	.282	.175	.288	
5602	β Boo	14 58.2	40 47	3.6	G8 III	MHJ	6	.336	.177	.256	
5616	ψ Boo	15 0.2	27 20	4.7	K2 III		3	.173	.240	.357	
5635		15 3.4	54 56	5.2	G8 III		3	.347	.144	.249	
5681	δ Boo	15 11.5	33 41	3.5	G8 III	JM	2	.351	.124	.244	
5714	11 UMi	15 17.2	72 11	5.1	K4 III		2		.308	.400	
5744	ι Dra	15 22.7	59 19	3.5	K2 III	JM	3	.195	.258	.342	
5823	ϕ Boo	15 34.2	40 41	5.4	G8 IV		2	.404	.110	.235	
5854	α Ser	15 39.3	6 44	2.8	K2 III	JM	10	.207	.286	.358	
5901	κ CrB	15 47.5	35 58	4.8	K0 III-IV		2	.285	.181	.305	
5947	ϵ CrB	15 53.4	27 10	4.2	K3 III	JM	2	.162	.231	.348	
5966	5 Her	15 56.8	18 06	5.3	K0 III		2	.326	.144	.282	
6018	τ CrB	16 5.3	36 45	4.9	K0 III	MHJ	2	.300	.181	.290	
6103	ξ CrB	16 18.2	31 07	4.7	K0 III		2	.301	.202	.288	
6126		16 22.0	69 20	5.4	K2 III		2	.229	.265	.315	
6132	η Dra	16 22.6	61 44	2.9	G8 III	MHJ	5	.348	.170	.246	
6199		16 36.0	56 13	5.4	K1 III		2	.308	.209	.279	
6220	η Her	16 39.5	39 07	3.6	G7 III-IV	M	2	.365	.140	.236	
6299	κ Oph	16 52.9	9 32	3.4	K2 III	MHJ	2	.205	.250	.338	
6603	β Oph	17 38.5	4 37	2.9	K2 III	JM	2	.201	.278	.351	

Table 1 (continued)

HR		(1900)		m	Sp		N	k	n	g	
6688	ξ Dra	17^h51^m8	$+56°53'$	3.9	K2 III	MHJ	2	0.178	0.239	0.354	
6703	ξ Her	17 53.9	29 16	3.8	G9 III	M	2	.365	.166	.265	
6705	γ Dra	17 54.3	51 30	2.4	K5 III	JM	3	.112	.301	.469	
6872	κ Lyr	18 16.3	36 01	4.3	K2 III		1	.200	.265	.346	
6895	109 Her	18 19.4	21 43	3.9	K2 III		2	.204	.228	.335	
6945	42 Dra	18 25.7	65 30	5.0	K2 III		2	.224	.218	.321	
7180	υ Dra	18 55.6	71 10	4.9	K0 III		2	.226	.246	.337	
7295	53 Dra	19 9.8	56 41	5.2	G8 III		2	.319	.222	.274	
7309	54 Dra	19 12.1	57 32	5.3	K2 III		3	.227	.243	.339	
7310	δ Dra	19 12.5	67 29	3.2	G9 III	MHJ	2	.301	.174	.275	
7328	κ Cyg	19 14.8	53 11	4.0	K0 III	MHJ	2	.318	.192	.266	
7352	τ Dra	19 17.5	73 10	4.6	K3 III		2	.174	.314	.395	
7462	σ Dra	19 32.5	69 29	4.8	K0 V	MHJ	3	.424	.067	.242	
7468		19 33.5	44 28	5.2	K0 III		3	.325	.167	.285	
7615	η Cyg	19 52.5	34 49	4.0	K0 III		3	.270	.193	.302	
7685	ρ Dra	20 2.4	67 35	4.7	K3 III		2	.148	.299	.394	
7796	γ Cyg	20 18.6	39 56	2.3	F8 Ib	JM	3	.533	.128	.178	
7806	39 Cyg	20 19.9	31 52	4.6	K3 III		2	.122	.280	.419	
7949	ϵ Cyg	20 42.2	33 36	2.6	K0 III	JM	3	.271	.167	.282	
7955		20 42.9	57 13	4.6	F8 V	M	1	.595	.078	.148	
7957	η Cep	20 43.2	61 27	3.6	K0 IV	M	9	.348	.123	.255	hv
8085	61 Cyg A	21 2.4	38 15	5.6	K5 V	JM	2	.248	.162	.427	hv
8173	1 Peg	21 17.5	19 23	4.2	K1 III	JM	2	.234	.215	.316	
8228	71 Cyg	21 25.8	46 06	5.3	K0 III		2	.310	.183	.272	
8232	β Aqr	21 26.3	- 6 01	3.1	G0 Ib	JM	2	.448	.145	.199	
8252	ρ Cyg	21 30.2	45 09	4.2	G8 III		3	.398	.142	.246	
8255	72 Cyg	21 30.7	38 05	5.0	K0 III	M	1	.260	.234	.304	
8308	ϵ Peg	21 39.3	9 25	2.5	K2 Ib	JM	2	.167	.346	.421	
8313	9 Peg	21 39.8	16 53	4.5	G5 Ib	JM	2	.282	.251	.292	
8317	11 Cep	21 40.4	70 51	4.8	K0 III		2	.224	.262	.331	
8324		21 41.8	71 52	5.4	K1 III		3	.262	.235	.310	
8414	α Aqr	22 0.6	- 0 48	3.2	G2 Ib	JM	2	.380	.168	.244	
8465	ζ Cep	22 7.4	57 42	3.6	K1 Ib	M	5	.176	.356	.418	
8468	24 Cep	22 7.9	71 51	5.0	G8 III		3	.376	.172	.242	
8475		22 8.4	34 07	5.4	K2 III		2	.222	.248	.328	
8485		22 9.6	39 13	4.6	K3 III		3	.238	.293	.380	
8538	3 Lac	22 19.6	51 44	4.6	G9 III		2	.306	.159	.275	
8551	35 Peg	22 22.8	4 12	4.9	K0 III-IV	M	2	.281	.158	.291	
8632	11 Lac	22 36.1	43 45	4.6	K3 III	M	4	.162	.250	.376	
8656	13 Lac	22 39.6	41 18	5.2	K0 III		2	.314	.212	.271	
8684	μ Peg	22 45.2	24 04	3.7	G8 III	MHJ	3	.338	.148	.268	
8694	32 Cep	22 46.1	65 40	3.7	K1 III		2	.265	.202	.301	
8702		22 47.9	82 37	5.0	K3 III	MHJ	2	.128	.319	.442	
8752		22 55.9	56 24	5.5	G0 Ia	JM	2	.418	.162	.210	
8779		22 59.7	66 40	5.5	K3 III		2	.180	.318	.371	
8780	3 And	22 59.7	49 30	4.9	K0 III		2	.278	.178	.288	
8832		23 8.5	56 37	5.6	K3 V	JM	1	.275	.150	.345	
8852	γ Psc	23 12.0	2 44	3.8	G7 III	M	2	.382	.119	.222	hv
8874	11 And	23 14.8	48 05	5.4	K0 III		3	.314	.171	.275	
8905	υ Peg	23 20.4	22 51	4.6	F8 IV	JM	1	.592	.082	.164	
8923	70 Peg	23 24.1	12 13	4.7	G8 III		3	.345	.171	.258	
8930	14 And	23 26.4	38 41	5.3	K0 III	M	2	.288	.169	.274	hv
8974	γ Cep	23 35.2	77 04	3.4	K1 IV	JM	3	.250	.197	.317	
9008	τ Cas	23 42.2	58 06	5.1	K1 III		3	.229	.211	.311	

SPECTRAL CLASSIFICATION OF G AND K STARS THROUGH PHOTOELECTRIC PHOTOMETRY WITH INTERFERENCE FILTERS

BENGT STRÖMGREN AND K. GYLDENKERNE
Yerkes Observatory and Copenhagen Observatory
Received July 3, 1954

ABSTRACT

A method of two-dimensional spectral classification of G and K stars, based on photoelectric photometry with interference filters, is described. Indices measuring the strength of the K line, the discontinuity at the G band, and the cyanogen band strength are utilized. A comparison is made with spectral classification on the Yerkes MK system and with color indices. An accuracy corresponding to a probable error (one determination) of about 0.02 of a spectral class is achieved.

I. INTRODUCTION

The results obtained through the methods of spectral classification from low-dispersion objective-prism spectra, developed by B. Lindblad about thirty years ago, indicated that it should be possible to achieve accurate spectral classification through photoelectric photometry of spectral regions containing strong absorption-line features, isolated through the use of interference filters.

Preliminary tests with the photoelectric method made at McDonald Observatory (B. Strömgren 1950) were encouraging, and it was decided to test the possibilities of the method in an empirical way. A filter-wheel containing 25 interference filters (made by Bausch and Lomb) with transmission peaks in the spectral range 3800–5500 A and an ultraviolet filter transmitting a region around 3550 A was constructed and first tested at the Copenhagen Observatory. The filter-wheel photometer was then mounted on the 32-inch reflector of the Observatoire de Haute-Provence. Measures were obtained here by one of the authors (K. Gyldenkerne) for 110 standard stars of all spectral classes and luminosity classes. Classifications by W. W. Morgan were available for these standard stars.

An analysis of the material showed that several of the intensity ratios measured were useful in spectral classification (for a summary of the results cf. B. Strömgren 1951).

A method for two-dimensional classification of B, A, and F stars through photoelectric photometry with interference filters has been developed by one of the authors at the McDonald Observatory (B. Strömgren 1952, 1955). The present paper summarizes the results obtained for G and K stars through observations made by K. Gyldenkerne with a photoelectric photometer equipped with interference filters and attached to the 10-inch reflector at the Sophienholm station of the Copenhagen Observatory, located about forty miles west of Copenhagen.

II. THE FILTERS AND THE PHOTOMETER

The observations with the filter-wheel photometer at the Observatoire de Haute-Provence referred to earlier indicated that three intensity ratios were particularly useful for two-dimensional classification of G and K stars, namely, 4360/4240, which measures the discontinuity at the G band; 3910/4030, measuring the strength of the K line; and 4240/4170, indicating the strength of cyanogen absorption. These ratios correspond closely to ratios used by Lindblad and his collaborators at the Stockholm Observatory in their photographic-spectraphotometric classification work (cf., in particular, B. Lindblad and E. Stenquist 1934).

The three intensity ratios were measured for a number of G and K stars with the Copenhagen Observatory 10-inch reflector. The spectral regions in question were isolated through the use of five Bausch and Lomb interference filters with half-widths about 100 A and maximum transmissions around 40 per cent.

An EMI photomultiplier (type 5060, photocathode diameter $\frac{3}{8}$ inch) with a multiplication factor of approximately 10^8 was used throughout this work. The photoelectric current was measured with a galvanometer (sensitivity 1.1×10^{-9} amp/mm at 1 meter, period 7 seconds), the deflections being recorded photographically. The deviations from linearity of the galvanometer were determined and found to be small. Corresponding corrections were applied to all the measures. The dark current was usually around 10^{-9} amp and remained satisfactorily constant. One set of observations of a star consisted of 15–21 deflections for the five filters. The total photometric observing time for one star was 12–25 minutes.

The reduction of the intensity through the various filters is shown in the accompanying table for three different types of stars. The reduction (filter compared to no filter) is expressed in magnitudes.

	3910 A	4030 A	4170 A	4240 A	4360 A
G5 III.....	4^m5	4^m3	4^m0	4^m2	4^m0
K0 III.....	4.9	4.5	4.2	4.3	4.0
K5 III.....	5.9	5.3	4.9	4.8	4.4

In comparison with photometry with standard blue and yellow filters, the reduction through the use of the interference filters corresponds to a loss of 3–4 mag. For the three filters 4170, 4240, and 4360 the loss is, on the average, 3 mag.

With the equipment used, measures of the desired precision could be conveniently made for stars brighter than 5.5 visual magnitude.

III. THE CLASSIFICATION INDICES

From the photoelectric intensity measures with the interference filters the three classification indices, defined as follows, were derived:

$$k = 2.5\,[\log I\,(3910) - \log I\,(4030)] + \text{const.}, \text{ K-line index};$$

$$g = 2.5\,[\log I\,(4360) - \log I\,(4240)] + \text{const.}, \text{ G-discontinuity index};$$

$$n = 2.5\,[\log I\,(4240) - \log I\,(4170)] + \text{const.}, \text{ cyanogen index}.$$

Extinction coefficients were determined on a number of nights. Corresponding to the relative smallness of the differences in the two wave lengths of any one of the indices, the extinction coefficients are small. In view of this and of the fact that, for about 80 per cent of the photoelectric measures, sec z was in the range from 1 to 1.25, it was considered sufficiently accurate to use mean extinction coefficients for the reduction to the zenith. The adopted mean extinction reductions to the zenith are, for k, $+0^m062$ (sec $z - 1$); for g, -0^m020 (sec $z - 1$); and for n, -0^m018 (sec $z - 1$).

Small differences in the indices obtained on different nights may be expected for two reasons: differences in the condition of the interference filters may cause variations from night to night, as will differences in the zenith extinction for the index in question. Repeated observations of a number of standard stars were made, to check the effect. These observations showed that it was not necessary to use separate corrections for each night. For periods of, on the average, several weeks, a constant correction could be adopted for

the reduction of an index observation to the mean system. The average correction, without regard to sign, was about 0.01 mag.

After the application of the period corrections mentioned, the internal agreement of the observations of standard stars on different nights was satisfactory, corresponding to a probable error of ± 0.004 mag. for one observation of a classification index. From repeated measures of ordinary program stars, a probable error of ± 0.006 mag. for one observation was derived. The program stars were, on the average, fainter than the standard stars, which explains the somewhat lower accuracy obtained for the former.

The three classification indices have been measured for 234 G and K stars, mostly brighter than 5.5 visual magnitude. Nearly all stars were observed on two different nights, a considerable fraction on three or more nights. A star list giving the observed values of the classification indices is published separately (K. Gyldenkerne 1955).

IV. COMPARISON WITH THE YERKES MK SYSTEM

For 80 of the program stars spectral classes and luminosity classes on the Yerkes MK system determined by W. W. Morgan were available. Similar classification data by Nancy G. Roman (1953) were available for all the remaining program stars.

TABLE 1

SPECTRAL INDICES AS FUNCTIONS OF SPECTRAL CLASS FOR STARS OF LUMINOSITY CLASS III

	No. of Stars	k	g	n
G8 III	29	$0^m.348$	$0^m.255$	$0^m.168$
K0 III	48	.295	.285	.194
K1 III	13	.240	.315	.217
K2 III	26	.202	.343	.253
K3 III	23	.149	.390	.282
K4 III	9	.112	.435	.297
K5 III	6	0.109	0.472	0.294

TABLE 2

PROBABLE ERROR OF SPECTRAL CLASSES DETERMINED FROM k OR g

G8 III–K1 III	$k \pm 0.017$ of a spectral class
K2 III–K3 III	$k \pm .011$
	$g \pm .013$
K4 III–K5 III	$g \pm 0.016$

The majority of the stars are of luminosity class III, with spectral classes in the range from G8 to K5. For stars of luminosity class III, mean values of the spectral indices were formed for each subgroup of spectral class represented. High-velocity stars and peculiar stars were excluded here. The results are shown in Table 1.

It is apparent that both k and g are suitable as spectral-class indices. The index k gives the best accuracy for G and early K stars, while g is the best for the range K3–K5. The index g can, however, be used over a range extending at least from K1 to K5.

From the data given in Table 1 the photometric probable error of a spectral class demined from k or g can be evaluated. The results are shown in Table 2. The probable error of one determination of a classification index was taken as ± 0.006 mag. For stars earlier

than G8 III, k should still be a good criterion. However, as is well known (cf. Roman 1952), only relatively few stars have classes from G0 III to G8 III.

A comparison of the spectral classes yielded by the k and g indices, respectively, was made for 107 stars of luminosity class III in the range G8 and K3 ($k > 0^m190$). High-velocity stars and peculiar stars were again excluded. Over this range a linear relation between k and g was assumed. The following relation resulted,

$$g = 0^m451 - 0.562k\,. \tag{1}$$

The residuals, observed g minus g computed from k according to equation (1), were analyzed and were found to correspond to a probable error of ± 0.007 mag. The contribution of the photometric errors of k and g to this quantity can be derived from the known photometric probable errors of one determination of k and g and the average number of observations per star, using equation (1). The result is ± 0.005 mag. Since this is significantly smaller than the probable error derived earlier, it can be concluded that there is a small scatter in the relation between k and g, in addition to that produced by the photometric uncertainties. Cosmical scatter caused by variations in chemical composition from star to star is probably a contributing factor.

It should be noted in this connection that about one-third of the variation of the indices k and g with spectral class is a color-index effect. Since the correlation of the color-index effects on k and g, respectively, is presumably quite high and hardly affected by cosmical scatter, the effect of cosmical scatter on the relation between k and g will appear somewhat reduced thereby.

Although the determination of the cosmical scatter through the comparison is rather uncertain, it is safe to conclude that the effect is small and that the corresponding scatter in the spectral classes derived from k or g is measured by a probable error of not much more than ± 0.01 of a spectral class. We shall return to the problem of cosmical scatter in connection with the discussion of correlation between the classification index k and color index.

We shall consider, next, the relation between the indices g and u, on one side, and spectral class and luminosity class, on the other, with a view to the feasibility of two-dimensional classification from g and u.

In Figure 1 the program stars are represented in a diagram with g as abscissae and u as ordinates. The spectral class and luminosity class on the Yerkes MK system are indicated for each star at the representing point. The figure shows that, for G and K stars, two-dimensional classification with the classification indices g and u is possible. The general agreement with the luminosity classes and spectral classes is satisfactory.

The luminosity classification depends primarily on the cyanogen index u. The range of variation of u from stars of luminosity class Ib to luminosity class V corresponds to a variation of u with absolute magnitude M_v of roughly 0.02 mag. per magnitude. The photometric probable error of one observation of u equal to ± 0.006 mag. then corresponds to a probable error of M_v of the order of $\frac{1}{3}$ mag.

With the help of Figure 2, the classification index u can be analyzed in terms of spectral class and luminosity class. For each spectral class from G0 to K5, the luminosity class and u are well correlated. From G8 to K5, mean points for class III are shown, not points for individual stars. A mean curve representing these points is drawn. In this connection reference is made to the spectrophotographic work on the cyanogen criterion by B. Lindblad and E. Stenquist (1934) and T. Setterberg (1947). Figure 2 shows that high-velocity stars (indicated by crosses) have, on the average, lower u for their luminosity than the remainder of the stars. The spread of stars of luminosity class III around the mean curve is, however, too large for the individual high-velocity stars to stand out unambiguously. This was to be expected from earlier spectrophotographic investigations of the cyanogen criterion (cf. Keenan and Keller 1953). The material represented in

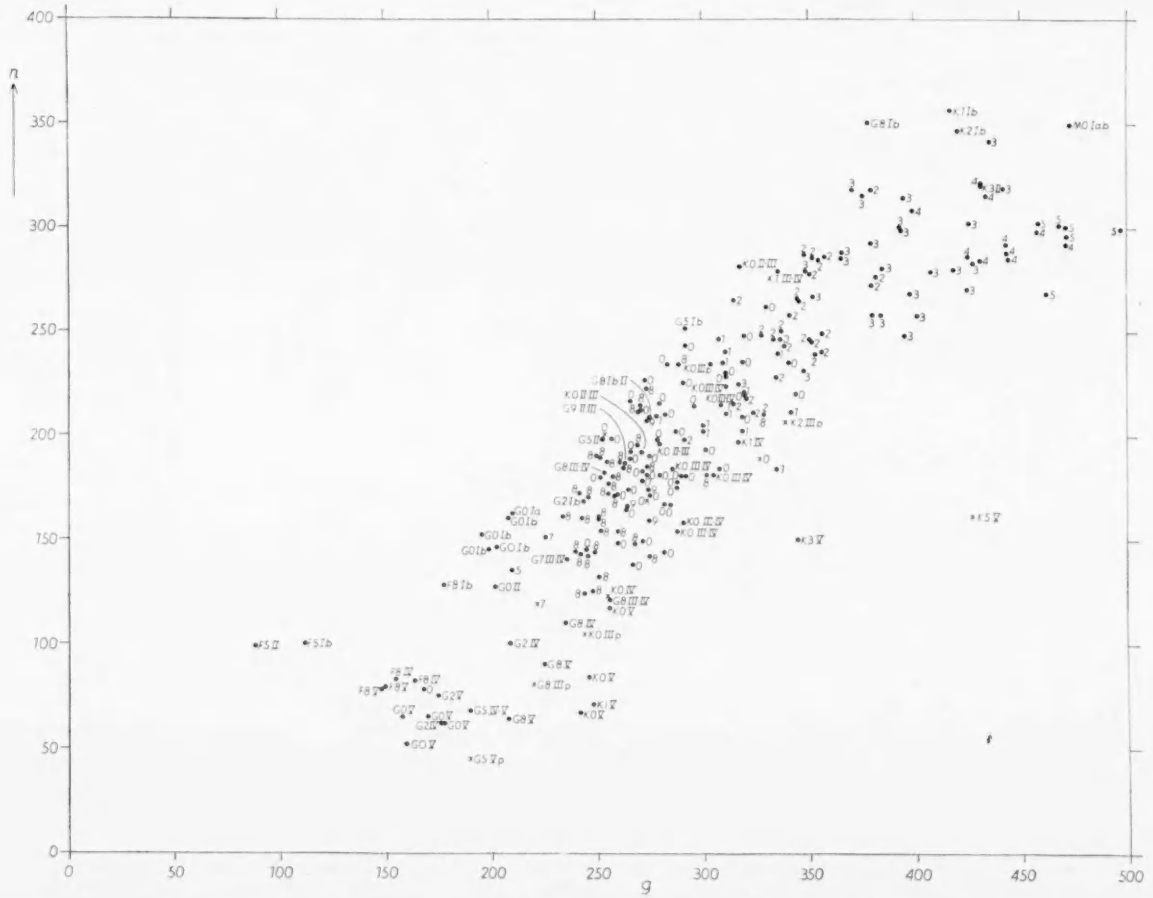

FIG. 1.—Representation of the program stars with g (G-discontinuity index) as abscissa and n (cyanogen index) as ordinate. The spectral class and luminosity class on the MK system are indicated. For stars of luminosity class III, only a figure indicating the spectral subclass (8 for G8 III, 3 for K3 III, etc.) is given. High-velocity stars are denoted by crosses. The following revised spectral types became available after this figure was prepared (cf. the star list in K. Gyldenkerne, *Ap. J.*, **121**, 38, 1955): HR 434, K4 III instead of K3 III, 824 K1 III for K0 III, 1407 K2 III for K1 III, 1907 G8 IIIp for K0 IIIp, 2427 K3 II–III for K2 III, 2459 K5 III for K4 III, 2477 K0 III–IV for K0 III, 8255 K0 III for K0 IIIp.

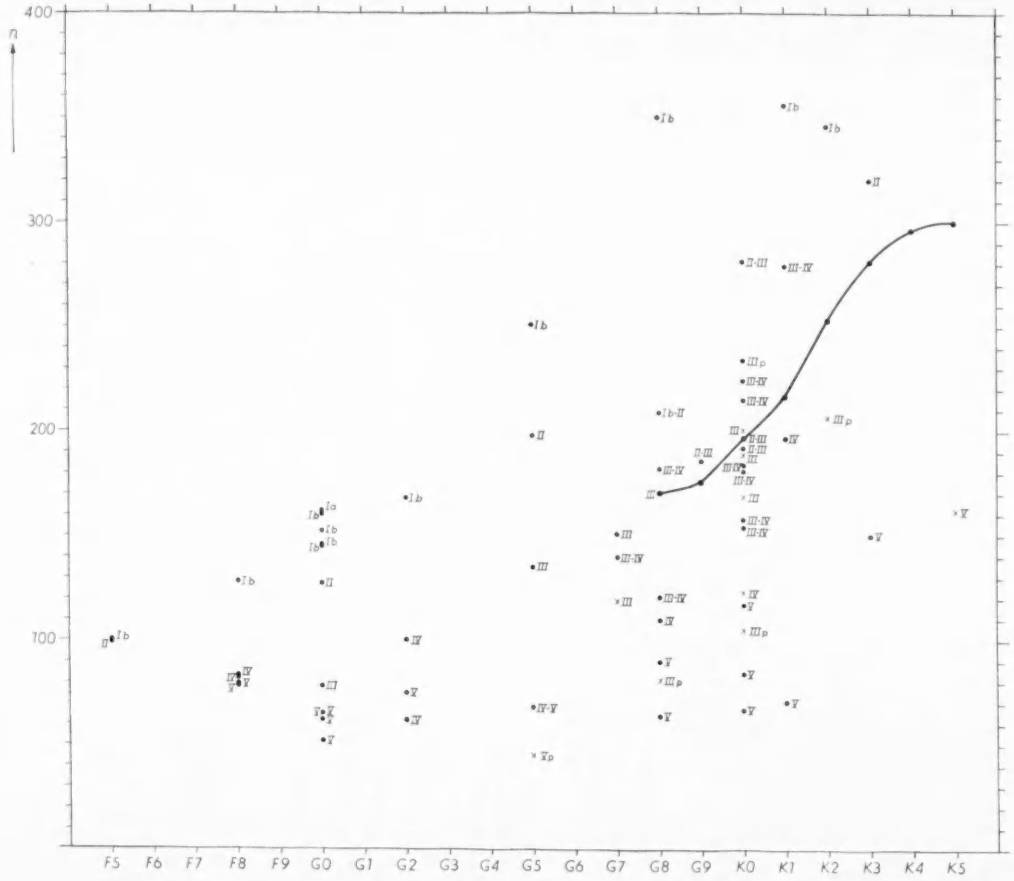

FIG. 2.—The abscissa is the MK spectral class; the ordinate the cyanogen index n. The luminosity class is given for individual stars except for luminosity class III in the range G8–K5, where representative points corresponding to mean values of n for each subclass are plotted.

Figure 1 is sufficient for a calibration of the g–n classification in terms of spectral classes and luminosity classes on the Yerkes MK system. A direct calibration in terms of color index and absolute magnitude, on the basis of trigonometric parallaxes, proper motions, and radial velocities, should preferably be based on a larger material and will not be attempted here.

It is to be expected that the absolute visual magnitude M_v can be expressed linearly in terms of g and n, or k and n, for a certain range of spectral class and absolute magnitude. For instance, the data in Table 1 indicate that $n + 0.5k$ is nearly independent of spectral class for G8–K5 giants and thus should be a good index of luminosity class and also of absolute visual magnitude, since the latter quantity does not change much with spectral class for the stars in question. The problem of calibration should be simplified thereby.

With regard to the effect of cosmical scatter on the determination of absolute magnitudes from g and n, it is intended to investigate this on the basis of larger material. In particular, the effect of a third parameter, which may be called the "population" parameter and which is to a certain extent correlated with space velocity, could be analyzed if a planned attempt to measure photoelectrically a third classification index (4077 *Sr* II index), very closely connected with the MK luminosity class, is successful.

V. COMPARISON WITH PHOTOELECTRIC COLOR INDICES

One of the principal aims of the present investigation has been the development of a method for accurate prediction of intrinsic color indices of G and K giants, with a view to the determination of color excesses for stars of this spectral group.

For stars of luminosity class III and in the spectral group G7 to K1 the classification index k proved very suitable for prediction of intrinsic color index. For 30 stars within this range, photoelectric color indices on Harold Johnson's $B - V$ system were available, according to measures by Daniel L. Harris and Harold Johnson with the 13-inch reflector of the McDonald Observatory. The color indices $B - V$ proved to be linearly related to the index k, and the following linear relation was derived:

$$B - V = 1^{m}420 - 1.385k\,, \qquad (2)$$

valid for G7 III–K1 III stars. The corresponding range of k is 0.24–0.39 mag.; of $B - V$, 0.9–1.2 mag. Two peculiar stars were omitted.

The residuals, observed $B - V$ minus $B - V$ computed from k according to equation (2), corresponded to a probable error equal to ± 0.016 mag. We shall attempt to make a breakdown of this scatter into its various components.

1. The probable error of an observed k value (determination on 2 nights) is ± 0.004 mag. The corresponding photometric probable error of a $B - V$ predicted according to equation (2) is ± 0.006 mag.

2. The probable error of the observed $(B - V)$ values is estimated by Harris to be ± 0.007 mag.

3. The cosmical scatter is not known, but an estimate can be made according to the results obtained in Section IV concerning the mutual agreement of spectral classes determined from k and g, respectively. This leads to a probable error between ± 0.01 and ± 0.015. We shall assume that the probable error due to cosmical scatter is ± 0.012 of a spectral class. Since the rate of change of the color index $B - V$ with spectral class is approximately 0.6 mag. per spectral class for the stars considered, this contributes a probable error equal to ± 0.007 mag.

4. The stars in question are at an average distance of about 50 parsecs. Although interstellar reddening is certainly small for these stars, its effect on the color indices $B - V$ is not entirely negligible. A rough estimate of the scatter due to this cause leads to a probable error of ± 0.006 mag.

The probable error resulting from the four components considered is ± 0.013 mag.,

thus in fair agreement with the actual value found. Although this analysis of the various contributions to the observed scatter is necessarily somewhat uncertain, it can be safely concluded that it is possible to predict intrinsic $B - V$ color indices from the k index, for the spectral group of stars considered, with a probable error of between ± 0.010 and ± 0.016 mag. (one determination). Since the variation of color index $B - V$ with spectral class is large, 0.6 mag. per class, for the stars considered, this compares favorably with the accuracy of color indices predicted from spectral classes determined with the help of the standard spectrophotographic methods. When more extensive observational material is available, it is intended to investigate the possibilities of prediction of $B - V$ from the g index.

VI. THE EFFECT OF INTERSTELLAR REDDENING UPON THE CLASSIFICATION INDICES

The effect of interstellar reddening upon the classification indices k, g, and n is small but not entirely negligible. As an example, let us consider the index k and the effect of interstellar reddening upon the $(B - V)$ values predicted from k. Assuming the standard wave-length dependence of interstellar absorption (van de Hulst 1949), it is found that visual absorption of 1 mag. gives a change of about 0.04 mag. in k. According to equation (2), the corresponding error in the predicted $B - V$ is 0.06 mag., while the actual reddening, $B - V$, for a visual absorption of 1 mag. is close to 0.33 mag. (cf. Morgan, Harris, and Johnson 1953). The error in the color excess as determined from k is thus somewhat less than 20 per cent of its value.

We conclude that when color excesses are determined, it is easy to correct with fair accuracy for the effect of interstellar reddening upon the observed classification indices. The possibility of interstellar absorption with a wave-length dependence differing significantly from the standard one must, however, be kept in mind.

In similar work on B, A, and F stars an $H\beta$ index is used that is completely independent of interstellar reddening (B. Strömgren 1955). If desirable, the same advantage could be achieved for the G and K stars through the use of one or two additional interference filters or if an index corresponding to the ratio 4360/4030 were utilized to correct for the considered effect of interstellar absorption. The photometric accuracy, for the same observing time, might prove to be somewhat reduced thereby, but presumably not very much, as atmospheric extinction effects would also be reduced.

The authors are very much indebted to Dr. W. W. Morgan for making available to us spectral classes and luminosity classes for a number of the program stars. We are grateful to Dr. Daniel L. Harris, who, in his program of photoelectric photometry of bright stars, very kindly gave preference to a number of our program stars and communicated photoelectric color indices in advance of publication. We wish to express our thanks to the Board of the Observatoire de Haute-Provence for the opportunity given one of us (K. Gyldenkerne) to use the 32-inch reflector at an early stage of the investigation of the photoelectric interference filter method of spectral classification.

REFERENCES

Gyldenkerne, K. 1955, *Ap. J.*, **121**, 38.
Keenan, P. C., and Keller, G. 1953, *Ap. J.*, **117**, 241.
Lindblad, B., and Stenquist, E. 1934, *Stockholm Astr. Iakttagelser och Undersökningar*, Vol. **11**, No. 12.
Morgan, W. W., Harris, D. L., and Johnson, H. L. 1953. *Ap. J.*, **118**, 92.
Roman, N. G. 1952, *Ap. J.*, **116**, 122.
Setterberg, T. 1947, *Stockholm Astr. Iakttagelser och Undersökningar*, Vol. **15**, No. 1.
Strömgren, B. 1950, *Trans. I.A.U.*, **7**, 404.
———. 1951, *A.J.*, **56**, 142.
———. 1952, *ibid.*, **57**, 200.
———. 1955. *Vistas of Astronomy*.
Van de Hulst, H. C. 1949, *Rech. Astr. Obs. Utrecht*, Vol. 11, Part 2.

THE COLORS OF THE BETA CANIS MAJORIS STARS*

D. H. McNAMARA AND A. D. WILLIAMS
Berkeley Astronomical Department, University of California
Received July 3, 1954

ABSTRACT

The colors of nine β Canis Majoris stars have been measured. A correlation between the periods and the colors of the stars is clearly indicated for stars with periods <5 hours. For stars with periods in the interval 5–6 hours the color appears to be constant.

I. INTRODUCTION

The β Canis Majoris or β Cephei variable stars form a very compact group with respect to spectral type. The ten stars that are known to belong to this class of variables have been assigned either to spectral type B1 or B2. In spite of the small range in spectral type, McNamara (1953*a*) has presented evidence that indicates the existence of a period-spectrum relationship for this group of stars. The present investigation was undertaken for the purpose of supplementing our knowledge of this relationship with accurate photometric color data. The recent Q method, developed by Johnson and Morgan (1953) from their three-color photometry, provides us with a unique method of overcoming the difficulties of interstellar reddening inherent in the determination of the intrinsic colors of early-type stars. Fortunately, the β Canis Majoris stars fall in the spectral type range in which the Q method is valid. The present discussion is based on colors determined by this method.

II. PHOTOELECTRIC OBSERVATIONS

The photoelectric observations of the β Canis Majoris stars were made on the nights of December 20/21 and December 21/22, 1953, with the Crossley reflector of the Lick Observatory. A description of an amplifier similar to the one used here is given elsewhere (Kron 1952). A 1P21 photomultiplier was used as the light-sensitive unit. The observations were made through three filter combinations; a Corning 9863 (ultraviolet), a Corning 3060 + Schott BG 12 (blue), and a Schott GG 14 (yellow). The effective wave lengths of the photomultiplier-filter combinations are approximately 3550, 4400, and 5420 A. The observations were recorded by means of a Brown recording potentiometer and were corrected for the sky background admitted through the diaphragm (diameter = 40 seconds of arc). The extinction reductions were made by making use of the condition that the colors of the extinction stars must be the same on both nights. The stars selected for extinction standards were: μ Eri, ι CMa, π^4 Ori, γ Peg, β Ari, and 10 Lac. These stars were selected because they are located close to the β Canis Majoris stars and, with the exception of β Ari, have colors almost identical to the variable stars. Although γ Peg is itself a β Canis Majoris star, its use as an extinction star is justified, since color changes with phase are probably negligible as its light-amplitude is only 0.015 mag. (Williams 1954). Following the notation of Johnson and Morgan (1953), the observed colors reduced to outside the atmosphere are given by:

$$C_y = C_{y0} - K_y \sec Z ,$$

$$C_u = C_{u0} - K_u \sec Z .$$

* The observational material presented in this paper was obtained at the Lick Observatory.

No attempt was made to determine the variation of K_y with color, since the stars are very similar in color. The star β Ari, which differs by the greatest amount in color from the other stars, was reduced to no atmosphere with its own yellow color-extinction coefficient.

The internal probable errors for the instrumental colors were computed for the β Canis Majoris stars which were observed several times, and were found to be:

$$\left.\begin{aligned} C_y\text{:p.e.} &= \pm 0.006 \text{ mag.} \\ C_u\text{:p.e.} &= \pm 0.009 \text{ mag.} \end{aligned}\right\} \text{ for one observation.}$$

A single observation consists of two deflections on the recorder.

The observed colors C_y and C_u were related to the $B - V$ and $U - B$ system of Johnson and Morgan by the transformation equations

$$B - V = A_1 + A_2 C_y ,$$
$$U - B = A_3 + A_4 C_u .$$

The five standard stars used to determine the transformation coefficients are listed in Table 1. The stars were given equal weight, with the exception of 10 Lac, which was

TABLE 1

COLORS OF STANDARD STARS

Star	Sp.	C_y	C_u	$(B-V)_{J,M}$	$(B-V)_C$	$(U-B)_{J,M}$	$(U-B)_C$
ι CMa	B3 II	−0.705	+0.046	−0.07	−0.075	−0.70	−0.703
π^4 Ori	B2 III	− .790	− .055	− .17	− .162	−0.81	−0.804
10 Lac	O9 V	− .832	− .304	− .200	− .205	−1.04	−1.051
ν And	B5 V	− .769	+ .196	− .15	− .141	−0.57	−0.554
β Ari	A5 V	−0.495	+0.848	+0.14	+0.140	+0.10	+0.093

given double weight in the solution of the $B - V$ coefficients, since its $B - V$ color is given to three decimals by Johnson and Morgan. From least-square solutions the coefficients were found to be:

$$A_1 = +0.646 \pm 0.013 ,$$
$$A_2 = +1.023 \pm 0.017 ,$$
$$A_3 = -0.749 \pm 0.004 ,$$
$$A_4 = +0.993 \pm 0.010 .$$

The $B - V$ and $U - B$ values were then computed for the standard stars and the β Canis Majoris stars. A comparison between the computed standard star colors and those given by Johnson and Morgan is given in Table 1.

An attempt was made to observe the β Canis Majoris stars near the mean light-positions in their light-curves, since the colors are known to vary with phase in the case of the stars with the larger light-amplitudes (Nikonov and Nikonova 1952; Kraft 1953; de Jager 1953; Walker 1954). BW Vulpeculae was observed near the light-minimum on December 21/22; the observed colors were corrected by −0.015 mag. and −0.040 mag. in the C_y and C_u colors, respectively, to bring them to the mean light-colors. The other stars were observed near the mean light-phases, and therefore no corrections were necessary.

The final results of the observations of the β Canis Majoris stars are given in Table 2. The first column contains the star names, listed according to increasing period. The second column lists the spectral types assigned on the M.K.K. system. The third column contains spectral types assigned on the basis of the color of the stars from the calibration of Q with respect to spectral type, as given by Johnson and Morgan. The fourth and fifth columns contain the periods (in hours) and the observed $B - V$ colors. The sixth column lists the $B - V$ colors for four of the stars, observed by Stoy (1953). The seventh, eighth, and ninth columns contain the observed $U - B$ colors, the values of Q computed by the equation $Q = (U - B) - 0.72\,(B - V)$, and the color excess given by $E_y = (B - V) - 0.337Q + 0.009$ (Johnson and Morgan 1953). The tenth and eleventh columns list the intrinsic $(B - V)_I$ and $(U - B)_I$ colors determined from the Q values. The twelfth column gives the number of observations. The colors listed in Table 2 are given to the nearest 0.005 mag.

TABLE 2

SPECTRAL TYPES AND COLORS OF THE β CANIS MAJORIS STARS*

Star	Sp.†	Spq	P	$B-V$	$(B-V)$‡	$U-B$	Q	E_y	$(B-V)_I$	$(U-B)_I$	No.
γ Peg	B2 IV	B2	3^{h}64	−0.215	.....	−0.840	−0.685	0.025	−0.240	−0.860	5
δ Cet	B2 IV	B2	3.87	− .210	−0.20	− .850	− .700	.035	− .245	−0.875	4
16 Lac	B2 IV	B1	4.06	− .145	.....	− .850	− .745	.115	− .260	−0.935	4
ν Eri	B2 III	B2	4.16	− .190	− .20	− .860	− .725	.065	− .255	−0.905	4
β Cep	B2 III	B1	4.57	− .225	.....	− .945	− .785	.050	− .275	−0.980	3
DD Lac	B2 III	B1	4.63	− .135	.....	− .860	− .765	.130	− .265	−0.955	4
BW Vul	B2 III	B1	4.82	− .130	.....	− .870	− .775	.140	− .270	−0.970	3
ξ_1 CMa	B1 IV	B1	5.03	− .240	− .25	− .980	− .805	.040	− .280	−1.010	6
β CMa	B1 II–III	B1	6.00	−0.235	−0.23	−0.970	−0.800	0.045	−0.280	−1.000	5

* The colors listed are given to the nearest 0.005 mag.

† M.K.K. spectral types. The spectral type of ξ' CMa was estimated by McNamara from Mills spectrograms on the basis of the classifications supplied by Morgan for the other stars listed.

‡ R. H. Stoy, *Cape Mimeogram*, No. 1, 1953.

III. DISCUSSION

The results given in Table 2 are depicted graphically in Figure 1. With the exception of σ Scorpii, all the known β Canis Majoris stars are shown in the figure. It is evident upon inspection of Figure 1 that there is a well-defined relation between the periods and the intrinsic colors of this group of variable stars. This is in agreement with the results announced earlier (McNamara 1953*a*). Figure 1 indicates that for stars with periods shorter than 5 hours the color is sensitive to the period. Excluding the star β Canis Majoris, we find from least-squares solutions that the colors can be represented by the regression lines

$$Q = -0.390 - 1.974\ P \text{ days},$$

$$(B - V)_I = -0.143 - 0.653\ P \text{ days}.$$

These straight lines are shown in the figure. If we use the first equation to compute the value of Q for β Canis Majoris, we find a value of $Q = -0.88$. Thus β Canis Majoris departs by a considerable margin from an extrapolation of this line to 6 hours. A Q value equal to -0.88 would require a spectral type near B0; β Canis Majoris is an M.K.K. standard of spectral type B1. A star of spectral type B1 should have a Q value near -0.78. Therefore, the observed Q value of -0.800 is in excellent agreement with the spectral type.

Although we have no color observations of σ Scorpii ($P = 5^h55^m$), its spectral type is identical to that of β Canis Majoris, and it would also probably fall off extrapolations

of the lines shown in Figure 1. Dr. A. R. Hogg of the Commonwealth Observatory, Mount Stromlo, has kindly supplied us with preliminary measures of the color of σ Scorpii. His results, which he stresses are subject to revision, indicate $Q = -0.76$; $(B - V)_I = -0.26$; and S_a = B1. Since the period of σ Scorpii is 5^h92, Hogg's Q and $(B - V)_I$ are considerably smaller than would be indicated by an extrapolation of the period-color relationship for shorter-period members of the group. Examination of the spectra of ξ_1 CMa, σ Sco, and β CMa indicate that they are practically identical with regard to line intensities. This can be seen by an inspection of the Mills spectrograms (original dispersion 11 A/mm at $H\gamma$) reproduced in Figure 2. While there is a considerable change in the intensities of a number of lines as we proceed from ξ_1 CMa to a star like 16 Lac, there is little, if any, change between ξ_1 CMa and β CMa, in spite of an equivalent change in period. Thus the observational evidence indicates that the β Canis Majoris stars are restricted to spectral type B1 or later. This result should be accepted only tentatively, in view of the small sample of stars.

It is of interest to note that, for stars with a declination greater than $-40°$ and a magnitude brighter than 7.00, the B0 stars outnumber the B1 stars in the ratio of 2 to 1 (Stebbins, Huffer, and Whitford 1940). This suggests that if the β Canis Majoris stars

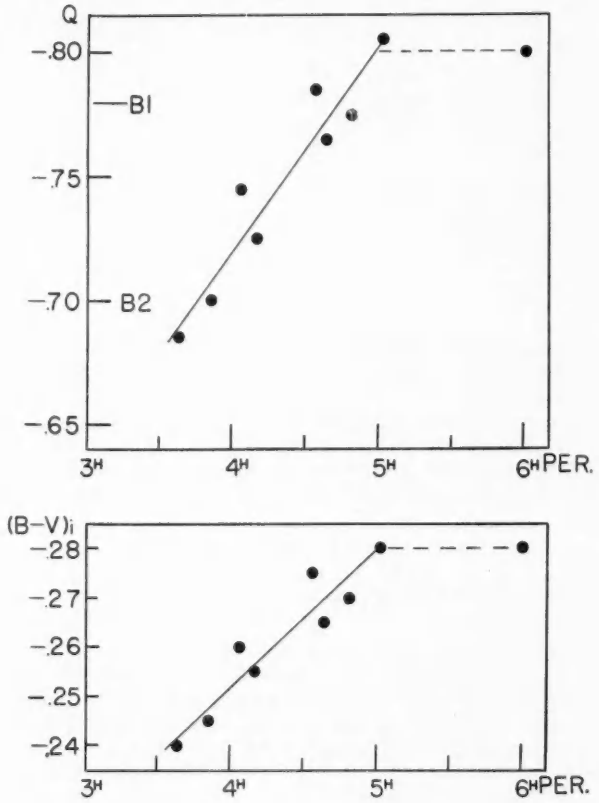

FIG. 1.—Color-period relationship of β Canis Majoris stars. *Upper*, the relationship between Q and period; *lower*, the relationship between the intrinsic $(B - V)_I$ color and the period.

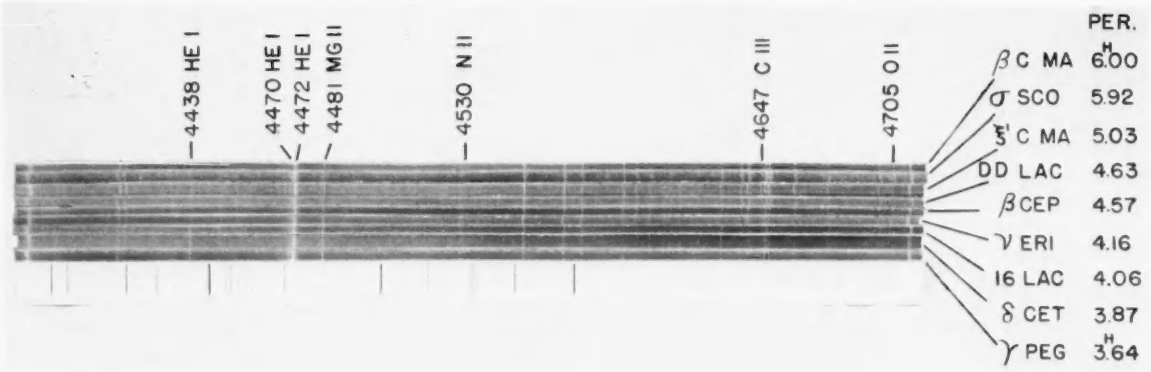

FIG. 2.—Spectra of the β Canis Majoris stars

are present among the B0 stars, it is with a lower frequency that their occurrence among the B1 stars.

This suggested cutoff at spectral type B1 raises some interesting questions regarding the position of the β Canis Majoris stars in the H-R diagram. Blaauw and Savedoff (1953) and also McNamara (1953*b*) have presented evidence favoring the existence of a period-luminosity relation for this group of stars. If the relation is valid through the interval of periods from 5 hours to 6 hours, the β Canis Majoris stars with periods longer than 5 hours would fall on a perpendicular sequence in the H-R diagram.

We wish to express our gratitude to Dr. G. E. Kron for the use of his photometer and for valuable suggestions.

REFERENCES

Blaauw, A., and Savedoff, M. P. 1953, *B.A.N.*, **12**, 69.
de Jager, C. 1953, *B.A.N.*, **12**, 81.
Johnson, H. L., and Morgan, W. W. 1953, *Ap. J.*, **117**, 313.
Kraft, R. P. 1953, *Pub. A.S.P.*, **65**, 45.
Kron, G. E. 1952, *Ap. J.*, **115**, 1.
McNamara, D. H. 1953*a*, *Pub. A.S.P.*, **65**, 155.
———. 1953*b*, *ibid.*, p. 286.
Nikonov, B. V., and Nikonova, E. K. 1952, *Izvestiia Krimskoi Astrophiizicheskoi Observatorii*, **9**, 135.
Stebbins, J. Huffer, C. M., and Whitford, A. E. 1940, *Ap. J.*, **91**, 20.
Stoy, R. H. 1953, *Cape Mimeogram*, No. 1.
Walker, M. F. 1954, *Ap. J.*, **119**, 631.
Williams, A. D. 1954, *Pub. A.S.P.*, **66**, 25.

THE ECLIPSING BINARY V356 SAGITTARII

DANIEL M. POPPER
Department of Astronomy, University of California, Los Angeles
Received April 23, 1954; revised July 23, 1954

ABSTRACT

The system V356 Sgr is found to be of special interest principally because of the presence of an A star of luminosity class II with unusual properties. The most striking of these are (1) departure from the mass-luminosity relation for main-sequence stars and (2) departure from the cosine law of limb darkening. The system is noteworthy also, in that it is one of the brightest eclipsing binaries which show the spectral lines of both components and which have well-defined total and annular eclipses.

Spectrographic and two-color photoelectric observations are combined to investigate the properties of the system. The velocity-curve of the hotter component and the light-curve are not obtained with high precision. The spectral types of the components are A2 II and B3: V, with the B star undergoing total eclipse at primary minimum. The masses and radii of the stars are such that the B star is nearly spherical, while the A star is distorted by tidal force. Ordinary rectification of the light-curve is not applicable. An approximate solution is based on the assumption that the orbital inclination is 90°. It is not possible to obtain a satisfactory interpretation of the principal features of the light-curve unless one assumes a distribution of light over the disk of the A star considerably more concentrated toward the center than is given by the cosine law of limb darkening. By way of illustration, it is found that one of the laws of darkening worked out by the Gaposchkins for an extended photosphere, combined with a gravity-darkening coefficient of unity, gives a satisfactory representation of the principal features of the light-curve.

The surface-brightness ratio of the two components and their difference of color index are in agreement with the values to be expected for stars of the observed spectral types. The principal properties of the stars are given in the accompanying table. The B star appears normal for its type in all respects. The A star is a new kind of object. It lies approximately 2 mag. above the mass-luminosity relation for main-sequence stars.

Spectral type	B3: V	A2 II	Luminosity (solar units)	2640	1350
Mass (solar units)	12.1	4.7	M_{pv}	−1.9	−2.7
Radius (solar units)	4.9	12.7			

INTRODUCTION

V356 Sgr[1] is one of the brightest known eclipsing binaries, in which the spectral lines of both components appear except during the minima and in which the light-curve shows two well-defined minima with constant phases of appreciable duration. Hence it should be a favorable object to study. Earlier observational work on the system consists of light-curves by Kanda (1930), Voûte (1931), and Gaposchkin (1953) and estimated spectral types of the components by Wyse (1934). The period is 8.90 days. Wyse (1934) and the Gaposchkins (Payne-Gaposchkin and Gaposchkin 1943) have published solutions of Voûte's light-curve. The present writer has published provisional values for the masses, radii, and luminosities of the components (Popper 1950). Principally because of the unsatisfactory nature of Voûte's light-curve, however, those results are quite different from the ones derived in this paper.

The present investigation is based on spectrograms obtained at the McDonald Observatory in 1946 and on photometric observations obtained at the Lick Observatory, principally in 1951.

SPECTROGRAPHIC MATERIAL

Appearance of the spectra.—Twenty-one spectrograms with a dispersion of 26 A/mm at $H\gamma$ were obtained in May and June, 1946. Four of them are reproduced in Figure 1,

[1] HD 173787, mag 6.9, Sp. B9, α_{1900} 18^{h}42^{m}0, δ_{1900} − 20°22′.

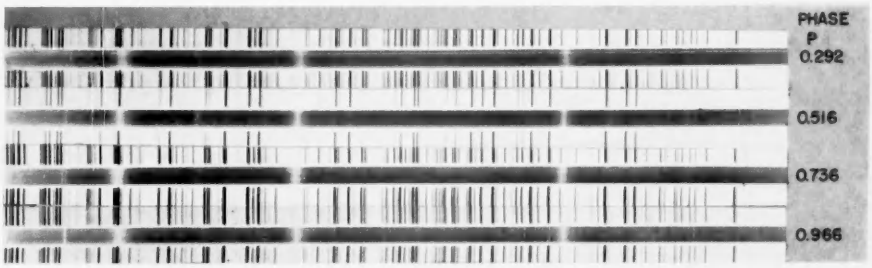

FIG. 1.—Spectrograms of V356 Sgr. The region covered is from approximately λ 3900 to approximately λ 4500, shorter wave lengths being at the left. Iron-arc comparison.

one having been photographed during each eclipse and one near each node. During primary minimum the spectrum is of type A, the *He* lines, present at all other phases, being absent and the lines of ionized metals being greatly strengthened (Fig. 1, phase *0.966*). Hence the deeper eclipse is total. The spectrum at this phase has been classified by W. W. Morgan (unpublished) as A2 II, the wings of the *H* lines being much weaker than in the spectra of main-sequence A stars. I am indebted to Drs. Burbidge, Bidelman, and Morgan for obtaining and classifying the necessary spectrograms. The spectral type at secondary eclipse is estimated as B5–B7 from *He/H* line ratios (Fig. 1, phase *0.516*). Since, according to the photometric analysis, the A star at this phase contributes about half the combined light, the hotter component must be considerably earlier than B5 and is estimated to be of type B2 or B3. We adopt type B3:. As was previously pointed out (Popper 1950), these spectral types remove the apparent discrepancy be-

TABLE 1

RADIAL VELOCITIES OF V356 SGR

PLATE CG	JULIAN DAY 2,431,000+	PHASE*	A STAR			B STAR	
			Velocity (Km/Sec)	Weight	O−C (Km/Sec)	Velocity (Km/Sec)	O−C (Km/Sec)
4890	964.88	0.382	+145	1	+10	−78	−36
4892	965.92	.500	+ 13	¼	+ 5		
4894	966.95	.616	−125	½	− 6	+42	−14
4899	967.96	.728	−172	½	+ 9	+88	+ 9
4902	970.97	.066	+ 77	½	− 7		
4904	971.94	.176	+177	1	0	−52	+ 6
4906	974.85	.504	+ 12	¼	+ 9		
4908	975.92	.624	−136	½	−10		
4910	976.92	.736	−186	1	− 4	+87	+ 7
4915	977.97	.854	−134	½	+10		
4916	978.80	.948	− 54	1	0		
4920	979.88	.068	+ 93	½	+ 7		
4921	980.84	.176	+175	1	− 2	−45	+13
4922	981.86	.292	+182	1	− 9	−71	− 8
4925	982.89	.406	+118	1	+ 5		
4927	983.82	.512	− 19	¼	− 5		
4951	985.80	.733	−183	½	− 1	+61	−19
4953	986.90	.858	−146	1	− 5		
4956	987.86	.966	− 28	1	+ 6		
4961	992.75	.516	+ 5	¼	+16		
4964	995.75	0.852	−142	½	+ 3	+62	− 4

* Fraction of the period since primary minimum.

tween the surface-brightness ratio of the components as derived from Wyse's spectral types (B9, A1), on the one hand, and from the light-curve, on the other. Near the nodes the K line shows two components (Fig. 1, phases *0.292* and *0.736*), one from the A star and one interstellar.

The *He* I lines of the B component appear markedly broadened by rotation, whereas the lines of the A star are relatively sharp, though the stellar K line is distinctly broader than the interstellar line. These observations are in qualitative agreement with the hypothesis that the periods of axial rotation and of orbital revolution of the A star are equal (equatorial velocity of rotation 75 km/sec deduced from data derived below), while the rotation period of the B star is considerably shorter. It is found later that the B star is essentially spherical, whereas the A star is strongly distorted by tidal force.

Spectrographic orbits.—A list of spectrograms and measured radial velocities is contained in Table 1. The phases, in fractions of the period from primary minimum, were

computed from the light-elements discussed below. The sharp metallic lines of the A star lead to relatively precise velocities. The velocities of the B star are quite uncertain because of the difficulty of measuring the broad, diffuse lines. Only λ 4026 and λ 4471 of *He* I could be used. The *H* lines of the two components are badly blended. The residuals of Table 1 and the curves of Figure 2 were obtained from the following circular elements:

$$K_A = 190 \pm 2 \text{ km/sec}, \qquad a \sin i = 3.22(\pm 0.08) \times 10^7 \text{ km},$$
$$K_B = 73 \pm 6 \text{ km/sec}, \qquad = 46.2 \pm 1.2 \text{ solar radii},$$
$$\gamma = +7 \pm 1 \text{ km/sec}, \qquad \mathfrak{M}_A \sin^3 i = 4.7 \pm 0.4 \text{ solar masses},$$
$$\mathfrak{M}_B \sin^3 i = 12.1 \pm 1.0 \text{ solar masses}.$$

The orbital eccentricity, if different from zero, is too small to be significant. The value of γ, which was computed from the velocities of the A component only, was adopted in

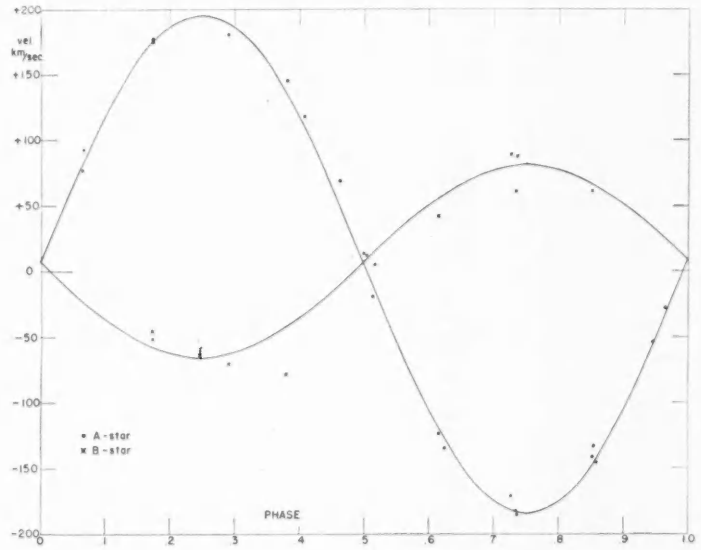

FIG. 2.—Radial-velocity observations of V356 Sgr. Abscissae are fractions of the period from primary minimum. The curves are based on the adopted elements.

computing K_B. Subscripts A and B as used throughout this paper refer to the A star and the B star, respectively. The interstellar K-line velocity is -1.7 ± 1.4 km/sec, or +11 km/sec when corrected for local solar motion.

PHOTOMETRIC MATERIAL

Observational procedure.—V356 Sgr was observed in blue and yellow light with a photoelectric photometer on the 12-inch refractor of the Lick Observatory in the summers of 1950 and 1951. The equipment has been described by Eggen (1950). The present discussion is based principally on the 1951 observations because of more satisfactory skies and more stable operation. The 1P21 photocell and Brown recorder employed in

1951 were the property of the Berkeley Astronomical Department of the University of California. The yellow filter used is similar to that used by Eggen, whereas the blue filter transmits less than his in the near ultraviolet. As determined by comparison with standard stars, the resulting 1951 magnitudes and colors are very nearly on the B, V system (Johnson and Morgan 1953).

Because of its southerly declination, V356 Sgr is not an ideal object for photometry at Mount Hamilton. Additional troublesome factors are the passage of the full moon quite near to the star in summer, the relatively long period of orbital revolution, and the near-equality of this period to 9 sidereal days.

The comparison star used throughout is HD 172696.[2] Its magnitude and color on the B, V system are $V = 7.1$, $B-V = +0.19$. This star is 0.03 mag. redder than the variable and 0.26 mag. fainter in the blue at maximum light. The declinations of the two stars differ by 2′, and their right ascensions by 6 minutes. Corrections for differential extinction were evaluated on the basis of extinction factors determined on 6 nights. The corrections amount to 0.01 mag. in the yellow at an hour angle of 2^h15^m and to 0.01 mag. in the blue at an hour angle of 1^h40^m.

Observations were obtained on 39 nights in July, August, and September, 1951. The length of "exposure" on a star for a single color averaged about 1 minute. In what follows, the term "observation" will refer to a set of one blue and one yellow exposure of the variable obtained between two sets of the comparison star. The quantities used in the discussion and shown in the diagrams are intensity ratios corrected for extinction:

$$\text{Yellow: } l_Y = \frac{\text{Deflection on variable with yellow filter}}{\text{Mean of preceding and following deflections on comparison star}} ;$$

$$\text{Blue: } \quad l_B = 0.969 \times (\text{corresponding ratio with blue filter}) ;$$

that is, the units of intensity, l, are the intensity of the comparison star in the yellow and 1.0320 times the intensity of the comparison star in the blue (the factor for the 1950 observations is 1.0256). In these units the variable star has, on the average, equal intensity in the two colors outside of minima.

Light-elements.—Times of minima of V356 Sgr have been published by Voûte (1931), Kanda (1930), and Gaposchkin (1953). My observed epoch of primary minimum is JD 2433900.827. The observed minima as well as the velocity-curve are satisfied by the following light-elements:

$$\text{JD}_{\text{helioc}} = 2433900.827 + 8.89610E .$$

The greater precision of the photoelectric observations justifies adoption without change of the epoch of minimum thus determined. The phases of the observations, θ, which are expressed throughout as fractions of the period from primary minimum, have been computed from these elements for both the photometric and the spectrographic observations.

Observed light-curve.—The observations are shown graphically. The individual data will be provided to anyone interested. Light-units rather than magnitudes are used. The appearance of the light-curve is shown in Figure 3, which contains the 1951 observations in yellow light. Each point represents the mean of from 4 to 7 observations. The curve in blue light has a similar appearance, whereas the curves obtained in 1950 show considerably greater scatter. Light-curves have been published previously for this star by Voûte (1931), Kanda (1930), and Gaposchkin (1953). None of these observers noted the marked variation of 0.16 mag. between eclipses, although a variation is suggested by Voûte's and Kanda's observations. Figure 4 shows the 1950 observations between

[2] Mag 6.9, Sp. B9, α_{1900} 18^h36^m5, δ_{1900} $-20°24'$.

minima. The ordinates are the same as those of Figure 3, except that the yellow and blue observations are averaged. Figure 5 shows the 1951 observations between minima. The straight lines drawn on these two diagrams are discussed below. Figure 6 contains the observations during primary minimum (1951), while Figure 7 shows secondary minimum. In Figures 6 and 7 each point represents a single observation. Although the 1950 observations during minima show too much scatter to be of use in the discussion, the observations between minima are of sufficient combined weight to be considered.

Discussion of the light-curve between minima.—The marked variation between minima must result from tidal distortion of the stars combined with the effects of gravity darkening and limb darkening. Although the reflection effect must also be present, the observations are of insufficient precision to evaluate it observationally.

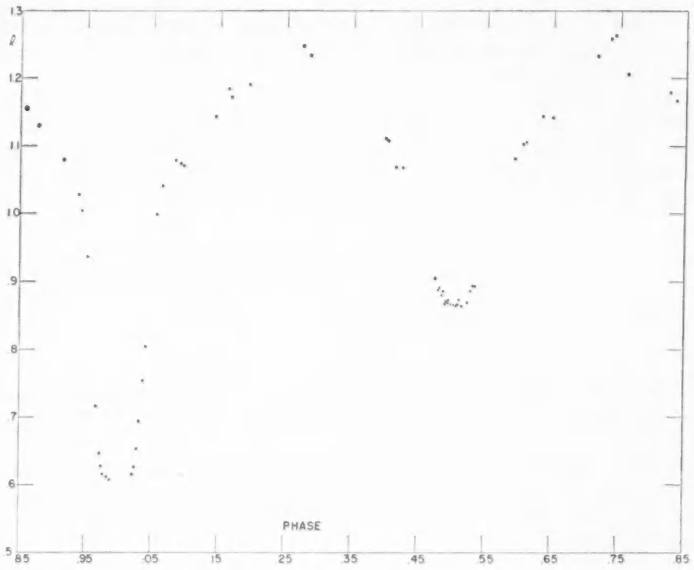

FIG. 3.—Light-curve of V356 Sgr. Observations in yellow light made in 1951. Each point is the mean of from 4 to 7 observations. Abscissae are as in Fig. 2. Ordinates are ratios of the light of the variable star to that of the comparison star.

In interpreting the variation between minima, one has a considerable advantage if the true shapes of the stars are known. They depend on the mass ratio of the components, on the size of each star in units of the distance between their centers, and to a minor extent on the degree of central condensation in their interiors (e.g., Russell 1948). Because the mass ratio of the components of V356 Sgr is known and because the sizes of the stars are quite well determined from the well-defined minima, the true shapes of the stars can be computed with reasonable accuracy. We adopt the followihg quantities for use in the computation. They are obtained from the spectrographic material discussed earlier and from the light-curve during minima, discussed later:

$$\frac{\mathfrak{M}_B}{\mathfrak{M}_A} = 2.6, \qquad \bar{r}_B = 0.10, \qquad \bar{r}_A = 0.28,$$

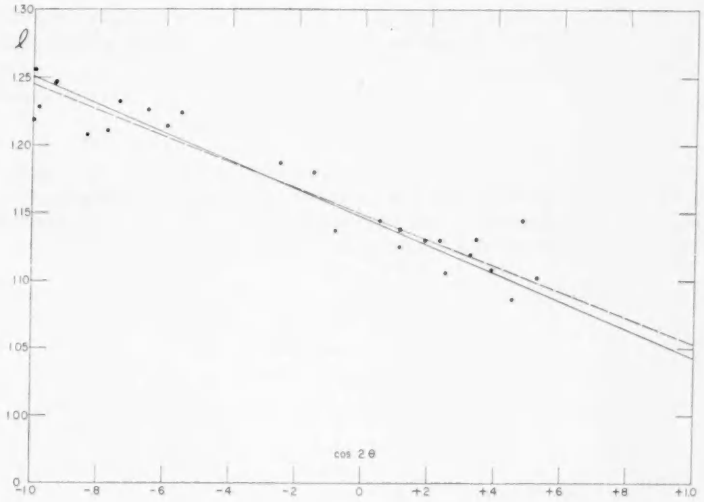

FIG. 4.—Light between minima, 1950 observations. θ is the phase in fraction of the period from primary minimum. Ordinates are as in Fig. 3. Each point represents the mean of from 4 to 7 observations, yellow and blue averaged. *Dashed line:* best straight-line fit; *solid line:* computed from adopted photometric ellipticity of the A star.

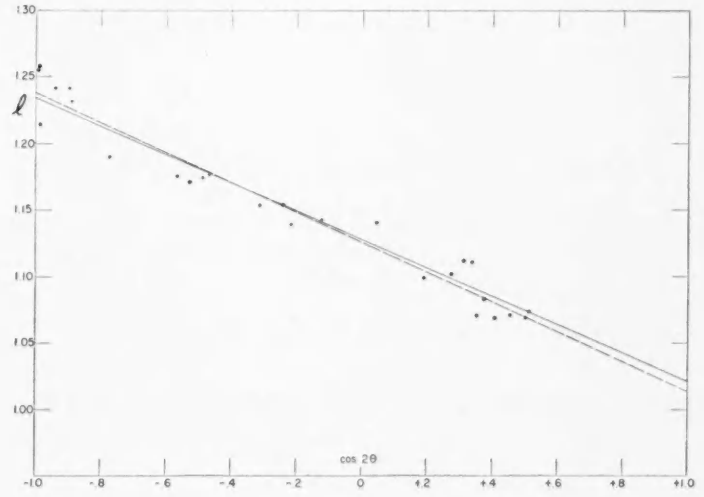

FIG. 5.—Light between minima, 1951 observations. Explanation as in Fig. 4

where $\bar{r}$ is the mean of the three axes of the distorted ellipsoid in units of the distance between centers of the two components. Then the ellipticities of those cross-sections lying in the orbital plane are

$$\epsilon_B = 0.001 , \qquad \epsilon_A = 0.078 .$$

We see that the shapes of the stars are so different that we may assume that *all* the variation of light between minima results from distortion of the A star. On the basis of this assumption we may determine the uneclipsed variation of each star separately. For the uneclipsed light we write for each color,

$$l_B = \text{Constant} ,$$

$$l_A = a_0 + a_2 \cos 2\theta ,$$

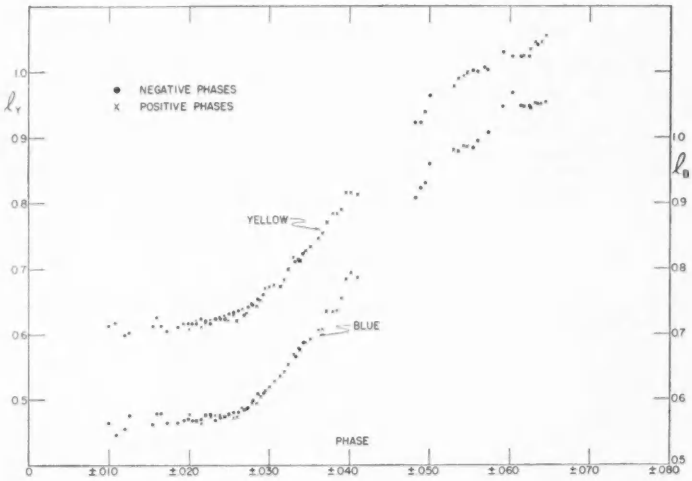

FIG. 6.—Primary minimum, 1951 observations. Each point represents a single observation. Abscissae and ordinates as in Fig. 3.

in which a_2 is negative, and

$$l = l_A + l_B = l_B + a_0 + a_2 \cos 2\theta .$$

The simplifying assumption is made that the photometric ellipticity of the A star,

$$(N\epsilon)_A = \frac{-2a_2}{a_0 - a_2},$$

is the same in the two colors; N_A is the ratio of the photometric ellipticity to the true ellipticity of the A star. More precise observations between minima are needed to justify a less simple assumption.

In order to evaluate l_B, a_0, and a_2, we need, in addition to the shape of the light-curve between minima (Figs. 4 and 5), the light of the A star alone, as observed at primary (total) eclipse, which light is equal to $a_0 + a_2$. The observed values of the light at primary minimum are given in the accompanying tabulation. The values of $(N\epsilon)_A$, ob-

	Yellow	Blue		Yellow	Blue
1950.....	0.605	0.552	1951.....	0.611	0.566

tained by a least-squares solution from the points of Figures 4 and 5, and the values of $a_0 + a_2$ just given are, for the mean of the two colors,

$$1950: (N\epsilon)_A = 0.25 , \qquad 1951: (N\epsilon)_A = 0.275 .$$

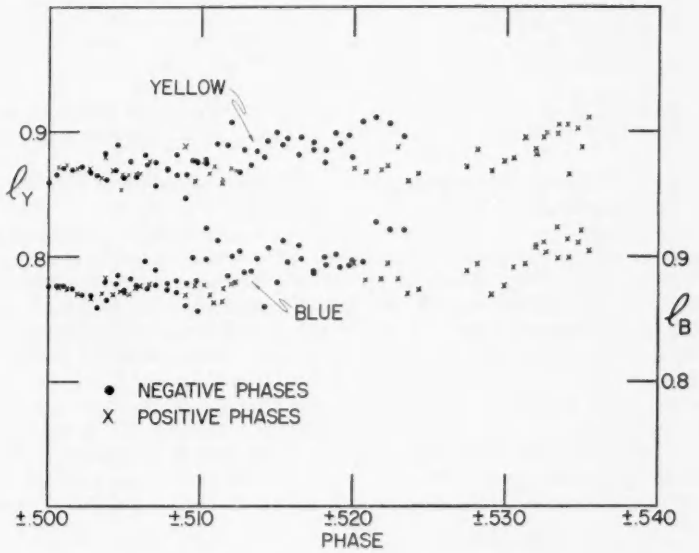

FIG. 7.—Secondary minimum, 1951 observations. Each point represents a single observation. Abscissae and ordinates as in Fig. 3.

The corresponding light-curves are shown in Figures 4 and 5 as dashed lines. I have adopted, for the photometric ellipticity of the A star,

$$(N\epsilon)_A = 0.265 .$$

The light-curves between minima corresponding to this value are shown in Figures 4 and 5 as solid lines. The values of l_B, a_0, and a_2 resulting from fitting the adopted value

of $(N\epsilon)_A = -2a_2/(a_0 - a_2)$ to the depths of primary minimum and to the points between minima, are given in the accompanying tabulation.

	1950		1951	
	Yellow	Blue	Yellow	Blue
l_B	+0.432	+0.496	+0.405	+0.460
a_0	+ .714	+ .652	+ .721	+ .668
a_2	−0.109	−0.099	−0.110	−0.102

If ϵ_A equals 0.078 as determined above, N_A, the ratio of photometric to dynamical ellipticity of the A star, is 3.4, considerably larger than the value of about 2.5 recommended by Russell (1948).

Thus far the reflection effect has not been considered. From the elements of the system adopted below, one may compute the coefficients of reflection to be expected (Russell 1948). They are negligible for the B star. If we write, for the variation of the light of the A star caused by reflection,

$$a_1' \cos\theta + a_2' \cos 2\theta ,$$

we find, from theory, $a_1' = -0.04$ and $a_2' = +0.01$. Although the observations between minima are not very precise, a value of $|a_1'|$ as large as 0.02 appears to be excluded by them.

Discussion of the light-curve within minima.—Because of the great difference in shape of the two components of V356 Sgr, it is clear that determination of an "intermediate model" of the system by the usual rectification procedures is not a satisfactory approach. As a matter of fact, attempts at such a determination failed to yield meaningful results ($\cos^2 i < 0$). Furthermore, the shape of the light-curve is not sufficiently well established to justify the application of Kopal's developments for distorted stars (e.g., Kopal 1946). On the other hand, the depths of minima and times of contact are quite well determined, so that it should be possible to obtain a preliminary set of elements. The assumptions I adopt for this purpose are that the true shapes of the stars are those obtained earlier from dynamical considerations and that the orbital inclination is 90°. The principal justification for this last assumption is that it enables us to obtain a solution of the light-curve with a minimum of difficulty. In addition, it is seen below that a value of i close to 90° is most reasonable.

The accompanying tabulation lists the quantities used in the analysis. They are taken

	Yellow	Blue
l_B	0.405	0.460
l_A	0.721−0.110 cos 2θ	0.668−0.102 cos 2θ
l (sec. min.)	0.870	0.874
θ'	0.0615	
θ''	0.0260	
ϵ_A	0.078	
i	90° (assumed)	

from the 1951 light-curve and from previous discussion. Here θ' and θ'' are the phases, in fractions of the period, of external and internal contact, respectively (see Fig. 6). The estimated uncertainties are ± 0.0020 in θ' and ± 0.0010 in θ''.

If i is given, the relative radii of the stars are determined from the phases of the contacts. For $i = 90°$ the relationships are

$$\sin \theta' = a_A(1 - e_A^2 \cos^2 \theta')^{1/2} + r_B ,$$
$$\sin \theta'' = a_A(1 - e_A^2 \cos^2 \theta'')^{1/2} - r_B ,$$

where a_A is the ratio ot that semiaxis of the A star along the line of centers to the distance between centers; r_B is the radius of the spherical B star; and e_A is the eccentricity of the A star corresponding to ϵ_A. Employing the quantities listed above, we obtain,

$$a_A = 0.290 , \qquad r_B = 0.106 .$$

The dynamical values of the other axes of the A star are $b_A = 0.268$ and $c_A = 0.258$, where c is the axis normal to the orbital plane. Some iteration is involved in determining a_A and r_B, since the dynamical eccentricity, e_A, depends on the sizes of the stars, which, in turn, depend to a lesser extent upon the adopted value of e_A.

The chief remaining problem in the interpretation of the light-curve during minima is the following: Given the variation of the light of each star with phase, the sizes and shapes of the stars, and an inclination of 90°, can we account satisfactorily for the light at secondary (annular) eclipse? From the numerical expressions for l_A and l_B and the observed values of the light at secondary minimum, the fraction of the light of the A star covered at mid-eclipse is found to be

$$\text{Fraction covered in yellow light} = 0.23 ,$$
$$\text{Fraction covered in blue light} = 0.27 ,$$

the unit being the uneclipsed light of the A star at the phase of mid-eclipse. The reflection effect has been neglected in the computations. The fractions of light covered are *greater* than the foregoing values if the reflection effect is present. This can be seen in principle as follows. When reflection is neglected, the light at secondary minimum, l_{sec}, is given by

$$l_{sec} = l_B + (1 - f)l_A ,$$

where l_A is the light of the A star as observed at primary minimum and f is the fraction of the light of the A star covered. Hence

$$f = 1 - \frac{l_{sec} - l_B}{l_A} .$$

But the light of the A star as seen at primary eclipse is less because of reflection than its true uneclipsed value at the time of secondary eclipse. Hence the value of f computed when reflection is neglected is less than it would be if reflection were included.

If the sizes of the stars are as adopted, the fraction of the *area* of the A star covered at secondary minimum is

$$\frac{(0.106)^2}{(0.268 \times 0.258)} = 0.16 .$$

The fraction of area covered is *less* than 0.16 if i is less than 90°, since in this case the radius of the A star would be larger and that of the B star smaller than the adopted values.

The differences between the geometrical fraction and the photometric fractions must be due to a concentration of light toward the center of the disk of the A star as it faces us during minimum. Sterne (1941) has developed the first-order theory for the distribution of light over the projected disk of a tidally distorted star, taking limb darkening and gravity darkening into account. The greatest concentration of light toward the center of the disk at the time of conjunction occurs if x, the coefficient of limb darkening, is unity (complete darkening) and y, the coefficient of gravity darkening, is zero (no gravity darkening). Under these conditions the central 16 per cent of the area of the disk contributes 23 per cent of the light. If x is less than 1 or y is greater than zero, the concentration is less. Thus these extreme and physically unsatisfactory values of x and y are the only ones that approach satisfying the observed light at secondary minimum, and that only in yellow light. An additional difficulty is that it is not possible to obtain agreement of theory with the observed light-variation between eclipses and with the dynamical ellipticity if these values of x and y (1 and zero, respectively) are adopted. Sterne's theory yields, for the photometric ellipticity, the expression[3]

$$N\epsilon = \frac{\epsilon \sin^2 i\,(1+y)\,(15+x)}{15-5x+(\epsilon/3)\sin^2 i\,(1+y)\,(15+x)}. \tag{1}$$

The observed value of $N\epsilon$ for the A star, 0.265, can be reconciled with the values $x = 1$, $y = 0$, only if $\epsilon_A = 0.18$. This value is so much greater than the dynamical value, 0.078, that we must conclude that theory and observation are incompatible. As seen earlier, consideration of reflection and of an orbital inclination less than 90° would only increase the discrepancy.

Another way of stating the discrepancy is the following. If we adopt any set of values of x and $\epsilon(1+y)$ in agreement with the photometric ellipticity of the A star according to expression (1), we cannot account for the large depth of secondary minimum with stars of the given sizes and brightnesses. In addition, any such set of values of x and $\epsilon(1+y)$ requires an intensity *minimum* at the center of the A star as seen at conjunction because of the effect of gravity "brightening" in the case of such a greatly distorted star. Such a minimum of intensity would require the light-curve at mid-secondary eclipse to be convex upward. This requirement does not appear borne out by the observed light-curve (Fig. 7).

The discrepancy between theory and observation depends, as far as the observations are concerned, upon only the phases of internal and external contacts (θ' and θ''); the light at primary and secondary minima; the single parameter, $(N\epsilon)_A$, describing the variation of light between minima; and the mass ratio. No reasonable alteration of the adopted values of these quantities can, in my opinion, remove the discrepancy. As noted previously, the adoption of a value of i less than 90° can only increase the discrepancy. Hence we must look to the theory of the distribution of light over the disk of the A star.

A consideration that immediately suggests itself is that the simple cosine expression for limb darkening may be inadequate. Limb darkening has been reasonably well observed only for main-sequence stars. Little or nothing is known of the structure of the photosphere of a star like the A component of V356 Sgr, spectral type A2 II, with a surface gravity 3 per cent that of the sun. Any extent of the photosphere, for example, which requires a departure from the plane approximation in the theory of radiation transfer leads to greater concentration of light toward the center of the stellar disk than does the simple cosine relation approximated by the plane theory (e.g., Chandrasekhar 1934). The Gaposchkins (Payne-Gaposchkin and Gaposchkin 1945) have worked out darken-

[3] This expression is nearly the same as that given by Russell (1939). The small differences are presumably due to different treatment of the approximations involved. I use Sterne's development because it gives more complete information on the distribution of light over the stellar disk.

ing distributions in the nonplane theory for a number of cases and have discussed some applications to stellar eclipses.

Although it is not to be expected that a photospheric model chosen arbitrarily from among those discussed by the Gaposchkins will represent the actual photosphere of the A component of V356 Sgr, it is of interest that application of the Gaposchkins' case $n = 3$ (least extended photosphere considered by them) just removes the discrepancy discussed here in the light-curve of V356 Sgr. In order to test any one of these cases in the simplest manner, I have altered Sterne's theory by replacing the cosine law of limb darkening by the intensity distribution given by the Gaposchkins. Then the fraction of the light covered may be computed for a given fraction of the area at central eclipse. I have retained the assumption $i = 90°$. In this computation the theoretical disks, which do not have sharp edges, were cut off a little way outside the radius corresponding to optical depth unity. Although the parts of the star outside this radius do affect the shape of the light-curve near outer contact, they contribute relatively little to the integrated light. Gravity darkening must also be taken into consideration in computing the light-fraction. For a given limb-darkening distribution, the coefficient of gravity darkening, y, may be obtained as follows from the variation between minima. It can be shown that in this simple alteration of Sterne's theory for an arbitrary limb-darkening distribution, the light-variation between minima depends on a photometric ellipticity, $N\epsilon$, which has precisely the same form as in equation (1), with the limb-darkening coefficient, x, replaced by an effective coefficient, x', which is computed in a definite way from the limb-darkening distribution. The value of this darkening coefficient effective for the variation of light *between* minima in the context of Sterne's theory is

$$x' = 1.5\,\frac{\int_0^{\pi/2} I(\gamma)\,(1 - 2\sin^2\gamma)\sin\gamma\cos\gamma\,d\gamma}{\int_0^{\pi/2} I(\gamma)\,(7 - 10\sin^2\gamma)\sin\gamma\cos\gamma\,d\gamma}, \tag{2}$$

in which γ is the angle at the surface of the star between a normal to the surface and the line of sight, and $I(\gamma)$ is the limb-darkening distribution. Then y can be computed from equation (1) for a given $N\epsilon$, ϵ, and x'. Given $I(\gamma)$ and y, the fraction of light covered by a given fraction of the area at central transit may be found by numerical methods.

In applying this theory to V356 Sgr, I have further simplified the model by assuming the cross-section of the A star to be circular at conjunction (no polar flattening), with a radius 2.50 times that of the B star. The other parameters adopted are $(N\epsilon)_A = 0.265$, $\epsilon_A = 0.078$, $i = 90°$, $n = 3$, where n is the parameter upon which depends the distribution of optical density in the photosphere of the A star. The results computed for this case are given in the accompanying tabulation. The predicted fractions would be in-

λT	Predicted Fraction of Light Covered at Central Eclipse	x'	y	Observed Fraction of Light Covered at Central Eclipse
4×10^7	0.27	1.3	0.9	0.27 (blue)
6×10^7	0.23	1.2	1.1	0.23 (yellow)

creased somewhat if reflected light from the B star was included. The last column is taken from the observations at secondary minimum. T is the photospheric temperature and λ the wave length is angstroms.

Thus the observed fractions of the light contained in the central 16 per cent of the area of the A star are reproduced for approximately the correct wave lengths if T is about 10,000°. An approximate computation of the blue light at internal contact predicted by the foregoing parameters [$I(\gamma)$ for $\lambda T = 4 \times 10^7$, $y = 0.9$] gives the value 0.93, whereas the observations (Fig. 7) show 0.90 or 0.91. The indication is that the theoretical distribution contains too low an intensity near the limb.

It would, of course, be a mistake to emphasize too strongly the agreement between observation and this simplified revision of the theory of limb darkening. There are many uncertainties in the theory (gray-body opacity, law of optical density variation) and in its application ($i = 90°$, first-order theory of tidal distortion, neglect of reflection effect and of polar flattening). But it is significant that these first observations of a star of the kind encountered here (type A2 II) seem to require a distribution of light of the nature expected for an extended photosphere. More precise observations of the entire light-curve in two or more colors, and particularly of the variation of light during secondary minimum, are needed for a more refined discussion than that given. From the spectroscopic standpoint, the mass ratio is not so well determined as it should be for an adequate interpretation of the light-curve. I shall undertake a redetermination of the mass ratio of V356 Sgr if someone else, preferably in the Southern Hemisphere, will obtain precise photometric observations.

One last problem in the interpretation of the photometric observations remains, namely, the evaluation of the light-ratios and surface-brightness ratios of the two stars in each color. This problem is complicated by the nonuniform distribution of light over the surface of the A star. As an approximation to the mean light of this star, we may take the mean of each of three mutually perpendicular faces. The light of those faces presented to us at quadrature and at conjunction is obtained directly from the observations. That of a face parallel to the orbit plane must be computed from the theory for the distribution of light. The result is not sensitive to the adopted darkening law. The light-ratios for the three cross-sections are 1.16/1/0.74, the corresponding ratios of area being 1.04/1/0.92. Here unity is the value for the face seen at quadrature. We obtain from the 1951 observations values for the light of the components, as shown in the accompanying table. The color difference between the two components of V356 Sgr is 0.22

	Light-Units of This Paper		Relative Light		Mag. Difference V356 − HD 172696		V	$B-V$
	Yellow	Blue	Yellow	Blue	Yellow	Blue		
A star	0.802	0.743	0.664	0.618	+0.24	+0.29	7.3	+0.24
B star	0.405	0.460	0.336	0.382	+0.98	+0.81	8.1	+0.02

mag. in the B, V system. This corresponds to a spectral-type difference of B5–A2 or B3–A1, in good agreement with the difference obtained from the spectrograms. The color excess of the system is approximately 0.20 mag. in the $B-V$ scale, corresponding to a visual absorption of 0.6 mag. (Morgan, Harris, and Johnson 1953).

A reason of fundamental importance for obtaining observations in more than one color is to make just such a check as that contained in the preceding paragraph of color difference against estimated difference of spectral type. It is well known that in a number of systems the difference in spectral type estimated from the spectrograms varies considerably from that obtained from the depths of minima (e.g., Wyse 1934), so that an additional check such as that afforded by the colors is highly desirable. In the case of V356 Sgr the surface-brightness ratio cannot be obtained directly from the minima

because of the large ellipticity effects. If we adopt, for the projected surface area of the A star, the mean of the areas of the three faces, we obtain the values given in the accompanying table. If we use Kuiper's (1938*a*) effective temperatures and bolometric cor-

RATIO: A STAR/B STAR

	Surface Area	Light	Surface Brightness
Yellow	6.60	1.98	0.30
Blue	6.60	1.61	0.24

rections, we find that the observed surface-brightness ratios correspond to a spectral-type difference B3–A2, in good agreement with the spectrograms and color difference. The conclusions of the last two paragraphs are not dependent on the assumption $i = 90°$.

RESULTS

In this section are gathered the principal results of the analysis of the system V356 Sgr. In computing the bolometric luminosities and absolute magnitudes, Kuiper's (1938*a*) temperature scale is adopted, and his bolometric corrections are used to find the absolute photovisual magnitudes. The effective temperature of an A star of luminosity class II is not particularly well known.

SPECTROGRAPHIC RESULTS

Spectral type	B3: V	A2 II
K (km/sec)	73 ±6	190±2
$\mathfrak{M} \sin^3 i$ (solar masses)	12.1±1.0	4.7±0.4
$a \sin i$ (solar radii)	46.2±1.2	
γ (km/sec)	7±1	
Orbital eccentricity (assumed)	0	

PHOTOMETRIC RESULTS

	B Star	A Star
Radius of star / Orbital radius	0.11	0.27 (mean)
Light of star (relative)		
Yellow	0.336	0.664
Blue	0.382	0.618
Apparent magnitude, V	8.1	7.3
Color index, $B-V$	+0.02	+0.24
Color excess	+0.20	
Orbital inclination (assumed)	90°	

Primary minimum: $JD_{helioc} = 2433900.827 + 8.89610E$

The concentration of light toward the center of the disk of the A star is greater than is given by the cosine law of limb darkening. The coefficient of gravity darkening of the A star is approximately unity.

The accompanying table lists the properties of the two stars. The estimated uncertainties are added. Although probable errors cannot, in general, be computed because of all

PROPERTIES OF THE STARS

Spectral type	B3: V	A2 II
Mass (solar units)	12.1±1.1	4.7±0.6
Radius (solar units)	4.9±0.3	12.7±1.0
Density (solar units)	0.10	0.0023
Ellipticity	0.001	0.078
Luminosity (solar units)	2640	1350
M_{bol}	−3.9±0.6	−3.2±0.3
M_{pv}	−1.9±0.7	−2.7±0.3

the factors involved in evaluating the properties of the stars, it is desirable to indicate estimates of the sizes of the uncertainties. As far as possible, they have been evaluated by the usual theory for the propagation for errors.

It is interesting to note that the B star has properties similar to those of other stars of the same spectral class, such as μ^1 Sco (Kuiper 1938*b*), the less massive component of V Pup (Popper 1943), and the more massive component of SX Aur (Popper 1943). The absolute photovisual magnitude of the B star in V356 Sgr is close to the value, −2.0, given by Keenan and Morgan (1951) for a B3 star on the main sequence. The absolute photovisual magnitude of the cooler component is also close to the rather uncertain value, −2.7:, given by Keenan and Morgan. This star is, however, a new type of object, as far as mass determinations are concerned. It is approximately 2 mag. more luminous bolometrically than main-sequence stars of the same mass. Combining the absolute magnitudes, apparent magnitudes, and interstellar absorption yields a distance of the system of 760 parsecs.

The 1951 photometric observations were carried out under a contract between the Office of Naval Research and the University of California. I am indebted to the director and staff of the Lick Observatory for the opportunity to use photoelectric photometers there in the summers of 1950 and 1951.

REFERENCES

Chandrasekhar, S. 1934, *M.N.*, **94**, 444.
Eggen, O. J. 1950, *Ap. J.*, **111**, 333.
Gaposchkin, S. 1953, *Harvard Ann.*, Vol. **113**, No. 2.
Johnson, H. L., and Morgan, W. W. 1953, *Ap. J.*, **117**, 313.
Kanda, K. 1930, *Tokyo Astr. Bull.*, Nos. 37–38.
Keenan, P. C., and Morgan, W. W. 1951, *Astrophysics*, ed. J. A. Hynek (New York: McGraw-Hill Book Co.), chap. 1.
Kopal, Z. 1946, *Eclipsing Variables* (Cambridge: Harvard Observatory), chap. 8.
Kuiper, G. P. 1938*a*, *Ap. J.*, **88**, 429.
———. 1938*b*, *ibid.*, p. 472.
Morgan, W. W., Harris, D. L., and Johnson, H. L. 1953, *Ap. J.*, **118**, 92.
Payne-Gaposchkin, C., and Gaposchkin, S. 1943, *Variable Stars* (Cambridge: Harvard Observatory), Table II, XXII.
———. 1945, *Ap. J.*, **101**, 56.
Popper, D. M. 1943, *Ap. J.*, **97**, 394.
———. 1950, *A.J.*, **55**, 78.
Russell, H. N. 1939, *Ap. J.*, **90**, 658.
———. 1948, *ibid.*, **108**, 388.
Sterne, T. E. 1941, *Proc. Nat. Acad. Sci.*, **27**, 99.
Voûte, J.-G. 1931, *Lembang Ann.*, **2**, D48.
Wyse, A. B. 1934, *Lick Obs. Bull.*, **17**, 37.

ON THE SUBGIANT COMPONENTS OF ECLIPSING BINARY SYSTEMS

J. A. CRAWFORD
Berkeley Astronomical Department, University of California
Received June 22, 1954

ABSTRACT

A recent paper by Parenago (1950) on the subgiant components of "single-line" eclipsing binary systems of the Algol type has been studied in the light of a result by Struve (1953), showing statistically that the luminosities of the subgiant secondaries depend not only on their masses and radii but on the mass ratio of the components. This mass ratio is directly related to the size of the zero-velocity surface passing through the inner Lagrangian point of the system, which sets an upper limit to the size of the star. From the photometric radii of the secondaries it was possible to obtain an upper limit to their masses. Those with mass limit less than 1 ⊙ were classified as definitely abnormal subgiants. These stars were found to lie, as a group, very near their maximum size. An evolutionary mechanism is proposed, relating the advanced "biological age" of these stars to the fact that they fill the inner zero-velocity surface.

I. INTRODUCTION

It has often been suggested that subgiant stars fall into two physically distinct classes, the first class containing all single stars, whereas members of the second class occur only in close binary systems, as exemplified by eclipsing systems with Algol-type light-curves. Such systems might also include the first or normal type of subgiant, whose prototype is the A component of the visual binary ζ Herculis. Eclipsing binaries are therefore a profitable field of study for clarifying this distinction. P. P. Parenago (1950) has recently listed 82 eclipsing variables for which spectroscopic determinations of the velocity-curve of the primary component alone are available. From these he selected 54 systems that also possess adequate photometric data. One of these systems has a supergiant primary. The remaining 53 all have main-sequence primaries and form the subject matter of this paper. The work of Parenago has recently been reviewed and discussed by Struve and Gould (1954). Struve (1953) has shown statistically that the luminosity of a subgiant secondary depends not only on its mass and radius but also on the mass ratio of the components of the binary system.

By choosing the mass of the primary in each case as the average main-sequence value corresponding to the observed spectral type, Parengo was able, from the spectroscopic and photometric data, to compute directly the mass and radius of the secondary, as well as the distance between the components. A survey of his list shows at once that the masses of the secondaries are, on the average, below the solar mass, while their radii are considerably larger than the sun's radius. Now the size of a star which is a member of a binary system is limited by the dimensions of the zero-velocity surface surrounding it, which passes through the inner Lagrangian point L_1. We shall refer to this as the inner zero-velocity surface. Its dimensions are always smaller for the less massive component. The question arises, then, as to whether in some cases the secondary component (assumed to be the less massive) fills this inner surface, as illustrated schematically in Figure 1.[1]

II. THE GROUP OF ABNORMAL SUBGIANTS

The stars of Parenago's list were therefore plotted on a diagram (Fig. 2) for which the abscissa was r_2 (the photometric radius of the secondary), and the ordinate the ratio μ

[1] In the case of contact binaries, the limiting size is given by the zero-velocity surface passing through the second Lagrangian point, L_2, as in the case of β Lyrae. However, if only one star fills the inner surface, a common envelope cannot exist, and one must take the inner surface as that of the swollen star.

of the mass of the secondary to the sum of the masses. On this same diagram a theoretical limiting curve was drawn, giving a lower limit to μ for a given r_2. To define this curve, it was necessary to ascertain that dimension of the inner surface which is measured as the photometric radius. For values of μ greater than 0.2, the mean radius of the inner surface as defined by Kuiper (1941, Table 3*c*) was used. This corresponds to the cube root of three radii defined as the distance from the center of the secondary to the surface, taken, respectively, parallel to the rotation axis, along the interstellar axis (x-axis) away from the primary, and perpendicular to these two. For $\mu < 0.2$ the curve was sketched so as to pass through the point $\mu = 0$, $r_2 = 0$. The theoretical curve is therefore quite rough. It could have been improved by making use of the asymptotic behavior of Kuiper's radius for very small μ. However, the exact location of the curve should not be regarded too seriously for several reasons. First, the curve is not really defined, since the photometric radius of the secondary also depends to some extent on the radius of the primary and on the inclination of the orbit, because of distortion from sphericity. Second, and most important, the data (Fig. 2) indicate that abnormal subgiants (see definition

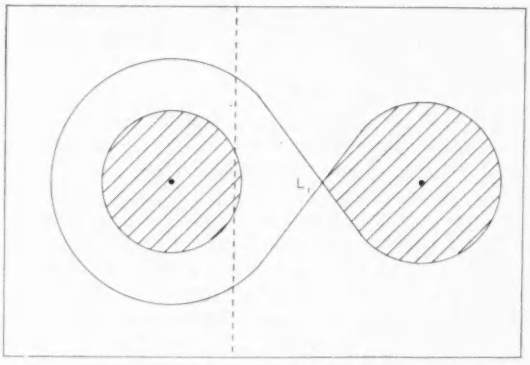

FIG. 1.—Schematic diagram of the zero-velocity surface passing through the inner Lagrangian point L_1, for the case $\mu = 0.25$. Section in xz-plane. Axis of rotation (through center of gravity) shown as broken line. The size of the primary star is drawn arbitrarily.

below) may tend, on the average, to overstep the limiting boundary (perhaps because of the effects of the dynamical equilibrium of the matter lying near the boundary). This indication would, for instance, be accentuated if we had used Wood's (1950) limiting curve, as some subgiants above the curve would cease to be classified as abnormal. It should be emphasized that a quantitative description of these systems is not intended in this paper.

The results of this comparison are shown in Figure 2. It appears that there is a significant separation between the main-sequence secondaries and the subgiant secondaries and, in addition, a tendency for the subgiants to cluster quite near the curve. This suggests that many of the subgiant components do fill the inner surface.

As was mentioned earlier, the position of the points in Figure 2 depends on Parenago's guess as to the mass of the primary. However, the mass function,

$$\frac{\mathfrak{M}_2^3}{(\mathfrak{M}_1 + \mathfrak{M}_2)^2} = \mu^2 \mathfrak{M}_2 ,$$

is known from observation (the inclination of the orbit is obtained from the photometric data). Since the secondary cannot lie below the curve, we can, by placing it on the curve

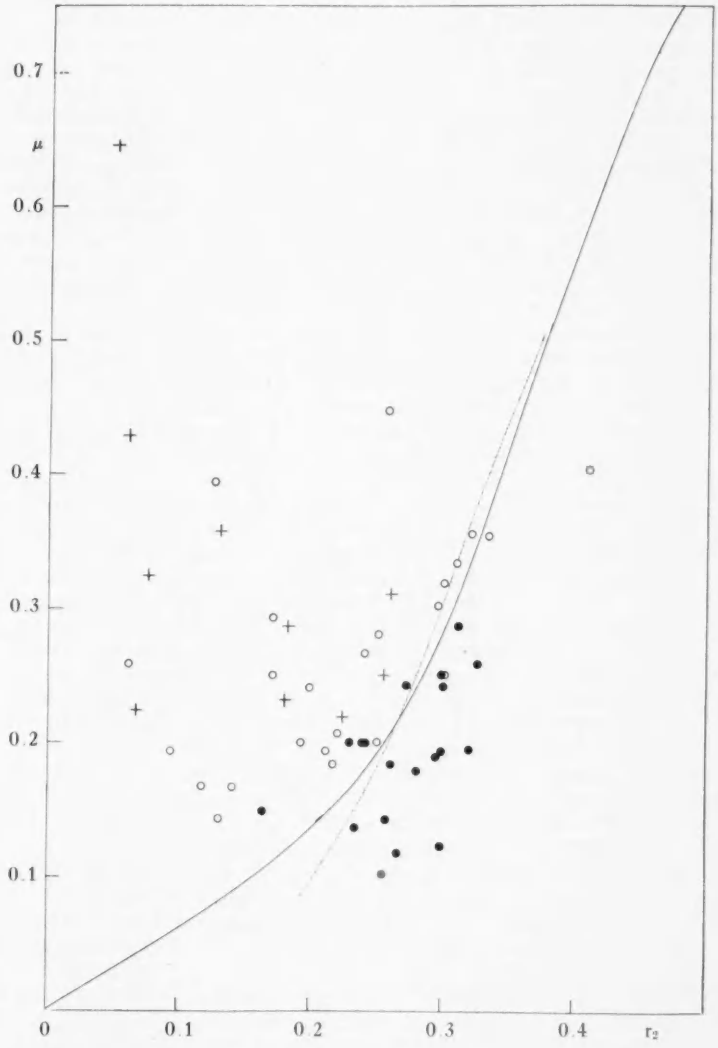

FIG. 2.—The quantity μ is plotted against the photometric radius of the secondary (in units of the semimajor axis of the orbit), r_2, for 53 systems, with the primary on the main sequence. Those with main-sequence secondaries are indicated by crosses. The 18 dots represent subgiant secondaries whose upper mass limit is less than $1\odot$. The open circles are other subgiants. One subdwarf is indicated by a crossed circle. The full curve is the limiting curve as defined in the text. The dotted curve is a limiting curve as defined somewhat differently by F. B. Wood (1950).

obtain a lower limit $\mu_{\min}$ for μ and an upper limit $\mathfrak{M}_{2\,\max}$ to its mass, given by the following expression:

$$\mathfrak{M}_{2\,\max} = \mathfrak{M}_2 \left(\frac{\mu}{\mu_{\min}}\right)^2.$$

This was done for all 53 secondaries. It was found that 19 stars had an upper mass limit less than one solar mass; 18 of these are classified by Parenago as subgiants and are indicated in Figure 2 as black dots (the remaining secondary is listed as a subdwarf). It is evident that they cluster nearer the curve than do the total group of subgiants.

It therefore appears justifiable to suppose that these 18 secondaries actually do lie on the curve, that is to say, fill the inner zero-velocity surface. On the other hand, these stars were chosen because they form a peculiar group, combining subgiant character with small mass ($<1\,\odot$). It is not possible to understand how stars with such small mass could have had enough time in five billion years to reach the advanced stage of evolution suggested by their subgiant characteristics, unless they had originally a very unusual chemical composition not shared by their companions. In the following section a hypothesis which relates the peculiar properties of these stars to the fact that they fill the inner zero-velocity surface will be discussed. First, however, a word should be said about luminosities. Parenago has obtained average luminosities of secondaries by fixing the absolute magnitude of the primary at the average value for main-sequence stars. The observed difference in magnitude and a bolometric correction are then applied to obtain an estimate of the luminosity of the secondary. However, one can do better than this when, as for these 18 stars, the mass of the secondary is known. From the value of $\mu_{\min}$, $\mathfrak{M}_1$ is then obtained. The radii of the two stars are then obtained from Parenago's values of μ, R_1, and R_2, by noting that the products μR_1 and μR_2 are constants directly derivable from the observations. Assigning to the primary an effective temperature corresponding to its spectral type (Kuiper's Tables 3 and 13 were used [1938], as the spectral types are listed in the older notation), the bolometric magnitude of the primary can be obtained. By subtracting the bolometric correction (Kuipei's Table 6) we then obtain a consistent value for the absolute magnitude of the primary and could proceed, as before, to obtain the luminosity of the secondary. The theoretical curve on which this procedure depends is, however, at present somewhat crude.

The absolute magnitudes of the primaries were calculated by the foregoing method. Their masses were also obtained. The results are given in Table 1. Here M_1 and M_2 are the absolute magnitudes of the components; $\Delta\mathfrak{M}_1$ and ΔM_1 are the increments over the values listed by Parenago (main-sequence averages). It was found that, except in one instance, the increase of mass of the primary over the main-sequence average had the same algebraic sign as the increase in luminosity (neglecting any change in the bolometric correction with absolute magnitude for a given spectral type). On the other hand, 13 of the 18 primaries have a mass lower than the main-sequence average, and, of these, 12 lie below the main sequence in luminosity. Because of the small number of stars and some uncertainty as to the position of the theoretical curve, it is not possible to infer that the primaries tend to be systematically underluminous and undermassive. It is essential to note that the masses $\mathfrak{M}_1$ are extremely sensitive to an error in the theoretical curve's position, whereas the values of M_1 are not. The values of $\mathfrak{M}_1$ in Table 1 may therefore be quite wrong in some cases. The data appear to indicate that there is no marked tendency for the primaries to lie above the average main sequence. This is an indication that these systems are comparatively young or average members of population I.

III. EVOLUTIONARY MECHANISM

Let us consider in a general way the evolution of a close binary system subsequent to its formation at a given date by some unknown mechanism. One of the stars will, in

general, be more massive than the other. The more massive star will, from the mass-luminosity relation, be much more luminous and will evolve more rapidly. At a certain point it will acquire an unstable depleted core (Schönberg and Chandrasekhar 1942) and begin to move very rapidly to the right in the H-R diagram (Sandage and Schwarzschild 1952), expanding its radius as it does so. It is then very probable that this expansion will continue until the star fills the inner zero-velocity surface. The star will then continue to expand but will not be able to hold on to the mass that passes out of the surface. This mass will either be collected by the companion or be ejected from the system by centrifugal force, probably depending on whether or not fairly violent ejection mechanisms, such as prominences, dominate. The material lost, lying at the surface of the star, will be rich in hydrogen; and, as mass is lost, the ratio of the mass contained in the depleted core to the total mass of the star will increase. This ratio is a measure of the "biological age" of the star. As this age increases, the expansion will continue. By this mechanism the star can gradually become less massive than its companion and eventually less luminous,

TABLE 1

Star	Sp1	Sp2	$\mathfrak{M}_2$	R_2	$\mathfrak{M}_1$	M_1	$\Delta\mathfrak{M}_1$	ΔM_1	M_2
RZ Cas	A2	.....	0.34	1.82	0.92	+2.1	−2.1	+1.1	+4.3
RS Cep	A5	G	.78	12.62	4.10	+0.8	+2.1	−1.3	+2.1
RW CrB	A8	.....	.62	1.29	3.02	+1.8	+1.2	−0.9	+5.6
WW Cyg	B8	G	.77	4.22	1.43	+1.2	−2.6	+1.7	+4.8
W Del	A0	G5	.29	3.76	1.24	+1.2	−1.8	+1.0	+3.8
Z Dra	A5	.....	.38	1.75	1.52	+2.1	−0.5	+0.1	+4.7
TW Dra	A6	K2	.68	3.69	1.51	+1.3	−0.5	−0.9	+3.5
RW Gem	B6	F0	.58	3.95	1.49	+0.3	−3.5	+1.5	+2.0
TT Her	A2	.....	.97	1.98	3.44	+0.1	+0.9	−1.0	+5.1
AK Her	F8	.....	.32	0.72	0.82	+4.0	−0.4	+1.7	+4.2
Y Leo	A3	.....	.52	2.15	1.34	+2.0	−0.9	+0.6	+5.2
T LMi	A0	.....	.13	1.91	0.49	+1.6	−2.5	+0.1	+4.7
Z Ori	B4	.....	.59	4.78	1.20	−1.2	−5.8	+0.7	+1.6
RT Per	dF2	.....	.21	1.01	0.70	+3.7	−0.9	+0.4	+5.5
RW Per	A5	gG0	.78	8.03	7.02	+0.7	+5.0	−1.3	+2.7
ST Per	A3	G–K	.23	1.85	1.12	+2.0	−1.1	+0.5	+4.1
Y Psc	A3	K0	.69	3.88	3.36	+1.1	+1.4	−0.4	+5.1
RZ Sct	B2	.....	0.27	7.68	0.69	−1.6	−9.3	+1.3	+0.6

becoming the secondary component. It should be noted that if the star lies wholly inside the zero-velocity surface without losing mass, the dimensions of this surface will not alter. There is therefore no possibility of the surface itself expanding faster than the star. The dimensions of the surface will, of course, change as the mass ratio continuously decreases. The exact manner of this change will depend on the extent to which angular momentum is conserved in the system, i.e., the extent to which mass is exchanged or lost from the system. The main features of the 18 stars—low mass and subgiant character—seem to be qualitatively explained on the basis of the foregoing evolutionary mechanism. Conversely, one should not expect to find stars of this type among the single subgiants or the subgiant components of visual binary systems.

The fact that the peculiar stars are found only among the secondaries can perhaps be accounted for by remarking that the greater the fraction of mass a star has lost in this way, the more peculiar it will become and the greater chance it will have of being so classified. In addition, the amount of time spent in the lower-mass region is probably greater, so that there is more of a chance of observing a peculiar subgiant when it has lost considerable mass and probably become the secondary component of its system. An important question which is difficult to decide is whether or not mass is exchanged between

the components. If so, the primary star would constantly have been receiving hydrogen-rich material from the outside and thus be kept "rejuvenated." The existence of such a process might enable one to attribute a greater age to such a system than is indicated by the early spectral type and moderate luminosity of the primary star.

In conclusion, we wish to cite an important paper by F. B. Wood (1950), in which a more detailed discussion of the mass-ejection mechanism in eclipsing binary systems is to be found. In this work Wood discusses the period fluctuations of eclipsing binaries and finds that they are associated with the same phenomenon (filling of the inner zero-velocity surface by the secondary component) as described here.

The writer desires to express his thanks to Professor O. Struve for stimulating this investigation, and to Professor H. Weaver and Dr. K. Franklin for helpful discussions.

REFERENCES

Kuiper, G. P. 1938, *Ap. J.*, **88,** 429–471.
———. 1941, *ibid.*, **93,** 133–177.
Moulton, F. R. 1914, *Celestial Mechanics* (2d ed.; New York: Macmillan Co.), p. 281.
Parenago, P. P. 1950, *Astr. Zhur.*, **27,** 41–47.
Sandage, A. R., and Schwarzschild, M. 1952, *Ap. J.*, **116,** 463–476.
Schönberg, M., and Chandrasekhar, S. 1942, *Ap. J.*, **96,** 161–172.
Struve, O. 1953, Les processus nucléaires dans les astres, *Mém. Soc. R. de Liége*, 4th Ser., **14,** 236–253.
Struve, O., and Gould, N. 1954, *Pub. A.S.P.*, **66,** No. 388, 28–31.
Wood, F. B. 1950, *Ap. J.*, **112,** 196–206.

A SPECTROSCOPIC STUDY OF THE DOUBLE STAR DELTA EQUULEI

WILLIAM H. WEHLAU*
Berkeley Astronomical Department, University of California
Received July 3, 1954

ABSTRACT

Curves of growth for the two components of δ Equulei, constructed from the resolved and unblended *Fe* I lines, and a direct comparison of the equivalent widths are discussed. The parameters of the curves of growth and the abundances of the elements in the atmospheres are found to be equal. Excitation and ionization temperatures, derived on the assumption that the electron pressures are the same, showed no differences. The formation of binaries with such similar components on the assumption of random selection of the components is shown to be unlikely.

Delta Equulei is a binary with a well-determined visual orbit. Data on the system are summarized in Table 1. The radial-velocity observations are not adequate for an independent determination of the orbit but suffice to determine the masses of the components. The difference in magnitude is difficult to measure because of the narrow separation of the components.

TABLE 1

PARAMETERS OF DELTA EQUULEI

Period	5.72 years	Magnitude difference	0.0–0.1 mag.†
Mass (total)	$3.6\odot$	Spectral type	F8 V‡
Mass ratio	1.03*	Abs. mag. (each component)	+3.9

* W. Luyten and E. Ebbighausen, *Pub. Astr. Obs. U. Minnesota*, **2**, No. 1, 25, 1934; P. van de Kamp and S. L. Lippencott, *A.J.*, **51**, 162, 1945.

† G. P. Kuiper, *Ap. J.*, **88**, 477, 1938; W. S. Finsen, *Circ. Union Obs., Johannesburg*, No. 112, p. 104, 1951.

‡ N. G. Roman, *Ap. J.*, **112**, 554, 1950.

On July 7, 1952, a spectrogram with a dispersion of 2.8 A/mm was obtained by Dr. O. Struve at the Mount Wilson Observatory. The lines are double and the components are well separated. The radial velocities of the two components are

$$V_v = -26.55\,, \quad V_r = -3.12\,.$$

The subscripts v and r refer to the violet and red components as observed on July 7, 1952. The difference in the velocities is almost twice the value predicted from the elements of the visual orbit (Luyten and Ebbighausen 1934) and the radial velocities determined at the Lick Observatory (Campbell and Moore 1928). This discrepancy can be attributed to small uncertainties in the elements of the visual orbit. The predicted and observed values can be brought into agreement if the period is taken as 5.72 years and the time of periastron passage as 1912.86. These elements adequately represent the visual double-star observations as well as the radial-velocity data. The mass ratio obtained from the Lick Observatory radial velocities is in the sense that the component giving rise to the lines displaced to the violet is the more massive, although the masses of the components are equal within the uncertainties in the measurements.

In order to compare the atmospheres of the two stars, visual estimates of line intensities were made for about 500 lines in the wave-length range 3850–4626 A. The intensities

* Now at the Warner and Swasey Observatory, Case Institute of Technology.

of the lines of each spectrum are reduced by the continuum of the other component. In addition, undetected absorption lines in one spectrum which happen to fall on lines of the other spectrum produce a scattering in the observed intensities. The degree of blending of each line was estimated by comparing the spectrum of δ Equulei and the very similar spectrum of Procyon. The identifications of the lines are taken from J. Swensson's (1946) study of Procyon. The comparison indicated that the lines shifted to the violet are slightly weaker than the ones shifted to the red. This difference appeared to be independent of the excitation potential, the stage of ionization, and the element producing the line.

To obtain a quantitative estimate of the differences in the spectra, equivalent widths for some of the lines which showed little or no blending were obtained from a microphotometer tracing of the plate. A number of additional *Fe* I lines were measured to improve the determination of the curves of growth. Since the features to be compared are always very similar and close to one another, the photometric errors, with the exception of plate-grain and local sensitivity effects, influence each component in the same way and do not affect the final result.

The equivalent widths of most lines were determined by the triangle approximation, which was calibrated by comparing the values for 28 of the lines with the values obtained by using the profiles for these lines. The equivalent widths of the stronger lines were obtained by planimetering the areas under the profiles. Since these lines are blended, the values obtained are less reliable than those for the weaker lines. The values determined for log W/λ in units of 10^{-6} are listed in Table 2. The weights depend upon the visual estimates of the blending and the appearance on the tracing.

The equivalent widths of the *Fe* I lines were used with K. O. Wright's (1948) solar log X_f-values to plot curves of growth for both components. These empirical curves were fitted with theoretical curves based on those published by Wright. It was found that both empirical curves could be fitted by using the same theoretical curve. These curves are shown in Figure 1, where the log X_f-values have been corrected for the difference in temperature between the sun and δ Equulei. The parameters of the curves of growth are listed in Table 3. The ratios of the number of *Fe* I atoms in the atmospheres of δ Equulei to the number in the atmosphere of the sun were obtained by correcting the horizontal displacements of the empirical curves of growth relative to the theoretical curve for the differences in the turbulent velocities of δ Equulei and the sun. The logarithms of these ratios, uncorrected for the differences in the continuous opacity, are listed in Table 3 as $\Delta \log X$. The provisional parameters determined by A. Pannekoek and G. B. van Albada (1946) are also given in the same table, where the value of v has been computed from their value of b. Both log s_0/k (sun/star) and $\Delta \log X$ give the logarithm of the ratio of the number of neutral atoms in the sun to the number in the star. The difference in these values is large, but the uncertainty in the determination of the curves of growth for the faint lines may be sufficient to account for the discrepancy.

The excitation temperatures of the two stars were determined by measuring the deviation, log X − log X_f, from the curve of growth and solving the equation

$$\log X - \log X_f = \chi_i 5040\left(\frac{1}{T_\odot} - \frac{1}{T_*}\right) + \text{constant}$$

by least squares. A separate solution for the difference in the temperatures of the two stars was made, using only those *Fe* I lines which were considered free from blending on visual inspection. The value obtained is

$$T_r - T_v = +72^\circ \pm 143^\circ .$$

TABLE 2

EQUIVALENT WIDTHS OF δ EQUULEI

λ	Elem.	Wt.	log W/λ		λ	Elem.	Wt.	log W/λ	
			v	r				v	r
3865.53	Fe I	2	1.52	1.54	4188.72	.....	2	0.88	1.18
3900.55	Ti II	2	1.42	1.53	4191.43	Fe I	1	1.16	.....
3922.93	Fe I	2	1.53	1.54	4191.68	Fe I	1	.....	1.08
3951.95	V II	2	1.11	1.18	4199.94	Fe I	2	1.16	0.86
3960.28	Fe I	1	0.92	0.84	4202.04	Fe I	2	1.35	1.46
3977.76	Fe I	2	1.14	1.28	4208.60	Fe I	1	1.35	.....
3985.38	Fe I	2	1.12	1.04	4213.64	Fe I	2	1.03	1.07
4002.94	V II	2	0.89	0.70	4216.20	Fe I	1	1.23	0.99
4014.54	Fe I	2	1.25	1.26	4219.37	Fe I	2	1.24	1.19
4016.43	Fe I	2	0.71	0.81	4222.22	Fe I	2	1.08	1.23
4021.89	Fe I	2	1.33	1.39	4231.02	CH	2	0.72	0.78
4023.39	V II	2	0.90	1.00	4233.61	Fe I	1	.....	1.22
4028.35	Ti II	2	1.15	1.18	4235.94	Fe I	1	1.51	1.54
4034.49	Mn I	2	1.45	1.42	4241.15	Fe I	1	0.88	0.67
4044.59	Fe I	2	1.05	1.21	4247.42	Fe I	1	1.34	1.31
4049.35	Fe I	1	0.87	0.96	4250.13	Fe I	2	1.39	1.39
4059.72	Fe I	2	1.09	1.01	4250.80	Fe I	2	1.48	1.45
4062.46	Fe I	1	1.08	1.07	4252.66	Cr II	1	0.87	0.94
4065.38	Fe I	2	1.00	0.94	4260.07	Fe I	1	1.39	.....
4067.99	Fe I	2	1.27	1.13	4260.50	Fe I	1	.....	1.62
4070.78	Fe I	1	0.96	1.09	4271.16	Fe I	1	1.54	1.69
4072.52	Fe I	1	.....	0.88	4271.77	Fe I	1	1.53	1.56
4073.77	Fe I	2	1.10	1.11	4276.69	Fe I	2	0.51	0.69
4082.11	Fe I	1	0.88	.....	4282.41	Fe I	1	1.15	1.32
4084.50	Fe I	1	1.20	.....	4291.46	Fe I	1	.....	0.95
4085.30	Fe I	1	.....	1.23	4293.10	Zr II	2	0.90	1.06
4087.11	Fe I	1	1.10	1.04	4316.81	Ti II	2	0.55	0.83
4091.56	Fe I	1	0.67	0.77	4318.66	Ca I	2	1.15	1.24
4107.49	Fe I	2	1.13	1.29	4346.57	Fe I	2	1.04	0.90
4114.46	Fe I	2	1.04	.....	4347.24	Fe I	1	0.44	0.36
4120.22	Fe I	2	1.12	1.10	4347.87	Fe I	2	0.81	0.91
4132.04	Fe I	1	1.55	1.68	4349.01	Fe I	2	0.68	0.64
4132.91	Fe I	1	1.49	1.17	4352.75	Fe I	2	1.25	1.20
4133.85	Fe I	1	1.08	1.15	4355.91	Ni I	2	0.69	0.86
4136.53	Fe I	1	0.64	.....	4359.65	Cr I	2	1.26	1.23
4139.94	Fe I	1	0.83	.....	4365.90	Fe I	2	0.40	0.40
4141.86	Fe I	1	0.76	.....	4375.95	Fe I	2	1.20	1.15
4143.44	Fe I	1	1.41	.....	4379.26	V I	2	0.93	0.93
4143.88	Fe I	1	.....	1.52	4389.24	Fe I	2	0.88	0.85
4147.69	Fe I	2	.....	1.17	4413.60	Fe II	1	0.38	0.66
4154.51	Fe I	1	1.19	.....	4415.15	Fe I	1	1.39	.....
4156.78	Fe I	1	.....	1.33	4415.57	Sc II	1	.....	1.10
4157.78	Fe I	2	1.17	1.27	4416.83	Fe II	2	0.92	0.94
4160.35	Fe II	2	0.94	0.97	4417.74	Ti II	2	1.10	1.09
4163.65	Ti II	2	1.11	1.17	4427.31	Fe I	1	1.15	1.22
4170.97	Fe I	2	1.22	1.27	4430.64	Fe I	1	1.15	1.20
4174.91	Fe I	2	1.22	1.21	4439.87	Fe I	1	0.39	0.47
4175.64	Fe I	2	1.10	1.16	4442.34	Fe I	1	1.10	1.34
4176.57	Fe I	2	1.06	1.12	4447.73	Fe I	1	1.00	1.08
4187.05	Fe I	1	1.39	1.32	4457.49	Ti I	2	0.88	0.95

TABLE 2—*Continued*

λ	Elem.	Wt.	log W/λ		λ	Elem.	Wt.	log W/λ	
			v	r				v	r
4468.50	*Ti* II	2	1.09	1.16	4558.66	*Cr* II	2	1.11	0.91
4476.04	*Fe* I	2	1.21	1.16	4563.77	*Ti* II	2	1.21	1.24
4485.69	*Fe* I	2	0.85	0.88	4571.98	*Ti* II	2	1.39	1.20
4491.41	*Fe* II	2	0.87	0.80	4576.34	*Fe* II	2	0.90	0.83
4496.88	*Cr* I	2	1.03	1.07	4578.55	*Ca* I	2	0.53	0.81
4501.26	*Ti* II	2	1.14	1.21	4580.93	*Cr* I	1	0.97	1.09
4502.22	*Mn* I	2	0.59	0.75	4582.85	*Fe* II	2	0.90	0.93
4504.78	*Fe* I	1	0.46	0.55	4588.21	*Cr* II	2	0.93	0.94
4508.29	*Fe* II	2	0.99	1.02	4589.95	*Ti* II	2	0.77	0.91
4515.34	*Fe* II	2	1.09	1.05	4602.02	*Fe* I	2	0.72	0.72
4517.54	*Fe* I	1	0.89	0.97	4602.95	*Fe* I	2	1.06	1.05
4520.23	*Fe* II	2	1.13	1.10	4607.64	*Fe* I	2	1.08	0.96
4534.80	*Ti* I	1	0.93	0.91	4611.28	*Fe* I	2	1.03	1.05
4541.54	*Fe* II	2	0.91	0.84	4620.54	*Fe* II	2	0.80	0.81
4542.43	*Fe* I	2	0.49	0.52	4625.05	*Fe* I	1	0.73	0.89
4545.96	*Cr* I	2	0.84	0.90	4637.51	*Fe* I	1	0.85	.....
4547.84	*Fe* I	2	0.69	0.77	4647.42	*Fe* I	1	.....	1.17
4552.44	*Ti* I	1	1.11	1.11	4662.00	*Fe* I	1	0.48	0.75
4554.05	*Ba* II	2	1.29	1.34	4691.42	*Fe* I	1	1.04	1.14
4555.00	*Cr* II	2	0.83	0.83	4710.27	*Fe* I	1	.....	0.82
					4736.79	*Fe* I	1	1.06	1.26

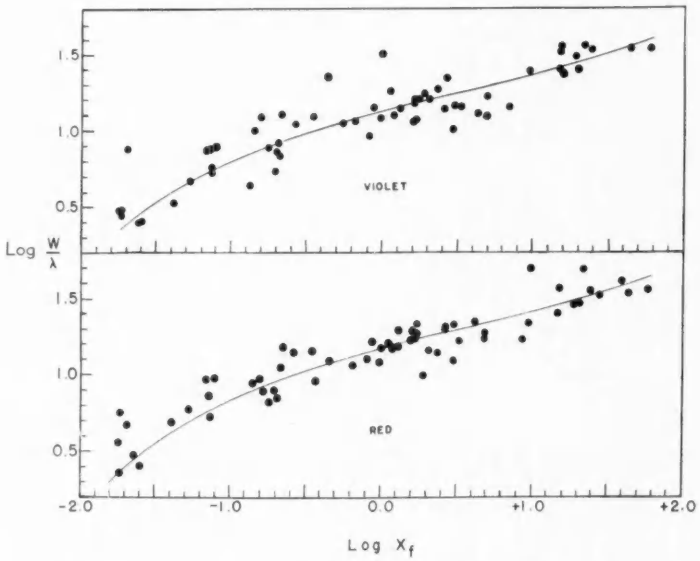

FIG. 1.—Curves of growth of *Fe* I for the components of δ Equulei

Another estimate of the temperature difference was obtained by comparing the ionization in the two stars. Since both stars lie on the main sequence, the electron pressures were assumed to be equal. Saha's equation was used, and the following mean difference obtained:

$$T_r - T_v = -29° \pm 42° .$$

The temperatures of the two stars are equal within the uncertainties.

To compare the equivalent widths more directly, the value of log W/λ for each *Fe* I line in one star was plotted against the value for the same line in the other star. If the two stars have identical spectra, the expected relation will be a straight line passing through the origin for a magnitude difference of zero. If any of the parameters which

TABLE 3

THE CURVE OF GROWTH

	Violet	Red	Pannekoek and van Albada
T	$5097° \pm 170°$	$5344° \pm 139°$	.....
v	2.4 km/sec		3.7 km/sec
Γ/ν	1.2×10^{-6}		.....
Γ/γ_{el}	7.4		16.6
$\Delta \log X$	−0.58	−0.53	.....
log s_0/k sun/star (atomic lines)	.....	.....	2.7

characterize the atmospheres differ, the relation between the equivalent widths becomes more complex. For the very weak or very strong lines of the same excitation potential, the curves would again be straight lines with slopes of 45°. The intercepts on the axes depend in a simple way on the differences in the magnitude, the excitation temperature, the number of atoms producing the lines, and, for strong lines, the values of $Z = (\Gamma/\nu)\ (v/c)$. No such simple relations exist for the lines of intermediate strength; however, theoretical curves may be easily constructed from the published curves of growth. In Figure 2 theoretical curves are shown for the following assumed differences in the parameters:

I: No differences ;

II: $\log \frac{N_r}{N_v} = 0.4$;

III: $\log \frac{N_r}{N_v} = 0.2$, $\log \frac{v_r}{v_v} = -0.2$;

IV: $\log \frac{N_r}{N_v} = -0.2$, $\log \frac{v_r}{v_v} = -0.2$,

where N is the number of atoms and v is the velocity parameter. In comparing the curves with the observed points, it should be remembered that there may be as much as 0.1 mag. difference between the two stars. This would correspond to a horizontal or vertical shift of the theoretical curves relative to the observational one of 0.04 in log W/λ. A comparison of the theoretical curves with the observational points indicates that the observations are consistent with the assumption that the curves of growth for the two stars are identical. However, the scatter in the points and the uncertainty in the magnitude difference allow a ratio of the number of atoms of *Fe* I as large as 1.5.

Since the temperatures are equal within the errors of measurement, the values of log X for each line read from the curves of growth are a direct measure of the relative abundances of the elements in the atmospheres. The ratios of the abundances thus derived are given in Table 4. There appears to be no evidence for any difference in abundances of the elements studied in the two stars. But, as stated above, the uncertainty in the difference in the magnitudes of the two stars leads to an uncertainty in the difference of the amount of *Fe* I present in the atmospheres of the two stars. Since the other elements were assumed to follow the same curves of growth as does *Fe* I, any error in these curves affects the determined abundances in the same manner as it affects *Fe* I.

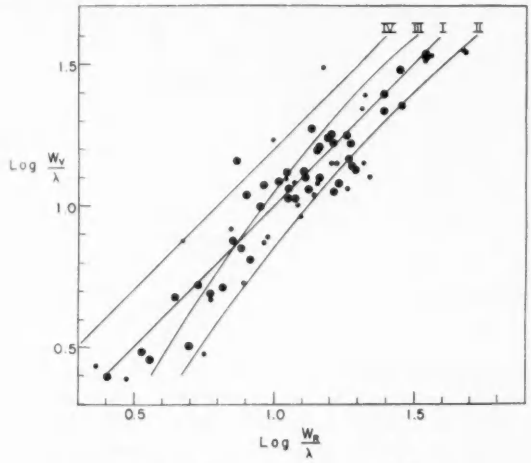

FIG. 2.—Direct comparison of the equivalent widths of *Fe* I for δ Equulei. The curves are theoretical relations explained in the text.

TABLE 4

ABUNDANCE RATIOS

Element	No. Lines	n_r/n_v	Element	No. Lines	n_r/n_v
Fe I	50	0.89±0.06	*Zr* II	1	2.46±....
Fe II	11	0.76± .05	*Ca* I	2	2.19±0.40
Ti I	3	0.93± .11	*Cr* I	4	0.91± .15
Ti II	10	1.12± .18	*Cr* II	4	0.55± .16
V I	1	0.81±....	*Ba* II	1	1.35±....
V II	3	2.14±0.49	*Mn* I	2	1.02±0.38

To obtain the difference in magnitude, the mean ratios of the equivalent widths were computed, with the following results:

$$Fe\ \text{I}: \frac{W_r}{W_v} = 1.048 \pm 0.021,$$

$$\text{All lines}: \frac{W_r}{W_v} = 1.075 \pm 0.017,$$

which correspond to differences in magnitude:

$$Fe\ \text{I}: m_v - m_r = +0.051 \pm 0.021\ ,$$
$$\text{All lines}: m_v - m_r = +0.079 \pm 0.017\ .$$

The star giving rise to the violet component appears to be less luminous than the one giving rise to the red component. In a study of γ Virginis Mrs. Gould (1952) found a difference in the ionization temperatures of the two components of 300°, while the observed difference in apparent magnitude, 0.03 mag., is consistent with a temperature difference of 30°.

It is of interest to compute the probability of finding a binary system with two components as nearly alike as δ Equulei among those systems which are accessible to observations of the type used in this discussion. For the formation of binary systems, the assumption may be made that the components are selected at random from the stars found in a unit volume of space in the vicinity of the sun and are combined to form pairs. The probability of finding a system for which the components differ by less than 0.1 mag. and less than 1 spectral subclass, corresponding to the temperature difference found, and with the primary brighter than a given apparent magnitude may be computed from the Hess diagram. This probability, P, may be evaluated from the formula

$$P = \sum \left[\frac{N(M, S)}{\Sigma N(M, S)} \frac{N(M, S \mid m < m_0)}{\Sigma N(M, S \mid m < m_0)} \right],$$

where $N(M, S)$ is the number of stars in the Hess diagram within an interval $\Delta M \Delta S$ around the point M, S; and $N(M, S \mid m < m_0)$ is the number of stars in the H-R diagram for stars brighter than apparent magnitude m_0 within an interval $\Delta M \Delta S$ around the point M, S.

The value of P obtained by using the Hess diagram given by C. Lonnqvist (1927) is 4×10^{-5}. The probability of finding even one such system as δ Equulei among the stars brighter than apparent magnitude 6 is small if the binary systems are formed by random selection. P. Muller (1951) lists four systems differing in magnitude by less than 0.10 and for which the spectral types are the same. In addition, two other systems are listed, for which spectral types of the individual stars are not available because of the narrow separation. Although the computations are based on the rather uncertain form of the Hess diagram, it seems unlikely that this uncertainty is sufficient to account for the discrepancy between the number of systems expected on the hypothesis of random formation and the number actually found.

It is a pleasure to thank Dr. O. Struve and Dr. H. F. Weaver for their advice and encouragement in this study.

REFERENCES

Campbell, W. W., and Moore, J. H. 1928, *Pub. Lick Obs.*, **16**, 311.
Gould, N. 1952, *A.J.*, **57**, 160.
Lonnqvist, C. 1927, *Meddel. Astr. Obs. Upsala*, No. 25.
Luyten, W., and Ebbighausen, E. 1934. *Pub. Astr. Obs. U. Minnesota*, **2**, No. 1, 25.
Muller, P. 1951, *Ann. Obs. Strasbourg*, Vol. **5**, No. 3.
Pannekoek, A., and van Albada, G. B. 1946, *Pub. Astr. Inst. U. Amsterdam*, No. 6, Part 2, p. 25.
Swensson, J. 1946, *Ap. J.*, **103**, 207.
Wright, K. O. 1948, *Pub. Dom. Ap. Obs. Victoria*, Vol. **8**, No. 1.

STUDY OF DOPPLER VELOCITIES IN STELLAR ATMOSPHERES THE SPECTRUM OF ALPHA CYGNI*

SU-SHU HUANG AND OTTO STRUVE
Berkeley Astronomical Department, University of California
Received July 3, 1954; revised August 9, 1954

ABSTRACT

In this paper the applicability of the curve of line-width correlation is rigorously examined. It is found that the curve can be used for most practical cases. Next, new methods are advanced for the study of Doppler velocity in stellar atmospheres. These methods emphasize the use of the profiles of weak lines. Calculation shows that the slope of the central-depth versus equivalent-width curve at the origin is a function of Doppler velocities. Consequently, Doppler velocities can be derived from a measurement of the slope. The limiting value of the half-width of very weak lines can be used in the same way. A coudé spectrogram of α Cygni was obtained and analyzed. The Doppler velocities in its atmosphere are investigated according to the methods mentioned above, the final results being given in Table 5. It appears from the empirical plot between central depths and equivalent widths that there might exist stratification of Doppler velocities in the atmosphere.

The present methods have also been applied to ρ Leonis and δ Canis Majoris, with results agreeing very well with the previous determinations.

I. SOME REMARKS ON THE CURVE OF LINE-WIDTH CORRELATION

In connection with a study of Doppler velocities in stellar atmospheres, we have previously developed a method of the so-called "curve of line-width correlation" (Huang and Struve 1952). By this method the Doppler velocities of both large and small eddies can be conveniently determined, provided that the broadening by macroscopic motion does not seriously alter the form of the original profile of the absorption line. This method was later used by Ruth F. Kilby (1953) in the study of ε Aurigae. She found that the small-scale turbulence determined by the curve of line-width correlation decreases with increasing excitation, a result agreeing with that which K. O. Wright and E. Van Dien (1949) obtained by means of the curve of growth. Mrs. Kilby further pointed out that for low excitation potentials the values found by means of the curve of line-width correlation are generally higher than Wright's, the disagreement being greater, on the whole, for lower excitation potentials. In the following paragraphs a more general formulation of the curve of line-width correlation is given, and the domain of its applicability is discussed.

Following a previous paper (Huang and Struve 1952), we use M. Minnaert's interpolation formula (1935) for the line profile before the line is broadened by the macroscopic motion:

$$R(v) = \frac{R_c x(v)}{R_c + x(v)}, \tag{1}$$

where

$$\frac{x(v)}{R_c} = \alpha Z H(v, a) . \tag{2}$$

In equations (1) and (2) the difference of frequency, v, from the center of an absorption line is measured in units of the Doppler width corresponding to the random velocity, ξ_s, of small eddies. The meaning of the other notations follows that given in the previous

* The observational material used in this investigation was obtained by Mr. Struve as guest investigator at the Mount Wilson Observatory; the theoretical discussion is by Mr. Huang.

paper. If $B(v)$ represents the normalized broadening function corresponding to the large-scale motion, the observed profile will be

$$R'(v) = \int_{-\infty}^{\infty} R(v - v')\, B(v')\, dv'. \tag{3}$$

The half-half-width, $v_{1/2}$, of a line should therefore be the root of the following equation:

$$\int_{-\infty}^{\infty} \frac{H(v, a)\, B(v_{1/2} - v)}{1 + aZH(v, a)}\, dv = \frac{1}{2} \int_{-\infty}^{\infty} \frac{H(v, a)\, B(v)}{1 + aZH(v, a)}\, dv. \tag{4}$$

Let us assume that the velocity distribution of large eddies is given by a Gaussian function (Unsöld and Struve 1949); hence

$$B(v) = \frac{\gamma}{\sqrt{\pi}}\, e^{-\gamma^2 v^2}, \tag{5}$$

where

$$\gamma = \frac{\xi_s}{\xi_l} \tag{6}$$

is the ratio of the random velocity of small eddies to that of large eddies. Substituting equation (5) in equation (4) and neglecting $1/\gamma^2$ and higher-order quantities, we obtain

$$\frac{H(v_{1/2}, a)}{1 + aZH(v_{1/2}, a)} - \frac{1}{2} \frac{H(0, a)}{1 + aZH(0, a)} = 0, \tag{7}$$

from which we computed $v_{1/2}$ in the previous paper. In other words, the curve of line-width correlation was computed for the case in which only a small amount of broadening by macroscopic motion is present. As the macroscopic motion becomes greater and greater, the form of the curve of line-width correlation changes accordingly. In principle we can compute a family of such curves corresponding to a series of values of γ, but the calculation involved is too tedious to be carried out. As a matter of fact, if γ is not too small, the curve of line-width correlation should retain its general shape: for weak lines the original profile can be approximated by a Gaussian curve. Hence the equivalent width is determined by the turbulent velocity ξ_s of small eddies, while the half-width is determined by the combined velocity $(\xi_s^2 + \xi_l^2)^{1/2}$ of both eddies. Therefore, the position and the shape of the nearly vertical branch of the curve of line-width correlation remain unchanged, because in using the curve we take the Doppler width corresponding to $(\xi_s^2 + \xi_l^2)^{1/2}$ as the unit for measuring the half-width, while we take the Doppler width corresponding to ξ_s as the unit for measuring the equivalent width. When the effect of damping dominates the line, the half-width becomes much larger than the Doppler width corresponding to ξ_l, and both half-width and equivalent width are determined by ξ_s, since the broadening effect of the macroscopic motion on the half-width will then be small. Hence the velocity factor which determines the half-width changes from $(\xi_s^2 + \xi_l^2)^{1/2}$ to ξ_s as the equivalent width increases from zero to infinity. In the theoretical curve of line-width correlation we have taken the Doppler width corresponding to $(\xi_s^2 + \xi_l^2)^{1/2}$ as a measure of the half-width; hence we have overestimated the half-width on the damping branch of the theoretical curve. The overestimation for extremely strong lines is $\frac{1}{2} \log [1 + (\xi_l/\xi_s)^2]$. In other words, the upper damping branch of the theoretical curve should move toward the left as γ decreases, while the vertical branch remains unmoved in the diagram. Different points on the intermediate portion of the theoretical curve should move toward the left a distance between zero and $\frac{1}{2} \log [1 + (\xi_l/\xi_s)^2]$; the higher the point, the more it should be displaced. The exact amount of displacement can, of course, be obtained only by actual calculation. Figure 1 shows qualitatively the present

argument. The solid line represents the curve for very large γ, and the broken line represents the curve that would be expected for smaller γ. Consequently, if we consider only the vertical and lower transition portion of the curve, the difference between the theoretical curve published in the previous paper and curves corresponding to any γ larger than, or of the same order of magnitude as, unity will be small. Hence we can use the published curve for all cases where $\gamma \gtrapprox 1$.

From the illustration given in Figure 1 we can see immediately that the value $(\xi_s^2 + \xi_l^2)^{1/2}$ determined by the published theoretical curve of line-width correlation is good for any value of γ, since it is the vertical branch which determines this quantity. But we slightly overestimate the turbulent velocity ξ_s of small eddies, if we use the theoretical curve corresponding to large γ as the standard of comparison when the actual value of

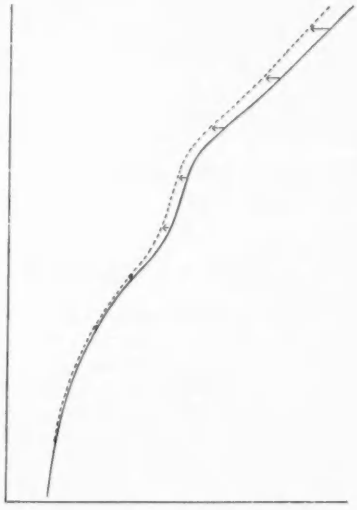

FIG. 1.—Change of the form of the curve of line-width correlation with increase of broadening by mass motion. The solid line represents the curve for small broadening by mass motion. As mass motion becomes larger and larger, the curve changes shape in the direction shown by the arrow; but the lower part of the curve, which is important in the actual application, does not alter very much. The figure shows only the qualitative behavior of the curve; hence no scale is given.

γ is of the order of unity. This is because ξ_s is determined by the transition branch of the curve. The difference will be small if we use only the lower part of the transition branch, as is the case for α Cygni.

For the convenience of anyone using the curve of line-width correlation, we publish its numerical values here in Table 1. In it we have denoted $A_\lambda/(2R_c\Delta\lambda_D)$ by V; hence the relation between V and Z simply represents the curve of growth based on formula (1) (Menzel 1936; Unsöld 1938), while the relation between $v_{1/2}$ and V shows the curve of line-width correlation.

If the macroscopic motion in a stellar atmosphere is extremely large, its velocity can be easily determined by a different method proposed by us in another paper (Huang and Struve 1953). Hence the most unsatisfactory case is the one in which ξ_l is comparable with ξ_s. Unfortunately, the spectrum of α Cygni falls into this category, and we shall devise a new method for investigating the Doppler velocity in its atmosphere. As a

matter of fact, the method developed here is very general and therefore can be used with accuracy in any case, although it does not give so much information as the two methods mentioned previously.

II. CHANGE OF LINE DEPTH WITH EQUIVALENT WIDTH

The central depth of an absorption line has been considered by J. A. Carroll (1928) in his investigation on stellar rotation. He expressed the projection of rotational velocity of a star on the line of sight, ξ_r, in terms of the central depth of the original line, $R(0)$, and the second derivative of the observed profile evaluated at the central point $(d^2R'/dv^2)_0$. Also, M. Schwarzschild and his associates (M. and B. Schwarzschild and W. S.

TABLE 1

THE CURVE OF LINE-WIDTH CORRELATION

LOG Z	$a=0$		$a=10^{-4}$		$a=10^{-3}$		$a=10^{-2}$	
	log $v_{1/2}$	log V	log $v_{1/2}$	log V	log $v_{1/2}$	log V	log $v_{1/2}$	log V
−0.8	−0.076	−1.886						
−0.4	− .073	−1.494						
0	− .064	−1.109						
+0.4	− .045	−0.747					−0.046	−0.747
+0.8	− .010	−0.427					−0.010	−0.426
+1.2	+ .051	−0.170					+0.052	−0.169
+1.6	+ .124	+0.014					+0.125	+0.018
+2.0	+ .195	+0.141					+0.196	+0.146
+2.4	+ .255	+0.228			0.255	0.229	+0.258	+0.240
+2.8	+ .310	+0.292			0.310	0.293	+0.314	+0.308
+3.2	+ .352	+0.340			0.354	0.343	+0.360	+0.377
+3.6	+ .389	+0.380	0.389	0.381	0.391	0.387	+0.400	+0.451
+4.0	+ .420	+0.414	0.420	0.415	0.422	0.429	+0.440	+0.545
+4.4	+ .448	+0.442	0.448	0.445	0.450	0.476	+0.494	+0.670
+4.8	+ .473	+0.467	0.473	0.475	0.477	0.536	+0.631	+0.833
+5.2	+ .496	+0.489	0.496	0.509	0.506	0.630	+0.822	+1.022
+5.6	+ .514	+0.509	0.514	0.550	0.559	0.762	+1.016	+1.210
+6.0	+ .532	+0.528	0.538	0.614	0.725	0.938	+1.210	+1.408
+6.4	+ .550	+0.545	0.564	0.710	0.917	1.113	+1.410	+1.607
+6.8	+ .565	+0.561	0.631	0.852	1.110	1.310	+1.610	+1.807
+7.2	+ .580	+0.575	0.822	1.022	1.310	1.507	+1.810	+2.007
+7.6	+ .594	+0.589	1.016	1.210	1.510	1.707	+2.010	+2.207
+8.0	+0.605	+0.602	1.210	1.402	1.710	1.907	+2.210	+2.407

Adams 1948; M. and B. Schwarzschild 1950) have investigated the dependence of the central depth of absorption lines on the number of absorbing atoms.

Here we shall investigate the effect of large-scale motion upon the relationship between the central depth of a line and its equivalent width. Let us use equation (1) as the formula for the original profile. We are aware that, because of incoherent scattering, etc., few intensity formulae correctly predict the central intensity of a strong line. But if we want only to illustrate the qualitative effect of the macroscopic motion on the central intensity, equation (1) will be adequate. The original profile is then broadened by macroscopic motion according to equation (3). Two possible broadening functions will be considered here, one representing random motion of large eddies and another rotation or a particular kind of convection described in the previous paper (Huang and Struve 1953). The broadening function corresponding to the first case is given by equation (5) (Unsöld and Struve 1949). According to the previous investigation, the broadening functions cor-

responding to rotation and to that particular kind of convection (the velocity distribution of convecting currents is given by a step function) are similar; thus

$$B(v) = \sigma\left[\frac{1}{\pi}(1-\sigma^2 v^2)^{1/2} + \frac{3}{8}(1-\sigma^2 v^2)\right], \tag{8}$$

where

$$\sigma = \frac{\xi_s}{\xi_r}. \tag{9}$$

In equation (8) a darking constant $\beta = \frac{3}{2}$ has been used.

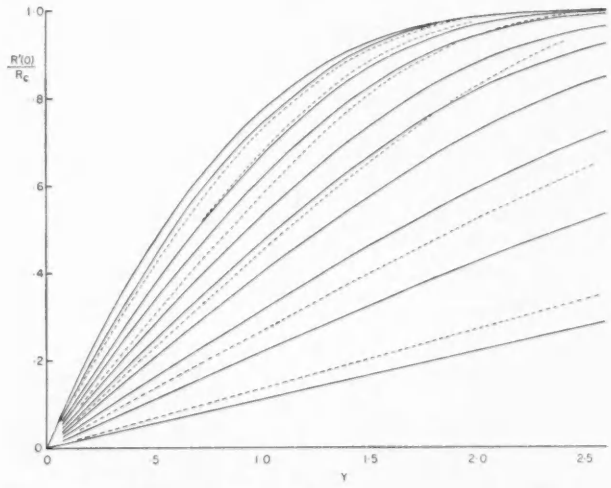

FIG. 2.—The effect of mass motion on the central depth of an absorption line. The central absorption is plotted against the equivalent width for different amounts of broadening by mass motion. If the solid line at the top of the diagram represents the depth-width relationship of a line in an ideal case, where there is no broadening by mass motion, the solid-line curves below it give the same relation when the absorption line is broadened by random motion, and the dotted-line curves, by rotation. Running downward, the different curves correspond to the cases of increasing large-scale motions.

In considering the central depth, the damping constant is not important and will be set equal to zero. Substituting equation (5) in equation (3) and letting $v = 0$, we obtain the central depth of an observed line, $R'(0)$,

$$\frac{R'(0)}{R_c} = \frac{2\gamma}{\sqrt{\pi}} \int_0^\infty \frac{aZ\, e^{-(\gamma^2+1)v^2}}{1 + aZ\, e^{-v^2}}\, dv\,. \tag{10}$$

The integral in equation (10) can be expanded into series for both large and small values of aZ in ways similar to those used when the special case ($\gamma = 0$) was expanded (A. Sommerfeld 1928). For other values of aZ we have to compute numerically the integral in equation (10); the final results are plotted as the solid curve in Figure 2. Going downward, the solid-line curves represent, respectively, the cases $\gamma = \infty$, 2, 1, 0.8, 0.6, 0.5, 0.4, 0.3, 0.2, and 0.1.

In a similar way we can compute the central depth $R'(0)$ when the broadening is due

to rotation (or convection). Substituting equation (8) in equation (3) and setting $v = 0$, we obtain

$$\frac{R'(0)}{R_c} = 2\sigma \int_0^{1/\sigma} \frac{aZ\, e^{-v^2}}{1 + aZ\, e^{-v^2}} \left[\frac{1}{\pi} (1 - \sigma^2 v^2)^{1/2} + \tfrac{3}{8} (1 - \sigma^2 v^2) \right] dv . \tag{11}$$

Before actual computation it is useful to define a function $f(m)$ such that

$$f(m) = 2 \int^1 e^{-mx^2} \left[\frac{1}{\pi} (1 - x^2)^{1/2} + \tfrac{3}{8} (1 - x^2) \right] dx . \tag{12}$$

For both large and small values of m, the function $f(m)$ as given in Table 2 was computed from its asymptotic forms. For intermediate values, numerical integration was used. With the aid of Table 2 we then compute $R'(0)/R_c$ according to equation (11). The final results are plotted as the broken curves in Figure 2. Running downward, the broken-line curves represent, respectively, the cases $\sigma = 1$, 0.707, 0.5, 0.354, 0.2, and 0.1.

TABLE 2

THE FUNCTION $f(m)$

m	$f(m)$	m	$f(m)$	m	$f(m)$
0	1.000	1.5	0.758	6	0.470
0.25	0.952	2	.703	8	.414
0.5	0.904	2.5	.656	12	.344
0.75	0.862	3	.618	16	0.300
1.00	0.824	4	.556		
1.25	0.789	5	0.508		

We shall now point out some general features in Figure 2. First, the linear part at small V covers a considerable portion of the curve. Hence the slope of the curve at $V = 0$ is a quantity that can be well determined in the observational curve. This fact will be utilized later. As the velocity of macroscopic motion becomes larger and larger, the linear portion of the curve extends farther and farther up. We would therefore expect that, for a star having large macroscopic motion (including rotation), most absorption lines should lie on the linear portion of the $R'(0) - V$ curve. While the form of the $R'(0) - V$ curves for small γ (or σ) is independent of the choice of the original profile formula, that for large γ (or σ) depends solely upon such a choice. In fact, the $R'(0) - V$ curves corresponding to large γ (or σ) follow nearly the relation between $R(0)$ and V. In other words, a slight broadening by the macroscopic motion or by the instrument will not seriously affect the form of the central-depth versus equivalent-width relationship. Another point that can be seen immediately from Figure 2 is that we will never be able to ascertain from such a diagram the nature of the macroscopic motion which is responsible for the broadening of lines. The broadenings by random motion and by rotation (or convection) give two families of curves (the solid-line ones and the broken-line ones) which can hardly be distinguished from each other, especially in view of the eventual large scatter of observational points.

III. SLOPE OF THE $R'(0) - V$ CURVE AT ORIGIN

Since

$$V = \frac{\Delta\lambda}{\lambda} \left(\frac{c}{2R_c \xi_s} \right), \tag{13}$$

the slope, $(1/R_c)[dR'(0)/dY]$, of the computed curve is connected with the slope, $dR'(0)/d(A_\lambda/\lambda)$, of the observed curve by the following formula:

$$\frac{1}{R_c}\frac{dR'(0)}{dY} = \frac{2\xi_s}{c}\frac{dR'(0)}{d(A_\lambda/\lambda)}. \tag{14}$$

We are interested in the slope at $Y = A_\lambda = 0$; hence the left side in equation (14) can be easily computed. Although equation (14) holds generally for any broadening function, $B(v)$, the actual expression for $(1/R_c)[dR'(0)/dY]$ depends upon the form of $B(v)$.

Let us consider, first, the Gaussian broadening function. The value of Y at small αZ is given by

$$Y = \frac{\sqrt{\pi}}{2}\alpha Z\left[1 - \frac{\alpha Z}{\sqrt{2}} + \frac{(\alpha Z)^2}{\sqrt{3}} - \cdots\right]. \tag{15}$$

To investigate the behavior of the slope at $Y = 0$, it is enough to take only the first-order quantities; hence equations (15) and (10) together give

$$\frac{1}{R_c}\left[\frac{dR'(0)}{dY}\right]_0 = \frac{2\gamma}{[\pi(1+\gamma^2)]^{1/2}}. \tag{16}$$

The subscript 0 means that the expression inside the bracket should be evaluated at $Y = A_\lambda/\lambda = 0$. Combining equations (16) and (14) and remembering $\gamma = \xi_s/\xi_l$, we readily obtain

$$\left[\frac{dR'(0)}{d(A_\lambda/\lambda)}\right]_0 = \frac{c}{\sqrt{\pi}}\frac{1}{(\xi_s^2+\xi_l^2)^{1/2}}. \tag{17}$$

The left side is a directly observable quantity; hence $(\xi_s^2 + \xi_l^2)^{1/2}$ can be determined.

Let us next consider the case of rotation. From equation (15) and the asymptotic expansion of $R'(0)/R_c$ for small αZ, it follows that

$$\frac{1}{R_c}\left[\frac{dR'(0)}{dY}\right]_0 = \frac{2}{\sqrt{\pi}} f\left(\frac{1}{\sigma^2}\right). \tag{18}$$

Combined with equation (14), equation (18) gives

$$\left[\frac{dR'(0)}{d(A_\lambda/\lambda)}\right]_0 = \frac{c}{\xi_s}\frac{1}{\sqrt{\pi}} f\left(\frac{1}{\sigma^2}\right), \tag{19}$$

where $f(x)$ is defined in equation (12). We should point out here that the different intensity formulae give the same profile for weak lines. The results expressed in equations (17) and (19) are therefore generally true and free from any approximation.

Equation (19) cannot be used directly without first determining one of the two unknowns, ξ_s and σ. Hence its applicability is limited. But if the rotational velocity (or the maximum velocity of convective currents) is much larger compared with ξ_s, we can substitute for $f(1/\sigma^2)$ in equation (19) its asymptotic expansion and obtain

$$\left[\frac{dR'(0)}{d(A_\lambda/\lambda)}\right]_0 = \frac{c}{\xi_r}\left(\frac{1}{\pi}+\frac{3}{8}\right) \qquad \text{(small } \sigma\text{)}. \tag{20}$$

On the other hand, if $\xi_r \ll \xi_s$, so that $1/\sigma^2$ can be neglected, we have

$$\left[\frac{dR'(0)}{d(A_\lambda/\lambda)}\right]_0 = \frac{c}{\sqrt{\pi}}\frac{1}{\xi_s} \qquad \text{(large } \sigma\text{)}. \tag{21}$$

Before using the limiting formula (21), we should be certain that not only the broadening by macroscopic motion in the stellar atmosphere but also the instrumental broadening are very small. For other formulae in the present paper we understand that the instrumental broadening is absorbed in $B(v)$; hence the determined velocity would be slightly larger than the true velocity. In the case of the Mount Wilson coudé spectrogram of 2.85 A/mm dispersion we found the average half-half-width of the weak comparison lines to be 3 km/sec; hence the correction of Doppler velocities for the instrumental broadening is quite small.

IV. BEHAVIOR OF THE $v_{1/2} - Y$ CURVE AT $Y = 0$

In the same manner as in the previous section we shall divide the present one into two parts: Gaussian broadening and rotational broadening. Substituting equation (5) in equation (4), we obtain, for small aZ and $a = 0$, an equation which determines $v_{1/2}$:

$$\int_{-\infty}^{\infty} e^{-v^2-\gamma^2(v_{1/2}-v)^2}(1-aZ\,e^{-v^2})\,dv = \frac{1}{2}\int_{-\infty}^{\infty} e^{-(1+\gamma^2)v^2}(1-aZ\,e^{-v^2})\,dv + O(a^2Z^2)\ . \tag{22}$$

With the aid of equation (15), equation (22) can be reduced to

$$\left[\exp\left(-\frac{\gamma^2 v_{1/2}^2}{1+\gamma^2}\right)-\frac{1}{2}\right]\left(\frac{2+\gamma^2}{1+\gamma^2}\right)^{1/2} = \frac{2Y}{\sqrt{\pi}}\left[\exp\left(-\frac{2\gamma^2 v_{1/2}^2}{2+\gamma^2}\right)-\frac{1}{2}\right]+O(Y^2)\ . \tag{23}$$

As $Y \to 0$,

$$v_{1/2} = \frac{1}{\gamma}\left[(1+\gamma^2)\ln 2\right]^{1/2} = (v_{1/2})_0\,, \qquad \text{say}\,. \tag{24}$$

The value $(v_{1/2})_0$ defines the intercept of the $v_{1/2} - Y$ curve on the $v_{1/2}$ axis.

The calculated $v_{1/2}$ is connected with the measured half-width, D_λ, in angstrom units by

$$v_{1/2} = \frac{D_\lambda}{\lambda}\left(\frac{c}{2\xi_s}\right). \tag{25}$$

Combining equations (24) and (25), we obtain

$$\left(\frac{D_\lambda}{\lambda}\right)_0 = \frac{2}{c}\left[(\xi_s^2+\xi_i^2)\ln 2\right]^{1/2}, \tag{26}$$

where $(D_\lambda/\lambda)_0$ is the observed limiting value of D_λ/λ as $A_\lambda/\lambda \to 0$. Hence we can see that both $[dR'(0)/d(A_\lambda/\lambda)]_0$ and $(D_\lambda/\lambda)_0$ determine the same physical quantity. In fact, the product of these two expressions is a constant.

Next we investigate $(dv_{1/2}/dY)_0$, i.e., the slope at the point $[(v_{1/2})_0, 0]$. Differentiate equation (23) with respect to Y and set $Y = 0$, and $v_{1/2} = (v_{1/2})_0$ in the resulting equation. In this way we obtain

$$R_c\left(\frac{d\,D_\lambda}{d\,A_\lambda}\right)_0 = \frac{F(\gamma)}{(\pi\ln 2)^{1/2}}, \tag{27}$$

where

$$F(\gamma) = \frac{1+\gamma^2}{\gamma(2+\gamma^2)^{1/2}}\left[1-(\tfrac{1}{2})^{\gamma^2/(2+\gamma^2)}\right]\ . \tag{28}$$

It can be easily shown that $F(0) = 0$ and $F(\infty) = 0.5$. Equation (27) determines γ from the observed value $(dD_\lambda/dA_\lambda)_0$.

The equation which determines $(v_{1/2})_0$ in the case of rotational broadening is given by

$$f\left(\frac{1}{\sigma^2}\right) = e^{-v_{1/2}^2} \int_{-1}^{1} \left[\frac{2}{\pi}(1-x^2)^{1/2} + \tfrac{3}{4}(1-x^2)\right] \exp\left(\frac{2x\,v_{1/2}}{\sigma} - \frac{x^2}{\sigma^2}\right) dx\,. \tag{29}$$

To avoid cumbersome expression, we have dropped the subscript 0 in equation (29) and following equations. For large σ we can expand the exponential part of the integrand as a power series of $1/\sigma$. Because the other factor in the integrand is an even function of x, all terms having odd powers of $1/\sigma$ vanish after integration. If $1/\sigma^4$ and higher-order terms can be neglected, we obtain

$$v_{1/2} = (\ln 2)^{1/2} \qquad (\text{large } \sigma)\,, \tag{30}$$

as expected. Or

$$\left(\frac{D_\lambda}{\lambda}\right)_0 = \frac{2\xi_s}{c}(\ln 2)^{1/2} \qquad (\xi_r \to 0)\,. \tag{31}$$

For small values of σ, the final profile resembles a pure rotational profile, We can therefore compute the limiting $(v_{1/2})_0$ for small σ by directly using the $B(v)$ profile; thus we obtain

$$\frac{2}{\pi}(1-\sigma^2 v_{1/2}^2)^{1/2} + \tfrac{3}{4}(1-\sigma^2 v_{1/2}^2) = \frac{1}{\pi} + \tfrac{3}{8}\,. \tag{32}$$

Solving the quadratic equation of the unknown, $(1-\sigma^2 v_{1/2}^2)^{1/2}$, and discarding the negative root, we obtain

$$v_{1/2} = \frac{0.782}{\sigma} \qquad (\text{small } \sigma)\,. \tag{33}$$

Hence

$$\left(\frac{D_\lambda}{\lambda}\right)_0 = \frac{1.564}{c}\,\xi_r \qquad (\xi_r \gg \xi_s)\,. \tag{34}$$

For intermediate values of σ, no simple method can be given for calculating $(v_{1/2})_0$; numerical iteration must therefore be used. Having known the asymptotic behavior of

TABLE 3

ROOTS OF EQUATION (29) FOR DIFFERENT VALUES OF σ

σ	$(v_{1/2})_0$	σ	$(v_{1/2})_0$	σ	$(v_{1/2})_0$
10	0.833	1	1.127	0.333	2.346
2	0.878	0.5	1.572	0.1	7.82

$(v_{1/2})_0$ (i.e., eqs. [30] and [33]), we can make a fair guess at the value of $(v_{1/2})_0$ for any value of σ, because $(v_{1/2})_0$ is a monotonically increasing function of $1/\sigma$. Substitute this value for the $v_{1/2}$ inside the integration sign in equation (29) and solve for the $v_{1/2}$ outside the integration sign as an unknown after numerical integration has been performed. A better value of $v_{1/2}$ is then obtained. Repeat this process until a correct value of $(v_{1/2})_0$ is found. The result of such iteration is given in Table 3.

The idea involved in the calculation of the present section is nothing more than that of the curve of line-width correlation. However, the present treatment does not limit its application to the case of Gaussian broadening, as does the curve of line-width correlation.

V. THE SPECTRUM OF α CYGNI

The coudé spectrogram used for the present analysis was taken on August 21, 1953 (U.T. 5:57) at the Mount Wilson Observatory. The dispersion is 2.85 A/mm. A direct photometric tracing of the spectrum was reduced by an automatic reducing instrument. Identification of the absorption lines was guided by O. Struve's (1939) and O. Struve and P. Swings's (1941) tables of wave lengths in the spectrum of α Cygni. We have selected those lines which are not seriously blended and have measured the equivalent width, A_λ, the half-width, D_λ, and the central depth, $R'(0)$, of each line. The results are listed in Table 4. The wave lengths given in the table follow the values given in C. E. Moore's recent compilation (1945).

The spectrum of α Cygni has been studied quantitatively by A. Pannekoek (1931), O. Struve and C. T. Elvey (1934), O. Struve and F. Sherman (1940), L. H. Aller (1942), G. A. Shajn and P. F. Shajn (1949), and W. Buscombe (1951). About one-third of the lines given in Table 4 overlap with Buscombe's determinations. We compared the equivalent widths of those overlapping lines and found that the two measurements agree very well except at the extreme ends—of very strong and very weak lines—where the present determination falls slightly below Buscombe's result. Also, the line λ 4242.38 *Cr* II, shows a large discrepancy between the two measurements. In Buscombe's paper, $\log (10^6 A_\lambda/\lambda)$ is given as 0.65, while we have 1.61 for the same quantity. Struve and Elvey's measurement gives the value 1.6.

Using the curve-of-growth method, Buscombe obtains for the turbulent velocity of small eddies a value of 13 km/sec. This value seems to be consistent with that derived from the curve of line-width correlation, as well be seen later.

VI. DETERMINATION OF DOPPLER VELOCITY IN ATMOSPHERE OF α CYGNI

Let us first plot an empirical curve of line-width correlation according to the values given in Table 4. Comparing it with the theoretical curve, we find that $\xi_s = 14.8$ km/sec and $\xi_l = 11.7$ km/sec, if we take $R_c = 1$. Hence $\gamma = 1.26$. As we mentioned in the first section, the theoretical curve of line-width correlation in Table 1 slightly overestimates ξ_s when γ is of the order of unity, as in the present case. Since ξ_l is computed from ξ_s and the well-determined quantity, $(\xi_s^2 + \xi_l^2)^{1/2}$, the velocity of large eddies is underestimated in the present measurements. We should therefore have

$$\xi_s \lesssim 14.8 \text{ km/sec} \qquad \text{and} \qquad \xi_l \gtrsim 11.7 \text{ km/sec} \tag{35}$$

where the sign $\lesssim$ means smaller than, but of the same order of magnitude as, the value following it. The first result in expression (35) is consistent with Buscombe's value of ξ_s (13 km/sec) obtained from the study of the curve of growth. Assuming $\xi_s = 12$, 13, and 14 km/sec, respectively, we obtain $\xi_l = 14.5$, 13.6, and 12.5 km/sec. In passing, we should mention that there is no systematic difference in any of the observed curves of line-width correlation for different species of atoms.

Next we plot in Figure 3 the central depths against the equivalent widths for different elements. Different diagrams in Figure 3 give consistently, for the slope of the curve at the origin, the following value:

$$\left[\frac{dR'(0)}{d(A_\lambda/\lambda)}\right]_0 = 9 \times 10^3, \tag{36}$$

which corresponds to $(\xi_s^2 + \xi_l^2)^{1/2} = 18.8$ km/sec if the Gaussian broadening is supposed. This value is in close agreement with 18.9 km/sec, determined from the line-width correlation method.

TABLE 4

EQUIVALENT WIDTHS, ETC., MEASURED IN SPECTRUM OF α CYGNI

Wave Length and Identification	Central Depth	$10^6 D_\lambda/\lambda$	$10^6 A_\lambda/\lambda$	E.P. (Ev)
3736.901 *Ca* II	0.592	179.1	107.3	3.14
3738.38 *Cr* II	.336	138.2	47.0	3.09
3741.633 *Ti* II	.501	138.9	70.1	1.57
3743.364 *Fe* I	.168	112.7	18.7	0.99
3746.56 *Fe* IIp	.248	134.0	31.8	2.27
3754.59 *Cr* II	.290	131.0	38.0	3.09
3755.563 *Fe* II	.174	113.4	19.4	4.72
3757.684 *Ti* II	.351	129.1	46.4	1.56
3762.894 *Fe* II	.197	94.1	20.2	5.93
3765.62 *Cr* II	.208	107.5	24.3	3.09
3776.062 *Ti* II	.170	107.2	18.9	1.57
3778.357 *V* II	.080	121.3	9.0	1.67
3779.58 *Fe* IIp	.146	118.0	17.1	2.53
3781.510 *Fe* II	.095	113.2	10.2	4.48
3783.347 *Fe* II	.382	126.9	51.5	2.27
3786.33 *Ti* IIp	.088	126.8	11.0	0.60
3815.842 *Fe* I	.202	112.3	22.4	1.48
3820.428 *Fe* I	.302	114.3	36.6	0.86
3821.92 *Fe* IIp	.180	122.1	20.7	2.33
3824.913 *Fe* II	.300	120.0	35.5	2.57
3825.884 *Fe* I	.264	112.0	29.3	0.91
3827.079 *Fe* II	.225	113.0	26.7	4.71
3829.355 *Mg* I	.260	116.1	32.9	2.70
3832.304 *Mg* I	.396	145.1	57.6	2.70
3838.29 *Mg* I	.445	150.4	68.6	2.70
3840.439 *Fe* I	.154	113.9	18.0	0.99
3845.18 *Fe* IIp	.193	120.9	24.3	4.46
3853.657 *Si* II	.384	126.2	52.4	6.83
3856.021 *Si* II	.600	162.7	104.6	6.83
3859.913 *Fe* I	.213	105.0	24.3	0
3862.592 *Si* II	.537	147.5	86.3	6.83
3865.59 *Cr* II	.205	106.8	24.4	5.30
3872.76 *Fe* IIp	.195	127.0	25.7	2.69
3900.546 *Ti* II	.478	139.1	74.9	1.13
3913.464 *Ti* II	.453	142.1	68.3	1.11
3930.299 *Fe* I	.254	122.0	34.6	0.09
3933.664 *Ca* II	.796	262.0	232.0	0
3935.942 *Fe* II	.241	129.6	34.8	5.54
3938.289 *Fe* II	.292	127.3	36.6	1.66
3938.969 *Fe* II	.203	129.3	25.5	5.89
3968.470 *Ca* II	.820	254.0	208.0	0
3974.160 *Fe* II	.254	122.2	30.5	2.69
3979.51 *Cr* II	.161	106.3	18.5	5.65
4024.552 *Fe* II	.240	111.1	27.4	4.48
4028.332 *Ti* II	.200	110.2	23.4	1.88
4032.946 *Fe* II	.144	105.9	14.5	4.48
4044.01 *Fe* II	.060	107.0	6.2	5.55
4045.815 *Fe* I	.229	125.6	29.3	1.48
4051.97 *Cr* II	.124	106.8	12.9	3.09
4053.814 *Ti* II	.188	123.3	24.4	1.88
4057.457 *Fe* II	.078	106.3	8.4	7.24
4063.597 *Fe* I	.148	114.3	18.7	1.55
4067.05 {*Cr* IIp, *Ni* II}	.276	117.9	33.6	{6.46, 4.01}
4069.883 *Fe* II	.045	105.1	4.5	5.89
4070.90 *Cr* II	.055	104.8	5.8	6.46
4071.740 *Fe* I	.127	112.0	13.3	1.60
4072.56 *Cr* II	.057	99.4	5.8	3.70
4076.87 *Cr* II	0.086	111.9	9.2	3.09

TABLE 4—*Continued*

Wave Length and Identification	Central Depth	$10^6\ D_\lambda/\lambda$	$10^6\ A_\lambda/\lambda$	E.P. (Ev)
4077.714 *Sr* II	0.181	125.7	22.1	0
4111.01 *Cr* II	.120	99.6	12.0	3.09 3.74
4122.638 *Fe* II	.286	112.7	34.2	2.57
4124.793 *Fe* II	.092	117.9	11.1	2.53
4128.053 *Si* II	.403	142.0	55.6	9.79
4128.735 *Fe* II	.237	124.7	30.5	2.57
4130.884 *Si* II	.393	150.2	63.0	9.80
4163.644 *Ti* II	.240	129.8	33.1	2.58
4171.897 *Ti* II	.208	121.0	26.0	2.59
4173.450 *Fe* II	.433	148.1	64.4	2.57
4177.70 *Fe* IIp	.275	122.7	34.3	2.53
4178.855 *Fe* II	.443	148.6	69.4	2.57
4187.802 *Fe* I	.087	125.0	10.9	2.41
4233.167 *Fe* II	.555	186.4	106.3	2.57
4242.38 *Cr* II	.292	135.0	40.7	3.85
4246.829 *Sc* II	.224	119.3	29.5	0.31
4254.346 *Cr* I	.066	117.6	7.3	0
4258.155 *Fe* II	.225	133.0	30.4	2.69
4259.203 *Mn* II	.052	106.3	5.4	5.37
4260.479 *Fe* I	.072	105.0	7.4	2.39
4261.92 *Cr* II	.248	114.8	30.2	3.85
4271.764 *Fe* I	.160	118.1	18.6	1.48
4273.317 *Fe* II	.253	134.0	38.9	2.69
4275.57 *Cr* II	.197	117.4	25.6	3.84
4284.21 *Cr* II	.173	108.7	18.7	3.84
4290.222 *Ti* II	.283	130.1	38.6	1.16
4294.101 *Ti* II	.295	128.1	40.6	1.08
4296.567 *Fe* II	.340	131.3	47.9	2.69
4300.052 *Ti* II	.405	126.1	52.3	1.18
4301.928 *Ti* II	.221	115.6	25.4	1.16
4303.166 *Fe* II	.458	138.1	70.0	2.69
4307.900 *Ti* II	.264	119.0	34.7	1.16
4312.861 *Ti* II	.235	117.0	30.0	1.18
4351.764 *Fe* II	.488	157.1	81.4	2.69
4354.358 *Fe* II	.052	102.8	5.8	7.62
4357.574 *Fe* II	.094	105.0	9.4	.....
4369.404 *Fe* II	.146	103.9	16.5	2.77
4383.547 *Fe* I	.226	112.1	25.6	1.48
4385.381 *Fe* II	.425	138.0	58.2	2.77
4395.031 *Ti* II	.389	144.0	59.5	1.08
4399.767 *Ti* II	.212	110.4	24.2	1.23
4402.875 *Fe* II	.121	108.6	13.9	.....
4411.080 *Ti* II	.098	118.8	11.3	3.08
4413.600 *Fe* II	.097	113.2	11.4	2.66
4416.817 *Fe* II	.426	151.0	62.2	2.77
4417.718 *Ti* II	.240	139.0	32.4	1.16
4443.802 *Ti* II	.326	130.0	43.2	1.08
4450.487 *Ti* II	.154	120.8	19.3	1.08
4451.545 *Fe* II	.142	110.2	16.4	.....
4455.258 *Fe* II	.095	99.8	9.7	.....
4468.493 *Ti* II	.401	122.4	60.0	1.13
4472.921 *Fe* II	.191	123.8	24.8	2.83
4481.327 *Mg* II	.800	190.3	156.1	8.83
4489.185 *Fe* II	.363	124.3	46.3	2.82
4491.401 *Fe* II	.408	136.4	59.0	2.84
4501.270 *Ti* II	.363	120.8	48.9	1.11
4520.225 *Fe* II	.528	137.2	76.5	2.79
4522.634 *Fe* II	.635	144.6	94.6	2.83
4541.523 *Fe* II	0.385	131.0	51.5	2.84

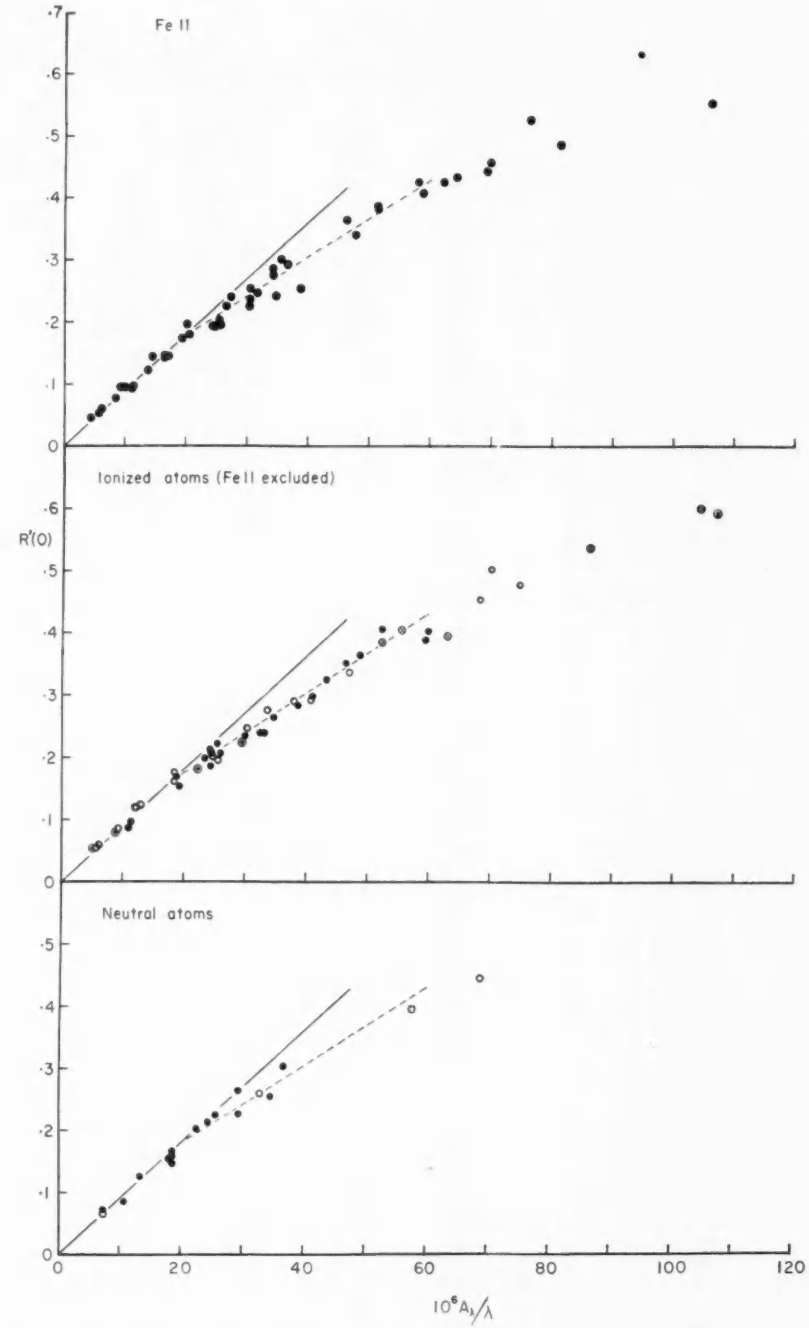

FIG. 3.—The relationship observed in α Cygni between the central absorption of a line and its equivalent width is shown. In the middle diagram the solid dot represents *Ti* II lines; the circle, *Cr* II lines; the cross-centered circle, *Si* II lines; and the dot-centered circle, lines of other singly ionized atoms.

If the broadening is due to rotation or convection having a broadening function similar to that of rotation, we cannot derive from equation (36) any significant result without first knowing the value of ξ_s. Taking $\xi_s = 12$, 13, and 14 km/sec, we obtain, from equations (19) and (36),

$$f\left(\frac{1}{\sigma^2}\right) = 0.638,\ 0.691 \quad \text{and} \quad 0.744,$$

which give, with the aid of Table 2,

$$\xi_r = 19.8,\ 19.0, \text{ and } 17.8 \text{ km/sec, respectively}.$$

Any formula for the line profile should predict, as in Figure 2, an $R'(0) - A_\lambda/\lambda$ curve with continuously changing slopes. But Figure 3 seems to indicate a discontinuous change in slope at a certain point. The observed points corresponding to weak lines lie on a straight line (i.e., the solid line in each diagram) the slope of which was utilized in the previous discussion. It is difficult to draw a smooth curve which extends from this straight line and which, at the same time, fits the observed points. If, however, we assume that the slope changes abruptly at about $10^6 A_\lambda/\lambda = 20$ and remains constant until $10^6 A_\lambda/\lambda$ reaches 60 (as shown by the broken line in each diagram in the figure), the fit to the observations is better. For $10^6 A_\lambda/\lambda > 60$ there are so few observed points that the trend of the curve cannot be definitely ascertained. Being independent of the nature of absorbing atoms, the discontinuity in slope of the observed curve of central depth and equivalent width seems to exist in each diagram and suggests stratification of the atmosphere. Either the mechanism of line formation changes sharply from one to another as the light passes through a certain layer, or the turbulent motions in the upper and the lower layers of the atmosphere have considerable differences either in nature or (and) in magnitude. The second possibility is consistent with our previous result found in ρ Leonis, that the outermost layers show random mass motion while the inner layers show regular rotation or convection.

Next we plot a $A_\lambda/\lambda - D_\lambda/\lambda$ diagram for those lines listed in Table 4. This is shown in Figure 4. We have combined all elements together in one figure, but different kinds of atoms are represented by different symbols. The scatter of the points is much larger than that in the plot between $R'(0)$ and A_λ/λ. From Figure 4 we obtain

$$\left(\frac{D_\lambda}{\lambda}\right)_0 = 1.07 \times 10^{-4}. \tag{37}$$

If the broadening is Gaussian-like, we have, from equations (26) and (37), $(\xi_s^2 + \xi_l^2)^{1/2} = 19.3$ km/sec. If the broadening is rotation-like, we derive, from equations (25) and (37), $v_{1/2} = 1.34$, 1.23, and 1.15, respectively, if we assume $\xi_s = 12$, 13, and 14 km/sec. The corresponding rotational velocities are 19.7, 18.7, and 18.1 km/sec. They are derived from the simple relation $\xi_r = \xi_s/\sigma$ and Table 3. The points in Figure 4 have such a large scatter that it is impossible to determine even approximately the slope of the empirical curve at any point. We shall therefore not apply the method of slope in the $A_\lambda/\lambda - D_\lambda/\lambda$ diagram to the present observational result.

Table 5 gives a summary of the results of the present determination of Doppler velocities in α Cygni. The half-widths of the five weak lines that Buscombe has measured also show large scatter. From his measured results we can estimate roughly the value of $(D_\lambda/\lambda)_0$ to be 188×10^{-6}. For the Gaussian broadening, this corresponds to $(\xi_s^2 + \xi_l^2)^{1/2} = 34.0$ km/sec, which agrees with Buscombe's own result of 35 km/sec. A mean profile of the five lines has also been given in Buscombe's paper. In taking the average, he used $\Delta\lambda$ instead of $\Delta\lambda/\lambda$ as the independent variable. His estimate for $(\xi_s^2 + \xi_l^2)^{1/2}$ from the average profile gives 31 km/sec (1954).

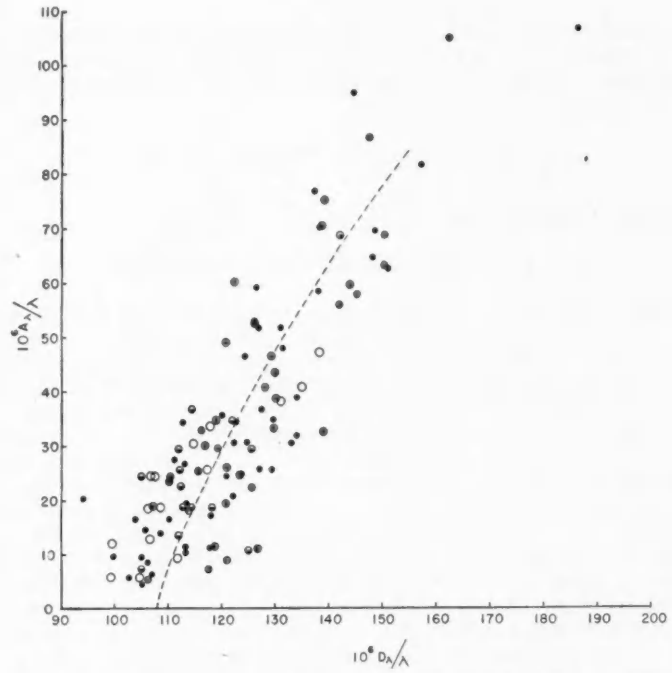

FIG. 4.—The relationship observed in α Cygni between the equivalent width and the half-width. Different kinds of absorbing atoms are represented by different symbols; thus *Fe* II is represented by dots; *Ti* II by dot-centered circles; *Cr* II by empty circles; *Fe* I by half-filled circles; and others by cross-centered circles. We can see that the scatter is much larger than that in Fig. 3.

TABLE 5

DOPPLER VELOCITIES (KM/SEC) IN α CYGNI* (AUGUST 21, 1953)

METHOD	$B(v)$ IS GAUSSIAN-LIKE		$B(v)$ IS ROTATION-LIKE	
	ξ_a	$(\xi_a^2+\xi_t^2)^{1/2}$	ξ_a (Assumed)	ξ_v
Curve of line-width correlation	<14.8	18.9	.....	.....
Slope of the $R'(0)-\frac{1}{2}A_\lambda/\lambda$ curve	.....	18.8	12.0 13.0 14.0	19.8 19.0 17.8
Limiting value of D_λ/λ	.....	19.3	12.0 13.0 14.0	19.7 18.7 18.1

* The instrumental broadening of an amount of 3 km/sec for the half-half-width has not been deduced from the tabulated values.

The ratio of Buscombe's value to the present value of the same quantity, $(\xi_a^2 + \xi_l^2)^{1/2}$, is $35/19 = 1.84$. This is a rather large discrepancy. As the equivalent widths measured by Buscombe and by us agree in general, ξ_a cannot differe appreciably, and the discrepancy can probably be attributed to a change of ξ_l with time. On the other hand, the general features of spectrograms of α Cygni taken at different times do not indicate, in our experience, such a large change of macroscopic motion. Hence the discrepancy remains unsettled.

VII. APPLICATION OF PRESENT METHOD TO OTHER STARS

We shall now apply the present method to other stars that have been studied by us. Let us first consider ρ Leonis. We have measured the central depths of those lines which were listed in the previous paper and have plotted an $R'(0) - A_\lambda/\lambda$ diagram in Figure 5. The slope at zero is measured to be

$$\left[\frac{dR'(0)}{d(A_\lambda/\lambda)}\right]_0 = 3.08 \times 10^3 . \tag{38}$$

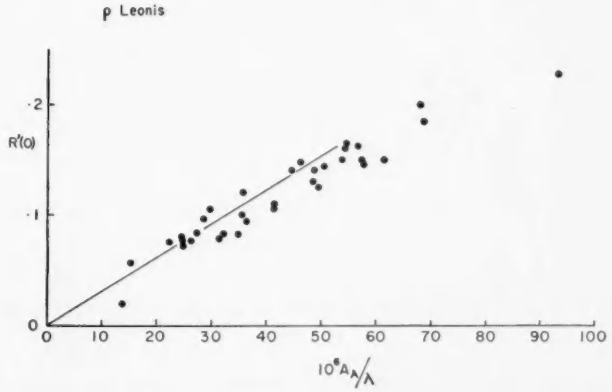

FIG. 5.—The relationship observed in ρ Leonis between the central absorption of a spectral line and its equivalent width.

If the broadening can be represented by a Gaussian function, we obtain from equation (38)

$$(\xi_a^2 + \xi_l^2)^{1/2} = 55.0 \text{ km/sec} .$$

If the broadening is rotation-like, we can use the asymptotic formula (20) to determine the rotational velocity, because the shallowness of the lines necessarily suggests a small value of σ. Hence

$$\xi_r = 0.693\left[\frac{dR'(0)}{d(A_\lambda/\lambda)}\right]_0^{-1} = 67.5 \text{ km/sec} ,$$

as compared with an average value of 62.2 km/sec determined previously from four groups of weak lines. In Figure 5 we also notice the change in slope at a certain point ($10^6 A_\lambda/\lambda = 30$), although the change is even smaller than that in α Cygni. It appears that the slope remains constant between $10^6 A_\lambda/\lambda = 30$ and 60.

Similarly, we plot in Figure 6 a diagram for δ Canis Majoris. We do not have lines weak enough to insure a good determination of the slope at the origin. The curve is first extrapolated to the origin, and its slope at that point is measured. It gives approximately

$$\left[\frac{dR'(0)}{d(A_\lambda/\lambda)}\right]_0 = 1.5 \times 10^4 ,$$

yielding a value

$$(\xi_s^2 + \xi_l^2)^{1/2} = 11.3 \text{ km/sec} .$$

In Figure 6 we can notice a discontinuity of the observed curve at $10^6 A_\lambda/\lambda = 120$. We have drawn two curves to represent the smoothed relationship between the observed

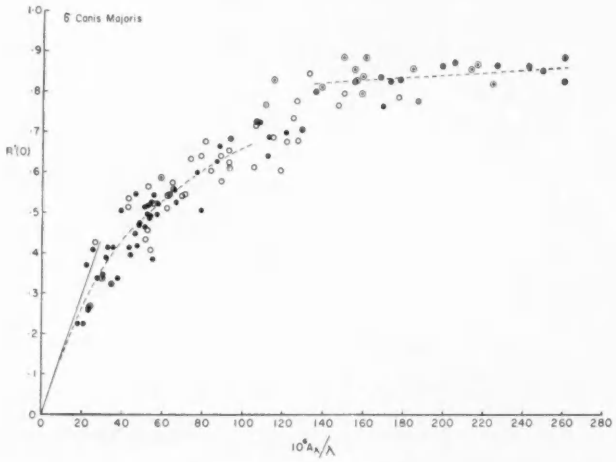

FIG. 6.—The relation observed in δ Canis Majoris between the central absorption of a spectral line and its equivalent width. All are *Fe* I lines: The different symbols refer to different excitation potentials of the lower level: cross-centered circles, lines of 0–1 e.v.; dot-centered circles, 1–2 e.v.; empty circles, 2–3 e.v.; filled circles, 3–4 e.v. We can notice a discontinuity of the observed points at about $10^6 A_\lambda/\lambda = 120$. We have drawn freehand two curves to represent the smoothed relation on both sides of the discontinuous point. This phenomenon seems to indicate an abrupt change in turbulent velocity of small eddies at a certain depth in the atmosphere.

$R'(0)$ and A_λ/λ, respectively, for $10^6 A_\lambda/\lambda < 120$ and $10^6 A_\lambda/\lambda > 120$. The discontinuity at $10^6 A_\lambda/\lambda = 120$ seems also to indicate the stratification of turbulent motions in the atmosphere. If the turbulent velocity of small eddies, ξ_s, increases abruptly at the outermost layers of the atmosphere, the phenomenon can be easily understood (Unsöld and Struve 1949; Huang 1952).

REFERENCES

Aller, L. H. 1942, *Ap. J.*, **95**, 73
Buscombe, W. 1951, *Ap. J.*, **114**, 73.
———. 1954, private communication.
Carroll, J. A. 1928, *M.N.*, **88**, 548.
Huang, S.-S. 1952, *Ap. J.*, **115**, 529.
Huang, S.-S., and Struve, O. 1952, *Ap. J.*, **116**, 410.
———. 1953, *ibid.*, **118**, 463.

Kilby, R. F. 1953, Master's dissertation, Berkeley Astronomical Department, University of California.
Menzel, D. H. 1936, *Ap. J.*, **84,** 462.
Minnaert, M. 1935, *Zs. f. Ap.*, **10,** 40.
Moore, C. E. 1945, *Contr. Princeton U. Obs.*, No. 20.
Pannekoek, A. 1931, *Proc. Kon. Akad. Wesentsch., Amsterdam*, Vol. **34,** No. 6.
Schwarzschild, M. and B. 1950, *Ap. J.*, **112,** 248.
Schwarzschild, M. and B., and Adams, W. S. 1948, *Ap. J.*, **108,** 207.
Shajn, G. A. and P. F. 1949, *Comm. Crimean Ap. Obs.*, **4,** 49.
Sommerfeld, A. 1928, *Zs. f. Phys.*, **47,** 1.
Struve, O. 1939, *Ap. J.*, **90,** 699.
Struve, O., and Elvey, C. T. 1934, *Ap. J.*, **79,** 409.
Struve, O., and Sherman, F. 1940, *Ap. J.*, **91,** 428.
Struve, O., and Swings, P. 1941, *Ap. J.*, **94,** 344.
Unsöld, A. 1938, *Physik der Sternatmosphären* (Berlin: Julius Springer).
Unsöld, A., and Struve, O. 1949, *Ap. J.*, **110,** 455.
Wright, K. O., and Van Dien, E. 1949, *J.R.A.S. Canada*, **43,** 15.

AXIAL ROTATION IN THE BRIGHTER STARS OF DRAPER TYPES B2–B5

ARNE SLETTEBAK AND ROBERT F. HOWARD
Perkins Observatory
Received May 25, 1954; revised July 23, 1954

ABSTRACT

Rotational velocities ($v \sin i$) of the stars of Draper types B2–B5, brighter than 5.51 mag. and north of declination $-20°$, were determined by comparing observed profiles of the *He* I 4471 line with sets of profiles computed by the graphical method of Shajn and Struve. Spectral types and luminosity classes on the MK system of classification were provided by Dr. W. W. Morgan.

The mean true rotational velocity of the main-sequence stars of MK types B2–B5 was found to be 201 km/sec, a value somewhat larger than the corresponding one for the B8–A2 stars. A subdivision of the main-sequence stars into MK types B1–B3 and B5–B7 shows that the B5–B7 stars appear to have the greatest axial rotation, with decreasing rotational velocities for both earlier and later types.

The stars of intermediate luminosity have smaller axial rotation than the main-sequence stars. This was also found to be the case for the B8–A2 stars, but the opposite situation was obtained for the F0–G0 stars.

A number of spectroscopic binaries included in this study are discussed from the point of view of possible synchronism between axial rotation and orbital revolution. The luminosity effect of the forbidden line of *He* I at λ 4470 is briefly discussed.

It is suggested that the observed relation of axial rotation to position on the H-R diagram may be interpreted in terms of the evolutionary sequences recently computed by Sandage and Schwarzschild.

I. INTRODUCTION

The present paper describes the B2–B5 phase in a program of obtaining rotational velocities for the brighter stars with Draper types between B2 and G0. The results for the Be stars (Slettebak 1949) and B8–A2 stars (Slettebak 1954) have been reported earlier, as have the preliminary results of the F0–G0 stars (Slettebak 1953). The ultimate aim of this work is to indicate how axial rotation varies across the H-R diagram and how this bears on problems of stellar evolution.

II. OBSERVATIONS

All stars brighter than 5.51 mag. with Draper types between B2 and B5 and north of declination $-20°$ are included in the present study. Of the total of 185 stars included, 106 have been observed only at the Perkins Observatory, 48 only at the Yerkes Observatory, and the remaining 31 at both observatories.

The Perkins material consists of one or more spectrograms of each star, taken with the two-prism spectrograph attached to the 69-inch telescope, giving a dispersion of 28 A/mm at $H\gamma$ and 32 A/mm at λ 4471. All spectra were considerably widened in order to increase the accuracy of spectral classification and to permit two independent microphotometer tracings to be made even if only one spectrogram was available. Eastman IIa-O plates, developed for 12 minutes in Promicrol at 69° F, were used for all stars. The plates were calibrated with the spectral sensitometer in the dome of the 69-inch telescope. The Perkins microphotometer, employing a magnification of about 100, was used to derive the line profiles. Figure 1, which shows the extremes in axial rotation measured in this study, illustrates the spectrograms employed.

The Yerkes material was described in detail earlier (Slettebak 1949). It consists of most of the more rapidly rotating bright B2–B5 stars and was originally prepared for purposes of comparison with the Be stars.

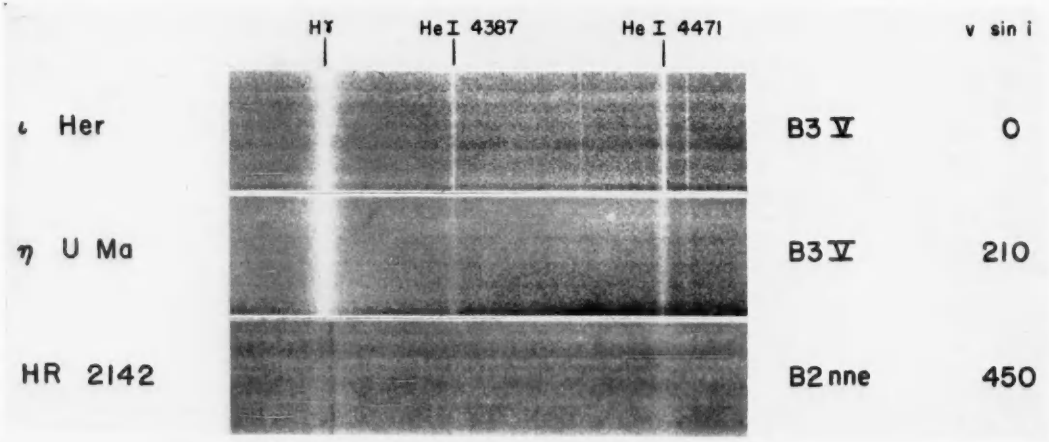

FIG. 1.—Line broadening by axial rotation in three representative B-type stars

III. ROTATIONAL VELOCITIES AND SPECTRAL TYPES

Rotational velocities for all stars were derived from the degree of line broadening with the aid of the graphical method of Shajn and Struve (1929). The method has been used and described by many writers and will not be discussed further here.

The absorption line *He* I 4471 was chosen for the determination of $v \sin i$ for all stars taken at the Perkins Observatory. It has the disadvantage of being subject to Stark effect and is blended with forbidden *He* I 4470 in stars on or near the main sequence, but it is nevertheless probably the most suitable choice with the observational material described above. Values of $v \sin i$ for the stars observed only at the Yerkes Observatory were derived from the *He* I 4026 line.

Two sharp-lined stars were chosen as zero-rotational-velocity standards for all determinations of $v \sin i$: ι Herculis (B3 V) for the stronger lines and ϵ Cassiopeiae (B2p) for the fainter lines. The latter actually has slightly broadened lines, corresponding to a $v \sin i$ of about 10 km/sec; the effect of this will be considered below. Sets of rotationally broadened contours were built up from the above standards, using the average of four independent contours of *He* I 4471 for each standard. A limb-darkened stellar disk was assumed, divided into 40 strips, as described earlier (Slettebak 1949). The inclusion of limb-darkening is probably an unnecessary refinement, however, since the uncertainties in the observed line profiles are large with respect to the small changes introduced by limb-darkening.

Two independent line profiles of *He* I 4471 were obtained for each of the stars observed at the Perkins Observatory. In most cases the resultant values of $v \sin i$ were simply averaged to give the rotational velocity of the star. For those stars which were observed both at the Yerkes and at the Perkins Observatory, the average Perkins $v \sin i$ was again averaged with the Yerkes value to give the final rotational velocity of the star. As a final check, all stars were arranged into groups of similar rotational velocity, spectral type, and luminosity class and were intercompared visually, great care being taken to obtain similar density matches. It was then found that a number of sharp-lined stars had been assigned values of $v \sin i$ which were too high, owing to the blending effect of the forbidden *He* I 4470 line. The final values of $v \sin i$ for these stars were determined visually, as were the values for a number of other stars of various degrees of line broadening, whose measured rotational velocities were inconsistent with those of the remainder of the stars. The rotational velocities of all stars are listed in Table 1.

In order to carry out the stated purpose of this investigation, the positions of the stars included must be known on the H-R diagram; that is, accurate spectral types and luminosity classes are required. These were very kindly provided by Dr. W. W. Morgan, of the Yerkes Observatory, and are on the MK system (Johnson and Morgan 1953). They are listed in Table 1. All spectral types and luminosity classes given there are due to him, with the exception of a few which were classified at Perkins. The latter are identified by an asterisk in Table 1.

IV. ACCURACY OF THE ROTATIONAL VELOCITIES

It is difficult to assess the internal accuracy of the set of $v \sin i$ values determined in this paper. This is because of the method employed, in which estimates from line profiles were combined with direct visual estimates to obtain final values of $v \sin i$. The agreement between the two values of the rotational velocity derived from line profiles for each star is good, but this is probably misleading as a gauge of internal accuracy, as direct visual estimates show. As a final check on the internal consistency of a set of $v \sin i$ values, direct visual estimates appear to be rather accurate, provided that the observational material is homogeneous and that comparisons are made between stars of the same spectral type and luminosity class, using spectra of comparable density.

TABLE 1

SPECTRAL TYPES AND ROTATIONAL VELOCITIES OF THE BRIGHTER DRAPER B2-B5 STARS

Star	α(1900)	δ(1900)	m_v	Sp(MK)	v sin i (Km/sec)	Notes
	$0^h\ 8^m.1$	$+14^\circ 38'$	2.87	B2IV	0	**
HR 91	0 18.9	+51 28	5.36	B5IV	230	
HR 144	0 30.6	+53 37	5.14	B8V*	60	
ζ Cas	0 31.4	+53 21	3.72	B2V	20	
π And	0 31.5	+33 10	4.44	B5V	$\leq$50	1
η Cas	0 36.5	+49 58	4.85	B2V	230	
o Cas	0 39.2	+47 44	4.70	B2V	260	2
ν And	0 44.3	+40 32	4.42	B5V	80	3
1 Per	1 45.4	+54 39	5.49	B2V	210	
ϵ Cas	1 47.2	+63 11	3.44	B2p	10	4
δ Cet	2 34.4	- 0 6	4.04	B2IV	20	5**
35 Ari	2 37.6	+27 17	4.58	B3V	135	
π Cet	2 39.3	-14 17	4.39	B7V	15	
π Ari	2 43.7	+17 3	5.30	B6IV*	75	6
σ Ari	2 46.0	+14 40	5.46	B7V*	195	
HR 890	2 53.7	+51 57	5.42	B7IV*	220	
λ Cet	2 54.4	+ 8 31	4.69	B5III*	150	
30 Per	3 11.1	+43 39	5.38	B8V*	250	
HR 985	3 11.2	+65 17	4.76	B2Ve	360	7
29 Per	3 11.5	+49 51	5.30	B3V	145	
31 Per	3 12.0	+49 44	5.08	B5V	320	
τ Ari	3 15.5	+20 47	5.17	B5Vp?	20	8
HR 1011	3 16.1	+48 51	5.30	B5V	250	
HR 1034	3 20.9	+48 43	4.94	B3V	50	
34 Per	3 22.2	+49 10	4.67	B5V*	180	
ψ Per	3 29.4	+47 52	4.26	B5e	390	9
δ Per	3 35.8	+47 28	3.10	B5III	255	
40 Per	3 36.0	+33 39	5.04	B0.5V	60	
16 Tau	3 38.9	+23 58	5.43	B7IV	235	
17 Tau	3 38.9	+23 48	3.81	B6III	245	10
19 Tau	3 39.3	+24 9	4.37	B6V	140	
20 Tau	3 39.9	+24 3	4.02	B7III	30	
29 Tau	3 40.4	+ 5 44	5.36	B3V	145	11
23 Tau	3 40.4	+23 38	4.25	B6IVnn	315	12
η Tau	3 41.5	+23 48	2.96	B7III	210	13
30 Tau	3 42.8	+10 50	5.03	B3V	20	
HR 1207	3 48.8	+47 35	5.34	B6V	300	
HR 1215	3 50.0	+34 47	5.48	B2V	130	
λ Tau	3 55.1	+12 12	3.8-4.1	B3V	$\leq$110	14
35 Eri	3 56.5	- 1 50	5.25	B5V	190	
40 Tau	3 58.5	+ 5 10	5.33	B3V	25	
48 Per	4 1.4	+47 27	4.03	B3Vp	250	15
HR 1288	4 4.8	-16 39	5.45	B3V	40	
HR 1289	4 5.0	+83 34	5.39	B5V	320:	
μ Tau	4 10.1	+ 8 39	4.32	B3V	80	
53 Per	4 14.3	+46 16	4.89	B6III	10	
72 Tau	4 21.3	+22 46	5.41	B6V	230	
HR 1423	4 24.5	-13 16	5.50	B1Vn	340	16
ν Eri	4 31.3	- 3 33	4.12	B2III	40	17**
HR 1469	4 32.1	+ 0 48	5.32	B7V	140	
τ Tau	4 36.3	+22 46	4.33	B3V	220	18
μ Eri	4 40.5	- 3 26	4.18	B5IV	190	
π^4 Ori	4 45.9	+ 5 26	3.78	B2III	40	19
π^5 Ori	4 49.0	+ 2 17	3.6-3.7	B2III	90	20
ψ Eri	4 56.6	- 7 19	4.81	B2*V*	90	

TABLE 1 (Continued)

SPECTRAL TYPES AND ROTATIONAL VELOCITIES OF THE BRIGHTER DRAPER B2-B5 STARS

Star	α (1900)	δ (1900)	m_v	Sp(MK)	v sin i (Km/sec)	Notes
11 Cam	$4^h57^m.5$	+58°50'	5.31	B2*V:p*	125	21
η Aur	4 59.5	+41 6	3.28	B3V	125	
103 Tau	5 2.0	+24 8	5.50	B2V	90	22
λ Eri	5 4.4	- 8 53	4.34	B2IV	325	
τ Ori	5 12.8	- 6 57	3.68	B5III	25	
ρ Aur	5 14.7	+41 42	5.12	B5V*	90:	
ν Lep	5 15.4	-12 25	5.29	B7:V:nn	370	
22 Ori	5 16.7	- 0 29	4.65	B2IV	20	
23 Ori(br)	5 17.6	+ 3 27	4.99	B1V	280	
8 Lep	5 18.9	-14 1	5.17	B2IV	20	
25 Ori	5 19.6	+ 1 45	4.73	B1V	295	23
γ Ori	5 19.8	+ 6 16	1.70	B2III	60	
115 Tau	5 21.3	+17 53	5.31	B5V	160	
ψ Ori	5 21.6	+ 3 1	4.66	B2IV		24
114 Tau	5 21.6	+21 51	4.83	B3V	10	
32 Ori	5 25.4	+ 5 52	4.32	B5IV	190	
ν Ori	5 27.1	- 7 23	4.64	BOV	10	
HR 1861	5 27.6	- 1 40	5.30	B1V	20	
120 Tau	5 27.7	+18 28	5.50	Bp	280	25
121 Tau	5 29.4	+23 58	5.28	B3V	115	
42 Ori	5 30.5	- 4 54	4.65	B2III	105	
ζ Tau	5 31.7	+21 5	3.00	B2IVp	310	26
125 Tau	5 33.5	+25 50	5.00	B2V	60	27
ω Ori	5 33.9	+ 4 4	4.54	B3IIIe	195	28
126 Tau	5 35.5	+16 29	4.87	B3IV	90	29
HR 1952	5 35.8	- 1 11	5.00	B2IV	65	30
133 Tau	5 42.1	+13 52	5.20	B2V	60	
55 Ori	5 46.5	- 7 33	5.32	B2V	145	
139 Tau	5 51.8	+25 56	4.90	B1Ib	$\leq$140	
χ^2 Ori	5 58.0	+20 8	4.71	B2Ia	0	
HR 2142	5 59.4	- 6 42	5.12	B2IV,V*nne	450	31
HR 2154	6 1.7	- 4 11	5.37	B5IV	10	
ν Ori	6 1.9	+14 47	4.40	B3V	30	32
ι Ori	6 6.3	+14 14	4.35	B3V	230	
69 Ori	6 6.3	+16 9	4.92	B5V	310	
HR 2205	6 7.0	- 6 32	5.09	B2V	15	
HR 2266	6 13.9	-19 56	5.31	B2V	75	
7 Mon	6 14.9	- 7 47	5.13	B2V	165	
HR 2284	6 16.8	-11 44	5.49	B1Vep	270	33
10 Mon	6 23.0	- 4 42	4.98	B2V	85	
ν Gem	6 23.0	+20 17	4.06	B7IV	220	34
β Mon A	6 24.0	- 6 58	4.73	B3Vpe	360	35
HR 2395	6 28.6	- 1 9	5.02	B6V	310	
42 Cam	6 40.5	+67 41	5.04	B3IV*	140	
43 Cam	6 42.9	+69 0	5.13	B7IV*	205	
HR 2522	6 44.4	-15 2	5.29	B6V	150	
ι CMa	6 51.7	-16 55	4.39	B3II	0	
19 Mon	6 58.0	- 4 6	4.89	B1V	350	
γ CMa	6 59.2	-15 29	4.07	B8II	$\leq$15	
HR 2678	7 2.0	-11 8	5.28	B0.5IV	165	36
HR 2825	7 20.2	-16 0	5.20	B3V	30:	37
16 Pup	8 4.6	-18 57	4.34	B5V	190	
η Hya	8 38.0	+ 3 45	4.32	B3V	135	
κ Hya	9 35.5	-13 53	4.96	B5V	190	
30 Sex	10 25.2	- 0 7	4.95	B6V	115	

TABLE I (Continued)

SPECTRAL TYPES AND ROTATIONAL VELOCITIES OF THE BRIGHTER DRAPER B2-B5 STARS

Star	α(1900)	δ(1900)	m_v	Sp(MK)	v sin i (Km/sec)	Notes
HR 4590	$11^h55.^m7$	$-19^\circ 6'$	5.28	B1.5V	135	38
κ Dra	12 29.2	+70 20	3.88	B7p	250	39
α Vir	13 19.9	-10 38	1.21	B1V		40
η UMa	13 43.6	+49 49	1.91	B3V	210	
θ CrB	15 28.9	+31 42	4.17	B7nn	400	41
HR 5780	15 29.0	- 8 51	5.15	B6IV-V	15	
λ Lib	15 47.5	-19 52	5.06	B3V	220	
48 Lib	15 52.6	-13 59	4.68	Bp	400	42
β Sco(ft)	15 59.6	-19 32	5.06	B2V	85	
ν Sco(br)	16 6.2	-19 12	4.29	B2IV?	210	
τ Her	16 16.7	+46 33	3.91	B5IV	20	
χ Oph	16 21.2	-18 14	4.85	B2IV†p	115	43
ζ Dra	17 8.5	+65 50	3.22	B6III	20	
68 Her	17 13.6	+33 12	4.6-5.3	Comp		44
HR 6502	17 22.5	+20 10	5.42	B6V:	250	
ι Her	17 36.6	+46 4	3.79	B3V	0	45
66 Oph	17 55.3	+ 4 22	4.81	B2Ve	$\leq$275	46
67 Oph	17 55.6	+ 2 56	3.92	B5Ib	0	
96 Her	17 58.1	+20 50	5.09	B3V	220	47
102 Her	18 4.5	+20 48	4.32	B2V	20	
HR 6845	18 12.5	+42 8	5.42	B6V:	235	
4 Aql	18 39.8	+ 1 57	5.04	B9V	350	
HR 7119	18 49.0	-15 44	5.04	B5III	10	
HR 7166	18 53.8	-12 59	5.36	B5V	190	48
HR 7202	18 57.2	+26 9	5.50	B5V	300	
HR 7210	18 57.7	+50 23	5.24	B3V	0	
HR 7249	19 2.4	-19 27	5.41	B2Ve?	220	49
ι Lyr	19 3.7	+35 57	5.13	B7IV	310:	
20 Aql	19 7.3	- 8 6	5.37	B3IV	170	
η Lyr	19 10.4	+38 58	4.46	B2IV	10	
1 Vul	19 11.9	+21 13	4.60	B3IV	130	
3 Vul	19 18.8	+26 4	4.92	B6III	45	
Σ Cyg	19 20.2	+29 26	4.86	B3IV	155	
8 Cyg	19 28.1	+34 14	4.85	B3IV	10	
ι Aql	19 31.6	- 1 31	4.28	B5III	95	
σ Aql	19 34.3	+ 5 10	5.0-5.2	B3V		50
12 Vul	19 46.8	+22 21	4.91	B3V	300	51
23 Cyg	19 51.2	+57 16	5.04	B5V	150	
22 Cyg	19 52.3	+38 13	4.87	B6III	120	
HR 7628	19 53.8	+40 6	5.43	B5Vp?	115	52
25 Cyg	19 56.3	+36 46	5.15	B3V	230	53
17 Vul	20 2.6	+23 20	5.08	B3V	240:	
28 Cyg	20 5.7	+36 33	4.82	B3V	310	54
HR 7739	20 11.0	+25 17	4.82	B3V	275	
ω^1 Cyg	20 27.0	+48 37	4.89	B2V	185	
ϵ Del	20 28.4	+10 58	3.98	B6III	40	
τ Cap	20 33.7	-15 18	5.30	B6III	180	55
28 Vul	20 34.2	+23 46	5.04	B5V	330	
51 Cyg	20 39.1	+49 59	5.41	B2V	30	
λ Cyg	20 43.5	+36 7	4.47	B5V	140	56
55 Cyg	20 45.5	+45 45	4.89	B3Ia	0	
57 Cyg	20 49.7	+44 1	4.68	B5V	$\leq$115	57
60 Cyg	20 57.7	+45 46	5.24	B1V	320:	58
υ Cyg	21 13.8	+34 29	4.42	B2Ve	280	59
6 Cep	21 17.3	+64 27	5.18	B3V	150	60

TABLE 1 (Continued)

SPECTRAL TYPES AND ROTATIONAL VELOCITIES OF THE BRIGHTER DRAPER B2-B5 STARS

Star	α(1900)	δ(1900)	m_v	Sp(MK)	v sin i (Km/sec)	Notes
70 Cyg	$21^h23^m.3$	$+36^\circ41'$	5.20	B3V	135	
7 Cep	21 25.8	+66 22	5.42	B7	300:	
ϵ Cap	21 31.5	-19 55	4.72	B3V:p	290	61
9 Cep	21 35.2	+61 38	4.87	B2Ib	0	
π^4 Cyg	21 38.6	+50 44	4.78	B3V	120	
π^3 Cyg	21 43.1	+48 51	4.26	B3III	35	
16 Peg	21 48.5	+25 27	5.05	B3V	150	62
o Aqr	21 58.2	- 2 38	4.66	B8V	300	63
38 Aqr	22 5.3	-12 3	5.40	B6III:	10	
30 Peg	22 15.4	+ 5 17	5.35	B5III	30	
31 Peg	22 16.6	+11 42	4.93	B2V	130	64
2 Lac	22 16.9	+46 2	4.66	B6IV		65
6 Lac	22 26.2	+42 37	4.54	B2IV	75	
12 Lac	22 37.0	+39 42	5.18	B2III	80	66**
HR 8731	22 52.7	+48 9	5.20	B2:p	340	67
o And	22 57.3	+41 47	3.63	B6*p	330	68
β Psc	22 58.8	+ 3 17	4.58	B5ne	145	69
ψ^2 Aqr	23 12.7	- 9 44	4.56	B5V	350	
HR 8926	23 25.4	+58 0	4.9-5.0	B3*V*	160	70
σ Cas	23 53.9	+55 12	4.93	B1V	190	

NOTES TO TABLE 1

1. Variable radial velocity, P = 144 days, two spectra. There are indications of two spectra on the Perkins plate. The He I 4471 line is shaded slightly to the violet and it is possible that the rotational velocity of 50 Km/sec is slightly too large.

2. MWC 8.

3. Variable radial velocity, P = 4.3 days, two spectra. Only one spectrum is visible on the Perkins plate.

4. Sharp-line standard star. Morgan (Morgan, Keenan and Kellman 1943) has called attention to the peculiar spectrum of this star, pointing out that the lines He I 4026 and 4471 are considerably weaker than in stars of similar type, while the broad H wings observed for stars of luminosity class V are not observed.

5. Variable radial velocity, P = 0.15 days.

6. Variable radial velocity, P = 3.9 days.

7. MWC 65. Also variable radial velocity, P = 4.5 years.

8. He I 4026 abnormally strong?

9. MWC 69. Shell star.

10. MWC 72.

11. Variable radial velocity, two spectra. Only one spectrum is visible on the Perkins plate.

12. MWC 73.

13. MWC 74.

14. Variable radial velocity, P = 4.0 days, two spectra. Some evidence of secondary spectrum on the Perkins plate, but the He I lines appear to be single.

15. MWC 81. Pole-on star.

16. MWC 86.

NOTES TO TABLE 1 (Continued)

17. Variable radial velocity, P = 0.19 days.

18. Variable radial velocity, P = 1.5 days.

19. Variable radial velocity, P = 9.5 days.

20. Variable radial velocity, P = 3.7 days.

21. MWC 96. Pole-on star.

22. Variable radial velocity, P = 58.4 days.

23. MWC 110.

24. Variable radial velocity, P = 2.5 days, two spectra. The spectrum is composite on the Perkins plate.

25. MWC 111. Pole-on star?

26. MWC 115. Shell star. Variable radial velocity, P = 133 days.

27. Variable radial velocity, P = 27.9 days.

28. MWC 117.

29. Close binary, $5^{m}.5$ and $5^{m}.7$ components. Only one spectrum visible on the Perkins plate.

30. Variable radial velocity, P = 27.2 days.

31. MWC 133

32. Variable radial velocity, P = 131 days.

33. MWC 138.

34. MWC 141.

35. MWC 143. Shell star.

36. Close binary, $5^{m}.6$ and $6^{m}.8$ components. The He I lines appear to be single on the Perkins plate.

37. MWC 177. Pole-on star.

38. Variable radial velocity, P = 3.0 days.

39. MWC 222. Variable radial velocity, P = 0.89 days.

40. Variable radial velocity, P = 4.0 days, two spectra. The spectrum is composite on the Perkins Plate.

41. MWC 237.

42. MWC 239. Shell star.

43. MWC 241. Pole-on star.

44. Variable radial velocity, P = 2.05 days, two spectra, eclipsing system. The spectrum is composite on the Perkins plate.

45. Sharp-line standard star. Variable radial velocity, P = 0.14 days?

46. MWC 278. Two spectra. The helium lines are very broad on the Perkins plate and it is uncertain whether there was doubling at that phase.

47. Variable radial velocity, P = 50.2 days?

48. Close binary, $5^{m}.9$ and $6^{m}.4$ components.

49. MWC 311.

50. Variable radial velocity, P = 2.0 days, two spectra, eclipsing system. The spectrum is composite on the Perkins Plate.

NOTES TO TABLE 1 (Continued)

51. MWC 323.

52. Hydrogen lines too strong?

53. MWC 624.

54. MWC 329. Variable radial velocity, P = 226 days.

55. Close binary, $5^{m}.6$ and $6^{m}.9$ components.

56. MWC 352. Close binary, $4^{m}.8$ and $6^{m}.1$ components. The helium lines appear single on the Perkins plate.

57. Variable radial velocity, P = 2.9 days, two spectra. Only one spectrum is visible on the Perkins plate.

58. MWC 360.

59. MWC 364. Pole-on star.

60. MWC 367.

61. MWC 373. Shell star.

62. MWC 644.

63. MWC 384.

64. MWC 387.

65. Variable radial velocity, P = 2.6 days, two spectra. The spectrum is composite on the Perkins plate.

66. Variable radial velocity, P = 0.19 days.

67. MWC 394. Shell star.

68. Shell star.

69. MWC 396. Pole-on star.

70. Eclipsing variable, AR Cassiopeiae, P = 6.1 days.

** These stars are β Cephei or β Canis Majoris stars. Struve ("The Present State of Our Knowledge of the β Canis Majoris or β Cephei Stars", Ann.d'ap.,15,157-168,1952) has shown that the members of this class of stars show variations in line broadening. The values of v sin i given here are based on one plate only, and therefore are measures of the line broadening at a particular phase.

The fact that one of the sharp-lined standard stars, ϵ Cassiopeiae, has slight rotational line broadening should tend to give values of $v \sin i$ for slowly rotating stars that are a trifle small and should have little effect on the more rapidly rotating stars. As was mentioned above, however, the rotational velocities for the stars with small line broadening were largely determined by visual inspection. For the more rapidly rotating stars, the agreement between rotational velocities estimated from computed line contours derived from ι Herculis and from ϵ Cassiopeiae was good.

A rough estimate of the accidental errors involved in the $v \sin i$ determinations is given in Table 2, in which the probable maximum errors are given for different values of the measured rotational velocities.

A word should be added concerning the effect of finite resolving power on the observed rotational velocities. With the dispersion employed in this study there is very little difference in the broadening of line contours corresponding to rotational velocities of 0 and 25 km/sec. Therefore, values of $v \sin i$ listed in Table 1 which are less than 25 km/sec

TABLE 2

PROBABLE MAXIMUM ERRORS OF MEASURED ROTATIONAL VELOCITIES

$v \sin i$ (Km/Sec)	Probable Maximum Error (Km/Sec)	$v \sin i$ (Km/Sec)	Probable Maximum Error (Km/Sec)
0–50	±20	205–300	±50
55–100	±30	>300	±75
105–200	±40		

should be treated cautiously. Coudé spectrograms would be required to give a reliable distribution of the rotational velocities of slowly rotating stars. On the other hand, the present resolution is quite adequate to handle the moderately and rapidly rotating stars, since the line contours computed by the Shajn-Struve graphical method are insensitive to the standard zero-rotational-velocity line contour for large values of $v \sin i$. Since the B-type stars are characterized by values of $v \sin i$ ranging up to 400–500 km/sec, the present moderate resolution is sufficient for a statistical study of axial rotation in these stars as a group, even though it provides only approximate values of $v \sin i$ for the slowly rotating stars.

A comparison of the rotational velocities of stars which were observed both at the Perkins and at the Yerkes Observatory is shown in Figure 2. The agreement is quite good, although there appears to be a tendency for the Yerkes values to run slightly higher. The star which is considerably off the left side of the diagram (Perkins, 50 km/sec; Yerkes, 250 km/sec) is π Andromedae, which is a double-lined spectroscopic binary. It is probable that the two-line phase was observed at Yerkes, thus giving too high a value of $v \sin i$.

Figure 3 illustrates the Perkins rotational velocities versus those of Miss Westgate (1933). In addition to a rather considerable scatter, the values of Miss Westgate are seen to run systematically lower than the Perkins values.

A similar comparison made with the recent observations of Huang (1953) is shown in Figure 4. The agreement here is satisfactory, but two points should be noted. First, the Perkins values of $v \sin i$ are systematically slightly larger than those of Huang for values in excess of about 200 km/sec. Second, Huang's rotational velocities are systematically larger for values of $v \sin i$ less than about 75 km/sec. As was mentioned above, the Perkins line-profile values were also found to run systematically higher than the direct

visual estimates for many slowly rotating stars, and this was interpreted as being due to the blending effect of the forbidden *He* I 4470 line. It appears probable that this same effect may have influenced Huang's measures of line widths for the stars with small line broadening.

V. DISCUSSION

Of the 185 stars in Table 1, only stars which could be located uniquely on the H-R diagram by spectroscopic means and which have noncomposite spectra on the Perkins

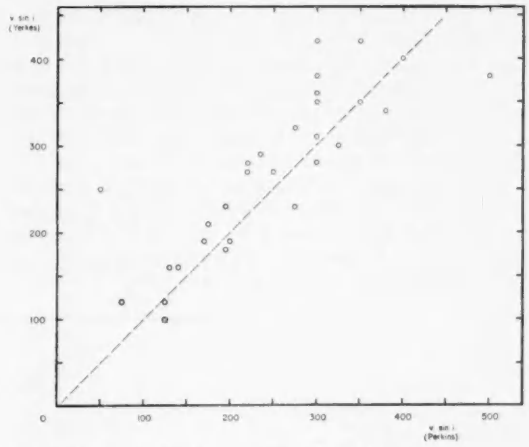

FIG. 2.—Comparison of rotational velocities measured at Perkins with those measured at Yerkes

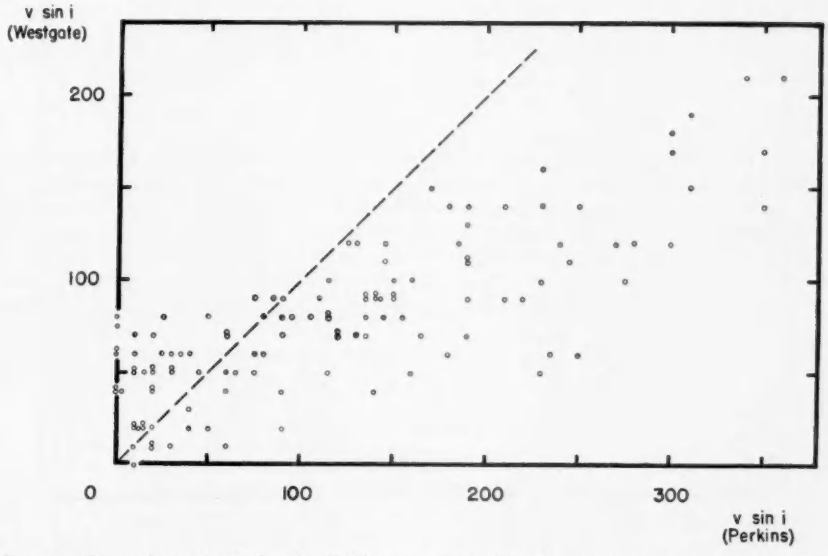

FIG. 3.—Comparison of rotational velocities measured at Perkins with those measured by Miss Westgate.

plates were included in the following statistical discussion. Thus a total of 12 stars has been eliminated because of difficulties of spectral classification, most of these being shell stars or pole-on stars. In addition, seven stars show some evidence of secondary spectrum on the Perkins plates and have also been eliminated. The remaining stars, plus one B2, one B5, and four B7 stars, whose rotational velocities were measured in a previous study (Slettebak 1954), are considered below.

1. MAIN-SEQUENCE STARS

A total of 78 stars with MK types in the range B2–B5 V has been found. The mean observed rotational velocity of this group is given in Table 3, with the mean true rotational velocity. The derivation of the latter quantity, given the former and assuming a random distribution of the axes of rotation, is due to Chandrasekhar and Münch (1950).

Included in the 78 B2–B5 V stars are 16 stars of type Be. Taken separately, these stars have a $\bar{v}$ of 284 km/sec—significantly larger than the value obtained for the corresponding non-emission stars, as has been shown previously. The Be stars have been included in this discussion because it appears likely from the work of Wilson (1941) and Smith (1947) that there is no significant difference in the luminosities of the emission and non-emission stars. Also, the spectra of Be stars in a non-emission phase appear no different from those of normal B-type stars of corresponding type. In this sense a Be star is probably a normal B-type star in rotational instability.

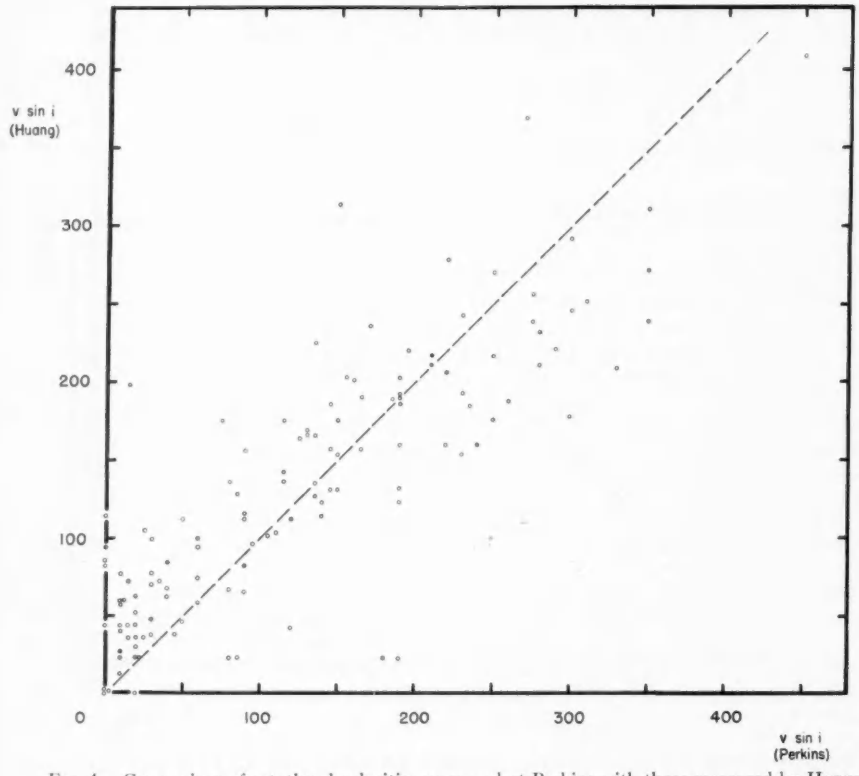

FIG. 4.—Comparison of rotational velocities measured at Perkins with those measured by Huang

The value of $\bar{v}$ of 201 km/sec for the B2–B5 V stars obtained here may be compared with the corresponding value, obtained by one of us (1954), for the B8–A2 V stars: 177 km/sec. The reality of the somewhat larger axial rotation found for the B2–B5 V stars is questionable. Besides errors arising from the relatively small number of stars considered, a systematic error of 25 km/sec between the two determinations is entirely possible and would be enough to obliterate the difference. It is safe to say that axial rotation at these two positions on the H-R diagram is not very different, with the B2–B5 V stars probably having somewhat greater rotation than the B8–A2 V stars.

Since a number of stars with MK types earlier than B2 and later than B5 are included in Table 1, an attempt to gain resolution on the main sequence was made by dividing the B1–B7 stars into two groups and comparing their axial rotation. Table 3 lists the mean observed rotational velocity and the mean true rotational velocity of the two groups, the B1–B3 V stars and the B5–B7 V stars. This grouping would tend to indicate

TABLE 3

AXIAL ROTATION OF THE B-TYPE STARS

Spectral Type (MK) and Luminosity Class	No. of Stars	$\overline{v \sin i}$ (Km/Sec)	$\bar{v}$ (Km/Sec)
B2–B5:			
V	78	158	201
IV	23	112	143
III	14	86	110
B1–B3:			
V	67	157	200
IV	17	110	139
III	8	81	102
B5–B7:			
V	35	203	257
IV	13	177	225
III	17	91	116

that the largest axial rotation among the B-type stars occurs in the B5–B7 V range, with the values dropping off as one goes to both earlier and later types. Again, it must be cautioned that the numbers of stars involved are relatively small.

It may be of some interest to derive the distribution of the true rotational velocities from the distribution of observed rotational velocities for the B2–B5 V stars, following the methods of Chandrasekhar and Münch (1950), although the physical significance of the derived true-rotational-velocity distribution is questionable with only 78 stars involved (Brown 1950).

Assuming random orientation of the axes of rotation and a frequency function for the true rotational velocities of the form

$$f(v) = \frac{j}{\sqrt{\pi}} \left[e^{-j^2(v-v_1)^2} + e^{-j^2(v+v_1)^2} \right],$$

the predicted distribution of $v \sin i$ is compared with the observed distribution of $v \sin i$ in Figure 5. The parameters of $f(v)$ are listed in Table 4, following the notation of Chandrasekhar and Münch (1950). Figure 5 may be compared with similar frequency-curves for the B8–A2 stars (Slettebak 1954) and for other groups of stars (Chandrasekhar and Münch 1950).

2. STARS OF INTERMEDIATE LUMINOSITY

A total of 55 stars was estimated to be of luminosity classes III and IV in the range of MK spectral types B1–B7. These are differentiated and broken down into groups of B2–B5, B1–B3, and B5–B7 stars in Table 3. In all cases the stars of intermediate luminosity have significantly less axial rotation than the corresponding main-sequence stars. This was also found to be the case among the B8–A2 stars (Slettebak 1954), but the opposite was found for the F0–G0 stars by Herbig and Spalding (1953) and independently by Slettebak (1953).

Table 3 shows further that axial rotation among the B-type stars appears to be smallest in the giant stars and increases with decreasing luminosity to the subgiant and finally to the main-sequence stars. As in the case of the main-sequence stars, the largest axial

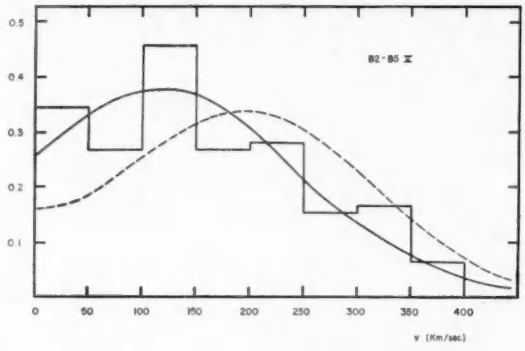

FIG. 5.—Comparison of the distribution of the observed rotational velocities of the B2–B5 main-sequence stars with that derived on the assumption of a true distribution of velocities of the form given in the text and for values of the parameters listed in Table 4. The observed distribution of $v \sin i$ is represented by the histogram, while the full-line curve represents the predicted distribution of $v \sin i$ for a true distribution of v given by the dashed curve.

TABLE 4

PARAMETERS OF ROTATIONAL-VELOCITY DISTRIBUTION OF B2–B5 MAIN-SEQUENCE STARS

$\overline{v \sin i}$ (km/sec)	158	$\bar{v}/[2\,(\overline{v^2} - \bar{v}^2)]^{1/2}$	1.33
$\overline{v^2 \sin^2 i}$ [(km/sec)^2]	34,560	j^{-1} (km/sec)	164
$\bar{v}$ (km/sec)	201	v_1 (km/sec)	197
$\overline{v^2}$ [(km/sec)^2]	51,840		

rotation among the stars of intermediate luminosity occurs in the B5–B7 range, the velocities decreasing as one goes to both earlier and later types. The B-type giants and subgiants probably have generally larger rotational velocities than the corresponding B8–A2 stars, but this result must be viewed with caution for two reasons: (1) the possibility of systematic errors in the two determinations and (2) the difficulty of accurate luminosity classification in the B8–A2 stars.

3. SUPERGIANT AND LUMINOUS GIANT STARS

Seven stars in Table 1 are in the range of luminosity classes I*a*–II. Of these, all but one were judged to have extremely small axial rotation, though the lines in some appear to be turbulence-broadened. The B1 I*b* star, 139 Tauri, has rather broad lines which have the appearance of being rotationally broadened. The observed rotational velocity

of this supergiant star is 140 km/sec, under the assumption that the line broadening is entirely due to axial rotation. It is possible that large-scale turbulence may also be an important broadening agent, however, as has been suggested by Struve (1952) for the early-type supergiant stars. The similarity in appearance of line profiles broadened by axial rotation and those broadened by large-scale turbulence has been pointed out by Huang and Struve (1953).

VI. MISCELLANEOUS REMARKS

1. SPECTROSCOPIC BINARIES

Of the stars listed in Table 1, twenty-one are also listed in the Lick Observatory "Fifth Catalogue of the Orbital Elements of Spectroscopic Binary Stars" (1948). Of these, six show evidence of secondary spectrum on the Perkins plates and have been eliminated from the following discussion. The remaining fifteen are listed in Table 5 with their MK spectral types and the corresponding visual absolute magnitudes and effective temperatures, determined from the calibration by Keenan and Morgan (1951).

The fifth column of Table 5 lists the computed radii (Russell, Dugan, and Stewart

TABLE 5

COMPARISON OF ORBITAL AND ROTATIONAL PERIODS FOR FIFTEEN SPECTROSCOPIC BINARIES

Star	Sp (MK)	M_v	T_{eff} (° K)	$R/R_\odot$	$v \sin i$ (Km/Sec)	$P_{rot}/\sin i$ (Days)	P_{orb} (Days)
ν And	B5 V	−1.3	15,600	4.2	80	2.7	4.3
π Ari	B6 IV	−2.0	14,500	6.2	75	4.2	3.9
λ Tau	B3 V	−2.0	18,000	5.1	≤ 110	≥ 2.4	4.0
τ Tau	B3 V	−2.0	18,000	5.1	220	1.2	1.5
π^4 Ori	B2 III	−4.1	20,300	12.4	40	15.6	9.5
π^5 Ori	B2 III	−4.1	20,300	12.4	90	7.0	3.7
103 Tau	B2 V	−2.6	20,300	6.2	90	3.5	58.3
125 Tau	B2 V	−2.6	20,300	6.2	60	5.2	27.9
HR 1952	B2 IV	−3.3	20,300	8.6	65	6.7	27.2
ν Ori	B3 V	−2.0	18,000	5.1	30	8.6	131.3
HR 4590	B1.5 V	−2.9	21,400	6.9	135	2.6	3.0
28 Cyg	B3 V	−2.0	18,000	5.1	310	0.9	226.0
57 Cyg	B5 V	−1.3	15,600	4.2	≤ 115	≥ 1.8	2.9
π^2 Cyg	B3 III	−3.7	18,000	11.3	35	16.3	72.0
HR 8926	B3 V	−2.0	18,000	5.1	160	1.6	6.1

1938) of the fifteen stars and the sixth column their measured rotational velocities. In the seventh and eighth columns the computed period of rotation divided by the sine of the inclination is compared with the orbital period as listed in the Lick catalogue (1948).

Synchronism between axial rotation and orbital revolution appears to be ruled out for seven of the systems in Table 1: 103 Tauri, 125 Tauri, HR 1952, ν Orionis, 28 Cygni, π^2 Cygni, and HR 8926. The latter is the eclipsing system AR Cassiopeiae, for which Luyten, Struve, and Morgan (1939) reached a similar conclusion. On the basis of the measured rotational velocities, synchronism also appears improbable for λ Tauri and 57 Cygni. However, it is possible that the secondary spectrum influenced the $v \sin i$ measures; hence synchronism should not be ruled out for these two systems.

2. THE FORBIDDEN LINE OF HELIUM, λ 4470

As has been mentioned previously, the forbidden line of *He* I at λ 4469.92 (2^3P-4^3F) is visible on the Perkins spectrograms of a number of stars. Since only moderate dispersion was available and the line is intrinsically diffuse, it is not completely resolved from *He* I 4471 but, rather, appears as a fuzzy violet asymmetrical edge on the Perkins plates.

Further, it was distinctly visible only for stars with observed rotational velocities less than about 50 km/sec; greater line broadening blends the two lines hopelessly.

The luminosity dependence of the forbidden λ 4470 line was first shown by Struve (1929): the smaller the luminosity of the star, the stronger the electric fields operating in its atmosphere and the greater the intensity of the line. The stars of high luminosity did not show the λ 4470 line on the Perkins plates, and the line was very weak in the spectra of the few luminosity class III stars in which it was present. All slowly rotating stars of luminosity classes IV and V of spectral type B5 or earlier showed some trace of λ 4470 on the Perkins plates, but no clear separation of the two luminosity classes could be made in terms of the strength of the line. Thus two of the stars with the strongest λ 4470 are the B2 IV stars δ Ceti and γ Pegasi. Again, although a number of main-sequence stars showed the forbidden line conspicuously, others of similar type and rotational broadening had it only weakly present on the Perkins spectrograms.

It should be emphasized that the above remarks are strictly qualitative, in view of the limited visibility of λ 4470 with the present resolution. A quantitative study of the λ 4470 line in the B-type stars with high dispersion plates would be very desirable.

VII. INTERPRETATION

The present investigation, as well as similar studies of the B8–A2 and F0–G0 stars described earlier, have brought out the following relationships between stellar axial rotation and position on the H-R diagram.

1. Axial rotation on the main sequence appears to reach a maximum in the range of spectral types B5–B7 and decreases as one moves to both earlier and later types. In view of the relatively small numbers of stars employed and the possibility of systematic errors, the possibility that the average axial rotation is approximately constant along the main sequence from B2 to A2 cannot be rejected. In any case, there is no question that stellar axial rotation on the main sequence has declined sharply in the early F-type stars and is, for all practical purposes, nonexistent in stars of spectral type F5 and later. The nature of the decline will be considered in a forthcoming paper concerning axial rotation in the A3–G0 stars.

2. Among the B2–A2 stars, axial rotation is greatest for the main-sequence stars and decreases as one goes to higher luminosities. The F0–G0 stars, on the other hand, show the greatest axial rotation in the stars of intermediate luminosity, with less rotation for the main-sequence stars. Further, the giants and subgiants exhibit rotational line broadening to spectral type G0, at least, while axial rotation on the main sequence stops at about F5, as mentioned above. The luminosity dependence of axial rotation in the A3–A7 stars will be considered in a forthcoming paper.

It is tempting to attempt to explain these results in terms of the evolutionary sequences computed recently by Sandage and Schwarzschild (1952). These authors have considered an initially homogeneous star with a convective core and radiative envelope (Cowling model), which is assumed to experience no mixing between the core and envelope and starts to exhaust the hydrogen supply in its core. The subsequent early stages of the evolution were computed by Schönberg and Chandrasekhar (1942). The core finally exhausts its hydrogen and becomes isothermal. The nuclear energy production is then confined to a shell between the exhausted core and the radiative envelope, and the burning continues outward until the core reaches the Schönberg-Chandrasekhar limit. During this process the star moves up about one magnitude from the main sequence, while its effective temperature remains approximately constant.

At this point, Sandage and Schwarzschild assume that a gravitational contraction of the core occurs, which results in a great expansion of the envelope. The star thus evolves rapidly to the right in the H-R diagram, into the giant region.

Following this picture, a main-sequence B- or A-type star with a given rotational velocity will first evolve into a subgiant star of the same spectral type, with a consequent

decrease in axial rotation, due to the conservation of angular momentum. It will then move to the right in the H-R diagram, keeping about the same luminosity while approaching later spectral types. The resultant increase in radius will lead to a further decrease in axial rotation.

The observed decrease in axial rotation in the B2–A2 stars of intermediate luminosity then follows as a result of the evolution of these stars from more rapidly rotating main-sequence stars of similar spectral type (resulting in subgiant stars) and of earlier spectral type (resulting in giant stars). Among the F-type stars, on the other hand, the stars of intermediate luminosity have evolved from rapidly rotating A-type main-sequence stars and therefore still exhibit considerable axial rotation, while the corresponding F-type main-sequence stars, for reasons as yet unknown, have intrinsically small axial rotation.

Perhaps the chief objection to the above interpretation concerns the assumption that no mixing occurs between the core and the envelope of stars with equatorial rotational velocities up to several hundreds of kilometers per second. However, Chandrasekhar (1951) has pointed out that, even if large-scale circulatory currents exist, keeping the envelope well mixed, the rigid-body rotation of the core would prevent mixing between it and the envelope. More recently, Mestel (1953) has shown that the nonsymmetrical distribution of matter set up by the mixing currents in rapidly rotating stars will have a large choking effect on the mixing. He concludes that, if the mixing zone is to extend at all into the radiative envelope, the angular velocity of the star must be so great that the centrifugal force at the surface equator nearly equals gravity.

We are extremely grateful to Dr. W. W. Morgan for generously supplying the spectral types which were used in this study. Thanks are also due our associates at the Perkins Observatory, particularly Dr. Geoffrey Keller, for many informative discussions.

REFERENCES

Brown, A. 1950, *Ap. J.*, **111**, 366–374.
Chandrasekhar, S. 1951, in J. A. Hynek (ed.), *Astrophysics* (New York: McGraw-Hill Book Co., Inc., chap. xiv.
Chandrasekhar, S., and Münch, G. 1950, *Ap. J.*, **111**, 142–156.
Herbig, G. H., and Spalding, J. F., Jr. 1953, *Pub. A.S.P.*, **65**, 192–193.
Huang, Su-Shu. 1953, *Ap. J.*, **118**, 285–303.
Huang, Su-Shu, and Struve, O. 1953, *Ap. J.*, **118**, 463–476.
Johnson, H. L., and Morgan, W. W. 1953, *Ap. J.*, **117**, 313–352.
Keenan, P. C., and Morgan, W. W. 1951, in J. A. Hynek (ed.), *Astrophysics* (New York: McGraw-Hill Book Co., Inc.), chap. i.
Luyten, W. J., Struve, O., and Morgan, W. W. 1939, *Pub. Yerkes Obs.*, Vol. **7**, Part IV.
Mestel, L. 1953, *Observatory*, **73**, 217–218.
Moore, J. H., and Neubauer, F. J. 1948, "Fifth Catalogue of the Orbital Elements of Spectroscopic Binary Stars," *Lick Obs. Bull.*, No. 521.
Morgan, W. W., Keenan, P. C., and Kellman, E. 1943, *An Atlas of Stellar Spectra* (Chicago: University of Chicago Press).
Russell, H. N., Dugan, R. S., and Stewart, J. Q. 1938, *Astronomy* (Boston: Ginn & Co.), Vol. **2**, chap. xxi.
Sandage, A. R., and Schwarzschild, M. 1952, *Ap. J.*, **116**, 463–476.
Schönberg, M., and Chandrasekhar, S. 1942, *Ap. J.*, **96**, 161–172.
Shajn, G., and Struve, O. 1929, *M.N.*, **89**, 222–239.
Slettebak, A. 1949, *Ap. J.*, **110**, 498–514.
———. 1953, *A.J.*, **58**, 228.
———. 1954, *Ap. J.*, **119**, 146–167.
Smith, B. 1947, *Ap. J.*, **105**, 489–491.
Struve, O. 1929, *Ap. J.*, **70**, 237–242.
———. 1952, *Pub. A.S.P.*, **64**, 118–119.
Westgate, C. 1933, *Ap. J.*, **77**, 141–152.
Wilson, R. E. 1941, *Mt. W. Contr.*, No. 646; *Ap. J.*, **94**, 12–20.

AXIAL ROTATION AND LINE BROADENING IN STARS OF SPECTRAL TYPES F0–K5*

GEORGE H. HERBIG AND JOHN F. SPALDING, JR.
Lick Observatory, University of California
Received June 18, 1954

ABSTRACT

The widths of weak lines in 656 stars of spectral types F0–K5 on the revised Yerkes *Atlas* system of Morgan and Keenan have been obtained from plates having a dispersion of 11 A/mm. These line widths have been expressed in terms of $v \sin i$, the projected equatorial velocity required of a rotating, spherical, limb-darkened star in order to reproduce the observed broadening. It seems reasonable that axial rotation is the principal macroscopic broadening agent in those stars less luminous than supergiants, but this is not necessarily the case for the high-luminosity stars. The main conclusions of the paper are as follows: (1) The mean rotational velocity diminishes through class F, but $v \sin i$ values of 20 km/sec or greater can be found in types as late as F8 (in luminosity classes II, IV–V, and V) or G0 (in classes III and IV). With the exception of two binaries, no stars of type later than G5 have been found with rotationally broadened lines, and the widening in a few single stars of types G2–G5 is marginal. (2) For a given spectral type between F0 and G0, the stars of luminosity classes III and IV have much higher mean rotational velocities than do those of class V. (3) There is no significant difference in the rotational velocities of the weak- and strong-line groups of F- and G-type stars. (4) The luminosity class I*a* supergiants have considerably wider lines than do those of class I*b*.

I. INTRODUCTION

Most of our knowledge of the statistics of the rotational velocities of stars of spectral types F and later depends upon the work done by O. Struve and his colleagues at the Yerkes Observatory about 20 years ago and upon a recent contribution by Su-Shu Huang (1953). References to earlier work in the field will be found in the latter paper or in a review article by Struve (1945). Very briefly, the more extensive published studies of projected rotational velocities for stars of type F0 and later are the following: (1) Struve and C. T. Elvey (1931) estimated rotational velocities for 31 F0–K0 stars from the line widths on Yerkes spectrograms of dispersion 10 A/mm at λ 4500; (2) Miss C. Westgate (1934) measured the width of *Sr* II λ 4215 with a micrometer microscope on Yerkes plates of dispersion 30 A/mm at λ 4500 for 112 F-type stars and a limited number of later type; (3) Su-Shu Huang (1953) measured micrometrically the width of *Mg* II λ 4481 in 313 F-type and 10 G-type stars on plates of dispersions 10, 13, and 26 A/mm at λ 4481 selected from the Lick collection of spectrograms.

Although the present investigation is, for the F-type stars, based on much of the same plate material as was used by Huang, it differs from his study in several ways. First, the present line widths (expressed here as rotational velocities) were determined, not from micrometer measures of line width but from careful visual comparison with the spectra of standard stars. The projected rotational velocities of the standard stars were determined from their line profiles. Second, only those stars were examined for which assignments of spectral type and luminosity class were available on the revised *Atlas* system (MK) of W. W. Morgan and P. C. Keenan (Johnson and Morgan 1953). Huang's types were taken from *Pub. Lick Obs.*, Vol. **18,** 1932, and are either HD assignments or types given by the radial-velocity observers; no distinction was made with respect to luminosity. Third, in our investigation, only plates taken with the "New" Mills spectrograph, of dispersion 11 A/mm at λ 4500, were used; furthermore, a considerable number of new spectrograms were taken with this instrument of stars for which additional material seemed desirable. Fourth, the spectral interval covered was F0–K5. All known double-

* *Contributions from the Lick Observatory*, Ser. II, No. 56.

line spectroscopic binaries in which the lines of the two components were not clearly separated and most unresolved visual binaries with $\Delta m \backsim 0$ were rejected. A number of unresolved visual binaries with small Δm, for which it is unlikely that line doubling contributes to the line width, were retained and are indicated in the notes to Table 2.

A preliminary report on this investigation was given by Herbig and Spalding (1953) at the Santa Barbara, California, meeting of the Astronomical Society of the Pacific in June, 1953. Not long after that paper was read, we learned of a parallel study of axial rotation in stars of type A7–G0 in progress by A. Slettebak, of the Perkins Observatory (1953, 1954). We wish to acknowledge the kindness of Dr. Slettebak in sending us in advance of publication a copy of his paper on "Axial Rotation in the F-Type Stars," which he prepared for the meeting of the American Astronomical Society in Boulder, Colorado, in August, 1953. The results of these two independent investigations are in substantial agreement.

II. THE BASIC DATA: ROTATIONAL VELOCITIES AND SPECTRAL TYPES

The quantity actually observed in an investigation of this kind is the width of spectral lines. We have proceeded on the assumption that in the case of lines of *Fe* I, any broadening in excess of that observed in narrow-lined F- and G-type stars is due entirely to axial rotation in those stars less luminous than supergiants. Therefore, the results of the line-width estimates for individual stars (contained in Tables 1 and 2) are expressed as projected equatorial velocities of rotation, in kilometers per second. This assumption seems to be a reasonable one in the light of present knowledge, but we cannot furnish assurance that it is entirely correct.

In order to set up a system of comparison stars of known apparent rotational velocity, it was first assumed that narrow, unblended *Fe* I lines, as observed on Mills 11 A/mm plates of the solar spectrum, contain in their profiles the effect of intrinsic line width in stars of that type, as well as the contribution of the finite resolution of the spectrograph. The lines chosen for profile determination were λ 4472.7 and λ 4476.0, both due mainly to *Fe* I. They were selected on the basis of their relative narrowness and their location in a spectral region where the position of the continuous spectrum is well defined on microphotometer tracings. In addition, *Fe* I λ 4404.8 was used for comparison with those stars in which large broadening rendered λ 4472 and λ 4476 excessively shallow and difficult to use.

The standards consisted of five stars of spectral types F5–G0, plus the sun, which were chosen after a preliminary survey of the plate material showed that they defined a wide range of line width without gaps that could not be spanned by visual interpolation. New spectrograms of photometric quality were obtained for the sun and for these standard stars with the Mills spectrograph. The slit-width projected on the plate was 19 μ, which corresponds to 14 km/sec at λ 4500. The spectra were uniformly broadened by drifting to a width of 0.3–0.5 mm. Kodak IIa-O plates were used throughout. The plates were traced in the modified Moll microphotometer of the Lick Observatory with a magnification of 424 times, and profiles were derived from a tube-sensitometer calibration in the usual manner. The differences in spectral type between some of the standard stars and the sun made it necessary to normalize the profiles in the stars of earliest type, in order that the increase in strength of the *Fe* I lines with spectral type should not confuse the determination of $v \sin i$. The profiles of the lines in the standard stars were then compared with sets of solar profiles as blurred by varying amounts of axial rotation. The method was the graphical one described by A. Unsöld (1938). A limb-darkening coefficient of $u = 0.6$ was used. The value of $v \sin i$ (the projected equatorial velocity of axial rotation) was adopted that yielded the best fit between the computed and the observed line profiles. The adopted values of $v \sin i$, rounded off to the nearest 5 km/sec for the stars with very broad lines, and other relevant data are given in Table 1.

Several spectrograms of different densities and slit widths were available for each standard star. With these at hand for ready reference, a survey of the entire collection of Mills spectrograms of stars with MK types between F0 and K5 was made with a hand magnifier. All stars having perceptibly wider lines than the sun were reserved for later examination. The second examination consisted of a careful comparison on a Hartmann spectrocomparator of the best spectrograms of each wide-lined star with those plates of the standard stars having the most comparable density and slit-width. It was necessary to exercise considerable judgment in the estimates of line width, on account of the large range in plate quality. Many of the older Mills spectrograms of fainter stars were taken with a slit-width of 38 μ (or 28 km/sec at λ 4500), which made them of limited value for the detection of small rotational velocities. The slit-width, therefore, had always to be taken into account in the assignment of $v \sin i$. The results for stars of luminosity classes II through V are contained in Table 2*a*. Because of the different character of the line broadening in supergiants, the data for the high-luminosity stars are given separately in Table 2*b*.

TABLE 1

ROTATIONAL VELOCITIES OF STANDARD STARS

Star	α_{1900}	δ_{1900}	MK Spectral Type	Adopted $v \sin i$ (Km/Sec)	Lines Used in Determination of $v \sin i$ (λ)	No. of Spectrograms
Sun*	.....	.....	G2 V	<15†	.....	4
π^3 Ori	4^h44^m4	+ 6°47′	F6 V	21	4472, 4476	3‡
11 Aql	18 54.5	+13 29	F8 IV	27	4472, 4476	2
ρ And	0 15.8	+37 25	F5 IV	45	4472, 4476	2
31 Com	12 46.8	+28 05	G0 III	85	4404, 4476	2
18 Com	12 24.4	+24 40	F5 IV	115	4404, 4476	2

* The sunlit sky and the moon were actually observed.

† Assumed.

‡ λ 4476 was utilized on all three plates of π^3 Ori, but λ 4472 on only one.

We believe that our estimates of $v \sin i$ are likely to be most uncertain, percentagewise, for those narrow-lined stars in which allowance for poor plate quality had to be made. The entries in the $v \sin i$ column of Tables 2*a* and 2*b* for narrow-lined stars are based on the following conventions. First, a star for which a plate or plates of good quality (i.e., narrow slit and proper exposure) were available and which exhibited weak absorption lines that were fully as sharp as those in the sun was assigned a $v \sin i$ of < 15 km/sec. For the best spectrograms, this value is probably too high a limit. Second, a star for which only poor plates were available but still showed no clear evidence of intrinsic line broadening was given a $v \sin i$ of < 20: km/sec. Third, those stars for which the plate quality was so low that a rotational velocity of 25 or even 30 km/sec would have been concealed were rejected. The choice between the second and third categories was sometimes difficult to make, and, although we have attempted always to err on the conservative side, it is not impossible that some stars of rotational velocity 20 or 25 km/sec are listed as < 20: km/sec in Tables 2*a* and 2*b*.

At the other extreme, for stars having $v \sin i$ of about 100 km/sec or more, a dispersion of 11 A/mm is inconveniently and unnecessarily large, at least when visual estimates are used for the determination of rotational velocity. We do not know whether the quality of our estimates of large $v \sin i$'s has suffered for this reason, but it is certain that the work on such stars would have been less difficult at a lower dispersion.

TABLE 2*a*

CATALOGUE OF LINE WIDTHS OF 624 STARS BETWEEN SPECTRAL TYPES F0 AND K5 AND OF LUMINOSITY CLASSES II–V, EXPRESSED AS ROTATIONAL VELOCITIES

No.*	Star	α_{1900}	δ_{1900}	Spectral Type	Source†	$v \sin i$ (Km/Sec)	Remarks‡
1	33 Psc	0^h00^m2	− 6°16′	K1 III	2	< 15	SB1
2	β Cas	0 03.8	+58 36	F2 IV	1	85	
3	22 And	0 05.1	+45 31	F2 II	1	40	
4	6 Cet	0 06.2	−16 01	F6 V w	2	< 15	
5	HR 37	0 07.1	−18 30	K5 III	2	< 20:	VV
6	ι Cet	0 14.3	− 9 23	K2 III	2	< 15	
7	ρ And	0 15.8	+37 25	F5 IV s	4	45	
8	HR 152	0 31.3	+43 56	K5 III	2	< 15	
9	ϵ And	0 33.3	+28 46	G8 III	2	< 15	
10	δ And	0 34.0	+30 19	K3 III	1	< 15	VV
11	α Cas	0 34.8	+55 59	K0 II–III	2	< 15	LV
12	32 And	0 35.7	+38 55	G8 III	2	< 15	
13	β Cet	0 38.6	−18 32	K0 III	2	< 15	
14	ϕ^1 Cet	0 39.2	−11 09	K0 III	2	< 15	
15*	ζ And	0 42.0	+23 43	K1 II	2	30	SB1
16	η Cas	0 43.0	+57 17	G0 V w	1	< 15	
17	δ Psc	0 43.5	+ 7 02	K5 III	2	< 20:	
18*	64 Psc	0 43.7	+16 24	F8 V s	2	< 15 < 15	SB2
19	ϕ^2 Cet	0 45.1	−11 11	F8 V s	4	< 15	
20	HR 244	0 47.1	+60 34	F8 IV–V s	4	< 15	
21	υ^1 Cas	0 49.1	+58 26	K2 III	2	< 15:	
22	υ^2 Cas	0 50.7	+58 38	G8 III–IV	2	< 15	
23	η And	0 51.9	+22 53	G8 III–IV	2	< 15 < 15	SB2
24	ϵ Psc	0 57.8	+ 7 21	K0 III	2	< 15	
25	μ Cas	1 01.6	+54 26	G5 Vp	1	< 15	
26	η Cet	1 03.6	−10 43	K2 III	2	< 15	
27	χ Psc	1 06.1	+20 30	K0 III	2	< 20:	
28	τ Psc	1 06.2	+29 34	K0 III–IV	2	< 15	VV
29	ϕ Psc	1 08.3	+24 03	K0 III	2	< 15	VV
30	ξ And	1 16.4	+45 00	K0 III–IV	2	< 15	VV?
31	ψ Cas	1 18.9	+67 36	K0 III	2	< 15	
32	θ Cet	1 19.0	− 8 42	K0 III	2	< 15	
33	46 Cet	1 20.7	−15 07	K3 III	2	< 15	
34	ω And	1 21.7	+44 53	F5 IV w	4	75	
35	49 And	1 24.1	+46 30	K0 III	2	< 20:	
36	μ Psc	1 24.9	+ 5 38	K4 III	2	< 15	
37	η Psc	1 26.1	+14 50	G8 III	1	< 20:	
38	χ Cas	1 27.4	+58 43	K0 III	2	< 20:	
39	40 Cas	1 30.5	+72 32	G8 II–III	2	< 20:	
40*	υ And	1 30.9	+40 54	F8 V w	1	< 15	
41	50 Cet	1 31.1	−15 54	K2 III	2	< 20:	
42	51 And	1 31.8	+48 07	K3 III	1	< 15	
43	χ And	1 33.4	+43 52	G8 III	2	< 15	VV
44	HR 483	1 35.7	+42 07	G2 V s	1	< 15	
45	ν Psc	1 36.2	+ 4 59	K3 III	2	< 20:	

* Additional remarks for stars noted by asterisks are given in "Notes to Table 2*a*."

† The sources are identified in the text (pp. 135 and 136).

‡ The abbreviations in the "Remarks" column have the following meanings:

SB1: single-line spectroscopic binary.
SB2: double-line spectroscopic binary.
VV: variable velocity.
VV?: possibly variable velocity.
LV: light variable.
VB: visual binary.

TABLE 2a—*Continued*

No.*	Star	α_{1900}	δ_{1900}	Spectral Type	Source†	$v \sin i$ (Km/Sec)	Remarks‡
46	107 Psc	1^h37^m1	+19° 47′	K1 V	1	< 20:	
47	HR 500	1 37.7	− 4 12	K3 II–III	2	< 20:	
48	τ Cet	1 39.4	−16 28	G8 Vp	1	< 15	
49	o Psc	1 40.1	+ 8 39	K0 III	2	< 15	
50	ζ Cet	1 46.5	−10 50	K2 III	2	< 20:	SB1
51	α Tri	1 47.4	+29 06	F6 IV w	1	115	SB1
52	ξ Psc	1 48.4	+ 2 42	K0 III	2	< 15	VV
53	ι Ari	1 51.9	+17 20	K1 p	2	< 15:	SB1
54	49 Cas	1 56.0	+75 38	G8 III	2	< 15	VV?
55	γ And A	1 57.8	+41 51	K2 III	2	< 15	
56	α Ari	2 01.5	+22 59	K2 III	1	< 15	
57	14 Ari	2 03.7	+25 28	F2 III	1	≥115	
58	60 And	2 07.0	+43 46	K4 III	2	< 15	SB1
59	η Ari	2 07.2	+20 44	F5 V s	2	< 20	
60	ξ^1 Cet	2 07.7	+ 8 23	G8 II	2	< 15	VV
61	δ Tri	2 10.9	+33 46	G0 V w	1	< 15	SB1
62	64 And	2 17.8	+49 33	G8 III	2	< 15	
63	65 And	2 19.0	+49 50	K4 III	2	< 15	
64	14 Tri	2 26.0	+35 42	K5 III	2	< 20:	
65	HR 737	2 26.3	+ 1 50	K3 III	2	< 20:	
66	σ Cet	2 27.4	−15 41	F5 IV–V s	4	20	
67	HR 743	2 28.5	+72 23	G8 III	2	< 20:	
68	ν Cet	2 30.6	+ 5 09	G8 III	2	< 15	
69*	θ Per	2 37.4	+48 48	F7 V w	1	< 15	
70	μ Cet	2 39.5	+ 9 42	F0 IV	1	45	VV
71	τ^1 Eri	2 40.4	−19 00	F6 V s	4	25	
72	39 Ari	2 42.0	+28 50	K1 III	2	< 15	
73	16 Per	2 44.3	+37 54	F2 III	1	>115	
74	17 Per	2 45.4	+34 39	K5 III	2	< 15	
75*	20 Per	2 47.4	+37 56	F4 V	2	85	VB
76	η Eri	2 51.5	− 9 18	K1 III–IV	2	< 15	
77	24 Per	2 52.9	+34 47	K2 III	2	< 15	
78	HR 918	2 58.0	+56 19	K0 II–III	2	< 20:	
79	ι Per	3 01.8	+49 14	G0 V w	1	< 15	
80	κ Per	3 02.7	+44 29	K0 III	2	< 15	VV
81	ω Per	3 04.8	+39 14	K1 III	2	< 20:	
82	δ Ari	3 05.9	+19 21	K2 III	2	< 15	
83	94 Cet	3 07.7	− 1 34	F8 V s	2	< 15	
84	HR 969	3 09.0	+50 34	G5 II	2	< 15	
85	HR 991	3 12.5	+33 51	K2 II	2	< 15	
86	κ Cet	3 14.1	+ 3 00	G5 V s	1	< 15	
87	HR 999	3 14.3	+28 41	K3 II–III	2	< 15	
88	63 Ari	3 17.0	+20 23	K3 III	2	< 20:	
89	o Tau	3 19.4	+ 8 41	G8 III	1	< 15	SB1
90	σ Per	3 23.6	+47 39	K3 III	2	< 15	
91	5 Tau	3 25.4	+12 36	K0 II–III	2	< 20:	SB1
92	36 Per	3 25.5	+45 43	F4 III	1	40	
93	ϵ Eri	3 28.2	− 9 48	K2 V	1	< 15	
94	10 Tau	3 31.8	+ 0 05	F8 V w	4	< 15	
95	ν Per	3 38.4	+42 16	F5 II	1	45	VV?

TABLE 2a—*Continued*

No.*	Star	α_{1900}	δ_{1900}	Spectral Type	Source†	$v \sin i$ (Km/Sec)	Remarks‡
96	δ Eri	3^h38^m4	$-10°06'$	K0 IV	1	< 15	
97	43 Per	3 49.2	+50 24	F5 V s	4	< 15 < 15	SB2
98	32 Eri A	3 49.3	− 3 15	G8 III	2	< 15	
99	HR 1242	3 56.1	+58 53	F0 II	1	< 20:	
100	HR 1249	3 57.5	− 0 33	F6 V s	2	25	
101	37 Tau	3 58.8	+21 49	K0 III	2	< 15	
102	HR 1257	3 58.9	+ 2 33	F6 IV w	2	25	
103*	46 Tau	4 08.2	+ 7 28	F3 V	1	65	VB
104	39 Eri	4 09.6	−10 30	K3 III	2	< 20:	
105	HR 1327	4 11.3	+64 54	G5 III	1	< 20:	
106	54 Per	4 13.9	+34 20	G8 III	2	< 20:	
107	γ Tau	4 14.1	+15 23	K0 III	1	< 15	
108	ϕ Tau	4 14.2	+27 07	K1 III	2	< 20:	
109	δ Tau	4 17.2	+17 18	K0 III	1	< 15	
110	HR 1390	4 19.7	+31 13	K1 III	2	< 20:	
111	π Tau	4 21.0	+14 29	G8 III	2	< 15	
112	75 Tau	4 22.7	+16 08	K2 III	2	< 20:	
113	ϵ Tau	4 22.8	+18 58	K0 III	1	< 15	
114	θ^1 Tau	4 22.8	+15 44	K0 III	1	< 20:	VV
115	45 Eri	4 26.8	− 0 16	K3 II–III	2	< 15	
116	HR 1452	4 29.4	− 9 11	K4 II–III	2	< 20:	
117	α Tau	4 30.2	+16 19	K5 III	1	< 15	
118	3 Cam	4 32.0	+52 53	K0 III	2	< 15	SB1
119	53 Eri	4 33.6	−14 30	K2 III	2	< 15	SB1
120	HR 1523	4 41.6	+81 02	K3 III	2	< 15	VV?
121	HR 1533	4 43.2	+37 19	K4 II	2	< 20:	
122	π^3 Ori	4 44.4	+ 6 47	F6 V s	1	20	
123	2 Aur	4 45.9	+36 32	K3 III	2	< 15	
124	ι Aur	4 50.5	+33 00	K3 II	1	< 15	
125	σ^2 Ori	4 50.8	+13 21	K2 III	2	< 15	
126	π^6 Ori	4 53.4	+ 1 34	K2 II	5	< 15	
127	68 Eri	5 03.8	− 4 35	F5 V w	2	< 15	
128	HR 1684	5 06.0	+15 55	K5 III	2	< 20:	
129	HR 1686	5 06.1	+79 07	F6 V w	2	< 20:	
130	ρ Ori	5 08.1	+ 2 45	K3 III	2	< 15	SB1
131*	α Aur	5 09.3	+45 54	.....	.....	.....	SB2
132	16 Aur	5 11.6	+33 16	K3 III	2	< 15	SB1
133*	λ Aur	5 12.1	+40 01	G0 V w	1	< 15:	
134	109 Tau	5 13.3	+22 00	G8 III	2	< 15	
135	21 Ori	5 14.0	+ 2 30	F5 II	2	85	
136	σ Aur	5 17.8	+37 18	K4 III	2	< 20:	
137	111 Tau	5 18.6	+17 17	F8 V s	2	25	
138	29 Ori	5 19.1	− 7 54	G8 III	2	< 15	
139	27 Ori	5 19.4	− 0 59	K0 III	2	< 20:	
140	ϕ Aur	5 21.0	+34 24	K3p	2	< 15	
141	β Lep	5 24.0	−20 50	G2 II	6	< 20:	
142	31 Ori	5 24.6	− 1 10	K5 III	2	< 20:	LV
143	51 Ori	5 37.3	+ 1 26	K1 III	2	< 15	
144	τ Aur	5 42.2	+39 09	G8 III	2	< 15	
145	132 Tau	5 42.9	+24 32	G8 III	2	< 20	

TABLE 2a—*Continued*

No.*	Star	α_{1900}	δ_{1900}	Spectral Type	Source†	$v \sin i$ (Km/Sec)	Remarks‡
146	ν Aur	5^h44^m6	+39° 07′	K0 III	2	< 15	
147	56 Ori	5 47.2	+ 1 50	K2 II	1	< 20:	
148	χ^1 Ori	5 48.5	+20 16	G0 V s	2	< 20:	
149	δ Aur	5 51.3	+54 17	K0 III	1	< 15	
150	1 Mon	5 54.3	− 9 24	F2 II	7	25:	
151	HR 2113	5 55.0	− 3 05	K2 III	2	< 15	
152	37 Cam	6 01.2	+58 57	G8 III	2	< 20:	
153	36 Cam	6 02.8	+65 44	K2 II–III	2	< 15	
154	71 Ori	6 09.0	+19 12	F6 V s	2	< 15	
155	κ Aur	6 09.0	+29 32	G8 III	2	< 20:	
156	74 Ori	6 10.8	+12 18	F5 IV–V w	2	20	
157	45 Aur	6 13.6	+53 30	F5 III s	2	20	SB1
158	5 Lyn	6 18.1	+58 28	K4 III	2	< 20:	
159	HR 2305	6 19.5	−11 28	K3 III	2	< 20:	
160	HR 2379	6 26.7	−12 19	K3 III	2	< 20:	
161	ψ^2 Aur	6 32.2	+42 35	K3 III	2	< 15	
162	ν^2 CMa	6 32.3	−19 10	K1 IV	2	< 15	
163	ν^3 CMa	6 33.5	−18 09	K1 III	2	< 15	
164	HR 2450	6 34.7	−14 03	K2 II	2	< 15	
165	ψ^4 Aur	6 35.8	+44 37	K5 III	2	< 15	
166	13 Lyn	6 38.3	+57 16	K0 III	2	< 20:	
167	30 Gem	6 38.4	+13 20	K1 III	2	< 20:	
168	ψ^5 Aur	6 39.5	+43 41	G0 V s	2	< 15	
169	ξ Gem	6 39.7	+13 00	F5 IV s	4	95	
170	ψ^6 Aur	6 40.0	+48 54	K1 III	2	< 20:	
171	17 Mon	6 41.9	+ 8 09	K4 III	2	< 20:	
172	18 Mon	6 42.6	+ 2 31	K0 III	2	< 15	VV
173	ψ^7 Aur	6 43.7	+41 54	K3 III	2	< 20:	
174	HR 2527	6 45.5	+77 06	K4 III	2	< 15	VV
175	θ CMa	6 49.6	−11 55	K4 III	2	< 20:	
176	ω Gem	6 56.3	+24 21	G5 II	1	< 20:	
177	HR 2649	6 58.1	+11 06	K3 III	2	< 20:	
178	τ Gem	7 04.8	+30 25	K2 III	2	< 15	
179	63 Aur	7 04.8	+39 29	K4 II–III	2	< 15	
180	20 Mon	7 05.3	− 4 05	K0 III	2	< 20:	
181	18 Lyn	7 07.2	+59 49	K2 III	2	< 20:	
182	δ Gem	7 14.2	+22 10	F2 IV–V	6	115	VV?
183	65 Aur	7 15.4	+36 57	K0 III	2	< 15	
184	66 Aur	7 17.2	+40 52	K0 III	2	< 20:	
185	57 Gem	7 17.4	+25 15	G8 III	2	< 20:	
186	ι Gem	7 19.5	+28 00	K0 III	2	< 15	
187	ϵ CMi	7 20.2	+ 9 28	G8 III	2	< 15	
188	22 Lyn	7 22.3	+49 53	F6 V s	2	< 20:	
189	γ CMi	7 22.7	+ 9 08	K3 III	2	< 15	SB1
190	ρ Gem	7 22.7	+31 59	F0 V	1	85	
191*	65 Gem	7 23.6	+28 07	K2 III	2	{< 15 < 15}	SB2
192	6 CMi	7 24.2	+12 13	K2 III	2	< 20:	
193	HR 2896	7 28.8	+31 11	K0 III	2	< 20:	
194	υ Gem	7 29.8	+27 07	K5 III	2	< 20:	
195	25 Mon	7 32.3	− 3 53	F5 III w	2	30	

TABLE 2a—*Continued*

No.*	Star	α_{1900}	δ_{1900}	Spectral Type	Source†	$v \sin i$ (Km/Sec)	Remarks‡
196	α CMi	7^h34^m1	+ 5° 29′	F5 IV–V s	1	< 15	VB
197	α Mon	7 36.5	− 9 19	K0 III	2	< 15	
198*	σ Gem	7 37.1	+29 08	K1 III	2	25	SB1
199	76 Gem	7 38.0	+26 01	K5 III	2	< 20:	
200	κ Gem	7 38.4	+24 38	G8 III	1	< 15	
201	β Gem	7 39.2	+28 16	K0 III	1	< 15	
202	81 Gem	7 40.3	+18 45	K5 III	2	< 15	VV
203*	9 Pup	7 47.1	−13 38	G1 V s	4	< 15	VB
204	11 Pup	7 52.6	−22 37	F8 II	7	25	
205	14 CMi	7 53.2	+ 2 29	K0 III	2	< 20:	
206	27 Mon	7 54.7	− 3 24	K2 III	2	< 20:	
207	28 Mon	7 56.1	− 1 07	K4 III	2	< 20:	
208	HR 3145	7 57.1	+ 2 37	K2 III	2	< 20:	
209	χ Gem	7 57.4	+28 04	K2 III	2	< 20:	VV
210	μ Cnc	8 01.9	+21 52	G2 IV s	4	< 20:	
211	HR 3182	8 02.9	+68 46	G8 II	2	< 20:	
212	ρ Pup	8 03.3	−24 01	F6 II	7	15	VV
213	19 Pup	8 06.6	−12 38	K0 III	2	< 15	
214	HR 3212	8 06.7	− 7 28	G8 III	2	< 20:	
215	β Cnc	8 11.1	+ 9 30	K4 III	1	< 15	
216	χ Cnc	8 14.0	+27 32	F6 V w	4	< 20:	
217	31 Lyn	8 16.0	+43 31	K5 III	2	< 20:	
218	HR 3306	8 20.6	+ 7 53	G8 II	2	< 20:	
219*	o UMa	8 22.0	+61 03	G2 II–III	3	15	
220	π^2 UMa	8 31.5	+64 41	K2 III	2	< 15	
221	σ Hya	8 33.5	+ 3 42	K2 III	2	< 15	
222	6 Hya	8 35.3	−12 07	K4 III	2	< 20:	
223	9 Hya	8 37.1	−15 35	K1 III	2	< 20:	
224	δ Cnc	8 39.0	+18 31	K0 III	2	< 15	
225	ι Cnc	8 40.6	+29 08	G8 II	2	< 20:	
226*	ϵ Hya AB	8 41.5	+ 6 47	G	.....	< 15	VB
227	12 Hya	8 41.7	−13 11	G8 III	2	< 15	SB1
228	35 Lyn	8 45.2	+44 06	K0 III	2	< 15	
229	ρ^2 Cnc	8 49.7	+28 19	G8 II–III	2	< 20:	
230	ζ Hya	8 50.1	+ 6 20	K0 III	2	< 15	
231*	HR 3579	8 54.2	+42 11	F5 V w	1	25	VB
232	σ^1 UMa	8 59.6	+67 17	K5 III	2	< 20:	
233	ω Hya	9 00.7	+ 5 30	K2 II–III	2	< 20:	
234*	σ^2 UMa	9 01.6	+67 32	F7 IV–V s	1	< 15	
235	τ Cnc	9 02.0	+30 03	G8 III	2	< 20:	
236	τ UMa	9 02.7	+63 55	A7 m	2	< 15	VV
237	ξ Cnc	9 03.6	+22 27	K0 III	2	< 15	SB1
238	17 UMa	9 08.4	+57 10	K5 III	2	< 20:	
239	23 Hya	9 11.7	− 5 56	K2 III	2	< 20:	SB1
240	26 Hya	9 15.0	−11 33	G8 III	2	< 20:	
241	27 Hya	9 15.6	− 9 08	G8 III–IV	2	< 20:	
242	κ Leo	9 18.8	+26 37	K2 III	2	< 20:	
243	α Hya	9 22.7	− 8 14	K3 III	2	< 15	
244	HR 3750	9 22.8	− 5 38	G2 V s	4	< 15	VV?
245	HR 3751	9 22.8	+81 46	K3 III	2	< 20:	

TABLE 2a—*Continued*

No.*	Star	α_{1900}	δ_{1900}	Spectral Type	Source†	$v \sin i$ (Km/Sec)	Remarks‡
246	τ^1 Hya	9h24m1	− 2° 20′	F6 V w	4	45	VV?
247	24 UMa	9 25.6	+70 16	G5 IV s	2	< 20:	
248	λ Leo	9 26.0	+23 25	K5 III	2	< 15	VV?
249	θ UMa	9 26.2	+52 08	F6 IV w	1	< 15	
250	6 Leo	9 26.6	+10 09	K3 III	2	< 15	
251	ξ Leo	9 26.6	+11 45	K0 III	2	< 20:	
252	10 LMi	9 28.1	+36 51	G8 III	2	< 20:	
253	HR 3809	9 28.8	+40 04	K0 III	2	< 20:	
254	11 LMi	9 29.7	+36 16	G8 IV–V	1	< 15	
255	10 Leo	9 31.9	+ 7 17	K1 III	2	< 15	VV
256	HR 3834	9 33.2	+ 5 06	K3 III	2	< 20:	
257	27 UMa	9 33.8	+72 42	K0 III	2	< 20:	
258	ι Hya	9 34.8	− 0 41	K3 III	2	< 15	
259	43 Lyn	9 35.8	+40 13	G8 III	2	< 20:	
260	ε Leo	9 40.2	+24 14	G0 II	1	< 15	
261	HR 3881	9 42.1	+46 29	G2 V s	4	< 15	
262	υ UMa	9 43.9	+59 31	F2 IV	1	115	
263	υ^1 Hya	9 46.7	−14 23	G8 III	2	< 20:	
264	μ Leo	9 47.1	+26 29	K2 III	2	< 15	
265	19 LMi	9 51.6	+41 32	F5 V s	4	< 20:	SB1
266	31 Leo	10 02.6	+10 29	K4 III	2	< 20:	
267	HR 3991	10 05.2	−12 19	F5 V s	2	≥115	
268	λ Hya	10 05.7	−11 52	K0 III	2	< 20:	SB1
269	ζ Leo	10 11.1	+23 55	F0 III	1	85	VV
270*	40 Leo	10 14.3	+19 59	F6 IV w	1	20	
271	γ Leo A	10 14.5	+20 21	K0 III	2	< 15	
272*	HR 4084	10 18.9	+83 04	F5 IV w	4	115	
273	μ Hya	10 21.2	−16 20	K4 III	2	< 20:	
274	31 LMi	10 22.1	+37 13	G8 III–IV	2	< 20:	
275	36 UMa A	10 24.2	+56 30	F8 V w	1	< 15	
276	HR 4126	10 26.6	+76 14	K0 III	2	< 20:	
277	48 Leo	10 29.6	+ 7 28	G8 II–III	2	< 20:	
278	37 LMi	10 33.1	+32 30	G2 II	2	< 20:	
279	φ Hya	10 33.7	−16 21	K0 III	2	< 15	SB1
280	38 UMa	10 35.1	+66 14	K2 III	2	< 20:	
281	HR 4181	10 35.9	+69 36	K3 III	2	< 20:	
282	ν Hya	10 44.7	−15 40	K2 III	2	< 15	
283	44 UMa	10 47.5	+55 07	K3 III	2	< 20:	
284	46 LMi	10 47.7	+34 45	K0 III–IV	1	< 20:	
285	HR 4251	10 48.6	−19 36	F6 V s	4	20	
286	46 UMa	10 50.2	+34 02	K1 III	2	< 20:	
287	47 UMa	10 53.9	+40 58	G0 V s	4	< 20:	
288	α Crt	10 54.9	−17 46	K0 III	2	< 20:	
289	58 Leo	10 55.4	+ 4 09	K1 III	2	< 20:	
290	61 Leo	10 56.7	− 1 57	K5 III	2	< 20:	VV
291	α UMa	10 57.6	+62 17	K0 III	1	< 15	VB
292	ψ UMa	11 04.0	+45 02	K1 III	1	< 20:	
293	73 Leo	11 10.6	+13 51	K3 III	2	< 20:	VV
294	ξ UMa	11 12.8	+32 06	G0 V w	4	< 15 A(btr.) SB1 < 20: B(ftr.) SB1	VB
295	ν UMa	11 13.1	+33 38	K3 III	1	< 20:	

TABLE 2a—*Continued*

No.*	Star	α_{1900}	δ_{1900}	Spectral Type	Source†	$v \sin i$ (Km/Sec)	Remarks‡
296	δ Crt	11^h14^m3	$-14°\,14'$	G8 III–IV	2	< 20:	VV
297	56 UMa	11 17.4	+44 02	G8 II	1	< 20:	
298	λ Crt	11 18.4	−18 14	F5 IV s	2	25	VV
299	ϵ Crt	11 19.6	−10 19	K5 III	2	< 20:	
300	τ Leo	11 22.8	+ 3 24	G8 II–III	2	< 20:	
301	87 Leo	11 25.2	− 2 27	K4 III	2	< 20:	
302	HR 4439	11 26.7	+61 38	F6 V w	4	< 20:	
303	2 Dra	11 30.2	+69 53	K0 III	2	< 20:	
304	υ Leo	11 31.8	− 0 16	G9 III	2	< 20:	
305	92 Leo	11 35.6	+21 54	K0 III	2	< 15	
306	61 UMa	11 35.8	+34 46	G8 V	1	< 15	
307	3 Dra	11 36.9	+67 18	K3 III	2	< 15	
308	ζ Crt	11 39.7	−17 48	G8 III	2	< 20:	
309	χ UMa	11 40.8	+48 20	K0 III	2	< 20:	
310	HR 4521	11 41.6	+56 11	K3 III	2	< 20:	
311	β Vir	11 45.5	+ 2 20	F8 V s	1	< 15	
312	o Vir	12 00.1	+ 9 17	G8 III	2	< 20:	
313	7 Com	12 11.3	+24 30	K0 III	2	< 15	
314	HR 4668	12 11.5	+33 37	K1 III	2	< 15	SB1
315	16 Vir	12 15.3	+ 3 52	K0 III	2	< 20:	
316	11 Com	12 15.7	+18 21	G8 III	2	< 20:	
317	HR 4699	12 15.8	−13 01	K1 III	2	< 20:	
318	5 CVn	12 19.2	+52 07	G7 III	2	< 15	
319	6 CVn	12 20.9	+39 34	G8 III–IV	2	< 20:	
320	15 Com	12 22.0	+28 49	K1 III–IV	2	< 15	
321	18 Com	12 24.4	+24 40	F5 IV s	4	115	
322	HR 4783	12 28.7	+33 48	K0 III	2	< 20:	
323	β CVn	12 29.0	+41 54	G0 V w	1	< 15	
324	β Crv	12 29.1	−22 51	G5 II	6	< 15	
325	χ Vir	12 34.1	− 7 27	K2 III	2	< 15	
326*	γ Vir	12 36.6	− 0 54	F0 V	1	25 (np) / 40 (sf)	VB
327	HD 110628	12 38.4	+26 40	F2n IV	7	110:	
328	27 Com	12 41.6	+17 07	K3 III	2	< 15	
329	31 Com	12 46.8	+28 05	G0 III s	1	85	
330	35 Com	12 48.4	+21 47	G8 III	2	< 15	
331	α^1 CVn	12 51.3	+38 51	F0 V	1	20:	
332	37 Com	12 55.5	+31 20	K1p	2	< 20:	
333	9 Dra	12 56.1	+67 08	G8 III	2	< 15	
334	78 UMa	12 56.4	+56 54	F2 V	1	105:	
335	ϵ Vir	12 57.2	+11 30	G9 III	2	< 15	
336	41 Com	13 02.4	+28 10	K5 III	2	< 15	
337	49 Vir	13 02.6	−10 12	K1 III	2	< 20:	
338	53 Vir	13 06.7	−15 40	F6 IV s	4	< 15	
339	β Com	13 07.2	+28 23	G0 V s	1	< 20:	
340	HR 4997	13 09.2	+40 41	K0 III	2	< 20:	
341	59 Vir	13 11.8	+ 9 57	G0 V s	4	< 15	
342	HR 5013	13 12.3	+14 12	K3 III	2	< 20:	
343*	61 Vir	13 13.2	−17 45	G6 V w	1	< 15	
344	γ Hya	13 13.5	−22 39	G5 III	6	< 15	
345	70 Vir	13 23.5	+14 19	G5 V w	1	< 15	

TABLE 2*a*—*Continued*

No.*	Star	α_{1900}	δ_{1900}	Spectral Type	Source†	$v \sin i$ (Km/Sec)	Remarks‡
346	76 Vir	13 27.7	− 9 39	K0 III	2	< 20:	
347*	τ Boo	13 42.5	+17 57	F7 V w	1	< 15	
348	89 Vir	13 44.4	−17 38	K1 III	2	< 20:	
349	υ Boo	13 44.6	+16 18	K5 III	2	< 15	
350	6 Boo	13 45.0	+21 46	K4 III	2	< 20:	
351	90 Vir	13 49.6	− 1 01	K2 III	2	< 15	
352	η Boo	13 49.9	+18 54	G0 IV s	1	20	SB1
353	9 Boo	13 52.0	+27 59	K3 III	2	< 20:	
354	κ Vir	14 07.6	− 9 48	K3 III	2	< 20:	
355	4 UMi	14 09.2	+78 01	K3 III	2	< 15	SB1
356	15 Boo	14 10.0	+10 34	K0 III	2	< 20:	
357	ι Vir	14 10.8	− 5 31	F6 IV s	4	20	
358	α Boo	14 11.1	+19 42	K2 IIIp	1	< 15	
359	HR 5361	14 13.8	+35 58	K1 III	2	< 15	SB1
360	υ Vir	14 14.4	− 1 48	G8 III	2	< 20:	
361	18 Boo	14 14.4	+13 28	F5 IV–V s	4	45	
362	20 Boo	14 15.0	+16 46	K3 III	2	< 15	
363*	θ Boo	14 21.8	+52 19	F7 V w	1	40	
364	ϕ Vir	14 23.0	− 1 47	G2 III	2	< 20:	
365	ρ Boo	14 27.5	+30 49	K3 III	1	< 15	VV?
366	5 UMi	14 27.7	+76 08	K4 III	2	< 15	
367	σ Boo	14 30.3	+30 11	F2 V	1	< 15	
368	31 Boo	14 36.7	+ 8 35	G8 III	2	< 15	
369	μ Vir	14 37.8	− 5 13	F5 IV w	4	85	VV
370	o Boo	14 40.6	+17 23	K0 III	2	< 15	
371	α^1 Lib	14 45.2	−15 35	F5 IV–V w	4	< 20:	
372	11 Lib	14 45.8	− 1 53	G8 III–IV	2	< 15	
373	HR 5541	14 46.6	+37 41	K0 III–IV	2	< 15	
374	β UMi	14 51.0	+74 34	K4 III	1	< 15	
375	ω Boo	14 57.7	+25 24	K4 III	2	< 15	
376	110 Vir	14 57.8	+ 2 29	K0 III	2	< 15	
377	β Boo	14 58.2	+40 47	G8 II–III	2	< 15	
378	ψ Boo	15 00.2	+27 20	K2 III	2	< 15	
379	45 Boo	15 02.9	+25 16	F5 V w	1	75	
380	HR 5635	15 03.4	+54 56	G8 III	2	< 20:	
381	δ Boo	15 11.5	+33 41	G8 III	1	< 20:	
382	HR 5691	15 13.5	+67 44	F8 V s	2	< 20:	
383	5 Ser	15 14.2	+ 2 09	F8 IV–V w	1	< 15	
384	6 Ser	15 16.0	+ 1 04	K3 III	2	< 15	
385	11 UMi	15 17.2	+72 11	K4 III	2	< 15	
386	ϵ Lib	15 18.8	− 9 58	F5 V s	4	< 20:	SB1
387	ι Dra	15 22.7	+59 19	K2 III	1	< 15	
388	ν^1 Boo	15 27.3	+41 10	K5 III	2	< 15	
389	37 Lib	15 28.7	− 9 43	K1 III	2	< 20:	
390	γ Lib	15 29.9	−14 27	G8 III–IV	2	< 15	
391	16 Ser	15 31.7	+10 21	K0p	2	< 15	VV
392	ϕ Boo	15 34.2	+40 41	G8 IV	2	< 20:	
393	θ UMi	15 34.4	+77 41	K5 III	2	< 15	
394	α Ser	15 39.3	+ 6 44	K2 III	1	< 15	
395	λ Ser	15 41.6	+ 7 40	G0 V w	1	< 15	

TABLE 2a—*Continued*

No.*	Star	α_{1900}	δ_{1900}	Spectral Type	Source†	$v \sin i$ (Km/Sec)	Remarks‡
396	ω Ser	15^{h}45^{m}2	+ 2°.30′	G8 III	2	< 15	
397	δ CrB	15 45.4	+26 23	G5 III–IV	2	< 15	
398	ρ Ser	15 46.9	+21 17	K5 III	2	< 15	
399	κ CrB	15 47.5	+35 58	K0 III–IV	2	< 15	
400	θ Lib	15 48.1	−16 26	G8 III–IV	2	< 20:	
401*	χ Her	15 49.2	+42 44	F9 V w	1	< 15	
402*	γ Ser	15 51.8	+15 59	F6 V w	1	< 20:	VV
403	ϵ CrB	15 53.4	+27 10	K3 III	1	< 15	
404	5 Her	15 56.8	+18 06	K0 III	2	< 15	
405	ρ CrB	15 57.2	+33 37	G2 V w	2	< 20:	
406	θ Dra	16 00.0	+58 50	F8 IV–V s	1	30	SB1
407	κ Her A	16 03.6	+17 19	G8 III	2	< 20:	
408	τ CrB	16 05.3	+36 45	K0 III	1	< 15	VV?
409	χ Sco	16 08.3	−11 35	K3 III	2	< 15	
410	ϵ Oph	16 13.0	− 4 27	G8 III	2	< 15	
411	γ Her	16 17.5	+19 23	F0 III	6	115	VV
412	ψ Oph	16 18.2	−19 48	K0 III	2	< 15	
413	ξ CrB	16 18.2	+31 07	K0 III	2	< 15	
414	ν^2 CrB	16 18.7	+33 56	K5 III	2	< 15	
415	HR 6126	16 22.0	+69 20	K2 III	2	< 20:	
416	η Dra	16 22.6	+61 44	G8 III	1	< 15	
417	HR 6136	16 23.5	+ 0 53	K4 IIIp	2	< 20:	
418	ϕ Oph	16 25.4	−16 24	G8 III	2	< 20:	
419	β Her	16 25.9	+21 42	G8 III	1	< 20:	SB1
420	HR 6152	16 26.2	+20 42	G8p	2	< 15	
421	29 Her	16 27.9	+11 42	K5 III	2	< 20:	
422	HR 6196	16 35.8	−17 33	G8 II	2	< 20:	
423	HR 6199	16 36.0	+56 13	K1 III	2	< 15	
424	ζ Her	16 37.5	+31 47	G0 IV w	1	< 15	VB
425	η Her	16 39.5	+39 07	G8 III–IV	2	< 15	VV?
426	18 Dra	16 40.2	+64 47	K1p	2	< 20:	
427	43 Her	16 41.0	+ 8 46	K5 III	2	< 15	
428	20 Oph	16 44.3	−10 36	F6 IV w	4	< 20:	
429	51 Her	16 47.6	+24 50	K2 II–III	2	< 15	
430	23 Oph	16 49.2	− 6 00	K2 III	2	< 20:	
431	HR 6287	16 50.6	+21 07	G8 III	2	< 15	
432	κ Oph	16 52.9	+ 9 32	K2 III	1	< 15	LV
433	19 Dra	16 55.5	+65 17	F6 V w	4	< 20:	SB1
434	30 Oph	16 55.8	− 4 04	K4 III	2	< 20:	
435	ϵ UMi	16 56.2	+82 12	G5 III s	2	25	SB1
436	HR 6388	17 06.3	+40 54	K3 III	2	< 15	VV
437	41 Oph	17 11.5	− 0 20	K2 III	2	< 15	
438	π Her	17 11.6	+36 55	K3 II	1	< 15	
439	HR 6433	17 13.9	+10 58	K4 II–III	2	< 15	
440*	72 Her	17 16.9	+32 36	G0 V w	1	< 15	
441	σ Oph	17 21.6	+ 4 14	K3 II	2	< 20:	
442	λ Her	17 26.7	+26 11	K4 III	2	< 15	
443	β Dra	17 28.2	+52 23	G2 II	1	< 15	
444	27 Dra	17 32.4	+68 12	K0 III	2	< 15	
445*	26 Dra	17 34.0	+61 57	G1 V w	1	< 20:	

TABLE 2a—*Continued*

No.*	Star	α_{1900}	δ_{1900}	Spectral Type	Source†	$v \sin i$ (Km/Sec)	Remarks‡
446	ω Dra	17h37m5	+68°48′	F5 V w	4	< 20:	SB1
447	β Oph	17 38.5	+ 4 37	K2 III	1	< 15	
448	μ Her	17 42.6	+27 47	G5 IV	1	< 15	
449	ψ Dra A	17 43.7	+72 12	F5 V s	4	15	
450	87 Her	17 44.8	+25 39	K2 III	2	< 15	
451	90 Her	17 50.0	+40 01	K3 III	2	< 20:	
452	ξ Dra	17 51.8	+56 53	K2 III	1	< 15	
453	θ Her	17 52.8	+37 16	K1 II	1	< 20:	
454	ν Oph	17 53.5	− 9 46	K0 III	2	< 15	
455	ξ Her	17 53.9	+29 16	K0 III	2	< 20:	
456	35 Dra	17 53.9	+76 59	F6 IV–V s	4	< 20:	
457	γ Dra	17 54.3	+51 30	K5 III	1	< 15	
458	ν Her	17 54.7	+30 12	F2 II	1	30	
459	ζ Ser	17 55.2	− 3 41	F3 V	1	110:	VV?
460	93 Her	17 55.6	+16 46	K0 II–III	2	< 15	
461	70 Oph A	18 00.4	+ 2 31	K0 V	1	< 20:	SB1, VB
462	71 Oph	18 02.5	+ 8 43	G8 III–IV	2	< 20:	
463*	99 Her	18 03.2	+30 33	F7 V w	1	< 20:	
464	HR 6791	18 04.5	+43 27	K0p	2	< 15	VV?
465	36 Dra	18 13.3	+64 22	F5 V w	2	< 15	
466	74 Oph	18 15.9	+ 3 20	G8 III	2	< 20:	
467	η Ser	18 16.1	− 2 55	K0 III–IV	1	< 20:	
468	κ Lyr	18 16.4	+36 01	K2 III	2	< 15	
469	ζ Sct	18 18.2	− 8 59	K0 III	2	< 15	SB1
470	HR 6885	18 18.4	+17 46	K3 III	2	< 15	
471	109 Her	18 19.4	+21 43	K2 III	2	< 15	
472	χ Dra	18 22.9	+72 41	F7 V	1	< 15	SB1
473	60 Ser	18 24.5	− 2 03	K0 III	2	< 15	SB1
474	42 Dra	18 25.7	+65 30	K2 III	2	< 15	
475	HR 6970	18 29.5	−11 03	G8 III	2	< 20:	
476	α Sct	18 29.8	− 8 19	K3 III	2	< 15	
477	HR 6983	18 31.7	+52 16	K0 III	2	< 15	VB
478	ϵ Sct	18 38.1	− 8 22	G8 II	2	< 20:	
479*	110 Her	18 41.4	+20 27	F6 V w	1	< 20:	
480	β Sct	18 41.9	− 4 51	G5 II	1	< 15	SB1
481	HR 7064	18 42.0	+26 33	K3 III	2	< 15	
482	HR 7117	18 48.3	+73 58	K0 II–III	2	< 15	
483	o Dra	18 49.7	+59 16	K0 II–III	2	< 20:	SB1
484	HR 7137	18 50.8	+50 35	G8 III	2	< 20:	
485	η Sct	18 51.7	− 5 58	K2 III	2	< 20:	
486	HR 7162	18 53.3	+32 46	G0 V w	2	< 15	
487*	11 Aql	18 54.5	+13 29	F8 IV w	4	25	
488	ϵ Aql	18 55.1	+14 56	K2 III	2	< 15	
489	υ Dra	18 55.6	+71 10	K0 III	2	< 15	VV
490	HR 7181	18 55.7	+26 05	K2 III	2	< 15	VV
491	λ Lyr	18 56.2	+32 00	K3 III	2	< 20:	
492	12 Aql	18 56.3	− 5 53	K1 III	2	< 15	
493	π Sgr	19 03.8	−21 11	F2 II	7	30	
494	53 Dra	19 09.8	+56 41	G8 III	2	< 20:	
495	43 Sgr	19 11.8	−19 08	G8 II	2	< 20:	

TABLE 2a—*Continued*

No.*	Star	α_{1900}	δ_{1900}	Spectral Type	Source†	$v \sin i$ (Km/Sec)	Remarks‡
496	54 Dra	19^h12^m1	+57° 32′	K2 III	2	< 20:	
497	δ Dra	19 12.5	+67 29	G9 III	2	< 15	
498	θ Lyr	19 12.9	+37 57	K0 II	1	< 20:	
499	23 Aql	19 13.4	+ 0 54	K2 II–III	2	< 20:	
500	κ Cyg	19 14.8	+53 11	K0 III	1	< 15	VV
501	26 Aql	19 15.2	− 5 36	G8 III–IV	2	< 15	SB1
502	τ Dra	19 17.5	+73 10	K3 III	2	< 15	VV
503	31 Aql	19 20.2	+11 44	G8 IV	2	< 15	
504	δ Aql	19 20.4	+ 2 55	F0 IV–V	8	85	VV
505	4 Vul	19 21.1	+19 36	K0 III	2	< 20:	
506	μ Aql	19 29.2	+ 7 10	K3 III	2	< 20:	
507	σ Dra	19 32.6	+69 29	K0 V	1	< 15	
508	HR 7468	19 33.5	+44 28	K0 III	2	< 20:	
509	θ Cyg	19 33.8	+49 59	F5 IV–V s	4	< 20:	
510	α Sge	19 35.6	+17 47	G0 II	1	< 15	
511	β Sge	19 36.6	+17 15	G8 II	2	< 20:	
512	10 Vul	19 39.6	+25 32	G8 III	2	< 15	
513	15 Cyg	19 40.7	+37 07	G8 III	2	< 20:	
514	γ Aql	19 41.5	+10 22	K3 II	1	< 15	
515	17 Cyg A	19 42.6	+33 30	F5 V w	1	< 20:	VV?
516	o Aql	19 46.2	+10 10	F8 V s	2	< 15	
517	20 Cyg	19 48.1	+52 44	K3 III	2	< 20:	
518	ϵ Dra	19 48.5	+70 01	G8 III	2	< 20:	
519	ξ Aql	19 49.4	+ 8 12	K0 III	2	< 20:	
520	β Aql	19 50.4	+ 6 09	G8 IV	1	< 20:	
521	η Cyg	19 52.6	+34 49	K0 III	2	< 20:	
522	HR 7633	19 54.0	+58 35	K5 II–III	2	< 20:	
523	γ Sge	19 54.3	+19 13	K5 III	2	< 15	
524	26 Cyg	19 58.5	+49 50	K1 II–III	2	< 20:	
525	η Sge	20 00.7	+19 42	K2 III	2	< 20:	
526	ρ Dra	20 02.4	+67 35	K3 III	2	< 20:	
527	23 Vul	20 11.6	+27 30	K3 III	2	< 20:	
528	α^2 Cap	20 12.5	−12 51	G9 III	2	< 15	
529	24 Vul	20 12.5	+24 22	G8 III	2	< 20:	
530	HR 7759	20 13.4	+40 03	K4 II	2	< 20:	
531	HR 7794	20 18.2	+ 5 01	G8 III–IV	2	< 20:	
532	39 Cyg	20 19.9	+31 52	K3 III	2	< 20:	
533	ρ Cap	20 23.2	−18 09	F2 IV	7	115:	
534	41 Cyg	20 25.3	+30 02	F5 II	1	< 15	
535*	β Del	20 32.9	+14 15	F5 IV s	4	55	VB
536	71 Aql	20 33.2	− 1 27	G8 III	2	< 20:	SB1
537	1 Aqr	20 34.3	+ 0 08	K1 III	2	< 20:	
538	κ Del	20 34.3	+ 9 44	G5 IV	2	< 20:	
539	30 Vul	20 40.6	+24 55	K2 III	2	< 15	VV
540	52 Cyg	20 41.5	+30 21	K0 III	2	< 15	
541	ϵ Cyg	20 42.2	+33 36	K0 III	1	< 15	VV
542	HR 7955	20 42.9	+57 13	F8 IV–V w	4	< 20:	
543	HR 7956	20 43.2	+34 00	K3 III	2	< 20:	
544	η Cep	20 43.2	+61 27	K0 IV	1	< 15	
545	31 Vul	20 47.8	+26 43	G8 III	2	< 20:	

TABLE 2a—*Continued*

No.*	Star	α_{1900}	δ_{1900}	Spectral Type	Source†	$v \sin i$ (Km/Sec)	Remarks‡
546	32 Vul	$20^h50^m.3$	$+27°41'$	K4 III	2	< 15	
547	17 Del	20 50.9	+13 20	K0 III	2	< 20:	
548*	1 Equ	20 54.1	+ 3 55	F5 IV w	4	75	VB
549	61 Cyg A	21 02.4	+38 15	K5 V	1	< 15	
550	ν Aqr	21 04.2	−11 47	G8 III	2	< 15	
551	ζ Cyg	21 08.7	+29 49	G8 II	1	< 15	VV
552	ι Cap	21 16.7	−17 16	G8 III	2	< 15	
553	1 Peg	21 17.5	+19 23	K1 III	1	< 15	
554	71 Cyg	21 25.8	+46 06	K0 III	2	< 20:	
555	ρ Cyg	21 30.2	+45 09	G8 III	2	< 20:	
556	72 Cyg	21 30.7	+38 05	K1 III	2	< 15	
557	25 Aqr	21 34.5	+ 1 48	K0 III	2	< 20:	
558*	42 Cap	21 36.1	−14 30	G2 IV s	2	15	SB1
559	κ Cap	21 37.1	−19 19	G8 III	2	< 20:	
560	46 Cap	21 39.7	− 9 32	G8 II–III	2	< 15	VV
561	μ Cyg A	21 39.7	+28 17	F6 V w	4	< 15	
562	11 Cep	21 40.4	+70 51	K0 III	2	< 15	
563	HR 8324	21 41.8	+71 52	K1 III	2	< 15	VV?
564	16 Cep	21 57.8	+72 42	F5 V s	2	35	
565	ν Peg	22 00.6	+ 4 34	K4 III	2	< 15	VV
566	HR 8424	22 02.0	+44 32	K5 III	2	< 15	
567	20 Cep	22 02.0	+62 18	K4 III	2	< 15	
568	ι Peg	22 02.4	+24 51	F5 V s	1	< 20:	SB1
569*	π Peg	22 05.6	+32 41	F5 III s	4	115:	
570	24 Cep	22 07.9	+71 51	G8 III	2	< 20:	VV?
571	HR 8472	22 08.2	+56 20	F8 V s	2	< 20:	
572	HR 8475	22 08.4	+34 07	K2 III	2	< 20:	VV?
573	HR 8485	22 09.6	+39 13	K3 III	2	< 15	VV?
574	ϵ Cep	22 11.4	+56 33	F0 IV	1	110	VV
575	θ Aqr	22 11.6	− 8 17	G8 III–IV	2	< 15	
576	1 Lac	22 11.6	+37 15	K3 II–III	2	< 20:	
577	3 Lac	22 19.6	+51 44	G9 III	2	< 15	
578	35 Peg	22 22.8	+ 4 12	K0 III	2	< 20:	
579	ζ Aqr	22 23.7	− 0 32	F5 IV w	4	75 np 75 sf	VB
580	37 Peg	22 24.9	+ 3 55	F5 IV s	4	85	VB
581	κ Aqr	22 32.6	− 4 45	K2 III	2	< 20:	
582*	31 Cep	22 33.3	+73 07	F4 III	7	100	
583	11 Lac	22 36.1	+43 45	K3 III	2	< 15	
584	66 Aqr	22 38.2	−19 21	K4 III	2	< 20:	
585	η Peg	22 38.3	+29 42	G2 II–III	1	< 15	SB1
586	13 Lac	22 39.6	+41 18	K0 III	2	< 20:	
587*	ξ Peg	22 41.7	+11 40	F7 V w	1	< 15	
588	λ Peg	22 41.7	+23 02	G8 II–III	2	< 20:	
589	μ Peg	22 45.2	+24 04	K0 III	2	< 15	
590	ι Cep	22 46.1	+65 40	K1 III	2	< 20:	
591*	σ Peg	22 47.3	+ 9 18	F7 IV s	1	< 15	
592	HR 8702	22 47.9	+82 37	K3 III	2	< 20:	
593	HR 8748	22 55.2	+83 49	K4 III	2	< 15	
594	3 And	22 59.7	+49 30	K0 III	2	< 15	
595	HR 8779	22 59.7	+66 40	K3 III	2	< 15	

TABLE 2*a*—*Continued*

No.*	Star	α_{1900}	δ_{1900}	Spectral Type	Source†	$v \sin i$ (Km/Sec)	Remarks‡
596	56 Peg	23^h02^m2	+24° 56′	K0 IIp	2	< 15	VV
597*	π Cep	23 04.7	+74 51	G2 III	6	≦ 15	SB1, VB
598	ψ^1 Aqr	23 10.6	− 9 38	K0 III	2	< 15	
599	γ Psc	23 12.0	+ 2 44	G8 III	2	< 15	
600	94 Aqr	23 13.8	−14 00	G5 IV	2	≦ 15	VV
601	o Cep	23 14.5	+67 34	K0 III	2	< 15	
602	11 And	23 14.8	+48 05	K0 III	2	< 20:	
603	7 Psc	23 15.2	+ 4 50	K2 III	2	< 20:	
604	66 Peg	23 18.0	+11 46	K3 III	2	< 20:	
605	v Peg	23 20.4	+22 51	F8 IV s	1	95	
606	θ Psc	23 22.9	+ 5 50	K1 III	2	< 15	
607	70 Peg	23 24.1	+12 13	G8 III	2	< 20:	VV?
608	14 And	23 26.4	+38 41	K0 III	2	< 20:	
609*	72 Peg	23 29.0	+30 46	K4 III	2	< 20:	VB
610	λ And	23 32.7	+45 55	G8 III–IV	1	< 20:	SB1
611*	ι Psc	23 34.8	+ 5 05	F7 V w	1	< 15	
612	γ Cep	23 35.2	+77 04	K1 IV	1	< 15	
613	104 Aqr	23 36.6	−18 22	G0 II	7	15	
614	HR 8987	23 37.3	−16 00	K4 III	2	< 15	VV?
615	78 Peg	23 39.0	+28 48	K0 III	2	< 20:	VV?
616	τ Cas	23 42.2	+58 06	K1 III	2	< 15	
617	27 Psc	23 53.6	− 4 07	G9 III	2	< 20:	
618	ω Psc	23 54.2	+ 6 19	F4 IV s	4	55	VV?

NOTES TO TABLE 2*a*

15 ξ And: Spectroscopic binary with $P = 17.8$ days. See the discussion by L. Gratton, *Ap. J.*, **111,** 31, 1950; *McDonald Contr.*, No. 185.
18 64 Psc: Double-line spectroscopic binary with $P = 14$ days.
40 v And: Miss Roman (1950) gives F8 IV on the MKK system.
69 θ Per: Miss Roman (1950) classifies this star as F6 V.
75 20 Per: The Δm is about 0.4 mag.
103 46 Tau: The Δm is about 0.3 mag.
131 a Aur: See text.
133 λ Aur: Miss Roman (1950) gives G2 IV–V.
191 65 Gem: Double-line spectroscopic binary with a period of several years.
198 σ Gem: Spectroscopic binary with $P = 19.6$ days. The line width is presumably due to rapid axial rotation associated with the orbital motion.
203 9 Pup: The Δm is about 0.7 mag.
219 o UMa: The type is given as G5 V in the Yerkes *Atlas*.
226 ϵ Hya AB: The type is given as G0 III in the Yerkes *Atlas* but does not appear in later lists. According to W. P. Bidelman, the brighter component of this close binary belongs to a later subdivision of class G.
231 HR 3579: This star (= 10 UMa) is a visual binary with a period of about 21 years. The line width was estimated on spectrograms that were taken in the interval February 8–March 23, 1953.
234 σ^2 UMa: Miss Roman (1950) gives F6 IV on the MKK system.
270 40 Leo: Miss Roman (1950) classifies this star as F6 V.
272 HR 4084: The type is given as F2 V by Bidelman (1951).
326 γ Vir: The difference in line width between the two components has been noted by Struve and Mrs. Gould (*Pub. A.S.P.*, **64,** 183, 1952; *A.J.*, **57,** 160, 1952).
343 61 Vir: The type is given as G5 V by Miss Roman (1950).
347 τ Boo: Miss Roman (1950) gives F6 IV on the MKK system.
363 θ Boo: Miss Roman (1950) classifies this star as F6 IV on the MKK system.
401 χ Her: The type is given as F8 V by Miss Roman (1950).
402 γ Ser: Miss Roman (1950) gives F6 IV on the MKK system.
440 72 Her: The type is given by Miss Roman (1950) as G2 V.
445 26 Dra: Miss Roman (1950) gives G2 V.
463 99 Her: The type is given as F8 V by Miss Roman (1950).
479 110 Her: Miss Roman (1950) classifies this star as F5 IV on the MKK system.
487 11 Aql: The type on the MKK system is F8 III–IV, according to Miss Roman. We have assumed that this corresponds to F8 IV on the MK system.
535 β Del: The Δm is about 0.6 mag.
548 1 Equ: The Δm is only about 0.2 mag.
558 42 Cap: The line widening is only marginally visible.
569 π Peg: No good Mills plates are available. The type is F5 II–III on the MKK system (Miss Roman 1950), and we have assumed that this is equivalent to F5 III on the MK system.
582 31 Cep: A type of F4 II–III on the MKK system was assigned by Bidelman. We have assumed that this is equivalent to F4 III on the MK system.
587 ξ Peg: Miss Roman (1950) assigned a type of F6 III–IV on the MKK system.
591 σ Peg: A type of F6 V was assigned by Miss Roman (1950).
597 π Cep: This star is a single-line spectroscopic binary ($P = 556$ days) and the brighter component of a visual binary with Δm about 2 mag. We are unable to explain the discrepancy between our value of $v \sin i$ (≤ 15 km/sec) and the value of 70 km/sec reported by Slettebak (1953).
609 72 Peg: The Δm is very small.
611 ι Psc: Miss Roman's (1950) type is F8 V.

TABLE 2*b*

CATALOGUE OF LINE WIDTHS OF 32 HIGH-LUMINOSITY STARS BETWEEN SPECTRAL TYPES F0 AND K5, EXPRESSED AS ROTATIONAL VELOCITIES

No.*	Star	α_{1900}	δ_{1900}	Spectral Type	Source†	$v \sin i$ (Km/Sec)	Remarks‡
619	ϕ Cas	1^h13^m8	+57°42′	F0 Ia	1	35	VV
620	η Per	2 43.4	+55 29	K3 Ib	1	<20:	
621	α Per	3 17.2	+49 30	F5 Ib	1	20	
622	μ Per	4 07.6	+48 09	G0 Ib	1	<15	SB1
623*	10 Cam	4 54.5	+60 18	G0 Ib	1	15	
624*	ϵ Aur	4 54.8	+43 40	F0p Ia	8	30	SB1
625	α Lep	5 28.3	−17 54	F0 Ib	1	15	
626	ϵ Gem	6 37.8	+25 14	G8 Ib	1	<15	
627	o^1 CMa	6 50.0	−24 04	K3 Iab	1	≤20	
628	δ CMa	7 04.3	−26 14	F8 Ia	1	25	
629	ζ Mon	8 03.6	− 2 42	G2 Ib	1	<15:	
630	HR 3459	8 38.8	− 6 52	G2 Ib	5	<15	
631	HR 3612	9 00.2	+38 51	G8 Ib–II	2	<20:	
632	89 Her	17 51.4	+26 04	F2 Ia	1	25	VV
633	45 Dra	18 30.8	+56 58	F7 Ib	7	<20:	
634	ν Aql	19 21.4	+ 0 08	F2 Ib	1	<20:	
635	22 Vul	20 11.2	+23 12	G2 Ib	1	15:	SB1
636	α^1 Cap	20 12.1	−12 49	G3 Ib	5	<15	VV
637	35 Cyg	20 14.8	+34 40	F5 Ib	1	<15	VV
638	γ Cyg	20 18.6	+39 56	F8 Ib	1	<15	
639	ξ Cyg	21 01.3	+43 32	K5 Ib	1	<15	VV
640*	DT Cyg	21 02.3	+30 47	.....	1	<15	LV
641	ζ Cap	21 21.0	−22 51	G4 Ib pec.	6	<20	VV
642	β Aqr	21 26.3	− 6 01	G0 Ib	1	<15	
643	ϵ Peg	21 39.3	+ 9 25	K2 Ib	1	<15	
644	9 Peg	21 39.8	+16 53	G5 Ib	1	<15	
645	α Aqr	22 00.6	− 0 48	G2 Ib	1	<15	
646	ζ Cep	22 07.4	+57 42	K1 Ib	1	<15	
647	HR 8752	22 55.9	+56 24	G0 Ia	1	35	VV?
648	ψ And	23 41.1	+45 52	G5 Ib	2	<20:	
649*	ρ Cas	23 49.4	+56 57	F8 Ia pec.	6	20:	LV
650	3 Cet	23 59.4	−11 04	K3 Ib	2	<15	

* Additional remarks for stars noted by asterisks:

623 10 Cam: The weak lines are slightly wider than those in the sun.

624 ϵ Aur: The type has been given by Bidelman (1951) as A8 *Ia;* the spectrum may be slightly variable, even outside eclipse.

640 DT Cyg: A cepheid variable with $P = 2.5$ days. The range in spectral type is given by A. D. Code (*Ap. J.*, **106**, 309, 1947) as F5.5 I–II to F7 I–II. The upper limit to $v \sin i$ quoted in the table was assigned on the basis of a plate exposed at phase 0.609 period (see W. H. Grasberger and G. H. Herbig, *Pub. A.S.P.*, **64**, 28, 1952).

649 ρ Cas: The value of $v \sin i = 20$: km/sec was estimated on a spectrogram taken on November 19, 1953. An examination of the width of weak lines on Mills plates of ρ Cas exposed in 1906, 1907, 1908, 1910, and 1923 yielded essentially the same result.

† The sources are identified in the text (see pp. 135 and 136).

‡ See note to Table 2*a*.

The estimates of line width were not made directly in kilometers per second but in units of an arbitrary scale in which the solar line width was set at 1.0, π^3 Orionis 1.3, 11 Aquilae 2.0, ρ Andromedae 3.0, 31 Comae 4.0, and 18 Comae 5.0. The conversion of estimates on this scale to $v \sin i$ in km/sec by means of a correlation diagram led to a spurious grouping of the $v \sin i$ values around certain rotational velocities, especially at those of the standard stars. The concentration of velocities around values ending in 5 is due to the same reason. No attempt has been made to correct the data in Tables 2*a* and 2*b* for this effect. All values of $v \sin i$ in those tables have, however, been rounded off to the nearest multiple of 5 km/sec.

For the supergiants, the turbulence-widened profiles of the strong lines made these lines unsuitable for estimating $v \sin i$, so that only weak lines were used for this purpose in stars of luminosity class I. Because of the marked difference in line character between the supergiants and the standard stars, it is entirely possible that determinations of $v \sin i$ for supergiants by some more appropriate method might differ systematically from the values in Table 2*b*. It should be emphasized that $v \sin i$ is used in that table only as a numerical index of the width of weak lines; its use is not intended to imply that the line-broadening agent in such stars is necessarily axial rotation.

Because of the manner in which the $v \sin i$'s in Tables 2*a* and 2*b* were determined, it is difficult to make any general statement as to their probable uncertainties. It is possible, however, to gain a limited idea of their reliability by comparing them with rotational velocities obtained for the same stars by other investigators. Such a comparison is shown in Table 3, in which the published $v \sin i$'s have all been obtained with dispersions comparable with that of the present work. The stars are identified by their numbers in Tables 2*a* and 2*b*. The main conclusions to be drawn are, first, that the present results for stars with narrow lines seem to be in good agreement with other work and, second, that the $v \sin i$'s for the supergiants are in reasonable agreement with rotational velocities assigned to those stars from detailed studies of their line profiles. However, the material in Table 3 is too scanty to furnish a good check on the accuracy of the data of this paper for stars with $v \sin i$ greater than about 25 km/sec.

A more detailed comparison is possible with the results of Huang (1953), which were obtained from micrometer measures of many of these same spectrograms. Figure 1 shows the correlation of Huang's rotational velocities ($\xi_r \sin i$, computed from his eqs. [1] and [2] with the parameter $\gamma = 2$, its compromise value) as determined from Mills plates, with the values of $v \sin i$ for the same stars given in this paper. For this comparison, 115 stars are available. The supergiants have been excluded because of the special nature of their line profiles. The points plotted in Figure 1 show the existence of a scale difference between the two series. Approximately the same difference in scale seems to be present in a comparison of Huang's velocities for stars with strong λ 4481 (i.e., stars of types late A, F, and G) with those determined by Elvey (see Fig. 3 of Huang's paper). As was suggested by Huang, this effect probably arises from a visual overestimation, when the micrometer settings were made, of the width of a strong, rotationally broadened line. Formally, Huang's series of rotational velocities of F- and G-type stars that are plotted in Figure 1 can be reduced to the scale of the present paper by using $\gamma \cong 1.4$.

The spectral types used in this paper are on or near the revised *Atlas* system of Morgan and Keenan. Other lists of spectral types in the Yerkes systems were also drawn upon, so that in Tables 2*a* and 2*b* the type is accompanied by a number that identifies the source. The sources and their designations are as follows.

1. H. L. Johnson and W. W. Morgan (1953): a list of standards for the MK system.
2. N. G. Roman (1952*a*): a list of types and luminosity classes for F5–K5 stars, expressed on the MK system.
3. N. G. Roman (1952*b*): classifications of a number of F- and G-type stars on the MK system.

4. N. G. Roman (1950): a list of the types and luminosity classes of F5–G5 stars, expressed on the MKK system of the *Atlas of Stellar Spectra* by W. W. Morgan, P. C. Keenan, and E. Kellman (1943). These classifications have been converted to the MK system as follows (see Johnson and Morgan 1953, p. 319, and Roman 1952*a*, p. 123): (*a*) all F2–F8 luminosity class III stars have been moved to class IV, and (*b*) all F2–F8 class IV stars have been changed to class IV–V.

TABLE 3

STARS FOR WHICH $v \sin i$ HAS BEEN MEASURED FROM LINE PROFILES BY ANOTHER INVESTIGATOR

Tables 2*a*, 2*b* No.	Star	Tables 2*a*, 2*b* $v \sin i$ (Km/Sec)	Published $v \sin i$ (Km/Sec)	Reference*
3	22 And	40	65	4
156	74 Ori	20	20	3
182	δ Gem	115	70; 70	1
196	α CMi	< 15	0; 0	1
270	40 Leo	20	15	3
326	γ Vir np	25	25; 50	1
	γ Vir sf	40	25; 50	1
329	31 Com	85	75	4
338	53 Vir	< 15	10	3
383	5 Ser	< 15	0	3
428	20 Oph	< 20:	10	3
463	99 Her	< 20:	5	3
504	δ Aql	85	100; 100	1
534	41 Cyg	< 15	0; 0	1
569	π Peg	115:	about 100	2
			125	4
611	ι Psc	< 15	0; 0	1
621	α Per	20	0; 0	1
624	ϵ Aur	30	0; 0	1
			30	6
628	δ CMa	25	$\approx$30	5

* The published $v \sin i$'s were drawn from the following sources:
1. C. T. Elvey, *Ap. J.*, **71,** 221, 1930. The two entries in the "Published $v \sin i$" column are independent estimates by Elvey and by O. Struve, respectively.
2. J. L. Greenstein, *Ap. J.*, **117,** 269, 1953.
3. M. and B. Schwarzschild, *Ap. J.*, **112,** 248, 1950.
4. A. Slettebak, *A.J.*, **58,** 228, 1953.
5. A. Unsöld and O. Struve, *Ap. J.*, **110,** 455, 1949; *McDonald Contr.*, No. 177.
6. K. O. Wright and E. Van Dien, *J.R.A.S. Canada*, **43,** 15, 1949; *Contr. Dom. Ap. Obs. Victoria*, No. 17.

5. W. W. Morgan and N. G. Roman (1950): a list of supergiant standards. These types have been used without change unless there is a conflict with a classification given in source 1, above, in which case the latter type has been used.

6. W. W. Morgan, P. C. Keenan, and E. Kellman, *Atlas of Stellar Spectra* (1943): this work defines the MKK system. The changes described under source 4 have been made for F2–F8 stars taken from this work. Other types have not been changed.

7. W. P. Bidelman (1951): a list of classifications of Miss Payne's c-stars, expressed on the MKK system. The treatment was the same as described under source 4, above.

8. P. C. Keenan and W. W. Morgan in *Astrophysics* (Hynek 1951), chap. 1.

III. DISCUSSION

The early Yerkes work on the spectral-type dependence of stellar rotation among stars less luminous than supergiants indicated that, in general, appreciable line broadening disappears among single stars[1] later than type F5. The results of the present paper demonstrate the existence of appreciable line widths in main-sequence stars as late as type F8. The slight difference between this and the Yerkes value of F5 is undoubtedly due to the higher dispersion that was used in this work. Among stars of somewhat higher luminosity, it has been known for many years that a few single objects of types later than F5 showed lines of appreciable width: for example, W. W. Campbell and J. H. Moore (1928) noted that the determination of the radial velocities of 31 Comae and

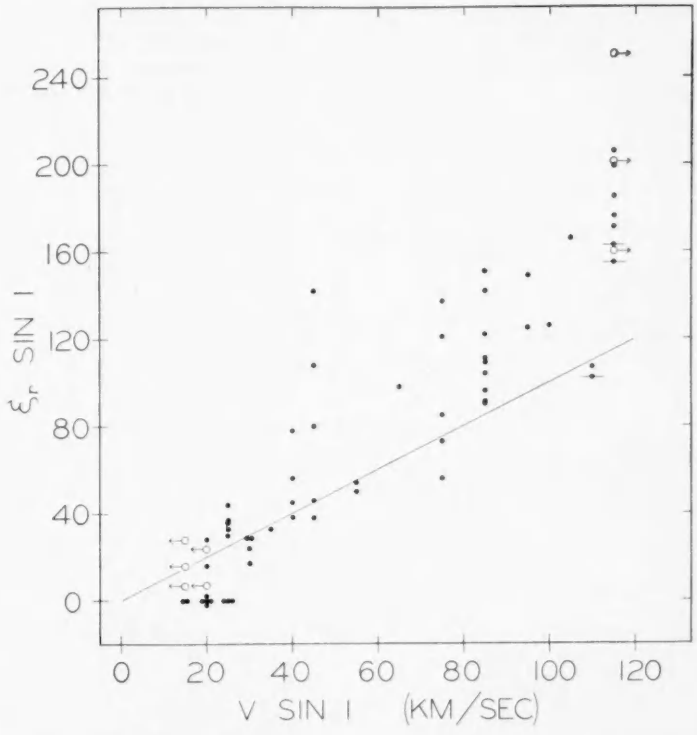

FIG. 1.—The scatter diagram relating rotational velocities measured by Su-Shu Huang ($\xi_r \sin i$) and those of this paper ($v \sin i$), both in km/sec. The scales of the ordinates and abscissae differ by a factor of 2, so the slope of the usual 45° regression line is decreased accordingly. Open circles with horizontal arrows represent stars for which only an upper or lower limit on $v \sin i$ was determined in the present investigation. A horizontal line through a filled circle indicates that the value of $v \sin i$ for that star is somewhat uncertain. In order to avoid congestion near the origin, 29 stars for which $\xi_r \sin i = 0$ and $v \sin i < 15$ km/sec, and 17 stars for which $\xi_r \sin i = 0$ and $v \sin i < 20$: km/sec have not been plotted. Furthermore, only stars of luminosity classes II through V are represented in the diagram.

[1] In addition to close binaries, we do not consider in the present discussion peculiar objects with broad lines, such as the T Tauri stars (G. H. Herbig, *J.R.A.S. Canada*, **46**, 222, 1952; *Contr. Dom. Ap. Obs. Victoria*, No. 27 [part 3]) and HD 117555 (P. W. Merrill, *Pub. A.S.P.*, **60**, 382, 1948).

v Pegasi, both of HD type G0, was difficult because of the poor quality of their spectral lines. More recently, J. L. Greenstein (1952, 1953), Slettebak (1953, 1954), Herbig and Miss Turner (1953), and others have noted that broad lines are very common among giant stars of types as late as early G.

The luminosity dependence of $v \sin i$ for the spectral interval F0–G5, as indicated by the data of this paper, is shown in Table 4. In this, as in the other collections of data that follow, each component of a visual binary or double-line spectroscopic binary has

TABLE 4

LUMINOSITY DEPENDENCE OF ROTATIONAL VELOCITY FOR SPECTRAL TYPES F0–G5

	Types F0–F4				
Luminosity class	II	III	IV	IV–V	V
No. stars with $v \sin i > 20$ km/sec	4	6	7	2	7
Total no. stars	5	6	7	2	9
Fraction with $v \sin i > 20$ km/sec	0.8	1.0	1.0	1.0	0.8
	Types F5–F7				
Luminosity class	II	III	IV	IV–V	V
No. stars with $v \sin i > 20$ km/sec	2	2	14	1	8
Total no. stars	4	3	20	8	37
Fraction with $v \sin i > 20$ km/sec	0.5	0.7	0.7	0.1	0.2
	Types F8–G0				
Luminosity class	II	III	IV	IV–V	V
No. stars with $v \sin i > 20$ km/sec	1	1	2	1	1
Total no. stars	4	1	4	4	28
Fraction with $v \sin i > 20$ km/sec	0.2	1.0	0.5	0.2	0.04
	Types G1–G5				
Luminosity class	II	III*	IV	IV–V	V
No. stars with $v \sin i > 20$ km/sec	0	0	0	.....	0
Total no. stars	7	5	6	0	10
Fraction with $v \sin i > 20$ km/sec	0.0	0.0	0.0	.....	0.0

* Includes one star of type G5 III–IV.

been entered with the integrated spectral type of the system, if the individual types are unknown. The last line of Table 4 gives the fraction of stars of each luminosity class that have projected rotational velocities greater than 20 km/sec. The entries in this line show that the tendency for a given star to have a $v \sin i > 20$ km/sec weakens rapidly through spectral type F but that rotation persists to later types in luminosity classes III and IV than in classes II or V. Rotation may be somewhat more common among the later F-type stars of luminosity class II than in those of class V, but the small sample of class II objects makes this point quite uncertain.

One type G5 star (ϵ Ursae Minoris) and two of type K (ζ Andromedae and σ Gemi-

norum) in Table 2*a* show broadened lines, very probably due to the fact that all are spectroscopic binaries of relatively short periods (39, 18, and 20 days, respectively) for such large stars. No other stars of types later than G5 have been found to have perceptibly wide lines. The line broadening observed in a few other objects of types G2–G5 is marginal ($v \sin i = 15$ km/sec). If these three binaries are rejected, then the latest spectral type at which at least one star with $v \sin i \geq 20$ km/sec is known is G0 for luminosity classes III and IV, and type F8 for classes II, IV–V, and V.

The dependence of rotational velocity upon luminosity class is shown also in Table 5, which has been obtained by combining the first three parts of Table 4. Table 5 gives the fractions of F0–G0 stars with $v \sin i > 20$ km/sec for each luminosity class from II to V. It must be emphasized, however, that the presentation of the data in the compressed form of Table 5 gives a somewhat misleading impression, because the mean spectral type is not the same for each luminosity class. For example, in the class III stars, 9 of the 10 objects between F0 and G0 are of types F0–F5, where the rotational velocities for any luminosity are fairly high. On the other hand, the bulk of the F0–G0 stars of class V represented in these statistics are of type F5 or later, where the average

TABLE 5

FRACTIONS OF F0–G0 STARS WITH $v \sin i > 20$ KM/SEC AS A FUNCTION OF LUMINOSITY CLASS*

Luminosity class	II	III	IV	IV–V	V
No. stars with $v \sin i > 20$ km/sec	7	9	23	4	16
Total no. stars	13	10	31	14	74
Fraction with $v \sin i > 20$ km/sec	0.5	0.9	0.7	0.3	0.2

* See the text for a caution regarding the interpretation of the data in this Table.

$v \sin i$ is small. A much fairer picture of the situation is shown by the same data in Table 4, where an effort was made to minimize the effect present in Table 5 by combining stars over a spectral-type range no larger than was necessary to obtain a reasonably significant number of stars.

The variation of the mean rotational velocities ($\bar{v}$, not $\overline{v \sin i}$) of groups of stars over the spectrum-luminosity class diagram between types F0 and G5 is shown in Table 6, which was constructed from the data of Tables 2*a* and 2*b*. The blocks indicate the regions of the diagram from which stars were drawn in order to form the mean velocities.[2] The mean $v \sin i$'s for stars of luminosity classes II–V were multiplied by the factor $4/\pi$ in order to obtain mean v's freed of the effect of an assumed random distribution in direction of the axes of rotation (Chandrasekhar and Münch 1950). This correction was applied throughout, although the number of stars in many of the groups is too small for it to be very meaningful. No allowance of this type was made for the supergiants (luminosity classes I*a* and I*b*), and so the mean velocities entered in Table 6 for these objects are straight averages of the velocities listed in the $v \sin i$ column of Table 2*b*. The figures in parentheses beneath the mean velocities in Table 6 are the numbers of stars used in forming the means.

Although the samples in many of the regions of Table 6 are very small, the observational data, when presented in this form, lead to the same conclusions with regard to the luminosity dependence of rotation as were drawn on the basis of Table 4. The arrangement of the material in Table 6 may be the more useful for theoretical workers.

We have assumed throughout the present work that the assignment of spectral type

[2] The remark appended to Table 6 discusses the convention used in computing these means.

TABLE 6

MEAN ROTATIONAL VELOCITIES IN SPECTRUM-LUMINOSITY CLASS DIAGRAM

Luminosity Class	Spectral Type													
	F0	F2	F3	F4	F5	F6	F7	F8	F9	G0	G1	G2	G3	G5
Ia	30 (3)							27 (3)						
Ib	<20 (2)				<20 (2)		<20 (2)			<15 (3)		<15 (4)	<20 (4)	
II	34 (5)				46 (5)					<19 (3)		<25 (3)		<25 (4)
II–III												<19 (2)		
III	146 (4)			78 (5)						108: (1)		<25 (2)		<25 (3)
IV	123 (6)			98 (13)		43 (10)				<25 (2)		<25 (2)		<25 (4)
IV–V	127 (2)				24 (6)	<25 (6)								
V	60 (6)		110 (3)		31 (15)	20 (15)	<25 (7)	<21 (12)	<21 (16)		<21 (7)			<19 (3)

and luminosity class is unaffected by the presence or absence of line width, since such classifications are generally made at a dispersion (about 125 A/mm) where line broadening of the magnitude found in stars of types F0 and later would be expected to be imperceptible. Nevertheless, the point is important enough to deserve a closer examination than we are in a position to make.

Among the stars of spectral types F5–G5 Miss Roman (1950, 1952*a*) has distinguished two groups, one characterized by weak and the other by strong lines. The space-velocity distribution of the weak-line stars has a larger dispersion than does that of the strong-line stars. In Table 2*a* the spectral types of stars between types F5 and G5 which have been assigned by Miss Roman to one group or the other, are followed by a "w" or an "s," even though the spectral type and luminosity class quoted there have been drawn from another source. Between types F5 and G0, there are available about 50 stars in each group. It is important to know whether axial rotation is correlated with membership in these groups. The answer is negative: there is no indication that the apparent rotational velocities of the two groups of stars differ in any significant way. There are about the same fractions of slowly rotating (or rapidly rotating) stars in each luminosity class for both weak- and strong-line objects.

As might be expected, the data of Table 2*b* indicate that the supergiants of luminosity class Ia ($M_v \backsim -7$) have systematically greater line widths than those of class Ib ($M_v \backsim -4.5$). In the spectral interval F0–G5, for which the data are probably most reliable for such spectra, the mean $v \sin i$ is 28 km/sec for 6 class Ia stars, and <15 km/sec for 17 class Ib supergiants. A comparable result has been obtained by Huang and Struve (1954).

We have not included our results for the components of α Aurigae in the statistical results, because no accurate spectral types are available. The Yerkes *Atlas* (Morgan, Keenan, and Kellman 1943) gives MKK types of G5 and F6 for the primary and secondary components, respectively, but states that "the separate values for the two components are very uncertain and may be in error by a considerable fraction of their separation." K. O. Wright (1954) gives spectral types of approximately G5 III and G0 III for the

NOTES TO TABLE 6

The entries in the table are $4/\pi$ times $\overline{v \sin i}$ for luminosity classes II through V, and $\overline{v \sin i}$ for classes Ia and Ib. It was sometimes necessary to combine the results for stars having definitely determined values of $v \sin i$ with those for which only an upper limit was available. This was done by assuming that it was permissible to use a value of 10 km/sec in those cases where $v \sin i <15$ or <20: km/sec, always provided that the resulting mean was not unrealistically small. The values contained in the table were computed in this way. So that one may judge the effect of this assumption upon the means, the notes below give for a number of tabular entries the extreme limits on the value of $4\,\overline{v \sin i}/\pi$ arising from error in this assumption. This range was obtained by regarding all stars for which $v \sin i$ has been observed to be <15 or <20: km/sec as having, first, $v \sin i = 0$ and, second, $v \sin i$ values equal to their upper limits. In cases where lower limits have been set on $v \sin i$ in Table 2, it was assumed that a value of ≥ 115 km/sec corresponds to 120 km/sec and that >115 km/sec may be replaced by 140 km/sec in order to compute the mean. The numbers in parentheses are the numbers of stars used in computing the corresponding value of $\bar{v} = 4\,\overline{v \sin i}/\pi$.

The ranges are as follows:

F0–F2 II: the range of $\bar{v}$ is 32–37 km/sec.
F5–F8 II: the range of $\bar{v}$ is 43–47 km/sec.
F6–F8 IV: the range of $\bar{v}$ is 36–44 km/sec.
F5 IV–V: the range of $\bar{v}$ is 18–30 km/sec.
F0–F2 V: the range of $\bar{v}$ is 58–62 km/sec.
F5 V: the range of $\bar{v}$ is 22–38 km/sec.
F6 V: the range of $\bar{v}$ is 11–27 km/sec.

One of the three stars entered under G5 III is actually of type G5 III–IV.

two components; the G5 star is usually regarded as the primary. The Lick spectrograms that we examined were taken in 1938–1939 on Process emulsion, but with a somewhat greater slit-width than we consider optimum. There is no difficulty, however, in assigning a value of $v \sin i < 15$ km/sec to the primary star. The lines of the earlier-type star are much wider. It is our impression from examining a number of our best spectrograms that the narrow features often seen flanking strong lines of the primary, which seem to shift from one side to the other in phase with the secondary spectrum, are frequently not lines of the fainter component at all. In many cases they seem to be only weak lines in the spectrum of the primary star, which strengthen or become faint, depending upon the position of the underlying, wide-lined spectrum of the secondary. In speaking of the line width of the secondary star, therefore, we refer not to these narrow components but to the hazy, ill-defined features that underlie the rich, sharp-lined spectrum of the G5 star. It is difficult to estimate the width of these wide lines, but it is our impression that the line breadth of the earlier-type component of α Aurigae is comparable to that of 31 Comae ($v \sin i = 85$ km/sec). If our interpretation of the spectrum is correct, it is interesting that the components of this binary, which lie on either side of the rotational "cutoff" slightly later than type G0 for stars of intermediate luminosity, have rotational velocities consistent with those of single stars of the same types.

The spectral interval F0–G5 is a region in which the transition from rapidly rotating to slowly rotating stars takes place, and for this reason it may be particularly important to have representative (i.e., extensive) data for stars of these types. The very small numbers of stars in some regions of the spectral-type luminosity-class diagram between F0 and G5 raises the question of how representative such small samples may be. The deterrent to the accumulation of more data is not the fact that somewhat fainter stars would have to be observed with moderately high dispersion but is the lack of accurate spectral-type and luminosity classifications for any significant number of additional objects. A systematic spectral classification of F0–G5 stars down to visual magnitude 6.5 or 7.0 would be very valuable. It not only would make possible a more thorough study of the matters discussed in this paper but might also render practical an examination of aspects of the phenomenon of rotation at which the present data only hint.

It is a pleasure to acknowledge the kindness of Dr. W. W. Morgan in furnishing us in advance of publication with a copy of the 1953 Johnson-Morgan paper that described the MK system. We are much indebted also to Miss Nancy G. Roman for giving us unpublished spectral classifications, and to Dr. W. P. Bidelman for valuable discussions. We also wish to thank Rev. F. C. Bertiau, S.J., for performing the greater part of the reductions of the microphotometer tracings of the standard stars.

REFERENCES

Bidelman, W. P. 1951, *Ap. J.*, **113**, 304; *McDonald Contr.*, No. 199.
Campbell, W. W., and Moore, J. H. 1928, *Pub. Lick Obs.*, Vol. **16**.
Chandrasekhar, S., and Münch, G. 1950, *Ap. J.*, **111**, 142.
Greenstein, J. L. 1952, *Carnegie Inst. Washington, Year Book*, No. 51; *Report of Director, Mt. Wilson and Palomar Obs.*, p. 13.
———. 1953, *Ap. J.*, **117**, 269.
Herbig, G. H., and Spalding, J. F., Jr. 1953, *Pub. A.S.P.*, **65**, 192.
Herbig, G. H., and Turner, B. A. 1953, *Ap. J.*, **118**, 477; *Lick Obs. Contr.*, Ser. II, No. 48.
Huang, Su-Shu. 1953, *Ap. J.*, **118**, 285.
Huang, Su-Shu, and Struve, O. 1954, *Ann. d'ap.*, **17**, 85.
Hynek, J. A. (ed.). 1951, *Astrophysics* (New York: McGraw-Hill Book Co.).
Johnson, H. L., and Morgan, W. W. 1953, *Ap. J.*, **117**, 313; *McDonald Contr.*, No. 216.
Morgan, W. W., Keenan, P. C., and Kellman, E. 1943, *An Atlas of Stellar Spectra* (Chicago: University of Chicago Press).

Morgan, W. W., and Roman, N. G. 1950, *Ap. J.*, **112**, 362.
Roman, N. G. 1950, *Ap. J.*, **112**, 554.
———. 1952*a*, *ibid.*, **116**, 122.
———. 1952*b*, private communication.
Slettebak, A. 1953, *A.J.*, **58**, 228.
———. 1954, *Ap. J.*, **119**, 146, n. 14.
Struve, O. 1945, *Pop. Astr.*, **53**, 201, 259.
Struve, O., and Elvey, C. T. 1931, *M.N.*, **91**, 663.
Unsöld, A. 1938, *Physik der Sternatmosphären* (Berlin: J. Springer), p. 317.
Westgate, C. 1934, *Ap. J.*, **79**, 357.
Wright, K. O. 1954, *Ap. J.*, **119**, 471.

ORIGIN OF ANOMALOUS ABUNDANCES OF THE ELEMENTS IN GIANT STARS

A. G. W. CAMERON*
Iowa State College, Ames, Iowa
Received July 9, 1954; revised September 14, 1954

ABSTRACT

Following the exhaustion of hydrogen in the cores of certain massive stars, it appears that the cores contract and the envelopes expand, the stars becoming red giants. When the central temperature and density have increased sufficiently, thermonuclear reactions involving the helium in the core can take place with the nuclei which have taken part in the carbon cycle. The rate of the $C^{13}(\alpha, n)O^{16}$ reaction is calculated; it is found to produce neutrons rapidly at a temperature of 10^8 ° K and a density of 5×10^4 gm/cm³. These neutrons are slowed down until they reach thermal equilibrium with their surroundings (neutron energies of about 10 kev) and are then captured by the surrounding nuclei in proportion to their cosmic abundances and neutron-capture cross-sections. The latter quantities are estimated for neutron energies of 10 kev as a function of the mass number of the capturing nucleus. The heavier nuclei each appear to capture many neutrons (about 35 neutrons at mass number 100). Nuclei with closed shells of 50, 82, and 126 neutrons have much smaller cross-sections and become concentrated by the neutron-capture processes. With the assumption of a moderate amount of mixing between core and envelope of the star, it is thus found that the distinctive features of S-type and *Ba* II–type spectra can be explained. The further evolution of the star should then lead to the production of excess carbon by the Salpeter reactions, and the spectrum should gradually turn into that of type R or N.

INTRODUCTION

In recent years refined studies of stellar models and better estimates of thermonuclear reaction rates have improved our understanding of stellar evolution. It has become apparent that the giant stars are composed of highly condensed cores and very tenuous envelopes. A recent detailed study (Sandage and Schwarzschild 1952) of these stars traces their course of evolution as follows: Such stars are more massive and much more luminous than the sun, and therefore they will exhaust the hydrogen in their convective cores in a time short compared to the age of the universe. The thermonuclear energy generation is then confined to a shell about the isothermal core, and this shell burns outward until the mass of material in the core reaches the Schönberg-Chandrasekhar (1942) limit. The further evolution of the star must involve the contraction of the core, which releases gravitational energy and raises the central temperature. At the same time the chemical discontinuity between the core and the envelope causes the envelope to expand, so that the radius of the star becomes very large and its spectrum approaches that of an M giant. Most of the energy continues to be supplied by the carbon-cycle thermonuclear reactions in the shell surrounding the core, and the luminosity remains approximately constant during the initial stages of the expansion. When the central temperature becomes high enough (about 2×10^8 ° K), the helium in the core will be burned into heavier elements (Salpeter 1952*a*), and the luminosity of the star will increase.

Most of the giant stars have normal spectra of the regular spectral classes F, G, K, and M. Some of the giants, however, belong to spectral classes which have been called "parallel" to the regular spectral series. These include classes S, R, N, and the recently suggested (Bidelman and Keenan 1951) *Ba* II class. The stars of the *Ba* II and S classes are characterized by anomalously large abundances of certain heavy elements (including the unstable element technetium [Merrill 1952]). The stars of the R and N classes are mainly characterized by an anomalously large abundance of carbon.

* Present address: Atomic Energy of Canada Limited, Chalk River, Ontario, Canada.

It is the purpose of this paper to consider some of the thermonuclear reactions which may be expected to accompany the evolutionary process described but which are of negligible importance for the energy generation in the star. As a result of these considerations, it appears possible to explain nearly all the abundance anomalies observed in these special spectral classes and to predict additional abundance anomalies which may provide a fruitful test of the theory.

Since these thermonuclear reactions occur at the center of the star, it is necessary to assume that a moderate amount of mixing takes place between the core and the envelope, in order that the anomalous abundances may be detected in the spectrum emitted at the surface. It is further assumed that this mixing will not affect the broad outlines of the stellar evolutionary process outlined earlier. The relative rarity of the stars of these unusual spectral types would appear to indicate that considerable restrictions must exist on the rate of mixing. In the majority of the red giant stars, which belong to spectral class M, the mixing is too slow for abundance anomalies to have become noticeable at the surface. Stars with much more rapid mixing may be expected to consume their hydrogen approximately uniformly, so that no chemical discontinuity develops between the core and the envelope and further evolution will produce dense superhot configurations (Crawford 1953).

THE SEQUENCE OF THERMONUCLEAR REACTIONS

It appears to be well established that the carbon cycle (von Weizsäcker 1938; Bethe 1938; Gamow and Critchfield 1949; Salpeter 1953) of thermonuclear reactions is mainly responsible for the consumption of hydrogen in the cores of the more luminous stars. The reaction steps involved in the cycle are

$$C^{12} + H^1 \rightarrow N^{13} + \gamma\,, \tag{1}$$

$$N^{13} \rightarrow C^{13} + \beta^+ + \nu\,, \tag{1a}$$

$$C^{13} + H^1 \rightarrow N^{14} + \gamma\,, \tag{2}$$

$$N^{14} + H^1 \rightarrow O^{15} + \gamma\,, \tag{3}$$

$$O^{15} \rightarrow N^{15} + \beta^+ + \nu\,, \tag{3a}$$

$$N^{15} + H^1 \rightarrow C^{12} + He^4\,. \tag{4}$$

When the hydrogen has been exhausted, the carbon and nitrogen nuclei remain behind in their equilibrium proportions, which are inversely proportional to the rates of the foregoing reactions.

Thermonuclear reaction rates are estimated by an extrapolation to low energies from laboratory measurements of reaction cross-sections (Salpeter 1953), assuming a superposition of single-level Breit-Wigner shapes for the resonances observed at laboratory energies. Such a procedure is valid only if the reactions do not possess resonances near the thermonuclear energy region. It appears that the rates of reactions (1), (2), and (4) are not appreciably affected by such resonances (Fowler 1954) but that the extrapolated rate of reaction (3) may have to be increased by a factor of as much as 20 through the influence of low-lying states in O^{15}.

The temperature in the hydrogen-burning shells of the giant star models of Sandage and Schwarzschild (1952) is 30×10^6 ° K. This is also the central temperature of these stars when they were part of the main sequence before their core hydrogen was exhausted. At this temperature it is expected (Fowler 1954) that the equilibrium ratio of C^{12} to C^{13} nuclei in the carbon cycle will be 4.7 ± 1.7. A value of 3.1 is here adopted for this ratio; an argument based on an astrophysical interpretation is given later as justification. The expected equilibrium ratio of C^{12} to N^{15} nuclei is 730 ± 230. If one makes

no allowance for the low-lying states of O^{15}, the expected equilibrium ratio of N^{14} to C^{12} nuclei is 4.2 ± 1.6; this ratio would become 0.21 if the resonances should increase the rate of reaction (3) by a factor of 20.

Of the carbon and nitrogen nuclei present initially in cosmic proportions in the young star, we may therefore expect that in the equilibrium proportions at least 6 per cent and perhaps as much as 22 per cent of the nuclei come to exist as C^{13}. In this paper it is hereafter assumed that the equilibrium abundance of C^{13} is 12 per cent. The adoption of a lower figure would not change the major conclusions reached later, although the details of the picture would be modified.

The loss of nuclei from the carbon cycle by the reaction

$$N^{15} + H^1 \rightarrow O^{16} + \gamma \tag{5}$$

has been neglected. It appears (Schardt, Fowler, and Lauritsen 1952) that the rate of reaction (5) is so much less than that of reaction (4) that, even after repeated cycling, the loss of nuclei is less than the uncertainty in the original cosmic abundance of those nuclei.

When, in the course of the evolution of a giant star, the central temperature of the contracting dehydrogenated core reaches about 2×10^8 ° K, a further set of thermonuclear reactions commences, in which the helium is converted into heavier elements:

$$He^4 + He^4 \rightarrow Be^8 + \gamma\,, \tag{6}$$

$$Be^8 \rightarrow He^4 + He^4\,, \tag{6a}$$

$$Be^8 + He^4 \rightarrow C^{12} + \gamma\,, \tag{7}$$

$$C^{12} + He^4 \rightarrow O^{16} + \gamma\,, \tag{8}$$

$$O^{16} + He^4 \rightarrow Ne^{20} + \gamma\,. \tag{9}$$

Reaction (6) is endothermic by 94.5 kev (Jones, Donahue, McEllistrem, Douglas, and Richards 1953), and its reverse, reaction (6*a*), has a half-life of order of magnitude 10^{-16} seconds. Nevertheless, according to Salpeter (1952*a*), at a temperature in the vicinity of 2×10^8 ° K, reaction (6) proceeds so rapidly that about 1 part in 10^{10} of He^4 is continuously present as Be^8. Since the rate of reaction (7) is greatly increased by a resonance near the thermonuclear energy region (Dunbar, Pixley, Wenzel, and Whaling 1953), it can then proceed rapidly. The resulting C^{12} nuclei can then capture further He^4 nuclei, as in reactions (8) and (9); but the rates of these reactions drop off as the charge of the capturing nucleus increases (Greenstein 1954).

Before the temperature has reached the level where reactions (6)–(9) give appreciable energy generation, it can be expected that the nuclei left over from the carbon cycle will undergo reactions with helium. The exothermic reactions which may take place are as follows:

$$C^{12} + He^4 \rightarrow O^{16} + \gamma\,, \tag{8}$$

$$C^{13} + He^4 \rightarrow O^{16} + n^1\,, \tag{10}$$

$$C^{13} + He^4 \rightarrow O^{17} + \gamma\,, \tag{11}$$

$$N^{14} + He^4 \rightarrow F^{18} + \gamma\,, \tag{12}$$

$$F^{18} \rightarrow O^{18} + \beta^+ + \nu\,, \tag{12a}$$

$$N^{15} + He^4 \rightarrow F^{19} + \gamma\,. \tag{13}$$

Most of these reactions involve the simple capture of alpha particles. Since the abundances of the carbon and nitrogen nuclei are not large compared to that of helium, these reactions do not give an important contribution to the energy generation of the star. However, it should be noted that reaction (10) produces neutrons. Such neutrons for the most part will be slowed down by collisions with the helium until they are in thermal equilibrium with their surroundings. It is shown later that these neutrons are then captured preferentially by the heavier nuclei in the cosmic mixture, a process which brings about a large transformation in the relative abundances of the heavier elements.

RATE OF THE $C^{13}(\alpha, n)O^{16}$ REACTION

The rate of a thermonuclear reaction may be written as

$$p = 434\,\rho x_1 S\,(A_1^2 Z_1 Z_2)^{-1}\tau^2 e^{-\tau}\ \text{sec}^{-1}, \tag{14}$$

where

$$\tau = 42.48\left[\frac{Z_1^2 Z_2^2 A_1 A_2}{A_1 + A_2}\right]^{1/3} T^{-1/3},$$

ρ is the density in gm/cm^3; x_1 is the concentration (by weight) of the bombarding particle (here helium nuclei); Z_1 and Z_2 are the atomic numbers of the reacting constituents; and T is the temperature in units of 10^6 ° K. The cross-section of the reaction can be written over a small energy region in terms of the approximate constant S as

$$\sigma = -\frac{S}{E}\exp\left(-\frac{2\pi e^2 Z_1 Z_2}{\hbar v}\right). \tag{15}$$

Here E and v are the kinetic energy and velocity of particle 1 (in laboratory co-ordinates), and S must be expressed in units of ev-barns for use in equation (14).

It is necessary to estimate the value of S in the thermonuclear energy region in order that the reaction rate may be evaluated. This energy region is centered about an optimum bombarding energy (Gamow and Critchfield 1949) (in center-of-mass co-ordinates):

$$E_{\text{opt}} = 1220\,[Z_1 Z_2 T]^{2/3}\left[\frac{A_1 A_2}{A_1 + A_2}\right]^{1/3}, \tag{16}$$

the energy being measured in electron volts. For the $C^{13}(\alpha, n)O^{16}$ reaction, the optimum energy is 2.00×10^5 ev at a temperature of 100×10^6 ° K.

Precision laboratory measurements of the cross-section of the $C^{13}(\alpha, n)O^{16}$ reaction at low bombarding energies have not yet been reported. Therefore, it is necessary to estimate the value of S for reaction (10) in the thermonuclear energy region on the basis of other information.

The energy of excitation (center-of-mass co-ordinates) with which we are concerned in the compound O^{17} nucleus is equal to the Q-value of reaction (11) plus 0.200 mev, or 6.544 mev. This is in the middle of an energy region which has been thoroughly explored by neutron scattering from O^{16}, the peak heights, peak shapes, and angular distributions of the scattered neutrons having been measured (Ajzenberg and Lauritsen 1952). From this information the spins, parities, and neutron widths of most of the resonances have been determined. Hence the cross-section for the $C^{13}(\alpha, n)O^{16}$ reaction can be calculated at an excitation energy of 6.544 mev from a superposition of Breit-Wigner resonance shapes (neglecting interferences between the levels), provided that the alpha-particle widths can be estimated.

The Breit-Wigner formula for the cross-section due to a single level is

$$\sigma(\alpha, n) = \frac{(2J+1)}{(2s+1)(2I+1)}\,\pi\lambda\!\!\!^{-2}_{\alpha}\,\frac{\Gamma_\alpha \Gamma_n}{(E-E_r)^2 + \frac{1}{4}\Gamma^2}, \tag{17}$$

where J, s, and I are the spins of the compound nucleus, the bombarding particle, and the target nucleus, respectively; $2\pi\lambda\!\!\!^{-}_{a}$ is the de Broglie wave length of the incident particle; E and E_r are the excitation and resonance energies, respectively; and Γ_n, Γ_a, and Γ are the neutron width, the alpha-particle width, and the total width (full width at half-maximum), respectively. All energies are in the center-of-mass system. The neutron experiments give us J, Γ_n, and E_r for each resonance. The radiation widths should be much smaller than the neutron widths (Blatt and Weisskopf 1952), so we may assume $\Gamma \approx \Gamma_n$. For reaction (10) we also have $s = 0$ and $I = \frac{1}{2}$ (Ajzenberg and Lauritsen 1952).

The alpha-particle width may be written as the product of the following terms (Blatt and Weisskopf 1952):

$$\Gamma_a = 2k_a P_a \gamma_a^2 , \tag{18}$$

where $k_a = \lambda\!\!\!^{-1}_{a}$ is the wave number of the incident particle, P_a is the barrier penetrability, and γ_a^2 is the reduced alpha-particle width for the particular resonance under consideration. The barrier penetration is readily calculated (Mott and Massey 1949),

TABLE 1

CHARACTERISTICS OF THE RESONANCES CONTRIBUTING TO THE $C^{13}(\alpha, n)O^{16}$ REACTION

O^{17} Excitation Energy (Mev)	Spin	Parity	Γ_n (Kev)	l_a	Cross-section (Barns)
4.570	$\frac{3}{2}$	−	40	2	0.005×10^{-17}
5.070	$\frac{3}{2}$	−	100	2	0.023
5.390	$\frac{3}{2}$	−	35	2	0.013
5.040	$\frac{1}{2}$	−	30	0	0.42
6.370	$\frac{1}{2}$	+	120	1	6.15
7.370	$\frac{3}{2}$	+	220	1	1.10
7.720	$\frac{5}{2}$	−	800	2	0.28
8.280	$\frac{1}{2}$	−	280	0	0.49

Total cross-section = 8.49×10^{-17} barns

but the reduced widths depend upon undetermined properties of the nuclear resonances. Teichman and Wigner (1952) have deduced a sum-rule limit for the reduced widths which states

$$\gamma_a^2 \leqslant \frac{3\hbar^2}{2Ma_a}, \tag{19}$$

where M is the mass of the incident particle and a_a is the "channel radius," assumed here to be the sum of the radii of the He^4 and C^{13} nuclei. The levels of interest to us in the O^{17} nucleus have reduced neutron widths of the order of magnitude of 1 per cent of the sum-rule limit, and, in the absence of better information, the reduced alpha-particle widths of these levels are also assumed here to be 1 per cent of the sum-rule limit.

In Table 1 are listed data of interest for the resonances which give the main contribution to the (α, n) cross-section at 6.544 mev. The resonances with very small neutron widths have been omitted, since they probably have higher angular momenta and they are not likely to make appreciable contributions to the cross-section. The first four columns list, respectively, the excitation energy, the spin, the parity, and the measured neutron width of each level. The fifth column gives the orbital angular momentum which

the alpha particle must have with respect to the C^{13} nucleus in order to excite the level (this quantity is of importance in the calculation of the barrier penetrability). The last column gives the cross-section contribution of each level at an excitation energy of 6.544 mev as calculated from equations (17), (18), and (19).

It follows from equation (15) that, in the thermonuclear energy region,

$$S = 3.9 \times 10^9 \text{ ev-barns} .$$

The corresponding reaction rate, from equation (14), is

$$p = 9 \times 10^{14} \exp (-322T^{-1/3}) \rho x_a T^{-2/3} \text{ sec}^{-1} .$$

At $\rho x_a = 5 \times 10^4$ and $T = 100$ (Sandage and Schwarzschild 1952), we have

$$p = 1.3 \times 10^{-12} \text{ sec}^{-1}$$
$$= 4 \times 10^{-5} \text{ year}^{-1} .$$

Under these conditions the mean reaction time of C^{13} with helium is of the order of magnitude of 25,000 years. These are therefore taken to be typical conditions under which neutron production takes place in the cores of giant stars. The relative neutron capture rates considered later are not sensitive to these conditions.

The neutrons are ejected from the compound O^{17} nuclei with an energy of about 2.3 mev and are slowed down mainly by collisions with the predominantly abundant helium nuclei until they come into thermal equilibrium with their surroundings. At $T = 100 \times 10^6$ ° K the Maxwell flux distribution of any type of particle peaks at 8.6 kev. Hence the fate of the thermalized neutrons depends on the neutron-capture cross-sections of the nuclei in the core of the star at neutron bombarding energies in the vicinity of 10 kev. These are estimated in the following section.

CAPTURE OF THE NEUTRONS

The only form of interaction which the thermalized neutrons can undergo with the predominantly abundant helium nuclei in the core is scattering, since He^5 is unstable. With any heavier nucleus, however, we may think of the neutron as entering and forming a compound system, which can decay in more than one way. The two principal modes of decay in which we shall be interested are the re-emission of a neutron and the emission of electromagnetic radiation. Other possibilities, such as the emission of protons or alpha particles or fission, are important in only a few of the nuclei under consideration. If a neutron is re-emitted, there is no net effect of the nuclear interaction, and therefore we shall be interested only in the neutron-capture cross-sections of the elements in the core of the star.

There is practically no experimental information concerning the radiative capture of neutrons having a few kev kinetic energy. Most experiments have been done with neutrons thermalized at about 300 ° K, which have Maxwell flux distributions peaking at 0.025 ev, and with fast fission neutrons with an average effective energy of 1 mev (Hughes, Garth, and Levin 1953). The laboratory thermal cross-sections vary over many orders of magnitude, since they depend on how close the thermal energy is to a resonance energy of the compound nucleus.

We shall be interested in the capture of neutrons having a spread of energies in the neighborhood of 10 kev. The capture process must therefore be averaged over many resonances in heavy nuclei but will depend on the location of individual resonances in the light nuclei. However, at an energy of 10 kev the variation in the cross-section at the peaks and troughs of the resonances probably lies within one order of magnitude, and hence there should not be extreme variations in capture cross-sections between neigh-

boring nuclei, with the exceptions noted below. The laboratory thermal cross-sections are of almost no help in the estimation of the 10-kev cross-sections.

The 1-mev capture cross-sections are quite regular (Hughes *et al.* 1953), since there is an average over resonances for nuclei throughout most of the periodic table. However, only for the lighter nuclei can there be a confident extrapolation of these cross-sections to the 10-kev region. The first few excited states of the heavier nuclei lie more than 10 kev, but less than 1 mev, above the ground state. Hence there can be only elastic scattering of 10-kev neutrons, but both elastic and inelastic scattering of 1-mev neutrons from such nuclei.

The procedure of this paper has therefore been to obtain the 10-kev capture cross-sections of the lighter nuclei by extrapolation from the 1-mev data. The cross-sections of the heavier nuclei have been calculated in a more direct manner, making use of the few experimental measurements in the kev region to normalize theoretical parameters.

The neutron-capture cross-section averaged over resonances may be written in the form (Blatt and Weisskopf 1952):

$$\sigma(n, \gamma) \approx \frac{\pi (\lambda\!\!\!^{-} - R)^2 T \Gamma_\gamma}{\Gamma}, \tag{20}$$

where $2\pi\lambda\!\!\!^{-}$ is the de Broglie wave length of the incoming neutron, R is the nuclear radius (here assumed to be $1.45 \times 10^{-13} A^{1/3}$ cm), Γ_γ is the radiation width, and Γ is the total width for the decay of the compound nucleus. For most nuclei of interest here, $\Gamma = \Gamma_n + \Gamma_\gamma$.

The gamma rays of neutron capture have been found to be emitted predominantly by electric dipole transitions (Kinsey and Bartholomew 1954). The capture of a slow neutron gives the compound nucleus an excitation energy of 7 or 8 mev, which is the binding energy of the last neutron in the capture product. Below this range of excitation there are normally a great many nuclear energy levels within one unit of angular momentum from, and of opposite parity to, the capturing level; the electric dipole transition may take place to any one of these levels. Hence it is not very surprising to find that the neutron-capture radiation widths are not sensitive functions of excitation energies, of the spins of the capturing states, or of the mass number of the capturing nucleus (Hughes and Harvey 1954). In this work the radiation widths have been assumed to be given by an empirical formula (Heidmann and Bethe 1951) of the form

$$\Gamma_\gamma = 1920\, A^{-2.06} \text{ ev}, \tag{21}$$

where A is the mass number of the capturing nucleus.

The other quantity which must be estimated in order to evaluate equation (20) is the neutron emission width, Γ_n. This may be written in the form (Blatt and Weisskopf 1952):

$$\Gamma_n = \frac{T D}{2\pi}, \tag{22}$$

where T is the transmission coefficient for the neutrons to escape from the nucleus and D is the average spacing between energy levels of a given kind in the neighborhood of the nuclear excitation energy.

The transmission coefficient T takes into account the fact that the outgoing neutrons can be reflected, because of the sudden change of wave number at the potential step marking the boundary of the nucleus. For the energies under consideration here, only s-wave neutrons have a significant probability of being emitted, so that no account need be taken of centrifugal barriers. The transmission coefficient then becomes (Blatt and Weisskopf 1952):

$$T = \frac{4kK}{(K+k)^2}, \tag{23}$$

where $k = \lambda\!\!\!^{-}^{-1}$ is the wave number of the neutron outside the nucleus, and $K = (K_0^2 + k^2)^{1/2}$ is the neutron wave number inside the nucleus. $K_0 \approx 1 \times 10^{13}$ cm^{-1}.

The level spacing D is the reciprocal of the level density ω; it is customary to write the latter quantity in the form

$$\omega(E) = C \exp(bE^{1/2}) \text{ mev}^{-1}, \tag{24}$$

where C and b are constants depending on the nucleus and E is the nuclear excitation energy. In this work, values of C and b (as functions of mass number A) were taken from graphs in the final report of the Fast Neutron Data Project (Feld, Feshbach, Goldberger, Goldstein, and Weisskopf 1951).

As a check on this procedure, the measurements of capture cross-sections for neutron energies in the range 1–50 kev (Hughes, Bonner, Goldstein, Havens, Kaplan, Muelhouse, Snell, Stehn, Snyder, Taschek, Wattenberg, and Zabel 1951) were used to calculate the appropriate level spacings in the excited nuclei from equations (20), (21), (22), and (23). These were then compared with the predictions of equation (24) with the constants of Feld *et al.* (1951). The logarithmically averaged ratio of the predicted to the "observed" level spacings came out to be 2.6; therefore, the values of C given by Feld *et al.* (1951) were increased by this factor (which includes the transmission factor T). The "observed" level spacings then had an average deviation of a factor of 2.3 from the adjusted predictions. This indicates the order of magnitude to be expected for individual fluctuations about the smoothly varying capture cross-sections computed below.

With these indicated procedures, the neutron-capture cross-sections at 10 kev were computed for the range of mass numbers $60 < A < 205$. The present knowledge of level densities for $A < 60$ appears much too crude to allow reliable predictions. The calculations used level densities at excitation energies corresponding to the average neutron-binding energy in each range of mass number (Feather 1953). The values so obtained for $100 < A < 205$ were somewhat smoothed and appear as part of Figure 1.

For mass numbers $A < 60$ the neutron-capture cross-sections were obtained by extrapolation from the 1-mev data. For this range of mass number, inelastic scattering of 1-mev neutrons does not appear to be important. Also in this range, $\Gamma_\gamma \ll \Gamma_n$ for 10-kev neutrons. Therefore, the ratio of the capture cross-sections for neutrons of energies E_1 and E_2 may be written

$$\frac{\sigma(E_1)}{\sigma(E_2)} = \left[\frac{R + \lambda\!\!\!^{-}(E_1)}{R + \lambda\!\!\!^{-}(E_2)}\right]^2 \frac{D(B+E_2)}{D(B+E_1)} \frac{\Gamma_\gamma(B+E_1)}{\Gamma_\gamma(B+E_2)}, \tag{25}$$

where B is the binding energy of the neutron in the nucleus under consideration. Here we place $E_1 = 0.01$ mev and $E_2 = 1$ mev. The first two ratio factors on the right-hand side of equation (25) can be readily evaluated as indicated previously.

The ratio of the radiation widths, which is the last factor in equation (25), was crudely estimated in the following way: If we assume that only electric dipole radiation is important, the transition probability for radiation that leaves the nucleus excited in the energy interval between E^* and $E^* + dE^*$ is proportional to the product $(B + E - E^*)^3\omega(E^*)dE^*$, E being the kinetic energy brought in by the neutron (Blatt and Weisskopf 1952). Hence the ratio of the radiation widths becomes

$$\frac{\Gamma_\gamma(B+E_1)}{\Gamma_\gamma(B+E_2)} = \frac{\text{Int.}(B+E_1)}{\text{Int.}(B+E_2)}, \tag{26}$$

where

$$\text{Int.}(x) = \int_0^x (x - E^*)^3 \omega(E^*)\, dE^*.$$

In this expression the level densities were assumed to be of the exponential form of equation (24), only the constant b being required, since the constant C cancels from the numerator and denominator of equation (26). For the lighter nuclei of interest here, the values of the constant b were taken from a paper by Heidmann and Bethe (1951). Equation (26) may then be readily evaluated in analytical form.

In this way the capture cross-sections for 10-kev neutrons were calculated for the range of mass numbers $20 < A < 100$. The two estimates did not agree very well in the overlap region $60 < A < 100$. After having been smoothed, the results appear as part of Figure 1, with a gradual transition from one calculation to the other in the overlap region.

There are certain nuclei whose neutron-capture cross-sections will depart from the smoothed line of Figure 1 by very large factors. These are the so-called "magic-number"

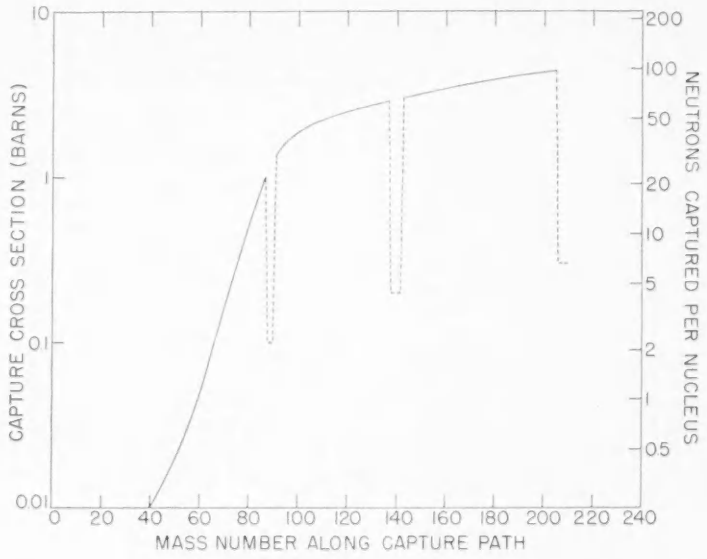

FIG. 1.—The neutron-capture cross-section of the nuclides lying on the main neutron-capture path. The scale on the right shows the number of neutrons captured per nucleus as calculated by the "static" method, which does not make allowances for the changing abundances.

nuclei, which have closed shells (Blatt and Weisskopf 1952; Hughes *et al.* 1953) of 50, 82, or 126 neutrons. The capture cross-sections for these nuclei are less than those of their neighbors for two reasons: (*a*) neutrons are very weakly bound to closed-shell nuclei; the smaller excitation energy implies larger level spacings according to equation (24); and (*b*) associated with the closed-shell structure the level spacings appear to be larger at a given excitation energy than predicted by equation (24). The larger values of the level spacing increase the neutron width, Γ_n, according to equation (22), and hence a much smaller fraction of the neutron interactions with these nuclei result in neutron capture. It appears from the 1-Mev data that the capture cross-sections of most closed-shell nuclei are reduced by a factor of 10–100. The regions in which these nuclei lie are indicated by the dotted "holes" in the cross-section–curve of Figure 1.

The probabilities of capture of the neutrons generated by the $C^{13}(\alpha, n)O^{16}$ reaction are proportional to the capture cross-sections of the surrounding nuclei, which are given

by Figure 1. The numbers of neutrons captured by nuclei of a given species are also proportional to the cosmic abundances of those species.

It is a common procedure to quote cosmic abundances in terms of the number of atoms of a given element present relative to 10,000 atoms of silicon. Let us therefore define a cosmic abundance unit as being that amount of matter which, in the original cosmic mixture from which the star was formed, contained 10,000 atoms of silicon. Alternatively, we may say that the cosmic abundance unit contains 10,000 cosmic abundance atoms (caa) of silicon.

Several determinations of cosmic abundances have recently been tabulated by Urey (1952). In the present work Urey's own values have been adopted where they exist; otherwise, among the lighter elements, Kuiper's values have been adopted. The abundances of the few heavier elements for which values do not exist have been interpolated from the abundances of their neighbors in the periodic table.

This gives a total of carbon plus nitrogen nuclei in the cosmic abundance unit of 1.32×10^5 caa. It has previously been assumed that 12 per cent of this, or 15,800 caa, becomes C^{13} during the operation of the carbon cycle. Hence reaction (10) will release 15,800 neutrons into the cosmic abundance unit.

Let P be the abundance (in caa) of any element or nuclide. Then the probability, f, that a neutron will be captured by a nucleus of any given species (Z, A) in the cosmic abundance unit is

$$f = \frac{P(Z, A)\,\sigma(Z, A)}{\sum_{Z,A} P(Z, A)\,\sigma(Z, A)}. \tag{27}$$

In the evaluation of equation (27) the abundances P were taken as adopted earlier, and the capture cross-sections, σ, were read from Figure 1, except for the lightest nuclei. For mass numbers $A < 20$ the spacings of the nuclear levels are quite large, and it is probable that the whole 10-kev energy region lies in the trough between nuclear resonances if the thermal capture cross-sections are small. If this is the case, then the capture cross-section at 10 kev can be extrapolated from laboratory thermal energies according to the $1/v$ law, where v is the neutron velocity. In this way it is found that the contribution of oxygen to the denominator of equation (27) is negligible. The contribution of neon to the denominator is unknown but has been similarly assumed to be negligible.

Neglecting, for the moment, neutron capture in N^{14}, it is found that the denominator of equation (27) has the value

$$\sum_{Z,A} P(Z, A)\,\sigma(Z, A) = 534 \text{ caa-barns}.$$

The interaction of neutrons with N^{14} leads to the exothermic $N^{14}(n, p)C^{14}$ reaction, which has a laboratory thermal cross-section of 1.70 barns, the large value indicating a close resonance, possibly below the neutron binding energy (Feld 1951). An extrapolation to 10 kev by the $1/v$ law leads to a cross-section of 0.0027 barns. If the equilibrium ratio of N^{14} to C^{12} should have the maximum value of 4.2 (Fowler 1954), then $P(7, 14)\sigma(7, 14) = 270$ caa-barns, which is comparable to the total due to all the other elements. Corresponding to the assumed 12 per cent C^{13} equilibrium abundance in the carbon cycle, $P(7, 14) = 66{,}000$ caa, and $P(7, 14)\sigma(7, 14) = 178$ caa-barns.

In Table 2 is given a list of all nuclides sufficiently abundant that their contribution to the denominator of equation (27) exceeds 1 caa-barn. It should be noted that 86 per cent of the entire summation (excluding the N^{14} reaction) is given by only five nuclides: Mg^{24}, Si^{28}, A^{36}, A^{38}, and Fe^{56}. Accordingly, the value of the denominator of equation (27) is quite sensitive to the values assumed for the abundances and capture cross-sections of these particular nuclides.

It follows that there are $15{,}800/(534 + 178) = 22.2$ neutrons absorbed per caa-barn. Alternatively, a nucleus with a capture cross-section of 1 barn would, on the average, capture 22.2 neutrons. The number of neutrons captured per nucleus is also plotted in Figure 1.

Most of these values are purely nominal. The calculation outlined is a "static" one, which takes no account of the changes in abundances produced by the neutron capture. However, the calculation should give the correct order of magnitude for the number of neutrons captured per nucleus in the actual dynamic case.

Most of the capture products are radioactive, with a fairly short half-life, and they decay into another stable form by negative beta emission before another capture process

TABLE 2

NUCLIDES GIVING MAJOR CONTRIBUTIONS TO NEUTRON ABSORPTION

Atomic No.	Element	Mass No.	P (Caa)	σ (Barns)	$P\sigma$ (Caa-barns)
7.....	*N*	14	66,000*	0.0027	178
11.....	*Na*	23	510	.0034	1.7
12.....	*Mg*	24	6850	.0036	25
12.....	*Mg*	25	880	.0038	3.3
12.....	*Mg*	26	967	.0040	3.9
13.....	*Al*	27	820	.007†	5.7
14.....	*Si*	28	9221	.0046	42.5
14.....	*Si*	29	470	.0049	2.3
14.....	*Si*	30	309	.0052	1.6
16.....	*S*	32	931	.0060	5.6
18.....	*A*	36	21,000‡	.0078	164
18.....	*A*	38	4000‡	.0088	35
20.....	*Ca*	40	542	.0098	5.3
24.....	*Cr*	52	69	.022	1.5
25.....	*Mn*	55	68	.029	2.0
26.....	*Fe*	54	389	.027	10.5
26.....	*Fe*	56	6050	.032	194
26.....	*Fe*	57	145	.035	5.1
27.....	*Co*	59	29	.043	1.2
28.....	*Ni*	58	265	.038	10.1
28.....	*Ni*	60	102	0.048	4.9

* Assumed carbon-cycle equilibrium abundance.
† Experimental value.
‡ Assuming negligible cosmic abundance of A^{40}.
For all elements $\Sigma P\sigma = 712$ caa-barns.

is likely to take place. All the nuclides of higher mass number are rapidly depleted by capture processes; only some of them are replenished by capture paths leading from nuclides of lesser mass number. Thus it is possible to define a main neutron-capture path in the following way: One starts with Ne^{20} and adds a succession of neutrons, allowing beta decays to intervene whenever the half-life of any product is less than (say) 1000 years. The nuclei in the original cosmic mixture will be led into and will then follow this main capture path by the successive addition of neutrons. The capture cross-sections given in Figure 1 refer explicitly to this capture path.

One can expect two important features to characterize the dynamical evolution of the chemical abundances. First, there will be approximate local equilibrium established along the main neutron-capture path, in which the abundances of the nuclides become inversely proportional to their neutron-capture cross-sections. This has an important

bearing on the question of technetium in giant stars. Mo^{98} lies on the main capture path; neutron capture leads to Mo^{99}, with a half-life of 67 hours. This quickly decays into Tc^{99}, which has a half-life of 2.1×10^6 years; we may therefore consider Tc^{99} to be a "stable" member of the capture path. Further neutron capture destroys Tc^{99}, giving Tc^{100}, which decays into Ru^{100}, with a half-life of 16 seconds. Hence, during the time that neutron production is operative, technetium is maintained in abundance comparable to its neighbors molybdenum and ruthenium. According to Figure 1, there is an average of 35 neutrons captured per nucleus in this region of mass number.

The second important feature is the presence of nuclei with closed neutron shells on the main neutron-capture path. These are shown as the dotted "holes" in the cross-section–curve of Figure 1. The abundance of these particular nuclei will be greatly increased as the neutron captures proceed. If local abundance equilibrium should also be reached in these regions of the main capture path, then the closed-shell nuclei would become more abundant than their neighbors by factors of 10–100.

These closed-shell nuclei are as follows: nuclei with 50 neutrons are Sr^{88},Y^{89}, and Zr^{90}. Nuclei with 82 neutrons are Ba^{138}, La^{139}, Ce^{140}, Pr^{141}, and Nd^{142}. At the top of the periodic table we have Pb^{208} and Bi^{209}, with closed shells of 126 neutrons. However, Pb^{206} and Pb^{207} have closed shells of 82 protons, and it appears that their neutron-capture cross-sections would also be somewhat reduced.

The main neutron-capture path is terminated at its upper end by a closed loop at the lead and bismuth nuclei. Further neutron captures lead to alpha-radioactive nuclei, which decay back into lead isotopes. This is an additional reason why the lead and bismuth abundances should be greatly increased by the neutron-capture processes.

FURTHER EVOLUTION OF THE STAR

The foregoing discussion deals with the changes in chemical abundances which may be expected to take place during the consumption of the carbon-cycle nuclei in thermonuclear reactions with helium. The only giant stars in which we can observe such changes by direct spectroscopic measurements are those in which it seems necessary to assume sufficient internal circulation of matter to bring the new nuclei formed in the star's core to the surface in a reasonably short length of time. This circulation will itself bring about a "spectroscopic" evolution of the star quite distinct from the processes which take place in the ordinary M-type giants.

A star with these internal currents will start with a regular K- or M-type spectrum. The onset of neutron production in the core may first become noticeable through the appearance of technetium in the spectrum, since local abundance equilibrium will be rapidly achieved among the heavier nuclei along the main neutron-capture path not in the closed-shell regions. As the neutron production continues, the next noticeable change may be increased abundances of elements with closed-shell nuclei on the main capture path. The prediction of the abundance changes in most of the other nonclosed-shell nuclei requires a detailed solution of the dynamical problem of the chemical evolution, which is not attempted here.

It may be seen that these abundance changes produce the characteristic features of the *Ba* II– and S-type spectra. We are led to expect different red giant stars to exhibit these abundance anomalies in different degrees, as is indeed observed in stars which are classified as "a mixture of M- and S-type" or "M-type with departures toward S-type."

In the normal course of evolution of the giant star the central temperature and density will continue to increase, and eventually there will be production of C^{12} at the center by reactions (6) and (7). This is particularly important in those stars with appreciable internal circulation. The currents can carry C^{12} to the core boundary and into the hydrogen-burning shell, where much of the C^{12} becomes transmuted to C^{13} by reactions (1) and (1*a*). When this C^{13} is returned to the core, it will produce more neutrons by reac-

tion (10). This process will henceforth be termed "carbon circulation." By this means many more neutrons will be captured per nucleus than indicated in Figure 1. In the first instance this will accentuate the abundance anomalies characteristic of the *Ba* II– and S-spectra.

However, the continued production of additional carbon will bring about considerably more spectacular changes in the spectrum of the star. It appears that most of the carbon at the surface of late-type stars is normally bound in unobservable *CO* molecules; the excess oxygen forms the other oxide molecules responsible for the most distinctive features of the ordinary late-type spectra. In this paper it has been assumed that in the carbon-cycle equilibrium proportions the number of carbon nuclei has grown at the expense of the nitrogen nuclei in the original cosmic proportions; in stars with circulation currents this would reduce somewhat the amount of excess oxygen available for oxide formation. When additional carbon becomes available from the Salpeter reactions, the excess oxygen available for the formation of oxides other than *CO* is rapidly reduced, and eventually we may expect that the carbon will become in excess. This would then produce the characteristic featues due to C_2, *CN*, and *CH* molecules in R- and N-type spectra. The later production of oxygen by reaction (8) may change the spectrum back to an S-type.

Thus it appears that the stars with R-, N-, and S-type spectra should not be thought to form "parallel branches" of the spectral sequence. We may expect a continuous gradation in spectral features going from M- to S- to R- or N-type spectra as the evolution of the star proceeds, in cases where there is appreciable mixing.

This evolutionary sequence readily accounts for the abnormally small abundances of C^{12} relative to C^{13} in most R- and N-type stars. This ratio has been found to be 3.1 ± 0.2 in a majority of R-type stars for which determinations have been possible (McKellar 1948). This may be presumed to occur when the excess C^{12}, produced in the core, becomes transmuted to the carbon-cycle nuclides in equilibrium proportions in the course of its passage through the hydrogen-burning shell. This is the basis for the choice of 3.1 as the equilibrium ratio in the earlier discussion. In a minority of the carbon stars the C^{12}/C^{13} ratio is greater than 30; this may perhaps result if the C^{12} passes through the hydrogen-burning shell too quickly for equilibrium to be achieved or if structural changes in the star suppress the hydrogen-burning shell.

DISCUSSION OF ASTROPHYSICAL OBSERVATIONS

There do not appear to be many precise determinations of the abundances of the elements in stars with S, R, and N spectra. When abnormal line intensities of certain elements have been observed in these spectral types, the usual procedure has quite properly been to try to explain them in terms of special physical conditions. There have been few determinations of absolute abundances by curve-of-growth methods; evidently, if the preceding theory is correct, there should be many more such determinations, in order to follow the details of the stellar evolution. In this section there follows a discussion of some papers from the more recent astrophysical literature which have come to the author's attention and which appear to have a bearing on these abundance questions. Since precise abundance information is very scarce, this discussion is necessarily quite speculative.

1. "The Spectrum of GP Orionis," by W. P. Bidelman (1950). It appears that this star has a basic S-type spectrum, but with a considerable increase in the carbon content. As a result, the abundances of the normally visible oxide molecules (*TiO*, *ZrO*, etc.) are greatly reduced. According to the evolutionary scheme suggested earlier, this star should be placed between the classes S and R or N.

2. "The Spectra of R Andromedae (Maximum) and Mu Cephei between 7400 and 8800 A," by L. H. Aller and P. C. Keenan (1951). These stars have S- and M-type spectra, respectively. The physical conditions in the two atmospheres appeared to be com-

parable, and the temperatures appeared high enough that the formation of molecules should have little effect on the comparison of atomic line strengths. It was found that the S spectrum contained stronger lines of *Rb*, *Zr*, and *Y;* the lines of *Ti* and *V* were of roughly equal strength; and the S spectrum contained weaker lines of *Fe*, *K*, *Na*, and *Ni*.

It appears not inconsistent with the theory outlined to attribute most of these differences to abundance anomalies in the S spectrum. The increase in the *Zr* and *Y* abundances is expected, since Zr^{90} and Y^{89} are closed-shell nuclei lying on the main neutron-capture path. The abundances of *Fe* and *Ni* should be reduced by the neutron capture, since these elements represent abundance peaks in the original cosmic mixture. The dynamic problem of the chemical evolution must be solved in detail before changes in the *Rb*, *Ti*, *V*, *Na*, and *K* abundances can be predicted.

3. "Lithium and the Internal Circulation of the Sun," by J. L. Greenstein and R. S. Richardson (1951). These authors show that lithium is depleted in the sun relative to terrestrial abundances. They believe this to indicate that the outer solar convection zone circulates material to regions where the temperature reaches 3.0×10^6 ° K. In a later paper (Greenstein and Tanberg-Hanssen 1954) it is shown that the lesser destruction of *Be* in the sun indicates that the convection zone does not reach temperatures as high as 3.6×10^6 ° K. Greenstein and Richardson then discuss the question of the very large abundances of lithium in stars with N spectra, which are comparable with terrestrial abundances, but quite variable (Sanford 1950). The authors believe this to indicate that the circulation of material in N-type stars cannot reach great depths. Since this belief is directly opposed to the evolutionary scheme outlined earlier, it is necessary to show that the present picture is consistent with large abundances of lithium in N-type stars.

In addition to the carbon-cycle process of reactions (1)–(4), some energy generation in massive stars will take place by the proton-proton chain:

$$H^1 + H^1 \rightarrow D^2 + \beta^+ + \nu\,, \tag{28}$$

$$D^2 + H^1 \rightarrow He^3 + \gamma\,, \tag{29}$$

$$He^3 + He^3 \rightarrow He^4 + 2H^1\,. \tag{30}$$

This chain may also go by an alternate route:

$$He^3 + He^4 \rightarrow Be^7 + \gamma\,, \tag{31}$$

$$Be^7 + e^- \rightarrow Li^7 + \nu\,, \tag{32}$$

$$Li^7 + H^1 \rightarrow 2He^4\,. \tag{33}$$

It has been shown by Salpeter (1952*b*) that, at a temperature of 30×10^6 ° K, reaction (30) takes place about 30 times as rapidly as reaction (31). However, for present purposes it is sufficient to note that a significant fraction of the proton-proton chain can be expected to lead to the formation of Be^7.

Under terrestrial conditions reaction (32) takes place with a half-life of 52.9 days; the Be^7 nucleus captures one of the *K* electrons. However, at a temperature of 30×10^6 ° K, the Be^7 nucleus is almost completely stripped of electrons; only a very small fraction of these nuclei contain a *K* electron at any one time. The electron-capture transition probability of reaction (32) is proportional to the square of the electron wave function at the surface of the nucleus (Blatt and Weisskopf 1952); this is very much smaller for free electrons under stellar conditions than for the Be^7 *K* electrons. Hence the laboratory half-life of Be^7 is lengthened nearly inversely proportionally to the degree of ionization of the Be^7 *K* shell electrons. A crude calculation carried out with Sandage and

Schwarzschild's (1952) red giant model No. VII shows that in the envelope, where temperatures are in excess of 1×10^{6} ° K, the half-life of Be^{7} lies in the range 50–100 years. This may well be long enough for the circulation currents postulated in N-type stars to bring substantial amounts of Be^{7} out to cooler regions before electron capture takes place. Eventually, the Li^{7}, which is then formed, will be carried back toward the center of the star and will be destroyed by reaction (33). It would appear that measurements of the equilibrium abundances of lithium which are built up in these stars should give valuable information about the nature of the circulation currents.

This explanation requires that there should be no very rapid thermonuclear reactions with the Be^{7} nuclei. The most likely reactions would be

$$Be^{7} + H^{1} \rightarrow B^{8} + \gamma\,, \tag{34}$$

$$B^{8} \rightarrow Be^{8} + \beta^{+} + \nu\,, \tag{34a}$$

$$Be^{8} \rightarrow 2He^{4}\,, \tag{34b}$$

$$Be^{7} + He^{4} \rightarrow C^{11} + \gamma\,, \tag{35}$$

$$C^{11} \rightarrow B^{11} + \beta^{+} + \nu\,. \tag{35a}$$

Reaction (34) is probably very slow because the proton-binding energy in B^{8} is only 0.3 ± 0.3 mev (Ajzenberg and Lauritsen 1952). A rough calculation of the rate of reaction (35) indicates that it is of negligible importance outside the core of the star. Hence the foregoing explanation appears reasonable.

4. "HD 26—An Unusual High-Velocity Star," by P. C. Keenan and G. Keller (1951). This star has approximately a G2 spectrum but with enhancement of *CH*, *Sr*, and *Ba*. There is not much enhancement of *CN* and C_2. This star may have nearly equal amounts of carbon and oxygen in the envelope. It appears that additional carbon has been produced and that neutron production has taken place.

5. "The *Ba* II Stars," by W. P. Bidelman and P. C. Keenan (1951). These authors define a class of peculiar G- and K-type stars whose spectra are characterized by the great strength of *CH*, *CN*, C_2, *Ba*, and *Sr*. The star HR 774 probably has strengthened lines of *La* as well. These stars would appear to be advanced along the evolutionary sequence discussed earlier. The carbon abundance has been increased, and lines due to closed-shell nuclei are greatly enhanced.

6. "Spectroscopic Observations of Stars of Class S," by P. W. Merrill (1952). This is the paper in which Merrill announced the presence of technetium in some stars with S spectra. As the spectral features of the stars departed more from the M type in the direction of "pure" S type, the intensity of the *Tc* I lines in the spectrum was found to increase.

It was indicated previously that the neutron-capture processes should quickly bring Tc^{99} into local abundance equilibrium with its neighbors along the main neutron-capture path. The half-life of Tc^{99} of 210,000 years may be comparable to the time required for the C^{13} consumption and for circulation currents to bring material from the core to the surface of the star. The increase in strength of the *Tc* I lines in going from M-type to S-type spectra may be taken as the result of slow mixing of matter between the core and the envelope rather than of progressive increases in the *Tc* abundance in the core.

7. "Intensities of Atomic Absorption Lines in the Spectra of Long-Period Variable Stars," by W. Buscombe and P. W. Merrill (1952). The equivalent widths were found for the lines of several elements in the stars R Leo (M type), *o* Ceti (intermediate between M and S types), and R And (S type). The authors found that, for every atom of *Zr* in the reversing layer of R Leo, there are 10 in *o* Ceti and 60 in R And. *Sr* was also enhanced in the S spectra. The abundances of other elements measured (*Mg* and *Ru*

appeared relatively strongest in *o* Ceti; *Sc*, *Ti*, and *Nb* were strongest in R And; and there was little change in the strengths of *V*, *Cr*, *Mn*, *Fe*, *Co*, and *Ni*) were changed much less, and some of the apparent changes may have been due to physical differences in the atmosphere of these stars. The spectacular increase in the *Zr* abundance is not out of line with the theory of this paper, since Zr^{90} is a closed-shell nucleus and its neutron-capture cross-section may be less than those of its neighbors by a factor of as much as 100.

8. "The Spectrum of ζ Capricorni," by R. H. Garstang (1952). This star is the brightest of Bidelman and Keenan's (1951) *Ba* II stars. Further investigation shows great strengthening of additional lines due to *Ba*, *La*, *Y*, *Sc*, *Fe*, *Zr*, *Nd*, *Pr*, *Sm*, and *Ce*.

Some of this strengthening may be due to atmospheric conditions in the star. Since there is an initial cosmic abundance peak at *Fe*, it is not expected that the abundance of this element should be increased by neutron-capture processes. However, it appears possible to explain most of the other line strengthening as resulting (at least in part) from neutron capture. *Sc* will be increased because of neutron capture in the more abundant *Ca* (the ratio of cosmic abundances is 3300 [Urey 1952]). Ba^{138}, La^{139}, Y^{89}, Zr^{90}, Nd^{142}, Pr^{141}, and Ce^{140} are all closed-shell nuclei on the main neutron-capture path. It seems probable that a great deal of neutron production must have taken place in this star for local abundance equilibrium to have been achieved in these closed-shell regions. This is particularly emphasized if the line strengthening of *Sm* is due to a real abundance increase; this can occur only if much of the original stock of the elements below the 82 neutron closed-shell region of the capture path can have moved through this region and then through five stable isotopes of *Nd*.

9. "Lines of the Rare-Earth Elements in the Spectrum of R Andromedae," by W. P. Bidelman (1953). The lines of all rare-earth elements except *Lu* and unstable *Pm* were found in the spectrum of the S-type star R And. All these lines, with the exception of those due to *Eu*, were found to be stronger in this spectrum than in that of the M-type star R Leo. If this line strengthening is due to increased abundances rather than to atmospheric conditions, it would have to be interpreted as indicating a very large neutron production by carbon circulation, as in the case of ζ Capricorni discussed earlier. This is consistent with the conclusions drawn concerning R And under paragraphs 2 and 7 above.

10. "Line Intensities in the Spectra of Cool Carbon Stars. I. R Stars in the Violet," by W. Buscombe (1953). There appeared to be ten times fewer *CH* molecules absorbing in the atmosphere of HD 182040 than in the other R stars studied. According to the evolutionary scheme proposed in this paper, this star would appear to be at a very advanced stage, in which hydrogen is becoming very deficient in the envelope, owing to the effects of the slow circulation currents in the star.

CONCLUSIONS

The hypothesis that the large changes in abundances of the elements in some stars arise from neutron production by the $C^{13}(\alpha, n)O^{16}$ reaction appears to be in agreement with the majority of the observations, and not to be in definite disagreement with any of them.

REFERENCES

Ajzenberg, F., and Lauritsen, T. 1952, *Rev. Mod. Phys.*, **24**, 321.
Aller, L. H., and Keenan, P. C. 1951, *Ap. J.*, **113**, 72.
Bethe, H. A. 1939, *Phys. Rev.*, **55**, 434.
Bidelman, W. P. 1950, *Ap. J.*, **112**, 219.
———. 1953, *ibid.*, **117**, 377.
Bidelman, W. P., and Keenan, P. C. 1951, *Ap. J.*, **114**, 473.
Blatt, J. M., and Weisskopf, V. F. 1952, *Theoretical Nuclear Physics* (New York: John Wiley & Sons).
Buscombe, W. 1953, *Ap. J.*, **118**, 459.

Buscombe, W., and Merrill, P. W. 1952, *Ap. J.*, **116**, 525.
Crawford, J. A. 1953, *Pub. A.S.P.*, **65**, 210.
Dunbar, D. N. F., Pixley, R. E., Wenzel, W. A., and Whaling, W. 1953, *Phys. Rev.*, **92**, 649.
Feather, N. 1953, *Adv. in Phys.*, **2**, 141.
Feld, B. T. 1951, *Phys. Rev.*, **82**, 308.
Feld, B. T., Feshbach, H., Goldberger, M. L., Goldstein, H., and Weisskopf, V. F. 1951, *Atomic Energy Commission Document NYO-636* (Washington, D.C.: Office of Technical Services, Dept. of Commerce).
Fowler, W. A. 1954; quoted by Aller, L. H., *Astrophysics* (New York: Ronald Press), **2**, 38.
Gamow, G., and Critchfield, C. L. 1949, *Theory of Atomic Nucleus and Nuclear Energy Sources* (Oxford: Clarendon Press).
Garstang, R. H. 1952, *Pub. A.S.P.*, **64**, 227.
Greenstein, J. L. 1954, *Mem. Soc. R. Sci., Liége*, **14**, 307.
Greenstein, J. L., and Richardson, R. S. 1951, *Ap. J.*, **113**, 536.
Greenstein, J. L., and Tanberg-Hanssen, E. 1954, *Ap. J.*, **119**, 113.
Heidmann, J., and Bethe, H. A. 1951, *Phys. Rev.*, **84**, 274.
Hughes, D. J., Bonner, T. W., Goldstein, H., Havens, W. W., Kaplan, I., Muelhouse, C. O., Snell, A. H., Stehn, J. R., Snyder, T. M., Taschek, R. F., Wattenberg, A., and Zabel, C. W. 1952, *Atomic Energy Commission Document AECU-2040* (Washington, D.C.: Office of Technical Services, Dept. of Commerce).
Hughes, D. J., Garth, R. C., and Levin, J. S. 1953, *Phys. Rev.*, **91**, 1423.
Hughes, D. J., and Harvey, J. A. 1954, *Nature*, **173**, 942.
Jones, K. W., Donahue, D. J., McEllistrem, M. T., Douglas, R. A., and Richards, H. T. 1953, *Phys. Rev.*, **91**, 879.
Keenan, P. C., and Keller, G. 1951, *Ap. J.*, **113**, 700.
Kinsey, B. B., and Bartholomew, G. A. 1954, *Phys. Rev.*, **93**, 1260.
McKellar, A. 1948, *Pub. Dom. Ap. Obs. Victoria*, **7**, 395.
Merrill, P. W. 1952, *Ap. J.*, **116**, 21.
Mott, N. F., and Massey, H. S. 1949, *The Theory of Atomic Collisions* (2d ed.; Oxford: ClarendonPress).
Salpeter, E. E. 1952*a*, *Ap. J.*, **115**, 326.
———. 1952*b*, *Phys. Rev.*, **88**, 547.
———. 1953, *Annual Review of Nuclear Science* (Stanford: Annual Reviews, Inc.), **2**, 41.
Sandage, A. R., and Schwarzschild, M. 1952, *Ap. J.*, **116**, 463.
Sanford, R. F. 1950, *Ap. J.*, **111**, 262.
Schardt, A., Fowler, W. A., and Lauritsen, C. C. 1952, *Phys. Rev.*, **86**, 527.
Schönberg, M., and Chandrasekhar S. 1942, *Ap. J.*, **96**, 161.
Teichman, T., and Wigner, E. P. 1952, *Phys. Rev.*, **87**, 123.
Urey, H. C. 1952, *Phys. Rev.*, **88**, 248.
von Weizsäcker, C. 1938, *Phys. Zs.*, **39**, 633.

THE LUMINOSITY FUNCTION AND STELLAR EVOLUTION

EDWIN E. SALPETER*
Australian National University, Canberra, and Cornell University
Received July 29, 1954

ABSTRACT

The evolutionary significance of the observed luminosity function for main-sequence stars in the solar neighborhood is discussed. The hypothesis is made that stars move off the main sequence after burning about 10 per cent of their hydrogen mass and that stars have been created at a uniform rate in the solar neighborhood for the last five billion years.

Using this hypothesis and the observed luminosity function, the rate of star creation as a function of stellar mass is calculated. The total number and mass of stars which have moved off the main sequence is found to be comparable with the total number of white dwarfs and with the total mass of all fainter main-sequence stars, respectively.

I. INTRODUCTION

Since Baade's early work on the two types of stellar populations, much has been learned about stellar evolution from studies of population II systems. Of particular importance are the H-R diagrams of globular clusters (Arp, Baum, and Sandage 1952), where main-sequence stars brighter than M_v about 3.5 are missing almost completely and a subgiant branch, leading to a giant branch, starts at the same magnitude. These results were explained theoretically by Sandage and Schwarzschild (1952), on the assumption of very poor mixing between the central core and the outer layer of a star. According to their theory, the more luminous main-sequence stars, which have converted more than about 12 per cent of their mass (the Schönberg-Chandrasekhar limit) from hydrogen into helium in their central core, change their internal structure and rapidly move off the main sequence toward the red-giant region. The amount of energy released in the conversion of 1 gm of hydrogen into helium is known from nuclear data to be 6.2×10^{18} ergs. For a star with $M_v = 3.5$ and mass about 1.3 $\mathfrak{M}_\odot$ it takes about 6×10^9 years for the nuclear conversion of 12 per cent of the stellar mass. The absence of more luminous main-sequence stars in a globular cluster then indicates that the cluster is about 5×10^9 years old, which agrees well with other estimates of the age of our galaxy. Further, the fact that the main sequence peters out fairly suddenly indicates that all the stars of a cluster have practically the same age. Because of this uniformity in age and because of the rapid evolution of stars along the subgiant branch, globular clusters mainly give information on the evolution of stars in a narrow range of main-sequence luminosity and hence a narrow range of mass (near 1.3 $\mathfrak{M}_\odot$).

Population I systems, on the other hand, the solar neighborhood in particular, contain stars with a large range of ages. From a large amount of observational data on stars in our neighborhood, tolerably accurate values are available for the luminosity function $\phi(M_v, \text{Sp})$, the density of stars of absolute visual magnitude between $(M_v - \frac{1}{2})$ and $(M_v + \frac{1}{2})$ in a certain range of spectral class. This luminosity function depends on three factors: (i) $\xi(\mathfrak{M})$, the relative probability for the creation of stars of mass near $\mathfrak{M}$ at a particular time; (ii) the rate of creation of stars as a function of time since the formation of our galaxy; and (iii) the evolution of stars of different masses after they have burned out an appreciable fraction of their hydrogen mass and have left the main sequence.

One cannot, of course, derive these three factors from a knowledge of the luminosity function. But we can test whether the following series of hypotheses is compatible with the luminosity function: (*a*) The rate of formation of stars in the solar neighborhood has

* This work was done at the Australian National University on leave of absence from Cornell University.

been uniform since the beginning of our galaxy (in contrast to population II systems, no very large number of stars were formed simultaneously in the beginning). (*b*) The factor $\xi(\mathfrak{M})$ is a smoothly varying function of mass $\mathfrak{M}$, independent of time. (*c*) Stars do not change their mass appreciably during their evolution, except at the last stages (accretion of matter, loss of matter by corpuscular radiation, etc., are unimportant). (*d*) Most stars are poorly mixed and move off the main sequence toward cooler surface temperature as soon as about 12 per cent of their mass has changed from hydrogen into helium.

II. OBSERVATIONAL DATA

The total luminosity function $\phi_t(M_v)$ is defined by

$$dN = \phi_t(M_v)\, dM\,, \tag{1}$$

where dN is the number of stars of all spectral classes per cubic parsec of absolute visual magnitude between M_v and $(M_v + dM)$. Among others, Van Rhijn (1925, 1936) has determined $\phi_t(M_v)$ between $M_v = -6$ and $M_v = +13$ from extensive observational data. For the low-luminosity part of this range, Luyten (1939, 1941) more recently has derived $\phi_t(M_v)$ from a detailed survey of faint stars in the Southern Hemisphere. We adopt a compromise between Van Rhijn's and Luyten's luminosity functions, similar to that of Bok (1941). This luminosity function, $\phi(M_v)$, is given in Table 2.

TABLE 1

FRACTION f OF MAIN-SEQUENCE STARS (TYPE EARLIER THAN Sp_d)

	M_v								
	−4.5	−3.5	−2.5	−1.5	−0.5	+0.5	+1.5	+2.5	+3.5
Sp_d	B0	B3	B6	B9	A1	A6	F0	F8	G7
f	0.10	0.25	0.48	0.51	0.43	0.40	0.60	0.70	0.90

We shall only consider the luminosity function in the range $M_v = -4.5$ to $+13.5$. Luyten's work indicates that the luminosity function decreases for M_v greater than 13 or 14, although this does not necessarily mean that the total number of these faint stars is small. Our adopted luminosity function does not refer to stars at a homogeneous distance from the galactic plane. Work by McCuskey (1951) and others indicates that the luminosity functions for various distances from the galactic plane differ only in minor details from Van Rhijn's up to distances of about 500 parsecs, except possibly for $M_v < -2$.

We shall not consider the detailed luminosity–spectral type function $\phi(M, \mathrm{Sp})$ (cf. Luyten 1936), but we shall want the luminosity function for main-sequence stars alone, separated from the giants. Trumpler and Weaver (1953) give the relative frequency of stars of different spectral types with the same value of M_v, based on results of Strömberg and of Öpik for stars brighter than apparent visual magnitude +6. The resolving power of this data is not sufficiently high to give a clear separation between main sequence and subgiants. For each value of M_v we chose, somewhat arbitrarily, a dividing spectral type Sp_d, shown in Table 1. Comparison with a table (Keenan and Morgan 1951) of average values of M_v on the two-dimensional spectral type–luminosity class classification shows that stars of type earlier than Sp_d should contain most of the main-sequence stars (class V), a reasonable fraction of the subgiants (class IV), and only few giants or supergiants. In Table 1 we give, for each value of M_v, the fraction f of the stars which have types earlier than Sp_d, taken from Trumpler and Weaver (1953).

We define the luminosity function $\phi(M_v)$ for the main sequence alone as $[f\phi_t(M_v)]$, with a small correction for the presence of white dwarfs in ϕ_t. No very accurate data on the frequency of white dwarfs is available, but data on the nearest 50–500 stars indicate that of the order of 10 per cent of all stars are white dwarfs. Luyten (1952) found the luminosity of white dwarfs to be scattered in the range $M_v = +9$ to $+16$. Our adopted luminosity function $\phi(M_v)$ for the main sequence is given in Table 2.

We shall need values for the average mass $\mathfrak{M}$ and absolute bolometric magnitude M_b as a function of M_v for main-sequence stars. The adopted values for the masses, given in Table 2, are a compromise between various compilations (cf. Becker 1950 and Hynek 1951). The adopted mass values are not very accurate but were chosen such that $\mathfrak{M}$ is a smoothly varying function of M_v. The values for M_b, also given in Table 2, were obtained by using Kuiper's (1938*b*) values for the bolometric correction for the average main-sequence spectral type (see Trumpler and Weaver, 1953) corresponding to each M_v.

TABLE 2

LUMINOSITY FUNCTION

M_v	$\log \phi_{tot}+10$	$\log \phi+10$	M_b	$\log(\mathfrak{M}/\mathfrak{M}_\odot)+1$	$\log \psi+10$	$\log \xi+10$
− 4	3.58	2.83	−6.64	2.23	5.81	6.63
− 3	4.12	3.68	−5.31	2.08	6.28	7.10
− 2	4.71	4.41	−3.90	1.93	6.54	7.36
− 1	5.32	4.99	−2.31	1.78	6.70	7.52
0	5.99	5.60	−0.90	1.63	6.89	7.72
+ 1	6.61	6.28	+0.49	1.48	7.16	8.00
+ 2	6.74	6.55	+1.71	1.33	7.09	7.98
+ 3	7.02	6.90	+3.00	1.20	7.05	7.98
+ 4	7.34	7.32	+4.01	1.09	7.32	8.32
+ 5	7.45	7.45	.....	1.00	7.45	8.50
+ 6	7.50	7.50	.....	0.93	7.50	8.60
+ 7	7.54	7.54	.....	0.86	7.54	8.70
+ 8	7.64	7.64	.....	0.80	7.64	8.83
+ 9	7.76	7.75	.....	0.74	7.75	8.97
+10	7.84	7.82	.....	0.68	7.82	9.04
+11	7.94	7.91	.....	0.62	7.91	9.13
+12	8.02	7.98	.....	0.56	7.98	9.20
+13	8.05	8.00	.....	0.50	8.00	9.22

III. THE "ORIGINAL MASS FUNCTION"

A portion of the luminosity function of Table 2 is plotted against magnitude in Figure 1. The finer details of this curve are most probably not significant, but the very marked change from a small slope for faint stars to a large slope for bright ones certainly is significant. This change of slope is already significant for ϕ_t, slightly more significant still for ϕ. For instance, $\phi(+8)/\phi(+3)$ is only about 6, as compared with a value of about 150 for $\phi(+3)/\phi(-2)$ for all stars and about 300 for main-sequence stars alone. This change of slope takes place somewhere between $M_v = +1$ and $M_v = +5$ (probably closer to the latter). Also, the main-sequence and giant branches start diverging in about the same magnitude region, which also brackets the magnitude, $M_v \approx +3.5$, at which the main sequence in globular clusters peters out. Further, this change in slope is not due to any peculiar dependence of M_v on variables of greater physical significance like mass. For instance, the mass function, defined as $[\phi dM_v/d(\log \mathfrak{M})]$, plotted against $\mathfrak{M}$, shows a change of slope almost as marked as that of ϕ.

It seems natural to explain the change of slope of the population I luminosity function

along lines similar to the explanation for the globular-cluster H-R diagram: There are no stars older than T_0 years (the age of the galaxy), and stars of visual magnitude M_L burn 12 per cent of their hydrogen mass in this time. Hence all stars fainter than this limiting magnitude have burned less and are still on the main sequence. For brighter stars only those sufficiently young to have burned less than 12 per cent of their mass are still on the main sequence, which leads to a rapid decline of main-sequence stars with increasing brightness for $M_v < M_{L,v}$.

More specifically, we wish to test the validity of the series of hypotheses stated at the end of Section I. We defined the "original mass function," $\xi(\mathfrak{M})$, by

$$dN = \xi(\mathfrak{M})\, d(\log_{10} \mathfrak{M}) \frac{dt}{T_0}, \tag{2}$$

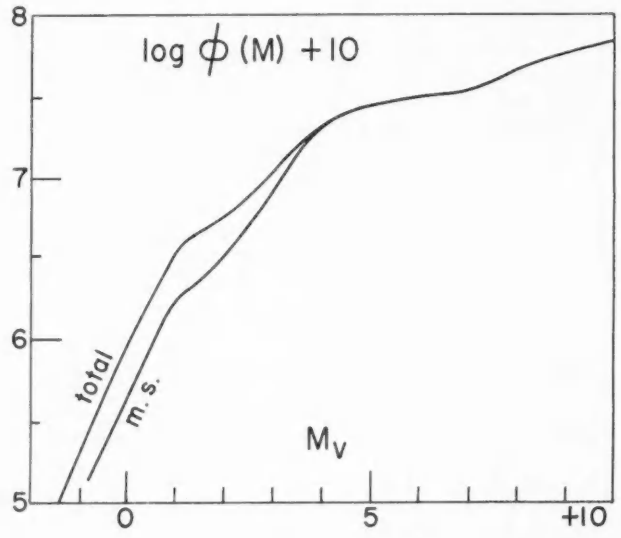

FIG. 1.—The logarithm of the luminosity function ϕ plotted against visual magnitude, M_v. The curve marked *total* denotes the total observed function. The curve marked *m.s.* denotes the derived function for main-sequence stars only.

where dN is the number of stars in the mass range $d\mathfrak{M}$ created in the time interval dt per cubic parsec. The corresponding "original luminosity function," $\psi(M_v)$, is then

$$\psi(M_v) = \xi(\mathfrak{M}) \frac{d(\log_{10} \mathfrak{M})}{dM_v}. \tag{3}$$

These mass and luminosity functions are, of course, not identical with the observed ones for stars brighter than the limiting magnitude $M_{L,v}$, but are the functions which would be observed if these stars remained on the main sequence forever. Let the average mass, bolometric luminosity, and bolometric magnitude of a main-sequence star of visual magnitude $M_{L,v}$ be $\mathfrak{M}_L$, L_L, and $M_{L,b}$, respectively. The time T spent on the main sequence by a brighter star (time taken to burn 12 per cent of the mass) is then $T_0(\mathfrak{M}/L)$

$(L_L/\mathfrak{M}_L)$. The relation between our "original luminosity function," $\psi(M_v)$, and the observed one, $\phi(M_v)$, is then

$$\log \phi\,(M_v) = \log \psi\,(M_v) + 0.4\,(M_b - M_{L,\,b}) + \log\left(\frac{\mathfrak{M}}{\mathfrak{M}_L}\right) \tag{4}$$

for $M_v < M_{L,\,v}$; $\phi = \psi$ for $M_v > M_{L,\,v}$.

Since the data on $\phi(M_v)$ are not sufficiently accurate to obtain a precise value of $M_{L,\,v}$ from the change of slope, we assume the value indicated by the globular-cluster data of $M_{L,\,v} = 3.5$. Using equation (4) and the values for mass $\mathfrak{M}$ and bolometric magnitude M_b given in Table 2, $\psi(M_v)$ was derived from the observed $\phi(M_v)$. Finally, using equation (3) and the adopted mass values, the function $\xi(\mathfrak{M})$ was derived. Both ψ and ξ are given in Table 2. A plot of ξ against $\mathfrak{M}$ is given in Figure 2, passing through all the points of Table 2, except for three points, marked with circles in the figure.

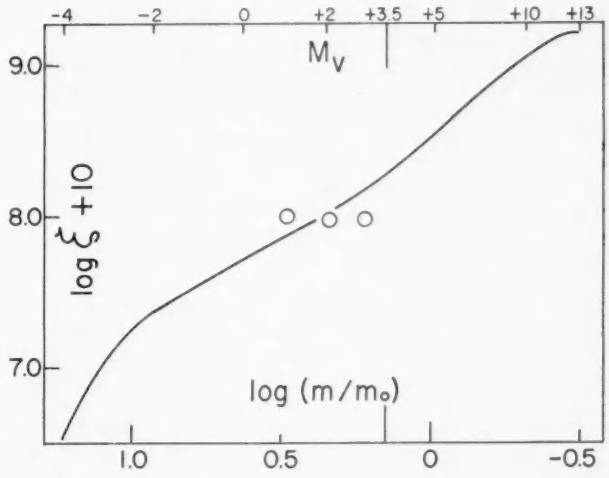

FIG. 2.—The logarithm of the "original mass function," ξ, plotted against the mass, $\mathfrak{M}$, in solar units.

IV. DISCUSSION

Figure 2 and Table 2 show that the "original" mass and luminosity functions ξ and ψ are, in fact, fairly smoothly varying functions without any very rapid change of slope. For $\log(\mathfrak{M}/\mathfrak{M}_\odot)$ between -0.4 and $+1.0$, ξ is given reasonably well by the approximation

$$\xi\,(\mathfrak{M}) \approx 0.03\left(\frac{\mathfrak{M}}{\mathfrak{M}_\odot}\right)^{-1.35}. \tag{5}$$

It is not yet clear whether the steeper drop of ξ for masses larger than $10\,\mathfrak{M}_\odot$ is a real effect, since in this region masses and bolometric corrections are not known very accurately and the number of such stars reasonably near the galactic plane is small.

The smoothness of the function ξ lends support to the hypotheses, stated in Section I, on which this paper is based (but of course does not prove them to be correct). Accept-

ance of these hypotheses, and hence of the mass function $\xi(\mathfrak{M})$, has some interesting consequences. Numerical integration shows that

$$\int_{0.15}^{\infty} d(\log \mathfrak{M}) [\mathfrak{M} \xi(\mathfrak{M})] \approx 0.8 \int_{-0.5}^{0.15} d(\log \mathfrak{M}) [\mathfrak{M} \xi(\mathfrak{M})], \tag{6}$$

$$\int_{0.15}^{\infty} d(\log \mathfrak{M}) \xi(\mathfrak{M}) \approx 0.12 \int_{-0.5}^{0.15} d(\log \mathfrak{M}) \xi(\mathfrak{M}). \tag{7}$$

The left-hand side of equation (6) represents the total mass per cubic parsec of all stars, created at any time since the origin of the galaxy, brighter than limiting magnitude $M_{L,v} = 3.5$. Since most of these stars burn their hydrogen very quickly, most of this mass is at present in some form other than main-sequence stars. The integral on the right-hand side of equation (6), on the other hand, is approximately equal to the total mass (per cubic parsec) contained in all stars (brighter than $M_v = 13.5$) which are in existence at present. In other words, the total mass which has been in the form of main-sequence stars once but has taken on different form by now is of the same order of magnitude as the total mass of present stars!

It is interesting to speculate what form this mass of vanished main-sequence stars has taken. One attractive hypothesis is that a massive and luminous star loses most of its mass to the interstellar medium during the last stages of its evolution, the small remnant becoming a white dwarf. Equation (7) lends support to this view: the integrals on the left- and right-hand sides of this equation represent roughly the total number of burned-out and present main-sequence stars, respectively. According to this hypothesis, then, roughly 10 per cent of existing stars should be white dwarfs, which agrees well with observational estimates of the abundance of white dwarfs.

Some workers have estimated that, in regions near the galactic plane, the total mass of existing stars is of the same order of magnitude as the mass of the interstellar gas. If all the assumptions of this paper should turn out to be at least roughly correct, it would then appear likely that an appreciable fraction of the interstellar gas present has at some time passed through the interior of stars. This conclusion, if true, would have some bearing on Hoyle's (1946) theory, which claims that all the chemical elements (except hydrogen) found in the universe today were formed in the interior of stars.

One should perhaps re-emphasize the various sources of error and limitations of the calculations of this paper. The various input data used for deriving the "original mass function" are sufficiently inaccurate so that the values given in Table 2 for $\log \psi$ and $\log \xi$ may be in error by more than ± 0.20. The numerical coefficients on the right-hand side of equations (6) and (7) could be in error by as much as a factor of 2. Further, the luminosity function discussed in this paper refers only to a relatively small region in the solar neighborhood. It is, of course, unlikely that the same stars and gas clouds have remained in this small region over several billions of years. For this reason, too, the quantitative conclusions of this section should be considered as quite tentative.

Neither the observed nor the "original" luminosity function used in this paper shows a marked sudden drop from the low-luminosity to the high-luminosity side of $M_v \sim 4$. The absence of this drop, so characteristic of population II systems, indicates that the region considered contains mainly population I stars. Nevertheless, a fair fraction of the very faint main-sequence stars and of the white dwarfs could belong to population II.

REFERENCES

Arp, H., Baum, W., and Sandage, A. R. 1952, *A.J.*, **57**, 4.
Becker, W. 1950, *Sterne und Sternsysteme* (Dresden: Steinkopf), p. 62.
Bok, B. J. 1951, *Ann. New York Acad. Sci.*, **42**, 219.
Hoyle, F. 1946, *M.N.*, **106**, 343.

Hynek, J. A. 1951, in J. A. Hynek (ed.), *Astrophysics: A Topical Symposium* (New York: McGraw-Hill Book Co., Inc.), chap. x, p. 466.
Keenan, P. C., and Morgan, W. W. 1951, in J. A. Hynek (ed.), *Astrophysics: A Topical Symposium* (New York: McGraw-Hill Book Co., Inc.), chap. i, p. 23.
Kuiper, G. P. 1938, *Ap. J.*, **88**, 429.
Luyten, William. 1939, *Pub. Astr. Obs. U. Minnesota*, Vol. 2, No. 7.
———. 1941, *Ann. New York Acad. Sci.*, **42**, 205.
———. 1952, *Ap. J.*, **116**, 283.
McCuskey, S. W. 1951, *Pub. Obs. U. Michigan*, **10**, 67.
Sandage, A. R., and Schwarzschild, M. 1952, *Ap. J.*, **116**, 463.
Trumpler, R. J., and Weaver, H. F. 1953, *Statistical Astronomy* (Berkeley: University of California Press), p. 409.
Van Rhijn, P. J. 1925, *Pub. Astr. Lab. Groningen*, No. 38.
———. 1936, *ibid.*, No. 47.

ON TOROIDAL MAGNETIC FIELDS IN THE SUN AND STARS

C. PLUMPTON AND V. C. A. FERRARO
Queen Mary College, University of London
Received June 4, 1954

ABSTRACT

Torsional oscillations of a liquid sphere of infinite electrical conductivity in the presence of a permanent axi-symmetric magnetic field are considered. It is shown that axially symmetric oscillations can be excited in which the sphere oscillates in shells generated by the rotation of the lines of force about the axis of symmetry.

The range of frequencies forms a continuous spectrum, but this degeneracy may be due to the approximations made and may disappear when a rotating sphere is considered. The bearing of this solution on problems of interest in solar magnetism is also discussed.

I. INTRODUCTION

It has been suggested by Cowling (1946) and also by Bullard that sunspots might result from the transport by convection to the sun's surface of the magnetic lines of force of a toroidal component of the sun's general magnetic field. Such a toroidal component of the field could arise as a result of torsional oscillations of the sun in the presence of the axially symmetric part of the field. Thus the problem of the torsional oscillations of a star in its own magnetic field is of considerable interest in this connection. Unfortunately, the problem is beset with mathematical difficulties, and it seems that progress can best be made by considering, in the first instance, simpler illustrative problems.

The simplest problem is that of the torsional oscillations of a liquid sphere of infinite electrical conductivity in the presence of a permanent magnetic field axially symmetric with respect to the axis of the oscillations. We shall first consider the case when the field is uniform (this appears to be the most important case) and shall subsequently generalize the results.

The case of the torsional oscillations of a highly conducting liquid sphere in a decaying magnetic field has, in fact, been treated by Jensen (1955); his discussion deals essentially with the case of asymmetric oscillations. His solution does not include, however, the case of axial symmetry as a special case.

This will be considered here, and it will be shown that the sphere oscillates in shells generated by the rotation of the lines of force about the axis of symmetry. The range of frequencies forms a continuous spectrum, and this novel feature in eigenvalue problems appears also to be present in Jensen's solution. It is possible, as has been suggested by Professor Cowling, to the writer, that this degeneracy may be removed by taking account of the rotation of the sphere.

II. THE ELECTROMAGNETIC FIELD EQUATIONS

Let $\boldsymbol{E}$ and $\boldsymbol{H}$ denote the electric and magnetic fields, respectively; ν and $\boldsymbol{j}$ the space charge and current density, respectively; and σ the electrical conductivity of the liquid (all in e.m.u.). The field equations are then, neglecting displacement currents,

$$\operatorname{curl} \boldsymbol{E} = -\dot{\boldsymbol{H}}\,, \tag{1}$$

$$\operatorname{curl} \boldsymbol{H} = 4\pi \boldsymbol{j}\,, \tag{2}$$

$$\operatorname{div} \boldsymbol{E} = 4\pi\nu\,, \tag{3}$$

$$\operatorname{div} \boldsymbol{H} = 0\,, \tag{4}$$

with the constitutive equation

$$\boldsymbol{j} = \sigma(\boldsymbol{E} + \boldsymbol{v} \times \boldsymbol{H}) . \tag{5}$$

Here dots denote partial derivatives with respect to time, and $\boldsymbol{v}$ is the velocity of a liquid element.

Consider a disturbance from the equilibrium state of the liquid sphere, in which the only nonvanishing resolute of the velocity is the toroidal component $\boldsymbol{w}$ (thus the velocity vector $\boldsymbol{v}$ has no resolutes in the meridian plane through the element). Denoting by $\boldsymbol{h}$ the (toroidal) variations of the magnetic field from the uniform field $\boldsymbol{H}_0$, so that

$$\boldsymbol{H} = \boldsymbol{H}_0 + \boldsymbol{h} , \tag{6}$$

equations (1), (2), (4), and (5) become

$$\operatorname{curl} \boldsymbol{E} = -\dot{\boldsymbol{h}} , \tag{7}$$

$$\operatorname{curl} \boldsymbol{h} = 4\pi \boldsymbol{j} , \tag{8}$$

$$\operatorname{div} \boldsymbol{h} = 0 , \tag{9}$$

$$\boldsymbol{j} = \sigma(\boldsymbol{E} + \boldsymbol{w} \times \boldsymbol{H}) , \tag{10}$$

since $\boldsymbol{w}$ and $\boldsymbol{h}$ are parallel vectors.

From equations (7), (8), and (10) we have

$$\dot{\boldsymbol{h}} = -\frac{1}{4\pi\sigma} \operatorname{curl} \operatorname{curl} \boldsymbol{h} + \operatorname{curl} (\boldsymbol{w} \times \boldsymbol{H}_0) . \tag{11}$$

Choose a set of cylindrical co-ordinates (ϖ, ϕ, z) in which the z-axis lies along the direction of $\boldsymbol{H}_0$ and the origin is the center of the sphere. Then the only nonvanishing resolute of equation (11) gives

$$\dot{h} = \frac{1}{4\pi\sigma} \Delta h + H_0 \frac{\partial w}{\partial z} , \tag{12}$$

where

$$\Delta h = \frac{\partial}{\partial \varpi} \left\{ \frac{1}{\varpi} \frac{\partial (\varpi h)}{\partial \varpi} \right\} + \frac{\partial^2 h}{\partial z^2} \tag{13}$$

and $h = |\boldsymbol{h}|$, etc.

When $H_0 = 0$, equation (12) reduces to the equation of decay of the magnetic field through ohmic resistance, and Cowling (1945) has shown that for an ordinary star like the sun the decay time is at least comparable with the life of the star, though this estimate may be reduced somewhat when turbulence is taken into account (Sweet 1950). However, hydromagnetic oscillations of a star have periods which are small compared with the decay time (Ferraro and Memory 1952), and it is legitimate to treat the electrical conductivity of the star as infinite to a high degree of approximation. Hence we replace equation (12) by the simpler equation

$$\dot{h} = H_0 \frac{\partial w}{\partial z} . \tag{14}$$

Outside the star, $j = 0$, and equation (8) then shows that the disturbance magnetic field $\boldsymbol{h}'$ is derived from a potential. But, on account of axial symmetry and the fact that $\boldsymbol{h}'$ is a toroidal vector, it follows that $h' = 0$ outside the star. The electric field inside the sphere is given by $\boldsymbol{E} = -\boldsymbol{v} \times \boldsymbol{H}$. Outside the sphere, by equation (7), it is derived from a potential.

III. BOUNDARY CONDITIONS

The magnetic field at the surface of the liquid sphere is continuous, so that h is continuous in crossing the surface. Since $h' = 0$ outside the sphere, it follows that h vanishes at the surface of the liquid, $r = a$(say).

The continuity of the tangential resolute of the electric field at the surface enables us to determine the potential of the external field, since, by expanding the tangential resolute of the internal electric field in a series of spherical harmonics, the expansion theorem then suffices to determine the potential. Thus the only boundary condition of the problem is that

$$h = 0 \text{ for } r = a\,. \tag{15}$$

IV. THE MECHANICAL EQUATIONS

Let p and V denote the pressure and gravitational potential at any point of the liquid, of density ρ. Then the equation of small motions is

$$\rho \frac{\partial \boldsymbol{w}}{\partial t} = j \times \boldsymbol{H} - \operatorname{grad}(p + \rho V)\,. \tag{16}$$

In the case of small toroidal oscillations, the surface of the liquid remains spherical during the oscillations. The only nonvanishing resolute of equation (16) then gives

$$\dot{w} = \left(\frac{H_0}{4\pi\rho}\right)\left(\frac{\partial h}{\partial z}\right). \tag{17}$$

Eliminating h or w between equations (14) and (17) yields Alfvén's equations

$$\ddot{w} = U^2 \frac{\partial^2 w}{\partial z^2}, \qquad \ddot{h} = U^2 \frac{\partial^2 h}{\partial z^2}, \tag{18}$$

where U is the velocity of the Alfvén waves given by

$$U = H_0 (4\pi\rho)^{-1/2}\,. \tag{19}$$

V. SOLUTION OF THE EQUATIONS

Writing

$$Ut = \tau\,, \tag{20}$$

the first of equations (18) may be written

$$\frac{\partial^2 w}{\partial \tau^2} = \frac{\partial^2 w}{\partial z^2}, \tag{21}$$

and equation (14) becomes

$$\frac{\partial h}{\partial \tau} = (4\pi\rho)^{1/2} \frac{\partial w}{\partial z}\,. \tag{22}$$

Let us now consider an initial disturbance such that, at $t = 0$ (that is, at $\tau = 0$), $h = 0$ and $w = \varpi\Omega(z, \varpi)$, so that Ω has the dimensions of an angular velocity. Assuming a solution of equation (21) of the form

$$w = F(z, \varpi) \cos \lambda\tau\,, \tag{23}$$

where λ is a constant, equation (21) becomes

$$\frac{\partial^2 F}{\partial z^2} + \lambda^2 F = 0\,, \tag{24}$$

the solution of which is

$$F = A(\varpi) \cos \lambda z + B(\varpi) \sin \lambda z \,, \tag{25}$$

where A and B are arbitrary functions of ϖ. Thus

$$w = \{A(\varpi) \cos \lambda z + B(\varpi) \sin \lambda z\} \cos \lambda \tau \,. \tag{26}$$

Substituting in equation (22), we then find

$$h = (4\pi\rho)^{1/2}\{-A(\varpi) \sin \lambda z + B(\varpi) \cos \lambda z\} \sin \lambda \tau \,, \tag{27}$$

so that the disturbance velocity and magnetic vectors differ in phase by a quarter-period. The boundary condition $h = 0$ at $r = a$ gives

$$h = 0 \text{ for } z = \pm (a^2 - \varpi^2)^{1/2} \,. \tag{28}$$

Hence

$$\begin{aligned} -A(\varpi) \sin \lambda(a^2 - \varpi^2)^{1/2} + B(\varpi) \cos \lambda(a^2 - \varpi^2)^{1/2} = 0 \,, \\ A(\varpi) \sin \lambda(a^2 - \varpi^2)^{1/2} + B(\varpi) \cos \lambda(a^2 - \varpi^2)^{1/2} = 0 \,. \end{aligned} \tag{29}$$

For a nonvanishing solution we must have

$$\sin 2\lambda z_0 = 0 \,, \tag{30}$$

where we have written $z_0 = (a^2 - \varpi^2)^{1/2}$. The solution of this equation is

$$2\lambda z_0 = k\pi \,, \tag{31}$$

where k is a positive integer or zero. Then we can take

$$w = \sum_{k=0}^{\infty} \left[A_k(\varpi) \cos \frac{k\pi z}{2 z_0} + B_k(\varpi) \sin \frac{k\pi z}{2 z_0} \right] \cos \frac{k\pi \tau}{2 z_0} \,. \tag{32}$$

Fitting the initial condition for $\tau = 0$, we have

$$\varpi\Omega(z, \varpi) = \sum_{k=0}^{\infty} \left[A_k(\varpi) \cos \frac{k\pi z}{2 z_0} + B_k(\varpi) \sin \frac{k\pi z}{2 z_0} \right] \tag{33}$$

in the range $-z_0 \leqslant z \leqslant z_0$, i.e., over the cylindrical shell of radius ϖ. The usual Fourier analysis gives, if k is a positive integer,

$$\begin{aligned} A_0 &= \frac{\varpi}{2 z_0} \int_{-z_0}^{z_0} \Omega(z, \varpi) \, dz \,, \\ A_{2k+1}(\varpi) &= 0 = B_{2k}(\varpi) \,, \\ A_{2k}(\varpi) &= \frac{\varpi}{z_0} \int_{-z_0}^{z_0} \Omega(z, \varpi) \cos \frac{k\pi z}{z_0} \, dz \,, \\ B_{2k+1}(\varpi) &= \frac{\varpi}{z_0} \int_{-z_0}^{z_0} \Omega(z, \varpi) \sin \frac{(2k+1)\pi z}{2 z_0} \, dz \,. \end{aligned} \tag{34}$$

These results also follow from equations (29) and (31), since when k is odd $\cos \lambda z_0 = 0$, so that $A_k = 0$, and when k is even $\sin \lambda z_0 = 0$ and $B_k = 0$. Thus, with the above definitions of the A's and B's, we have, finally,

$$w = \sum_{k=0}^{\infty} A_{2k} \cos \frac{k\pi z}{z_0} \cos \frac{k\pi Ut}{z_0} + \sum_{k=0}^{\infty} B_{2k+1} \sin \frac{(2k+1)\pi z}{2z_0} \cos \frac{(2k+1)\pi Ut}{2z_0} \tag{35}$$

for the toroidal disturbance velocity and

$$h = \frac{H_0}{U}\Big[- \sum_{k=0}^{\infty} A_{2k} \sin \frac{k\pi z}{z_0} \sin \frac{k\pi Ut}{z_0} + \sum_{k=0}^{\infty} B_{2k+1} \cos \frac{(2k+1)\pi z}{2z_0} \sin \frac{(2k+1)\pi Ut}{2z_0}\Big]. \tag{36}$$

This solution may be conveniently analyzed into odd and even modes; in each it will be seen that the liquid will vibrate in cylindrical shells parallel to the axis. We consider each mode in turn.

Odd modes ($A_k = 0$).—Considering the shell $\varpi = \varpi_1$, the periods of the toroidal oscillations of this shell are $4z_0/(2k+1)U$, $k = 0, 1, \ldots$, the period of the fundamental mode being $4z_0/U$, where $z_0 = (a^2 - \varpi_1^2)^{1/2}$. We note, however, the novel feature that, as we pass from shell to shell from the axis to the equator, this period varies continuously from $4a/U$ to 0.

Even modes ($B_k = 0$).—The periods of the toroidal oscillations of the same shell in this case are $2z_0/kU$, $k = 1, 2, \ldots$; the period of the fundamental mode is $2z_0/U$, and again these periods vary continuously from shell to shell from $2a/U$ to 0 as we pass from the axis to the equator.

VI. TOROIDAL OSCILLATIONS IN A POLOIDAL FIELD

We now generalize the above results to the case of a general poloidal magnetic field. Assuming the conductivity to be infinite, equation (11) may be written

$$\dot{\boldsymbol{h}} = \operatorname{curl} (\boldsymbol{w} \times \boldsymbol{H}_0), \tag{37}$$

and, if $\boldsymbol{\xi}$ denotes the displacement of a particle in a shell from its steady-state motion, we have

$$\boldsymbol{w} = \frac{\partial}{\partial t}, \tag{38}$$

and, substituting in equation (37) and integrating, we find

$$\boldsymbol{h} = \operatorname{curl} (\boldsymbol{\xi} \times \boldsymbol{H}_0). \tag{39}$$

Again, from equation (16),

$$\rho \frac{\partial \boldsymbol{w}}{\partial t} = \boldsymbol{j} \times \boldsymbol{H}_0, \tag{40}$$

and, using equations (8), (38), and (39), the equation for $\boldsymbol{\xi}$ is found to be

$$4\pi\rho \ddot{\boldsymbol{\xi}} = [\operatorname{curl} \operatorname{curl} (\boldsymbol{\xi} \times \boldsymbol{H}_0)] \times \boldsymbol{H}_0. \tag{41}$$

A poloidal potential magnetic field is derivable from a stream function ψ, the same for all meridian planes. Using spherical polar co-ordinates (r, θ, ϕ) in which the axis of symmetry of the field coincides with the θ-axis, the radial and transverse resolutes in a meridian plane are given by

$$H_r = -\frac{1}{r^2 \sin\theta}\frac{\partial\psi}{\partial\theta}, \qquad H_\theta = \frac{1}{r\sin\theta}\frac{\partial\psi}{\partial r}. \tag{42}$$

Introducing the angular displacement η corresponding to the torsional displacement ξ, where

$$\eta = \frac{\xi}{\varpi}, \tag{43}$$

and writing

$$Q = \frac{\partial(\psi, \eta)}{\partial(r, \theta)}, \tag{44}$$

the only nonvanishing resolute of equation (41) is

$$4\pi\rho r^4 \sin^3\theta\,\ddot{\eta} = \frac{\partial(\psi, Q\sin\theta)}{\partial(r, \theta)}, \tag{45}$$

and this is the equation to determine η.

If we now change the independent variables to ψ and Φ, the magnetic potential of the poloidal field, and use the identity

$$\frac{\partial(\psi, \eta)}{\partial(r, \theta)} = \frac{\partial(\psi, \eta)}{\partial(\psi, \Phi)}\frac{\partial(\psi, \Phi)}{\partial(r, \theta)}, \tag{46}$$

we find

$$Q = -H^2 r^2 \sin\theta\frac{\partial\eta}{\partial\Phi}, \tag{47}$$

and, finally, from equation (45),

$$4\pi\rho\ddot{\eta} = H^4\frac{\partial^2\eta}{\partial\Phi^2} + \frac{H^2}{\varpi^2}\frac{\partial\eta}{\partial\Phi}\frac{\partial(H^2\varpi^2)}{\partial\Phi}, \tag{48}$$

where $\varpi = r\sin\theta$.

This equation shows that the medium behaves as an anisotropic elastic fluid in which a disturbance is propagated as a wave form along the magnetic lines of force, as was inferred by Alfvén.

The results already obtained above for a uniform magnetic field suggest that the torsional oscillations of the sphere will be in shells formed by the magnetic lines of force.

VII. SOME REMARKS ON THE PRESENT EIGENVALUE PROBLEM

The unexpected result that the frequencies of the fundamental modes of vibrations of the isorotational shells form a continuous spectrum is not without mathematical interest. The continuous spectrum arises because the boundary of the liquid is not a "natural" boundary of the co-ordinate system appropriate to the equations of the problem; that is to say, if q is such a co-ordinate, the equation of the boundary is not of the form $q =$ Constant. It also explains the fact that a "line" spectrum was obtained for the natural frequencies of the oscillations considered by Ferraro and Memory (1952) and Plumpton and Ferraro (1953), for here the sphere was a natural boundary in the spherical polar co-ordinate system in terms of which the equation of the problem was in its simplest form.

The result obtained in Section V can also be discussed in the light of Alfvén's picture of the lines of force as taut strings. It is clear that in this case, if these are twisted about

the axis of rotation, each will behave as a taut string with its ends fixed. It will therefore vibrate with frequencies corresponding to the length of the string, the "tension" being the same for all strings in the case of a uniform permanent field. Since the lengths of the "strings" vary continuously from their maximum (equal to the diameter of the sphere) to zero at the equator, the spectrum of the frequencies of the fundamental modes is continuous.

The longest period for the odd modes found in Section V is $4a/U$, i.e., twice the time an Alfvén wave would take to travel from one pole of the sphere to the other; equation (48) also shows that in the more general case considered in Section VI similar conclusions hold good.

However, as Professor Cowling has pointed out to the writer, any effect which creates linking between neighboring shells as they twist will serve to replace the continuum by a discrete set of frequencies. Further, the above analysis is not applicable to the case of a rotating star. Pure torsional oscillations are impossible in a rotating star; an unbalanced Coriolis term arises in the equation of motion, and it is necessary to consider both meridianal and torsional oscillations together.

VIII. CONCLUSION

It is of interest to consider the order of magnitude of the periods of oscillations to be expected in the case of a liquid sphere of the dimensions of the sun in a magnetic field of the same order of magnitude as that to be expected in the solar interior. It seems unlikely that this can exceed a few thousand gauss.

Thus, taking $\rho = 1.4$ and $H_0 = 1000$ gauss, the longest periods to be expected are those for shells of the smallest radius. These are of the order of $4a/U$ for the fundamental odd mode and $2a/U$ for the fundamental even mode. Taking $a = 6.9 \times 10^{10}$ cm, we find these periods to be of the order of 37 and 18 years, respectively. For shells of greater radius the periods of the fundamental mode would be smaller but still of the order of 10 years, and so comparable with the period of 22 years of the complete sunspot cycle. This coincidence was noted by Grotrian (1950), among others.

It seems not unlikely that, if toroidal oscillations can be excited in the sun or in magnetic stars, the period of oscillation to be expected is likely to be of the order of magnitude found above. This, however, can only be ascertained by a more complete investigation which, in particular, takes into account the rotation of the sun.

As was shown in Section III, the toroidal field h will vanish at the surface, so that such a field could not be observed at the surface of the sun. In so far as a theory of sunspots is concerned in which part of the toroidal field is supposed to be carried by convection to the surface, one would have to suppose that this toroidal field has opposite directions in the Northern and Southern hemispheres. This would correspond to an even mode of oscillation, defined in section V. In such a mode the toroidal velocity at any instant is directed in the same sense in both hemispheres. There is, however, no a priori reason why the even modes should be excited in preference to the odd modes or any reason why the higher harmonics of the oscillation should not be excited. Thus it seems necessary to invoke an additional mechanism to insure that only an "even" mode is excited. This suggests that a theory of sunspots based on torsional oscillations alone is likely to raise more difficulties than it resolves.

REFERENCES

Cowling, T. G. 1945, *M.N.*, **105**, 166.
———. 1946, *ibid.*, **106**, 218.
Ferraro, V. C. A., and Memory, D. J. 1952, *M.N.*, **112**, 361.
Grotrian, W. 1950, *Naturwissenschaften*, **37**, 163.
Jensen, E. 1955, *Ap. J.* (in press).
Plumpton, C., and Ferraro, V. C. A. 1953, *M.N.*, **113**, 647.
Sweet, P. A. 1950. *M.N.*, **110**, 69.

THE TRANSFER OF RADIATION BY AN EMITTING ATMOSPHERE. IV

CHARLES A. LUNDQUIST AND HENRY G. HORAK
University of Kansas
Received July 26, 1954

ABSTRACT

The problem of the radiation intensities for a plane-parallel atmosphere containing a distribution of emission sources given by an arbitrary polynomial of the optical depth is solved for isotropic scattering. Both finite and semi-infinite atmospheres are considered. The quadratic case is considered in detail as an example.

I. INTRODUCTION

The equation of transfer for a plane-parallel layer of finite optical thickness in which the source function, ϵ, for the emission sources is a function of the optical depth, for the case of isotropic scattering with an albedo ϖ_0, has the form

$$\mu \frac{dI(\tau, \mu)}{d\tau} = I(\tau, \mu) - \varpi_0 J(\tau) - \epsilon(\tau), \tag{1}$$

where

$$J(\tau) = \frac{1}{2}\int_{-1}^{+1} I(\tau, \mu)\, d\mu. \tag{2}$$

The appropriate boundary conditions are given by the specification of the radiation incident on the boundaries. The solution of any general problem may be expressed as the sum of the solutions of two other problems, one having the specified boundary conditions and no emission sources and a second having the given distribution of sources and no incident radiation. The complete solution of the first problem has been given by Chandrasekhar (1950). The second problem was solved for a uniform distribution of sources by Horak (1952) and for a linear distribution of sources by Horak and Lundquist (1954). The solution will be given here for a distribution of sources given by an arbitrary polynomial of the optical depth.

II. THE SEMI-INFINITE ATMOSPHERE

The invariance principles for plane-parallel emitting atmospheres have been given by Horak (1952, eqs. [2] and [3]). For a semi-infinite atmosphere one of these is

$$I(\tau, +\mu) = \mathfrak{J}(\tau, +\mu) + \frac{1}{2\mu}\int_0^1 S(\infty, \mu, \mu')\, I(\tau, -\mu')\, d\mu', \tag{3}$$

where $\mathfrak{J}(\tau, \mu)$ is the solution of the problem for the semi-infinite atmosphere from τ to ∞, if there were no layer from 0 to τ. Differentiating equation (3) with respect to τ, using the equation of transfer to express derivatives of I, taking the limit of the resulting expression as τ approaches 0, and, finally, using the definition of the H-function (Chandrasekhar 1950, p. 105) yield the expression

$$I(0, +\mu) = \mu\left[\frac{d\mathfrak{J}(\tau, +\mu)}{d\tau}\right]_{\tau=0} + [\varpi_0 J(0) + \epsilon(0)]\, H(\mu). \tag{4}$$

From the form of the equation of transfer, it follows that, if I and I^* are the solutions for the distributions of sources ϵ and ϵ^*, respectively, then $I + I^*$ is the solution for $\epsilon + \epsilon^*$. The solution for a distribution of sources given by a polynomial in τ may then be expressed as the corresponding linear combination of the solutions for the distributions $\epsilon_N(\tau) = \tau^N$ (N an integer ≥ 1). It is therefore sufficient to solve the problem for the distributions $\epsilon_N(\tau)$.

The independent variable will temporarily be represented by τ', and the boundary of the atmosphere will be assumed to be $\tau' = 0$. In addition to the distribution $\epsilon_N(\tau')$, an auxiliary distribution $\epsilon_N^*(\tau') = (\tau' + \tau)^N$ will be introduced (Fig. 1). Expanding ϵ_N^* by the binomial expansion gives

$$\epsilon_N^*(\tau') = \tau'^N + \sum_{i=0}^{N-1} \binom{N}{i} \tau'^i \tau^{N-i} . \tag{5}$$

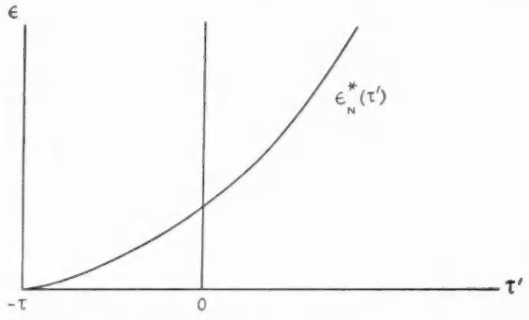

FIG. 1.—The auxiliary source distribution in the semi-infinite case

If I_N is the solution for ϵ_N and I_N^* is the solution for ϵ_N^*, then from equation (5) it follows that

$$I_N^*(\tau', \mu) = I_N(\tau', \mu) + \sum_{i=0}^{N-1} \binom{N}{i} \tau^{N-i} I_i(\tau', \mu) , \tag{6}$$

and, in particular,

$$I_N^*(0, +\mu) = I_N(0, +\mu) + \sum_{i=0}^{N-1} \binom{N}{i} \tau^{N-i} I_i(0, +\mu) . \tag{7}$$

By making a simple translation of the origin of the co-ordinate system, it is easily shown that

$$\mathfrak{I}_N(\tau, +\mu) = I_N^*(0, +\mu) . \tag{8}$$

Substitution of equation (8) into equation (4) gives

$$I_N(0, +\mu) = N\mu I_{N-1}(0, +\mu) + \varpi_0 J(0) H(\mu) . \tag{9}$$

The quantity $J(0)$ may be evaluated by integrating this equation and solving for $J(0)$:

$$J(0) = \frac{N}{2 - \varpi_0 \alpha_0} \int_0^1 I_{N-1}(0, +\mu)\, \mu d\mu , \tag{10}$$

where α_0 is the zero moment of the H-function.

The emergent intensity $I_N(0, +\mu)$ has thus been simply expressed in terms of the emergent intensity $I_{N-1}(0, +\mu)$ for the preceding case.

III. THE FINITE ATMOSPHERE WITH NONCONSERVATIVE SCATTERING

For a finite layer extending from 0 to τ_1 there are four invariance principles (Horak and Lundquist 1954, eqs. [6]–[9]). Differentiating two of these with respect to τ, using the equation of transfer to eliminate derivatives of I, taking the limit as τ approaches the boundary τ_1, either adding or subtracting the resulting expressions, and, finally, using the definitions of the X- and Y-functions (Chandrasekhar 1950, p. 183) yield the relations:

$$I(\tau_1, -\mu) = -\mu \left\{ \frac{d}{d\tau} [\mathfrak{J}(\tau, -\mu) + \mathfrak{J}(0, +\mu)] \right\}_{\tau=\tau_1} + [\varpi_0 J(\tau_1) + \epsilon(\tau_1)][X(\mu, \tau_1) + Y(\mu, \tau_1)], \tag{11}$$

and

$$I(\tau_1, -\mu) = -\mu \left\{ \frac{d}{d\tau} [\mathfrak{J}(\tau, -\mu) - \mathfrak{J}(0, +\mu)] \right\}_{\tau=\tau_1} + [\varpi_0 J(\tau_1) + \epsilon(\tau_1)][X(\mu, \tau_1) - Y(\mu, \tau_1)]. \tag{12}$$

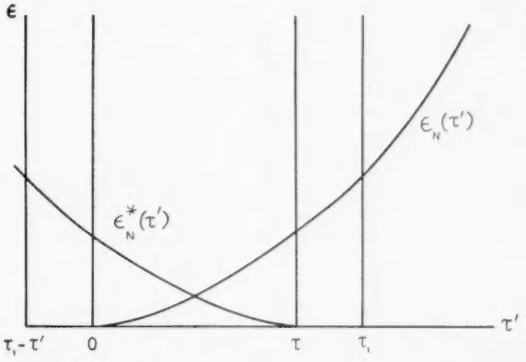

FIG. 2.—The source distributions for the finite atmosphere

In these equations $\mathfrak{J}$ represents the emergent intensity from the layer from 0 to τ if there were no layer from τ to τ_1. If the sum or the difference of the intensities $\mathfrak{J}$ at the two boundaries 0 and τ could be expressed as a known function of τ and μ and if $J(\tau_1)$ could be evaluated, then the above expressions would yield a solution for the emergent intensities. This will indeed be possible. In the layer extending from 0 to τ, the independent variable will be indicated by τ'. In addition to the distribution of sources $\epsilon_N(\tau') = \tau'^N$, it is convenient to introduce an auxiliary distribution $\epsilon_N^*(\tau') = (\tau - \tau')^N$ (Fig. 2). This auxiliary distribution is just the distribution into which $\epsilon_N(\tau')$ is carried under a reflection of the layer from 0 to τ through its middle plane. If $\mathfrak{J}_N(\tau', \mu)$ is the solution of the equation of transfer for the original distribution and $\mathfrak{J}_N^*(\tau', \mu)$ is the solution for the auxiliary distribution, then, by symmetry,

$$\mathfrak{J}_N^*(0, +\mu) = \mathfrak{J}_N(\tau, -\mu). \tag{13}$$

The expression for $\epsilon_N^*(\tau')$ may be expanded by the binomial expansion thus:

$$\epsilon_N^*(\tau') = (-\tau')^N + \sum_{i=0}^{N-1}\binom{N}{i}(-1)^i\tau'^i\tau^{N-i}. \tag{14}$$

From this it follows that

$$\mathfrak{J}_N^*(\tau, -\mu) = (-1)^N\mathfrak{J}(\tau, -\mu) + \sum_{i=0}^{N-1}\binom{N}{i}(-1)^i\tau^{N-i}\mathfrak{J}_i(\tau', \mu). \tag{15}$$

Evaluating this at the boundary $\tau' = 0$ and using the symmetry given in equation (13) yield

$$\mathfrak{J}_N(\tau, -\mu) - (-1)^N\mathfrak{J}(0, +\mu) = L_N(\tau, \mu), \tag{16}$$

where

$$L_N(\tau, \mu) = \sum_{i=0}^{N-1}\binom{N}{i}(-1)^i\tau^{N-i}\mathfrak{J}_i(0, +\mu). \tag{17}$$

For N even, equation (16) gives the difference of the emergent intensities at the two surfaces of the layer as a combination of the emergent intensities for the cases $\epsilon_M(\tau') = \tau'^N$ $(M < N)$. For N odd it gives the sum of the emergent intensities as a combination of the cases with smaller exponents. These are just the expressions needed to substitute into equation (11) or (12). The useful forms of equations (11) and (12) may be combined into the single equation

$$I_N(\tau_1, -\mu) = -\mu\left[\frac{d}{d\tau}L_N(\tau, \mu)\right]_{\tau=\tau_1} + [\varpi_0 J_N(\tau_1) + \tau_1^N][X(\mu, \tau_1) - (-1)^N Y(\mu, \tau_1)]. \tag{18}$$

The quantity $J_N(\tau_1)$ may be evaluated by integrating equation (18) over the range of μ thus:

$$J_N(\tau_1) = \frac{-\int_0^1\left[\frac{d}{d\tau}L_N(\tau, \mu)\right]_{\tau=\tau_1}\mu d\mu + \tau_1^N[\alpha_0 - (-1)^N\beta_0]}{2 - \varpi_0[\alpha_0 - (-1)^N\beta_0]}, \tag{19}$$

where α_0 and β_0 are the zero moments of the X- and Y-functions, respectively.

Equations (18) and (19) give $I_N(\tau_1, -\mu)$ as a function of $L_N(\tau, \mu)$. Since $L_N(\tau, \mu)$ is a combination of the emergent intensities for distributions of sources τ^M $(M < N)$, the emergent intensity $I_N(\tau_1, -\mu)$ depends on all the preceding cases. The other emergent intensity may be obtained by using equations (18) and (16).

IV. THE FINITE ATMOSPHERE WITH CONSERVATIVE SCATTERING

For conservative scattering, $\varpi_0 = 1$, the formalism of the preceding section remains valid, but the procedure used to evaluate $J_N(\tau_1)$ no longer works in general. It is necessary to consider the quantities $F(\tau)$ and $K(\tau)$ (Chandrasekhar 1950, pp. 10, 13). These can be shown to satisfy the relations

$$F_N(\tau) - F_N(0) = -\frac{4}{N+1}\tau^{N+1} \tag{20}$$

and

$$K_N(\tau_1) - K_N(0) = \tfrac{1}{4}F_N(0)\,\tau_1 - \frac{1}{(N+1)(N+2)}\tau_1^{N+2}. \tag{21}$$

On the other hand, $F_N(0)$, $K_N(0)$, and $K_N(\tau_1)$ may also be obtained by multiplying the expressions for the emergent intensities by $2\mu d\mu$ for F or $\frac{1}{2}\mu^2 d\mu$ for K and integrating over the range of μ. The three equations so obtained, together with equations (20) and (21), constitute a set of equations which may be solved for $J_N(\tau_1)$. The final expression resulting from these equations is

$$\begin{aligned} J_N(\tau_1) &= \{(-1)^N \tau_1 [\alpha_1 - (-1)^N \beta_1] - [1 - (-1)^N][\alpha_2 - (-1)^N \beta_2]\} \\ &= -[1 - (-1)^N] \int_0^1 \left[\frac{d}{d\tau} L_N(\tau, \mu)\right]_{\tau=\tau_1} \mu^3 d\mu \\ &+ \tau_1 (-1)^N \int_0^1 \left[\frac{d}{d\tau} L_N(\tau, \mu)\right]_{\tau=\tau_1} \mu^2 d\mu + (-1)^N \int_0^1 L_N(\tau_1, \mu)\, \mu^2 d\mu \\ &+ \tau_1 (-1)^N \int_0^1 L_N(\tau_1, \mu)\, \mu d\mu + \tau_1^N [1 - (-1)^N][\alpha_2 - (-1)^N \beta_2] \\ &- \tau_1^{N+1} (-1)^N [\alpha_1 - (-1)^N \beta_1] + \frac{2}{(N+2)(N+1)} \tau_1^{N+2}. \end{aligned} \tag{22}$$

If it is desired to express the solutions of the conservative case in terms of the standard solutions, the expressions relating the X- and Y-functions of the preceding discussion to the standard solutions are (Chandrasekhar 1950, pp. 190 ff.)

$$\begin{aligned} X(\mu) &= X^s(\mu) + Q[X^s(\mu) + Y^s(\mu)], \\ Y(\mu) &= Y^s(\mu) - Q[X^s(\mu) + Y^s(\mu)], \end{aligned} \tag{23}$$

where

$$Q = \frac{-(\alpha_1^s - \beta_1^s)}{(\alpha_1^s + \beta_1^s) + 2(\alpha_2^s + \beta_2^s)}. \tag{24}$$

V. THE QUADRATIC SOURCE DISTRIBUTION

As an example, the quadratic distribution case will be worked out in detail. For a semi-infinite atmosphere, from equation (9) it follows that

$$I_2(0, +\mu) = 2\mu I_1(0, +\mu) + \varpi_0 J_2(0) H(\mu). \tag{25}$$

The solution for the linear case is known to be (Horak and Lundquist 1954)

$$I_1(0, +\mu) = \left[\frac{1}{(1-\varpi_0)^{1/2}} \mu + \frac{\varpi_0 \alpha_1}{2(1-\varpi_0)}\right] H(\mu). \tag{26}$$

Using this in equation (25) gives

$$I_2(0, +\mu) = \left[\frac{2\mu^2}{(1-\varpi_0)^{1/2}} + \frac{\varpi_0 \alpha_1 \mu}{1-\varpi_0} + \frac{\varpi_0 \alpha_2}{1-\varpi_0} + \frac{\varpi_0^2 \alpha_1^2}{2(1-\varpi_0)^{3/2}}\right] H(\mu). \tag{27}$$

For the finite atmosphere with nonconservative scattering, the function $L_2(\tau, \mu)$ must be computed from the relation

$$L_2(\tau, \mu) = \tau^2 \mathfrak{J}_0(0, +\mu) - 2\tau \mathfrak{J}(0, +\mu). \tag{28}$$

Using the known solutions for the uniform (Horak 1952) and linear (Horak and Lundquist 1954) cases, this becomes

$$L_2(\tau, \mu) = \frac{2\tau^2}{2-\varpi_0(a_0-\beta_0)}[X(\mu, \tau) + Y(\mu, \tau)] - \frac{4\varpi_0\tau(a_1-\beta_1-\beta_0\tau)}{[2-\varpi_0(a_0-\beta_0)][2-\varpi_0(a_0+\beta_0)]}[X(\mu, \tau) + Y(\mu, \tau)] - \frac{4\tau\mu}{2-\varpi_0(a_0-\beta_0)}[X(\mu, \tau) - Y(\mu, \tau)]. \quad (29)$$

The desired derivative of L_2 is

$$\frac{dL_2(\tau, \mu)}{d\tau} = \frac{1}{\mu}\left\{\frac{4\tau\mu^2}{2-\varpi_0(a_0-\beta_0)}X - \frac{2\tau^2}{2-\varpi_0(a_0-\beta_0)}Y - \frac{4\mu^2}{2-\varpi_0(a_0-\beta_0)}(X-Y) - \frac{4\varpi_0\mu(a_1-\beta_1-\beta_0\tau)}{[2-\varpi_0(a_0-\beta_0)][2-\varpi_0(a_0+\beta_0)]}(X+Y) + \frac{4\varpi_0\tau(a_1-\beta_1-\beta_0\tau)}{[2-\varpi_0(a_0-\beta_0)][2-\varpi_0(a_0+\beta_0)]}Y\right\}. \quad (30)$$

Substituting this into equation (18) gives

$$I_2(\tau_1, -\mu) = \frac{2\tau_1^2}{2-\varpi_0(a_0-\beta_0)}X - \frac{\varpi_0\tau_1^2(a_0-\beta_0)}{2-\varpi_0(a_0-\beta_0)}(X-Y) - \frac{4\tau_1\mu}{2-\varpi_0(a_0-\beta_0)} - \frac{4\varpi_0\tau_1(a_1-\beta_1-\beta_0\tau_1)}{[2-\varpi_0(a_0-\beta_0)][2-\varpi_0(a_0+\beta_0)]}Y + \frac{4\varpi_0\mu(a_1-\beta_1-\beta_0\tau_1)}{[2-\varpi_0(a_0-\beta_0)][2-\varpi_0(a_0+\beta_0)]}(X+Y) + \frac{4\mu^2}{2-\varpi_0(a_0-\beta_0)}(X-Y) + \varpi_0 J_2(\tau_1)(X-Y). \quad (31)$$

From equation (19) it follows that

$$J_2(\tau_1) = \frac{2\tau_1^2 a_0}{[2-\varpi_0(a_0-\beta_0)]^2} - \frac{\tau_1^2(a_0-\beta_0)^2}{[2-\varpi_0(a_0-\beta_0)]^2} + \frac{4(a_2-\beta_2-\tau_1 a_1)}{[2-\varpi_0(a_0-\beta_0)]^2} + \frac{4(a_1-\beta_1-\beta_0\tau_1)(a_1+\beta_1-\beta_0\tau_1)}{[2-\varpi_0(a_0-\beta_0)]^2[2-\varpi_0(a_0+\beta_0)]}. \quad (32)$$

The analytical expressions for the emergent intensities have been evaluated for a layer of thickness $\tau_1 = 0.20$ and for $\varpi_0 = 0.90$. These values are given in Table 1. Figure 3 shows this same information plotted in polar co-ordinates.

VI. THE FINITE APPROXIMATION METHOD

The equation of transfer can be solved in the nth approximation by Chandrasekhar's method. The integral $J(\tau)$ is replaced by a sum, using the Gaussian quadrature formula, and the equation of transfer, equation (1), is replaced by a simultaneous system of ordinary differential equations thus:

$$\mu_i\frac{dI(\tau, \mu_i)}{d\tau} = I(\tau, \mu_i) - \frac{\varpi_0}{2}\sum_j a_j I(\tau, \mu_j) - \epsilon(\tau) \qquad (i, j = \pm 1, \ldots, \pm n), \quad (33)$$

where a_i and μ_i are, respectively, the Gaussian weights and divisions. The solution of the homogeneous part is known to be (Chandrasekhar 1950, p. 195, eq. [73])

$$I(\tau, \mu_i) = \sum_{a=-n}^{+n} \frac{L_a e^{-k_a \tau}}{1 + \mu_i k_a} \qquad (i = \pm 1, \ldots, \pm n), \quad (34)$$

where the L_a's are integration constants and the k_a's are the roots of the characteristic equation

$$1 = \varpi_0 \sum_{j=1}^{n} \frac{a_j}{1 - \mu_j^2 k^2}. \quad (35)$$

TABLE 1

THE EMERGENT RADIATION FIELD, $\tau_2 = 0.20$, $\varpi_0 = 0.90$

μ	$I_2(0, +\mu)$	$I_2(\tau_1, -\mu)$	μ	$I_2(0, +\mu)$	$I_2(\tau_1, -\mu)$
0.00	0.0031	0.0448	0.40	0.0069	0.0081
.02	.0041	.0381	0.50	.0061	.0068
.05	.0076	.0300	0.60	.0056	.0061
.10	.0102	.0216	0.70	.0053	.0056
.15	.0101	.0168	0.80	.0051	.0052
.20	.0094	.0137	0.90	.0051	.0051
0.30	0.0080	0.0101	1.00	0.0050	0.0050

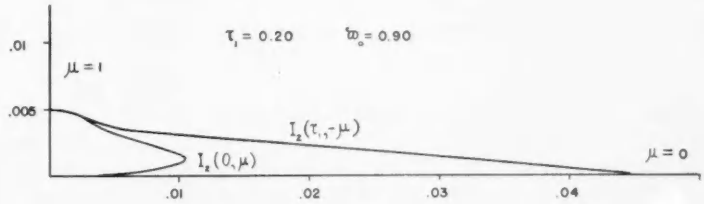

FIG. 3.—Emergent intensities for a layer of optical thickness $\tau_1 = 0.20$, with $\varpi_0 = 0.90$ and with a quadratic distribution of sources.

The particular integral depends on the form of ϵ, which is, by initial assumption, a polynomial of degree N in τ. It can be shown that the particular integral for a source distribution τ^N is expressed by the series

$$\frac{1}{1 - \varpi_0} \sum_{r=0}^{N} \frac{N!}{(N - r)!} \tau^{N-r} \mu^r \qquad (\varpi_0 < 1), \quad (36)$$

$$\frac{-3}{(N+2)(N+1)} \sum_{r=0}^{N+2} \frac{(N+2)!}{(N+2-r)!} \tau^{N+2-r} \mu^r \qquad (\varpi_0 = 1), \quad (37)$$

together with the particular integrals for the following source distributions of lower degree in τ:

$$\frac{\varpi_0}{1-\varpi_0}\sum_{n=1}^{\substack{N/2\,(N\text{ even})\\(N-1)/2\,(N\text{ odd})}}\frac{N!}{(N-2n)!\,(2n+1)}\,\tau^{N-2n} \qquad (\varpi_0<1)\,, \tag{38}$$

$$-3\sum_{n=1}^{\substack{N/2\,(N\text{ even})\\(N-1)/2\,(N\text{ odd})}}\frac{N!}{(N-2n)!\,(2n+3)}\,\tau^{N-2n} \qquad (\varpi_0=1)\,. \tag{39}$$

Thus the particular integral for any value of N can always be readily computed. The first four integrals are given in Table 2.

TABLE 2

PARTICULAR INTEGRALS

N	$\varpi_0<1$
0....	$\dfrac{1}{1-\varpi_0}$
1....	$\dfrac{1}{1-\varpi_0}(\tau+\mu)$
2....	$\dfrac{1}{1-\varpi_0}\left[\tau^2+2\tau\mu+2\mu^2+\dfrac{\varpi_0}{1-\varpi_0}\left(\dfrac{2}{3}\right)\right]$
3....	$\dfrac{1}{1-\varpi_0}\left[\tau^3+3\tau^2\mu+6\tau\mu^2+6\mu^3+\dfrac{2\varpi_0}{1-\varpi_0}(\tau+\mu)\right]$
	$\varpi_0=1$
0....	$-\frac{3}{2}\tau^2-3\tau\mu-3\mu^2$
1....	$-\frac{1}{2}\tau^3-\frac{3}{2}\tau^2\mu-3\tau\mu^2-3\mu^3$
2....	$-\frac{1}{4}\tau^4-\tau^3\mu-3\tau^2\mu^2-6\tau\mu^3-6\mu^3-\frac{2}{3}(\frac{3}{2}\tau-3\tau\mu-3\mu^2)$
3....	$-\frac{3}{20}\tau^5-\frac{3}{4}\tau^4\mu-3\tau^3\mu^2-9\tau^2\mu^3-18\tau\mu^4-18\mu^5$ $-\frac{18}{5}(-\frac{1}{2}\tau^3-\frac{3}{2}\tau^2\mu-3\tau\mu^2-3\mu^3)$

The remainder of the solution can then be carried out, as has been indicated in previous papers, by defining a function $T(\tau, \mu)$ and then using the formal solution of the equation of transfer.

REFERENCES

Chandrasekhar, S. 1950, *Radiative Transfer* (Oxford: Clarendon Press).
Horak, H. G. 1952, *Ap. J.*, **116**, 477.
Horak, H. G., and Lundquist, C. A. 1954, *Ap. J.*, **119**, 42.

THE TRANSFER OF RADIATION BY AN EMITTING ATMOSPHERE. V

CHARLES A. LUNDQUIST
Ordnance Research Laboratory, Pennsylvania State University
Received August 31, 1954

ABSTRACT

Finite and semi-infinite plane-parallel atmospheres with source functions for emission sources of the form $\epsilon(\mu) = \mu^n$ and $\epsilon(\tau, \mu) = \mu^n \tau^m$, with m and n being positive integers, are considered for isotropic scattering. The emergent intensities are found for the case of the first source function, and a similar method is indicated for the second case.

I. INTRODUCTION

The problem of determining the specific intensity of the emergent radiation from an atmosphere or layer of material whose absorption and scattering properties for radiation of a fixed frequency or energy are characterized by a phase function, $p(\cos\theta)$, where θ is the angle between the incident and scattered radiation, has been solved by Chandrasekhar (1950) for the case of incident radiation on the bounding plane of a semi-infinite layer or a layer of finite thickness. If τ is the optical depth into the layer, normal to the bounding plane, $\tau = 0$; if μ is the cosine of the angle between an arbitrary direction and the outward normal to the bounding plane, $\tau = 0$; and if the phase function is a constant, ϖ_0, then the equation of transfer for this situation is

$$\frac{dI(\tau, \mu)}{d\tau} = I(\tau, \mu) - \varpi_0 J(\tau) , \tag{1}$$

where

$$J(\tau) = \frac{1}{2}\int_{-1}^{1} I(\tau, \mu)\, d\mu . \tag{2}$$

If $I(\tau, +\mu)$ and $I(\tau, -\mu)$ represent the intensity at the level τ within the layer in the direction ranges $\mu = 0$ to $+1$ and $\mu = -1$ to 0, respectively, then the appropriate boundary conditions are given when $I(0, -\mu)$ for the semi-infinite layer or $I(0, -\mu)$ and $I(\tau_1, +\mu)$ for a finite layer of optical thickness τ_1 are known. The quantities $I(0, +\mu)$ and $I(\tau_1, -\mu)$ were obtained by Chandrasekhar in terms of $H(\mu)$ function for a semi-infinite layer and $X(\mu)$ and $Y(\mu)$ functions for a finite layer through the use of sets of "invariance principles."

Horak (1952) considered the case where there is no incident radiation on the layer but, instead, a uniform distribution of sources of radiation within the layer. The equation of transfer for this situation is obtained by subtracting from the right side of equation (1) a constant term, ϵ_0, representing the uniform distribution of sources. By formulating invariance principles for this situation, Horak obtained the quantities $I(0, +\mu)$ in terms of $H(\mu)$ functions for a semi-infinite layer and $I(0, +\mu)$ and $I(\tau_1, -\mu)$ in terms of $X(\mu)$ and $Y(\mu)$ functions for a finite layer.

The cases with a linear source function $\epsilon(\tau) = \epsilon_1\tau$ subtracted from the right side of equation (1) (Horak and Lundquist 1954), and later with an arbitrary polynomial in τ, were considered by Lundquist and Horak (1955).

This paper will consider the cases with isotropic scattering where source functions of the forms $\epsilon(\mu) = \mu^n$ and $\epsilon(\tau, \mu) = \tau^m\mu^n$, with m and n positive integers, have been sub-

tracted from the right side of equation (1). The solution for a linear combination of terms of these forms is just the corresponding linear combination of the solutions for the individual terms. The generalization of the results of this paper to cases with more involved phase functions can be carried out by applying the methods presented by Horak (1954).

II. FINITE LAYER WITH NONCONSERVATIVE SCATTERING AND $\epsilon(\mu) = \mu^n$

For the finite layer with emission source function $\epsilon(\tau, \mu)$, two of the invariance principles formulated by Horak (1952) are

$$I(\tau, +\mu) = \Im_{\tau_1-\tau}(\tau, +\mu) + \frac{1}{2\mu}\int_0^1 S(\tau_1-\tau; \mu, \mu')\, I(\tau, -\mu')\, d\mu', \tag{3}$$

$$I(\tau_1, -\mu) = \Im_{\tau_1-\tau}(\tau_1, -\mu) + e^{-(\tau_1-\tau)/\mu} I(\tau, -\mu) + \frac{1}{2\mu}\int_0^1 T(\tau_1-\tau; \mu, \mu')\, I(\tau, -\mu')\, d\mu'. \tag{4}$$

The intensity $\Im_{\tau_1-\tau}$ refers to the intensity that would exist if there were no layer from 0 to τ; and S and T are, respectively, scattering and transmission functions.

Proceeding in the usual manner, equations (3) and (4) are differentiated with respect to τ, equation (1) is used to eliminate derivatives of $I(\tau, \mu)$, and the resulting relations are evaluated in the limit as τ approaches 0. These operations yield the equations

$$I(0, +\mu) = \mu\left[\frac{d\Im_{\tau_1-\tau}(\tau, +\mu)}{d\tau}\right]_0 + \epsilon(0, +\mu) + \varpi_0 J(0)\, X(\mu) + \frac{1}{2}\int_0^1 S(\tau_1; \mu, \mu')\,\epsilon(0, -\mu')\frac{d\mu'}{\mu'}, \tag{5}$$

$$0 = \mu\left[\frac{d\Im_{\tau_1-\tau}(\tau_1, -\mu)}{d\tau}\right]_0 + \epsilon(0, -\mu)\, e^{-\tau_1/\mu} + \varpi_0 J(0)\, Y(\mu) + \frac{1}{2}\int_0^1 T(\tau_1; \mu, \mu')\,\epsilon(0, -\mu')\frac{d\mu'}{\mu'}. \tag{6}$$

Equations (5) and (6) may be added or subtracted to obtain the fundamental equations:

$$I(0, +\mu) = \mu\left\{\frac{d}{d\tau}\left[\Im_{\tau_1-\tau}(\tau, +\mu) \pm \Im_{\tau_1-\tau}(\tau_1, -\mu)\right]\right\}_0 + \epsilon(0, +\mu) \pm \epsilon(0, -\mu)\, e^{-\tau_1/\mu} + \varpi_0 J(0)\left[X(\mu) \pm Y(\mu)\right] + \frac{1}{2}\int_0^1 S(\tau_1; \mu, \mu')\,\epsilon(0, -\mu')\frac{d\mu'}{\mu'} \pm \frac{1}{2}\int_0^1 T(\tau_1; \mu, \mu')\,\epsilon(0, -\mu')\frac{d\mu'}{\mu'}. \tag{7}$$

The situation where the emission source function, $\epsilon(\tau, \mu)$, has the form $\epsilon(\mu) = \mu^n$, with n a positive integer, will be divided into two cases according to whether n is even or odd. If n is even, the source function is symmetric about the direction $\mu = 0$. The solution of the equation of transfer must therefore be symmetric about the middle plane of the layer. Thus, for the single layer extending from τ to τ_1,

$$\Im_{\tau_1-\tau}(\tau, +\mu) = \Im_{\tau_1-\tau}(\tau_1, -\mu). \tag{8}$$

If the minus sign is used in equation (7), equation (8) shows that the first term on the right side of equation (7) vanishes for the case being considered.

If n is an odd positive integer, applying to the equation of transfer the transformation which changes the sign of μ and reflects the layer about its midpoint shows that

$$\Im_{\tau_1-\tau}(\tau, +\mu) = -\Im_{\tau_1-\tau}(\tau_1, -\mu). \tag{9}$$

Equation (9) shows that if the plus sign is used in equation (7), then in this special case the first term on the right side of this equation is zero.

Using the minus sign for even n and the plus sign for odd n, equation (7) may be rewritten

$$I(0, +\mu) = \mu^n [1 - e^{-\tau_1/\mu}] + \varpi_0 J(0) [X(\mu) - (-1)^n Y(\mu)] + \frac{(-1)^n}{2} \int_0^1 S(\tau_1; \mu, \mu') \mu'^n \frac{d\mu'}{\mu'} - \frac{1}{2} \int_0^1 T(\tau_1; \mu, \mu') \mu'^n \frac{d\mu'}{\mu'}. \tag{10}$$

The relations (Chandrasekhar 1950, p. 181)

$$S(\tau_1; \mu, \mu') = \frac{\varpi_0 \mu \mu'}{\mu + \mu'} [X(\mu) X(\mu') - Y(\mu) Y(\mu')], \tag{11}$$

$$T(\tau_1; \mu, \mu') = \frac{\varpi_0 \mu \mu'}{\mu - \mu'} [Y(\mu) X(\mu') - X(\mu) Y(\mu')], \tag{12}$$

may be substituted in equation (10). This results in integrals of the form

$$\frac{\varpi_0 \mu}{2} \int_0^1 [X(\mu) X(\mu') - Y(\mu) Y(\mu')] \frac{\mu'^n}{\mu + \mu'} d\mu', \tag{13}$$

$$\frac{\varpi_0 \mu}{2} \int_0^1 [Y(\mu) X(\mu') - X(\mu) Y(\mu')] \frac{\mu'^n}{\mu - \mu'} d\mu'. \tag{14}$$

In the integrals of this form, the following substitution may be made:

$$\frac{\mu'^n}{\mu + \mu'} = \sum_{i=0}^{n-1} (-1)^i \mu^i \mu'^{n-i-1} + (-1)^n \frac{\mu^n}{\mu + \mu'}, \tag{15}$$

$$\frac{\mu'^n}{\mu - \mu'} = -\sum_{i=0}^{n-1} \mu^i \mu'^{n-i-1} + \frac{\mu^n}{\mu - \mu}. \tag{16}$$

Using the definitions of the moments of the X and Y functions and the equations (Chandrasekhar 1950, p. 181),

$$X(\mu) = 1 + \frac{\mu \varpi_0}{2} \int_0^1 [X(\mu) X(\mu') - Y(\mu) Y(\mu')] \frac{d\mu'}{\mu + \mu'}, \tag{17}$$

$$Y(\mu) = e^{-\tau_1/\mu} + \frac{\mu \varpi_0}{2} \int_0^1 [Y(\mu) X(\mu') - X(\mu) Y(\mu')] \frac{d\mu'}{\mu - \mu}, \tag{18}$$

the integrals (13) and (14) can be carried out.

The expression for $I(0, +\mu)$ then becomes

$$I(0, +\mu) = \mu^n [X(\mu) - Y(\mu)] + \varpi_0 J(0) [X(\mu) - (-1)^n Y(\mu)] + \frac{\varpi_0}{2} \sum_{i=0}^{n-1} \mu^{i+1} (-1)^{n+i} [\alpha_{n-i-1} - (-1)^{n+i} \beta_{n-i-1}] [X(\mu) + (-1)^{n+1} Y(\mu)] . \quad (19)$$

Integrating this equation with respect to μ from 0 to 1 and solving for $J(0)$ gives

$$J(0) = \frac{[\alpha_n - \beta_n] + \frac{\varpi_0}{2} \sum_{i=0}^{n-1} (-1)^{n+i} [\alpha_{n-i-1} - (-1)^{n+i} \beta_{n-i-1}] [\alpha_{i+1} + (-1)^{n+i} \beta_{i+1}]}{2 - \varpi_0 [\alpha_0 - (-1)^n \beta_0]} . \quad (20)$$

Substituting equation (20) in equation (19) yields the final expression for $I(0, +\mu)$ for the case of a source function of the form $\epsilon(\mu) = \mu^n$ and nonconservative scattering. For n even, $I(\tau_1, -\mu)$ equals $I(0, +\mu)$; and for n odd, $I(\tau_1, -\mu)$ equals $-I(0, +\mu)$.

III. FINITE LAYER WITH CONSERVATIVE SCATTERING AND $\epsilon(\mu) = \mu^n$

In the case of conservative scattering, $\varpi_0 = 1$, and a layer of finite thickness, equation (19) remains valid. However, the method used to calculate $J(0)$ for the nonconservative case is no longer satisfactory. To find $J(0)$ it is convenient to use the quantities $F(\tau)$ and $K(\tau)$ defined by the following relations (Chandrasekhar 1950, secs. 8 and 10):

$$F(\tau) = 2 \int_{-1}^{1} I(\tau, \mu) \mu d\mu , \quad (21)$$

$$K(\tau) = \frac{1}{2} \int_{-1}^{1} I(\tau, \mu) \mu^2 d\mu . \quad (22)$$

Integrating the equation of transfer over the range of μ gives

$$\frac{dF(\tau)}{d\tau} = -\frac{2}{n+1} [1 + (-1)^n] . \quad (23)$$

Multiplying the equation of transfer by μ and integrating over the range of μ gives

$$\frac{dK(\tau)}{d\mu} = \tfrac{1}{4} F(\tau) - \frac{1}{2(n+2)} [1 - (-1)^n] . \quad (24)$$

If n is even, integrating equation (23) gives

$$F(\tau) - F(0) = -\frac{4}{n+1} \tau , \quad (25)$$

and, in particular, since $F(\tau_1) = -F(0)$,

$$F(0) = \frac{2}{n+1} \tau_1 . \quad (26)$$

If n is odd, equation (23) shows only that F is a constant. Integrating equation (24) for n odd gives

$$K(\tau) - K(0) = \tfrac{1}{4} F\tau - \frac{1}{n+2} \tau . \quad (27)$$

Inasmuch as $K(\tau_1) = -K(0)$, it follows that

$$K(0) = -\tfrac{1}{8}F\tau_1 + \frac{1}{2(n+2)}\tau_1 . \tag{28}$$

Expressions for $F(0)$ and $K(0)$ may also be obtained from equation (19), with ϖ_0 set equal to 1. Multiplying this equation by μ and integrating over the range of μ gives

$$F(0) = 2[\alpha_{n+1} - \beta_{n+1}] + 2J(0)[\alpha_1 - (-1)^n\beta_1] + \sum_{i=0}^{n-1}(-1)^{n+i}[\alpha_{n-i-1} - (-1)^{n+i}\beta_{n-i-1}][\alpha_{i+2} + (-1)^{n+i}\beta_{i+2}] . \tag{29}$$

Similarly, multiplying equation (19) by μ^2 and integrating over the range of μ gives

$$K(0) = \tfrac{1}{2}[\alpha_{n+2} - \beta_{n+2}] + \tfrac{1}{2}J(0)[\alpha_2 - (-1)^n\beta_2] + \frac{1}{4}\sum_{i=0}^{n-1}(-1)^{n+i}[\alpha_{n-i-1} - (-1)^{n+i}\beta_{n-i-1}][\alpha_{i+3} + (-1)^{n+i}\beta_{i+3}] . \tag{30}$$

For n even, equations (26) and (29) may be used to evaluate $J(0)$:

$$J(0) = \frac{\frac{1}{n+1}\tau_1 - [\alpha_{n+1} - \beta_{n+1}] - \frac{1}{2}\sum_{i=0}^{n-1}(-1)^i[\alpha_{n-i-1} - (-1)^i\beta_{n-i-1}][\alpha_{i+2} + (-1)^i\beta_{i+2}]}{\alpha_1 - \beta_1} . \tag{31}$$

For n odd, equations (28), (29), and (30) may be used to evaluate $J(0)$:

$$J(0) = \frac{2/(n+2)\,\tau_1 - \tau_1[\alpha_{n+1} - \beta_{n+1}] - 2[\alpha_{n+2} - \beta_{n+2}]}{\tau_1[\alpha_1 + \beta_1] + 2[\alpha_2 + \beta_2]} + \frac{\sum_{i=0}^{n-i}(-1)^i[\alpha_{n-i-1} + (-1)^i\beta_{n-i-1}][\alpha_{i+3} - (-1)^i\beta_{i+3}]}{\tau_1[\alpha_1 + \beta_1] + 2[\alpha_2 + \beta_2]} + \frac{\tau_1\frac{1}{2}\sum_{i=0}^{n-1}(-1)^i[\alpha_{n-i-1} + (-1)^i\beta_{n-i-1}][\alpha_{i+2} - (-1)^i\beta_{i+2}]}{\tau_1[\alpha_1 + \beta_1] + 2[\alpha_2 + \beta_2]} . \tag{32}$$

The expressions for $I(0, +\mu)$ for the two foregoing cases are obtained when the foregoing values for $J(0)$ are substituted in equation (19), with $\varpi_0 = 1$.

IV. SEMI-INFINITE LAYER WITH $\epsilon(\mu) = \mu^n$

For a semi-infinite layer with an emission source function $\epsilon(\tau, \mu)$, an invariance principle is (Horak 1952, eq. [24])

$$I(\tau, +\mu) = \mathfrak{I}_\tau(\tau, +\mu) + \frac{1}{2\mu}\int_0^1 S(\infty; \mu, \mu')\, I(\tau, -\mu')\, d\mu' , \tag{33}$$

where $\mathfrak{I}_\tau(\tau, +\mu)$ is the emergent intensity for the semi-infinite layer remaining after the layer from 0 to τ has been removed. Differentiating this equation, using the equation

of transfer to eliminate derivatives of I, and taking the limit of the resulting equation as τ approaches 0 gives the equation

$$I(0, +\mu) = \varpi_0 J(0) H(\mu) + \epsilon(0, +\mu) + \mu\left[\frac{d}{d\tau} \Im_\tau(\tau, +\mu)\right]_0 + \frac{1}{2}\int_0^1 S(\infty; \mu, \mu') \epsilon(0, -\mu') \frac{d\mu'}{\mu'}. \tag{34}$$

For an emission source function of the form $\epsilon(\mu) = \mu^n$, with n as an even or odd positive integer, the emergent intensity, $\Im_\tau(\tau, +\mu)$ does not depend upon the location of the bounding surface, and its derivative with respect to τ is zero. Thus

$$I(0, +\mu) = \varpi_0 J(0) H(\mu) + \mu^n + \frac{1}{2}\int_0^1 S(\infty; \mu, \mu') (-\mu')^n \frac{d\mu'}{\mu'}. \tag{35}$$

The scattering function $S(\infty; \mu, \mu')$ may be expressed as (Chandrasekhar 1950, p. 97)

$$S(\infty; \mu, \mu') = \frac{\varpi_0 \mu \mu'}{\mu + \mu'} H(\mu) H(\mu') . \tag{36}$$

Using this and equation (14), equation (35) becomes

$$I(0, +\mu) = \varpi_0 J(0) H(\mu) + \mu^n H(\mu) + \frac{\varpi_0}{2}\left[\sum_{i=0}^{n-1} (-1)^{n+i} \mu^{i+1} a_{n-i-1}\right] H(\mu) . \tag{37}$$

Integrating equation (37) over μ from -1 to 1 and solving for $J(0)$ gives

$$J(0) = \frac{a_n + \frac{1}{2}\varpi_0 \sum_{i=0}^{n-1} (-1)^{n+i} a_{i+1} a_{n-i-1}}{2 - \varpi_0 a_0} . \tag{38}$$

When equation (38) is substituted in equation (37), this completes the solution.

V. LAYERS WITH $\epsilon(\tau, \mu) = \tau^m \mu^n$

The emergent intensities for a semi-infinite or finite layer with an emission source function of the form $\epsilon(\tau, \mu) = \tau^m \mu^n$, with m and n positive integers, may be obtained by combining the methods used by Lundquist and Horak (1955) and in the preceding sections of this paper. For a finite layer of thickness τ_1, equation (7) is still valid. To calculate the term within the braces, it is convenient to define two auxiliary emission source functions, $\epsilon^*(\tau, \mu) = (\tau_1 - \tau)^m \mu^n$ and $\epsilon^+(\tau, \mu) = -(\tau_1 - \tau)^m \mu^n$. The solutions of the equation of transfer for a finite layer from τ to τ_1 with these two emission source functions will be represented by $\Im^*_{\tau_1 - \tau}(\tau', \mu)$ and $\Im^+_{\tau_1 - \tau}(\tau', \mu)$, respectively, where τ' is the independent variable of optical depth.

From the symmetry of the emission source functions, it follows that, for n even,

$$\Im_{\tau_1 - \tau}(\tau', +\mu) = \Im^*_{\tau_1 - \tau}(\tau_1 - \tau', -\mu) , \tag{39}$$

and, for n odd,

$$\Im_{\tau_1 - \tau}(\tau', +\mu) = \Im^+_{\tau_1 - \tau}(\tau_1 - \tau', -\mu) . \tag{40}$$

The auxiliary emission source functions can be expanded as follows:

$$\epsilon^*(\tau', \mu) = -\epsilon^+(\tau', \mu) = \mu^n(-\tau')^m + \mu^n \sum_{i=0}^{m-1} \binom{m}{i} (-1)^i \tau'^i \tau^{m-i}. \quad (41)$$

Using equation (41), $\mathfrak{I}^*_{\tau_1-\tau}$ or $\mathfrak{I}^+_{\tau_1-\tau}$ may be represented as the sum of $\pm \mathfrak{I}_{\tau_1-\tau}$ and a linear combination of solutions for emission source functions of the form $\epsilon(\tau', \mu) = \mu^n \tau'^p$, with $p < m$. By utilizing equations (39) and (40) and the induction process used by Lundquist and Horak (1955), the desired emergent intensities may be found. An argument similar to the foregoing may also be used for a semi-infinite layer.

REFERENCES

Chandrasekhar, S. 1950, *Radiative Transfer* (1st ed.; Oxford: Clarendon Press).
Horak, H. G. 1952, *Ap. J.*, **116**, 477.
———. 1954, *ibid.*, **119**, 640.
Horak, H. G., and Lundquist, C. A. 1954, *Ap. J.*, **119**, 42.
Lundquist, C. A., and Horak, H. G. 1955, *Ap. J.*, **121**, 175.

FORMATION OF ABSORPTION LINES*

JAMES W. WARWICK
Sacramento Peak Station, Harvard College Observatory, Sunspot, New Mexico
Received June 9, 1954; revised July 22, 1954

ABSTRACT

The proposed new equation gives a phenomenological description of the combination of thermal emission and scattering in the formation of an absorption or emission line. A feature of the equation is the dependence of thermal emission on the radiation field. The equation reduces to the standard ones for line formation if one assumes a two-state atom. Finally, we show that the constancy of ϵ in the Milne-Eddington equation implies a definite excitation temperature.

In recent years, noncoherent scattering of light by atoms has assumed an important role. Numerous investigations (see Stibbs 1953 for bibliography) have led to the conclusion that noncoherent scattering produces different line profiles than pure absorption. The conclusion is essentially mathematical rather than physical.

In the hope that it may elucidate physical questions such as the difference between pure absorption and noncoherent scattering, we propose a new transfer equation (13) for the formation of a line under conditions of scattering and thermal emission. As a secondary feature, we exhibit the fact that equation (13) contains all earlier transfer equations, except for interlocking equations (Woolley and Stibbs 1953). However, it is not equivalent to them in general. Also, we investigate briefly one consequence of assuming a constant ϵ in the Milne-Eddington (Milne 1928; Eddington 1929) equation. Finally, we show that the Milne-Eddington description of noncoherent scattering is identical *in form* to pure absorption.

1. Let the absorption coefficient per atom, at frequency ν, be a_ν. It is convenient to introduce the frequency dependence of a_ν, which we call ϕ_ν:

$$\phi_\nu = \frac{a_\nu}{\int a_\nu d\nu}. \tag{1}$$

Let R be that fraction of the light absorbed from (ν', ω'), which is scattered into (ν, ω) per unit frequency interval and per unit solid angle of both incident and scattered light. In isotropic monochromatic scattering,

$$R = \frac{1}{4\pi}\,\delta\,(\nu' - \nu)\,, \tag{2}$$

where $\delta(\nu' - \nu)$ is the Dirac δ-function. For completely noncoherent scattering, the scattering is isotropic, with the frequency dependence (1):

$$R = \frac{1}{4\pi}\,\phi_\nu\,. \tag{3}$$

An atom scatters by first absorbing a photon and then spontaneously emitting another photon in the same line. When the atom has absorbed, however, we can only speak of the probability that the atom in the upper level will spontaneously emit in the line. This

* The work reported herein was accomplished under the sponsorship of the Air Force Cambridge Research Center, Geophysics Research Directorate, through Contract AF 19(604)-146 with Harvard University.

probability will be less than 1 for an atom with many energy levels. Call the probability q. Then

$$q = \frac{\text{Prob. per second of spont. transitions from upper level to lower level}}{\text{Total prob. per second of all types transitions from upper level}} . \quad (4)$$

The Einstein coefficients for absorption and induced emission may be conveniently defined so that the number of (upward or downward) jumps per unit time caused by radiation of intensity I_ν incident on unit volume of gas containing N_1 or N_2 atoms is

$$\frac{1}{\varpi_1} N_1 B \phi_\nu I_\nu \quad \text{or} \quad \frac{1}{\varpi_2} N_2 B \phi_\nu I_\nu . \quad (5)^1$$

The numbers of atoms in the lower and upper levels are N_1 and N_2, respectively. The statistical weights of the levels are ϖ_1 and ϖ_2. The spontaneous emission coefficient is defined so that the total number of spontaneous emissions from the upper level is given by

$$\frac{1}{\varpi_2} N_2 4\pi A . \quad (6)$$

The second part of expressions (5), the induced emissions, is written in a form which assumes that their frequency-dependence is the same as that of the absorptions.

The number of scatterings into (ν, ω) is

$$\frac{1}{\varpi_1} N_1 B \int\int R q \phi_{\nu'} I_{\nu'} d\nu' d\omega' . \quad (7)$$

The total number of scatterings into all frequencies and directions is the integral of (7) over all (ν, ω):

$$\frac{1}{\varpi_1} N_1 B \int\int\int q \phi_{\nu'} I_{\nu'} d\nu' d\omega' . \quad (8)$$

The emission, by assumption, is solely a combination of scattering and thermal emission. Therefore, if there were no scattering, all emission would be thermal. The total thermal emission into ν and ω would then be

$$\frac{1}{\varpi_2} N_2 A \phi_\nu . \quad (9)$$

Redistribute the total number of scatterings, (8), over all line frequencies and directions according to the function $\phi_\nu/4\pi$:

$$\frac{1}{\varpi_1} N_1 B \phi_\nu \int\int q \phi_{\nu'} I_{\nu'} d\nu' \frac{d\omega'}{4\pi} . \quad (10)$$

Formula (10) gives the amount by which the actual thermal emission is less than expression (9) for each frequency and direction. Subtract (10) from (9):

$$\frac{1}{\varpi_2} N_2 A \phi_\nu - \frac{1}{\varpi_1} N_1 B \phi_\nu \int\int q \phi_{\nu'} I_{\nu'} d\nu' \frac{d\omega'}{4\pi} ; \quad (11)$$

expression (11) is the thermal emission for scattering according to the arbitrary R-function.

[1] B is equal to a constant, dependent only on line frequency, times the line strength (Condon and Shortley 1951).

Expression (11) is a function of the radiation field. This fact results directly from our assumptions that (1) scattering contributes to the population N_2; (2) only scattering and thermal emission are present. Those atoms which are in level 2 as the intermediate state in a scattering process cannot, by definition, participate in thermal emission. The remaining atoms in level 2, by definition, produce all the thermal emission. The dependence of expression (11) on the radiation is removed when, for example, the ratio of N_1 and N_2 is fixed by statistical equilibrium (see expression [20], below).

Finally, the number of absorptions at (ν, ω), reduced by the number of induced emissions, is

$$\left(\frac{1}{\varpi_1} N_1 - \frac{1}{\varpi_2} N_2\right) B\phi_\nu I_\nu . \tag{12}$$

If x is the linear height in a plane-parallel atmosphere, the equation of radiative transfer can be written

$$-\frac{\mu}{h\nu}\frac{dI_\nu}{dx} = \left(\frac{1}{\varpi_1} N_1 - \frac{1}{\varpi_2} N_2\right) B\phi_\nu I_\nu - \frac{1}{\varpi_1} N_1 B \int\int R q \phi_{\nu'} I_{\nu'} d\nu' d\omega' - \left[\frac{1}{\varpi_2} N_2 A\phi_\nu - \frac{1}{\varpi_1} N_1 B\phi_\nu \int\int q\phi_{\nu'} I_{\nu'} d\nu' \frac{d\omega'}{4\pi}\right]. \tag{13}$$

As written, equation (13) does not contain the usual terms in the continuous absorption coefficient, but they may be added without loss of generality.

2. For $q = 0$, equation (13) reduces immediately to the pure absorption equation. For the R-function, (3), equation (13) reduces to the same form as the pure absorption equation. The only difference between the two is (possibly) the ratio N_1/N_2 of populations in the two levels. This difference leads to different line profiles. It is the physical basis for the differences between noncoherent scattering and pure absorption.

Equation (13) can be reduced to the form of the Milne-Eddington equation, written for scattering according to an arbitrary R-function. Assume that the atom has only two energy levels. Collisions, as well as radiation, play a role in populating these energy levels. We assume q as defined by equation (4). Let $4\pi c_{12}$ be the probability per second of a collisional transition from level 2 to level 1. The probability per atom per second for an induced transition to level 1 is $B\int\int \phi_{\nu'} I_{\nu'} d\nu' d\omega'$. Therefore,

$$q = \frac{A}{A + B\bar{J} + c_{12}}, \tag{14}$$

where

$$\bar{J} = \int\int \phi_{\nu'} I_{\nu'} d\nu' \frac{d\omega'}{4\pi} . \tag{15}$$

Following Milne (1928), set

$$\frac{1}{\varpi_1} N_1^{(e)} c_{21} = \frac{1}{\varpi_2} N_2^{(e)} c_{12} . \tag{16}$$

Let

$$\frac{\varpi_2 N_1^{(e)}}{\varpi_1 N_2^{(e)}} \equiv \exp\left[\frac{h\nu}{kT}\right], \tag{17}$$

where T is a kinetic temperature, measuring the effects of collisions. And, finally,

$$c_{12} = c_{21}\left[1 + \frac{A}{B}\frac{1}{B(T)}\right], \tag{18}$$

where $B(T)$ is the Planck function for T.

The equation of statistical equilibrium for the populations of the two levels is

$$\frac{1}{\varpi_2} N_2 [A + B\bar{J} + c_{12}) = \frac{1}{\varpi_1} N_1 [B\bar{J} + c_{21}] . \tag{19}$$

Equation (19) allows us to write the thermal emission, expression (11), in the form

$$\frac{A}{(A + B\bar{J} + c_{12})} \frac{1}{\varpi_1} N_1 c_{21} \phi_\nu . \tag{20}$$

Here q, as introduced in expression (4) and specialized in equation (14), has a straightforward physical interpretation. To obtain the Milne-Eddington formalism from equation (13), however, one must introduce, in place of q, a similar parameter, q', defined by

$$q' = \frac{A}{(A + B\bar{J} + c_{12})} \frac{(1/\varpi_1) N_1}{[(1/\varpi_1) N_1 - (1/\varpi_2) N_2]} . \tag{21}$$

If N_2 can be neglected in equation (21), $q = q'$. Equations (18) and (19) allow us to write

$$\frac{1}{\varpi_1} N_1 c_{21} = (1 - q') \left(\frac{1}{\varpi_1} N_1 - \frac{1}{\varpi_2} N_2 \right) BB(T) \frac{(A + B\bar{J} + c_{12})}{A} . \tag{22}$$

The thermal emission, expression (20), then becomes

$$(1 - q') \left(\frac{1}{\varpi_1} N_1 - \frac{1}{\varpi_2} N_2 \right) B \phi_\nu B(T) . \tag{23}$$

Substitute equations (21) and (14) in the scattering term of equation (13). Substitute expression (23) for the thermal term. There results

$$\frac{-\mu}{[(1/\varpi_1) N_1 - (1/\varpi_2) N_2] B \phi_\nu} \frac{dI_\nu}{dx} = I_\nu - q' \iint \left(\frac{R}{\phi_\nu} \right) \phi_{\nu'} I_{\nu'} d\nu' d\omega' - (1 - q') B(T) . \tag{24}$$

Equation (24) is the form of the Milne-Eddington equation.

We conclude with one remark on the assumption of constant ϵ (or $1 - q'$) with depth. This assumption fixes the ratio of atomic populations and its variation in depth. For equations (18), (19), and (21), regarded as simultaneous equations in c_{12}, c_{21}, and N_1/N_2, are determined if q' is given.

REFERENCES

Condon, E. U., and Shortley, G. H. 1951. *The Theory of Atomic Spectra* (Cambridge: At the University Press) (reprint with corrections).
Eddington, A. S. 1929, *M.N.*, **89**, 620.
Milne, E. A. 1928, *M.N.*, **88**, 943.
Stibbs, D. W. N. 1953, *M.N.*, **113**, 493.
Woolley, R. v. d. R., and Stibbs, D. W. N. 1953, *The Outer Layers of a Star* (Oxford: ClarendonPress).

QUANTUM THEORY OF LINE BROADENING BY AN IONIC PLASMA*

H. MARGENAU
Yale University

AND

R. MEYEROTT†
Argonne National Laboratory

Received June 7, 1954; revised August 6, 1954

ABSTRACT

It is shown how Holtsmark's theory is related to first principles of line broadening, and its connection with other so-called "statistical" theories is indicated. The quantum-mechanical derivation is restricted to perturbations by a single ion but retains the terms which correspond to the nonuniformity of the field. Ions and electrons are treated simultaneously, and the shifts caused by the electrons are computed in a simple manner. Unpublished work dealing with line broadening by electrons, not included in this paper, is briefly summarized; it is noted that broadening as well as shifts by electrons amount to only a few per cent of the ion width. While the method employed is applicable to all hydrogen lines, the details are given only for the Lyman-α line.

I. GENERAL CONSIDERATIONS

The broadening of hydrogen lines by an ionized gas is a problem of long standing; available solutions have much plausibility and enjoy an impressive wealth of experimental support. Nevertheless, the theory is far from satisfactory. Its weakness lies primarily at two points, to which the present paper draws attention and which it is intended to clarify.

It is customary to treat the effect of the heavy ions and that of the electrons separately. The heavy ions produce a Stark effect which Holtsmark's theory (1924) describes in satisfactory fashion. That theory, however, is a classical one whose structure is difficult to incorporate into a general theory of line broadening that includes all effects. It is statistical to be sure and has similarities to quantum-statistical theories (Margenau 1932, 1935; Kuhn 1934; Foley 1946), with which it is frequently classified. But this similarity is superficial, for Holtsmark computes the probability of a given *electric field* resulting from all possible ion configurations and assumes it to be proportional to the line intensity at the Stark frequency corresponding to that field, whereas the statistical quantum theories fix attention upon the probability of a given *energy perturbation* $\Delta\epsilon$, a *scalar* quantity, and identify this probability with the intensity of the line at $h\Delta\nu$.

The equivalence of these procedures can be proved fairly simply and is hardly worth a note as long as this. To be sure, it is one of the points we wish to clarify. It will not be developed separately, however; it forms one feature among others that emerge in our general treatment, which develops the Holtsmark theory from first principles.

The second moot point in the treatment of plasma effects on lines is in the role it assigns to the electrons. These are admittedly hard to handle, even separately. Hence they are often ignored on the supposition that they move too fast to cause line broadening. A semicritical analysis of this phase of the problem is contained in an important paper by Inglis and Teller (1939), who state conditions under which electrons cease to

* Work supported by the United States Atomic Energy Commission.

† Present address: RAND Corporation, Santa Monica, California.

broaden a line. Their results lend credibility to the assumption that the electrons may often be ignored. They do not settle the question whether ion broadening and electron broadening may be treated as separate effects. The most careful study to date of the effects by electrons was made by Unsöld (1943).

In this paper we describe the action of ions and electrons initially by a single Hamiltonian. However, in the course of the work, we use results similar to those of Inglis and Teller, albeit in a modified form determined by more rigorous considerations. Since these latter considerations are at present available only in progress reports (Bloom, Kivel, and Margenau 1951, 1953), we summarize here briefly the physical conclusions to which they lead.

Broadening by electron collisions is determined by the product of two factors (defined below), f and S. (The broadening here discussed does not include the effects of quenching. See Bloom, Kivel, and Margenau 1951, 1953.) The line width is roughly equal to $(1 + fS)\gamma$, γ being the natural width arising from radiation damping. When $fS \gg 1$, the electrons make their presence felt largely through a static interaction with the atom and, therefore, cause primarily a shift of the line. While this statement is an oversimplification, it is true for the Lyman lines of hydrogen, the case treated systematically in this paper. Here the width caused by electrons is only a few per cent of the Holtsmark width.

The function f is the ratio of the lifetime of the excited atomic state to the interval between atomic collisions or, equivalently, the number of electron collisions during the life of the upper state:

$$f = \frac{2 n v \sigma}{\gamma},$$

where v = the electron speed, n = the number of electrons per unit volume, and σ is a kind of collision cross-section, defined by

$$\sigma = \pi \left(\frac{\hbar}{m v} \right)^2 .$$

S is a numerical factor which reaches a constant magnitude of order 1 when the speed of the colliding electron approaches that of the atomic electron v_0; for small v it is proportional to $(v/v_0)^2$. Its detailed form and final value depend on the specific interaction between the perturbing electron and the atom (linear Stark effect, polarization), and in the case of Lyman-α (Bloom, Kivel, and Margenau 1951, 1953) the proportionality factor was about $\frac{1}{100}$. The function S is a measure of the dynamic efficiency of an electron collision in broadening the line.

When the broadening effects of interest are much larger than the natural width, the starting point of our theory is the Fourier integral formula (Anderson 1949; Bloom and Margenau 1953)

$$I(\omega) = \text{const} \times \text{Tr} \left\{ \rho \int_{-\infty}^{+\infty} dt \mu^H(t)\, e^{-i\omega t} \int_{-\infty}^{+\infty} dt' \mu^H(t')\, e^{i\omega t'} \right\} . \tag{1}$$

"Tr" means "trace." $I(\omega)$ is the intensity at angular frequency ω; ρ is the statistical matrix of the entire radiating (or absorbing) system, including the electrons; and μ^H is the atomic dipole moment in the Heisenberg representation. This quantity satisfies

$$\mu^H = U^+ \mu U ,$$

where μ is the ordinary, stationary matrix and the matrix U obeys the Schrödinger equation

$$i\hbar \dot{U} = H U . \tag{2}$$

We regard as our radiating system the atom emitting a line, plus the circumambient electrons. If the ions were held fixed, the Hamiltonian H would be independent of the time, and the solution of equation (2) would be

$$U_{LM} = e^{-(i/\hbar)E_L t}\delta_{LM} ,$$

provided that E_L represents the elements of H in a diagonal representation. The ions, however, are not stationary but move slowly, and H is a slowly varying function of t. A satisfactory solution of equation (2) in that case is the adiabatic one,

$$U_{LM} = \exp\left\{-\frac{i}{\hbar}\int_0^t E_L(t')\,dt'\right\}\delta_{LM} . \tag{3}$$

Here the E_L are eigenvalues of the equation

$$H\psi_L(t) = E_L(t)\,\psi_L(t) . \tag{4}$$

With the use of equation (3), μ^H becomes

$$\mu^H_{LM} = \mu_{LM}\exp\left\{\frac{i}{\hbar}\int_0^t [E_L(t') - E_M(t')]\,dt'\right\},$$

and equation (1), with ρ diagonal, assumes the form

$$I(\omega) \propto \sum_{IF}\rho_I |\mu_{IF}|^2 \left|\int_{-\infty}^{+\infty} dt\,\exp\{i[\phi_{IF}(t) - \omega t]\}\right|^2 ,$$

$$\phi_{IF} = \hbar^{-1}\int_0^t [E_I(t') - E_F(t')]\,dt' .$$

By changing one of the variables from t' to $\tau = t' - t$, this result can be written in terms of a correlation function $C(\tau)$:

$$I(\omega) \propto \int_{-\infty}^{+\infty} d\tau\, e^{i\omega\tau}C(\tau) ,$$

where

$$C(\tau) = \sum_{IF}\rho_I\int_{-\infty}^{+\infty} |\omega_{IF}|^2 \exp\{-i[\phi_{IF}(t+\tau) - \phi_{IF}(t)]\}\,dt .$$

At this point we make the transition to the statistical theory of pressure broadening (Margenau 1933). Lyman Spitzer has given a detailed analysis of the ion-broadening problem and has thereby provided specific justification for this procedure in the case to which it is here applied (1939). In accordance with the adiabatic assumption, we take E_I and E_F to vary slowly with t and expand

$$\phi(t+\tau) = \phi(t) + \hbar^{-1}[E_I(t) - E_F(t)]\,\tau + \ldots ,$$

neglecting time derivatives of E. Then, with the abbreviation $\omega_{IF} = \hbar^{-1}(E_I - E_F)$,

$$c(\tau) = \sum_{IF}\rho_I |\mu_{IF}|^2\int_{-\infty}^{+\infty} dt\,\exp\{-i\omega_{IF}(t)\,\tau\} ,$$

and I becomes an integral over a δ-function:

$$I(\omega) \propto \sum_{IF}\rho_I |\mu_{IF}|^2\delta[\omega, \omega_{IF}(t)]\,dt . \tag{5}$$

In our application there will be but one initial state I and one final state F. The result may be interpreted by saying that the intensity at ω is proportional to three factors: the population of the initial state, ρ_I; the strength of the transition $|\omega_{IF}|^2$; and the sum of the time intervals during which $\omega_{IF}(t)$ equals ω.

In the solution of equation (4) E_L is a function of t through the ion configuration $\boldsymbol{R}(t)$, and ω_{IF} is a function of $\boldsymbol{R}$. In view of this circumstance we finally invoke the ergodic hypothesis and claim that the time in which $\omega_{IF}(t) = \omega$ is proportional to that portion of configuration space in which $\omega_{IF}(\boldsymbol{R}) = \omega$, i.e.,

$$\int \delta\,(\omega, \omega_{IF})\, dt \propto \int \delta\,[\omega, \omega_{IF}\,(\boldsymbol{R})\,]\, d\boldsymbol{R}\,.$$

We now turn to the solution of equation (4) and the computation of $\omega_{IF}(\boldsymbol{R})$.

II. HOLTSMARK THEORY OF BROADENING OF HYDROGEN LINES BY IONS AND ELECTRONS

To keep the theory simple and to exhibit throughout the connections with the well-known features of the ordinary Stark effect, we restrict our considerations henceforth to a radiating one-electron atom surrounded by simply charged ions and electrons. The co-ordinate of the atomic electron is $\boldsymbol{r}_0$; the perturbing electrons are situated at $\boldsymbol{r}_i$ and the ions at $\boldsymbol{R}_i$. A treatment of the complete Hamiltonian is needlessly complex for our purposes. When carried through, it yields results which differ from those obtained here in the same respects in which the Holtsmark treatment for many ions differs from its simpler version, namely, the confinement of a single ion in a sphere of volume $n^{-1/3}$. Hence the model employed is this: The atom is placed at the center of a sphere of volume $n^{-1/3}$ containing, besides, one ion and one electron. This model is not wholly without mathematical justification, for it can be arrived at by reducing the full Hamiltonian in the spirit of Hartree's method.

An unperturbed state of this system will have the form $\psi(\boldsymbol{r}_0)\Phi(\boldsymbol{r})$, and we shall usually assume Φ to be a free-electron function corresponding to a sharp energy. In that case μ_{IF}, which is, of course, $[\mu(\boldsymbol{r}_0) + \mu(\boldsymbol{r})]_{IF}$, contains no contribution from the perturbing electron, since a free electron does not radiate; μ is diagonal in the states of the perturber $\Phi(\boldsymbol{r})$, and the subscripts I and F can be replaced by letters $(a, b, \ldots)$ designating the states of the atom. We deal in particular with the ground state ψ_a; the first excited state ψ_b, which has degenerate components ψ_{bi}; and other excited states ψ_c.

To assume that Φ is a free-electron function belonging to a sharp energy simplifies the results in a manner that is not always justified. Such a function smears the electron uniformly over its cell and prejudges the case against the possibility of fluctuations in electron positions, multiple versus single impacts, and the like. Furthermore, it will never allow the electron, because of its ubiquity, to exercise a Stark effect in Holtsmark fashion. Since the electron is often said to be capable of such an effect, attention to this point is in order. (The present qualitative argument will be supplemented elsewhere by a more detailed account which actually constructs the wave packet in accordance with thermodynamic energy fluctuations.)

If the electron is to produce an ordinary Stark effect, i.e., if it is to act as an individual upon the atom, it must be moving sufficiently slowly relative to some characteristic atomic time τ to produce a well-defined perturbation at the atom. This fact is generally recognized and respected. But there is another condition, coming from the fact that $\Phi(\boldsymbol{r})$, to be granular in space, must be a wave packet, and this packet must stay together long enough to allow the electron to act as an individual. Now the time of diffusion of a wave packet has nothing to do with its speed of motion; it is determined solely by its size. If the packet fills a volume of radius s (to be precise, has a half-width s), the speed of diffusion is $\hbar/ms$. The criterion for the capability of an electron to act individually

is clearly that it shall not diffuse out of its cell during the atomic time τ. That is, say, if $s = n^{-1/3}$, $s/(\hbar/ms) > \tau$.

The identification of τ is probably difficult to settle without elaborate calculation. If it is chosen to be the lifetime of the excited atomic state $1/\gamma$, we find $m\gamma/\hbar n^{2/3} > 1$. For example, if $\gamma \approx 10^9$ sec^{-1}, n must be 10^{13} cm^{-3} or less. This choice of γ is qualitatively in accord with the considerations at the beginning of Section I.

If, in reliance on classical theory, we take τ to be the time of revolution in an orbit, we obtain a criterion which is true but trivial. For in that case

$$\frac{m s^2}{\hbar} \gg \frac{\hbar^3}{m e^4},$$

and this leads to $s \gg$ radius of Bohr orbit.

In our work we permit ourselves to ignore the granularity of the electrons. The state function $\psi(r_0)\Phi(r)$ is perturbed by a potential energy having two parts, one arising from the free electron in the cell, the other from the ion:

$$V = V_- + V_+; \qquad V_- = -\frac{e^2}{r} + \frac{e^2}{|r - r_0|}; \qquad V_+ = \frac{e^2}{R} - \frac{e^2}{R - r_0}. \tag{6}$$

The effect of V on the two atomic states connected by radiation will be calculated by ordinary perturbation theory, and it will be seen that the first-order perturbation yields the Holtsmark theory, while the second produces line shifts which correspond physically to a mutual polarization of the atom and the surrounding electron cloud.

For the ground state of the atom, which has spherical symmetry and is nondegenerate, the first-order energy is simply the mean of V with respect to the weighting function $|\psi_a(r_0)^2\Phi(r)|^2$. The part V_- contributes nothing to this average, provided that we exclude the free electron from the interior of the atom and take the cell to be spherical, for then the mean of $1/r$ is the same as that of $1/|r - r_0|$. The error made in this procedure is $2\pi n e^2 r_0^2$. Since it does not depend on R, it will, in any case, not affect the line breadth.

In forming the mean of V_+, the integration over dr introduces the factor 1. To integrate over dr_0, we expand:

$$V_+ = -\sum_{l=1}^{\infty} \frac{e^2 r_0^l}{R^{l+1}} \sum_{m=l}^{l} \frac{(l-m)!}{(l+m)!} P_l^m(\cos\theta_0)\, e^{im\phi_0} P_l^m(\cos\theta)\, e^{-im\phi}. \tag{7}$$

Here again the interior of the atom is taken to be inaccessible to the ion, $R > r_0$; θ_0 and ϕ_0 refer to the atomic electron, θ and ϕ to the ion. Because of the spherical symmetry of $\psi_a(r_0)$, the mean of V_+ is zero. It may also be noticed from equation (7) that states of higher angular momentum have diagonal elements with respect to equation (7) which are proportional to R^{-3}, for every $|\psi_{lm}|^2$ has axial symmetry and therefore receives contributions from V_+ only through the terms in $m = 0$. Hence l must be even, if the integral over $\cos\theta_0$ is to survive, and $l = 2$ is the lowest even value in the sum. The nondiagonal elements between degenerate states of higher angular momentum, however, contribute terms proportional to R^{-2} and are therefore more important. We calculate them for the first excited states, 2s and 2p.

The effect of the free electrons, V_-, can again be ignored because it drops out in the integration over r. If we write i and j for any of the space-degenerate states of 2s and 2p, we find from equation (7):

$$(i|\, V_+ \,|j) = -\sum_{l=1}^{\infty} \frac{e^2}{R^{l+1}} \sum_{m} \frac{(l+m)!}{(l-m)!}\, a_{ij}^{lm} P_l^m(\cos\theta)\, e^{-im\phi}, \tag{8}$$

with

$$a_{ij}^{lm} = \int \psi_i^* (\mathbf{r}_0)\, r_0^l P_l^m (\cos\ \theta_0)\ e^{im\phi_0} \psi_j (\mathbf{r}_0)\, d\mathbf{r}_0 . \tag{9}$$

The coefficients a_{ij}^{lm} are listed in Table 1. We note that they are not Hermitean in i and j; indeed, $a_{ij}^{lm} = a_j^{l-m}$. The letter a denotes the first Bohr radius. From the a coefficients one derives the matrix elements in Table 2 by using equation (8). When the determinantal equation

$$\det \{ (i \mid V_+ \mid j) - E\delta_{ij} \} = 0$$

is solved with these elements, the roots are found to be

$$E = \begin{cases} 2a\rho - a\,(1 + 4\rho^2)^{1/2} , \\ -2a\rho , \\ -2a\rho , \\ 2a\rho + a\,(1 + 4\rho^2)^{1/2} . \end{cases} \tag{10}$$

TABLE 1

COEFFICIENTS a_{ij}^{lm}, AS DEFINED IN EQUATION (9)

i	$j = 2s$	$j = 2p_0$	$j = 2p_{-1}$	$j = 2p_1$
2s	0	$-3a\delta_{l1}\delta_{m0}$	$-(\sqrt{2})3a\delta_{l1}\delta_{m1}$	$(-\sqrt{2})3a\delta_{l1}\delta_{m-1}$
$2p_0$	.....	$12a^2\delta_{l2}\delta_{m0}$	$(\sqrt{2})18a^2\delta_{l2}\delta_{m1}$	$(\sqrt{2})18a^2\delta_{l2}\delta_{m-1}$
$2p_{-1}$	.....	.....	$-6a^2\delta_{l2}\delta_{m0}$	$72a^2\delta_{l2}\delta_{m-2}$
$2p_1$	.....	.....	.....	$-6a^2\delta_{l2}\delta_{m0}$

TABLE 2

MATRIX ELEMENTS OF V_+ BETWEEN DEGENERATE STATES*

i	$j = 2s$	$j = 2p_0$	$j = 2p_{-1}$	$j = 2p_1$
2s	0	$-a\cos\theta$	$(-a/\sqrt{2})\sin\theta\, e^{-i\phi}$	$(-a/\sqrt{2})\sin\theta\, e^{i\phi}$
$2p_0$	.....	$2a\rho(3\cos^2\theta - 1)$	$3(2a)^{1/2}\rho\cos\theta\sin\theta\, e^{-i\phi}$	$3(2a)^{1/2}\rho\cos\theta\sin\theta\, e^{i\phi}$
$2p_{-1}$	.....	.....	$-a\rho(3\cos^2\theta - 1)$	$3a\rho\sin^2\theta\, e^{2i\phi}$
$2p_1$	.....	.....	.....	$-a\rho(3\cos^2\theta - 1)$

* The abbreviations used in Table 2 are $a = 3e^2a/R^2$; $\rho = a/R$.

The linear combinations of degenerate functions which correspond to these energies are

$$\psi = \begin{cases} \dfrac{1}{\sqrt{2}} [1 - 2\rho\,(1 + 4\rho^2)^{1/2} + 4\rho^2]^{-1/2} \{\psi_{2s} + [\,(1 + 4\rho^2)^{1/2} - 2\rho]\,\psi_{2p_0}\} , \\ \psi_{2p_{-1}} , \\ \psi_{2p_1} , \\ \dfrac{1}{\sqrt{2}} [1 + 2\rho\,(1 + 4\rho^2)^{1/2} + 4\rho^2]^{-1/2} \{\psi_{2s} - [\,(1 + 4\rho^2)^{1/2} + 2\rho]\,\psi_{2p_0}\} . \end{cases} \tag{11}$$

In writing these, we have assumed θ to be zero, i.e., the ion to be on the Z-axis.

For large R, ρ may be negligible. In that case, the results of equation (10) reduce to the ordinary Stark effect,

$$E=\left(-\frac{3e^2a}{R^2},\ 0,\ 0,\ \frac{3e^2a}{R^2}\right).$$

The energies are proportional to the field, and we have recovered the starting point of the Holtsmark theory, which, beyond this state, is nothing more than an evaluation of equation (5) with $\omega_{IF}(R)$ given by the three values of $\omega_0 + E/\hbar$, ω_0 being the normal frequency of the line.

The equivalence of the statistical theory, which operates with the probabilities of energies, and the Stark effect theory, which takes averages over electric fields, is thus apparent for the case of single ions. But the situation is perhaps not quite so clear when two ions collaborate in shifting the line, since the fields may cancel, whereas the energies, classically at least, are added. What happens here can be read from equation (11). They show that the atom, when perturbed by an ion, stretches a lobe of charge toward the ion. When two ions are present, they compete in producing this reaction, and, when they are situated on opposite sides of the atom, the atomic charge is spherical. For that reason, then, there is no Stark effect, although the classical (Coulomb) potential energy under these conditions has twice the value produced by a single ion.

III. EFFECT OF NONUNIFORMITY OF THE FIELD

Terms in ρ arise from the nonuniformity of the field at the atom. For sufficiently large R the energies become $-a(1-2\rho)$, $-2a\rho$, $a(1+2\rho)$.

It is easy to calculate the effect of the terms in $a\rho$ upon the wings of the line, where the Holtsmark theory based on single-ion perturbations is valid. For the outer Stark components the perturbed frequency is

$$\omega=\frac{u}{R^2}+\frac{v}{R^3},\qquad u=\pm 3e^2a\ ,\qquad v=6e^2a^2\ . \tag{12}$$

If R' is the radius of the sphere in which the ion moves ($4\pi R'^3/3 = n^{-1}$), the probability of a particular R is, approximately,

$$p\ (R)\ dR=\frac{3R^2}{R'^3}\ dR\ .$$

This can be expressed in terms of ω by equation (12). We assume that $R \gg v/u = b$ and find $R=\sqrt{(u/\omega)}+b/2$. From this,

$$p\ (R)\ dR=\left(\frac{3u}{2R'^3\omega^2}\right)\left[\sqrt{\left(\frac{u}{\omega}\right)}+b\right]\ |\ d\omega\ |\ =I\ (\omega)\ d\omega\ . \tag{13}$$

It is customary to introduce the parameter $\beta=\omega/\omega'$, where ω' is the frequency perturbation corresponding to R' (with neglect of v), $\omega'=u/R'^2$. In terms of it,

$$I\ (\omega)\ d\omega=I\ (\beta)\ d\beta\ ,\qquad I\ (\beta)\ =\frac{3}{2}\left[\beta^{-5/2}+\left(\frac{\omega'}{u}\right)^{1/2}\ b\beta^{-2}\right]$$

or, explicitly,

$$I\ (\beta)\ =\frac{3}{2}\left(\beta^{-5/2}+\frac{2a\beta^{-2}}{R'}\right). \tag{14}$$

The term in $\beta^{-5/2}$ is the ordinary Holtsmark result for a single ion. The correction is not important for the simple case we have considered. At $\beta = 10$, for example, R' would have to be 60 Bohr radii if the second term is to be 10 per cent of the first, and this would correspond to an ion density of 10^{19} cm^{-3}. However, lines arising from higher

levels of the atom will be subject to this correction because of the rapid increase in the atomic radius with principal quantum number.

We see that the central Stark component also suffers a slight shift and broadening. For it, $|\omega| = 6e^2a^2/R^3$, $p(R)dR = (6e^2a^2/R'^3\omega^2)d\omega$. In terms of $\gamma = \omega/\omega'$, ω' being the frequency perturbation for this component corresponding to R', $I(\gamma) = 1/\gamma^2$. An idea of the half-width of this line may be obtained by remembering that $I_{\max} = I(1) = 1$. Hence, the half-width is given by $I(\gamma_{1/2}) = \frac{1}{2}$, and $\gamma_{1/2} = \sqrt{2}$, $\omega_{1/2} = \sqrt{2}\omega' = 2e^2a^2n$. Comparison shows that the ratio of the half-width of the central component to that of the outer components is of the order of a/R'.

It should be observed, in addition, that the central line is not symmetric, for the sign of the two middle roots for E is negative. There will be a shift to the red, which is also of the order of magnitude of a/R'.

IV. SECOND-ORDER EFFECT

Second-order perturbation theory requires the calculation of matrix elements of the form $(a\alpha|V|b\beta)$ or $(b\alpha|V|c\beta)$, Roman letters referring to atomic, Greek letters to electronic, states. At least one of the letters on the right must differ from its partner on the left. If a transition $a \rightarrow b$ or $\alpha \rightarrow \beta$ corresponds to a large energy difference, its effect on our answer is small. This is generally true for the atomic states unless they are degenerates. Thus we neglect all elements of the type $(a\alpha|V|b\beta)$, where a denotes the ground state. But $(a\alpha|V|a\beta) = 0$; hence there is no second-order effect on the lowest state. Physically, this means that an s-state does not polarize the medium around it (in this approximation).

Thus we are left with elements of the form $(i\alpha|V|j\beta)$, in which the letters i, j denote degenerate components of the excited state b. Only V_- contributes to these elements, for V_+ does not depend on r, and the states α, β are orthogonal. Hence

$$(i\alpha \mid V \mid j\beta) = e^2 \sum_{l=1}^{\infty} \sum_{m} \frac{(l-|m|)!}{(l+|m|)!} a_{ij}^{lm} A_{\alpha\beta}^{lm}, \tag{15}$$

$$A_{\alpha\beta}^{lm} = \int \Phi_a^* (\mathbf{r}) \frac{P_l^m (\cos\theta)}{r^{l+1}} e^{im\phi} \Phi_b (\mathbf{r})\, d\mathbf{r}. \tag{16}$$

The most important term in this sum is that with lowest l, since the terms go roughly with $(a/R')^l$, R' being the linear dimension of the average volume per electron. We therefore retain only the contribution of $l = 1$.

As to i and j, we combine the degenerate states in the manner of formulae (12), taking $\rho = 0$. Let $i = 1$ denote the first degenerate combination, $\sqrt{\frac{1}{2}}(\psi_{2s} + \psi_{2p_0})$. One then finds $a_{11}^m = -3a\delta_{l1}\delta_{m0}$, and $(1\alpha|V|1\beta) = e^2 a_{11}^{10} A_{\alpha\beta}^{10}$. Furthermore, the second-order energy in question is

$$\Delta E = e^4 |a_{11}^{10}|^2 \sum_{\beta} \frac{|A_{\alpha\beta}^{10}|^2}{E_\alpha - E_\beta}. \tag{17}$$

At this point it would seem to be necessary to calculate the $A_{\alpha\beta}^{10}$, and this would require detailed knowledge of the functions $\Phi(r)$, which is very difficult to obtain. A physical consideration permits us to circumvent this difficulty.

Formula (17) is the quantum-mechanical expression for the energy of a dipole immersed in a medium of electrons. A fixed and rigid dipole of moment μ directed along the Z-axis gives rise to a potential energy

$$V' = e\mu \frac{p_1 (\cos\theta)}{r^2},$$

so that $(\alpha|V'|\beta) = \mu A^{10}_{\alpha\beta}$. This dipole polarizes the atmosphere of charge around it, producing a polarization energy

$$\Delta E' = -e^2\mu^2 \sum_\beta \frac{|A^{10}_{\alpha\beta}|^2}{E_\alpha - E_\beta}. \tag{18}$$

Thus, if we can calculate $\Delta E'$, we need only replace the dipole moment in the formula for E' by the *transition moment* $ea^{10}_{11} = -3ea$ to get ΔE. But the polarization energy of a dipole in an atmosphere of charge is computable by the method of Debye and Hückel.

Although we have already disposed of the ions (by putting them in fixed places and thereby preventing them from taking part in any polarizing rearrangement), it is more realistic to restore to them their sensitivity to the presence of an atomic dipole and to treat the atmosphere as a neutral one. The uncertainty arising from this procedure, if there be any, does not affect the order of magnitude of our result.

V. POLARIZATION ENERGY OF A DIPOLE IMMERSED IN A PLASMA; DEBYE-HÜCKEL THEORY; LINE SHIFT

Adopting the method of Debye and Hückel, we assume that the density of positive ions at a point, whose electrostatic potential (produced by the dipole) is U, can be represented as $ne^{-eU/kT}$. Likewise, the density of electrons is $ne^{eU/kT}$. Hence the charge density ρ is equal to

$$ne(e^{-eU/kT} - e^{eU/kT}) \doteq \left(-\frac{2ne^2}{kT}\right)U,$$

if the temperature is high enough, which we shall suppose. Poisson's equation

$$\nabla^2 U = -4\pi\rho = \kappa^2 U,$$

where $\kappa^2 = 8\pi ne^2/kT$, has solutions of the form

$$U = \sum_i c_i \frac{e^{-\kappa|\mathbf{r}-\mathbf{r}_i|}}{|\mathbf{r}-\mathbf{r}_i|}.$$

Let the charges $\pm q$ of the polarizing dipole be situated at $\mathbf{r}_+$ and $\mathbf{r}_-$. Since, at these two points, the potentials are $q/|\mathbf{r}-\mathbf{r}_+|$ and $-q/|\mathbf{r}-\mathbf{r}_-|$,

$$U = q\left(\frac{e^{-\kappa|\mathbf{r}-\mathbf{r}_+|}}{|\mathbf{r}-\mathbf{r}_+|} - \frac{e^{-\kappa|\mathbf{r}-\mathbf{r}_-|}}{|\mathbf{r}-\mathbf{r}_-|}\right),$$

and therefore the potential produced by the polarized medium alone is

$$\Delta U = q\left(\frac{e^{-\kappa|\mathbf{r}-\mathbf{r}_+|}-1}{|\mathbf{r}-\mathbf{r}_+|} - \frac{e^{-\kappa|\mathbf{r}-\mathbf{r}_-|}-1}{|\mathbf{r}-\mathbf{r}_-|}\right).$$

The energy of an infinitesimal dipole with charges $\pm dq$ in this potential is

$$dq[\Delta U(\mathbf{r}_+) - \Delta U(\mathbf{r}_-)] = qdq\left(-\kappa - \frac{e^{-\kappa d}-1}{d}\right) - qdq\left(\frac{e^{-\kappa d}-1}{d} + \kappa\right) \quad (d \equiv |\mathbf{r}_+ - \mathbf{r}_-|),$$

$$= \frac{2qdq}{d}(x + e^{-x} - 1) \qquad (x \equiv kd).$$

For small x this is $-qx^2dq/d$; for large x it is $-2qxdq/d$.

The energy of the dipole in its induced potential is obtained by integrating these expressions with respect to q from 0 to q. For large x we find twice the Debye-Hückel result for monopoles; for small x

$$\Delta E = -\frac{q^2 x^2}{2d} = -\frac{\kappa^2 \mu^2}{2d}. \tag{19}$$

Comparison of formulae (17) and (18) shows that

$$E = -\tfrac{1}{2}\kappa^2 \frac{9e^2a^2}{3a}$$

$$= 3a^2\kappa^2 E_H ,$$

where E_H is the ground-state energy of hydrogen.

This shift is in general very small in comparison with the broadening caused by ions and is rarely of interest. We have computed it here only for one of the atomic states; because these states differ only with respect to orientation in space, its value is the same for the others. Numerically the shift is of the same order of magnitude as the broadening by electrons computed elsewhere (Bloom, Kivel, and Margenau 1951, 1953).

REFERENCES

Anderson, P. W. 1949, *Phys. Rev.*, **76**, 647.
Bloom, S., Kivel, B., and Margenau, H. June 1, 1951; April 1, 1953, *Progress Reports, Contract N7 onr-288*, Task Order 2 (to appear in *Phys. Rev.*).
Bloom, S., and Margenau, H. 1953, *Phys. Rev.*, **90**, 791.
Foley, H. M. 1946, *Phys. Rev.*, **69**, 616.
Holtsmark, J. 1924, *Phys. Zs.*, **25**, 73.
Inglis, D., and Teller, E. 1939, *Ap. J.*, **90**, 439.
Kuhn, H. 1934, *Phil. Mag.*, **18**, 987.
Margenau, H. 1932, *Phys. Rev.*, **40**, 387.
———. 1933, *ibid.*, **43**, 129.
———. 1935, *ibid.*, **48**, 755.
Spitzer, L. 1939, *Phys. Rev.*, **55**, 699.
Unsöld, A. 1943, *Verh. d. Astr. Gesellsch. Leipzig*, **78**, 213.

A STATISTICAL ANALYSIS OF SPECTROHELIOGRAMS

JOHN B. ROGERSON, JR.
Princeton University Observatory
Received August 4, 1954

ABSTRACT

The intensity fluctuations appearing on hydrogen and calcium spectroheliograms of the quiet sun have been analyzed to obtain a distribution of the scale lengths of the fluctuations. The Mount Wilson spectroheliograms used were taken in the center of the *Hα* line and the center of the K line. Two sizes of spectroheliogram image were analyzed. The intensity was measured at equidistant points along straight lines across the image. Mean lagged products were then computed from these intensities. The smallness of their probable errors indicates that the amount of data used (5820 points in each wave length) is sufficient to provide statistically stable results.

The Fourier transform of the mean-lagged-product function gave the power spectrum of the intensity variations along straight lines. Assuming the fluctuations to be two-dimensionally isotropic, it is possible to derive a two-dimensional spectrum from the one-dimensional spectrum. The two dimensional spectra thus obtained suggest that for *Hα* the intensity fluctuations have scale lengths principally in the range 5000–30,000 km, while for K the scale lengths are much longer and are largely confined to the range 25,000–70,000 km.

I. INTRODUCTION

Spectroheliograms of the inactive sun (to which this investigation is restricted) show large-scale intensity fluctuations to be present in the solar atmosphere. Furthermore, the intensity pattern on the solar disk changes with time. It will be assumed in this paper that the intensity fluctuations are statistically steady, and on that basis an exploratory attempt is made to provide a quantitative statistical description.

The work is divided into four sections: (1) the measurement of the intensity at a large number of equidistant points lying in straight lines across the spectroheliograms; (2) the calculation of mean lagged products, which essentially measure the degree of correlation existing between the intensities of pairs of points separated by a fixed distance; (3) the calculation from the mean lagged products of the Fourier power spectrum of the intensity variations along a line; and (4) the transformation of the one-dimensional spectrum into a two-dimensional spectrum of the intensity fluctuations over the disk, under the assumption that the intensity fluctuations are two-dimensionally isotropic.

Because of the exploratory nature of this work only two types of spectroheliograms are analyzed: those taken in the center of *Hα* (λ 6563) and those taken in the center (k_{2-3}) of the K line of ionized calcium (λ 3934). Judging from their appearance, these two types apparently picture different layers of the solar atmosphere.

II. OBSERVATIONAL MATERIAL

Large- and small-image spectroheliograms were used to study small- and large-scale intensity fluctuations, respectively. All spectroheliograms were taken at the 60-foot solar tower at Mount Wilson under the conditions listed in the accompanying tabulation. All fourteen plates used here were taken between June 10 and August 5, 1953, be-

Aperture for large images	12	inches
Effective aperture for small *Hα* images	6.9	inches
Effective aperture for small K images	2.8	inches
Diameter of large solar image	$6\frac{2}{3}$	inches
Diameter of small solar image	2	inches
Length of spectroheliograph slits	8	cm

Width of first spectroheliograph slit	0.07 mm
Width of second spectroheliograph slit	0.10 mm
Dispersion for *Hα*	3.4 A/mm
Dispersion for K	1.7 A/mm
Plate scale for large image	1 mm = 8210 km on sun
Plate scale for small image	1 mm = 27,360 km on sun

tween sunrise and 7 A.M. P.S.T. The large K images were taken on Eastman 33 plates; the small K images were taken on Cramer Contrast plates; both the large and the small *Hα* images were taken on Eastman IV-F plates.

The large-image plates were selected from twenty plates taken in each wave length especially for this program. The small-image plates were selected from approximately eighty plates in each wave length taken between May 19 and August 6, 1953, in the regular solar program of the Mount Wilson Observatory. Plates taken before May 19 were not included in the selection, since they were taken with a diffraction grating of poorer quality. The selection criteria were (1) good seeing, (2) freedom from large disturbed regions on the sun, (3) freedom from lines due to dust on the spectroheliograph slits (dust lines), (4) freedom from lines due to irregularities in the spectroheliograph carriage motion (jump lines), (5) freedom from plate blemishes, (6) satisfactory average density, and (7) good optical definition. The reasons for criteria 1, 5, 6, and 7 are self-evident. Criterion 2 follows from the desire to study the relatively quiet sun. The importance of criteria 3 and 4 are amply illustrated by the spectroheliogram on page 362 of *The Sun* (ed. Gerard P. Kuiper [Chicago: University of Chicago Press, 1953]). In this reproduction the vertical lines are jump lines, and the horizontal lines are dust lines. Only one large-image plate was chosen for analysis in each wave length, since in each case the chosen plate was markedly superior to the rest. Of the small-image plates, six in each wave length were selected.

The method used in getting the equidistant intensity measurements was to make a microdensitometer trace across the spectroheliogram, read off the density at equidistant points, and convert these to intensities by a calibration-curve. The choice of tracing direction on the spectroheliogram resolved into either the scanning direction of the spectroheliograph (which is roughly parallel to the solar equator) or the direction perpendicular to it. The difficulties of using the scanning direction are due to jump lines and bad seeing. The difficulties of the perpendicular direction are due to the dust lines and to the fear that the second spectroheliograph slit was not completely perpendicular to the dispersion, so that the two ends of the slit looked at somewhat different parts of the spectrum. In any event the scanning direction was chosen, since the dust-line problem was quite acute. The tracing length on large images was 440,000 km in length on the sun; that on small images was 590,000 km. All traces were chosen as near the center of the disk as possible to minimize foreshortening effects. In the worst case the foreshortening is somewhat less than 10 per cent.

Six parallel traces, separated from each other by at least 6 mm, were made on the large images. This separation makes the traces independent for all intensity fluctuations of scale length less than 49,000 km. For each wave length twelve traces were made on the six selected small-image plates. Some plates had one trace, some had two, and some had three. On the plates with multiple traces the separation was not less than 3 mm, so that the traces were independent for all intensity fluctuations of scale length less than 82,000 km.

The traces were made on the Mount Wilson microdensitometer with a scanning window of dimensions 0.1×0.1 mm on the plate and a linear magnification of 20 from the plate to the trace.

The microdensitometer traces were read at 540 equidistant points for the large images and at 215 equidistant points for the small images. For all traces the distance between

consecutive points was 2 mm, which corresponds to 821 km on the sun for the large images and to 2736 km on the sun for the small images. With twelve short traces and six long traces, the total number of measured points amounts to 5820 in each of the two wave lengths.

Calibration marks were put on the large-image plates, so that these could be readily calibrated. No calibration marks were available, however, for the small-image plates. The small *Hα* images, though, were on the same emulsion type as the large *Hα* images and were developed in a similar manner. It was decided, therefore, to use the large-*Hα*-image calibration for both large and small *Hα* images. Special Cramer Contrast calibration exposures were made for the small-K-image calibration. It is recognized that the small images suffer from insecure calibration, but it is felt that the results of the present analysis do not strongly depend on accurate calibration. The calibration-curves were fitted by interpolation formulae, and the actual computation of intensities from the transparency at each point was performed on IBM computing machines at the James Forrestal Research Center Computing Laboratory in Princeton, New Jersey.

III. MEAN LAGGED PRODUCTS

The mean lagged products computed in this paper are defined by

$$Q_p \equiv \overline{I_i I_{i+p}} = \frac{1}{N-p} \sum_{i=1}^{N-p} I_i I_{i+p}, \tag{1}$$

where I_i is the residual intensity measured at the ith point along the trace, N is the total number of measured points along the trace (either 215 or 540), and p is the lag parameter. From (1) it is seen that Q_p is just $\overline{I_i^2}$ times the correlation coefficient for the intensities of pairs of points which are separated by p points. By "residual intensity" is meant the difference between the measured intensity and the local mean intensity.

In removing the mean value from the intensities, it was found that the mean value was not constant along the trace. The variation of the mean value along the trace can, however, be satisfactorily represented by a second-order polynomial of the form $ai^2 + bi + c$, where i is the position variable along the trace. The parameters a, b, and c were fitted for each trace. The fitting was fairly rough and was accomplished as follows: consecutive means of 30 points were plotted against the midpoint abscissae; a smooth hand-drawn curve was fitted to the plotted points; and the second-order polynomial was fitted to three points of the hand-drawn curve, the beginning, the middle, and the end. The analytical curve was then plotted to check whether the fit was satisfactory. For some traces the parameter c needed a slight adjustment to give a mean residual intensity equal to zero. The residual intensity is then given by

$$I_i = I_i' - ai^2 - bi - c, \tag{2}$$

where I_i' is the full intensity at point i.

The computation of the residual intensities and the mean lagged products for lags of $p = 0, 1, 2, \ldots, 23$ was accomplished by the IBM computing machinery mentioned earlier.

Before combining the mean lagged products from different traces, each mean lagged product was divided by the square of the mean intensity of the trace from which it was computed. This procedure essentially reduces all images to the same effective exposure time, thus making the different traces comparable.

The mean Q_p-values, along with their internal probable errors, are given in Table 1 and plotted in Figure 1. The average is taken over all traces of images of the same size

and spectral line, and the probable error given is $0.6745/\sqrt{N}$ times the root-mean-square deviation of the individual Q_p-values from their mean, where N is the number of traces entering the average. The four plots in Figure 1 show separately the curves for large *Hα* images, small *Hα* images, large K images, and small K images.

The smallness of the probable errors indicates that the Q_p's can be considered a valid statistical description of the intensity fluctuations along a trace in a spectroheliogram. The larger probable errors for the large K images are due almost entirely to one trace, which, though rather discordant, was included, since no valid reason for excluding it was found.

It will be noticed that Q_0 is just the mean-square residual intensity divided by the

TABLE 1

MEAN LAGGED PRODUCTS AND PROBABLE ERRORS

p	Small Images			Large Images		
	Δx (in 10^3Km)	$Q_p \times 10^3$		Δx (in 10^3Km)	$Q_p \times 10^3$	
		Hα	K		*Hα*	K
0	0.0	+74.2±3.5	+1132±88	0.0	+154.3±5.4	+1540±84
1	2.7	+41.8±2.5	+ 895±77	0.8	+120.3±5.2	+1366±85
2	5.5	+11.1±1.5	+ 503±56	1.6	+ 68.7±4.1	+1118±89
3	8.2	+ 0.1±1.3	+ 238±41	2.5	+ 28.9±2.3	+ 875±93
4	10.9	− 1.1±1.5	+ 111±31	3.3	+ 8.0±2.6	+ 685±92
5	13.7	− 0.6±1.4	+ 63±28	4.1	− 0.1±2.6	+ 537±89
6	16.4	− 2.7±1.1	+ 45±28	4.9	− 3.2±2.3	+ 419±86
7	19.2	− 3.6±1.0	+ 21±28	5.7	− 4.7±2.0	+ 316±82
8	21.9	− 3.2±1.1	− 14±30	6.6	− 4.6±1.8	+ 233±77
9	24.6	− 1.2±1.3	− 51±28	7.4	− 5.6±1.9	+ 172±73
10	27.4	− 0.8±1.8	− 72±24	8.2	− 4.9±2.4	+ 138±72
11	30.1	− 0.4±1.8	− 66±24	9.0	− 5.0±2.5	+ 120±70
12	32.8	+ 0.3±1.4	− 45±27	9.9	− 3.4±2.2	+ 108±67
13	35.6	+ 1.2±1.3	− 29±24	10.7	− 0.1±2.3	+ 96±69
14	38.3	+ 1.4±1.2	− 11±20	11.5	+ 2.6±2.8	+ 82±70
15	41.0	+ 2.2±1.3	+ 18±18	12.3	+ 3.3±3.2	+ 68±71
16	43.8	+ 2.2±1.1	+ 34±26	13.1	+ 2.0±3.4	+ 51±70
17	46.5	+ 0.4±1.4	+ 13±34	14.0	0.0±3.7	+ 24±68
18	49.2	− 3.6±1.8	− 37±36	14.8	− 2.4±3.6	− 2±66
19	52.0	− 4.9±1.3	− 79±32	15.6	− 4.4±2.5	− 24±64
20	54.7	− 2.1±0.9	− 94±24	16.4	− 5.0±1.3	− 42±60
21	57.5	− 0.5±1.0	− 87±17	17.2	− 3.6±2.4	− 49±53
22	60.2	+ 0.7±1.4	− 66±16	18.1	− 3.1±3.9	− 70±46
23	62.9	+ 0.9±1.2	− 46±22	18.9	− 2.8±4.2	− 85±37

square of the mean intensity, from which it is found that in the light of *Hα* the root-mean-square intensity variation is about 3 per cent, while for K it is about 12 per cent. These values may be compared with a value of 4 per cent for the photosphere at an effective wave length of approximately 5800 A, found by Richardson and Schwarzschild (1950).

For *Hα* the Q_p-curve falls to zero for lags corresponding to distances of roughly 6000 km, while for K the curve falls to zero at distances of around 16,000 km. For all curves it appears that, having once fallen to zero, they do not in general significantly depart from it, either positively or negatively.

IV. POWER SPECTRUM

The power spectrum, $F(k)$, can be obtained from the mean lagged products by the Fourier transform

$$F(k) = \frac{2}{\pi}\int_0^\infty Q_p \cos kx\, dx\,, \tag{3}$$

where $x = pD$ is the distance along the trace, with $D = 821$ km for the large images and $D = 2736$ km for the small images. Because Q_p is only available in the finite range from

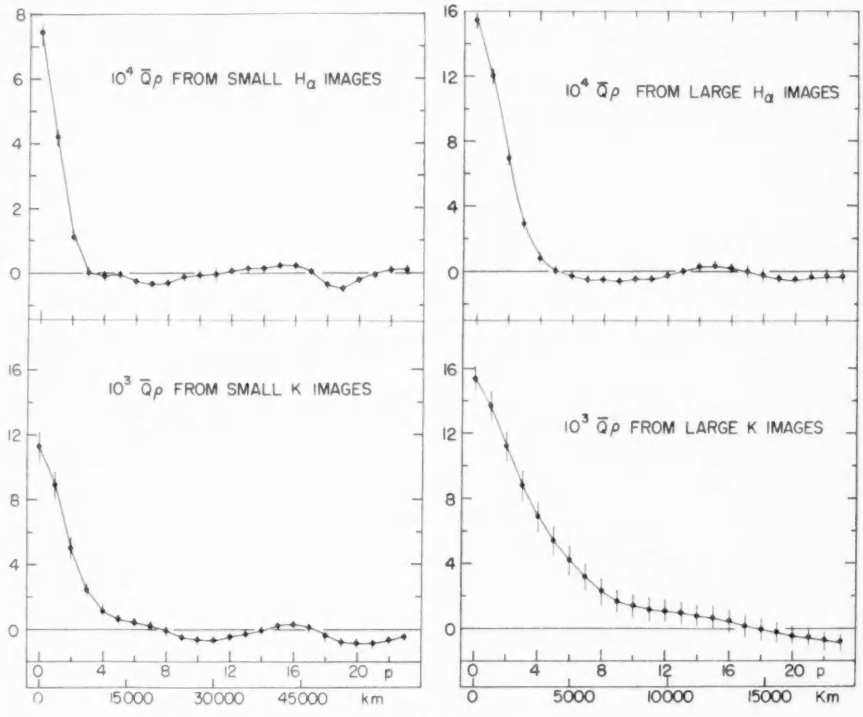
$10^4\ \bar{Q}\rho$ FROM SMALL H_α IMAGES
$10^4\ \bar{Q}\rho$ FROM LARGE H_α IMAGES
$10^3\ \bar{Q}\rho$ FROM SMALL K IMAGES
$10^3\ \bar{Q}\rho$ FROM LARGE K IMAGES
0 4 8 12 16 20 p
0 15000 30000 45000 km
0 5000 10000 15000 Km

FIG. 1.—Mean lagged products with probable errors

0 to M (say), equation (3) assumes the following form:

$$L_h = \frac{2}{M}\sum_{p=0}^{M} \epsilon_p Q_p \cos\frac{\pi hp}{M}, \qquad h = 0, 1, 2, \ldots, M\,, \tag{4}$$

$$\epsilon_p = \begin{cases} \frac{1}{2}\,, & p = 0\,,\ M\,, \\ 1\,, & \text{otherwise}\,. \end{cases}$$

Here the integration has been replaced by a simple sum. Since only $M + 1$ values of Q_p are available, equation (4) is designed to furnish only $M + 1$ values of L_h.

An important consequence of having only $M + 1$ values of Q_p is that equation (4), instead of giving $F(k)$, yields a function L_h, which is given very nearly by

$$L_h = \int_0^\infty F(k) \frac{\sin(MDk - \pi h)}{(MDk - \pi h)} dk . \quad (5)$$

Thus with equation (3) one is looking at the spectrum through a monochromatic filter, whereas with L_h one is looking at the spectrum through a filter having a transmission-curve given by the $(\sin x)/x$ factor. The biggest disadvantage of this filter is that it has significant negative transmission lobes, thus making L_h difficult to interpret. The trouble may be largely overcome by using, instead of L_h, a function U_h, defined as

$$U_h = \tfrac{1}{4}L_{h-1} + \tfrac{1}{2}L_h + \tfrac{1}{4}L_{h-1} . \quad (6)$$

Although the filter associated with U_h has a wider transmission band than that associated with L_h, the negative lobes are much less important. The transmission-curves of the

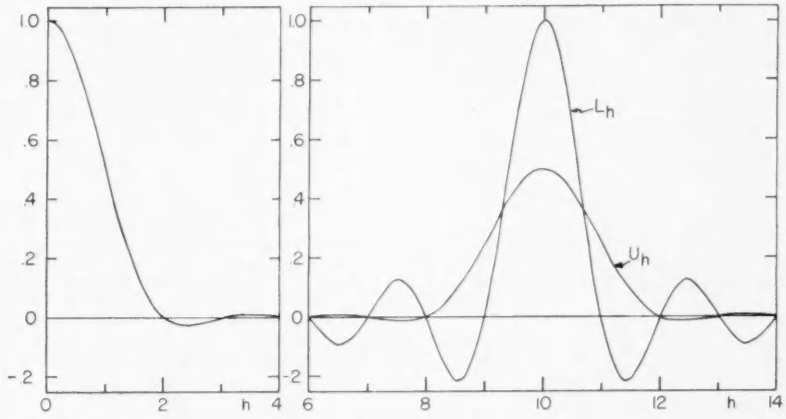

FIG. 2.—Representative transmission-curves for the arithmetical filters U_0 at the left and U_h and L_h at the right.

U_h filters are symmetrical except near $h = 0$. Figure 2 shows the transmission-curve for U_h at $h = 0$ and the L_h and U_h transmission-curves for $h = 10$.

It can be easily shown that, if the factor $\frac{1}{2}[1 + \cos(\pi p/M)]$ is inserted under the summation sign of equation (4), then L_h becomes U_h, and the computation of U_h in this manner is simpler than computation by equation (6). It should be noted that this factor vanishes for $p = M$, so that it is necessary to compute Q_p only up to $p = M - 1$. The equation finally used in this investigation is given by

$$U_h = \sum_{p=0}^{24} \epsilon_p Q_p \left(\tfrac{1}{2} + \tfrac{1}{2}\cos\frac{\pi p}{24}\right)\cos\frac{\pi h p}{24}, \qquad h = 0, 1, 2, \ldots, 24 . \quad (7)$$

The U_h-values computed from this equation and averaged over the appropriate traces are given in Table 2, along with their internal probable errors. The computation of these quantities was carried out on the IBM machines mentioned previously.

Equation (7) will analyze the power spectrum of the intensity measures made from the tracing, but this is not exactly what one desires, since the true intensity variations on

the sun will be partly smoothed out by the finite width of the spectroheliograph slits. For example, suppose that the intensity variation on the sun (along the trace path) were sinusoidal and of wave length just equal to the slit-width; then each wave length would be averaged to zero by the slit, and the photographic plate would show no intensity variation. The washing-out effect on longer wave lengths is, of course, less. An attempt has been made to estimate the washing-out effect as a function of k and to apply corrections to the measured spectrum on this basis.

TABLE 2

ONE-DIMENSIONAL SPECTRA AND PROBABLE ERRORS UNCORRECTED BY α

h	SMALL IMAGES				LARGE IMAGES				α
	λ in 10^3 Km	k in 10^{-4} Km^{-1}	$U_h \times 10^5$		λ in 10^3 Km	k in 10^{-4} Km^{-1}	$U_h \times 10^3$		
			$H\alpha$	K			$H\alpha$	K	
0	∞	0.0	73.4±9.4	2286±261.6	∞	0.0	273±16.4	6408±941	1.000
1	131.3	0.5	79.5±6.8	2320±226.8	39.4	1.6	282±13.7	5442±539	1.002
2	65.7	1.0	87.5±6.0	2206±216.4	19.7	3.2	285±14.8	3548±124	1.008
3	43.7	1.4	92.7±5.6	1856±223.5	13.1	4.8	264±17.8	2156± 52	1.020
4	32.8	1.9	86.7±5.4	1355±142.9	9.9	6.4	214±11.1	1297± 50	1.034
5	26.3	2.4	70.9±5.0	1020± 61.1	7.9	8.0	162±10.4	733± 50	1.056
6	21.9	2.9	63.9±5.5	954± 74.0	6.6	9.6	132± 6.4	500± 31	1.078
7	18.8	3.3	56.7±5.4	773± 60.8	5.6	11.2	101± 2.1	383± 12	1.111
8	16.4	3.8	49.5±3.2	565± 65.2	4.9	12.8	69± 2.3	285± 11	1.147
9	14.6	4.3	47.1±3.4	410± 51.3	4.4	14.4	50± 2.1	202± 8	1.190
10	13.1	4.8	40.1±3.1	259± 21.1	3.9	15.9	37± 0.5	132± 6	1.238
11	11.9	5.3	33.0±2.4	195± 16.0	3.6	17.5	26± 1.0	93± 7	1.297
12	10.9	5.7	26.2±1.5	161± 18.8	3.3	19.1	17± 0.4	76± 7	1.362
13	10.1	6.2	18.7±1.0	109± 12.3	3.0	20.7	13± 0.6	60± 3	1.445
14	9.4	6.7	15.5±0.8	77± 7.7	2.8	22.3	10± 0.6	49± 4	1.536
15	8.8	7.2	13.5±0.9	63± 5.2	2.6	23.9	8± 0.4	44± 3	1.636
16	8.2	7.7	11.3±0.7	48± 3.9	2.5	25.5	6± 0.6	38± 2	1.756
17	7.7	8.1	9.8±0.7	35± 3.3	2.3	27.1	6± 0.4	34± 1	1.889
18	7.3	8.6	8.5±0.5	26± 2.6	2.2	28.7	6± 0.4	34± 2	2.048
19	6.9	9.1	8.0±0.5	20± 2.5	2.1	30.3	5± 0.6	31± 1	2.228
20	6.6	9.6	7.5±0.4	16± 2.2	2.0	31.9	4± 0.6	28± 1	2.458
21	6.3	10.0	7.0±0.4	12± 1.6	1.9	33.5	3± 0.6	30± 2	2.684
22	6.0	10.5	6.2±0.3	12± 1.5	1.8	35.1	3± 0.5	31± 2	3.002
23	5.7	11.0	5.0±0.3	11± 1.3	1.7	36.7	4± 0.3	33± 2	3.313
24	5.5	11.5	4.3±0.3	11± 1.5	1.6	38.3	4± 0.5	34± 3	3.755

Let a particular Fourier component of the intensity variation along the tracing line on the spectroheliogram be represented by

$$I(x) = a \cos (kx + \phi) , \tag{8}$$

where x is the position co-ordinate measured along the trace. Let the first and second slits have widths D_1 and D_2, respectively. Let the middle of the first slit be initially at $x = y$. The first slit is in the plane of the telescope image, and the second slit is nearly in the plane of the photographic emulsion. Then the average intensity in the spectral region investigated admitted through the first slit is given by

$$\bar{I}(y) = \frac{1}{D_1} \int_{y-D_1/2}^{y+D_1/2} I(x)\, dx . \tag{9}$$

At the moment when the first slit is at y, a fresh point of the photographic plate is uncovered. The assumption is now made that the mean intensity, $\bar{I}(y)$, after passing through the optics of the spectroheliograph, is spread evenly over the second slit, so that an intensity of $\bar{I}(y)/D_2$ falls on the freshly exposed point. This point will be exposed so long as it falls under the second slit, i.e., the spectroheliograph carriage must move a distance D_2 before the point is covered up again. Thus the total intensity, A, falling on the point will be given by

$$A = \int_0^{D_2} \frac{1}{D_2} \bar{I}(y)\, dy . \tag{10}$$

When equation (10) is carried out, A is given as a function of a, k, D_1, D_2, and ϕ. What is desired, however, is the quantity $\overline{A^2}$, where the averaging is carried out over all possible phases ϕ. When equation (10) is squared and averaged, there results

$$\overline{A^2} = \frac{a^2}{2}\left[\frac{\sin\ (k D_1/2)}{k D_1/2}\right]^2 \left[\frac{\sin\ (k D_2/2)}{k D_2/2}\right]^2 . \tag{11}$$

Since $a^2/2$ is the average power of the true wave, the slit effects are given by the $[(\sin x)/x]^2$ factors. Thus the "true" power is reduced by the two similar factors, and, to retrieve the true power from the measured power, the measured power should be multiplied by the reciprocals of these factors. Hence the slit correcting factor, α, is given by

$$\alpha\,(k) = \left[\frac{k D_1/2}{\sin\ (k D_1/2)}\right]^2 \left[\frac{k D_2/2}{\sin\ (k D_2/2)}\right]^2 . \tag{12}$$

The factor α is tabulated in Table 2.

If U_h is corrected by α and multiplied by $2D/\pi$, where D (different for large and small images) is the length of the spacing interval in kilometers, then there results the power per unit wave-number interval, $F(k)$, with k measured in reciprocal kilometers. $F(k)$, with its internal probable errors, is shown in Figure 3, with the large- and small-image results for each wave length given individually.

From Figure 3 it may be seen that in each spectral line the spectra from large and small images are roughly similar. It must be noted that at very long wave lengths neither the large- nor the small-image spectrum is statistically very trustworthy. However, the small-image spectrum is derived from a total trace length nearly three times as great as that of the large images, which suggests that, at the very long wave lengths, the small-image spectrum is to be preferred. At shorter wave lengths, however, both spectra have good statistical certainty, which increases with decreasing wave length. It may well be that seeing quality accounts for the difference between the large- and small-image spectra at these shorter wave lengths. Bad seeing tends to smear out all wave lengths, but with an efficiency that increases toward shorter wave lengths. Since the large-image spectrum is based on one plate taken with excellent seeing and the small-image spectrum is based on six plates taken under seeing conditions ranging from good to excellent, it may be expected that the large-image spectrum is the more reliable at shorter wave lengths.

The effect of random measuring errors, rounding errors, and computing errors is to add a small and relatively constant amount of power at all wave lengths to the uncorrected spectrum. For small wave lengths, where α is large, the power due to errors, magnified by α, becomes so large that it distorts somewhat the "true" spectrum.

V. TWO-DIMENSIONAL SPECTRA

In Section IV a power spectrum has been obtained for a one-dimensional intensity trace across a spectroheliogram. In reality, the spectroheliogram is an area of fluctuat-

ing intensities and should be described by a two-dimensional Fourier analysis. In the special case where the intensity fluctuations are two-dimensionally isotropic (that is, a trace in any direction would yield the same one-dimensional spectrum), it is possible to compute the two-dimensional spectrum, which is here taken to mean the power per unit wave number as a function of the two-dimensional wave number. A visual inspection of the spectroheliograms suggests that the isotropy requirement is met on the sun, and it will be so assumed in this section.

For this analysis let the wave number of the one-dimensional spectrum already found be denoted by k_x. Let the power per unit area in the wave-number plane be denoted by $W(k, \theta)$ or $W(k_x, k_y)$, where $k^2 = k_x^2 + k_y^2$ and θ is the angle whose tangent is k_y/k_x. What is desired is $F_2(k)$, the power per unit total wave number. Now $F_2(k)$ is given by

$$\begin{aligned} F_2(k) &= \int_0^{2\pi} W(k,\theta)\, k\, d\theta \\ &= 2\pi k W(k,\theta)\,. \end{aligned} \tag{13}$$

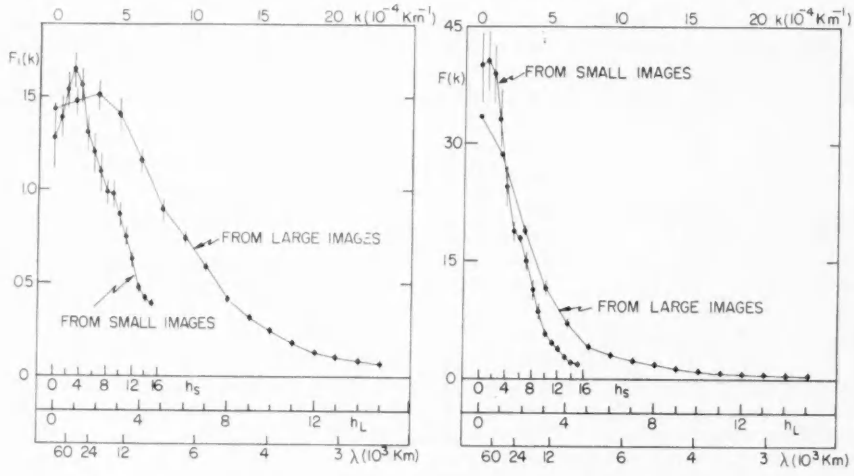

FIG. 3.—One-dimensional spectra with probable errors. Left figure for $H\alpha$ and right figure for K

The last equality holds, since $W(k, \theta)$ is assumed to be independent of θ. Let the one-dimensional spectrum computed in Section IV be denoted by $F_1(k_x)$, which, in terms of the present quantities, is given by

$$\begin{aligned} F_1(k_x) &= 2\int_{-\infty}^{\infty} W(k_x, k_y)\, dk_y = 4\int_{k_x}^{\infty} W(k,\theta)\, \frac{dk}{\sqrt{(k^2 - k_x^2)}} \\ &= \frac{2}{\pi}\int_{k_x}^{\infty} \frac{F_2(k)\, dk}{\sqrt{(k^2 - k_x^2)}}\,. \end{aligned} \tag{14}$$

This is an integral equation of Abel's type, the solution of which is given by

$$F_2(k) = -\frac{d}{dk}\int_k^{\infty} F_1(k_x)\, d\{\sqrt{(k_x^2 - k^2)}\}, \tag{15}$$

which gives $F_2(k)$ explicitly as a function of $F_1(k_x)$.

The computation indicated in equation (15) has been carried out on the four one-dimensional spectra shown in Figure 3. The results of the computation are given in Table 3.

Before discussing these results, it is necessary to take into account the averaging effect of the microdensitometer window. Since this window acts both across and along the tracing direction, it can properly be taken care of only in the two-dimensional, not in the one-dimensional, spectrum. Consider a two-dimensional wave of wave number k. The wave normal may be oriented at any angle with respect to the side of the microdensitometer window. The average power seen through the window at wave number k will be

TABLE 3

TWO-DIMENSIONAL SPECTRA UNCORRECTED BY β

h	SMALL IMAGES				LARGE IMAGES				β
	λ in 10^3 Km	k in 10^{-4} Km^{-1}	$F(k)$		λ in 10^3 Km	k in 10^{-4} Km^{-1}	$F(k)$		
			$H\alpha$	K			$H\alpha$	K	
0	∞	0.0	0.000	0.000	∞	0.0	0.000	0.000	1.000
1	131.3	0.5	−0.054	11.125	39.4	1.6	0.254	19.668	1.002
2	65.7	1.0	+0.216	24.918	19.7	3.2	0.735	20.201	1.005
3	43.7	1.4	+0.838	33.124	13.1	4.8	1.224	15.511	1.013
4	32.8	1.9	+1.287	26.144	9.9	6.4	1.305	11.165	1.024
5	26.3	2.4	+0.946	15.678	7.9	8.0	1.043	5.957	1.037
6	21.9	2.9	+1.000	23.251	6.6	9.6	1.066	3.930	1.053
7	18.8	3.3	+1.029	24.537	5.6	11.2	1.022	3.511	1.072
8	16.4	3.8	+0.831	20.186	4.9	12.8	0.718	3.046	1.096
9	14.6	4.3	+1.235	18.005	4.4	14.4	0.557	2.494	1.125
10	13.1	4.8	+1.244	9.927	3.9	15.9	0.479	1.528	1.153
11	11.9	5.3	+1.205	7.385	3.6	17.5	0.364	0.878	1.192
12	10.9	5.7	+1.155	8.587	3.3	19.1	0.225	0.763	1.236
13	10.1	6.2	+0.644	5.927	3.0	20.7	0.162	0.563	1.277
14	9.4	6.7	+0.512	3.665	2.8	22.3	0.146	0.378	1.334
15	8.8	7.2	+0.531	3.656	2.6	23.9	0.087	0.333	1.387
16	8.2	7.7	+0.425	3.329	2.5	25.5	0.040	0.287	1.458
17	7.7	8.1	+0.390	2.595	2.3	27.1	0.024	0.122	1.533
18	7.3	8.6	+0.286	1.902	2.2	28.7	0.077	0.322	1.614
19	6.9	9.1	+0.336	1.541	2.1	30.3	0.122	0.266	1.709
20	6.6	9.6	+0.444	1.263	2.0	31.9	0.085	0.110	1.825
21	6.3	10.0	+0.601	0.826	1.9	33.5	0.010	0.251	1.933
22	6.0	10.5	+0.831	0.948	1.8	35.1	0.012	0.493	2.081
23	5.7	11.0	+0.834	1.474	1.7	36.7	0.139	1.205	2.233

smaller than the true average power by a factor $g(k)$ (say). It is clear that $g(k)$ depends on the relative orientation of the wave and the window, and therefore $g(k)$ was computed for the two most widely differing orientations, the wave normal parallel to the side and parallel to the diagonal of the window. Since the two resulting $g(k)$ functions at the worst differ by less than 5 per cent, the mean of the two was taken to hold for all orientations. Thus the "true" two-dimensional spectrum is obtained by multiplying the observed two-dimensional spectrum by $\beta(k) \equiv (\bar{g}[k])^{-1}$. The window correction factor, β, is given in Table 3. The two-dimensional spectra, corrected by β, are shown in Figures 4 and 5, where it is seen that the main result of the transformation has been to take energy from the extreme long wave lengths and distribute it throughout the shorter wave lengths.

The *Hα* spectrum shows a broad maximum covering the wave lengths from 5000 to 30,000 km, which corresponds roughly with visual impressions, if the wave lengths are interpreted as distances between near-by intensity maxima. From the present material it cannot be decided whether the fall-off for wave lengths shorter than 5000 km is real or whether it is caused by the washing-out of finer details on the spectroheliograms by seeing.

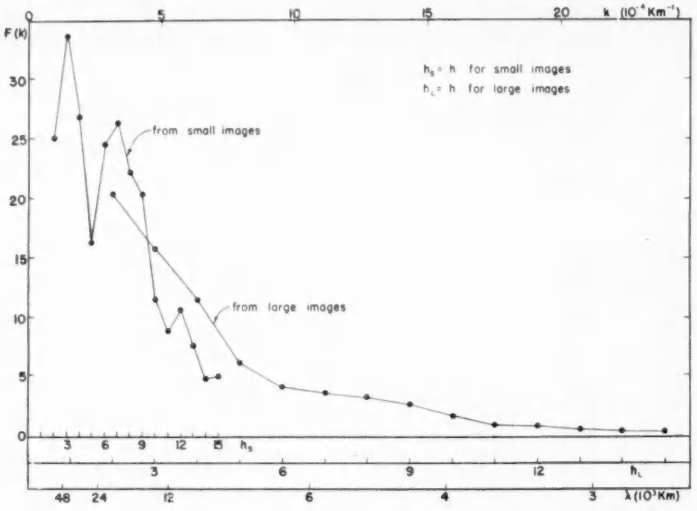

FIG. 4.—Two-dimensional spectra for K spectroheliograms

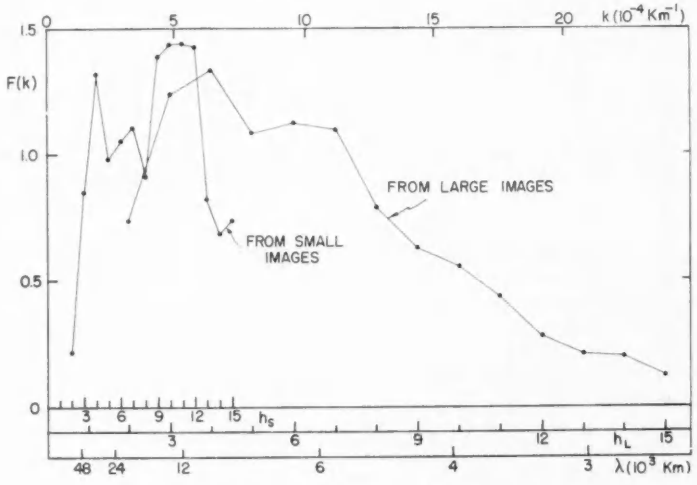

FIG. 5.—Two-dimensional spectra for *Hα* spectroheliograms

The K spectrum shows a good deal of power at wave lengths ranging from 25,000 to 70,000 km, with relatively little elsewhere. This large-scale phenomenon, which clearly corresponds to the well-known calcium flocculi, seems to be virtually absent in the photospheric turbulence spectrum (Frenkiel and Schwarzschild 1954). The flocculi should therefore be rather shallow, in agreement with De Jager's (1953) recent conclusion. To the right of the maximum in the K spectrum, the power fall-off is approximately represented by $F(k) \propto k^{-2.6}$. This fall-off appears likely to be real, since it occurs at wave lengths too large to be much affected by seeing.

The author would like to record his deep gratitude to Dr. Martin Schwarzschild for his continuing stimulation and guidance. Thanks are also due to Dr. Ira S. Bowen, director of the Mount Wilson and Palomar Observatories, for making possible this investigation; to Mr. Joseph Hickox for taking the special spectroheliogram plates; to Dr. J. W. Tukey, of Princeton University, for valuable advice on the method of analysis; and to Mr. Robert Goerss, of the James Forrestal Research Center Computing Laboratory, for his generous aid in the computation.

REFERENCES

Frenkiel, F. W., and Schwarzschild, M. 1954, *Ap. J.*, **121**, 216.
Jager, C. de. 1953, *The Hydrogen Spectrum of the Sun* (doctoral thesis, University of Utrecht [The Hague: Excelsiors Foto-offset]), pp. 70–71.
Richardson, R. S., and Schwarzschild, M. 1950, *Ap. J.*, **111**, 351.

ADDITIONAL DATA FOR TURBULENCE SPECTRUM OF SOLAR PHOTOSPHERE AT LONG WAVE LENGTHS*

F. N. Frenkiel and M. Schwarzschild
Applied Physics Laboratory, Johns Hopkins University,
and Princeton University Observatory
Received August 4, 1954

ABSTRACT

A plate showing the granulation with exceptional definition was selected from the regular Mount Wilson solar program. On this plate 8000 intensity measurements were made. The measurements were analyzed in terms of a turbulence spectrum of photospheric intensities. The spectrum, when corrected for the finite resolution of the photograph, is found to be fairly constant in the wave-length band from 2000 to 30,000 km. This result for the turbulence spectrum of photospheric intensities is similar to the earlier indications found for the turbulence spectrum of velocities, in showing that the spectrum contains much energy in the wave-length band around 15,000 km, but disagrees with them in not showing in the corrected spectrum a large decrease from 15,000 to 4000 km.

I. INTRODUCTION

In a previous paper (Frenkiel and Schwarzschild 1952) the turbulence in the solar photosphere was analyzed on the basis of a small set of velocity measurements. It was found that the photospheric turbulence spectrum of velocities may have a maximum at the long wave length of 15,000 km. This tentative result was recently substantiated by Rush and Stuart (1954). It is the aim of the present paper to determine the form of the photospheric turbulence spectrum of intensity with improved accuracy for all wave lengths that are resolvable on presently available plates. It should be noted that the present analysis is based on intensity, not velocity measurements.

II. OBSERVATIONS AND REDUCTIONS

The measurements were all made on one direct photograph of the sun of exceptionally fine definition, taken from the routine solar program of the Mount Wilson Observatory. The plate had been obtained with the 60-foot solar tower, with the objective diaphragmed down to 4 inches. A Solar Green A plate was used which has fine grain and high contrast and, in combination with an orange filter, gives an effective wave length of approximately 5800 A. The solar image on the plate had a radius of 8.45 cm.

Four straight lines were selected for the measurements on this plate. One pair of lines was oriented north-south and the other pair east-west. The locations of the lines were chosen so as to avoid any spots or faculae. In each pair one line had a normal distance from the disk center of 2.5 cm on the plate, and the other 1.7 cm. Hence the distance between the two lines of a pair was 8 mm on the plate or 66,000 km on the sun. Since this distance exceeds all wave lengths of interest here, one may consider the measurements on the separate lines as statistically independent.

On each of the four lines a segment 10 cm long and centered symmetrical to the center of the disk was used for the measurements. On these segments the points nearest to the limb have a distance from the disk center of 5.59 cm on the plate or 0.661 solar radii. At these points any length on the solar surface is foreshortened in the projection on the

* This investigation was made possible by a stay of one of the authors as guest investigator at the Mount Wilson and Palomar Observatories. This work was supported in part by the U.S. Navy Bureau or Ordnance under Contract NOrd 7386 and in part by funds of the Eugene Higgins Trust allocated to Princeton University.

plate by a factor of, at most, 0.75. Since for all the other points in the segments the foreshortening factor is even nearer to 1, this foreshortening has here been ignored.

The four segments on the plate were registered with the recording microphotometer of the Mount Wilson Observatory, with a magnification of 20. The photometer slit was set to correspond on the plate to a square 0.05 mm on the side, which corresponds on the tracings to 1 mm or on the sun to 410 km. The values of the deflections were read from the tracings every millimeter, which gave two thousand values for each of the four segments. The distance between adjacent readings, being 1 mm on the tracings, corresponded to 410 km on the sun.

The calibration-curve for the plate was derived by correlating the mean deflection as a function of the distance from the disk center with the known intensity variation on the solar disk from center to limb. The calibration-curve was found to be representable in a simple analytical form. With the help of this calibration-curve, all deflections were transformed into intensities.

III. NUMERICAL ANALYSIS

The 200 intensity readings for each of the four segments showed not only the fluctuations caused by the granulation but also smooth changes in the means from one end to the other. The latter changes were caused by the limb darkening of the sun, by unevenness in the vertical tank development, and by deceleration of the shutter in passing over the image during the exposure. To eliminate these changes, moving averages were computed by averaging over 201 successive brightness readings, according to the equation

$$\bar{b}_n = \frac{1}{201} \sum_{i=-100}^{+100} b_{n+i} . \tag{1}$$

The moving averages were then subtracted from the individual intensity readings, and thus corrected intensities were obtained. In this procedure 100 points were lost at each end of each segment, since, to compute the moving averages at a given point, 100 readings on either side are needed. The 1800 corrected intensities of each segment were divided into two sets of 900 values each for convenience in the subsequent mechanical computations. Finally, it was still necessary to normalize the intensities which were originally derived in arbitrary units. This was done by forming the over-all mean, $\bar{b}$, of the 900 uncorrected intensity readings for each set and by dividing the individual corrected intensities by this mean. Thus the corrected and normalized intensities, b'_n, were derived from the original intensity readings, b_n, by the equation

$$b'_n = \frac{b_n - \bar{b}_n}{\bar{b}} . \tag{2}$$

These b'_n values then represent the deviation of the intensity at one point from the mean intensity at the neighboring 201 points in units of the average intensity of the whole set.

The first main step in the analysis was the computation of the covariances $Q(y)$. These covariances can be transformed into an autocorrelation function by normalizing to 1 at $y = 0$. They were computed according to

$$Q(y) = \frac{1}{N-m} \sum_{n=1}^{N-m} b'_n b'_{n+m} , \tag{3}$$

with

$$y = m D , \qquad D = 411 \text{ km} , \qquad N = 900 .$$

The covariances were computed separately for the eight sets and then averaged over the eight sets for each y-value. These averages are given in Table 1, together with probable

errors which were derived for each y-value from the deviations of the individual sets from the average in the usual way.

The second main step of the analysis was the derivation of the one-dimensional spectrum of the intensity fluctuations according to

$$F(k) = \frac{D}{\pi}\left[Q(0) + 2\sum_{m=1}^{M-1} Q(mD)\cos\left(\frac{hm\pi}{M}\right) + Q(MD)\cos(h\pi)\right] \tag{4}$$

with

$$k = \frac{2\pi}{\lambda} = h\frac{\pi}{MD}, \qquad M = 60, \qquad \lambda = \frac{2MD}{h} = \frac{49{,}300}{h}\ \text{km}.$$

Here again the computations were performed separately for the eight sets and were afterward averaged at each wave number over the eight sets. The averages are given in Table 2, together with probable errors derived from the deviations of the individual sets from the averages.

TABLE 1

COVARIANCES (UNNORMALIZED CORRELATION FUNCTION) OF GRANULATION INTENSITIES

m	y (Km)	$10^4 \times Q$	$10^4 \times$p.e.	m	y (Km)	$10^4 \times Q$	$10^4 \times$p.e
0	0	+10.649	0.284	31	12,740	−0.160	0.106
1	410	+ 7.719	.259	32	13,150	− .457	.113
2	820	+ 3.394	.198	33	13,560	− .584	.122
3	1230	+ 0.950	.120	34	13,970	− .480	.130
4	1640	+ 0.223	.060	35	14,380	− .327	.115
5	2060	+ 0.071	.065	36	14,800	− .264	.118
6	2470	− 0.019	.130	37	15,210	− .359	.119
7	2880	− 0.071	.166	38	15,620	− .530	.090
8	3290	− 0.188	.161	39	16,030	− .644	.089
9	3700	− 0.317	.164	40	16,440	− .639	.080
10	4110	− 0.399	.147	41	16,850	− .511	.070
11	4520	− 0.402	.142	42	17,260	− .382	.078
12	4930	− 0.258	.132	43	17,670	− .304	.087
13	5340	− 0.209	.226	44	18,080	− .218	.083
14	5750	− 0.177	.194	45	18,500	− .079	.089
15	6160	− 0.217	.177	46	18,910	+ .030	.105
16	6580	− 0.251	.138	47	19,320	+ .047	.109
17	6990	− 0.222	.113	48	19,730	− .097	.088
18	7400	− 0.219	.147	49	20,140	− .328	.059
19	7810	− 0.377	.188	50	20,550	− .422	.062
20	8220	− 0.529	.196	51	20,960	− .309	.086
21	8630	− 0.544	.186	52	21,370	− .168	.097
22	9040	− 0.437	.187	53	21,780	− .053	.113
23	9450	− 0.347	.170	54	22,190	+ .058	.112
24	9860	− 0.279	.124	55	22,600	+ .034	.102
25	10,280	− 0.195	.099	56	23,020	− .114	.101
26	10,690	− 0.286	.081	57	23,430	− .194	.119
27	11,100	− 0.284	.130	58	23,840	− .076	.140
28	11,510	− 0.160	.127	59	24,250	− .058	.116
29	11,920	+ 0.045	.127	60	24,660	−0.052	0.079
30	12,330	+ 0.074	0.108				

TABLE 2

TURBULENCE SPECTRUM OF GRANULATION INTENSITIES

h	k (Km^{-1})	λ (Km)	$F(k)$	p.e.	$F_s(k)$	p.e.	α
0	0.00000	∞	0.1013	0.0229	0.2709	0.0265	1.000
1	.00013	49,320	.4700	.0439	.4075	.0296	1.002
2	.00025	24,660	.5677	.0420	.5167	.0390	1.009
3	.00038	16,440	.4429	.0586	.4860	.0430	1.021
4	.00051	12,330	.5049	.0283	.4864	.0248	1.036
5	.00064	9860	.4872	.0374	.4656	.0240	1.058
6	.00076	8220	.3757	.0399	.4044	.0310	1.084
7	.00089	7050	.3969	.0363	.4079	.0274	1.116
8	.00102	6160	.4656	.0292	.4287	.0237	1.154
9	.00115	5480	.3738	.0359	.3847	.0245	1.199
10	.00127	4930	.3306	.0290	.3369	.0162	1.251
11	.00140	4480	.3153	.0354	.3031	.0226	1.311
12	.00153	4110	.2473	.0260	.2838	.0190	1.380
13	.00166	3790	.3380	.0240	.2972	.0177	1.459
14	.00178	3520	.2513	.0180	.2678	.0162	1.550
15	.00191	3290	.2371	.0368	.2520	.0245	1.654
16	.00204	3080	.2882	.0218	.2583	.0187	1.773
17	.00217	2900	.2096	.0158	.2246	.0106	1.909
18	.00229	2740	.1955	.0190	.1920	.0162	2.064
19	.00242	2600	.1661	.0187	.1892	.0162	2.242
20	.00255	2470	.2379	.0180	.2018	.0132	2.447
21	.00268	2350	.1515	.0150	.1606	.0102	2.682
22	.00280	2240	.1052	.0067	.1205	.0054	2.952
23	.00293	2140	.1248	.0098	.1186	.0055	3.27
24	.00306	2060	.1166	.0062	.1135	.0037	3.63
25	.00319	1970	.0950	.0105	.0985	.0048	4.05
26	.00331	1900	.0903	.0093	.0891	.0054	4.54
27	.00344	1830	.0809	.0061	.0844	.0052	5.11
28	.00357	1760	.0864	.0086	.0797	.0053	5.78
29	.00369	1700	.0624	.0058	.0644	.0044	6.56
30	.00382	1640	.0467	.0097	.0506	.0036	7.49
31	.00395	1590	.0487	.0079	.0479	.0046	8.58
32	.00408	1540	.0467	.0021	.0479	.0027	9.88
33	.00420	1490	.0491	.0034	.0440	.0020	11.35
34	.00433	1450	.0294	.0023	.0345	.0022	13.27
35	.00446	1400	.0306	.0029	.0275	.0018	15.49
36	.00459	1370	.0177	.0017	.0224	.0007	18.15
37	.00471	1330	.0243	.0012	.0216	.0005	21.37
38	.00484	1300	.0188	.0016	.0196	.0011	25.28
39	.00497	1260	.0165	.0027	.0169	.0015	30.0
40	.00510	1230	.0157	.0015	.0149	.0009	35.8
41	.00522	1200	.0130	.0020	.0137	.0010	42.9
42	.00535	1170	.0141	.0013	.0133	.0010	51.7
43	.00548	1150	.0118	.0015	.0114	.0010	62.5
44	.00561	1120	.0082	.0014	.0090	.0009	76.0
45	.00573	1100	.0079	.0010	.0079	.0005	92.7
46	.00586	1070	.0079	.0011	.0079	.0004	.....
47	.00599	1050	.0086	.0012	.0079	.0006	.....
48	.00612	1030	.0090	.0013	.0079	.0010	.....
49	0.00624	1000	0.0079	0.0023	0.0075	0.0013	.....

TABLE 2—*Continued*

h	k (Km^{-1})	λ (Km)	$F(k)$	p.e.	$F_s(k)$	p.e.	α
50	0.00637	990	0.0067	0.0012	0.0071	0.0011	
51	.00650	970	.0075	.0015	.0075	.0011	
52	.00662	950	.0075	.0012	.0079	.0011	
53	.00675	930	.0082	.0015	.0079	.0012	
54	.00688	910	.0063	.0012	.0063	.0009	
55	.00701	900	.0059	.0010	.0059	.0006	
56	.00713	880	.0059	.0013	.0059	.0009	
57	.00726	870	.0055	.0014	.0055	.0011	
58	.00739	850	.0055	.0012	.0055	.0011	
59	.00752	840	.0063	.0015	.0063	.0012	
60	0.00764	820	0.0063	0.0012	0.0063	0.0012	

The final step in the analysis was the derivation of a smooth spectrum according to

$$F_s(k) = 0.23F\left(k - \frac{\pi}{MD}\right) + 0.54F(k) + 0.23F\left(k + \frac{\pi}{MD}\right). \tag{5}$$

The averaged results for this smooth spectrum, together with their probable errors, are also given in Table 2.

The computations indicated by equations (3), (4), and (5) were performed for each of the eight sets in one run on the UNIVAC of the Applied Mathematics Laboratory, David Taylor Model Basin, which had been coded for this combined operation.

It remains to investigate how the results are affected, at both ends of the wave-length band covered, by the numerical procedure and by the finite resolution of the photograph used. The cutoff at the long-wave-length end is essentially determined by the use of the moving averages defined in equation (1). Since they are obtained by averaging over 201 points corresponding to a distance on the sun of 82,000 km, wave lengths of this order or longer are severely affected. Correspondingly, the data given in the first line of Table 2 have virtually no significance. It was found, however, that the wave lengths to which the second line of Table 2 refers are already sufficiently short to be only moderately affected by the use of the moving averages and that the data from the third line on are essentially unaffected by this procedure.

At short wave lengths the cutoff should be caused mainly by the finite resolution of the photograph used. Since the plate used was of unusually fine definition, it seems likely that the resolution on the plate was largely determined by the diffraction pattern of the 4-inch aperture, which can be represented roughly by the relation,

$$i(d) = \frac{1}{\delta\sqrt{\pi}} \exp\left(-\frac{d^2}{\delta^2}\right), \qquad \text{with} \qquad \delta = 525 \text{ km}. \tag{6}$$

If one takes into account only the smoothing effects of this instrumental profile in the direction of the photometer tracings but not across them, then these smoothing effects can be represented by a correction factor α according to the relation

$$F_{\text{true}}(k) = \alpha(k) F_{\text{obs}}(k), \qquad \text{with} \qquad \alpha(k) = \exp\left(+\frac{k^2\delta^2}{2}\right). \tag{7}$$

The values of the correction factor α are listed in the last column of Table 2.

IV. RESULTS

The results of the computations are represented in Figures 1 and 2. Figure 1 shows the covariances (which are the unnormalized autocorrelation function). Significant positive correlations are obtained out to a distance of about 2000 km. The covariance at $y = 0$ indicates a root-mean-square intensity fluctuation of 0.0326, i.e., 3.3 per cent of the mean intensity.

The results for the turbulence spectrum are shown in Figure 2. The probable errors indicated by the vertical bars are seen to be encouragingly small. Hence the 8000 readings here used were apparently sufficient in number to give results of satisfactory statistical accuracy.

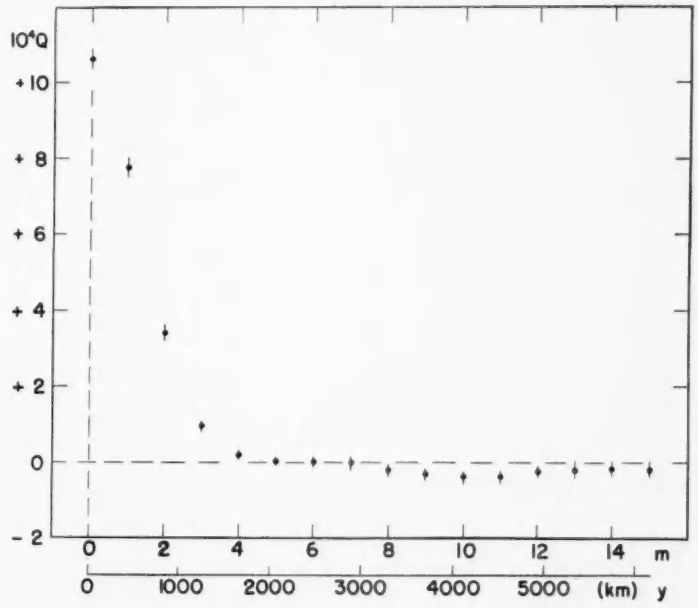

FIG. 1.—Covariances (unnormalized correlation function) from photospheric intensities as a function of the lag (distance between two points). The vertical bars give the probable errors.

The observed spectrum indicated by the dots shows high values for wave lengths between 7000 and 30,000 km. This is similar to the earlier result (Frenkiel and Schwarzschild 1952; Rush and Stuart 1954) that the turbulence spectrum of the solar photosphere contained much energy in the wave-length band around 15,000 km.

Toward shorter wave lengths (toward the right in Fig. 2) the observed spectrum decreases steadily. The question arises whether this apparent decrease is, at least in part, actually occurring on the sun or whether it is entirely due to the finite instrumental resolution. If the tentative derivation of the correction factor a given in the preceding section is accepted, one may remove the effects of finite resolution by multiplying the observed spectrum by this factor. The results are indicated by the circles in Figure 2.

One may conclude that the true turbulence spectrum of the granulation intensities

may very well be essentially constant throughout the wave-length range from 2000 to 30,000 km.

This last result is somewhat in disagreement with the earlier result (Frenkiel and Schwarzschild 1952), that the turbulence spectrum of the vertical granulation velocities decreased noticeably from the wave-number band between 0.000 and 0.001 to the band between 0.001 and 0.002. This discrepancy may be caused either by an actual difference between the spectra for intensities and for vertical velocities or by an overestimate of the definition of the plate used in the earlier investigation—an error which, with the present experience, does not seem implausible.

It is again tempting to speculate how the photospheric turbulence spectrum continues toward smaller, as yet completely unresolved, wave lengths. If one assumes that

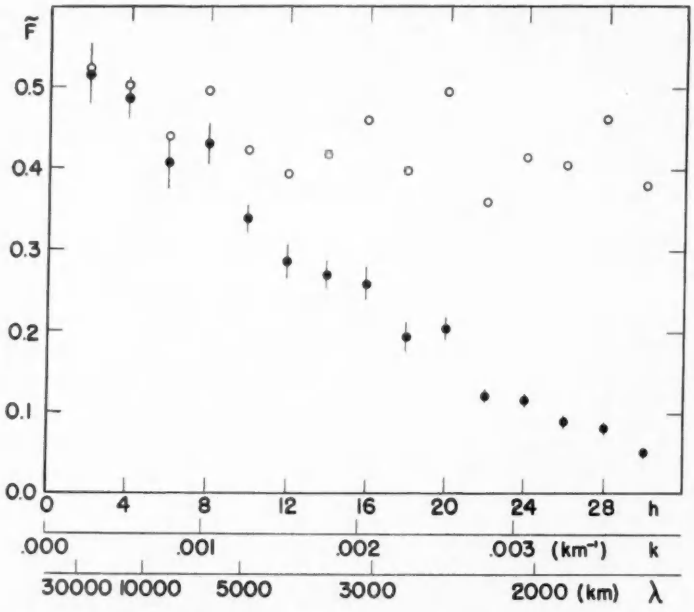

FIG. 2.—Turbulence spectrum in terms of photospheric intensities. The dots show the observed spectrum, with the vertical bars giving the probable errors. The circles show the spectrum corrected for the finite resolution of the plate used.

the spectrum continues essentially constant down to wave lengths of about 300 km (twice the photospheric scale height), then the total spectrum would contain about ten times more energy than the energy contained in the partial spectrum observed thus far. If this factor should turn out applicable also to the turbulence spectrum of the vertical velocities (not only to that of the intensities), then it would be of the right order of magnitude to explain the discrepancy between the small measured Doppler shifts of the resolved granules and the large total turbulent velocities, as judged by the line profiles.

Further studies of the turbulence spectrum in the solar photosphere and of the mathematical analysis of the data are planned.

The authors wish to acknowledge the assistance of Owen J. Deters (Applied Physics Laboratory) in some parts of this work and of Arthur Shapiro (David Taylor Model Basin) in the numerical computations on the high-speed computor.

REFERENCES

Frenkiel, F. N., and Schwarzschild, M. 1952, *Ap. J.*, **116**, 422.
Rush, J. H., and Stuart, F. E. 1954, *Ap. J.*, **120**, 245.

THE PROMINENCE OF JULY 25, 1951*

KURT ROTHSCHILD, JEAN-CLAUDE PECKER, AND WALTER ORR ROBERTS
Montana State College, High Altitude Observatory
Received June 21, 1954; revised August 4, 1954

ABSTRACT

The motions of 49 knots in the large prominence of July 25, 1951, have been measured. For 17 of them, a definite variation of acceleration vectors has been found. The dynamics of the motion still remains obscure. It seems difficult to represent them by a coherent field of forces. Moreover, gravity seems to play no role in this prominence.

INTRODUCTION

On July 23, 24, and 25, 1951, a very interesting quiescent limb prominence of the tree-shaped type was observed at the east solar limb by R. G. Athay and W. R. Allen, who used the coronagraph at the High Altitude Observatory station at Climax, Colorado. The same prominence was also recorded at other observatories (Mohler 1954; d'Azambuja 1954). It had appeared as a dark filament and limb prominence for several rotations prior to its *disparition brusque* on July 25 and subsequent thereto, when a similar prominence re-formed on the disk. Line-of-sight velocities also were observed at McMath-Hulbert Observatory (Mohler 1954) on July 24 and 25.

On July 25 the seeing and the weather conditions were good at Climax, and the film obtained was very suitable for motion studies. The prominence appeared at about heliographic longitude 140° and latitude 35° N.; the time of observation was U.T. 14^h51^m to 18^h2^m, with two interruptions of 24 and 13 minutes, respectively. Six pictures per minute were taken throughout the observing period. A birefringent filter, designed and built by J. W. Evans, of 4 A half-width centered at $H\alpha$ was used to isolate the prominence.

GENERAL FORM OF THE PROMINENCE MOTION

When the film starts, at U.T. 14^h51^m, the prominence exhibits an upward motion in the shape of the trunk of the tree, with branches extending to both sides. The motion proceeds from the stem outward. Streamers then develop from the extremities of the branches back to the surface of the sun, along curved paths; some of the branches apparently again cross the trunk. As the crown becomes more transparent, masses are seen to travel along paths that suggest that they are roughly circular, with the plane of the circle approximately perpendicular to the radius of the sun. As the material moves, however, the masses appear to change their curvature and to return to the solar surface.

Toward the end of the film, the motion becomes more violent; the stem begins to break, the lower part returns to the surface, while the upper part follows the general direction of the branches. Most of the material seems to fall back to the sun. However in the uppermost part of the crown the circular motion becomes more distinct, and, at the same time, explosion-like projections toward outer space can be seen, indicating an eruptive character. Unfortunately, the film ends at this point (U.T. 18^h2^m).

An especially interesting feature of the first part of the film is the fact that the prominence material seems to be constrained to remain inside a dome-shaped volume, whose limit is very sharp, as can be seen in Figures 1 and 2, and very constant in time.

* This research was supported by the Office of Naval Research.

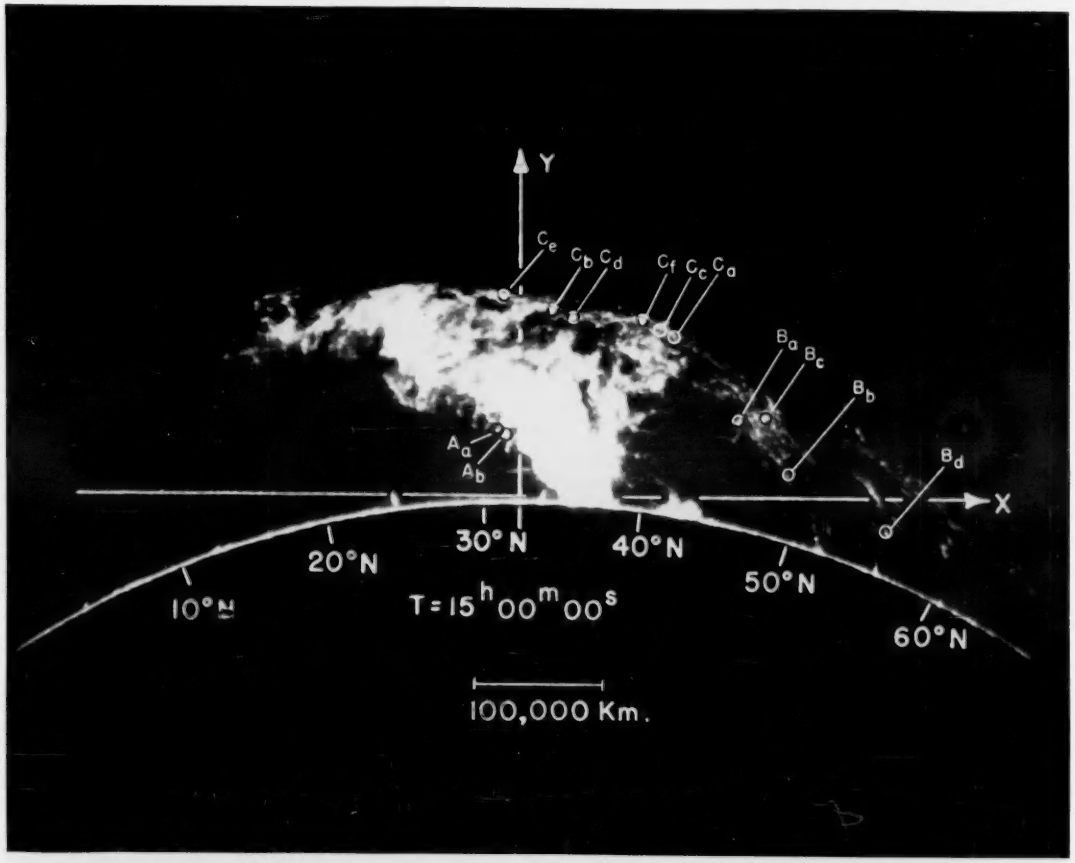

FIG. 1.—The prominence of July 25, 1951, at $15^h00^m00^s$. All knots observed at this time are labeled

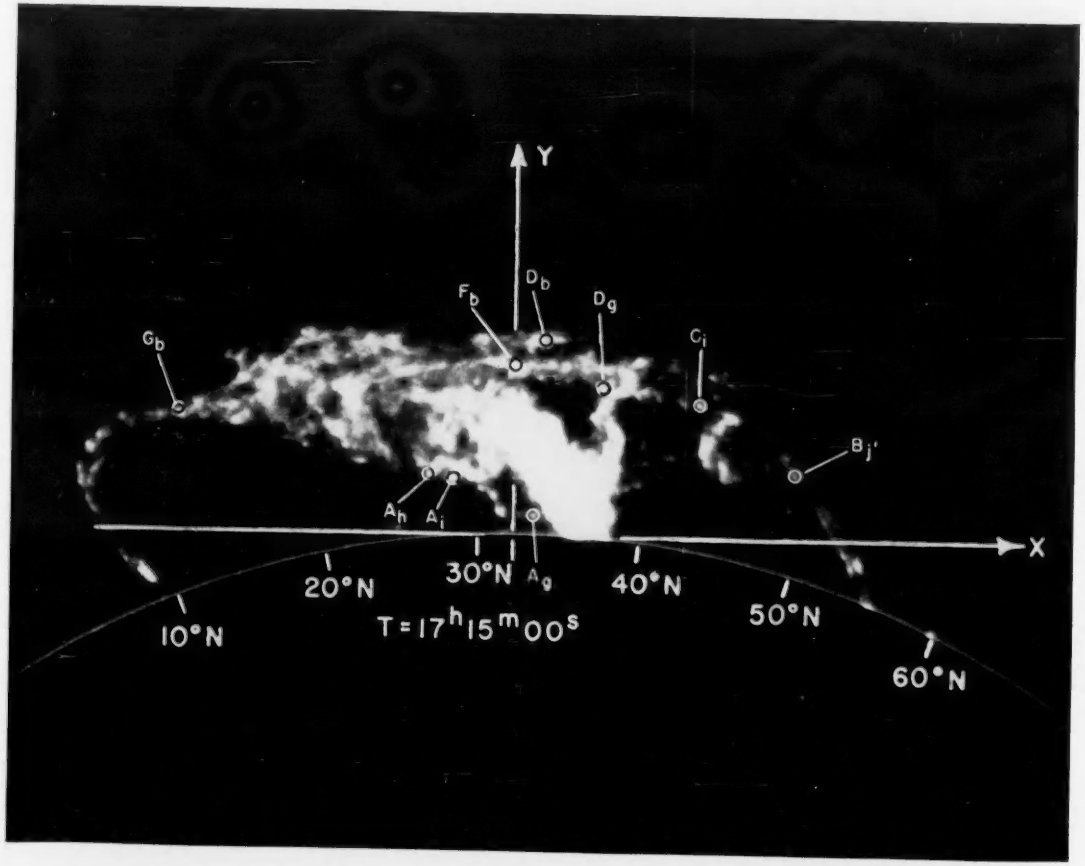

FIG. 2.—The prominence of July 25, 1951, at $17^h15^m00^s$. All knots observed at this time are labeled

PURPOSE AND DESCRIPTION OF THE MEASUREMENTS

The purpose of this investigation was to observe quantitatively the apparent motions of a maximum number of knots over as long a time as possible, in order to obtain a general picture of the accelerations over the whole visible extent of the prominence. This particular film was selected because of its photographic excellence, with good contrast, and well-defined knots showing throughout and because of its intrinsic interest as a very typical "common active" of type I*b* in Pettit's classification (1943, 1951) or of AN_e in that of Menzel and Evans (1952).

It was possible to follow the motion of 49 knots, though most of these had lifetimes of the order of only 15–20 minutes. These knots are labeled according to the region or streamer in which they are observed (A, B, . . .) and with a small letter (a, b, . . .) designating each individual knot. Table 1 gives the times of observation of these knots. The positions of some of them at two different times are shown in Figures 1 and 2.

FIGURES 1 AND 2

The measurements were made by Rothschild, frame by frame, from a positive copy, by means of a projector especially constructed for this purpose by Dr. J. H. Rush, of the High Altitude Observatory at Boulder; and the positions of the knots were read directly from the co-ordinate paper on which the film was projected. The origin of the system of co-ordinates was the point on the limb at 32° N. latitude, with the positive x-axis tangential to the limb pointing north and the positive y-axis pointing radially outward.

The measurements involved certain difficulties. In order to utilize the maximum resolution of the telescope, Rothschild sought to measure the position of the knots to at least 0.5 mm on the paper (about 500 km at the sun). This is generally not feasible; for even if the knot is well defined, one has to decide upon a reference point on it; but the knot changes shape and size; it may split or combine with other masses and thus make any reference point illusory. This situation becomes even worse when the knot has a hazy outline, as is usually the case, and if, in addition to that, the intensity of radiation changes with time. In several instances an interesting situation occurred when the paths of two knots intersected, both becoming faint before the intersection, but only one remaining visible afterward. In such cases an observer can easily be deceived into following the wrong knot and can thus conclude incorrectly that there is a discontinuous change of velocity at the time when the knots intersected. In all knots observed, however, there was no evidence of sudden changes of either velocity or accelerations, with the sole exception of the knot A_g, where such a misidentification may possibly have been involved.

ANALYSIS OF MEASUREMENTS

The data thus collected were evaluated by means of the method of least squares, as described by Birge and Weinberg (1947) and used for a similar study by Bartlett, Witte, and Roberts (1953). This method furnishes for each co-ordinate, to fit the prominence trajectories, a polynomial expression with the time as a variable and with coefficients giving position, velocity, and velocity derivatives. The method gives the errors in the polynomial expression as well. Thus we can be confident that we have carried the polynomial to a sufficiently high order when the errors of the coefficients are small compared to the coefficients. Further extension to higher orders of expression can only be misleading, as pointed out in the earlier paper (Bartlett *et al.* 1953). In 17 features (marked by an asterisk in Table 1) a third-degree equation has been found necessary to represent at least one co-ordinate of the motion. In all other cases, second- or even first-degree equations were sufficient to represent the measurements. Figure 3 shows, as an example, the precision one obtains. All computed coefficients are collected in Table 1, which summarizes all available measurements. For only one feature (the knot A_g) does the three-degree representation seem to be insufficient.

TABLE 1

COMPUTED TRAJECTORIES FOR 49 PROMINENCE KNOTS

I	II	III	IV (Km)	V (Km/Sec)	VI (10^{-3} Km/Sec^2)	VII (10^{-5} Km/Sec^3)
A_a*	$14^h56^m35^s$	$15^h14^m45^s$	− 600± 80	+ 9.6± 0.3	+ 9.4± 0.9	+ 2± 0.6
	15 15 15	(18 40)	+ 32,950± 90	−21.6± 0.3		
A_b*	14 57 0	15 4 0	− 530± 130	+ 9.8± 0.4	+ 5.0± 1.7	− 18± 9.0
	15 11 0	(14 0)	+ 41,840± 120	−49.0± 0.4	+ 5.0± 1.7	− 28± 9.0
A_c	15 9 5	15 13 5	− 27,980± 120	+30.2± 0.8	+22.7± 7.0	
	15 17 5	(8 0)	+ 58,500± 80	−14.3± 0.4		
A_d	15 14 50	15 22 20	− 28,160± 60	−19.9± 0.3	+ 3.0± 1.2	
	15 29 50	(15 0)	+ 10,610± 120	−13.0± 0.6	− 6.0± 1.8	
A_e	15 19 30	15 24 0	− 45,900± 90	−19.1± 0.5	−10.1± 3.0	
	15 28 30	(9 0)	+ 6520± 80	−14.1± 0.5		
A_f	16 52 0	16 55 0	+ 19,360±1600	+24.6±13.0		
	16 58 0	(6 0)	+ 11,160± 110	−48.3± 1.0		
A_g**	17 0 50	17 8 20	+ 3990± 180	+53.5± 0.6	+18.1± 1.8	
	17 15 50	(15 0)	+ 19,200± 130	+33.3± 0.3	+ 6.6± 1.3	+ 90+ ?
A_h	17 9 20	17 17 40	− 83,850± 140	+51.0± 0.7	+12.7± 1.8	
	17 26 0	(16 40)	+ 46,170± 150	−19.0± 0.7	−10.9± 1.8	
A_i*	17 14 10	17 25 0	− 44,880± 150	+41.7± 0.3	− 5.4± 1.0	
	17 35 50	(11 40)	+ 24,690± 120	−22.7± 0.3	+ 1.8± 0.9	+ 1± 0.2
B_a*	14 53 10	15 0 10	+177,000± 100	+ 9.05±0.5		
	15 7 10	(14 0)	+ 56,190± 80	−25.7± 0.3	−10.1± 1.2	+ 40± 5.0
B_b	14 53 0	15 0 30	+216,300± 120	+32.3± 0.7	+12.1± 1.8	
	15 8 0	(15 0)	+ 11,850± 200	−56.2± 0.7	−12.1± 2.4	
B_c	14 54 30	15 0 0	+199,100± 80	+29.2± 0.4	+23.5± 1.7	
	15 5 30	(9 0)	+ 64,690± 80	−37.7± 0.4	−35.4± 1.7	
B_d	14 55 10	15 0 40	+293,400± 300	+34.7± 1.5	− 8.4± 8.0	
	15 6 10	(11 0)	− 35,200±2100	−79.0±10.0		
B_e*	15 2 0	15 10 20	+229,500± 60	+37.8± 0.6	−10.9± 0.5	− 2± 0.4
	15 18 40	(16 40)	+ 26,030+ 80	−66.7± 0.6	−14.5± 0.7	+ 30± 2.0
B_f	15 19 0	15 28 10	+138,400± 80	+21.1± 0.2	+ 4.8± 0.6	
	15 37 20	(18 20)	+ 74,590± 120	−29.6± 0.3	+12.1± 1.8	
B_g	15 30 40	15 41 30	+220,700±1300	+43.8± 4.0		
	15 52 20	(21 40)	+ 30,850± 200	−71.3± 0.7	−14.5± 1.8	
B_h	15 52 50	15 55 10	+186,300±1200	+22.7± 1.4		
	15 57 30	(4 40)	+ 53,890± 50	+ 4.1± 0.6		
B_i*	16 29 20	16 44 30	+174,600± 270	+29.4± 0.4	+ 7.4± 1.0	+ 1.1± 0.2
	16 59 40	(30 20)	+ 77,800± 130	−48.8± 0.2	− 3.7± 0.4	+ 0.6± 0.1
B_j*	16 36 40	16 47 30	+186,600± 130	+32.3± 0.3	+ 3.6± 1.0	
	16 58 20	(21 40)	+100,300± 150	−41.1± 0.3	−18.1± 1.0	+ 1.4± 0.4
B_j'	17 0 0	17 9 10	+227,900± 150	+51.3± 0.6	+24.2± 1.8	
	17 18 20	(18 20)	+ 37,120± 450	−59.4± 2.0	−12.1± 4.8	
B_k	16 38 10	16 49 0	+185,600± 600	+46.8± 2.0		
	16 59 50	(21 40)	+ 16,470± 240	−80.0± 0.7	−18.1± 1.8	
B_l	18 0 50	18 3 50	+283,600±1000	+41.7± 9.0	+100.8±80.0	
	18 6 50	(6 0)	− 14,450± 290	−111.2± 2.0	+84.0±24.0	
B_m*	18 1 0	18 7 40	+251,900±1500	+58.3± 6.0		
	18 14 20	(13 20)	+ 49,410± 30	−50.1± 1.8	−18.1± 5.0	− 10± 2.0
C_a	14 56 30	15 14 30	+167,200± 330	+44.9± 0.4	+ 3.7± 0.9	
	15 32 30	(36 0)	+ 93,300± 380	−49.9± 0.4	−13.0± 0.9	
C_b	14 59 0	15 1 30	+ 43,000± 150	+50.3± 1.5		
	15 4 0	(4 30)	+139,700± 150	+ 4.5± 1.5	+84.0±17.0	
C_c*	14 59 30	15 4 30	+135,000± 100	+49.3± 0.5	+25.2± 1.0	+ 46 ± 1.0
	15 9 30	(10 0)	+119,700± 90	−35.2± 0.5	+40.3± 1.0	+ 130±10.0
C_d*	14 59 30	15 10 20	+ 64,320± 15	+28.7± 0.1	− 7.2± 0.5	
	15 21 10	(21 40)	+130,500± 300	−32.6± 0.6	−18.1± 0.5	+ 1.9± 0.1
C_e*	14 59 40	15 3 10	+ 6430±1000	+27.2± 1.0	+40.3± 5.0	
	15 6 40	(7 0)	+150,000±1000	− 9.1± 1.0	+35.3± 5.0	− 230±40
C_f*	15 0 0	15 11 40	+146,700± 15	+58.9± 0.3		
	15 23 20	(23 20)	+121,300± 540	−24.8± 1.2	−18.1±3.0	− 100±50
C_g	15 3 50	15 6 50	− 2010± 100	+45.8± 1.0		
	15 9 20	(5 30)	+158,600± 200			

TABLE 1—*Continued*

I	II	III	IV (Km)	V (Km/Sec)	VI (10^{-2} Km/Sec^2)	VII (10^{-4} Km/Sec^2)
Ch	15h 4m20s	15h 8m20s	+115,600± 310	+19.1± 2.0		
	15 12 20	(8 0)	+128,900± 100	−37.2± 0.5	−33.6± 5.0	
Ci*	16 58 40	17 13 50	+155,100± 270	+43.4± 0.4	− 5.5± 0.9	
	17 29 0	(30 20)	+ 91,910± 80	− 9.1± 0.2	+ 5.5± 0.3	− 1.4± 0.1
Da	15 33 50	15 38 0	+ 86,180± 80	+37.4± 0.6	−12.1± 3.6	
	15 42 10	(8 20)	+140,500± 150	−19.3± 0.9	−18.1± 6.0	
Db*	15 34 40	15 49 50	+ 50,030± 120	+27.2± 0.2	− 5.5± 0.5	+ 1.5± 0.1
	16 5 0	(30 20)	+126,400± 450	−28.1± 0.8		
Dc	15 39 0	15 48 10	+ 21,200± 160	+44.7± 0.6	+ 4.8± 1.2	
	15 57 20	(22 20)	+150,000± 110	−16.3± 0.3	−12.1± 0.6	
Dd	15 47 0	15 51 30	+ 59,690± 90	+34.2± 0.5		
	15 56 0	(9 0)	+131,400± 120	−42.2± 0.5	−15.1± 5.0	
De	15 47 20	15 56 30	− 41,090± 80	+64.6± 0.3	+ 3.6± 0.6	
	16 5 40	(18 20)	+157,700± 180			
Df	15 48 0	15 52 10	+ 98,120± 720	+20.2± 4.5	+18.1±36.0	
	15 56 20	(8 20)	+118,300± 30	−29.9± 1.5	−18.1±12.0	
Dg*	16 32 20	17 10 20	+ 66,560± 650	+40.1± 0.5	− 1.7± 0.3	+0.03±0.03
	17 48 20	(1 16 0)	+119,600± 690	−27.8± 0.5	− 1.7± 0.4	+0.35±0.03
Dh	16 47 30	17 5 30	+ 11,660± 210	+54.3± 0.4		
	17 23 30	(36 0)	+145,600± 90	− 1.3± 0.2	− 5.6± 0.2	
Ea*	15 21 40	15 41 10	−185,300±1400	−17.6± 2.0	− 3.3± 3.3	
	16 0 40	(39 0)	+127,600± 130	− 0.8± 0.2	+ 7.8± 3.3	+0.47± 0.03
Fa	15 16 20	15 40 10	+ 42,570± 330	+23.2± 0.4	− 5.6± 0.4	
	16 4 0	(47 40)	+113,300± 280	−16.6± 0.3	− 7.5± 0.4	
Fb	16 31 50	16 57 30	− 11,610± 380	+28.5± 0.3	+ 5.0± 0.2	
	17 23 10	(51 20)	+126,400± 160	+ 1.4± 0.2		
Ga	16 29 50	16 49 20	−317,700± 630	+14.1± 0.8	+22.3± 1.7	
	17 8 50	(39 0)	+ 39,360± 300	−48.0± 0.3	−16.7± 0.6	
Gb	16 33 20	17 5 50	−244,400± 200	+30.8± 0.2		
	17 38 20	(1 5 0)	+ 93,410± 170	+ 9.9± 0.1	− 2.0± 0.1	
Gc	18 0 50	18 3 50	−251,500± 220	+71.9± 0.2		
	18 6 50	(6 0)	− 10,870± 690	−158.4± 0.6		
Gd	18 0 50	18 7 30	−281,100± 650	+52.2± 0.3		
	18 14 10	(14 0)	− 12,190± 240	−70.7± 0.9	−12.1± 4.8	
Ha	18 1 30	18 14 20	+ 75,030± 370	+19.4± 0.8	−18.5± 2.0	
	18 27 10	(25 40)	+ 97,020± 220	+22.7± 0.4		
Hb	18 9 0	18 17 20	+ 62,000± 240	+11.5± 0.9	−18.1± 3.6	
	18 25 40	(16 40)	+191,300± 220	+83.3± 0.9	− 9.1± 2.7	

NOTES TO TABLE 1

Column I gives the designation of the features studied. The first letter represents the region. The second one represents the individual knot: knots are classified following the time of their first distinct appearance.

Column II gives time, in U.T., of the first and last observation of each knot.

Column III gives the time, U.T., t_0, and the duration of the observation of each knot.

Column IV and others give the coefficients a, b, c, d, and a′, b′, c′, d′, of the equations

$$x = a + b\,(t - t_0) + c\,(t - t_0)^2 + d\,(t - t_0)^3 \quad \text{(first line)},$$

$$y = a' + b'\,(t - t_0) + c'\,(t - t_0)^2 + d'\,(t - t_0)^3 \quad \text{(second line)},$$

as well as the mean errors of those coefficients (i.e., the position, velocity, acceleration, and derivative of the acceleration at the time t_0).

An asterisk (*) indicates the knots for which we measured variations of acceleration. A double asterisk (**) indicates the knot for which this variation could not be represented by a linear function of time.

Figure 4 shows the apparent motions of all the knots. On Figure 5 we have represented, on the same scale, the apparent motion on each of the 17 most interesting knots. These were the most precisely measured knots. We also show a graphical representation of the computed apparent accelerations.

GENERAL CONCLUSIONS

In the majority of cases there is a tendency for the accelerations to reverse at a certain point in the trajectory (examples C_f, A_a). This could occur either if the three-di-

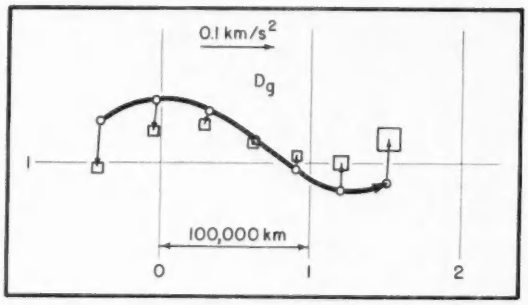

FIG. 3.—Example showing the precision of measurements for knot Dg. The squares show the mean errors of acceleration; the circles, the mean errors of position.

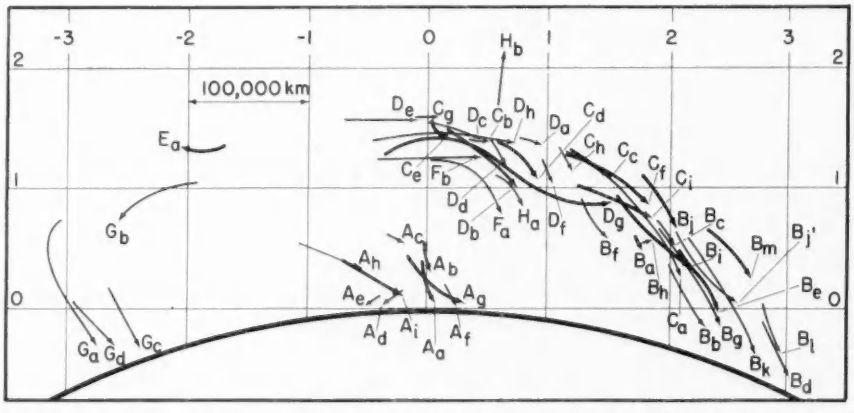

FIG. 4.—The apparent motions of the 49 knots. Heavy lines represent knots for which a variation of acceleration was detected. The scale is 100,000 km for each unit. The arrows indicate the direction of the motion.

mensional acceleration of the prominence knot actually becomes small or, alternatively, if the vector acceleration turns without changing in magnitude. The latter would be true for helical motion. The former might suggest sinusoidal motion, perhaps in a plane. Often reversal of the vector occurs in a very short path and involves substantial change of accelerations. This is the case, for example, of C_c or C_e. In the case of C_e, the acceleration does not go through a vanishing value, suggesting that we may be confronted here with helical motion.

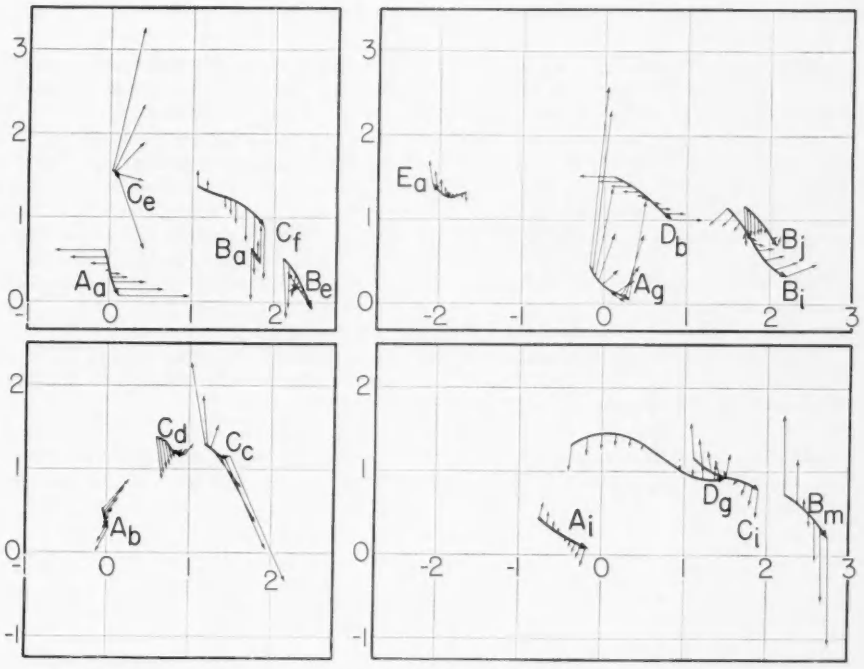

FIG. 5.—Apparent accelerations for the 17 knots for which the accelerations vary with time

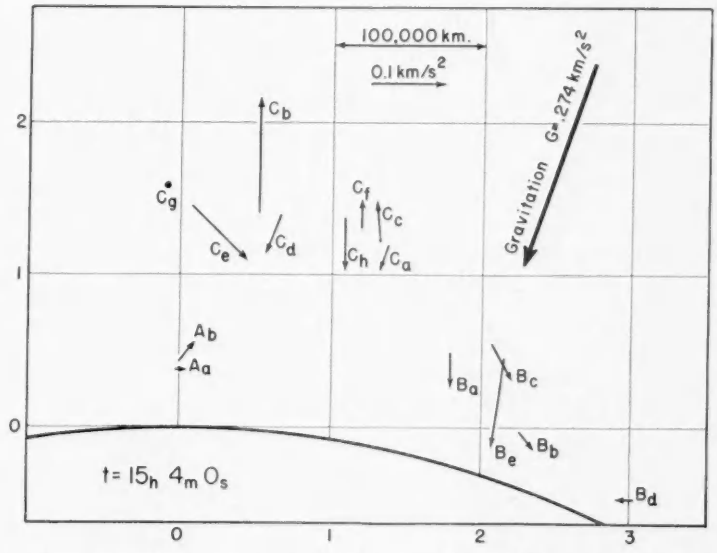

FIG. 6.—Apparent acceleration vectors at the time: $t = 15^h4^m0^s$. Solar gravity is shown in the same units. The figure shows that at the arbitrarily chosen time, as probably at all other times, there is no qualitatively apparent simple pattern of accelerations in the prominence.

Some knots (B_e) seem not to have the same tendency: if their motion is helical, the axis of helix must be roughly normal to the plane of projection. They appear to exhibit a tendency toward having a center of force, but this appearance may be illusory.

As is well known, the origin of prominence motion is still obscure. From the appearance of the accelerations of all knots at a certain time (Fig. 6), it appears clear that it is difficult to represent them by any simple coherent field of forces. Probably this is truly the case, though perhaps the impression is due to the fact that we are considering only a two-dimensional projection. Such a result is not unexpected, since previous authors have also found, in such prominences, accelerations smaller than gravitational, with little or no relationship even to the direction of gravity (Pettit 1925; Dodson 1948). Gravitational acceleration seems to play no role in the motion of knots, despite the fact that this acceleration is significantly larger than the observed accelerations.

In further research, we intend to introduce some dynamical hypotheses and use them to interpret the observed trajectories in an effort to compute a coherent three-dimensional model of the prominence (Billings and Pecker 1954).

The authors express their appreciation to Mr. Bruno Witte for his valuable advice in the work and to the whole staff of the High Altitude Observatory for their frequent discussions with us.

REFERENCES

Bartlett, T. J., Witte, B., and Roberts, W. O. 1953, *Ap. J.*, **117**, 292.
Billings, D. E., and Pecker, J. C. 1954, *C.R.*, **238**, 1690.
Birge, R. T., and Weinberg, J. W. 1947, *Rev. Mod. Phys.*, **19**, 298.
d'Azambuja, Mme M. 1954, private communication.
Dodson, H. W. 1948, *M.N.*, **108**, 383.
Menzel, D. H., and Evans, J. W. 1953, *Conv. Volta Accad. naz. dei Lincei*, **11**, 119, Fig. 8.
Mohler, D. 1954, private communication.
Pettit, E. 1925, *Pub. Yerkes Obs.*, **3**, 205.
———. 1943, *Ap. J.*, **98**, 6.
———. 1951, *Astrophysics*, ed. J. A. Hynek (New York: McGraw-Hill Book Co., Inc.), p. 291.

CORONAL LINE INTENSITIES AT THE KHARTOUM ECLIPSE

R. G. Athay and W. O. Roberts
High Altitude Observatory, Boulder, Colorado
Received July 26, 1954; revised August 27, 1954

ABSTRACT

Coronal line and continuum intensities were measured at several position angles on the limb and as a function of height above the limb on the slitless spectrograms obtained at Khartoum by the High Altitude Observatory. The lines λλ 5303, 6374, and 7892 and the continuum were measured at fifteen points around the limb. The relative line and continuum intensities around the limb showed large variations. In one active region where the emission in some lines was intense, the yellow coronal line λ 5694 was observed. In this same region the lines λ 6702 and λ 7060 were intense enough to measure, and it was found that lines of high ionization potential were at maxima in intensities, whereas lines of low ionization potential were at minima. The yellow line was at maximum in this region, confirming that it is a high-ionization-potential line. The correlation between line and continuum intensities was found to increase markedly as the ionization potential increased for the three lines studied. The correlation between line intensities was found to increase as the difference in ionization potential decreased.

Intensities of λ 5303, λ 7892, and the continuum were measured as a function of height above the limb in four regions. Two of these regions were active centers, one of which showed the yellow line, and two were more nearly average regions. The change of λ 7892 intensities with height in the latter two regions showed that the maximum intensity occurred below 10,000 km. Changes in the relative intensities of the two lines with height showed that in the yellow-line region the temperature decreased with height, but in the other regions the temperature increased with height. A comparison of the changes in line intensities to the changes in continuum intensities showed that the average temperature in the active regions was above the value at which the line λ 5303 had a maximum intensity, but in the two more normal regions the temperature was between the limits where the lines λ 5303 and λ 7892 have maxima. The active regions were found to be regions of high density.

I. INTRODUCTION

Some interesting features of coronal emission lines can be measured on the slitless spectrograms obtained by the High Altitude Observatory at the solar eclipse of February 25, 1952, at Khartoum. The coronal lines λλ 5303, 6374, and 7892 and the continuum were suitably exposed to allow measurements throughout a wide range in position angles, and λ 6702 and λ 7060 can be measured at one position angle. Several other lines can be identified at the position where λ 6702 and λ 7060 are most intense. The line λ 5694 is among these, and an upper limit to its intensity can be determined. There are several lines in the ultraviolet that are fairly intense, but on all usable spectrograms there are too many near-by chromospheric lines to allow reliable measurements. Because our instruments were slitless, the intensities that we can measure are integrated both along the line of sight and from the moon's limb outward. However, in some respects the integration is advantageous because it averages conditions over large sections of the corona, and small local perturbations are smoothed. Lyot and Dollfus (1953) made observations with slit spectrographs that are more suitable for registering faint lines and for isolating given sections of the corona. Their paper gives an extensive discussion of the lines observed.

On our spectrograms the line λ 7892 was sufficiently intense and the exposures were such that the intensities can be measured as a function of height between 3000 and 46,000 km. The height assigned to a given spectrogram is the height of the moon's limb above the solar limb at the middle of the exposure and represents the lower limit of the integration referred to in the preceding paragraph. The line λ 5303 can be measured on several spectrograms near the extreme heights, but not at intermediate heights because of overexposure of the spectrograms. The photometric standardization of the spectrograms was discussed in a previous paper (Athay, Billings, Evans, and Roberts 1954).

Our objectives in this paper are as follows: (1) to determine the correlation between the relative intensities of the various lines and the continuum at different positions around the limb; (2) to determine the height above the limb at which the emission in the coronal lines reaches maximum intensity; (3) to determine the changes in the relative intensities of the lines and continuum with height above the limb; and (4) to determine the sign of the temperature gradient and the temperature limits in selected regions from the data obtained in the first three objectives.

The identifications and ionization potentials of the lines considered in this paper are given in Table 1.

II. INTENSITIES VERSUS POSITION ANGLE

The intensities of λλ 5303, 6374, and 7892 were measured at points on the limb wherever significant changes were apparent to a visual examination. The microdensitometer tracings were made along lines parallel to the dispersion of the spectrographs, which corresponded to the line of contacts through 23° N. on the east limb and 23° S. on the west limb. Thus the integration over height was along nonradial lines in most cases. The intensities can be approximately corrected to a radial integration by multiplying by cos θ, where θ is the angle between the line of contacts and the latitude where the measurements

TABLE 1

LINE DATA

	Line						
	λ 6374	λ 7892	λ 5303	λ 7060	λ 6702	λ 8024	λ 5694
Identification	*Fe* X	*Fe* XI	*Fe* XIV	*Fe* XV	*Ni* XV	*Ni* XV	*Ca* XV?
Ionization potential (volts)	233	261	355	390	422	422	814

were made. An additional correction should be applied to account for the fact that the height of the moon's limb above the solar limb also varies with θ. The correction to be applied to the heights is $\Delta h \sim 25{,}000(1 - \cos\theta)$. Over the extreme ranges in the positions measured, $\Delta h \sim 10{,}000$ km. The curves of line intensity, E, versus height (see Fig. 2 in Sec. III below) show that log E for the lines decreased by about 0.20 over this height range. However, log (cos θ) also changed by about 0.2 over the ranges of positions measured, and this correction was applied in the opposite sense. Thus the combined effects of changes in the height of the moon's limb and integration along nonradial lines very nearly cancel, and no corrections were made for these effects.

The intensity of λ 7892 was measured on two spectrograms separated by a relatively small difference in height at each position angle, and the results were averaged; the same was done for λ 5303. The intensities of λ 6374 were averaged from measurements on two infrared and two visible spectrograms. The average probable error for repeated measurements was ±0.03 in log E. The continuum intensities corresponding to an integration over the same slice of atmosphere were also measured at each point on the limb. A complication in the continuum measurements arises from the overlapping of many monochromatic images of the sun, and, as a result, at a given position in the spectrograms the continuum consists of light from both sides of the sun. Fortunately, however, the contributions from the east and west limbs can be separated. This separation was described by Athay, Billings, Evans, and Roberts (1954) and will be discussed in more detail in a forthcoming paper dealing with the analysis of the chromospheric data.

The line and continuum intensities are shown graphically in Figure 1, and they are tabulated, along with the ratios of intensities of different lines, and equivalent widths of

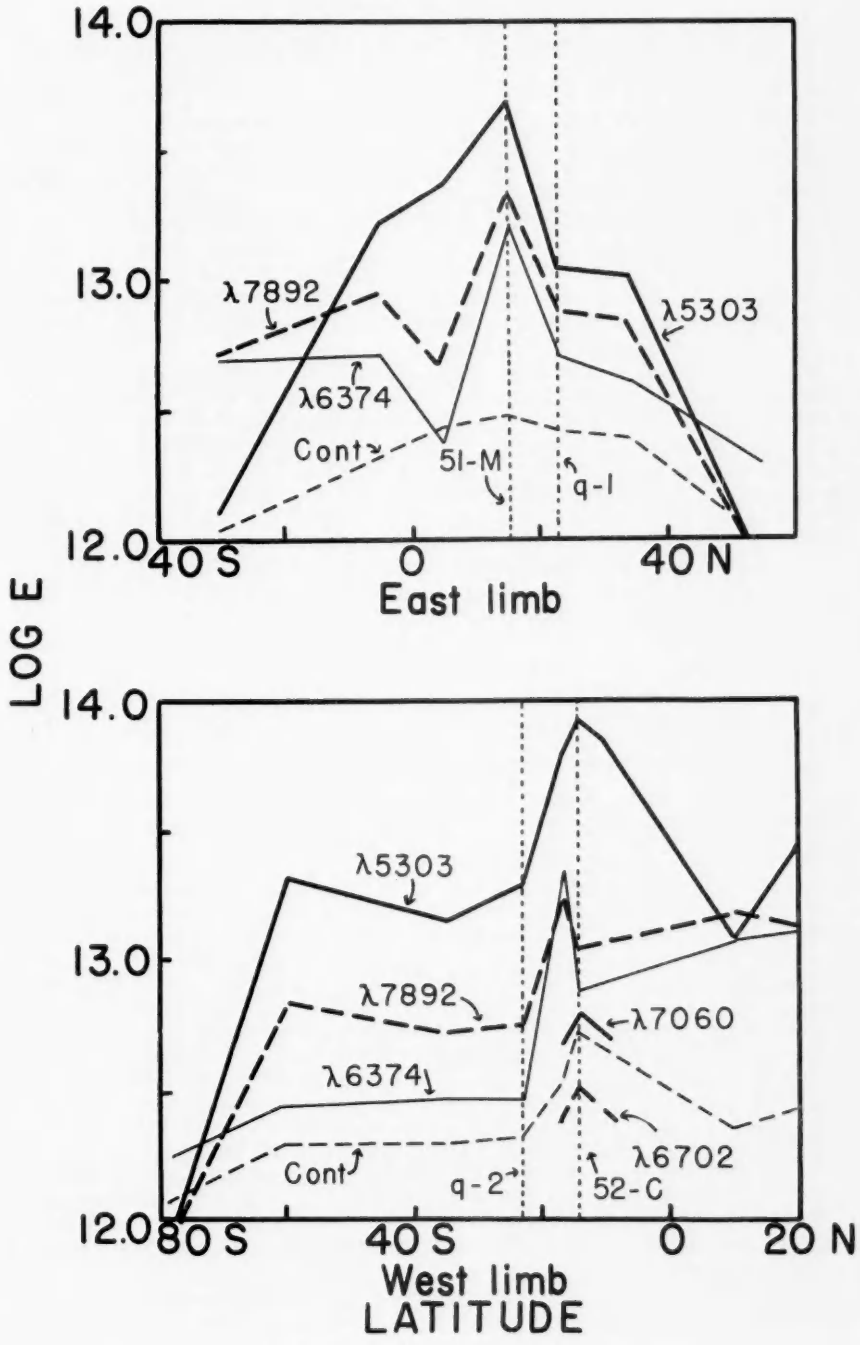

FIG. 1.—Intensities versus latitude

the lines, in Table 2. The correlation coefficients for various combinations of lines and continuum are given in Table 3. The coefficients were computed from the values of log E. The coefficients computed from E would be different, but the trends would be the same. For these data the correlation coefficients between line and continuum intensities increase as the ionization potential increases, and the correlation coefficients between line pairs increase as the difference in ionization potential decreases. The latter result is well known and expected a priori. Menzel (1946) pointed out that a visual inspection of eclipse spectrograms showed a stronger correlation between λ 5303 and the continuum

TABLE 2

LINE AND CONTINUUM INTENSITIES*

Position Angle (Degrees)	log E				$(E_L/E_{L'})$			$W=(E_L/E_C)$		
	Cont., λ 6375	λ 5303	λ 6374	λ 7892	λ 5303/ λ 6374	λ 5303/ λ 7892	λ 7892/ λ 6374	λ 5303/ λ 5304	λ 6374/ λ 6375	λ 7892/ λ 7893
30 SE.	2.04	2.10	2.68	2.70	0.3	0.2	1.0	0.5	2.3	3.6
5 SE.	2.32	3.23	2.70	2.94	3.4	2.0	1.7	7.2	2.4	6.3
5 NE.	2.42	3.37	2.37	2.68	10.0	4.9	2.0	7.9	0.9	2.7
15 NE.†	2.47	3.67	3.21	3.31	2.9	2.3	1.3	14.0	5.5	10.0
23 NE.‡	2.41	3.05	2.70	2.88	2.2	1.5	1.5	3.9	2.0	4.5
34 NE.	2.40	3.02	2.60	2.85	2.6	1.5	1.8	3.7	1.6	4.2
55 NE.	2.00	<2.00	2.30	<2.00	< 0.5	.....	<0.5	.....	2.0	.....
21 NW.	2.41	3.45	3.09	3.12	2.2	2.1	1.1	9.8	4.8	7.7
10 NW.	2.35	3.07	3.07	3.16	1.0	0.8	1.2	4.6	5.2	9.8
11 SW.§	2.73	3.84	2.88	3.05	9.1	6.2	1.5	12.0	1.4	3.2
14 SW.	2.53	3.92	3.33	3.24	3.9	4.8	1.2	22.0	6.3	7.7
23 SW.‖	2.32	3.29	2.45	2.75	6.9	3.5	2.0	8.6	1.3	4.1
35 SW.	2.30	3.15	2.45	2.72	5.0	2.7	1.9	6.3	1.4	3.9
61 SW.	2.29	3.31	2.44	2.84	7.4	3.0	2.5	8.9	1.4	5.3
78 SW.	2.08	<2.00	2.10	<2.00	< 0.8	.....	<0.8	.....	1.0	.....
Average	2.39	3.27	2.77	2.94	4.0	2.7	1.5	8.9	2.7	5.9

* Add 10.00 to get log 10 of the intensity in ergs sec^{-1} for lines and ergs sec^{-1} A^{-1} for continuum for a slice of corona 1 cm wide.

† 51-M. ‡ q-1. § 52-C. ‖ q-2.

TABLE 3

CORRELATION COEFFICIENTS

λ 5303–Cont.	λ 6374–Cont.	λ 7892–Cont.	λ 5303–λ 6374	λ 5303–λ 7892	λ 6374–λ 7892
0.87	0.41	0.54	0.43	0.60	0.94

than between λ 6374 and the continuum; these measurements therefore confirm Menzel's observation. There is a suggestion from Figure 1 that the strong correlation between λ 5303 and the continuum may break down in high latitudes. This is evidenced mainly by the points at 55° N. on the east limb and 78° S. on the west limb. At these points both λ 5303 and λ 7892 showed strong decreases compared to λ 6374 and the continuum. Since the continuum arises mainly from electron scattering, it is very insensitive to temperature changes when the temperature is high enough completely to ionize hydrogen. The fact that λ 5303 correlated more strongly with the continuum than did λ 6374 or

λ 7892 suggests that λ 5303 is less sensitive to temperature changes than the other two lines. A possible explanation of this is that the average coronal temperature is near the value at which *Fe* XIV is the most abundant ion, so that a small percentage change in temperature produces a relatively small change in the concentration of *Fe* XIV atoms. The apparent breakdown of the correlation at high latitudes may be due to a general temperature decrease in high latitudes, as is suggested by the well-known trend toward a decrease in the ratio E_{5303}/E_{6374} in high latitudes.

It should be pointed out that the regions of high continuum intensity did not correspond to coronal streamers of any appreciable size. White-light pictures of the corona at the Khartoum eclipse taken by the Naval Research Laboratory show that the strong increase in the continuum intensity at 11° S. on the west limb (hereafter referred to as "region 52-C"; see Trotter and Roberts 1953) was confined mainly to the lower levels of the corona.

The line-intensity ratios showed rather large variations around the limb. The ratio E_{5303}/E_{6374} varied by a factor of 33 in the integrated emission. It must be remembered that these intensities are integrated both along the line of sight and from the moon's limb outward, and local changes in the emission will be strongly suppressed by the integration. Thus E_{5303}/E_{6374} probably changed by much larger factors in local areas. In view of this, changes in relative intensities are hard to interpret in terms of temperature changes, and doing so may lead to large errors.

It is well known that some regions of the corona show wide departures from average conditions. At 30° S. and 55° N. on the east limb and 78° S. on the west limb we found $E_{5303}/E_{6374} < 1$. At these latitudes the values of E_{5303} were somewhat uncertain, but the errors were not likely to be large enough to reverse this ratio. It is significant that the low values of E_{5303}/E_{6374} in these regions were caused more by decreases in E_{5303} than by increases in E_{6374} as compared to the continuum intensities. In one other region, 10° N. on the west limb, $E_{5303}/E_{6374} = 1$. In this region the abnormality seems to be caused mostly by an increase in E_{6374} rather than by a decrease in E_{5303}. At 5° N. on the east limb and in region 52-C there were abnormally large values of E_{5303}/E_{6374}. Again, these large ratios seemed to be caused primarily by decreases in E_{6374} rather than by increases in E_{5303}.

Region 52-C is of special interest because many of the high-excitation lines, λλ 6702, 7060, and 8024, appeared only in this region. The region first appeared at the east limb two weeks before eclipse (Trotter and Roberts 1953). Coronagraphic and disk observations reveal that it was precisely at the limb at eclipse and had exhibited substantial flare activity as it crossed the solar disk. It was the region of greatest activity on the sun during February, 1952, though this activity was moderate compared with that experienced earlier in the sunspot cycle. The yellow line λ 5694 appeared on the eclipse spectra only in this region. The continuum was abnormally intense in this region, indicating a large increase in density. However, both λ 7892 and λ 6374 were at distinct minima compared to adjacent regions. The fact that λ 5694 was at a maximum in this region, along with the lines of *Fe* XIV, *Fe* XV, and *Ni* XV of higher ionization potential, strongly suggests that it originates from an ion of high ionization potential. This is consistent with Edlén's (1942) identification of λ 5694 as *Ca* XV. Further evidence for the validity of this identification was recently given by Pecker, Billings, and Roberts (1954). Region 52-C also showed abnormal properties in the chromosphere. Some of these properties were pointed out by Athay, Evans, and Roberts (1953, 1954).

The wide variations in relative intensities around the limb make it difficult to give representative values for each line. If we average the intensities around the limbs, we obtain the relative intensities given in Table 4. The relative intensities in region 52-C are also given. The values agree reasonably well with those reported by other authors; however, there are some interesting differences. Van de Hulst (1953) adopted a set of relative intensities that represents the combined results of several authors. With $E_{5303} =$

100, he has $E_{6374} = 20$ and $E_{7892} = 15$. On the other hand, Lyot (1939) has $E_{6374} = 23$ and $E_{7892} = 24$ on the same scale. It is doubtful whether such comparisons indicate anything other than the well-known fact that the relative intensities change with both position on the limb and time. It is surprising, however, to find such large differences between E_{6374} and E_{7892}, since the ionization potentials differ by only 28 volts. Similar variations are found for E_{6702} and E_{7060}, where the ionization potentials differ by 32 volts. Again, van de Hulst has the order reversed compared to our results, with $E_{6702} = 4.5$ and $E_{7060} = 2.5$, whereas Lyot has the same order as ours, with $E_{6702} = 2.8$ and $E_{7060} = 3.3$. The equivalent widths given in Table 3 show similar differences when compared to the results of others. It should be remembered, however, that our intensities are integrated over height, and we are comparing the results to observations usually made at a given height.

III. INTENSITY VERSUS HEIGHT

We chose four regions for measuring the intensities of λ 7892 and λ 5303 as a function of the height of the moon's limb in the corona. Two of these regions were in active centers, and two were in regions of about average intensities. The active centers were located

TABLE 4

RELATIVE INTENSITIES

	Line					
	λ 5303	λ 6374	λ 7892	λ 7060	λ 6702	λ 5694
Average	100	25	37	.....	.....	.....
52-C	100	11	16	8	4.5	~1

at 15° N. on the east limb (hereafter referred to as "region 51-M"; see Trotter and Roberts 1953) and 11° S. on the west limb (region 52-C). The two "quiet" or "normal" regions were located at 23° N. on the east limb and 23° S. on the west limb. These regions will be referred to as "q-1" and "q-2" respectively. Regions q-1 and q-2 were selected for the following reasons: (1) both were at the line of contacts, and, therefore, the integration over height was along radial lines. (2) Region q-1 is at the same position at which most of our chromospheric line measurements were made (Athay, Billings, Evans, and Roberts 1954). A detailed analysis of this region in the chromosphere, based on both line and continuum intensities, is being prepared for publication, and the behavior of the corona in this region is of interest in connection with the chromospheric model obtained. (3) The isophotes of the green line λ 5303 obtained from coronagraph observations at Climax and Sacramento Peak (Trotter and Roberts 1953) showed that on the day of the eclipse the emission at these latitudes was more intense at the longitudes at the limb than it was at longitudes on either side of the limb. This is of importance in insuring that the observed emission is representative of the regions above the limb rather than of those at some other point in the line of sight.

In order to reduce random errors as much as possible, we measured the line intensities on all spectrograms on three different occasions and averaged the results. At low heights, where the lines were fairly intense, the random errors due to all the reduction processes were less than ± 0.08 in log E. At large heights, where the intensities were approaching the sensitivity of the films, the dispersion between repeated measurements was sometimes as high as ± 0.20 in log E. By averaging the results, we considerably reduced the random errors in the reduction process.

a) λ 7892 IN REGIONS q-1 AND q-2

The final values of log E_{7892} in regions q-1 and q-2 were plotted against height in Figure 2. The data were not accurate enough to give the detailed shapes of the log E_{7892}–versus-height-curves. However, the straight-line representations used in Figure 2, with slightly different slopes for the two regions, appear to be good approximations. We hoped to determine from the data in Figure 2 the height at which the surface brightness, F, of the corona was at maximum intensity. In terms of our intensities, $F = 2.303\ E\ d\ \log\ E/dh$. Hence, in order to have a maximum in F, there must be a decrease in $d\ \log\ E/dh$ at low heights. The data in Figure 2 show clearly that, if such a decrease occurred, it occurred below 10,000 km, and we conclude that the maximum surface brightness in λ 7892 was below 10,000 km. There are two possible interpretations of this result: (1) either regions below 10,000 km actually emitted with relatively strong intensity per unit volume, or (2) most of the observed emission at these apparent eclipse heights comes from higher levels in the corona that lie either before or beyond the limb but along the line of sight.

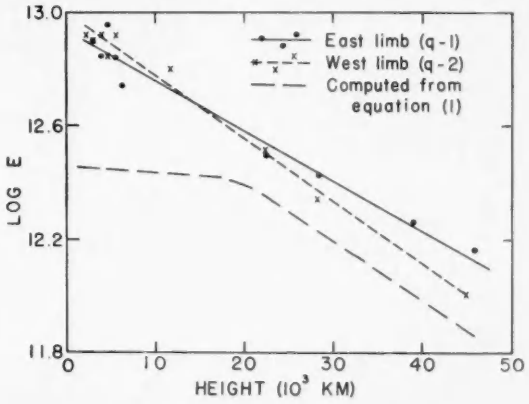

FIG. 2.—Intensities of λ 7892 versus height

We selected regions q-1 and q-2 in such a way as to insure that the emission from a given volume above the limb was stronger, or at least as strong, as the emission from similar volume elements in adjacent longitudes. Thus we can safely ignore the possibility of any localized centers of intense emission in the line of sight, and the second alternative stated above is actually very improbable.

A simple calculation demonstrates the improbability of the second alternative. In this calculation we computed the shape of the curve that would be observed if the coronal emission were of the form

$$\epsilon = \epsilon_0 \exp\left[-\beta(h - h_0)\right] \quad (h \geq h_0),\ \epsilon = 0 \quad (h < h_0)\ , \tag{1}$$

where ϵ is the emission per cubic centimeter. The observations give $\beta \sim 5 \times 10^{-10}$ cm^{-1}. The computed curve for $h_0 = 20{,}000$ km (the assumption that no emission originates below 20,000 km) is shown in Figure 2. There is a well-defined knee at h_0. However, h_0 determines only the position of the knee and not the general shape of the curve. If such a knee were present at a height above 10,000 km, it would be shown by the data. The conditions expressed by equation (1) are rather extreme, but the actual emission must be approximately of that form. The lack of any marked tendency for a knee in the ob-

served curves in Figure 2 requires that the maximum in ϵ occur below 10,000 km, as stated by the first alternative given above.

Petri (1952) has analyzed five years of coronagraphic observations of λ 5303 made by Muller. He found a statistical maximum in F_{5303} at ~18,000 km. The maximum in F_{5303} should be statistically the same as the maximum in ϵ_{5303}. Since λ 5303 is from *Fe* XIV with a much higher ionization potential than *Fe* XI, the source of λ 7892, and since the state of ionization most likely increases with height in the lower part of the region in question, the maximum in ϵ_{5303} is expected to occur at a greater height than the maximum in ϵ_{7892}. There is also the possibility that the height of maximum intensity varies throughout the sunspot cycle. H. D. and H. W. Babcock (1934) observed λ 5303 and λ 6374 in the chromospheric spectrum outside of eclipse, which also suggests that much of the emission originates at low heights; but it is possible that they may have observed regions in the line of sight that were not at the limb. The statement, sometimes found in textbooks (Aller 1953) and often quoted by astronomers, that the coronal emission lines are not observed below 5 minutes of arc above the limb is, however, highly dubious and certainly in conflict with our result.

The presence of coronal line emission at heights below 10,000 km indicates that a substantial part, if not all, of the increase in temperature between the photosphere and the

TABLE 5

$\Delta \log E = \log [E(3000 \text{ KM})/E(46{,}000 \text{ KM})]$

	Region			
	q-1	q-2	51-M	52-C
$\Delta \log E_{7892}$	0.75	0.90	0.79	0.12
$\Delta \log E_{5303}$	.17	.13	.53	.38
$\Delta \log E_{C}$	0.30	0.26	0.27	0.42

corona occurs below 10,000 km. This is in agreement with the large positive temperature gradient and the high temperatures in the upper chromosphere that were found by Athay, Pecker, Thomas, and Menzel (1954) from the continuum data. The maximum height of the observed *Hα* emission on our spectra of the Khartoum eclipse was ~8000 km. However, above a height of ~5500 km all the remaining chromospheric lines showed a distinctly nonuniform structure, as shown by the reproductions of some of the chromospheric lines in Figure 3. We interpret this nonuniformity as spicule activity in the upper chromosphere. Between the spicules there is very little if any chromospheric line emission. The coronal line emission apparently begins to be important near the top of the chromosphere, perhaps even in the regions between the spicules. A further implication of the presence of coronal line emission near the top of the chromosphere is that the spicules extending above the average top of the chromosphere and emitting *Hα* radiation must be cold in comparison with the surrounding regions, as was suggested earlier by Thomas (1948).

b) RELATIVE LINE AND CONTINUUM CHANGES

In Table 5 we give the observed changes in intensity between 3000 and 46,000 km for λ 7892, λ 5303, and the continuum. The continuum intensities are integrated over the same slice of atmosphere as the lines. We can use the data in Table 5 to determine some of the characteristics of the temperature structure of the corona in these regions if we make a few plausible assumptions. If we knew that the changes in intensity occurred uniformly throughout the entire height range indicated, the interpretation would be

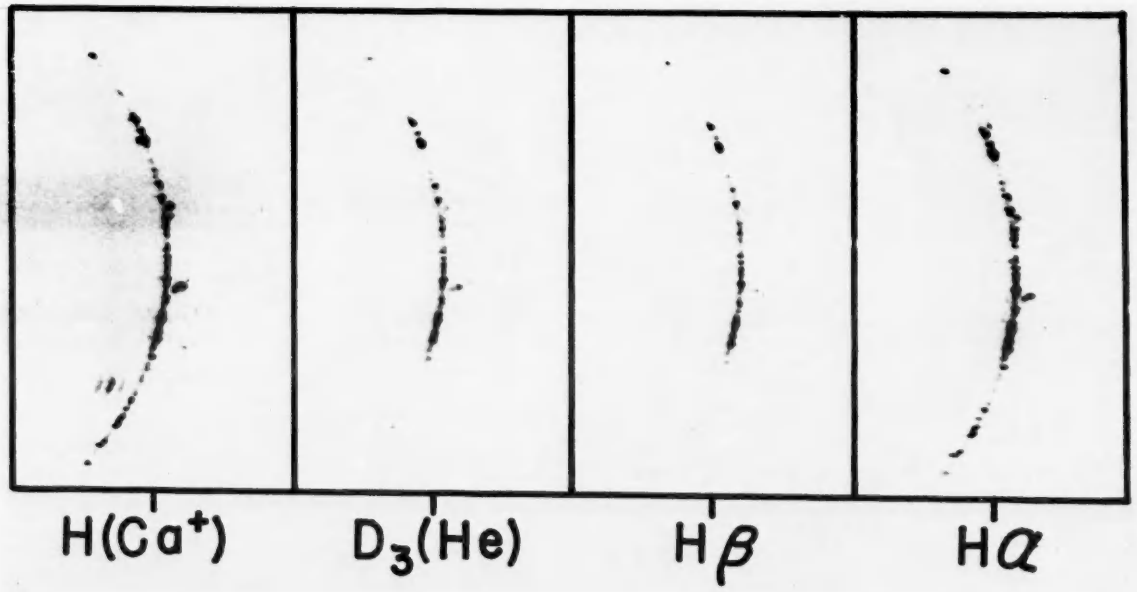

FIG. 3.—Reproductions of chromospheric lines on slitless spectrograms. H (Ca^+) was reproduced from a visible spectrogram with the height of the moon's limb at 6300 km, D_3 (He) and $H\beta$ from a visible spectrogram at 5500 km, and $H\alpha$ from an infrared spectrogram at 6300 km.

straightforward. However, the intensities in Table 5 may be constant over the lower part of the height range with all the changes in log E coming in the higher layers. We know from our discussion of Figure 2 that the emission in λ 7892 in regions q-1 and q-2 has maxima somewhere below 10,000 km. For purposes of the following discussions we assume that the maxima in λ 7892 in regions 51-M and 52-C are also below 10,000 km and that the maxima in λ 5303 occur somewhere below 18,000 km in all four regions. Actually, for our present interpretation, our assumptions need be that strict only in region 51-M, as an inspection of Table 5 will show. If we make the above assumptions, the data in Table 5 show that the ratio E_{5303}/E_{7892} increases with height in regions q-1, q-2, and 51-M and decreases with height in 52-C. The theory of coronal ionization (Woolley and Allen 1948; Shklovsky 1951) predicts that the relative line intensities will be a function of T_e only. Therefore, it appears reasonable to assume that the increase in E_{5303}/E_{7892} in regions q-1, q-2, and 51-M indicates an increase in T_e, and the decrease in E_{5303}/E_{7892} in 52-C indicates a decrease in T_e. These temperature gradients, however, apply only to the intervals between the maxima in λ 5303 and 46,000 km and not necessarily to lower heights.

It is of further interest to compare the observed changes in line intensities to the changes in continuum intensities. The intensity in a line can be written, assuming collisional ionization, electron-capture recombination with emission of radiation and collisional excitation (Woolley and Allen 1948),

$$E_L \propto \int_h^\infty \int_{-\infty}^\infty N_e^2 f(T_e)\, dy dx\,, \tag{2}$$

and the continuum intensity can be written

$$E_C \propto \int_h^\infty \int_{-\infty}^\infty N_e dy dx\,, \tag{3}$$

where y is the co-ordinate in the line of sight and x is the co-ordinate measured perpendicular to y along a solar radius. The data in Figure 2 show that E_{7892} is approximately exponential with height. A study of the continuum data in region q-1 (Athay, Pecker, Thomas, and Menzel 1954) also showed an approximately exponential decrease with height over the interval 5000–46,000 km. If we assume that the line and continuum intensities in all four regions are, to a first approximation, adequately represented by exponential functions of height, then

$$\Delta \log E_L = \Delta \log [N_e^2 f(T_e)] \tag{4}$$

and

$$\Delta \log E_C = \Delta \log N_e\,. \tag{5}$$

For an isothermal atmosphere, equations (4) and (5) give $\Delta \log E_L = 2\Delta \log E_C$, and, if a temperature gradient exists, $\Delta \log E_L - 2\Delta \log E_C = \Delta \log f(T_e)$. By comparing the values of $\Delta \log E_L$ and $\Delta \log E_C$, we should be able to determine the effect of $f(T_e)$ on the line intensities. We again make the same assumptions about the heights of maximum emission in λ 7892 and λ 5303 that were stated in the preceding paragraph. The data in Table 5 show $\Delta \log E_{5303} < 2\Delta \log E_C < \Delta \log E_{7892}$ in regions q-1 and q-2. Thus in these regions $f(T_e)$ causes an increase in E_{5303} with height and a decrease in E_{7892}. Since the line emission will go through maxima at higher values of T_e for higher stages of ionization, the above results can occur only if T_e is increasing with height and is between the limits where $f(T_e)$ has maxima for λ 7892, $T(7892)$, and λ 5303, $T(5303)$. The sign of the temperature gradient in these regions is in agreement with that obtained from the changes in E_{5303}/E_{7892}. In region 51-M $\Delta \log E_{5303} \sim 2\,\Delta \log E < \Delta \log E_{7892}$. This requires that T_e increase with height with $T_e \sim T(5303)$. This is also in agreement with the tempera-

ture gradient obtained from the changes in E_{5303}/E_{7892} in this region. In region 52-C $\Delta \log E_{5303} < 2\ \Delta \log E > \Delta \log E_{7892}$, and $f(T_e)$ causes an increase in both E_{5303} and E_{7892}. This is compatible with the decrease of T_e with height that was obtained from the decrease of E_{5303}/E_{7892} if $T_e > T(5303)$. Further evidence for a high T_e in this region comes from the abnormally large values of E_{5303}/E_{7892} and E_{5303}/E_{6374} and the presence of λλ 5694, 6702, 7060, and 8024, all of which are from ions of high ionization potential.

The ionization equations used by Woolley and Allen (1948) and Shklovsky (1951) give $T(7892) = 6.4 \times 10_5{}^\circ$ K and $T(5303) = 1 \times 10^6{}^\circ$ K. However, Werner (1954) obtained $T(5303) \sim 2 \times 10^6{}^\circ$ K from similar considerations, but with improved values of the recombination coefficients. Line-profile measurements consistently give $T_e \sim 2 \times 10^6{}^\circ$ K for average coronal regions (Billings, Pecker, and Roberts 1954), and, since the strong correlation between the continuum intensities and λ 5303 suggests that $T_e \sim T(5303)$, the value given by Werner may be more nearly correct.

We conclude from the above discussions that the quiet coronal regions below 46,000 km had temperatures between the values where *Fe* XIV and *Fe* XI are the most abundant ions of iron, and temperature increased with height in these regions. The two active regions studied were found to be regions of higher electron density and higher temperature than the two quiet regions. The highest temperature and density were found in the youngest active region. In this region the temperature was above the value at which *Fe* XIV is the most abundant iron ion. Similar concepts of active regions were arrived at by Piddington and Davies (1954) from a recent study of radio noise data.

The work reported in this paper was supported in part by the Office of Naval Research and in part by the Geophysics Research Directorate, Air Force Cambridge Research Center. The work was carried out in co-operation with the Naval Research Laboratory.

REFERENCES

Aller, L. H. 1953, *Astrophysics* (New York: Ronald Press Co.).
Athay, R. G., Billings, D. E., Evans, J. W., and Roberts, W. O. 1954, *Ap. J.*, **120**, 94.
Athay, R. G., Evans, J. W., and Roberts, W. O. 1953, *Observatory*, **73**, 244.
———. 1954, *A.J.*, **59**, 182.
Athay, R. G., Pecker, J.-C., Thomas, R. N., and Menzel, D. H. 1954, paper presented at meetings of American Astronomical Society, Ann Arbor, Michigan, *A.J.*, **59**, 314.
Babcock, H. D., and Babcock, H. W. 1934, *Pub. A.S.P.*, **46**, 132.
Billings, D. E., Pecker, C., and Roberts, W. O. 1954, paper presented at meetings of American Astronomical Society, Ann Arbor, Michigan, *A.J.*, **59**, 316.
Edlén, B. 1942, *Zs. f. Ap.*, **22**, 30.
Lyot, B. 1939, *M.N.*, **99**, 580.
Lyot, B., and Dollfus, A. 1953, *C.R.*, **237**, 855.
Menzel, D. H. 1946, *A.J.*, **52**, 47.
Pecker, C., Billings, D. E., and Roberts, W. O. 1954, *C.R.*, **238**, 1101.
Petri, W. 1952, *Forschungsber. Obs. Wendelstein*, Vol. **2**.
Piddington, J. H., and Davies, R. D. 1954, *M.N.*, **113**, 582.
Shklovsky, I. S. 1951, *Izvest. Krymsk. Ap. Obs.*, **6**, 105.
Thomas, R. N. 1948, *Ap. J.*, **108**, 130.
Trotter, D. E., and Roberts, W. O. 1953, *HAO-NBS Report No. 15* (February 15, 1953), available from High Altitude Observatory, Boulder, Colorado.
Van de Hulst, H. C. 1953, in G. P. Kuiper (ed.), *The Sun* (Chicago: University of Chicago Press).
Werner, A. 1954, *Australian J. Phys.*, **7**, 25.
Woolley, R. v. d. R., and Allen, C. W. 1948, *M. N.*, **108**, 292.

THE PHYSICAL THEORY OF METEORS. VII. ON METEOR LUMINOSITY AND IONIZATION*

FRED L. WHIPPLE
Harvard College Observatory
Received July 21, 1954

ABSTRACT

The relative frequencies of occurrence of radio and bright photographic meteors suggest either (*a*) that the ratio of meteoric ionization to luminosity varies as (velocity)^2 or (*b*) that there exists a surprising dependence of particle size upon orbital characteristics. The writer prefers the first alternative, which leads to about a (velocity)^5 law for the ionizing efficiency per gram. An order-of-magnitude deficiency in radio meteors at velocities above 60 km/sec may well arise from a suppression of radio-velocity measures for faint meteors above an altitude of about 110 km by rapid diffusion of the ion column. Meteor ionization, like a persistent meteor train, probably also decays extremely rapidly below about 82 km. The combined effects of rapid electron diffusion at high altitude and decay at lower altitudes would reduce the slope of the mean height-velocity curve for radio meteors as compared to photographic meteors. In this manner, conflicting data concerning the efficiencies of ionization versus luminosity for meteors may be reconciled.

The Harvard Photographic Meteor Project (Whipple 1954) has derived 144 meteor velocities by double-station photography with small cameras in Massachusetts and in New Mexico through 1951. The photographs have been analyzed largely under the direction of L. Jacchia (1952) at the Numerical Analysis Laboratory of the Massachusetts Institute of Technology under the sponsorship of the U.S. Office of Naval Research and the U.S. Army Office of Ordnance Research. These photographic determinations of velocity are now sufficiently numerous to allow a preliminary statistical comparison with those obtained by radio techniques, for the purpose of possibly determining the velocity dependence of a meteor's ionization as compared to its photographic radiation. The radio data used here were obtained at a frequency of 30.02 Mc/sec by D. W. R. McKinley (1951*a*), at Ottawa, Canada.

The Geminid and the Perseid meteor showers were eliminated from both sets of data, reducing the photographic material to 115 meteoric velocities, of which 64 have been allocated to showers and 51 remain sporadic. The radio data were reduced correspondingly by the omission from McKinley's data of his Tables A2 (Geminids) and A11 (Perseids). Table A16 was omitted because of incompleteness. The radio data were further reduced from 10,933 determinations to about one-third that number by a selection of meteors observed between the limits of evening and morning twilight, measured in terms of the local mean time. The distribution of the photographic meteors by months of the year is shown in Table 1. Because the sensitivity of radios is rather variable from time to time and because the photography of meteors has been concentrated in the winter months of long nights, the numbers of radio meteors in the night intervals were further weighted per month proportionally to the number of photographic meteors observed. The third column of Table 1 indicates McKinley's tables of radio velocities adopted each month, all tables in each month being given equal weight after being corrected to a standard number of meteors per table.

The adjusted frequencies of radio meteors are given in the third column of Table 2, for which the argument is the velocity range, in kilometers per second, shown in the first column, with mean velocities adopted in the second column. The velocity limits set by

* An investigation carried out partly with the U.S. Office of Naval Research and the U.S. Army Office of Ordnance Research.

McKinley were used in this compilation, although his separation of divisions occurs at velocities approximately 0.5 km/sec smaller than the present limits. This choice was made because the radio velocities had not been corrected for deceleration in the earth's atmosphere, as were the photographic velocities. The deceleration correction for radio meteors will be discussed later. It is of considerable interest to note that the radio distribution of velocities without the elimination of daylight meteors and without the weighting per month gives almost identically the distribution shown in Table 2.

The velocity frequencies of the 115 photographic meteors appear in the fourth column of Table 2 on a percentage basis. The common logarithm of the ratio of radio to photographic frequencies is given in the fifth column, while the sixth column lists the deviations from the arbitrary relation.

TABLE 1

SEASONAL DISTRIBUTION OF METEOR VELOCITIES

Month	No. Phot. Meteors	McKinley Tables	Month	No. Phot. Meteors	McKinley Tables
January	7	A17	July	3	A7, A8, A9
February	5	A17, A18	August	15	A10, A12
March	10	A19	September	2	A13
April	7	A4	October	16	A14
May	2	A5	November	22	A14, A15
June	4	A6	December	22	A15, A17

TABLE 2

METEOR VELOCITY DISTRIBUTIONS

Velocity Range (Km/Sec)	Mean Velocity (Km/Sec)	Radio (Per Cent)	Phot. (Per Cent)	$\log_{10}$ (Radio/Phot.)	$\Delta \log_{10}$ (Radio/Phot.) O−C
10–20	16	1.6	13	−0.90	+0.01
20–30	25	13.5	31	− .37	− .03
30–40	34	26.7	22	+ .09	+ .05
40–50	44	21.1	9	+ .38	+ .03
50–60	55	16.5	5	+ .50	− .14
>60	67	20.6	20	+0.01	−0.89
Sum		100.0	100		

$$\log (\text{rad.}/\text{phot.}) = -4.37 + 2.88 \log V \qquad (1)$$

where V is the velocity in kilometers per second. This equation appears as a straight line in Figure 1, where the logarithmic frequency ratio is plotted as a function of $\log V$.

The meteor frequency ratios in Table 2 and Figure 1, to be entirely comparable, should be corrected to a common height and for observational effects of velocity. If we neglect the effect of velocity, the height (h) dependence of sensitivity should vary roughly as $1/h$ photographically and $1/h^3$ for radio. The area of the sky covered by radio antennae varies roughly as h^2, however, while for doubly photographed meteors the dependence is not very uniform and is somewhat complicated because of the overlapping of two observational cones from the two stations. The cones were generally directed at rather high

altitudes. The correction can safely be omitted from the photographic meteors, making the height corrections roughly equal for the two methods of observation. The velocity selection for photographic meteors, on the other hand, favors slower meteors as the inverse angular velocity, h/V. There appears to be no such correction for the radio meteors observed by McKinley. Thus the coefficient of log V in equation (1) should be reduced to about 2.

On a comparable observational basis for radio and photographic meteors, we find, then, from the preceding paragraph and equation (1), that in the range of velocities up to 50 km/sec *the ratio of the number of radio to photographic meteors increases about as the square of the velocity.* Even though the statistics are weak in the range $40 < V < 60$ km/sec, the relation is clearly indicated. Above $V = 60$ km/sec, there appears to be a

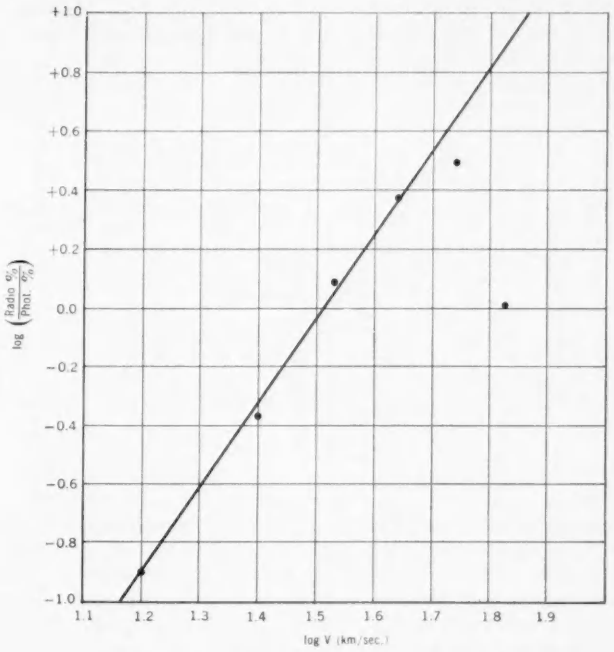

FIG. 1.—Meteor frequency ratios versus velocities

clear-cut deviation, in the sense that radio meteors are about an order of magnitude less frequent than the relation demands.

A comparable conclusion can be drawn from the radio-meteor velocities observed by the group at Manchester, England, and presented by M. Almond, J. G. Davies, and A. C. B. Lovell (1952). In their Figure 1, which shows the measured velocity distribution for the observations in 1950, near the apex of the earth's motion, a remarkable deficiency of meteors is shown in the range above 65 km/sec, as compared with the prediction based on the assumption of uniformly distributed parabolic meteors. The Manchester observations are made at a radio frequency of about 72 Mc/sec. The photographic observations indicate that the high-velocity meteors near the apex are very nearly randomly distributed, in so far as orbital characteristics about the sun are concerned, and that their velocities lie close to the parabolic limit.

Now the photographic meteors discussed here are generally brighter than zero magnitude visually, while the radio meteors correspond to much fainter magnitudes, mostly in the range fourth to fifth, with a limit near the seventh or the eighth. One might be tempted to ascribe the velocity relationships to some peculiarities in the relative distribution of particle sizes according to orbits among the bright and faint meteors. The velocities of fainter meteors photographed with the Baker-Super-Schmidt cameras in New Mexico, discussed below, show, however, much the same frequency distribution as the brighter ones, although the selection is not quite random.

In our present ignorance concerning the detailed physical processes in meteors, the writer believes that it is safer to adopt the working hypothesis that the orbital distribution of meteoroids is independent of dimension over the range involved (less than one order of magnitude) and to ascribe the effects here discussed to physical causes. This belief is strengthened by the writer's lack of success in searching for observational evidence indicating systematic orbital effects dependent on meteor brightness among shower meteors. Theoretical calculations (in preparation) do indicate, however, that meteoroids within the size range of this discussion are, in the main, eliminated finally from the solar

TABLE 3

MEAN HEIGHTS OF RADIO METEORS

MANCHESTER		OTTAWA	
V (Km/Sec)	h (Km)	V (Km/Sec)	h (Km)
22.5	88.1	35.5	91.6
27.5	89.7	40.5	93.9
32.5	92.3	46.5	95.7
37.5	93.8	60.0	99.3
42.5	96.6		
47.5	96.3		
53.0	99.6		

system by collision with zodiacal particles. Just possibly, the reduced relative numbers of fast radio meteors actually reflect such an attenuation for the faster and smaller retrograde particles. Let us now look at the physical evidence and arguments.

The mean heights of brighter radio meteors as a function of velocity are presented in Table 3; the Manchester data are by Evans (unpublished) as presented by T. R. Kaiser (1953), while the Ottawa data are by D. W. R. McKinley and P. M. Millman (1954).

Dr. L. Jacchia has kindly made available recently reduced heights obtained from photographs made with the Baker-Super-Schmidt meteor cameras of the Harvard Meteor Project. The first four columns of Table 4 contain, for 75 meteors, the means of velocity, beginning height, height at maximum light, and end height. The last two columns contain the number in each sample and the mean visual magnitude at maximum light. To show the dependence of height on magnitude for the Super-Schmidt photographic meteors, Figure 2 depicts the beginning and end heights of those meteors with velocities exceeding 60 km/sec. The mean heights of the radio meteors at Manchester and Ottawa have been extrapolated to the mean velocity of 67.2 km/sec for comparison purposes.

The Super-Schmidt photographic meteor heights of Table 4 and the mean radio-curve from Table 3, as derived by Millman, are plotted in Figure 3. In a private communication, Millman and McKinley state that the visual magnitudes of the radio meteors in Table 3 are much brighter than those for which the velocities have been determined,

i.e., in the range of -0.5 to $+1$ mag. and comparable to the Super-Schmidt photographic meteors. Figure 3 shows clearly that the slope of the height-velocity–curve is steeper for the photographic meteors than for the radio meteors, whether the comparison is made with heights at the beginning, mean, maximum light, or end. Nevertheless, the mean heights of the radio meteors lie well within the mean photographic range. If the photographic heights were corrected to apply at a constant visual magnitude, the curve would become still steeper and the radio-photographic discrepancy larger.

The slope of the height-velocity–curve is, in fact, a measure of the luminous or ionizing efficiency of the meteoric process. A steep slope indicates a high positive dependence of the efficiency upon velocity, since the slower meteoroids must be larger and penetrate more deeply into the atmosphere to give luminosity or ionization comparable to that from faster meteoroids. Indeed, Kaiser (1953) has recently used this small slope for the radio meteors as evidence that the ionization efficiency per gram of meteoroid is independent of velocity. Earlier, J. A. Clegg (1952) and Kaiser and Closs (1952) reached the same conclusion. On the other hand, the Harvard bright and faint photographic meteors indicate about a V^1 dependence for the luminous efficiency, measured in terms

TABLE 4

HEIGHTS FOR SUPER-SCHMIDT METEORS

V (Km/Sec)	h Beg. (Km)	h Max. (Km)	h End (Km)	No.	Max. Mag. (Vis.)
17.0	90.0	81.2	77.8	10	+2.4
25.5	96.6	87.3	82.7	17	+2.1
33.3	100.0	85.2	79.9	12	+0.7
44.2	102.0	93.9	88.9	13	+1.2
58.6	108.7	99.4	95.0	10	+0.8
68.6	115.6	102.9	97.1	13	+0.5

of luminous to kinetic energy or about V^3 measured per gram. From the early arguments of this paper, the ionization efficiency per gram should then vary about as V^5, if we accept F. G. Watson's (1941) inverse relation between meteoric luminosity and numbers. W. Liller (1949) and D. W. R. McKinley (1951*b*), indeed, have found evidence for such an increase, although Kaiser (1953) has criticized McKinley's conclusion. We have, then, a specific contradiction in our a priori interpretation of the data given by Figures 1 and 3. We cannot resolve the contradiction by assuming a space loss of faster meteoroids in the fainter radio region without tampering similarly with the slow ones in small orbits. Another approach is needed.

Let us first consider the relative deficiency of fast, faint radio meteors. Whether or not ionization actually occurs copiously at extreme altitudes, diffusion may well inhibit radio observation at these altitudes. The Manchester investigators have given considerable attention to this problem of diffusion in meteoric trails. In the altitude range near 90 km, J. S. Greenhow and G. S. Hawkins (1952) and T. R. Kaiser and R. L. Closs (1952) have settled on a value of the diffusion coefficient, D, of 3×10^4 cm^2/sec, as adequate to explain the observed durations of radio meteors. In the simple theory

$$D = \tfrac{4}{3} l_i v_i , \tag{2}$$

where l_i is the mean free path of ions and v_i is their mean speed.

If we assume that mean free paths of ions do not differ markedly from neutral molecules, then the Rocket Panel (1952) atmosphere gives $l_i = 4.5$ cm at 95 km. The mean speed of heated ions must exceed the speed of the atmospheric molecules, i.e., must

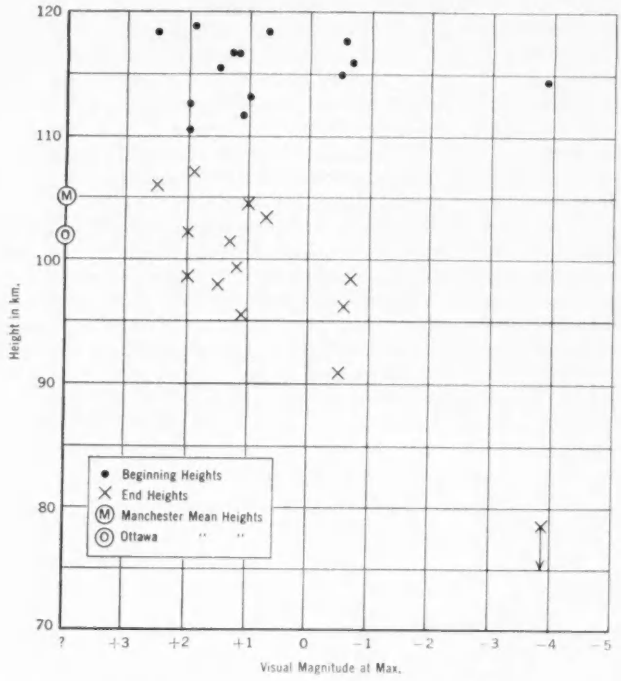

FIG. 2.—Height of Super-Schmidt meteors versus maximum visual magnitude. Velocity > 60 km/sec

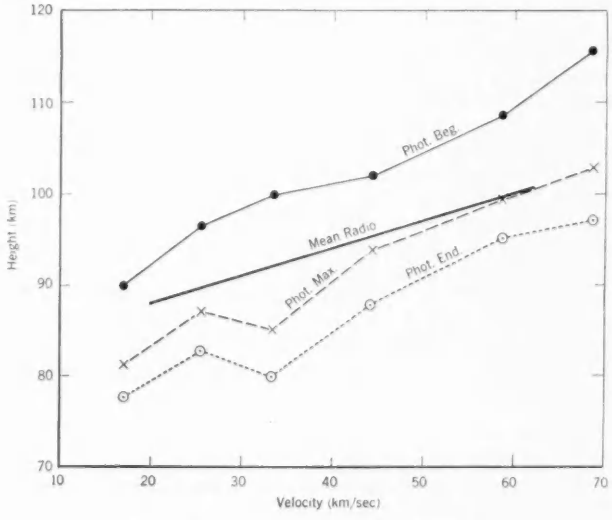

FIG. 3.—Height versus velocity for meteors

exceed about 3×10^4 cm^2/sec. Hence the adopted value of D seems small, but perhaps acceptable to an altitude of 95 km. By 110 km, however, the mean free path will have increased by an order of magnitude, and $D = 3 \times 10^4$ cm^2/sec becomes an incredibly small value.

An increase of the diffusion coefficient by 10 or more times will seriously curtail the durations of faint radio meteors, by the same factor. Thus the column of ionization will spread rapidly enough to prevent the measurement of velocity for low values of electron density and correspondingly increase the limiting dimensions of detectable meteoroids. Kaiser and Closs (1952) have discussed quantitatively the effects of very short duration on velocity determinations.

It appears, then, from the foregoing argument and the preliminary observations that the fainter radio meteors may be appreciably suppressed in the altitude range above about 110 km. Perhaps only the lower fringe of the altitude-frequency distribution can be observed except among the larger meteoroids. The effect can easily be velocity-sensitive enough to account for the results of Figure 1 for $V > 60$ km/sec and still not

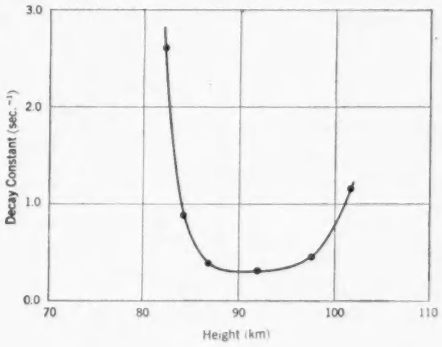

FIG. 4.—Decay constant versus height

affect appreciably the height data of Figures 2 and 3 for brighter meteors. If we accept this explanation and a high dependence of ionization upon velocity, we must account for the small slope of the height-velocity line applying to bright radio meteors in Figure 3. Since the upper end of the curve to 60 km/sec is not much affected by the diffusion, some effect must be raising the mean heights of the slower radio meteors. The most obvious physical effect is rapid recombination of the electrons produced by the increased atmospheric density at lower altitudes.

Direct evidence for some type of recombination effect at an altitude of about 81–82 km is afforded by persistent meteor trains. Visual trains of longer duration are limited, according to C. C. Trowbridge (1907), to an altitude range of 81–113 km. Exactly the same limits have been found in photographic meteor trains by Liller and Whipple (1954). For one photographic train, the rate of decay has been measured as a function of height. On the basis of a decay law of the form $(1 + kt)^{-2}$, where t is the time in seconds, the observed values of k are reproduced in Figure 4. The rate of decay increases extremely rapidly with decreasing height below about 85 km. Now Millman (1950) has shown that the durations of meteor trains and meteor ionization are intimately connected and that both exhibit the same dependence on meteoric velocity. Hence a measure of train decay may justifiably be taken as a measure of ionization decay or, at lower altitudes, electron attachment plus recombination. Thus we may expect velocity measures of fainter meteors to become more difficult at altitudes near or below about 82 km.

If, then, the ionization efficiency of meteoroids varies as a fairly high power of the velocity, as indicated by Figure 1, the slower radio meteors will be relatively brighter photographically and visually than faster ones. As a consequence, a relatively greater number will be detected photographically than by radio. Let us now predict on the basis of our postulates. Among radio meteors of moderate brightness, such as those of Figure 3, the mean heights of the slower ones should be raised by the electron decay at lower altitudes. Hence the slope of the height-velocity line should appear spuriously flat. Among fainter radio meteors, the heights of the slower ones should be little affected, but the heights of the faster ones should be depressed by diffusion at great altitudes, producing much the same result on the height-velocity–curve. Only among the extremely bright radio meteors, whose velocities are measured by the head echo alone (if such an effective echoing area exists), should the heights agree at all velocities with similar photographic meteors. Numerical calculations based on our postulates can well await the observational confirmation of these predictions.

If fast, faint radio meteors are suppressed at high altitudes and the slow, brighter ones at low altitudes, the effects should be apparent in the measured velocities of shower meteors. The data are not adequate for a thorough velocity comparison with the more

TABLE 5

COMPARISON OF RADIO AND PHOTOGRAPHIC VELOCITIES

Shower	Radio Velocity (Km/Sec)	Phot. Velocity (Km/Sec)	Per Cent Diff. Velocity	Per Cent ΔV and Position in Trail
Quadrantids	40.9	44.1	7	.....
δ Aquarids	40.3	43.0	6	4 0.90
Perseids	60.5	60.44	0	1 .60
Geminids	35.3	36.44	3	3 0.76

accurate photographic determinations, but the available data for four showers are compared in Table 5. The fourth column gives the percentage differences of the mean photographic velocities of the third column *minus* the mean radio velocities of the second column for the showers of the first column. The radio data, uncorrected for atmospheric deceleration, are taken from Millman (1954) and the photographic data, corrected for deceleration, from Whipple (1953) for the Quadrantids and Geminids; from F. W. Wright and F. L. Whipple (1953) for the Perseids; and from Wright, Whipple, and Jacchia (1954) for the δ Aquarids. Only a single photographic Quadrantid makes the comparison for this shower of low significance. The velocity differences in Table 5 should represent the deceleration of radio meteors by the atmosphere above the point of observation. The fifth column contains the mean measure of the relative position along the photographic trail at which the velocity is reduced by the percentage listed beside it. These data do not allow a positive conclusion but do suggest an eventually fruitful method of checking our postulates.

Other effects than diffusion can undoubtedly suppress ionization and also radiation at great altitudes for very fast meteors. In the preceding paper of this series, A. F. Cook (1954) has shown how the photographic light near the beginning of a bright meteor can be so suppressed; black-body radiation can spirit away the energy available for ablation. In the limit, for micrometeorites (Whipple 1950), the energy available for ionization will be markedly reduced. Even for micrometeorites, however, some radiation and ionization may be expected at great heights when ablation is absent. Atmospheric molecules encountered by the meteoroid and carried along momentarily will collide with

the atmosphere at high velocities and can produce a certain amount of both radiation and ionization. The radiation, if detectable, would probably occur in the nitrogen bands recently discovered by A. F. Cook and P. M. Millman (1954).

The major weaknesses in the physical conclusions concerning radio meteors arise from the lack of measurements of meteoric drag or mass. The arguments are, therefore, highly indirect. It is to be hoped that deceleration measurements, such as the three by McKinley, will soon be made in quantity, so that the drag equation, which is fairly reliable, can be used extensively. Almost certainly the masses of progressively fainter meteors, below the bright photographic range, decrease more slowly than their light or their ionization, because of reduced luminosity and ionization efficiency.

Laboratory and ballistic range measurements of most of the fundamental ballistic quantities involved in radio and photographic meteor studies are not difficult technically and are urgently needed to clarify several of these theoretical questions and observational discrepancies.

I am very grateful to Drs. P. M. Millman and D. W. R. McKinley for critical discussion and suggestion on various aspects of this paper.

REFERENCES

Almond, M., Davies, J. G., and Lovell, A. C. B. 1952, *M.N.*, **112**, 21.
Clegg, J. A. 1952, *M.N.*, **112**, 399.
Cook, A. F. 1954, *Ap. J.*, **120**, 572.
Cook, A. F., and Millman, P. M. 1955, *Ap. J.*, **121**, 250.
Greenhow, J. S., and Hawkins, G. S. 1952, *Nature*, **170**, 355.
Jacchia, L. G. 1952, *Harvard Reprint Ser. II*, No. 44.
Kaiser, T. R. 1953, *Phil. Mag. Suppl.*, **2**, 495.
Kaiser, T. R., and Closs, R. L. 1952, *Phil. Mag. Suppl.*, Ser. 7, **43**, 1.
Liller, W. 1949, *Tech. Report No. 65* (Cruft Laboratory, Harvard University).
Liller, W., and Whipple, F. L. 1954, *Rocket Exploration of the Upper Atmosphere*, ed. R. L. Boyd and M. J. Seaton (Cambridge, England: Pergamon Press), pp. 112–130.
McKinley, D. W. R. 1951*a*, *Ap. J.*, **113**, 255.
———. 1951*b*, *J. Appl. Phys.*, **22**, 202.
Millman, P. M. 1950, *J.R.A.S. Canada*, **44**, 209.
———. 1954, *Science*, **120**, 325. Paper presented at the Symposium on the Origin of Meteorites at the A.A.A.S. meeting, December, 1953.
Rocket Panel. 1952, *Phys. Rev.*, **88**, 1027.
Trowbridge, C. C. 1907, *Ap. J.*, **26**, 95.
Watson, F. G. 1941, *Between the Planets* (Philadelphia: Blakiston Co.).
Whipple, F. L. 1950, *Proc. Nat. Acad. Sci.*, **36**, No. 12, 687.
———. 1954, *A.J.*, **59**, 201.
Wright, F. W., Jacchia, L. G., and Whipple, F. L. 1954, *A.J.* (in press).
Wright, F. W., and Whipple, F. L. 1953, *Harvard Reprint Ser. II*, No. 47.

PHOTOMETRIC ANALYSIS OF A SPECTROGRAM OF A PERSEID METEOR*

ALLAN F. COOK
Harvard College Observatory, Cambridge, Massachusetts

AND

PETER M. MILLMAN
Dominion Observatory, Ottawa, Ontario, Canada
Received March 24, 1954; revised August 16, 1954

ABSTRACT

A good transmission grating spectrogram of a Perseid meteor has been obtained, the meteor also being well observed visually and by radar. The spectrogram has been subjected to a complete photometric reduction. From the zero-order image the light-curve of the meteor was found. The most prominent part of the spectrum consisted of the atomic lines of *H* I, *Na* I, *Mg* I, *Mg* II, *Si* I, *Si* II, *Ca* I, *Ca* II, *Fe* I, and *Fe* II. A background continuum was also found which can best be explained by a combination of a Planck curve at 7000° K and the first and second positive groups of bands of molecular nitrogen, these bands being unresolved. Abundances of atoms in various excited states were deduced. The range in height was too small to permit any conclusions concerning changes in the spectrum with height, but some evidence does appear for relative intensity changes of two lines with luminosity.

INTRODUCTION

Observational data in the form of photographic meteor spectra are difficult to secure in any quantity, since, even with the best cameras, it is seldom that a meteor fainter than magnitude −2 will produce a measurable spectrographic image. The number of spectra now available for study, however, is between 100 and 150 (Millman 1952, 1953*a*), and some of these show considerable detail.

The early photographic spectra were taken on blue-sensitive or orthochromatic plates and lacked photometric calibration. The photometric reduction possible was therefore limited and in most cases was of a rather qualitative nature (Millman 1932, 1935). Since 1945, the number of meteor spectra photographed with panchromatic emulsions has been considerably increased, and, in particular, a number of good-quality grating spectra with step-wedge calibration were secured during the course of the combined meteor program carried out in Ottawa since 1947 by the Dominion Observatory and the National Research Council. The dispersion of these spectra in the longer wave lengths is much larger than for the earlier prismatic spectra. With the present increased interest in the physical theory of meteoric phenomena, it is important to develop a detailed quantitative method for the photometric analysis of meteor spectra. This present paper is intended to serve as a guide to future work in this field.

The meteor spectrum studied here was photographed during the Ottawa Perseid observations in 1950. The relevant observational data are listed below.

OBSERVATIONAL DATA

Observing stations.—A—Ottawa, latitude 45°20′.5 N., longitude 75°38′.1 W. B—Arnprior, latitude 45°24′.9 N., longitude 76°21′.6 W. C—Carleton Place, latitude 45°9′.3 N., longitude 76°5′.3 W.

Visual data.—Station A: Meteor at $21^h45^m17^s$ E.S.T., August 11, 1950. Perseid, visual magnitude estimates: −4, −5, −7. Train duration: 14 seconds with naked eye,

* Work partially supported by the Office of Naval Research, Washington, D.C., Contract No. N5 ori-07647. Issued as *Contributions from the Dominion Observatory*, Vol. 2, No. 16.

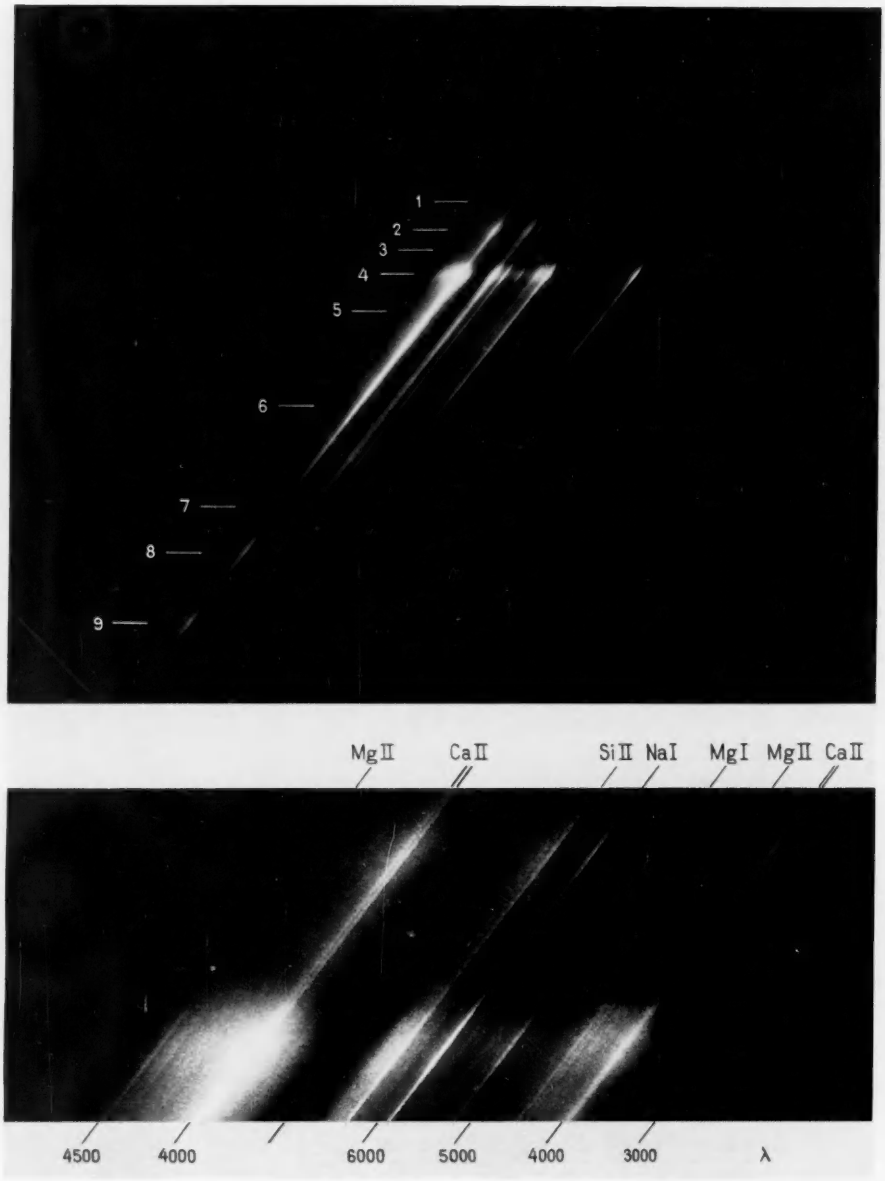

FIG. 1.—Spectrum No. 110, the Perseid meteor of 1950, August $11^{d}21^{h}45^{m}18^{s}$ E.S.T. Photographed from Ottawa.

21 seconds with binoculars. Color blue, two bursts, 7 visual plots on star charts. Stations B and C: No visual observations made.

Photographic data.—Station A: Camera R, Williamson aerial F24 camera, lens Pentac type, stationary altazimuth mounting, no rotating shutter. Focal length 8.0 inches, aperture 2.75 inches, field 35° × 35°. Grating: Wood replica-transmission grating mounted in front of camera lens as an objective grating, 1500 lines per inch, blazed for maximum intensity near 7500 A in the first order on one side; approximate first-order dispersion at center of camera field is 810 A/mm. Emulsion, Eastman Aero Super XX, 5½-inch-wide roll film. Exposure $21^h11^m0^s$ to $21^h45^m40^s$ E.S.T. Station B: No photograph obtained. Station C: No photographic equipment used at this station.

Radar data on 33 mc/sec.—Station A: Echo-type Ahbf, duration 90 seconds; Station B: Echo-type Ahb, duration 75 seconds; Station C: Echo-type Ahb5, duration 70 seconds.

The photographic spectrum is reproduced in Figure 1. The meteor crossed the camera field at an angle of approximately 50° to the dispersion and showed one bright burst and three fainter bursts. These four bursts correspond, in general position, with the second burst observed on the visual trail. The photographic trail extends for a total length of 18°, as compared with a length of 46° for the mean of the visual plots. The meteor trail ends near Corona Borealis, and the spectrum of α Coronae Borealis is the brightest stellar spectrum appearing on the film. A combination of all the visual, photographic, and radar data indicated a radiant near R.A. 43°, Decl. +60°. The mean visual trail has a distance from this radiant of 43°–89°; the photographic trail, from 71° to 89°. As an essential basis for the photometric reduction of the spectrogram, sensitometer spots in integrated light were impressed on the roll of film. These spots take the form here of a step-wedge. It is recognized that objections may be raised to the use of a calibration-curve derived from integrated light rather than from a number of separate wave-length regions. However, experience has shown that errors arising from this cause are small, and in this case it is considered that such errors are negligible compared to those due to other causes.

This meteor was photographed with only one camera, but the three radar echoes, when combined with the photographic and visual data, make possible a height determination for each position on the trail. Dr. D. W. R. McKinley has kindly provided the radar computations on the meteor. Details of the method used were published in 1949 (McKinley and Millman 1949). The height data, together with the range and other figures for each numbered trail position indicated in Figure 1, are given in Table 1. These trail positions correspond to those used in a preliminary photometric study of this spectrum, where values of the color index were determined (Millman 1951). The best mean geocentric velocity determined from the radar records is 61 km/sec, and this agrees satisfactorily with photographic determinations of Perseid velocities.

An additional calibration besides the sensitometer step-wedge impressed on the role of film is needed, i.e., a calibration of the sensitivity of the combination lower atmosphere, grating, optics, and emulsion as a function of wave length. To this end, stellar spectra may be employed. Unfortunately, none appear which are sufficiently dense on the photograph showing the meteor spectrum to give the sensitivity as a function of wave length. A later exposure made with the same camera on the same night at the same altitude and azimuth contains a well-exposed spectrum of α Lyrae, and this was used to obtain the relative run of this calibration. The spectrum of α Coronae Borealis appearing on the same exposure with the meteor is sufficiently dense that, given the relative calibration for sensitivity versus wave length, it may be used to obtain the absolute conversion factor for this relative calibration.

WAVE LENGTHS AND IDENTIFICATIONS OF EMISSION LINES

This meteor spectrum, No. 110 of the basic list (Millman 1952, 1953*a*), appeared to be of a type very similar to Perseid spectra previously photographed (Millman 1953*b*).

The approximate wave lengths of a number of the brightest lines were checked, using the standard dispersion constant for the grating. All detail visible at position 4 was then measured in a direction parallel to the dispersion. Preliminary wave lengths were computed assuming a linear dispersion between the ionized calcium lines in the first and second orders. A correction-curve was then drawn on the basis of the known wave lengths for a number of the strong sharp lines, and final wave lengths were computed by using this correction-curve. Identification with multiplets of *Fe* I, *Fe* II, *Ca* I, *Ca* II, *Si* I, *Si* II, *Mg* I, *Mg* II, *Na* I, and *H* I satisfactorily accounted for all the measured detail. This identification was made certain by comparison with a more detailed Perseid spectrum (No. 126) photographed by Millman in 1952 with higher dispersion. The study of the 1952 spectrum was particularly valuable in confirming the presence of ionized iron and hydrogen. The final wave lengths and identifications are listed in Table 2.

TABLE 1

DATA FROM THE OTTAWA STATION

Position on Trail	Azimuth	Elevation	Range (Km.)	Approx. Elong.*	Height† (Km.)
Vis. (beg.)	342°	55°			
Phot. (beg.)	294	54			
1	280°6	49°6	119.4	80°0	91.4
2	280.0	49.4	119.3		90.9
3	279.3	49.0	119.2		90.5
4	278.7	48.8	119.1		90.2
5	278.0	48.4	119.0		89.5
6	275.4	47.2	118.5		87.5
7	273.2	45.9	118.2		85.5
8	272.2	45.4	118.1		84.7
9	270.7	44.8	118.0	88.0	83.4
End	270	44			

* Approximate elongation from radiant.
† Above sea-level.

THE FIELD CORRECTION OF THE CAMERA

The well-known decrease in intensity transmitted to the image as the direction of the object becomes more inclined to the optical axis is an effect which must be allowed for in this work. The reduction to the center of the plate, known as the *field correction*, is usually expressed in stellar magnitudes. For determining this correction, the method described by Jacchia (1949) was used, with certain modifications. Dr. Jacchia has kindly supplied the authors with the designations, positions, and adopted photographic magnitudes of his standard stars for use with a field center near right ascension 19^h30^m, declination 0°. He recommended 3-minute trails rather than the 5-minute exposures mentioned in his paper. Three successive films were exposed, bracketing meridian passage. This process was repeated on a second night. Variation of trailing velocity with angular distance from the film frame center and with declination was neglected, since Jacchia's Table I (1949) indicated that this will not introduce an error greater than about ± 0.1 mag. As is usually the case, no detectable dependence of the field correction on the angle of the trailing direction to the radius from the center of the frame was found. The field correction of camera R is exhibited in Figure 2. Each point represents a single determination of the field correction from a single star.

TABLE 2

LINES IDENTIFIED AND MEASURED

Wave Length (A)	Atom or Ion	Mult. No.*	J–J†	Excit. Pot.‡ (e.v.)	Atom or Ion	Mult. No.*	J–J†	Excit. Pot.‡ (e.v.)
3666.8	*Fe* I	5	.....	3.37	.....	.....	.....	.....
3705.6–3760.2	*Fe* I	5	.....	3.36	*Fe* I	21?	.....	4.21
3846.2	*Fe* I	4	.....	3.22	*Fe* I	20?	.....	4.14
	(*Si* II)	(1)	.....	10.03	.....	.....	.....	.....
3881	*Fe* I	4	.....	3.25	*Fe* I	20?	.....	4.14
	(*Mg* I)	(3)	.....	5.92	.....	.....	.....	.....
3934.0	*Fe* I	4	.....	3.23	*Fe* I	20?	.....	4.09
	Ca II	1	$\frac{1}{2}$–$1\frac{1}{2}$§	3.14	.....	.....	.....	.....
3966.9	*Fe* I	43	4–3	4.59	*Ca* II	1	$\frac{1}{2}$–$\frac{1}{2}$§	3.11
4019.0	*Fe* I	43	3–2	4.63	.....	.....	.....	.....
4061.2	*Fe* I	43	.....	4.57	.....	.....	.....	.....
4092	*Si* I	2	0–1	4.91	.....	.....	.....	.....
4140.5	*Fe* I	42	4–3	4.45	*Fe* I	43	.....	4.56
	Fe II	27	$2\frac{1}{2}$–$1\frac{1}{2}$?	5.56	*Fe* II	28	$2\frac{1}{2}$–$2\frac{1}{2}$?	5.57
	Si II	3	.....	12.78	.....	.....	.....	.....
4196	*Fe* I	42	4–4	4.42	*Fe* II	27	$2\frac{1}{2}$–$2\frac{1}{2}$?	5.53
	Fe II	28	$2\frac{1}{2}$–$3\frac{1}{2}$?	5.52	.....	.....	.....	.....
4226.0	*Fe* II	27	$2\frac{1}{2}$–$3\frac{1}{2}$?	5.49	*Ca* I	2	0–1‖	2.92
4268.3	*Fe* I	42	.....	4.40	*Fe* II	27	$1\frac{1}{2}$–$\frac{1}{2}$?	5.58
	Fe II	28	$1\frac{1}{2}$–$1\frac{1}{2}$?	5.59	.....	.....	.....	.....
4320.8	*Fe* I	41	.....	4.37	*Fe* I	42	.....	4.43
	Fe II	27?	.....	5.54	*Fe* II	28	$1\frac{1}{2}$–$2\frac{1}{2}$?	5.57
4387.7	*Fe* I	2	.....	2.84	*Fe* I	41	.....	4.34
	Fe II	27	$\frac{1}{2}$–$\frac{1}{2}$?	5.58	*Fe* II	28	$\frac{1}{2}$–$1\frac{1}{2}$?	5.59
4425.4	*Fe* I	2	.....	2.85	*Fe* I	41	2–3	4.40
	Fe II	27	$\frac{1}{2}$–$1\frac{1}{2}$?	5.56	(*Ca* I)	(4)	.....	4.66
4482.9	*Fe* I	2	.....	2.86	*Fe* II	37	.....	5.59
	Fe II	38	.....	5.57	*Mg* II	4‖	.....	11.58
4594.2	*Fe* II	37	.....	5.49	*Fe* II	38	.....	5.57
4714	*Mg* I	11	1–2	6.95	.....	.....	.....	.....
4920.2	*Fe* I	16	5–4?	3.35	*Fe* I	318	.....	5.34
	(*Fe* II)	(42)	($2\frac{1}{2}$–$1\frac{1}{2}$)?	5.39	.....	.....	.....	.....
5037.2	*Fe* I	16?	.....	3.36	*Fe* I	318	.....	5.31
	(*Fe* II)	(42)	($2\frac{1}{2}$–$2\frac{1}{2}$)?	5.34	(*Si* II)	(5)	.....	12.47
5176.5	*Fe* I	16?	.....	3.36	(*Fe* II)	(42)	($2\frac{1}{2}$–$3\frac{1}{2}$)?	5.27
	Mg I	2‖	.....	5.09	.....	.....	.....	.....
5261.1	*Fe* I	15	5–4	3.20	(*Fe* II)	(48)	($2\frac{1}{2}$–$1\frac{1}{2}$)	5.56
5319.0	*Fe* I	15	4–3	3.23	(*Fe* II)	(48)	.....	5.51
5423.8	*Fe* I	15	.....	3.23	(*Fe* II)	(48)	.....	5.49
5588.3	*Ca* I	21	.....	4.72	.....	.....	.....	.....
5686.7	*Na* I	6	.....	4.27	*Si* I	10	.....	7.08
	Si I	11	2–1	7.10	.....	.....	.....	.....
5686.7–5893.3	*Si* I	9	.....	7.05	*Si* I	10	2–1	7.08
5893.3	*Na* I	1§	.....	2.10	*Si* I	9	2–2	7.04
5987.1	(*Si* I)	(16)	(1–2)	7.14	*Si* II	4	.....	12.09
6152.9	*Fe* II	74	.....	5.88	(*Ca* I)	(3)	.....	3.89
	(*Ca* I)	(20)	.....	4.52	*Na* I	5	.....	4.10
6249.2	*Fe* II	74	.....	5.85	.....	.....	.....	.....
6358.9	*Fe* II	74	$1\frac{1}{2}$–$2\frac{1}{2}$?	5.80	*Si* II	2§	.....	10.03
6456.4	*Fe* II	74	$3\frac{1}{2}$–$3\frac{1}{2}$	5.80	.....	.....	.....	.....
6471.2	*Ca* I	18	.....	4.42	.....	.....	.....	.....
6565.8	*H* I	1	.....	12.04	.....	.....	.....	.....

* From Miss Moore's (1945) table. The identifications given in parentheses are expected contributors to the line not independently identified.

† Lower level and upper level, respectively.

‡ Upper level.

§ Overwhelmingly dominant contributor.

‖ Dominant contributor.

REDUCTIONS TO RELATIVE INTENSITY

Tracings with the microdensitometer were made at or near the nine numbered trail positions in Figure 1. Two magnifications of the horizontal scale were used, 50× for detailed studies and 7× for investigating changes with position and brightness. Tracings at 7× were also made on α Coronae Borealis near the end of the trail, so as to coincide in time with the appearance of the meteor. For the sensitivity versus wave-length calibration, a tracing was also made of the spectrogram of α Lyrae taken on the same night. The zero order of the meteor was traced along its length to obtain the light-curve.

The basic photometric analysis was made from a 50× tracing near position 4, the brightest burst of the photographic trail. The characteristic curve of galvanometer displacement versus logarithm of intensity was established from the sensitometer spots, and this curve was used to rectify the tracing into relative sensitivity. Thus any possible variation of the characteristic curve with wave length was neglected. The intensity of the K line in the second order was taken as unity. The resulting rectified curve is exhibited in Figure 3. The sky fog was found to be 0.093 intensity units, and the scattered light between orders, 0.032. Since no better approximation is available, the scattered light was taken as constant throughout, giving a total background at 0.125 intensity units, indicated by a horizontal solid line in Figure 3. The tracing of the step-wedge sensitometer spots was also available to reduce the tracings of α Lyrae and α Coronae Borealis to relative intensity units and to reduce the zero-order meteor tracing to the light-curve on a relative scale.

REDUCTION FOR SENSITIVITY VERSUS WAVE LENGTH

RELATIVE SENSITIVITY

The tracing at 7× on α Lyrae was used to establish the relative sensitivity of the combination lower atmosphere, grating, camera, and film, the wave-length scale being established by using the hydrogen lines. The maximum intensity appearing in the first order at 6390 A was taken as unity on an arbitrary scale. Sky fog on this scale stood at 0.096, and scattered light at 0.060 outside the second order, at 0.057 between the second and first orders, and at 0.027 between the first and zero orders. The corresponding total backgrounds were 0.156, 0.153, and 0.123. The central position in this range—scattered light 0.044 and total background 0.140—was adopted.

Since the sensitivity as a function of wave length is desired, it is apparent that two quantities are required for any given wave length: the measured relative intensity cleared of background and the flux of energy from α Lyrae at this wave length. To obtain this latter quantity, recourse was had to the values of the fluxes at the surface of various stars tabulated by Milford (1950*a*, *b*, *c*). He (1950*c*) tabulates $\log F_\lambda$ for various values of λ and various spectral types and luminosity classes in his Table 7, where F_λ denotes the flux in ergs A^{-1} cm^{-2} sec^{-1} at the surface of the star and λ the wave length. He established these tabular values from spectrophotometric measurements of an absolute nature by various workers. These were made on individual stars, so that, in general, one or two prototypes served to establish the fluxes for a particular spectral type and luminosity class.

In establishing the absolute sensitivity, $\log F_\lambda$ is not the quantity actually required but rather $\log F^*_\lambda$, where F^*_λ is the flux from the star at the earth outside the atmosphere. This flux is ultimately a function of spectral type, luminosity class, and apparent magnitude. It can then be shown that

$$\log F^*_\lambda = (-8.425 - 0.4\Delta I_{pv}) + (\log F_\lambda - \log F_{5450}) - 0.4\, I_{pv} , \qquad (1)$$

where I_{pv} is the apparent visual magnitude of the star and ΔI_{pv} is a correction for the line absorption to F_{5450} given by Milford (1950*b*) in his Table 2.

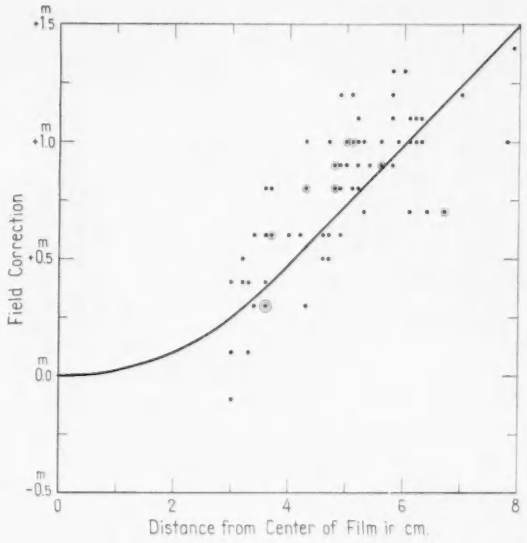

FIG. 2.—The field correction of camera R in units of photographic magnitude. The circles represent coinciding additional points. The curve is extrapolated to determine the origin, applying the condition that its slope must vanish there.

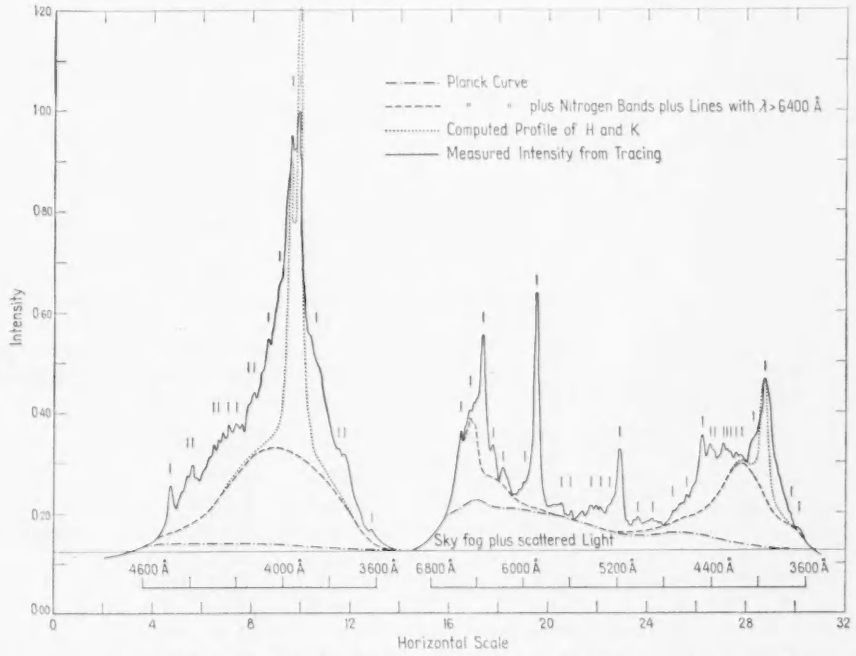

FIG. 3.—The rectified tracing of the meteor spectrum near position 4. Intensities are relative, in arbitrary units. The short vertical lines indicate the positions of identified spectral lines.

Keenan and Morgan (1950) give A0 V for the spectral classification of α Lyrae. Mrs. Payne-Gaposchkin (1938*a*, *b*) gives for its apparent magnitude, $I_{pv} = 0.18$. For A0 V, $\Delta I_{pv} = 0.00$. Milford (1950*b*) has selected various wave lengths for their freedom from line absorption depressing the continuum at low dispersions. In this case the wave lengths are 4022, 4640, 5066, 5336, 5450, 5851, and 6293 A. Log F_λ^* was calculated for α Lyrae by equation (1) for these wave lengths, and a smooth curve was plotted through the points found. From this curve, log F_λ^* was read for 4130, 4530, 5730, 5980, and 6390 A, as these values were also required in the reduction. Values of the sensitivity S on an arbitrary scale were found by dividing the net relative intensity cleared of background by F_λ^*. These were then adjusted by a scale factor to make the maximum value of S unity. The resulting points and the sensitivity-curve passed through them are shown in Figure 4. Since the continuum may be depressed by the absorption, the values of log F_λ^* read from the curve at the supplementary wave lengths may be slightly too large and the corresponding values of S may be too small. This possibility is indicated by these points being plotted in Figure 4 as upward-pointing arrows with heads at the computed values of S.

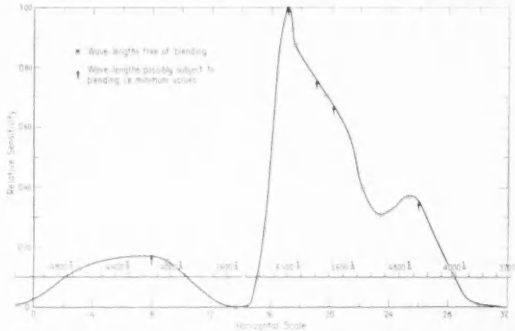
Wave lengths free of blending
Wave lengths possibly subject to blending, i.e. minimum values
Relative Sensitivity
Horizontal Scale

FIG. 4.—The relative sensitivity as a function of the wave length

It is obvious that the foregoing results may require further revision to allow for the field correction. The pertinent values of this quantity for the various orders and positions on the spectra of the meteor, α Coronae Borealis, and α Lyrae are given in Table 3. The difference in field correction, first order minus second, is, for position 4, +0.11 mag., while for α Lyrae it is +0.10 mag.; whence this difference may be neglected. Thus Figure 4 gives the correct relative sensitivity-curve for reducing Figure 3 from relative intensity to intensities differing only by a constant factor independent of wave length from ergs A^{-1} cm^{-2} per radian path length. The relative intensities of Figure 3 are to be *divided* by the relative sensitivities of Figure 4 to obtain these results.

REDUCTION FOR SENSITIVITY VERSUS WAVE LENGTH

ABSOLUTE SENSITIVITY

It is now necessary to supply the constant factor needed to convert the relative sensitivity to absolute sensitivity. The constant factor mentioned in the preceding paragraph is to be supplied as a coefficient of the intensity found by dividing the relative intensity from Figure 3 by the corresponding quantity S from Figure 4. For the determination of this conversion factor, the spectrum of α Coronae Borealis was used. The well-known decrease in sensitivity during exposure of an emulsion to humid air was in evidence here, so that the tracing was made at a point on the stellar trail and spectrum corresponding as nearly as possible to the time of appearance of the meteor.

Again the field correction must be considered. In this case the difference, second order *minus* first, is −0.01 mag.; and, since this value for α Lyrae is −0.10, the correction to the relative sensitivity-curve is +0.09 mag. in the second order, to reduce it to correspondence with the curve to be anticipated for α Coronae Borealis. This reduction corresponds to a factor of 0.920. The reduction, meteor *minus* α Coronae Borealis, in the first order is −0.01 mag., giving a factor of 1.010.

A further complication is introduced by the presence of reciprocity failure. The effective exposure times of the meteor and the star are required to evaluate this effect. The two factors determining the effective exposure time are, first, the velocity of the image on the film and, second, the width of the trail left for each spectral line, and, in the case of the continuum, the width of the continuous line image moving across the film. A convenient measure for these widths can be obtained from the half-half-width of an unblended spectral line. The half-half-width is defined as the interval from maximum intensity at the center of the line to the point on either side where the intensity has fallen to half its

TABLE 3

FIELD CORRECTIONS AND MAGNITUDES OF THE METEOR

OBJECT	POSITION	FIELD CORRECTION			APP. PHOT. MAG. (MG.)	ABS. PHOT. MAG. (MG.)	$\mathfrak{I}$* (OMG SEC)
		Zero Order (Mg.)	First Order (Mg.)	Second Order (Mg.)			
α Lyr		0.80	0.64	0.54	+0.18†		
α CrB		.68	.64	.63	+2.26†		
Meteor	1	.78	.65	.54	−3.5	−3.9	199.0
	2	.74	.64	.54	−7.3	−7.7	193.7
	3	.74	.64	.52	−6.6	−7.0	185.0
	4	.72	.63	.52	−8.9	−9.3	158.6
	5	.71	.63	.51	−7.7	−8.1	114.1
	6	.71	.63	.52	−7.2	−7.6	31.3
	7	.71	.63	.58	−4.7	−5.1	9.3
	8	.74	.68	.60	−5.9	−6.3	4.7
	9	0.76	0.70	0.64	−5.5	−5.9	0.8

* The symbol denotes the integral $\mathfrak{I} = \int_t^\infty I dt$.

† These are the apparent visual magnitudes, the color indices being assumed to be zero.

maximum and central value. From Figure 3, a half-half-width of the line at 5893 A, the sodium D line, was found from its profile to be 26.50 A, using an estimated level for the local background. By measurement on the tracing, 1 cm = 166.8 A, whence a half-half-width of 0.1588 cm at a magnification of 50× and hence on the original film a half-half-width of 3.176×10^{-3} cm. This value is widened by the inclination of the meteor trail to the perpendicular to the dispersion. The factor that must be applied to the actual half-half-width of the line is the sine of the angle between the meteor trail and the dispersion, which is 50° in this case, whence the value 2.435×10^{-3} cm is found.

Let T denote the effective exposure time, a the half-half-width just found, θ the angle between the dispersion and the trailing direction of the image of the star, and v the linear velocity of the star image on the plate. Then

$$T = \frac{4a}{v} \operatorname{cosec} \theta . \qquad (2)$$

Let R denote the focal length of the camera in centimeters and ω the angular velocity of the star in radians per second. Then

$$v = \omega R . \tag{3}$$

For α Coronae Borealis, $\omega = 6.52 \times 10^{-5}$ sec^{-1} (declination +26°.9), $R = 20.52$ cm, whence $v = 1.336 \times 10^{-3}$ cm sec^{-1}. Also $\theta = 48°$, whence $T = 9^{s}.82$.

For the meteor spectrum there are two cases. For the continuous background, equation (2) applies. For the line spectrum, the correct expression is

$$T = \frac{4a}{v} . \tag{4}$$

In both cases ω is given by

$$\omega = \frac{V}{r} , \tag{5}$$

where V is the velocity of the meteor and r is the distance of closest approach. In this case $V = 61$ km sec^{-1}, $r = 118.0$ km; whence $\omega = 0.517$ sec^{-1}, $v = 10.60$ cm sec^{-1}. Now $\theta = 50°$, whence, by equation (2), $T = 1.199 \times 10^{-3}$ sec for the continuum and by equation (4) $T = 9.18 \times 10^{-4}$ sec for the lines. The logarithms of these exposure times were used to find the factors for reducing the total energy received from α Coronae Borealis to the same scale as for the meteor. To this end, use was made of a reciprocity failure-curve kindly supplied by Mr. W. F. Swann, of the Eastman Kodak Company. The corresponding reduction factors are 0.2907 for the continuum and 0.2955 for isolated lines, blends lying somewhere in between. The value 0.293 was adopted as sufficiently accurate for all cases.

The formulae for reduction of relative intensity from Figure 3 and relative sensitivity from Figure 4 to absolute intensity must now be derived. Keenan and Morgan (1950) give for the spectral classification of α Coronae Borealis A0 V. Mrs. Payne-Gaposchkin (1938*a*, *b*) gives for its apparent magnitude $I_{pv} = 2.26$. With $\Delta I_{pv} = 0.00$, equation (1) becomes

$$\log F_{\lambda}^{*} = -9.33 + (\log F_{\lambda} - \log F_{5450}) \tag{6}$$

for α Coronae Borealis. Using Figure 4, the values of TSF_{λ}^{*} were formed for the same wave lengths as those used on α Lyrae. These values were multiplied by the reciprocity failure factor 0.293 and the field correction factor 1.010. Also the values in the second order were multiplied by the differential field correction factor 0.920. The resultant factors were, for the first order, 0.2959 and, for the second order, 0.2723. These products for each wave length were summed. Also the sum of the intensities on the same scale as Figure 3 was formed for the same wave lengths. The quotient found by division of the former sum by the latter gives the calibration factor for Figure 4, so that intensities on the scale of Figure 3 may be converted into absolute intensities in ergs A^{-1} cm^{-2}. The two sums were found to be 4.28×10^{-8} ergs A^{-1} cm^{-2} and 0.237, whence

$$I' = \frac{1.806 \times 10^{-7}}{S} I_m , \tag{7}$$

where I_m denotes the measured intensity on the scale of Figure 3, S the relative sensitivity from Figure 4, and I' the absolute intensity in ergs A^{-1} cm^{-2}. Then I_m is replaced by its equivalent in angstroms when used for lines to give a result in ergs cm^{-2}. For lines the angular length along the meteor path to which the result applies will be $4a/R = 4.75 \times 10^{-4}$ radians and, for the continuum, $(4a/R)$ cosec $\theta = 6.19 \times 10^{-4}$ radians. Hence I'

must be divided by these results to obtain intensities per radian path length, whence, for the continuum,

$$I = \frac{2.912 \times 10^{-4}}{S} I_m , \tag{8}$$

and, for the lines,

$$I = \frac{3.804 \times 10^{-4}}{S} I_m . \tag{9}$$

To determine the apparent and absolute magnitudes of the meteor as a function of position, equation (4) is used both for α Coronae Borealis and for the meteor, since the zero order presents itself as a line. For α Coronae Borealis, $T = 7.29$ seconds; for the meteor, $T = 9.19 \times 10^{-4}$ sec. The resulting factor for reciprocity failure is 0.3241; its logarithm is -0.490. The exposure times are in the ratio 7.94×10^3, logarithm, 3.900, whence the logarithm of the ratio of the brightnesses is 3.410, corresponding to 8.52 mag. The reduction to standard distance 100 km is -0.36 mag. for 118.0 km, the distance of closest approach. The zero order of α Coronae Borealis has a net intensity $I_m = 0.042$.

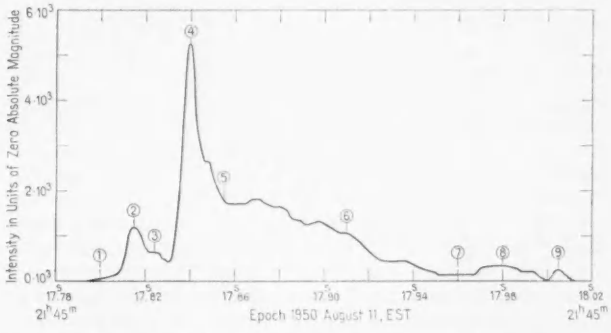

FIG. 5.—The light-curve of the meteor. The numbered positions are those of Fig. 1

The corresponding absolute and apparent photographic magnitudes are given in Table 3, the color index of α Coronae Borealis being assumed to be zero. The light-curve in units of zero absolute magnitude is exhibited in Figure 5. The integral of the intensity with respect to time forward to disappearance was planimetered from the light-curve and is tabulated for the nine positions in Table 3.

ANALYSIS OF THE SPECTRUM IN THE RED AND YELLOW

The first task approached was the analysis of the line spectrum in the red and yellow, to establish the position of the background continuum. It is necessary to adopt a standard intensity profile for all the emission lines. By plotting this profile individually for each line, overlapping profiles can be blended, and a summed intensity-curve drawn. This can now be used to subtract the intensity of any group of emission lines from the observed intensity-curve, thus obtaining the intensity of the background.

Starting from the minimum intensity at 5567 A, the region of longer wave lengths is examined. All the component lines of the multiplet forming the line at 5588 A are sufficiently close together that the profile will be indistinguishable from that of a single line. The central intensity is 0.203, the estimated local background continuum is 0.187; whence the net central intensity is 0.016. For the line profile, the form of instrumental

profile recommended by Unsöld (1938) in his equation (58, 28) was adopted; whence we obtain

$$I'_m(w) = \frac{a}{\pi} \frac{I_m}{a^2 + w^2}, \tag{10}$$

where I_m is the total strength of the line, I'_m is the intensity at distance w from the center of the line, and a is the half-half-width of the line in the same units as w. The half-half-width a was found, from the *Na* D line at 5893 A, to be, in the first order, 26.50 A and, in the second order, 13.20 A To convert the central intensity $I'_m(0)$ into an equivalent width, I_m, the following expression is used:

$$I_m = \pi a I'_m(0). \tag{11}$$

It is apparent that

$$I_m = \int_{-\infty}^{+\infty} I'_m(w)\, dw$$

is the width of a square line having the same total strength and a height of one relative intensity unit on the scale of Figure 3, so that the equivalent width is defined here in terms of the unit intensity on this scale. In the first order $\pi a = 83.3$ A, and, in the second order, $\pi a = 41.5$ A. Application of the former value gives $I_m = 1.3$ A for 5588.

Next the intensity of the line at 5893 A was considered. The measured central intensity is 0.636, the estimated background intensity is 0.192, whence the net central intensity is 0.444 and the equivalent width 37.0 A. Using an estimated curve for the wings of this line, the blend running from the line at 5687 A toward 5893 was measured from its area as 2.4 A. Also measured from its area was the line at 5987 A, found to be 0.1 A.

For the line at 6359 A the overwhelming contributor is produced by *Si* II, multiplet No. 2 of Miss Moore's (1945) tables. The two lines produced occur at 6347.1 and 6371.4 A, the former having double the intensity of the latter. The two values of S were found from Figure 4 to correct this ratio, and then individual profiles, according to equation (10), were computed and summed. Next the half-half-width point on the shorter-wave-length side is found from the computed profile, and the intensity value read off from Figure 3 at this point. This gives an estimated value of the central intensity (twice the difference center of line *minus* half-half-width point) and, by subtraction, an estimated local background intensity. The half-half-width point on the longer-wave-length side is blended and cannot be used.

Attention must now be directed to the line at 6249 A. The three component lines producing this blend are sufficiently close together to justify use of the instrumental profile for a single line. The central intensity and the intensity at the half-half-width point toward the shorter wave lengths were read and corrected for overlap by 6359; whence $I_m = 3.2$ A. For the line at 6153 A, due to *Na* I, multiplet No. 5, and *Fe* II, multiplet No. 74, all contributory lines fall close enough together to justify again the use of a single-line instrumental profile for this blend. Here the overlaps from 6249 and 6359 were computed, and the half-half-width point toward the blue was again used to establish $I_m = 2.7$ A. Computation of the overlap of 6153 and 6249 upon 6359 leads to a revised central intensity, $I'_m(0) = 0.271$. The reduction in central intensity as compared to that for the same total intensity concentrated in a single line is 0.886, so that the corresponding central intensity of an equally strong single line is 0.306 and $I_m = 25.4$ A. To the red of 6359 there is a complicated blend of *Ca* I, multiplet No. 18, and one line of *Fe* II, multiplet No. 74. Furthermore, the relative sensitivity S is very uncertain for $\lambda > 6400$ A, as can be seen from Figure 4. The area of the line at 6566 A due to *Ha* can be measured as 0.5 A but cannot be further dealt with, owing to the pronounced uncertainty of S.

The instrumental profiles of 5588, 5893, 6153, 6249, and 6359 have been subtracted from the observed intensity-curve to find the local background, which is indicated by a dashed line in Figure 3. This line is interpolated by eye under the blend from 5687 to 5893 A. The smoothness of the resulting curve until the blend to the red of line 6359 is reached confirms the intensities already found.

THE BACKGROUND CONTINUUM

The local background continuum, the red and yellow portions of which were found earlier, must now be studied in more detail. Various points were read from the observed intensity-curve in Figure 3 and reduced to absolute intensities by equation (8), after subtracting the sky fog plus scattered light. Two points were chosen that were the lowest in intensity, so placed as to define a Planck curve everywhere lower than the other points. These were at $\lambda\,\lambda = 5567$ and 4815 A. The intensities, less sky fog and scattered light, were $I_m = 0.061$ and 0.049, the relative sensitivities were $S = 0.594$ and 0.347; whence $I = 2.988 \times 10^{-5}$ and 4.11×10^{-5} ergs A^{-1} cm^{-2}. This continuum was then assumed to be due to Planck radiation from the surface of the meteor. From the ratio of the observed intensities and Planck's law, the absolute temperature, $T = 10{,}300°$ K, was deduced.

On plotting the corresponding preliminary Planck curve, it was immediately obvious that there were two unexplained large rises in the continuum, one in the red and the other in the blue. For the source of these, inspection of a spectrogram of an air-filled Geissler tube (Herzberg 1950*a*) immediately suggests the answer; in the red, the first positive group of the neutral nitrogen molecule, N_2, $B^3\Pi_g \rightarrow A^3\Sigma_u^+$; and, in the blue-violet, the second positive group, N_2, $C^3\Pi_u \rightarrow B^3\Pi_g$.

THE NITROGEN BANDS

Inspection of the first positive group shows that only the two diagonal sequences $\Delta v = +3$ and $+4$ are apparently present, those for $\Delta v > +4$ being absent in the meteor spectrum and in the Geissler tube. The dip in intensity between the two sequences in the Geissler tube did not appear in the meteor spectrum. The implication is a very high rotational and vibrational excitation temperature. The absence of the sequences for which $\Delta v > +4$ may be explained by the uniformly low vibrational transition probabilities for these bands (Jarmain and Nicholls 1952).

Attention must now be directed to the second positive group. The $C^3\Pi_u$ state is broken off in its vibrational structure above vibrational quantum number $v = 4$. Thus the energy range involved is small, 9810 cm^{-1} or 1.09 electron volts. It seemed best to put $1/T$ equal to zero in computing the intensity distribution in the band system.

The intensities of the individual lines must first be considered. Since these lines are not resolved, the problem actually reduces to that of finding the intensity of the apparent continuum produced. The triplet splitting may be ignored, as it fails to appear at the dispersion given in Herzberg's (1950*a*) spectrogram, which is much higher than that of the meteor spectrogram. This particular case is one in which both states proceed from Hund's coupling case (*a*) at low total rotational angular momentum quantum number, J, to coupling case (*b*) at high J. The intensities for both cases are given by Budó's (1937) formulae. For case (*b*), advantage may be taken of the usual near-equality between the coupling constants Y' and Y'' for the two states, the double prime denoting the lower electronic state. This is done as suggested by Budó (1937) by putting $Y' = Y''$. For case (*a*) neglect of the triplet splitting implies addition of the strengths for the same J', where the single prime denotes the upper electronic state. For case (*b*) the addition is for the same rotational quantum number, neglecting electron spin, K', i.e., the subscripts 1, 2, 3 on K' correspond to $J' = K' - 1$, K', and $K' + 1$, respectively. Since the Q-branch is, in any case, very weak, it will be more convenient to set the strengths $S_{K'}^{Q} = 0$, $S_{K'}^{Q} = 0$,

a superscript denoting a branch, in this case Q. To this approximation, it is possible to adopt, for both case (a) and case (b),

$$S^P_{K'} = 3K' , \qquad S^Q_{K'} = 0 , \qquad S^R_{K'} = 3(K'+1) . \tag{12}$$

The distinction between J' and K' is pointless, once the multiplicity of the state is neglected.

Herzberg (1950b), quoting Büttenbender and Herzberg (1935), gives the rotational quantum number K'_v above which the vibrational level v' breaks off. These are $K'_1 = 65$, $K'_2 = 55$, $K'_3 = 43$, and $K'_4 = 28$. For this paper, $K'_0 = 73$ was adopted by extrapolation. The vibrational overlap integrals have been computed by Jarmain and Nicholls (1952).

For the limits on the bands, the various constants of the electronic states are required. Herzberg (1950b) gives, for the $C^3\pi_u$ state, the electronic energy $T'_e = 89147.3$ cm^{-1} and the constants in the following formula for the vibrational energy:

$$G'(v') = 2035.1(v'+\tfrac{1}{2}) - 17.08(v'+\tfrac{1}{2})^2 - 2.15(v'+\tfrac{1}{2})^3 , \tag{13}$$

and the following formula for the rotational constant:

$$B_{v'} = 1.8259 - 0.0197(v'+\tfrac{1}{2}) . \tag{14}$$

Equation (13) applies only to $v' = 0, 1, 2, 3$. For the perturbed state $v' = 4$, a correction to the formula of -12.5 cm^{-1} is indicated by the results of Büttenbender and Herzberg (1935). Herzberg (1950b) gives, for the $B^3\pi_g$ state, $T''_e = 59626.3$ cm^{-1} and the following formulae:

$$G''(v'') = 1734.11(v''+\tfrac{1}{2}) - 14.47(v''+\tfrac{1}{2})^2 , \tag{15}$$

$$B_{v''} = 1.6380 - 0.0184(v''+\tfrac{1}{2}) . \tag{16}$$

Then, for the band zeros, ν_0,

$$\nu_0 = [T'_e + G'(v')] - [T''_e + G''(v'')] , \tag{17}$$

and for the vertices (here on the P-branches), ν_{vertex},

$$\nu_{\text{vertex}} = \nu_0 - (B_{v'} - B_{v''}) - \frac{(B_{v'} + B_{v''})^2}{4(B_{v'} - B_{v''})} , \tag{18}$$

and for the limit imposed on the P-branch by the breaking-off of the rotational structure,

$$\nu^{P'}_{v'v''} = \nu_0 + B_{v'}(K'^2_{v'} + K'_{v'} - 1) - B_{v''}(K'^2_{v'} + 3K'_{v'} + 1) , \tag{19}$$

and for the further displaced limit imposed on the R-branch,

$$\nu^{R'}_{v'v''} = \nu_0 + B_{v'}(K'^2_{v'} + K'_{v'} - 1) - B_{v''}(K'^2_{v'} - K'_{v'} - 1) . \tag{20}$$

Equations (17), (18), (19), and (20) were applied to all the bands in the diagonal sequences $\Delta v = -6$ to $\Delta v = -1$ inclusive.

It can be shown that for $1/T = 0$ no band head should be distinguishable, even in the second order.

For calculation of the general intensity distribution over the entire band system, now seen to appear effectively as a continuum not showing resolvable bands, a few further simplifications are possible. Average values of $B_{v'}$ and $B_{v''}$ are adopted for each diagonal sequence. For a given sequence a given point on the R-branch corresponds in wave number to a point for which K' is $\Delta K'$ greater than on the P-branch. It can be shown that

$$\Delta K' = \frac{B_{v'} + B_{v''}}{B_{v'} - B_{v''}} - 1 . \tag{21}$$

It can also be shown that

$$K' \lim_{\to \infty} \left(\frac{dI_{em}}{d\nu^{P}_{v'v''}} + \frac{dI_{em}}{d\nu^{R}_{v'v''}} \right) = \psi \frac{p^2_{v'v''} \nu^4}{B_{v'} - B_{v''}}, \tag{22}$$

$$\psi = \frac{4h^4 c}{3m^2 e^2} N' \overline{R_e^2} \frac{1}{15{,}740}, \tag{23}$$

where I_{em} is the emission per unit solid angle in a given vibrational state v' and rotational state K'; ν is wave number; h is Planck's constant; c is the velocity of light; m is the mass of an electron; e is the electronic charge; N' is the number of molecules in the upper electronic state; R_e is the electronic moment integral for the two electronic states in atomic units; and $p_{v'v''}$ is the vibrational overlap integral for the two electronic states. This limit is, in fact, attained at rather low K', i.e., close to ν_0. For the extension of the R-branch beyond the breaking-off point $\nu^{P'}_{v'v''}$ in the P-branch,

$$K' \lim_{\to \infty} \frac{dI_{em}}{d\nu^{R}_{v'v''}} = \frac{\psi}{2} \frac{p^2_{v'v''} \nu^4}{B_{v'} - B_{v''}}, \tag{24}$$

a limit which is not, in fact, attained even at $\nu^{R'}_{v'v''}$, $dI_{em}/d\nu^{R}_{v'v''}$ being very slowly varying but noticeably less than the value indicated in equation (24). Of course, the corresponding limit for the P-branch is exceeded by an amount nearly equal to the defect in the R-branch, thus serving to make equation (22) valid. An adequate approximation was adopted for the relative intensity distribution by assuming for the total intensity the limiting value (22) in the range $\nu_{\text{vertex}} \leq \nu \leq \nu^{P'}_{v'v''}$ and for the range $\nu^{P'}_{v'v''} \leq \nu \leq \nu^{R'}_{v'v''}$,

$$\frac{dI_{em}}{d\nu_{v'v''}} = \psi \frac{p^2_{v'v''} \nu^4 K'_{v'}}{(B_{v'} + B_{v''}) + 2(B_{v'} - B_{v''}) K'_{v'}}. \tag{25}$$

To find the weighted mean position of the band, adopting the weight W as unity for $\nu_{\text{vertex}} \leq \nu \leq \nu^{P'}_{v'v''}$, the following expressions are obvious:

$$\nu_{\text{vertex}} \leq \nu \leq \nu^{P'}_{v'v''} \qquad W = 1,$$

$$\nu^{P'}_{v'v''} \leq \nu \leq \nu^{R'}_{v'v''}, \qquad W = \frac{K'_{v'}}{\Delta K' + 1 + 2K_{v'}} = \frac{1}{2 + (\Delta K' + 1)/K'_{v'}};$$

whence

$$\bar{\nu}_{v'v''} = \frac{1}{2} \frac{[(\nu^{P}_{v'v''})^2 - (\nu_{\text{vertex}})^2] + 1/[2 + (\Delta K' + 1)/K'_{v'}][(\nu^{R'}_{v'v''})^2 - (\nu^{P'}_{v'v''})^2]}{(\nu^{P'}_{v'v''} - \nu_{\text{vertex}}) + 1/[2 + (\Delta K' + 1)/K'_{v'}](\nu^{R'}_{v'v''} - \nu^{P'}_{v'v''})}. \tag{26}$$

To find the weighted mean position of a particular diagonal sequence, it is apparent that

$$\bar{\nu}_{\Delta v} = \frac{\sum_{v'} p^2_{v'(v'-\Delta v)} Q_r(v') \bar{\nu}_{v'(v'-\Delta v)}}{\sum_{v'} p^2_{v'(v'-\Delta v)} Q_r(v')} = \frac{\sum_{v'=0}^{4} p^2_{v'(v'-\Delta v)} K'_{v'}(K'_{v'}+2) \bar{\nu}_{v'(v'-\Delta v')}}{\sum_{v'=0}^{4} p^2_{v'(v'-\Delta v)} K'_{v'}(K'_{v'}+2)} \tag{27}$$

where $Q_r(v')$ is the rotational partition function and again employing $1/T = 0$. The total intensity of the sequence is also required. It can be shown that

$$I^P_{em} = \psi p^2_{v'v''} \nu^4 K' , \tag{28}$$

$$I^R_{em} = \psi p^2_{v'v''} \nu^4 (K' + 1) , \tag{29}$$

where the superscripts on I_{em} denote the branches. Summing equations (28) and (29) and then summing over $0 \leq K' \leq K'_{v'}$ gives the total intensity of a band. Then, for the total intensity of a diagonal sequence, we have

$$I_{\Delta v} = \psi \bar{\nu}^4_{\Delta v} \sum_{v'=0}^{4} p^2_{v'(v'-\Delta v)} K'_{v'} (K'_{v'} + 2) . \tag{30}$$

Equations (26), (27), and (30) were applied to all the diagonal sequences $-6 \leq \Delta v \leq -1$. The $\bar{\nu}_{\Delta v}$'s were converted to wave lengths $\bar{\lambda}_{\Delta v}$. Then these intensities were assumed

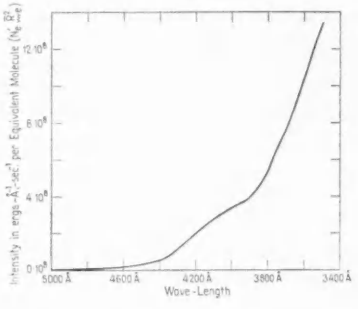

FIG. 6.—The computed intensity distribution for the second positive group of nitrogen bands, N_2, $C^3\Pi_u \rightarrow B^3\Pi_g$, for low dispersion and very high temperature.

to be averaged over the distance between mid-points of adjacent centroids of diagonal sequences, and these averages were taken as applying at the centroids, following which a smooth curve was drawn through the resulting points. This curve was taken to be the absolute intensity distribution in the group and is exhibited in Figure 6.

FINAL INTENSITIES OF THE PLANCK CURVE, N_2 AND *Ca* II

The curve of intensity versus wave length given in Figure 6 for the second positive group of nitrogen must be transformed into a form appropriate for use with the relative intensity-curve of Figure 3. This is done by multiplying the curve in Figure 6 by the relative sensitivity-curve in Figure 4. Division by r^2 reduces the result from ergs A^{-1} sec^{-1} to ergs A^{-1} cm^{-2} sec^{-1} at the distance of the meteor, division by ω to ergs A^{-1} cm^{-2} per radian path length and division by the numerical coefficient in equation (8) reduces the final result to the intensity on the scale of Figure 3 per "effective molecule" $(N'\overline{R^2_e})$, i.e.,

$$I_m = 4.77 \times 10^{-11} S I_\lambda (N'\overline{R^2_e}) . \tag{31}$$

To find $(N'\overline{R_e^2})$ various points in Figure 3 were chosen which appeared to be as nearly as possible free of overlap from the profiles of near-by lines, and I_m was read off for these points. The sum of sky fog, scattered light, and Planck continuum was removed by subtraction to find the remainder presumed due to N_2, $C^3\Pi_u \rightarrow B^3\Pi_g$. Equation (31) was then used to find $(N'\overline{R_e^2})$, and the lowest value was then adopted as a preliminary abundance. This occurred at horizontal scale position 28.00, corresponding to $\lambda = 4099$ A with an intensity 0.298, from which 0.142 was subtracted, leaving 0.156 due to the second positive group. At this wave length, $4.77 \times 10^{-11} SI_\lambda = 1.837 \times 10^{-19}$, giving $(N'\overline{R_e^2}) = 8.49 \times 10^{17}$ molecules. The corresponding intensity at horizontal scale position 24.62 ($\lambda = 4815$ A) is 0.008. This must be subtracted to redetermine the Planck temperature, whence $I_m = 0.041$, $I = 3.438 \times 10^{-5}$ ergs A^{-1} cm^{-2} and $T = 6940°$ K. The corresponding Planck curve is plotted in Figure 3 as a dash-dotted line. The solid angle filled by this source of continuous radiation is 2.75×10^{-12}, and the radiating area at $r = 1.18 \times 10^7$ cm is 383 cm^2.

The values of the Planck temperature and source area are of approximately one-figure accuracy but are given to three significant figures for use in the discussion of the continuum.

A further improvement upon $(N'\overline{R_e^2})$ is obtainable by taking into account the overlap of the blended profiles of the H and K lines of *Ca* II, multiplet No. 1 of Miss Moore's (1945) tables, appearing here at 3934 and 3967 A. A combined profile for the first order was prepared, using the instrumental profile and the sensitivities S from Figure 4. After a little adjusting, a satisfactory fit was found, using the above Planck curve at $T = 6940°$ K and solid angle 2.75×10^{-12}, along with $(N'\overline{R_e^2}) = 7.94 \times 10^{17}$ molecules and $I_m = 26.0$ A for H and K. The computed profile of the unresolved blend of H and K is shown by the dotted curve in the first order of Figure 3. The computed combined Planck and second positive group intensity-curve is shown in both orders to the violet of 5200 A by the dashed curve in Figure 3.

A comparison of this computed profile of H and K in the first order with the observed profile shows a distortion, presumably due to accidental causes, and extra intensity to the violet, perhaps due to unresolved blends of lines. Thus the area under the line including this extra intensity is not a good indication of its strength. In the second order, the mean of the two maximum intensities and the intervening minimum was fitted to the same quantity from the computed profile. The resulting equivalent width of H and K together is $I_m = 53.9$ A. The computed profile is again shown by a dotted line. The observed profile appears to suffer from blending by other lines on both sides, and, furthermore, there is an obvious distortion of the intensity distribution across the two peaks. A fit cannot be obtained by increasing a, the half-half-width of the instrumental profile.

LINE INTENSITIES AND ABUNDANCES OF EXCITED ATOMS

From this point forward, there remained the straightforward task of measuring the intensities of all the lines in the spectrum. Where central intensities could be measured by finding the drop to the half-half-width points, they were obtained. In all cases the area between the minima imposed by the blending of adjacent lines was measured. Both determinations of I_m are tabulated in Table 4 when available. A computed blend was used for *Fe* I, multiplet No. 15.

The relative sensitivities S are tabulated also, with the resulting values of the absolute intensity I in ergs cm^{-2}. Where values are available from both orders, an adopted value is given in Table 4. A slight systematic trend to larger values of I from the second order than from the first is indicated, but it is of the same order of magnitude as the errors of measurement. To convert these measured intensities into abundances in the upper states,

TABLE 4

LINES MEASURED AND ABUNDANCES IN THE UPPER STATES

WAVE LENGTH (A)	ORDER	EQUIVALENT WIDTH, I_m			INTENSITY, I			INTENSITY PER ATOM, I/N_m (ERGS CM^{-2})	NO. OF ATOMS IN UPPER STATE, N_m
		Central Intensity (A)	Area (A)	Adop. Value (A)	Sensitivity	From Order (Ergs Cm^{-2})	Adopted Value (Ergs Cm^{-2})		
3666.8	1st	.....	0.6	0.6	.....	.....	.....	.....	.....
	2d	.....	0.5	0.5	.....	.....	.....	.....	.....
3705.6									
3760.2	1st	.....	0.7	0.7	.....	.....	.....	.....	.....
3705.6	2d	.....	3.9	3.9	.....	.....	.....	.....	.....
3760.2	2d	.....	2.3	2.3	.....	.....	.....	.....	.....
3846.2	.....	.....	.....	.....	.....	.....	.....	.....	.....
3881	.....	.....	.....	.....	.....	.....	.....	.....	.....
3934.0	1st	26.0	.....	26.0	0.070	1.41×10^{-1}	1.53×10^{-1}	8.50×10^{-19}	1.80×10^{17}
3966.9	2d	53.9	.....	53.9	.125	1.64×10^{-1}			
4019.0	.....	.....	.....	.....	.....	.....	.....	.....	.....
4061.2	1st	.....	2.8	2.8	.123	9×10^{-3}	1.1×10^{-2}	8.94×10^{-19}	1.2×10^{16}
	2d	.....	5.6	5.6	.162	1.3×10^{-2}			
4092	2d	.....	4.0	4.0	.166	9×10^{-3}	9×10^{-3}	.....	.....
4140.5	1st	.....	1.4	1.4	.157	3×10^{-3}	5×10^{-3}	.....	.....
	2d	.....	3.0	3.0	.170	7×10^{-3}			
4196	1st	.....	1.4	1.4	.185	3×10^{-3}	5×10^{-3}	.....	.....
	2d	.....	3.0	3.0	.170	7×10^{-3}			
4226.0	1st	.....	1.6	1.6	.199	3×10^{-3}	5×10^{-3}	1.474×10^{-18}	3×10^{15}
	2d	.....	2.8	2.8	.169	6×10^{-3}			
4268.3	1st	.....	1.9	1.9	.218	3×10^{-3}	4×10^{-3}	.....	.....
	2d	.....	1.7	1.7	.168	4×10^{-3}			
4320.8	1st	.....	3.5	3.5	.246	5×10^{-3}	5×10^{-3}	.....	.....
	2d	.....	2.4	2.4	.166	5×10^{-3}			
4387.7	1st	.....	4.5	4.5	.283	6×10^{-3}	6×10^{-3}	.....	.....
	2d	.....	2.5	2.5	.162	6×10^{-3}			
4425.4	1st	.....	5.4	5.4	.304	7×10^{-3}	6×10^{-3}	.....	.....
	2d	.....	2.2	2.2	.160	5×10^{-3}			
4482.9	1st	.....	11.2	11.2	.331	1.3×10^{-2}	1.1×10^{-2}	1.097×10^{-18}	1.0×10^{16}
	2d	3.7	3.3	3.5	.154	9×10^{-3}			
4594.2	1st	.....	1.7	1.7	.368	2×10^{-3}	2×10^{-3}	.....	.....
4714	1st	.....	1.4	1.4	.367	2×10^{-3}	2×10^{-3}	9.99×10^{-20}	2×10^{16}
4920.2	1st	.....	1.5	1.5	.325	2×10^{-3}	2×10^{-3}	.....	.....
5037.2	1st	.....	2.2	2.2	.311	3×10^{-3}	3×10^{-3}	.....	.....
5176.5	1st	13.6	13.5	13.5	.330	1.6×10^{-2}	1.6×10^{-2}	4.94×10^{-19}	3.16×10^{16}
5261.1									
5319.0	1st	10.3	8.3	9.3	.419	8×10^{-3}	8×10^{-3}	1.444×10^{-20}	6×10^{17}
5423.8									
5588.3	1st	1.3	0.5	0.9	.607	6×10^{-4}	6×10^{-4}	3.054×10^{-19}	2×10^{15}
5686.7									
5686.7	1st	.....	2.4	2.4	.672	1.4×10^{-3}	1.4×10^{-3}	.....	.....
5893.3									
5893.3	1st	37.0	31.3	34.2	.724	1.80×10^{-2}	1.80×10^{-2}	2.332×10^{-19}	7.7×10^{16}
5987.1	1st	0.1	0.1	0.1	.759	1×10^{-4}	1×10^{-4}	4.26×10^{-19}	(2×10^{14})
6152.9	1st	2.7	2.4	2.5	.817	1.2×10^{-3}	1.2×10^{-3}	.....	.....
6249.2	1st	3.2	3.3	3.3	.851	1.5×10^{-3}	1.5×10^{-3}	.....	.....
6358.9	1st	25.4	20.8	23.1	0.973	9.0×10^{-3}	9.0×10^{-3}	2.510×10^{-19}	3.6×10^{16}
6456.4	.....	.....	.....	.....	.....	.....	.....	.....	.....
6471.2	.....	.....	.....	.....	.....	.....	.....	.....	.....
6565.8	1st	0.5	0.5	0.5	.....	.....	.....	.....	.....

the assumption was made that the levels of an individual term were populated in direct proportion to the statistical weights, and the following formulae were used:

$$A_{nm} = \frac{8\pi^2 e^2}{m c \lambda_{nm}^2} \frac{g_n}{g_m} f_{mn}, \tag{32}$$

$$\frac{j_{nm}}{N_m} = \frac{h c}{4\pi \lambda_{nm}} A_{nm}, \tag{33}$$

$$\frac{I}{N_m} = \frac{1}{\omega r^2} \frac{j_{nm}}{N_m}, \tag{34}$$

where f_{mn} is the absorption oscillator strength of the transition from lower level n to upper level m; g_n and g_m are the statistical weights of the two levels; λ_{nm} is the wave length of the transition; j_{nm} is the emission in ergs sec^{-1} per unit solid angle; and N_m is the number of atoms in the upper state. The quantities I/N_m are tabulated in Table 4, the quantities f_{mn} and j_{nm}/N_m being tabulated in Table 5, together with references for their sources. Finally, division of the observed values of I by I/N_m gives observed values of N_m, also tabulated in Table 4. It is apparent upon inspection of the values from the two orders in Table 4 and of Figure 3 that, while a precision of perhaps $\pm$ 20 per cent might be claimed for numbers of radiating atoms deduced from the strongest lines, only order-of-magnitude accuracy at best may be expected for the faintest lines.

The intensities in Table 4 refer only to position 4 on the meteor trail. From tracings made at a number of different positions, a study was made of the ratio of the maximum intensities of various lines to that of the second-order K line. A comparison of the K line with the zero order shows no deviation from direct proportionality. Only two lines showed an apparent deviation from proportionality to K. They were the lines at 5176 and 5893 A, both increasing in ratio to K with increasing brightness of K. This behavior is exhibited in Figure 7. It is evident that the measures really determine only two points on each curve; hence the exhibited straight-line representation is only schematic. For 5893 the change seems fairly well established, although not its course of variation. For 5176 it appears to be on the border line of detectability. Over the relatively small range in height available, no change could be detected as a function of position along the trail.

LINE DENSITY OF ELECTRONS FROM THE RADAR OBSERVATIONS

The radar echoes of this meteor give some evidence of the number of electrons produced per centimeter of path length, but the present state of the theory of radio reflections from meteoric ionization makes it difficult to calculate good quantitative values. If use is made of Greenhow's (1952) formula for the relation between number of electrons and echo duration for high-density trails,

$$N = 4\pi D N_c \tau, \tag{35}$$

where N is the number of electrons per centimeter of path length, D is the coefficient of diffusion, N_c is the critical electron density for the frequency used, and τ is the echo duration; and if it is assumed, after Greenhow (1952), that $D = 4 \times 10^4$ cm^2/sec, then

$$N = 6 \times 10^{14} \text{ electrons cm}^{-1}.$$

The calculated height of the enduring meteor echo in this case was 89 km, essentially at the position of the brightest photographic burst. The above value of N is probably a lower limit, as in this formula no account is taken of recombination and, from the general evidence of bright echoes photographed at Ottawa, recombination must become important somewhere below 90 km.

The foregoing value of N cannot at present be compared directly with the abundances of ionized atoms listed in Table 4 because of our lack of knowledge of the relevant cross-sections.

CONCLUSIONS

The important conclusions to be drawn from the foregoing discussion and analysis are that there is a detectable background continuum present, presumed to be Planck in form, and also that the first and second positive groups of bands of the neutral nitrogen

TABLE 5

OSCILLATOR STRENGTHS AND LINE INTENSITIES

Element, Multiplet No., and J-Values	Oscillator Strength (f_{mn})	Intensity per Atom in Upper Level, J_{nm}/N_m (Ergs Sec^{-1})	References
Ca I (2), 0–1	2.27	1.06×10^{-4}	Filippov (1932)
Ca I (21), 3–3	0.325*	1.96×10^{-4}	Filippov and Kremenevski (1932)
Ca I (21), 2–2	0.253*	1.52×10^{-5}	Steinhäuser (1935, 1936)
Ca I (21), 1–1	0.273*	1.64×10^{-5}	Hartree and Hartree (1938)
Ca I (21), 3–2	0.040*	3.4×10^{-6}	
Ca I (21), 2–1	0.054*	5.4×10^{-6}	
Ca I (21), 2–3	0.057*	2.5×10^{-6}	
Ca I (21), 1–2	0.091*	3.3×10^{-6}	
Ca II (1), $\frac{1}{2}$–$1\frac{1}{2}$	0.713	6.17×10^{-5}	Green and Weber (1950)
Ca II (1), $\frac{1}{2}$–$\frac{1}{2}$	0.357	6.02×10^{-5}	
Fe I (15), 5–4	0.0091	8.0×10^{-7}	King and King (1938)†
Fe I (15), 4–3	0.0079	7.1×10^{-7}	King (1942)
Fe I (15), 3–2	0.0066	6.3×10^{-7}	Kopfermann and Wessel (1951)
Fe I (15), 2–1	0.0073	8.1×10^{-7}	
Fe I (15), 1–0	0.0066	1.3×10^{-6}	
Fe I (15), 4–4	0.00278	1.87×10^{-7}	
Fe I (15), 3–3	0.00442	2.91×10^{-7}	
Fe I (15), 2–2	0.0052	3.40×10^{-7}	
Fe I (15), 1–1	0.0073	4.7×10^{-7}	
Fe I (43), 4–4	0.406	6.5×10^{-5}	
Fe I (43), 3–3	0.369	5.8×10^{-5}	
Fe I (43), 2–2	0.460	7.2×10^{-5}	
Mg I (2), 2–1	0.156	1.97×10^{-5}	Kersten and Ornstein (1941)
Mg I (2), 1–1	0.156	1.19×10^{-5}	Trefftz (1950)‡
Mg I (2), 0–1	0.156	3.97×10^{-6}	
Mg I (11), 1–2	0.119	7.2×10^{-6}	
Mg II (4), $2\frac{1}{2}$–$3\frac{1}{2}$	0.40	7.9×10^{-5}	Biermann (1946)
Mg II (4), $1\frac{1}{2}$–$2\frac{1}{2}$	0.95	7.4×10^{-5}	Biermann (1948)
Mg II (4), $2\frac{1}{2}$–$2\frac{1}{2}$	0.048	5.6×10^{-6}	
Na I (1), $\frac{1}{2}$–$1\frac{1}{2}$	0.650	1.68×10^{-5}	Stephenson (1951)
Na I (1), $\frac{1}{2}$–$\frac{1}{2}$	0.325	1.67×10^{-5}	
Si II (2), $\frac{1}{2}$–$1\frac{1}{2}$	0.88	1.81×10^{-5}	Biermann (1946)
Si II (2), $\frac{1}{2}$–$\frac{1}{2}$	0.44	1.79×10^{-5}	Biermann (1948)
Si II (4), $1\frac{1}{2}$–$\frac{1}{2}$	0.206*	2.04×10^{-5}	
Si II (4), $\frac{1}{2}$–$\frac{1}{2}$	0.206*	1.03×10^{-5}	

* Oscillator strengths calculated by means of the tables of Bates and Damgaard (1949), together with Goldberg's (1935) tables for supermultiplets in Russell-Saunders coupling. In finding oscillator strengths for individual lines of multiplets for all elements other than iron, Russell-Saunders coupling has been used, for which Russell's (1936) tables were employed.

† Relative values only are given by King and King (1938) but are calibrated by R. B. King (1942). This calibration requires further application of a factor 3.27, as indicated by absolute measurements by Kopfermann and Wessel (1951), the values in this table being so corrected.

‡ Kersten and Ornstein (1941) give relative values only but these may be calibrated by computed values of Trefftz (1950).

molecule are present, although they are not resolved. A Planck temperature of 7000° K and a source area of 400 cm² are found for the continuum. The elements and levels of ionization found in the spectrum are *Fe* I, *Fe* II, *Ca* I, *Ca* II, *Si* I, *Si* II, *Mg* I, *Mg* II, *Na* I, and *H* I. Particular attention is drawn to the identification of the *Fe* II and *H* I. Finally, there is some evidence for the variation of the relative intensities of two neutral lines with respect to the brightness of the meteor as a function of that brightness.

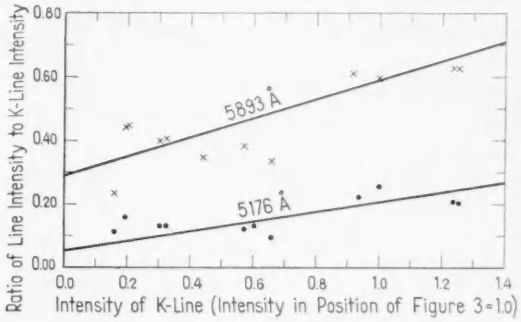

FIG. 7.—The variation of the ratios of the central intensities of two strong neutral lines to that of the K line of *Ca* II versus the actual intensity of the K line.

Thanks are due to Mr. D. R. Whittemore for running off the microphotometer tracings of the spectra and to Mr. L. A. Flower for making the exposures used in determining the field correction of camera R; also to Mr. W. F. Swann, of the Eastman Kodak Company, for providing the reciprocity failure-curve for the emulsion used; to Dr. Luigi Jacchia for furnishing the standard star sequence and the details of the method for finding the field correction; and to Dr. D. W. R. McKinley for supplying the values of height based on the radar echoes.

REFERENCES

Bates, D. R., and Damgaard, Agnette. 1949, *Phil. Trans. R. Soc. London*, *A*, **242**, 101.
Biermann, L. 1946, *Nachr. Akad. d. Wiss. Göttingen Math.-phys. Kl.*, p. 116.
———. 1948, *Zs. f. Ap.*, **25**, 325.
Budó, A. 1937, *Zs. f. Phys.*, **105**, 579.
Büttenbender, G., and Herzberg, G. 1935, *Ann. d. Phys.*, **21**, 577.
Filippov, A. 1932, *Phys. Zs. d. Sowjet-Union*, **1**, 289.
Filippov, A., and Kremenevski, N. 1932, *Phys. Zs. d. Sowjet-Union*, **1**, 299.
Goldberg, L. 1935, *Ap. J.*, **82**, 1.
Green, L. C., and Weber, N. E. 1950, *Ap. J.*, **111**, 582.
Greenhow, J. S. 1952, *Proc. Phys. Soc.*, **658**, 169.
Hartree, D. R., and Hartree, W. 1938, *Proc. R. Soc. London*, *A*, **164**, 167.
Herzberg, G. 1950*a*, *Molecular Spectra and Molecular Structure*, Vol. **1**: *Spectra of Diatomic Molecules* (New York, D. van Nostrand Co.), Fig. 8, p. 32.
———. 1950*b*, *ibid.*, Table 39, p. 552.
Jacchia, L. G. 1949, *Tech. Rept. No. 3* (Harvard Coll. Obs., and Center of Anal., M.I.T.), pp. 6–8.
Jarmain, W. R., and Nicholls, R. W. 1952, *Sci. Rept. No. 4* (Univ. Western Ontario, Dept. Physics).
Keenan, P. C., and Morgan, W. W. 1950, *Astrophysics: A Topical Symposium*, ed. J. A. Hynek (New York: McGraw-Hill Book Co.), chap. i.
Kersten, J. A. H., and Ornstein, L. S. 1941, *Physica*, **8**, 1124.
King, R. B. 1942, *Ap. J.*, **95**, 78.
King, R. B., and King A. S. 1938, *Ap. J.*, **87**, 24.
Kopfermann, H., and Wessel, G. 1951, *Zs. f. Phys.*, **130**, 100.

McKinley, D. W. R., and Millman, P. M. 1949, *Canad. J. Res., Sec. A.*, **27**, 53.
Milford, N. 1950*a*, *Ann. d'Ap.*, **13**, 243.
———. 1950*b*, *ibid.*, p. 251.
———. 1950*c*, *ibid.*, p. 263.
Millman, P. M. 1932, *Harvard Ann.*, **82**, 113.
———. 1935, *ibid.*, p. 149.
———. 1951, *A.J.*, **56**, 45.
———. 1952, *J. R. Astr. Soc. Canada*, **46**, 121.
———. 1953*a*, *ibid.*, **47**, 217.
———. 1953*b*, *Nature*, **172**, 853.
Moore, C. E. 1945, *Contr. Princeton U. Obs.*, No. 20.
Payne-Gaposchkin, C. 1938*a*, *Harvard Obs. Mimeograms*, Ser. III, No. 1.
———. 1938*b*, *ibid.*, No. 2.
Russell, H. N. 1936, *Ap. J.*, **83**, 129.
Steinhäuser, A. 1935, *Zs. f. Phys.*, **95**, 669.
———. 1936, *ibid.*, **99**, 300.
Stephenson, G. 1951, *Proc. Phys. Soc. London, A*, **64**, 458.
Trefftz, E. 1950, *Zs. f. Ap.*, **28**, 67.
Unsöld, A. 1938, *Physik der Sternatmosphären* (Berlin: Julius Springer), chap. xi, Secs. 58, 59, pp. 208–218.

FIG. 1.—Still photograph of an aluminum pellet in flight. The boxlike object behind the flight line is the spectrograph

SUPPRESSION OF *AlO* IN THE WAKE OF ULTRASPEED PELLETS

WILLIAM C. WHITE
Michelson Laboratory, United States Naval Ordnance Test Station,
Inyokern, China Lake, California
Received July 3, 1954; revised July 29, 1954

ABSTRACT

Time-resolved spectrograms of aluminum ultraspeed pellets have been obtained along their trajectories. The *AlO* bands were observed to be suppressed for a length of time depending upon the position of the pellet along its trajectory. The time of suppression is a few microseconds at the beginning of the trajectory, reaches a maximum of about 180 microseconds at 1.8 meters, and goes to 5 microseconds at approximately 3.5 meters.

INTRODUCTION

Two previous reports (White, Rinehart, and Allen 1952; Allen and Mayfield 1953) have discussed time-resolved spectroscopy of ultraspeed pellets. The results of one investigation (Allen and Mayfield 1953) indicated that the various features of the spectra of aluminum pellets were separated in time and appeared in the following order: ballistic shock, atomic spectra of the metallic constituents of the pellet, and *AlO* bands. The time delay in the appearance of the *AlO* bands was several microseconds after the ballistic shock.

A subsequent report (Thomas and White 1953) presented a semiquantitative interpretation of the time delay in the appearance of the *AlO* bands. Several mechanisms for the production of *AlO* in the wake of ultraspeed pellets were investigated. That process which gave the best explanation of the phenomena observed in the time-resolved spectra (Allen and Mayfield 1953) predicted that the time delay should decrease with decreasing velocity of the pellet. As a result of this prediction, a systematic investigation of the spectra along the trajectory of aluminum ultraspeed pellets was undertaken.

Time-resolved spectrograms were obtained at different positions along the pellet trajectory. As the pellet velocity decreases with distance along its trajectory, the time-resolved spectrograms furnish data on the possible dependence on velocity of the time delay in the appearance of *AlO* bands. This report presents the results of the above investigation.

EXPERIMENTAL ARRANGEMENT AND PROCEDURE

In the previous investigation conducted by Allen and Mayfield (1953), the time-resolving spectrographic camera was placed a sufficient distance from the line of flight so that a length of the luminous trail of the pellet could be used as a slit. Because the light was integrated over a length of trail, time-resolved spectrograms of good photographic density were obtained which showed the atomic spectra in fine detail.

The above method has the disadvantage of not allowing the changes of the spectra with time to be observed at a specific point on the trajectory of the pellet. To overcome this disadvantage, the data presented in the present report were obtained by placing the same spectrographic camera at one end of a 6-foot box which contained a slit 1 mm wide at the opposite end. The pellets were fired across the slit and normal to the slit length. The film was moved in a direction parallel to the slit length. Although this arrangement does have the advantage of allowing observation of the spectra essentially at a point, in general the spectrograms are fainter and show few or no atomic spectra. Figure 1 is a photograph of the luminous trail of a pellet as it passes in front of the spectrograph.

The spectra of the pellets were studied at several specific points along the flight line.

The distance from the position of firing to the point of study ranged from 0.88 to 3.55 meters. One or more time-resolved spectrograms were obtained for each point. A separate pellet was fired for each spectrogram.

A continuously moving film camera was operated in conjunction with the time-resolving spectrograph. The film was moved perpendicular to the trajectory of the pellet. Using the procedure of a previous paper (Allen, Rinehart, and White 1952), the velocities of the pellets were computed for the points at which the spectra were observed. Figure 2 is a reproduction of one of the "streak" photographs from which the velocities were measured.

RESULTS

Figure 3, *a*, is a time-resolved spectrogram taken at 0.88 meter along the trajectory. Below the spectrogram (Fig. 3, *b*) is a reproduction of a microdensitometer trace taken normal to the dispersion of the spectra. Figures 4 and 5 are microdensitometer traces of spectrograms taken at 1.71 and 3.02 meters, respectively. The ballistic shock, region of

TABLE 1

DISTANCES, VELOCITIES, AND TIMES OF SUPPRESSION

s (Meters)	v_{obs} (Meters/ Msec)	v_{calc} (Meters/ Msec)	t_{obs} (μsec)	t_{calc} (μsec)	s (Meters)	v_{obs} (Meters/ Msec)	v_{calc} (Meters/ Msec)	t_{obs} (μsec)	t_{calc} (μsec)
0.88	4.8	4.29	23	17	1.71	4.1	4.00	163	167
0.88	4.1	4.29	20	17	2.34	*	3.79	96	167
0.88	3.9	4.29	14	17	2.42	4.2	3.77	97	105
1.39	3.9	4.11	97	103	3.02	3.7	3.59	25	17
1.51	4.4	4.07	145	131	3.02	3.5	3.59	12	17
1.71	3.9	4.00	184	167	3.55	2.8	3.43	4	3

* Data not obtained.

the suppression of *AlO*, and maximum intensity of the *AlO* bands occur in that order. The time of suppression of *AlO* is taken to be the time between the appearance of the ballistic shock and the maximum intensity of the *AlO* bands. Table 1 lists (*a*) the distances along the trajectory, (*b*) observed velocities, (*c*) calculated velocities computed in a manner described below, (*d*) the time of suppression, t_{obs}, which is an average of several visual and microdensitometer measurements, and (*e*)t_{calc}, calculated from formula (2).

Figure 6 is a plot of times of suppression, t_{obs}, against distance along the trajectory. The time delay in the appearance of the maximum intensity of the *AlO* bands is about 20 microseconds at 0.88 meter along the trajectory, increases to a maximum of about 180 microseconds at 1.82 meters, and then decreases to approximately 5 microseconds at 3.55 meters. As the film velocity of the spectrographic camera was 0.1 mm/μsec and the imaged slit length was 1 mm or less, the resolution in time is 10 microseconds.

The observed velocities listed in Table 1 show considerable scatter. This scatter arises both from experimental errors of measurement and from uncontrollable small differences in the shape of each pellet. It is known (Allen, Rinehart, and White 1952) that the trajectory of each pellet can be described by the empirical velocity-distance relationship

$$v = v_0 e^{-\alpha s}, \tag{1}$$

where v is the velocity at any point along the trajectory, v_0 is the initial velocity, α is a constant, and s is the distance along the trajectory. Values for v_0 and α were computed

FIG. 2.—Streak photograph of a pellet. The long luminous streaks at the bottom of the photograph are due to the explosive products.

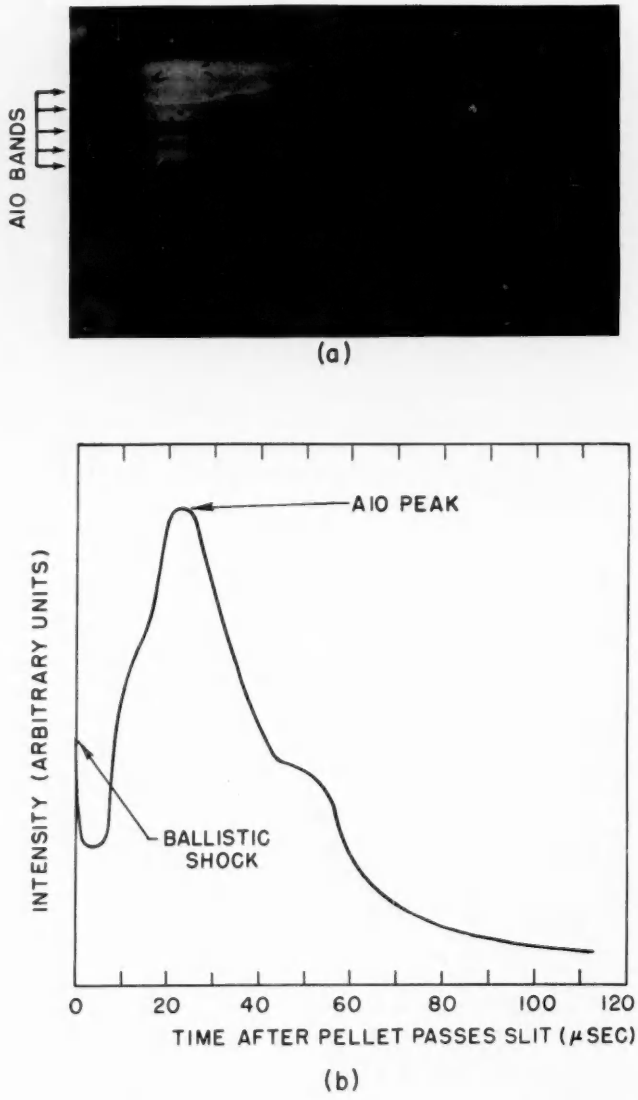

FIG. 3.—*a:* Time-resolved spectrogram of an aluminum pellet taken at a distance of 0.88 meter along the trajectory. Pellet velocity is 4.29 meters/msec. Time delay in the appearance of the maximum intensity of the AlO bands is 23 microseconds. *b:* Microdensitometer trace of the spectrogram shown in Fig. 3, *a*.

from the velocity data for each pellet. In order to smooth the velocity data, the average values of v_0 and a were used to calculate the velocity of the pellet for the distances at which the spectrograms were taken. The average value for v_0 was 4.62 ± 0.09 meters/msec. The average value for a was 0.084 ± 0.011 inverse meters. Figure 7 is a semilog

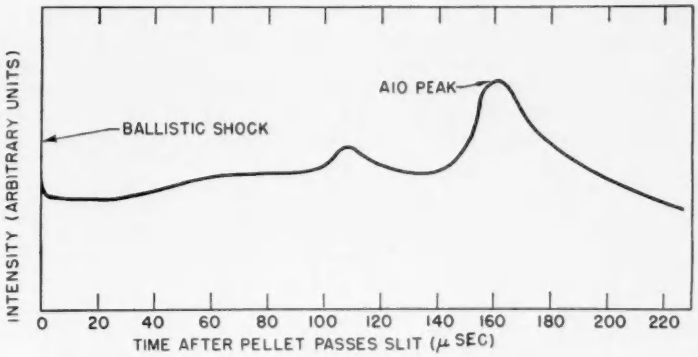
AlO PEAK
BALLISTIC SHOCK
INTENSITY (ARBITRARY UNITS)
0 20 40 60 80 100 120 140 160 180 200 220
TIME AFTER PELLET PASSES SLIT (μ SEC)

FIG. 4.—Microdensitometer trace of a time-resolved spectrogram of an aluminum pellet taken at a distance of 1.71 meters along the trajectory. Pellet velocity is 4.00 meters/msec. Time delay in the appearance of the maximum intensity of the A10 bands is 160 microseconds.

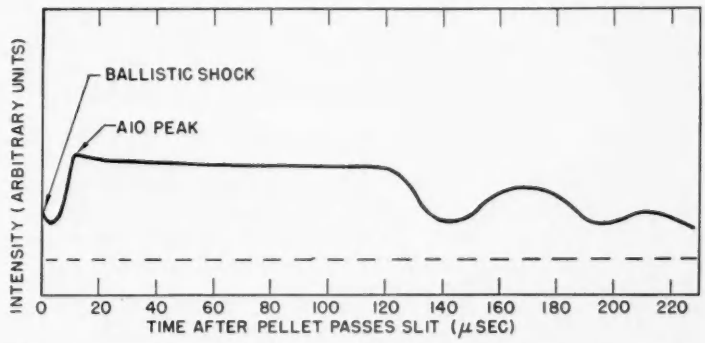
BALLISTIC SHOCK
AlO PEAK
INTENSITY (ARBITRARY UNITS)
0 20 40 60 80 100 120 140 160 180 200 220
TIME AFTER PELLET PASSES SLIT (μ SEC)

FIG. 5.—Microdensitometer trace of a time-resolved spectrogram of an aluminum pellet taken at a distance of 3.02 meters along the trajectory. Pellet velocity is 3.59 meters/msec. Time delay in the appearance of the maximum intensity of the A10 bands is 17 microseconds.

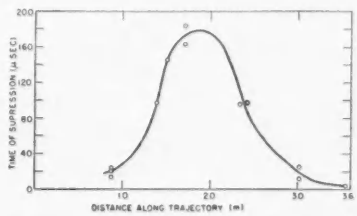

FIG. 6.—Time of suppression as a function of distance along the trajectory

plot of pellet velocities for the distances given in Table 1. The circles represent observed velocity values. The straight line represents the calculated velocities. Figure 8 is a plot of the times of suppression, t_{obs}, against the calculated velocities.

DISCUSSION

The mechanism proposed (Thomas and White 1953) for the suppression of *AlO* in the wake of ultraspeed pellets is that the formation of *AlO* is inhibited by the region of high kinetic temperature near the shock wave of the pellet. This inhibition continues until a point is reached in the wake of the pellet where the temperature has dropped to a value that allows a maximum concentration of *AlO* to occur. As a consequence, it was predicted (Thomas and White 1953) that, if the "inhibition mechanism" was correct,

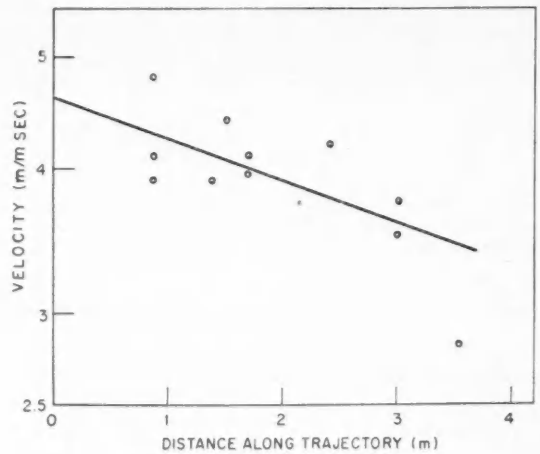

FIG. 7.—Pellet velocity as a function of distance along the trajectory

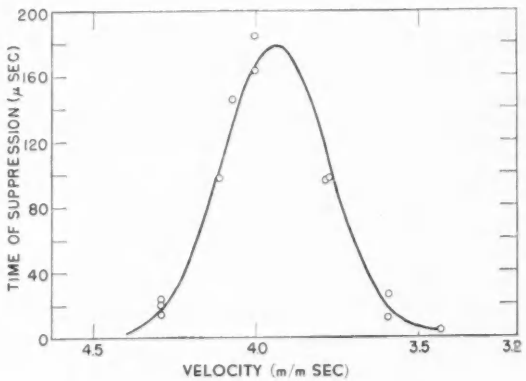

FIG. 8.—Time of suppression as a function of pellet velocity

the time of suppression of *AlO* should become shorter with lower velocities. As the pellet moves along its trajectory, its velocity decreases. The decrease in velocity decreases the kinetic temperature, and, therefore, the time of suppression of *AlO* should be shorter.

Figures 6 and 8 are in agreement with the prediction of the dependence of the time of suppression on velocity after the pellet has moved 1.82 meters along the trajectory and has slowed down to a velocity of 3.94 meters/msec. The maximum time of suppression is approximately 180 microseconds at 3.94 meters/msec. At 3.5 meters/msec the time of suppression of *AlO* has been reduced to approximately 5 microseconds.

Before the pellet has reached a point 1.82 meters along its trajectory, the dependence of the time of suppression on velocity is the reverse of the predicted behavior of the *AlO* bands. The time of suppression becomes greater with lower velocities until the maximum is reached at 180 microseconds.

The reason for the reverse of the predicted behavior for the initial part of the time-velocity or time-distance curve is not fully understood. One proposal is that the products of explosion[1] exert effectively a pressure at the rear of the pellet's wake. This pressure would decrease with distance along the trajectory and would have the effect of increasing the rate of expansion, with a subsequent increase of the rate of cooling of the ablated material in the wake. For such a condition, *AlO* would form rapidly, and the maximum intensity of the *AlO* bands would occur sooner. However, the experimental evidence indicates that, for the size of explosive charge used, the luminous front of the explosive products does not travel more than 1 meter from the point of initiation. Furthermore, the streak photographs (Fig. 2) show that the pellet is a considerable distance ahead of the explosive products at a point 1 meter along the trajectory.

A possible alternate explanation is that the high kinetic temperature behind the shock wave not only acts as an inhibitor for the formation of *AlO* but also affects the expansion rate of the material in the wake. For the initial portion of the trajectory, the temperature may be high enough so that the maximum amount of *AlO* may not be reached in the wake until after the density of the ablated material has dropped to a value such that the *AlO* bands are no longer visible. However, a *maximum density* of *AlO* could still occur.

As the pellet moves along its trajectory, the kinetic temperature behind the shock drops because of the decreasing velocity. This drop in temperature decreases the rate of expansion, and the maximum density of *AlO* occurs farther back in the wake. As a result, the time delay in the appearance of the maximum intensity of the *AlO* bands increases. At some point on the trajectory, the maximum density and the maximum amount of *AlO* probably occur at the same time. After this point is reached, the behavior of the *AlO* bands is in accordance with the previously mentioned inhibition process. Before the pellet reaches this position, the behavior can be explained by a combination of the inhibition process and a decreasing rate of expansion of the ablated material in the wake.

The shape of the time-velocity curve suggests the relationship:

$$t = t_m e^{-\beta(v-v_m)^2} \tag{2}$$

where t is the time of suppression, t_m is the maximum t, β is a constant, v is the velocity of the pellet, and v_m is the velocity at t_m. From Figure 6, t_m is 180 microseconds and v_m is 3.94 meters/msec. Using these graphical values of v_m and t_m and the values of t_{obs} and v from Table 1, values of β were calculated and averaged. The resulting average value of β was 19 ± 1 (μsec/meter)^2. The values of t were then recalculated and are given as t_{calc}. The circles indicate values of t_{obs}.

[1] The pellet is fired by an explosive charge.

SUMMARY

1. The hypothesis of "temperature dependence" of the formation of *AlO* in the wake was reviewed.

2. The time of suppression of *AlO* is correlated with velocity directly and with temperature indirectly. After 1.82 meters along the trajectory of the pellet, the time of suppression decreases with decreased velocity.

3. Before 1.82 meters the time-velocity curve may possibly be explained by back pressure of the explosive products or, tentatively, by an effect produced by a combination temperature and density variation. The latter explanation is probably preferable.

4. The time-velocity curve can probably be expressed empirically by equation (2).

It is a pleasure to acknowledge the assistance of Mr. E. B. Mayfield, who indoctrinated the author in the use of the time-resolving camera and also assisted in the experimental work. Mr. J. W. Rogers handled the experimental arrangements and Mr. J. C. McLaughlin the ordnance work.

REFERENCES

Allen, William A., and Mayfield, Earle B. 1953, *J. Appl. Phys.*, **24**, 131.
Allen, William A., Rinehart, John S., and White, W. C. 1952, *J. Appl. Phys.*, **23**, 132.
Thomas, R. N., and White, W. C. 1953, *Ap. J.*, **118**, 555.
White, W. C., Rinehart, John S., and Allen, William A. 1952, *J. Appl. Phys.*, **23**, 198.

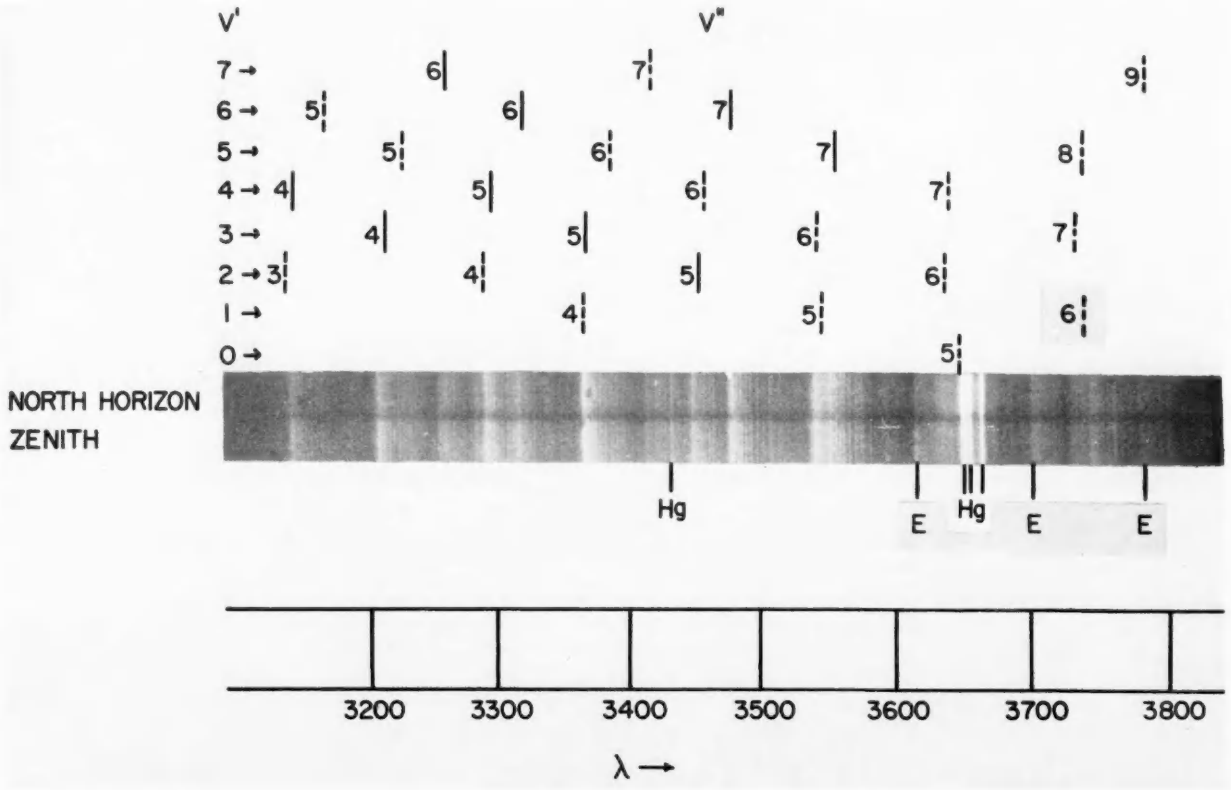

FIG. 1.—Spectrum of the ultraviolet airglow. Solid lines indicate Herzberg O_2 bands well established. Dashed lines indicate bands not positively identified but probably present. An E indicates an unidentified emission.

THE ULTRAVIOLET AIRGLOW SPECTRUM*

JOSEPH W. CHAMBERLAIN
Yerkes Observatory
Received August 2, 1954; revised August 18, 1954

ABSTRACT

A spectrum of the ultraviolet airglow has been obtained with high dispersion (23 A/mm) and superior resolution. The rotational structure, which is clearly resolved except near the band heads, shows conclusively that most of these airglow bands arise from the forbidden Herzberg system of O_2. Longward of 3600 A the starlight continuum becomes noticeable and in the blue tends to obscure the O_2 emission. A few emission features remain unidentified. The relative intensities of the bands, the excitation of the upper state, the rotational temperature, and the importance of de-exciting collisions in the emitting region are discussed.

I. INTRODUCTION

The identification of the ultraviolet airglow bands has been a perplexing problem for many years. J. Dufay (1941, 1947) originally suggested that the forbidden Herzberg ($A\ ^3\Sigma_u^+ \rightarrow X\ ^3\Sigma_g^-$) system of O_2 might be responsible for these bands, and Swings (1943) concurred in this proposal, assigning many additional Herzberg bands to the airglow spectrum. Barbier (1947*a*) also supported these identifications on the basis of his careful studies of the spectrum between 3000 and 5000 A (Barbier 1945).

Still, there has been considerable reluctance among workers in the subject to accept most of these bands. One of the main difficulties has been the apparent disagreement between the theoretical and observed relative intensities (J. Dufay 1947). Moreover, the accuracy of measurement of the bands on low-dispersion plates has been too poor to exclude the possibility of fortuitous coincidences between observed and computed band positions (J. Dufay and Déjardin 1946). For example, Auberger (1953) recently proposed a number of alternative band systems for the ultraviolet and blue airglow and expressed the opinion that the Herzberg system could not account for more than a few of the observed features.

In an effort to settle this problem, several long-exposure plates of the ultraviolet spectrum have been obtained (Chamberlain 1954*a*). The spectrograph utilizes a grating with 600 lines per millimeter and an $F/0.8$ flat-field Schmidt camera, 23 cm in diameter, designed by A. B. Meinel. The grating is used in the third-order ultraviolet, giving a dispersion of 23 A/mm, which is quite high for airglow spectra. The projected slit-width, for the best plate obtained, was 34 μ (= 0.78 A), and the exposure was 75 hours on Eastman 103*a*-O emulsion. By means of a field lens and mirror in front of the slit, the zenith and north horizon are photographed simultaneously. Thus, if any auroral emissions are present, they are much stronger on the horizon part of the spectrum and are easily recognized. In the ultraviolet the airglow spectrum is somewhat stronger in the zenith than on the horizon, in spite of the former's shorter emitting-path length, owing to the large amount of atmospheric scattering. A *Ne* comparison spectrum was used to calibrate the wave-length measurements. In addition, a few *Hg* lines arising from artificial lights in a neighboring village serve as wave-length standards but otherwise are a source of irritation, since they obliterate a small part of the airglow spectrum.

II. IDENTIFICATIONS

1. HERZBERG BANDS

The ultraviolet spectrum is shown in Figure 1, and microphotometer tracings are presented in Figures 2 and 3. In these figures the Herzberg bands of O_2 are indicated,

* The research reported in this paper has been supported in part by the Geophysics Research Directorate of the Air Force Cambridge Research Center under Contract AF 19(122)-480.

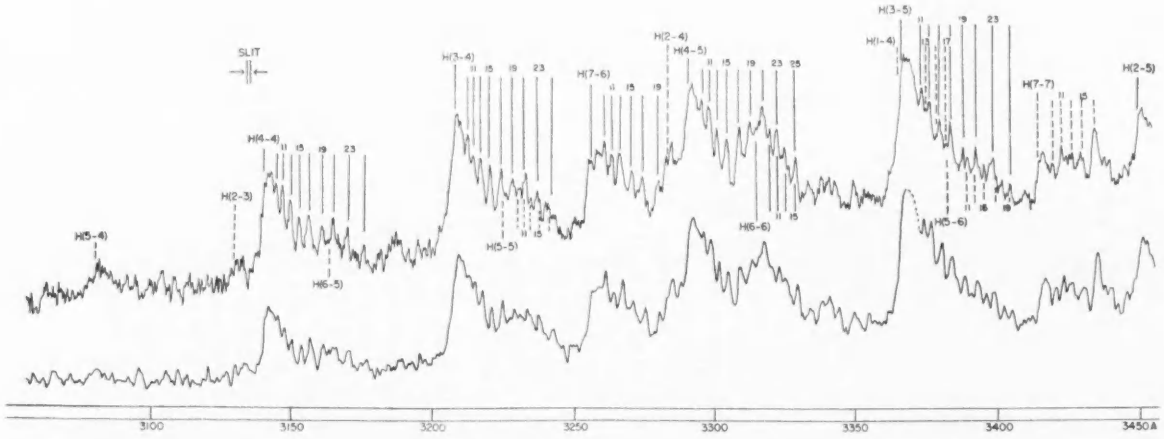

FIG. 2.—Microphotometer tracing of spectrum shown in Fig. 1, 3060–3450 A. Upper tracing is from the zenith spectrum; lower tracing, from the horizon spectrum. The heads of the Herzberg bands are marked with an *H*. Also indicated are the rotational lines and their *K* numbers for many bands.

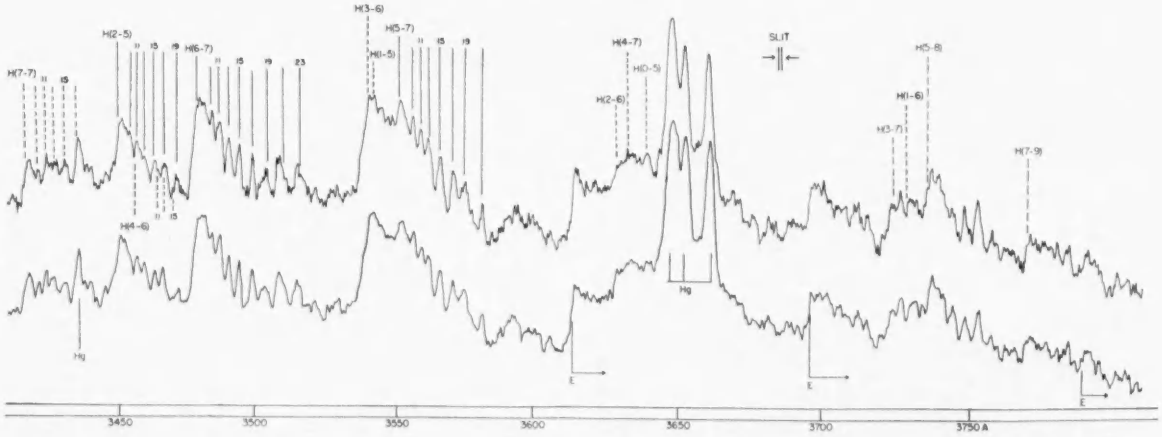

FIG. 3.—Microphotometer tracing of spectrum shown in Fig. 1, 3400–3800 A. Unidentified emissions are indicated by an *E*

where the adopted vibrational numbering is that recently proposed by Broida and Gaydon (1954), who have produced these bands in emission in a laboratory afterglow.

For the stronger bands the rotational structure, which consists of a single Q-form branch,[1] is clearly resolved for $K \geq 9$, and in these cases there can be no doubt of the identification. Other bands in the system, which are probably present but whose rotational structure is not sufficiently strong and sharp for a positive identification, are indicated by dashed lines.

In Table 1 are listed the wave lengths of clearly defined features identified as Herzberg band heads or rotational lines (a number of other bands indicated in Figs. 2 and 3, not quite so conspicuous, are omitted from this table). In his high-dispersion analysis of the absorption bands, Herzberg (1952) showed that the fine structure in each "line" covers a range of about 10 cm^{-1}; that is, in the wave-length region considered in this paper, each "line" will have a width of the order of 1 A. Therefore, the computed wave lengths in Table 1 have been obtained for the ${}^{Q}R_{12}$ branch, since these components lie close to the centers of the Q-form "lines."

For these computations Herzberg's (1952, Table 8) predicted band origins have been adopted, with the change in v' numbering mentioned above. The lower (rotational) level of a ${}^{Q}R_{12}$ transition is the F_2'' component (with $J'' = K''$) of the ${}^3\Sigma_g^-$ state, and its energy above its vibrational level depends only on the accurately known rotational constants, $B_{v''}$ and $D_{v''}$ (Herzberg 1950, Table 39). For the F_1' levels ($J' = K' + 1$) in the upper state I have used Herzberg's (1952, Table 2) rotational constants to obtain F_2' and added the small correction $F_1' - F_2'$ (Herzberg 1952, Table 3).

In nearly all cases the agreement between observed and computed wave lengths in Table 1 is excellent: for unblended rotational lines the mean residual, averaged without regard to algebraic sign, is approximately 0.2 A. This band system is discussed more fully in Section III.

2. CONTINUUM

Although J. Dufay (1923, 1928) and later Cabannes and Dufay (1944) listed a number of coincidences with solar absorption lines in the blue and ultraviolet night-sky spectrum, most observers have felt that starlight and zodiacal light were not significant sources of the light of the night sky. Barbier (1945, 1947*b*), in particular, has disagreed with these identifications of absorption lines. Recently, the question was reopened by Meinel (1953) and by Chamberlain and Oliver (1953), who pointed out, on plates with improved resolution, some rather striking similarities with stellar and solar spectra in the blue. On the basis of recent photometric studies, however, Barbier (1954) has again objected to the assignment of a major portion of the night-sky light to extraterrestrial sources.

Careful examination of the ultraviolet spectrum and comparison with the solar spectrum indicates that starlight and/or zodiacal light are clearly discernible at wave lengths as short as 3600 A. Below this point the stellar continuum is too weak to be definitely identified but probably has some effect on the apparent structure of emission bands (e.g., around 3500 A).

The faint, broad "emission" feature at λ 3600 probably belongs to the stellar continuum, as it compares favorably with the corresponding part of the solar spectrum. Several other features between 3600 and 3800 A suggest a stellar spectrum; still, some of the most convincing evidence is the appearance of absorption lines in the blue region. At longer wave lengths, however, a true airglow continuum may become important. Broida and Gaydon (1954) observed the air-afterglow continuum on their O_2 plates and suggested that the same reaction contributed to the night-sky continuum.

[1] In the laboratory absorption spectra Herzberg (1952) detected O- and S-form branches, but they were quite weak. Also, under high resolution he observed the six components in each "line." The transitions giving rise to this fine structure have been diagramed by Herzberg (1950, 1952).

TABLE 1

O_2 HERZBERG BANDS IN ULTRAVIOLET AIRGLOW

Band ($v'-v''$)	Line (K)	λ_{air} Computed*	λ_{air} Measured	Band ($v'-v''$)	Line (K)	λ_{air} Computed*	λ_{air} Measured
4–4	Max.	(3141.2)	3143.1	3–5	11	3374.6	3374.3#
4–4	9	3145.7	3145.7	3–5	13	3377.5	3377.2#
4–4	11	3147.9	3148.0	3–5	15	3380.9	3380.8#
4–4	13	3150.6	3150.8	3–5	17	3384.7	3384.5**
4–4	15	3153.8	3153.8	3–5	19	3389.1	3388.7
4–4	17	3157.4	3157.0	5–6	11	3389.7	3390.3
4–4	19	3161.4	3161.8	3–5	21	3393.9	3393.6
4–4	21	3165.9	3165.9†	5–6	13	3392.9	
4–4	23	3170.8	3170.3†	5–6	15	3396.2	3396.6
4–4	25	3176.2	3176.0†	3–5	23	3399.1	3399.5
3–4	Max.	(3209.3)	3209.8	3–5	25	3404.9	3405.6
3–4	9	3213.8	3213.7	7–7	Max.	(3414.7)	3416.8
3–4	11	3216.0	3215.9	7–7	9	3420.4	3420.3
3–4	13	3218.7	3218.4	7–7	11	3423.2	3423.2§
3–4	15	3221.9	3222.1	7–7	13	3426.6	3426.7§
3–4	17	3225.5	3225.3‡	7–7	15	3430.6	3430.8§
3–4	19	3229.6	3229.1‡	7–7	17	3435.1	3435.2††
3–4	21	3234.0	3234.1	2–5	Max.	(3450.1)	3451.5
5–5	11	3232.1		2–5	9	3454.9	3454.9
3–4	23	3239.0	3238.7	2–5	11	3457.3	3457.5
5–5	15	3238.4		4–6	Max.	(3456.5)	
3–4	25	3244.4	3244.1	2–5	13	3460.2	3460.5
5–5	17	3242.1		2–5	15	3463.6	3463.4
7–6	Max.	(3257.1)	3257.9§	4–6	11	3464.2	
7–6	9	3262.3	3262.0	2–5	17	3467.5	3467.5
7–6	11	3265.0	3265.2	4–6	13	3467.2	
7–6	13	3268.2	3268.1	2–5	19	3471.9	3472.2
7–6	15	3271.9	3272.1	6–7	Max.	(3479.5)	3479.8
7–6	17	3276.1	3275.7	6–7	9	3484.8	3484.6
7–6	19	3280.9	3280.9	6–7	11	3487.6	3487.3
2–4	Max.	(3284.3)	3285.6	6–7	13	3490.9	3490.5
7–6	21	3286.2		6–7	15	3494.8	3494.6
4–5	Max.	(3292.6)	3293.4	6–7	17	3499.2	3499.7
4–5	9	3297.3	3296.8	6–7	19	3504.2	3504.2‡‡
4–5	11	3299.7	3299.6	6–7	21	3509.8	3508.9‡‡
4–5	13	3302.6	3302.5	6–7	23	3515.9	3515.5‡‡
4–5	15	3306.0	3305.9	3–6	Max.	(3539.2)	3541.3
4–5	17	3309.8	3309.9	1–5	Max.	(3541.0)	3543.3
4–5	19	3314.1	3314.3‖	5–7	Max.	(3552.5)	3553.6
4–5	21	3318.9	3318.6‖	5–7	9	3557.9	3557.9
6–6	9	3320.9	3320.9	5–7	11	3560.7	3560.8
4–5	23	3324.1	3323.6	5–7	13	3564.0	3564.0
6–6	11	3323.5		5–7	15	3567.8	3567.6
6–6	13	3326.6	3326.2	5–7	17	3572.2	3572.1
4–5	25	3329.9	3330.0	5–7	19	3577.2	3576.7
6–6	15	3330.2		5–7	21	3582.7	3582.7
1–4	Max.	(3366.5)	3369.8				
3–5	Max.	(3367.5)					

* The computed band origins, λ_0, are given in parentheses in place of computed maxima. The observed band maxima would be expected at slightly longer wave lengths than these computed origins.

† Blend with weak 6–5 band.

‡ Blend with head of weak 5–5 band.

§ Peculiar structure.

‖ Blend with head of 6–6 band.

Possibly blended with lines of faint 1–4 band.

** Blend with head of weak 5–6 band.

†† Blend with H_β, λ 3434.7 (artificial-light contamination).

‡‡ Blend with stellar feature.

It does not seem likely that much of the ultraviolet and blue continuum is emitted by the upper atmosphere, since the H and K lines of *Ca* II are extremely deep on well-resolved spectra. The G band at λ 4300 seems to be partially "filled in" with O_2 emission (see Table 2); otherwise, it too would probably be quite deep. A photometric study by Roach, Pettit, and Meinel (1955) indicates that a considerable portion (about 80 per cent) of the night-sky continuum at wave lengths as long as 5300 A is extraterrestrial.

In the blue region (say, 3800–4500 A) the continuum makes the identification of true emissions quite difficult. However, with the definite assignments of the Herzberg bands in the ultraviolet, about eight bands arising from $v' = 0$, 1, and 2 can be identified in the blue with some confidence (see Table 2).

3. OTHER EMISSIONS

The Herzberg bands and stellar continuum by no means completely explain the entire ultraviolet spectrum. The most conspicuous unidentified feature is a band degraded toward the red with a sharp head at 3615 A. Other bands at 3698 and 3789 A may belong to the same system. Also, there are some peculiar features in the structure of the 7–6 and 7–7 bands that suggest underlying emission bands.

There seems to be no evidence, however, for any of the other band systems that have been proposed for the ultraviolet airglow. In particular, the N_2 Vegard-Kaplan bands, the O_2 Schumann-Runge bands, and the recently discovered $^1\Sigma_u^- \rightarrow {}^3\Sigma_g^-$ bands of O_2 (Herzberg 1953) are apparently absent.

III. HERZBERG BANDS OF O_2

1. BAND INTENSITIES

Figure 4 is a Deslandres table, showing theoretical and observed relative intensities of those bands lying in the wave-length range 3100–3800 A. More complete tables of band positions are given in wave-number units by Herzberg (1952) and in wave lengths by Pillow (1953). It should be pointed out that Pillow's vibrational numbering is the same as that used here, in which v' (upper level) is one unit greater than in the numbering tentatively assigned by Herzberg.

Within progressions with $v' = 2$, 3, and 4 the agreement between theoretical and observed intensities is quite acceptable.[2] For higher progressions, however, the comparison is much worse. Some of the differences may be due to errors in the theoretical intensities, which are based only on overlap integrals—i.e., the electronic transition moment, R_e, has been assumed constant with r, the internuclear distance. Overlap integrals computed by Fraser, Jarmain, and Nicholls (private communication) show little difference from those of Pillow; however, R. W. Nicholls (private communication) has found evidence for a strong dependence of R_e upon r, by comparing Broida and Gaydon's laboratory intensities with the computed overlap integrals.

On the other hand, some of the intensity anomalies probably arise from the underlying stellar continuum and from unidentified emission bands. Both these sources may be important, as I pointed out in Section II.

2. EXCITATION

R. W. Nicholls (private communication) has recently analyzed Broida and Gaydon's eye estimates of intensity to derive the relative populations in the upper-state vibrational levels. Briefly, he finds a rapid decrease in populations between $v' = 0$ and $v' = 2$, followed by a steady increase from $v' = 2$ to $v' = 7$.

[2] In these progressions there is also good agreement between the airglow and laboratory estimates of intensity. In lower and higher progressions the bands are weak in this part of the ultraviolet (note the primary Condon parabola in Fig. 4) and were not observed by Broida and Gaydon.

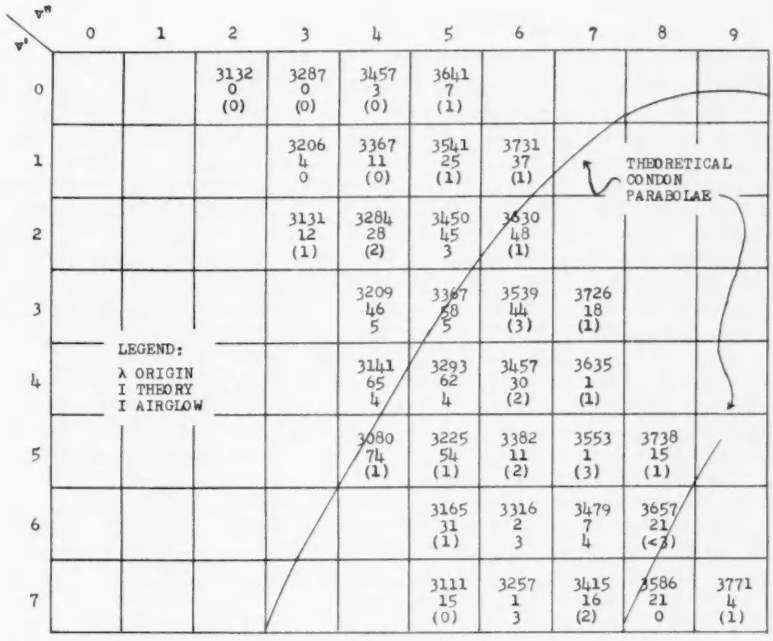

FIG. 4.—O_2 Herzberg bands, 3100–3800 A. The figure gives the following for each band with $v' \leq 7$ in the 3100–3800 A region: wave-length of the band origin; the relative theoretical intensity for equal populations of the upper (v') levels; and an eye estimate of the relative intensities in the airglow. The latter are on a scale of 5 for the strongest bands and are put in parentheses when there is an appreciable uncertainty in the band's intensity because of blends with other features.

TABLE 2

PROBABLE O_2 AIRGLOW BANDS, 3800–4500 A*

v'	v'' = 6	7	8	9
0	3842 16	4064 26	4308† 34	.....
1	Cf. Fig. 4	3940‡ 43	4169 33	4422 17
2	Cf. Fig. 4	3827 36	4044 13	4282§ 0

* Wave length and theoretical intensity (for equal populations in the upper levels) are given for each band found in the blue region (see Chamberlain and Meinel 1954, Fig. 15, p. 552).

† Band head and G-band absorption distort one another.

‡ Situated between H and K lines of *Ca* II, which affect band's appearance.

§ This band is uncertain. A portion of the band may fill in part of G-band absorption.

Because of the uncertainties in the relative intensities, especially outside the range 3100–3600 A, a quantitative excitation analysis of the airglow bands is not now practicable. The eye estimates presented in Figure 4, however, do suggest an increase in populations with increasing v'. One of the objections often cited against the identification of this band system in the ultraviolet airglow was that the bands in the visible spectrum should be extremely strong. Part of their faintness is probably due to relatively low populations in $v' = 0$ and $v' = 1$, although obscuration produced by the continuum is also an important factor.

The laboratory O_2 afterglows show the green line of [O I] and the red Atmospheric system of O_2 in common with airglow spectra, and it is quite likely that the excitation mechanisms in the two sources are similar. If the mechanism for exciting O_2 in the airglow is reassociation of two oxygen atoms (in the presence of a third body), one would expect the emission to be formed in the O_2–O transition zone. It is generally believed that this transition takes place over the altitude range 80–120 km, but mixing and diffusion will transport some O_2 to much greater heights (cf. Nicolet 1954, pp. 670–680).

Emitting heights are extremely difficult to determine in the ultraviolet, largely because of the great amount of Rayleigh scattering. From a photometric study of the ultraviolet, Barbier (1953) places the emitting layer at 200 km but emphasizes the very large uncertainty in this figure. We might also expect the O_2 Herzberg and Atmospheric systems to be formed at the same level, but Chamberlain (1954*b*) has shown that, because of a fluorescence effect, the Atmospheric emission band may appear to originate below the true emitting layer (see, however, paragraph 4, below). Thus we have no clear idea on the height of formation of the O_2 emission.

3. ROTATIONAL TEMPERATURE

Considerable interest is often attached to spectroscopic determinations of ionospheric temperatures. Rotational temperatures based on the profiles of bands with unresolved structure are likely to be quite inaccurate, but several such determinations for various band systems have been widely quoted in the literature.

For the Herzberg bands in the airglow, the maximum of intensity appears to fall within the unresolved band head, and it is thus difficult to determine accurately the position or K number of this maximum. An attempt to determine $K_{\max}$ by measuring the distance between band head and observed band maximum would be implying much greater accuracy than the plate contains, even if the profile of the band head were computed by summing idealized profiles of the rotational lines.

A temperature might conceivably be derived from the relative intensities of the higher rotational lines ($K \geq 11$) on calibrated plates. Even here, there will be difficulties in that photographic photometry becomes quite uncertain with such long exposures; and, unless the rotational lines are completely separated, their relative intensities may be affected by one another. Moreover, Herzberg (1952) has pointed out that the temperature cannot be obtained accurately from the relative intensities of the lines, because the line strengths are unknown in this case of intermediate coupling.

Hence it does not seem feasible at this time to derive more than a maximum rotational temperature. Herzberg obtained $K_{\max} = 9$ in his absorption spectrum produced at 300° K. Allowing for the difference in rotational constants, B_v, between the upper and lower states, and assuming that the maximum is indeed within the band head ($K_{\max} \leq 9$), we obtain for the airglow emission

$$T_{\text{rot}} \leq 200^\circ \text{ K} .$$

Since these bands are forbidden, it should be safe to interpret T_{rot} as a kinetic temperature. The fact that the Atmospheric O_2 band also gives a very low temperature (Meinel 1950) is some support for the suggestion that both systems are formed in the

same region of the atmosphere. Moreover, the low temperature is more in accord with excitation in the region of 80–100 km than in the higher layers indicated by Barbier's (1953) photometric investigation.

4. COLLISIONAL DE-EXCITATION

The absence in the airglow of the Herzberg II ($^1\Sigma_u^- \rightarrow {}^3\Sigma_g^-$) system of O_2 suggests that collisional de-excitation may be an important factor in the emitting layer. That is, nearly all molecules in the $^1\Sigma_u^-$ excited state may be collisionally de-excited, whereas an appreciable fraction of those in $^3\Sigma_u^+$ radiate. Moreover, collisions might keep the forbidden Herzberg and Atmospheric emissions well below the quite high intensity expected on theoretical grounds for excitation by three-body association (Bates 1954, p. 619).[3]

Nicolet (1948) has already emphasized that superelastic collisions probably have a strong influence on the relative intensities and altitude of emission of the [*O* I] lines in the airglow and aurora.[4] There are two other observations that suggest that collisional de-excitation may indeed be an important factor in quenching forbidden radiation in the airglow.

In a recent paper (1954*b*) I discussed a resonance-scattering process for the O_2 Atmospheric system and showed that, in the absence of collisional de-excitation, a large part of the observed 0–1 band would originate in a thick layer at about 50 km. Hence one would expect the rotational temperature to be much higher than the observed value of approximately 150° K. It was demonstrated that this low apparent temperature could be explained if de-exciting collisions become important in the lower part of the resonance-scattering layer. It was necessary to assume, however, that above this de-exciting region collisions are not even effective enough to redistribute the molecules over their rotational levels before re-emission occurs! An alternative explanation is that collisional de-excitation is actually important up to very great heights, so that the resonance effect would not have a chance to operate. Presumably the rotational temperature would then indicate the kinetic temperature of the region where the excitation occurs. Quantitative data on the importance of collisions could be obtained from a comparison of the intensity distribution with height for the Atmospheric 0–1 band (λ 8645), as obtained by a night-fired rocket, with the author's computations for the case of resonance scattering in the absence of de-exciting collisions.

The other observation suggesting strong collisional de-excitation of airglow forbidden radiations was made by M. Dufay (1953). He has found that the weak twilight line at λ 5200, apparently due to the nebular transition of [*N* I], invariably disappears within about two hours after sunset. This line is not detected in the nightglow, and in twilight it originates from an undetermined height. However, the upper term for the [*N* I] doublet has a lifetime of 26 hours, according to transition probabilities calculated by Garstang (1952), and it thus seems unusual that the daytime excitation does not persist throughout the night.

I am greatly indebted to Dr. A. B. Meinel for a number of stimulating discussions and helpful suggestions throughout the progress of this work.

REFERENCES

Auberger, L. 1953, *J. Geophys. Res*., **58**, 231.
Barbier, D. 1945, *Ann. de Géophys*., **1**, 224.
———. 1947*a*, *Ann. d'ap*., **10**, 47.

[3] Professor Bates (private communication) has recently pointed out, however, that the figure quoted in his article "may be rather high, since recent rocket work shows that the solar intensity in the Schumann-Runge region is less than originally supposed."

[4] More recently, Seaton (1954) discussed possible de-excitation processes in the aurora.

Barbier, D. 1947*b*, *ibid.*, p. 141.
———. 1953, *ibid.*, **16**, 96.
———. 1954, *ibid.*, **17**, 97.
Bates, D. R. 1954, in G. P. Kuiper (ed.), *The Earth as a Planet* (Chicago: University of Chicago Press), chap. xii.
Broida, H. P., and Gaydon, A. G. 1954, *Proc. R. Soc. London, A*, **222**, 181.
Cabannes, J., and Dufay, J. 1944, *Ann. de Géophys.*, **1**, 1.
Chamberlain, J. W. 1954*a*, *C.R.*, **238**, 1329.
———. 1954*b*, *Ap. J.*, **119**, 328.
Chamberlain, J. W., and Meinel, A. B. 1954, in G. P. Kuiper (ed.), *The Earth as a Planet* (Chicago: University of Chicago Press), chap. xi.
Chamberlain, J. W., and Oliver, N. J. 1953, *Ap. J.*, **118**, 197.
Dufay, J. 1923, *C.R.*, **176**, 1290.
———. 1928, *Bull. Obs. Lyon*, **10**, No. 9, 81.
———. 1941, *C.R.*, **213**, 284.
———. 1947, *Ann. de Géophys.*, **3**, 1.
Dufay, J., and Déjardin, G. 1946, *Ann. de Géophys.*, **2**, 249.
Dufay, M. 1953, *Ann. de Phys.*, **8**, 813.
Garstang, R. H. 1952, *Ap. J.*, **115**, 506.
Herzberg, G. 1950, *Spectra of Diatomic Molecules* (2d ed.; New York, Toronto, and London: D. Van Nostrand Co.), p. 276.
———. 1952, *Canadian J. Phys.*, **30**, 185.
———. 1953, *ibid.*, **31**, 657.
Meinel, A. B. 1950, *Ap. J.*, **112**, 464.
———. 1953, *ibid.*, **118**, 200.
Nicolet, M. 1948, *Emission Spectra of the Night Sky and Aurora* ("Reports of the Gassiot Committee" [London: Physical Society]), p. 36.
———. 1954, in G. P. Kuiper (ed.), *The Earth as a Planet* (Chicago: University of Chicago Press), chap. xiii.
Pillow, M. E. 1953, *Proc. Phys. Soc. London, A*, **66**, 1064.
Roach, F. E., Pettit, H. B., and Meinel, A. B. 1955, *Ap. J.* (in press).
Seaton, M. J. 1954, *J. Atm. Terr. Phys.*, **4**, 295.
Swings, P. 1943, *Ap. J.*, **97**, 72.

NOTES

AN IDENTIFICATION OF THE CORONAL LINE λ 5694

The yellow coronal line λ 5694 is well known to exhibit a very erratic behavior; sometimes it is practically invisible, whereas at other times it may be the brightest coronal line. It is generally believed that the line appears near regions of high solar activity (Dolder, Roberts, and Billings 1954).

Edlén (1942) tentatively identified this line with the transition $2p^2\ {}^3P_1-{}^3P_0$ in *Ca* XV, but this identification is quite controversial (cf. Waldmeier 1951; Shklovsky 1950; Naqvi 1951*a*; Garstang 1952). Another line of *Ca* XV arising from the transition $2p^2\ {}^3P_2-{}^3P_1$ lies in the observable region and has a higher transition probability than the ${}^3P_1-{}^3P_0$ transition (Naqvi 1951*a*). If Edlén's identification is correct, this line should also be present in the corona. Waldmeier (1951) suggested the new line λ 5445, and Naqvi (1951*a*) suggested one of the lines λ 4567 and λ 4586, as due to the ${}^3P_2-{}^3P_1$ transition.

TABLE 1

${}^3P$ LEVEL INTERVALS FOR C I ISOELECTRONIC SEQUENCES

Ion	$[{}^3P_1-{}^3P_0]_{obs}$	$[{}^3P_1-{}^3P_0]_{calc}$	Δ(Obs−Calc)	$[{}^3P_2-{}^3P_1]_{obs}$	$[{}^3P_2-{}^3P_1]_{calc}$	Δ(Obs−Calc)
C I	16.4	16.5	−0.1	27.1	27.1	0
N II	49.1	48.7	+0.4	82.2	82.3	−0.1
O III	113.4	113.4	0	193.4	193.4	0
F IV	225.2	226.6	−1.4	388.2	388.1	+0.1
Ne V	414	411.8	+2.2	698	698.2	−0.2
Na VI	698	699.3	−1.3	1160	1159.7	+0.3
Mg VII	1127	1126.9	+0.1	1812	1812.3	−0.3
Al VIII	1740	1739.8	+0.2	2700	2699.8	+0.2
Si IX	2590	2590.0	0	3870	3870.0	0

The main difficulty is that the wave lengths of the lines due to the highly ionized atoms are not known, since their spectra have not been produced and analyzed in the laboratory so far. These wave lengths, therefore, have to be determined by some method of extrapolation, involving substantial and often unascertainable errors. Naqvi (1951*b*) adopted a procedure wherein the known intervals along an isoelectronic sequence are fitted to a suitable polynomial by the least-squares method. The fits obtained are generally good, and in the case of the *C* I isoelectronic sequence, to which *Ca* XV belongs, the fit is excellent, as is shown in Table 1. The level intervals are given in cm^{-1}. The observed values are taken from the Atomic Energy Levels by Miss Moore (1949). PX is not included here as its observed level intervals appear to be erroneous (Naqvi 1953).

From this fit the extrapolated wave lengths of the *Ca* XV lines are ${}^3P_2-{}^3P_1 = 4998$ A, ${}^3P_1-{}^3P_0 = 6055$ A. Our estimate is that the error in these values does not much exceed 50 A. The identification of λ 5694 as well as of λλ 5445, 4586, and 4567 as due to transitions in *Ca* XV therefore seems most unlikely. The coronal wave lengths mentioned above can be shown to be irreconcilable with the trend along the *C* I isoelectronic sequence.

As an illustration of the accuracy to be expected from our method of extrapolation,

we give in Table 2 the extrapolated wave lengths along with the actual coronal wave lengths of several lines for which Edlén's identifications are regarded as established. We have determined the extrapolated wave lengths for all relevant highly ionized atoms having configurations p, p^2, p^4, p^5, and sp. We find that only two transitions (see Table 3) have wave lengths close to 5694 A.

The wave length of the *Cl* XIII line is quite close to 5694 A, whereas that of the *A* XV line is within the limits of error of extrapolation. We determined the wave lengths of other lines of these atoms, including other stages of ionization. Except for the lines which

TABLE 2

COMPARISON OF THE CORONAL WITH THE EXTRAPOLATED WAVE LENGTHS

Ion	Transition	Coronal Wave Length	Extrapolated Wave Length	Remarks on Fit
Fe XIV	$3p^2P_{3/2}-{}^2P_{1/2}$	5303	5293	Good
Ni XVI	$3p^2P_{3/2}-{}^2P_{1/2}$	3601	3589	
Fe XIII	$3p^2\,{}^3P_1-{}^3P_0$	10747	10732	Good
Ni XV	$3p^2\,{}^3P_1-{}^3P_0$	6701	6736	
Ni XIII	$3p^4\,{}^3P_1-{}^3P_2$	5116	5200	Fair
Fe XI	$3p^4\,{}^1D_2-{}^3P_1$	3986	3911	Bad
Ni XIII	$3p^4\,{}^1D_2-{}^3P_1$	3643	3482	
A X	$2p^5\,{}^2P_{1/2}-{}^2P_{3/2}$	5536	5535	Good

TABLE 3

EXTRAPOLATED WAVE LENGTHS FOR SUGGESTED IDENTIFICATIONS OF THE YELLOW LINE

Ion	Transition	Wave Length	A*	I.P.† (Volts)
A XV	$2s2p^3P_2-{}^3P_1$	5765	70	755
Cl XIII	$2p^2P_{3/2}-{}^2P_{1/2}$	5707	47	592

* Transition probability (Naqvi 1951b).

† Extrapolated values for the next lower stage of ionization.

lie outside the observable range or which have low transition probabilities, we found that they are either present in the corona or are probably blended with other coronal lines. The transition probability of the argon line is larger than that of the chlorine line. The abundances of these elements in the sun are not known. In γ Pegasi (Aller 1949), the only star where their abundances have been determined, the ratio *A*/*Cl* is 5, but even this is only an estimate. The difficulty of a companion line, found in the case of *Ca* XV identification, does not exist with either of these transitions.

In a recent paper Pecker, Billings, and Roberts (1954*a*, *b*) have found the atomic weight of the atom responsible for the yellow line to be nearly 40. This atomic weight corresponds to that of *Ca* (40.1) as well as to that of *A* (39.9). Since *Ca* XV identification seems improbable, this can be regarded as a confirmation of the identification with argon. The atomic weight of *Cl* (35.5) is perhaps a little beyond the limits of accuracy

of the measurements. We favor the identification with *A* XV, although the possibility of the *Cl* XIII transition cannot be ruled out entirely at present.

It is noteworthy that the ionization potential for the production of the *A* XV ion is 755 volts, rather close to that for *Ca* XV (814 volts). The excitation potential for the production of the *A* XV line is also rather high, about 30 volts.

ALI M. NAQVI
S. P. TALWAR

UNIVERSITY OF DELHI
DELHI, INDIA
July 7, 1954

REFERENCES

Aller, L. H. 1949, *Ap. J.*, **109**, 244.
Dolder, F. P., Roberts, W. O., and Billings, D. E. 1954, *Ap. J.*, **119**, 120.
Edlén, B. 1942, *Zs. f. Ap.*, **22**, 30.
Garstang, R. 1952, *Ap. J.*, **115**, 569.
Moore, C. E. 1949, *Atomic Levels* (Circ. No. 467, National Bureau of Standards, Washington, D.C.).
Naqvi, A. M. 1951*a*, *A.J.*, **56**, 135.
———. 1951*b*, thesis, Harvard University.
———. 1953, *Proc. Nat. Inst. Sci. India*, **19**, 461.
Pecker, J. C., Billings, D. E., and Roberts, W. O. 1954*a*, *C.R.*, **238**, 1101.
———. 1954*b*, *Ap. J.*, **120**, 509.
Shklovsky, I. S. 1950, *Izvest. Krymsk. Ap. Obs.*, **5**, 86.
Waldmeier, M. 1951, *Zs. f. Ap.*, **29**, 29.

ANNOUNCEMENT

Since January, 1948, the annual subscription to the *Astrophysical Journal* has been $12.00. For members of the American Astronomical Society a reduced rate ($7.00 a year) has been applicable in accordance with a special arrangement between the University of Chicago and the American Astronomical Society. Apart from the receipts from subscriptions, the *Astrophysical Journal* has depended for its maintenance on the generous support which it has received from the observatories and astronomical departments of this country in the payment of page charges for publication of papers in the *Astrophysical Journal* and the "Supplement Series." Unfortunately, the inflationary increase in prices since the end of the war, coupled with the increased astronomical productivity in the country, have made it impossible for the *Journal* to balance its budget. Thus during the fiscal year 1953–1954, the *Astrophysical Journal* incurred a deficit of nearly $3,000.00 in its operating budget. It is clear that the *Journal* cannot continue to incur such deficits and that prompt steps should be taken to prevent their recurrence. The steps which the Editorial Board of the *Astrophysical Journal* has approved are the following:

The annual subscription to the *Astrophysical Journal* has been increased to $15.00. The new rate starts with this issue. This applies to all subscribers except those who are members of the American Astronomical Society; the current reduced rates will continue to apply to them for the time being. Along with this increase in subscription, the current page charge for publication in the *Astrophysical Journal* and its "Supplements" has also been increased. The new rates are: $10.00 per page for articles which do not have an excess of mathematical formulae or tabular material; $15.00 per page for articles which are largely mathematical or tabular; $6.00 per page for material submitted in a form suitable for planographing; and $15.00 per page of half-tone illustrations. A modest increase in the cost of reprints has also been approved.

The Editorial Board has postponed as long as it possibly could the foregoing increases; but they now seem inevitable. The University of Chicago Press and the Editorial Board of the *Astrophysical Journal* sincerely hope that, in spite of the increased burden which it has been forced to place on its subscribers and on its contributors, its actions to balance the budget of the *Journal* will be understood and that it will continue to receive the cordial co-operation it has had during its nearly sixty years of publication.

S. CHANDRASEKHAR
Managing Editor

The Second Volume in a Distinguished Series

THE EARTH AS A PLANET

The Solar System—Volume II

Edited by GERARD P. KUIPER

This is the second of four volumes designed to collect and systematize our knowledge of the solar system. Like its predecessor, *The Sun*, it is conceived as both a reference book for the specialist and a source of general information for the general reader with some knowledge of the physical sciences.

Consisting of authoritative articles written by internationally eminent specialists, *The Earth as a Planet* is a complete and fully documented handbook, covering the entire range of physics, geochemistry, oceanography, and biochemistry as they apply to the earth in its planetary aspect. Among the many topics treated are the rotation of the earth; the nature of the earth's interior; the growth of continents; current systems of oceans and atmospheres; the life-cycles of methane, carbon dioxide, oxygen, and nitrogen; the absorption spectrum of the atmosphere; the physics and chemistry of the upper atmosphere; and the appearance of the earth from interplanetary space.

Contributions by

SIR HAROLD SPENCER JONES
FRED L. WHIPPLE
J. TUZO WILSON
D. R. BATES
HORACE R. BYERS
LEO GOLDBERG
SIR EDWARD BULLARD
A. B. MEINEL
BRIAN MASON
CLYDE T. HOLLIDAY
ANDRÉ DANJON
SIR HAROLD JEFFREYS
J. W. CHAMBERLAIN
H. U. SVERDRUP
M. NICOLET
G. E. HUTCHINSON

752 pages *$12.50*

The remaining two volumes in the series will consist of *Planets and Comets, Part 1, Planets and Satellites* and *Planets and Comets, Part 2, Minor Planets, Meteorites, Comets, Origin of the Solar System.*

from your bookseller or from

THE UNIVERSITY OF CHICAGO PRESS
5750 ELLIS AVENUE CHICAGO 37, ILLINOIS

COMPANION VOLUMES

ASTROPHYSICS

THE ATMOSPHERES OF THE SUN AND STARS

LAWRENCE H. ALLER, *University of Michigan*

THOROUGH COVERAGE of present-day knowledge concerning the atmospheres of the sun and stars and solar-terrestrial relationships. Provides a short introduction to astronomy and a review of relevant physics. Treats all major astrophysical principles—atomic structure and spectra, gas laws and velocity distribution, ionization, excitation, etc.—and applies them to the radiation of the sun and stars, to their continuous and dark-line spectra, to solar phenomena, and to solar-terrestrial relationships. Each principle is applied to a definite numerical problem concerned with the interpretation of stars and nebulae. *116 ills., 44 tables, 412 pages.* **$12**

"Hard to overemphasize the importance of this book . . . presents the subject of stellar atmospheres as it is known and accepted today."

—Publications of the Astronomical Society of the Pacific

CONTENTS: Survey of Basic Data—Atomic and Molecular Spectra—Gas Laws and Equations of State, Turbulence—Excitation, Ionization, and Dissociation—Emission and Absorption of Radiation—Radiation of Stars—Continuous Spectra of Sun and Stars—The Fraunhofer Spectrum—Solar Phenomena

ASTROPHYSICS

NUCLEAR TRANSFORMATIONS, STELLAR INTERIORS, AND NEBULAE

also by **LAWRENCE H. ALLER**

NEWLY PUBLISHED. A thorough study of thermal nuclear reactions, the interiors of stars, pulsating variable stars, and the interstellar medium. Covers fundamentals and major modern developments in the field. Emphasis is placed on the methods and procedures by which results are obtained. The book treats of the properties of matter at high temperatures, stellar energy generation, internal constitution of stars, stellar evolution and the origin of the elements, novae and supernovae, gaseous nebulae, with particular attention to discoveries achieved by radio astronomy. Illustrated with numerous diagrams and photographs, many reproduced here for the first time. *52 ills., 16 tables, 291 pages.* **$12**

CONTENTS: Stellar Interiors and Nuclear Transformations—Model Stars—The Cepheids and Long-Period Variables—Stars with Extended Envelopes, Novae, and Supernovae—The Planetary Nebulae—The Interstellar Medium

Order through your bookstore or from:

THE RONALD PRESS COMPANY · 15 E. 26th St., N.Y. 10